
Cancer
Cell
Volume 21
Number 4
April 17, 2012
www.cellpress.com
Visualizing Host Contribution
to Chemoresistance

CALming Down T Cell Acute Leukemia

Emilio Hirsch[1,*] and Roberto Chiarle[2,3]
[1]Molecular Biotechnology Center
[2]Department of Biomedical Sciences and Human Oncology and CERMS
University of Torino, 10126 Torino, Italy
[3]Department of Pathology, Children's Hospital, Harvard Medical School, Boston, MA 02215, USA
*Correspondence: emilio.hirsch@unito.it
DOI 10.1016/j.ccr.2012.03.025

Signaling from class I phosphoinositide 3-kinase (PI3K) is often deregulated in leukemia and lymphoma, but which isoforms are involved in T cell acute lymphoblastic leukemia (T-ALL) was not known. In this issue of *Cancer Cell*, Subramaniam et al. show that T-ALL can be tamed by inhibiting γ and δ PI3K isoforms.

Class I phosphoinositide 3-kinase (PI3K) activate fundamental pathways controlling survival, proliferation, and metabolism and thus represent crucial players in cancer development. Despite activating similar signaling cascades, the four human class I PI3Ks, each of which is composed of a regulatory subunit and one of the four p110 catalytic subunits (p110α, β, γ, and δ), show non-redundant roles in oncogenesis. For example, *PIK3CA*, the gene encoding p110α, is frequently mutated in cancers originating from different organs, including the mammary gland, colon, prostate, and brain (Wong et al., 2010). On the contrary, the p110β isoform does not accumulate mutations but plays a critical role in specific tumors, such as PTEN-deficient (Jia et al., 2008) or ErbB2-driven (Ciraolo et al., 2008) cancers. Similarly, the leukocyte-specific p110δ isoform is usually intact in human cancers, yet it drives B cell malignancies including chronic lymphocytic leukemia and mantle cell lymphoma (So and Fruman, 2012).

The fourth PI3K catalytic isoform, p110γ, is mainly expressed in leukocytes, and its role in cancer is only now starting to emerge. In white blood cells, p110γ usually drives G protein coupled receptor (GPCR)-mediated responses and shapes various forms of inflammatory reactions by controlling macrophage and neutrophil migration to chemotactic cues (Ghigo et al., 2010). Similar to p110δ, p110γ is also highly expressed in B and T lymphocytes but with a role considered minor so far, probably not affecting trafficking but rather specific differentiation steps. In T cell development, p110γ and p110δ together control the β selection process, allowing thymocytes to mature to the double positive (DP) stage. In these maturation steps, p110δ is required to modulate signals that originate from the pre-T cell receptor (TCR) complex, whereas p110γ is necessary for signals that derive from CXCR4 activation (Figure 1). Deletion of *PTEN* from developing thymocytes allows an unopposed activation of both p110s, resulting in abnormal passage to the DP stage in the absence of a mature TCR as well as in the development of T cell leukemia (So and Fruman, 2012).

Despite the ability of p110γ to cause transformation when overexpressed in cultured cells (Kang et al., 2006), direct evidence for its role in human cancer was missing. The ability of PI3Kγ to activate the classical PI3K pathway, triggering AKT, GSK3, and S6K phosphorylation, was long considered a business mainly for innate immunity aficionados. Nonetheless, recent evidence indicates that PI3Kγ is a key player in the inflammatory reactions that contribute to tumor progression and spreading (Schmid et al., 2011). In addition, PI3Kγ has also been found to drive, in immunocompromised patients, angioproliferative tumors induced by the Kaposi's sarcoma-associated virus, where its oncoviral receptor vGPCR couples to PI3Kγ to induce AKT/mTOR signaling (Martin et al., 2011).

The article by Subramaniam et al. (2012) in this issue of *Cancer Cell* further extends this notion and shows that PI3Kγ functions in concert with its cousin PI3Kδ to support development of T cell acute lymphoblastic leukemia (T-ALL). How did Subramaniam et al. (2012) discover these unexpected findings? They reasoned that the PI3K/AKT signaling pathway is frequently activated in T-ALL driven by PTEN loss (found in about 40% of T-ALL patients) rather than by activating mutations of *PIK3CA* that are found commonly in solid cancers (Wong et al., 2010). Therefore, other class I PI3Ks likely were involved in T-ALL. Developing thymocytes are thought to be the normal counterpart of transformed T-ALL cells, and the activities of both PI3Kδ and PI3Kγ are required to sustain normal thymic development and thymocyte survival (So and Fruman, 2012). Thus, Subramaniam et al. (2012) set out to define the PI3K isoform involved in T-ALL by introducing null mutations in *Pik3cg* and *Pik3cd*, which encode for p110γ and p110δ respectively, in a mouse model of T-ALL induced by conditional PTEN loss in T cells. To their surprise, in strict similarity with normal T cell development, both p110δ and p110γ were necessary to sustain T-ALL development, whereas single mutants had no antitumor effect (Figure 1). Deletion of PTEN in the absence of both p110δ and p110γ was not associated with increased AKT phosphorylation, thus indicating a negligible role for the other two class I PI3K isoforms, PI3Kα and PI3Kβ, in the development of either normal T cells or leukemia.

These findings are interesting for several reasons. First, they reaffirm the concept of a strong interconnection between T cell development and T cell leukemia, similarly to other T-ALL oncogenes. For example, Notch1 plays crucial roles in T cell differentiation and is frequently mutated in T-ALL (Aifantis et al., 2008). The essential PI3Kδ and PI3Kγ signaling functions in T cell development could thus be retained and exploited by leukemic cells. Second, these results clearly show an additive role for p110δ and p110γ in T cell leukemia but

interaction with ETS1, a critical component of the complex that binds and activates Eα (Figure 1). To test the biological significance of this interaction on the enhancer element, the authors silenced TLX1/3 in human T-ALL cell lines and observed increases in differentiation and cell death, suggesting abortive differentiation and induction of apoptosis. Ectopic expression of rearranged TCRα caused identical effects. These findings therefore connect proper TCR rearrangement and expression to tumor differentiation state.

Altogether, the work of Dadi et al. (2012) presents a novel mechanism of differentiation arrest orchestrated by the TLX oncogenes in the induction and maintenance of T-ALL. To this end, it will be important to determine whether additional transcriptional targets that are potentially perturbed by TLX1/3 are also important for progression of the disease. This is an important question as the differentiation defects seen in *TLX1* transgenic mice are distinct from those caused by paucity of TCRα rearrangement in human leukemia. One such example could be the downregulation *BCL11B*, a target of TLX1 that is essential for T cell commitment. Further investigation on the potential synergistic role other factors play in the TCR recombination (Polycomb complex, the CTCF insulator protein, and others) and on the mechanisms leading to sustained expression of the TLX proteins will shed light on the intricacies of this leukemia. Ultimately, the most intriguing implication of this study is whether there are means of regulating TLX function using targeted therapies to enforce differentiation of TLX1/3$^+$ T-ALL. A similar approach of "differentiation therapy" has been extremely effective in the treatment of acute promyelocytic leukemia with all-trans retinoic acid (Kogan and Bishop, 1999). Given that their expression is normally restricted to embryonic development, TLX1/3 could prove to be ideal targets in the treatment of large fraction T cell leukemias with limited potential for adverse side effects.

REFERENCES

Aifantis, I., Raetz, E., and Buonamici, S. (2008). Nat. Rev. Immunol. *8*, 380–390.

Dadi, S., Le Noir, S., Payet-Bornet, D., Lhermitte, L., Zacarias-Cabeza, J., Bergeron, J., Villarèse, P., Vachez, E., Dik, W.A., Millien, C., et al. (2012). Cancer Cell *21*, this issue, 563–576.

De Keersmaecker, K., Real, P.J., Gatta, G.D., Palomero, T., Sulis, M.L., Tosello, V., Van Vlierberghe, P., Barnes, K., Castillo, M., Sole, X., et al. (2010). Nat. Med. *16*, 1321–1327.

Gutierrez, A., Kentsis, A., Sanda, T., Holmfeldt, L., Chen, S.C., Zhang, J., Protopopov, A., Chin, L., Dahlberg, S.E., Neuberg, D.S., et al. (2011). Blood *118*, 4169–4173.

Hatano, M., Roberts, C.W., Minden, M., Crist, W.M., and Korsmeyer, S.J. (1991). Science *253*, 79–82.

Kogan, S.C., and Bishop, J.M. (1999). Oncogene *18*, 5261–5267.

Mullighan, C.G., and Downing, J.R. (2009). Leukemia *23*, 1209–1218.

Schatz, D.G., and Swanson, P.C. (2011). Annu. Rev. Genet. *45*, 167–202.

Sleckman, B.P., Bassing, C.H., Bardon, C.G., Okada, A., Khor, B., Bories, J.C., Monroe, R., and Alt, F.W. (1998). Immunol. Rev. *165*, 121–130.

Van Vlierberghe, P., Palomero, T., Khiabanian, H., Van der Meulen, J., Castillo, M., Van Roy, N., De Moerloose, B., Philippé, J., González-García, S., Toribio, M.L., et al. (2010). Nat. Genet. *42*, 338–342.

Personalized Medicine: Patient-Predictive Panel Power

Paul Workman,[1,*] Paul A. Clarke,[1] and Bissan Al-Lazikani[2]
[1]Signal Transduction and Molecular Pharmacology Team
[2]Computational Biology and Chemogenomics Team
Cancer Research UK Cancer Therapeutics Unit, Division of Cancer Therapeutics, The Institute of Cancer Research, Haddow Laboratories, 15 Cotswold Road, Sutton SM2 5NG, UK
*Correspondence: paul.workman@icr.ac.uk
DOI 10.1016/j.ccr.2012.03.030

Two recent papers published in *Nature* demonstrate the power of systematic high-throughput pharmacologic profiling of very large, diverse, molecularly-characterized human cancer cell line panels to reveal linkages between genetic profile and targeted-drug sensitivity. Known oncogene addictions are confirmed while surprising complexities and biomarker relationships with clinical potential are revealed.

The need to identify predictive biomarkers of tumor response has intensified with the era of molecularly-targeted therapies that exploit addictions and vulnerabilities in tumors with identifiable molecular traits, in contrast to the one-size-fits-all approach that dominated cytotoxic chemotherapy (Yap and Workman, 2012). Two recent *Nature* articles describe a systematic large-scale approach to this challenge by high-throughput profiling many targeted agents against hundreds of clinically-relevant human cancer cells lines with detailed genetic annotation (Garnett et al., 2012; Barretina et al., 2012).

There are three important general take-home messages from these two studies. (1) The articles provide the most extensive

validation to date for systematic large-scale analyses of human tumor cell panels that link drug sensitivity to cancer cell genetics. (2) They reveal examples of previously unsuspected genetic-pharmacologic relationships and complexities, some with immediate clinical potential. (3) They make available publicly the pharmacologic screening data alongside extensive genetic and other molecular characterization of the cancer cell panel (http://www.broadinstitute.org/ccle; http://www.cancerrxgene.org/), providing powerful tools and resources for use by the cancer community. Researchers can now mine the datasets to generate and test hypotheses, while new compounds can be submitted to the panel screens for pharmacogenomic interrogation.

A caveat of these studies is that both use the artificial two-dimensional adherent growth of established cancer cell lines on plastic and also lack the environmental and cellular complexity of clinical cancers. Nevertheless, very large diverse cancer cell line panels provide the only means currently available with which to model the enormous genetic and epigenetic heterogeneity present in human cancers and hence to identify predictive response biomarkers that address the molecular diversity seen in the clinic (Caponigro and Sellers, 2011).

The systematic large-scale pharmacologic and genetic analysis approach has its origins in the pioneering NCI60 tumor cell line panel (Weinstein et al., 1997). This led to use of larger cancer cell line panels that identified genotype-correlated sensitivity to kinase inhibitors within and between cancer histologies. However, it became clear that hundreds of cancer cell lines must now be used to mimic clinical heterogeneity and to account for pathogenic driver mutations present in only, say, 5% or even less of cancers (Caponigro and Sellers, 2011; Garnett and McDermott, 2012).

Figure 1A summarizes the workflow used for the two studies. Several clear high-level trends emerge from the analysis. Certain agents, e.g., the microtubule stabilizer paclitaxel and the pan-histone deacetylase inhibitor panobinostat, show broad activity whereas a few, including p53-MDM2 antagonists, are active in a small minority of cancer cell lines. Outlier cell lines with unusual sensitivity are often informative. Sensitivity to most agents is associated with at least one gene mutation, importantly demonstrating the very broad potential applicability of predictive biomarkers. Known oncogene addiction paradigms are reconfirmed in the large scale panels for several approved or developmental kinase inhibitors, including those targeting BCR-ABL, BRAF, MEK, ALK, ERBB2, EGFR, FLT3, and PIK3CA. Interestingly, however, gene expression features often correlate as well or even better with sensitivity than kinase mutation. Furthermore, mutation-sensitivity relationships are frequently modified by tissue-specific or gene expression biomarkers, suggesting the need for multigene signatures of sensitivity and reinforcing the importance of mechanistic drug combinations.

Some specific examples are illustrative (Figure 1B). Both studies conclusively demonstrate that expression of the quinone reductase metabolizing enzyme NQO1 was the strongest predictor of sensitivity to the benzoquinone ansamycin HSP90 molecular chaperone inhibitor 17-AAG (tanespimycin), as initially discovered using the NCI60 panel (Kelland et al., 1999), but not to the non-quinone chemotype NVP-AUY922, thus exemplifying differences in predictors between chemotypes hitting the same target.

The now clinically-validated synthetic-lethal relationship between inhibitors of the DNA repair enzyme poly(ADP-ribose) polymerase (PARP) and *BRCA* mutations could not be revealed in the short, 3 day drug exposures used. Thus other synthetic lethal relationships might also be missed. However, Garnett et al. (2012) do confirm the very recent discovery that PARP inhibitors (here olaparib and AG-014699) are highly active against Ewing's sarcoma cells with the characteristic *EWS-FLI1* rearrangement (Brenner et al., 2012), analogous to the sensitivity to PARP inhibition of prostate cancer cells with related *ETS* gene fusions (Brenner et al., 2011). Sensitivity may relate to PARP1 acting as a cofactor for the transcriptional activity of *ETS* family proteins or to a known EW1-FLI1-PARP positive feedback loop in transcriptional activation. Although sensitivity does not appear to be due to a defective DNA damage response per se, PARP inhibition may potentiate EST-mediated DNA damage. Thus there is exciting potential for evaluating PARP inhibitors in Ewing's sarcoma patients.

An unexpected and unexplained finding is that expression of *SLFN11*, encoding a member of the schlafen family of proteins with unknown function, is predictive of sensitivity to two camptothecin-based topoisomerase I inhibitors in several cancer cell lineages including, again, Ewing's sarcoma lines (Barretina et al., 2012). Clinical trials with topoisomerase inhibitors are already underway in Ewing's sarcoma.

BRAF and *NRAS* mutations are reconfirmed in both large-scale studies as single-gene predictors of sensitivity to MEK inhibitors. Expression of a group of genes, including those encoding known regulators of MAP kinase signaling, is found to modulate MEK inhibitor sensitivity. A novel observation is that expression of the aryl hydrocarbon receptor gene (*AHR*) strongly correlates with sensitivity to MEK inhibition in cancer cells with *NRAS* mutations and may be a predictive biomarker for increased MEK sensitivity in such cancers (Barretina et al., 2012). The causal link was confirmed by *AHR* silencing, which suppresses the growth of high but not low *AHR* expressing *NRAS* mutant cancer lines. Interestingly, Garnett et al. (2012) find that resistance to MEK inhibitors is also associated with the driver *EWS-FLI1* translocation.

Our own preliminary analysis of these data sets reveals, with a few notable exceptions, a surprising lack of correlation between the cellular effects of groups of drugs that supposedly have the same primary molecular mechanism, indicating polypharmacology and complex response drivers other than the declared targets. Interestingly, among the exceptions that are tightly correlated, the highly selective MEK inhibitors AZD-6244 and PD-0325901 show identical effector gene associations. In contrast, PARP and HSP90 inhibitors exhibit different effector gene associations that suggest a more complex basis for their action (Figure 1B).

For most drugs, sensitive cell lines are distributed across multiple cancer types. However, both articles show examples of cell lineage, rather than genetics, being the predominant predictive feature. Multiple myeloma cell lines with elevated IGF1 and IGF1R expression exhibit enhanced sensitivity to an IGF-1 receptor inhibitor, renal cell carcinomas to SRC inhibitors, and gliomas to a ROCK inhibitor. A hematologic lineage was predictive

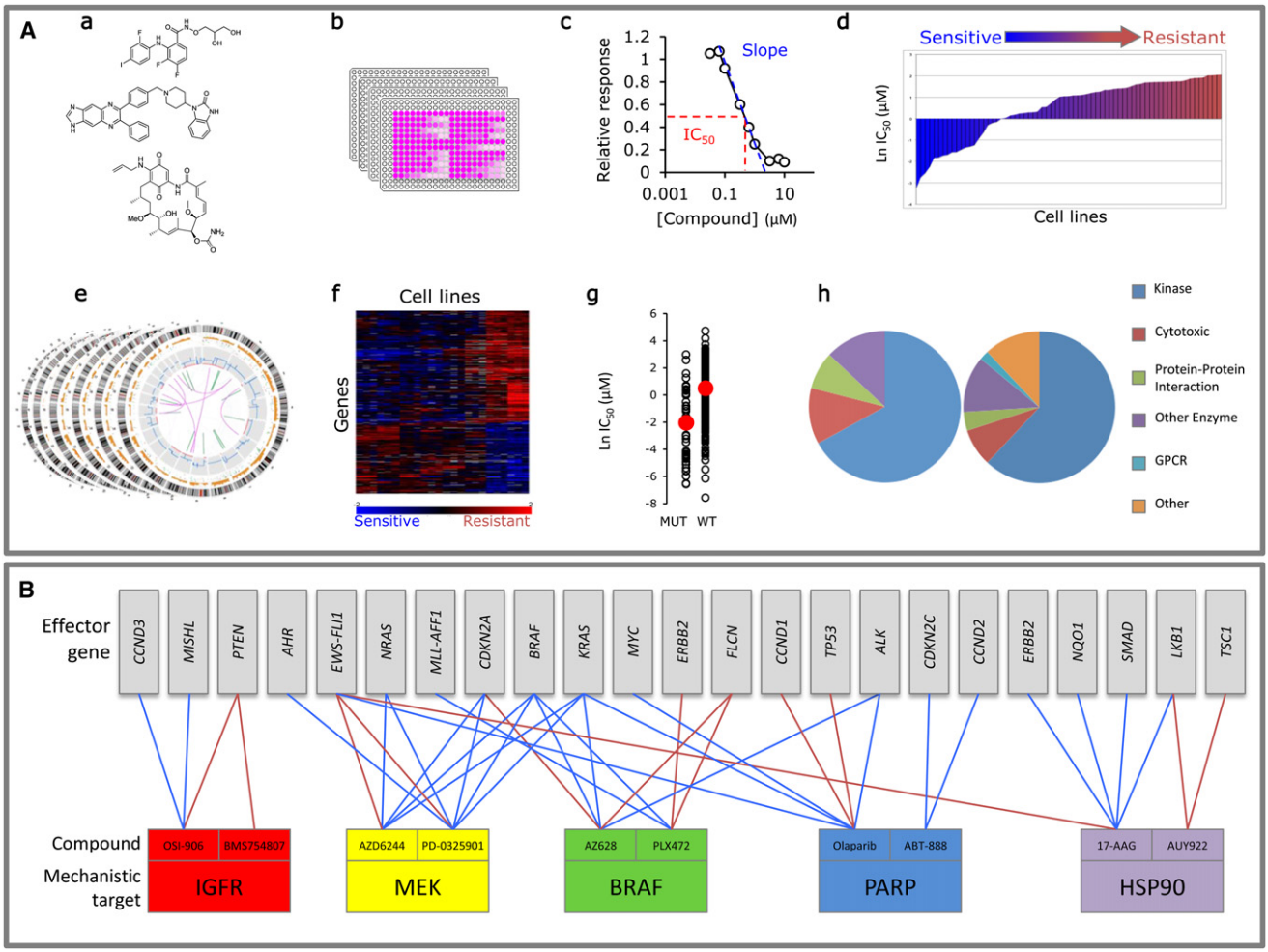

Figure 1. Systematic Large-Scale Pharmacologic and Genetic Profiling of Extensive Human Cancer Cell Line Panels

(A) Schematic of the workflow for screening human tumor cell line panels to identify factors that influence response to small-molecule drugs or tool compounds. A library of compounds (a) was screened in microplate format (b) against a diverse panel of cancer cell lines using an eight- to nine-point dose-response curve (c) from which sensitivities were calculated either as the concentration causing half-maximal inhibition of growth (IC_{50}) or from the slope of the responsive part of the curve. This generated a response profile across the cancer cell line panel for each compound (d). Garnett et al. (2012) profiled 130 agents against 275–507 cancer cell lines using a nine-point dose-response following 72 hr continuous exposure to compounds and assessed sensitivity by cell fixation and staining with a fluorescent DNA-binding dye as the end-point. Barretina et al. (2012) assessed 24 compounds across a panel of 479 tumor cell lines with an eight-point dose-response and measured total ATP using a luciferase-based assay following 72–84 hr continuous exposure. The sensitivity profile was then correlated with genomic features (e), gene expression patterns (f), or oncogenic mutations (g) using statistical methods. Both groups used the same chip-based methodology to determine single nucleotide polymorphism status and gene copy number. Garnett et al. (2012) profiled expression of 14.5k genes using oligonucleotide-based microarray technology. Barretina et al. (2012) profiled more genes with a later version of the same system. Point mutation status was determined by capillary sequencing of all coding exons for 64 genes frequently mutated in cancer by Garnett et al. (2012) or by targeted massively parallel sequencing of 1651 protein coding genes by Barretina et al. (2012) (h) Distribution of mechanistic classes of tested compounds in Barretina et al. (2012) (left) and Garnett et al. (2012) (right). (B) Examples of targeted drugs and corresponding effector genes identified in the two studies to be associated with sensitivity (blue lines) or resistance (red lines).

of panobinostat sensitivity, in agreement with the majority of clinical responses to panobinostat and other HDAC inhibitors being in hematological cancers.

Overall, these two important new studies firmly establish the value of systematic large-scale automated human cancer cell panel profiling for discovering cancer cell vulnerabilities, defining the cellular mechanism of action of small-molecule inhibitors, and identifying predictive biomarkers. The analytical power of the panels will grow as more compounds are profiled, including the important need to confirm biological associations using compounds of diverse chemotypes that hit the same target (Workman and Collins, 2010) and will also increase as the depth of genetic annotation rises, with the planned inclusion of the sequencing data for the coding exons of all ~22,000 human genes (Caponigro and Sellers, 2011; Garnett and McDermott, 2012). Additional cancer cell line annotations, including epigenomic, proteomic, and metabolomic features, would add further mechanistic and predictive power. Future iterations of the screens could involve use of more physiological growth conditions and longer incubation times.

Thus patient-predictive human cancer cell panels are set to become an

increasingly powerful platform for systematic mechanistic studies and especially for biomarker discovery. This, in turn, will facilitate the development and widespread application of personalized cancer medicine.

REFERENCES

Barretina, J., Caponigro, G., Stransky, N., Venkatesan, K., Margolin, A.A., Kim, S., Wilson, C.J., Lehar, J., Kryukov, G.V., and Sonkin, D. (2012). Nature *483*, 603–607.

Brenner, J.C., Ateeq, B., Li, Y., Yocum, A.K., Cao, Q., Asangani, I.A., Patel, S., Wang, X., Liang, H., Yu, J., et al. (2011). Cancer Cell *19*, 664–678.

Brenner, J.C., Feng, F.Y., Han, S., Patel, S., Goyal, S.V., Bou-Maroun, L.M., Liu, M., Lonigro, R.J., Prensner, J.R., Tomlins, S.A., and Chinnaiyan, A.M. (2012). Cancer Res. *72*, 1608–1613.

Caponigro, G., and Sellers, W.R. (2011). Nat. Rev. Drug Discov. *10*, 179–187.

Garnett, M.J., and McDermott, U. (2012). Drug Discov. Today *17*, 188–193.

Garnett, M.J., Edelman, E.J., Heidorn, S.J., Greenman, C.D., Dastur, A., King, L.W., Greninger, P., Thompson, R., Luo, X., Soares, J., et al. (2012). Nature *483*, 570–575.

Kelland, L.R., Sharp, S.Y., Rogers, P.M., Myers, T.G., and Workman, P. (1999). J. Natl. Cancer Inst. *91*, 1940–1949.

Weinstein, J.N., Myers, T.G., O'Connor, P.M., Friend, S.H., Fornace, A.J., Jr., Kohn, K.W., Fojo, T., Bates, S.E., Rubinstein, L.V., Anderson, N.L., et al. (1997). Science *275*, 343–349.

Workman, P., and Collins, I. (2010). Chem. Biol. *17*, 561–577.

Yap, T.A., and Workman, P. (2012). Annu. Rev. Pharmacol. Toxicol. *52*, 549–573.

Cancer Cell
Previews

Breaking the LSD1/KDM1A Addiction: Therapeutic Targeting of the Epigenetic Modifier in AML

Alyson A. Lokken[1] and Nancy J. Zeleznik-Le[1,2,*]
[1]Oncology Institute
[2]Department of Medicine
Loyola University Chicago, Maywood, IL 60153, USA
*Correspondence: nzelezn@lumc.edu
DOI 10.1016/j.ccr.2012.03.027

KDM1A/LSD1, a histone H3K4/K9 demethylase and epigenetic regulator with roles in both gene activation and repression, has increased expression in multiple cancer types. Harris et al., in this issue of *Cancer Cell*, and Schenk et al. show that KDM1A may be a viable therapeutic target in treating AML.

Epigenetic regulation of gene expression, through both histone modification and DNA methylation, provides cells with a heritable mechanism for controlling gene expression without altering the DNA nucleotide sequence. KDM1A/lysine specific demethylase 1 (LSD1) was discovered in 2004 as the first histone demethylase, with specificity for mono- and dimethyl histone H3 lysine 4 and mono- and dimethyl histone H3 lysine 9. Prior to its identification, methylation of histones was thought to be a relatively permanent epigenetic mark. KDM1A is a member of the flavin adenine dinucleotide (FAD)-dependent family of amine oxidases, which require FAD to oxidize the mono- or dimethyl lysine to an imine intermediate that is further hydrolyzed to unmodified lysine and formaldehyde (Shi et al., 2004).

KDM1A was originally identified as a member of the CoREST repressor complex (You et al., 2001) (Figure 1A). When this complex is targeted to lineage-specific genes, KDM1A demethylates the activating H3K4me2 mark to silence their expression. Additional repressive complexes containing KDM1A have since been identified (Wang et al., 2007).

Conversely, KDM1A has been found to interact with multiple proteins/complexes that function in gene activation (Figure 1A). KDM1A is required for transcription of androgen receptor (AR) and estrogen receptor (ER) target genes, where it is recruited via interaction with AR or ER, respectively, and is thought to demethylate the repressive H3K9me2 mark to allow for gene activation (Metzger et al., 2005). KDM1A is also a member of a transcription elongation complex composed of ELL (elongation factor RNA polymerase II), pTEFb, AF4, and AFF4 (Biswas et al., 2011). Additionally, KDM1A is a component of an MLL supercomplex associated with active transcription (Nakamura et al., 2002). MLL itself is an epigenetic modifier as a histone methyltransferase with specificity for H3K4.

In normal hematopoietic development, hematopoietic stem cells undergo a series of changes in gene expression which both promote differentiation to mature blood cell lineages and repress genes necessary for maintaining stem cell identity. These changes are mediated, in part, by epigenetic modifiers such as KDM1A and MLL (Figure 1B). In leukemia, this normal process of cellular maturation goes awry; the leukemic stem cells (LSCs) do not differentiate appropriately, with resultant accumulation of immature blast cells.

The mixed lineage leukemia gene (*MLL*) is frequently involved in chromosomal translocation with one of a variety of partner genes in acute leukemias of myeloid (AML) or lymphoid lineage. As a result, functional oncogenic fusion proteins are produced that promote the constitutive expression of MLL target genes, thereby blocking differentiation and promoting proliferation of immature blast cells. Recent studies have shown increased KDM1A expression in AML regardless of subtype/cytogenetic status (http://www.proteinatlas.org; Berglund et al., 2008) as well as in a variety of other tumor types (Hayami et al., 2011). This raises the hypothesis that KDM1A may be an attractive target for therapeutic development.

One therapeutic approach that has been successful in treating the acute promyelocytic leukemia (APL) subset of leukemias is forced differentiation of immature leukemic cells into mature myeloid cells. In the majority of APLs, chromosomal translocations involving the retinoic acid receptor alpha gene (*RARA*) and the promyelocytic leukemia gene (*PML*) produce the PML-RARα fusion protein. PML-RARα aberrantly interacts with co-repressor molecules such as NCOR and HDAC to prevent expression of RAR target genes necessary for differentiation. The use of all-*trans* retinoic acid (ATRA) can lift the differentiation block by promoting expression of RAR-responsive genes. However, the ability of ATRA to promote differentiation of PML-RARα AML cells is specific to this subset of leukemia; non-APL AML, such as AML harboring a *MLL* translocation, requires other treatment modalities.

In this issue of *Cancer Cell*, Harris et al. (2012) used microarray data from murine models of MLL leukemia to determine a correlation between KDM1A expression level and the leukemia colony-forming ability, often used as a surrogate assay to quantify LSC potential. Using both shRNAs and pharmacological inhibitors synthesized to target the enzymatic activity of KDM1A, the authors show that inhibition of KDM1A results in induction of differentiation in both murine and primary human MLL-fusion cells (Figure 1C). Cells without active KDM1A were unable to form colonies (indicative of loss of LSC potential), exhibited differentiated cell morphology and could not cause leukemia when introduced into mice. Gene expression analysis suggested that KDM1A is responsible for promoting the oncogenic gene program associated with MLL-AF9 leukemia. KDM1A co-localized to genes bound by MLL-AF9,

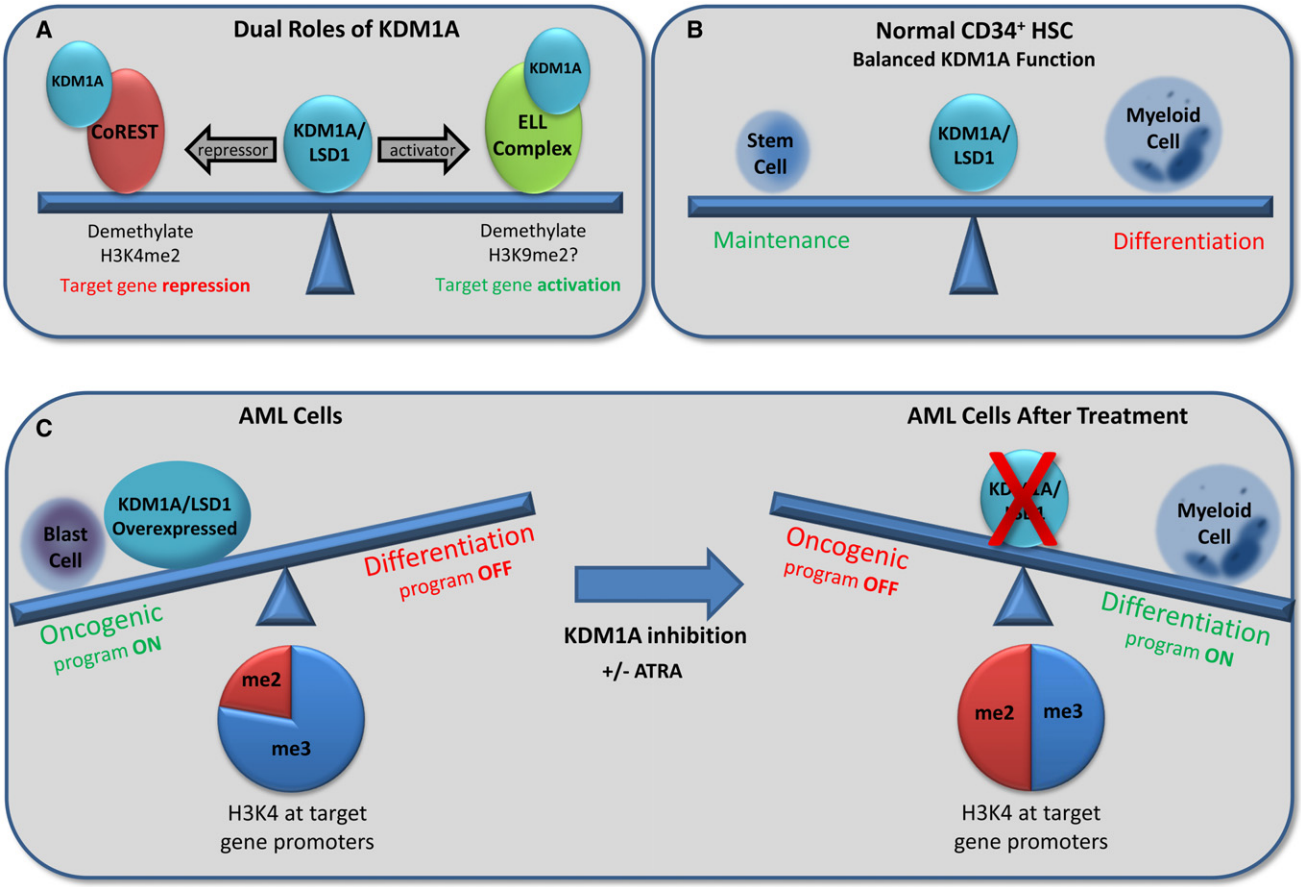

Figure 1. KDM1A/LSD1 Maintains a Balance in Gene Expression through Activating and Repressive Mechanisms that Are Disrupted in Acute Myeloid Leukemia

(A and B) In normal cells, KDM1A activates or represses genes through its histone demethylase activity (A), maintaining the balance between hematopoietic stem cells and differentiation to mature myeloid cells (B).

(C) In AML, increased KDM1A expression promotes an oncogenic gene expression program, causing a block in differentiation associated with increased H3K4me3 to H3K4me2 ratio at the promoter of target genes. Inhibition of KDM1A restores this balance, promoting blast cell differentiation.

and the presence of KDM1A correlated with a decreased ratio of H3K4me2 to H3K4me3 on these target genes. Upon inhibition of KDM1A, no global changes in H3K4me2 were evident, but the genes targeted by MLL-AF9 showed an increase in the H3K4me2 mark at their promoter and 5′ gene regions. This regional increase in H3K4me2 marks increased the ratio of H3K4me2 to H3K4me3 at the locus, making the prevalence of the marks more equal.

Complementary findings were recently reported in *Nature Medicine* (Schenk et al., 2012). The authors examined the effect of combining ATRA differentiation therapy with KDM1A inhibition in AML cells. They found that KDM1A inhibition, in combination with ATRA therapy, could sensitize otherwise ATRA-insensitive cells toward differentiation. This caused decreased leukemia-initiating activity (i.e., engraftment) as well as decreased tumor burden in human xenograft models. These combination-treated cells demonstrated increased expression of genes associated with myeloid-lineage differentiation and a concomitant increase in H3K4me2 at their promoters.

Together, these two studies illustrate the importance of KDM1A in maintaining expression of oncogenic gene programs and blocking differentiation in multiple subtypes of AML and highlight the potential therapeutic implications of targeting this important epigenetic regulator in leukemia. Despite these exciting findings, some very important questions remain to be addressed. First, what is the mechanism by which KDM1A functions at these target genes in AML? The presence of KDM1A at MLL-AF9 target genes decreases the H3K4me2 to H3K4me3 ratio, but how does KDM1A demethylation of H3K4me2/me1 lead to an increase in H3K4me3? Additionally, what proteins/protein complexes are recruited to these loci when KDM1A is present? Finally, what will be the long-term effect on normal hematopoietic stem cells and hematopoietic cell homeostasis and differentiation programs when treated with KDM1A inhibitors? Harris et al. (2012) start to address this question in their article. They found that while the overall frequency of colony forming cells remains the same upon KDM1A inhibition, erythroid lineage differentiation is decreased. In mice, this manifested as lethal anemia. How will these in vitro and in vivo results translate to patients that may be treated long-term with KDM1A inhibitors? Although the questions are plentiful in this

emerging field of targeting epigenetic regulators in cancer, the results presented in these articles highlight the potential of using such therapies, not only in AML, but perhaps in other cancers that are dependent on aberrant epigenetic activity for survival.

REFERENCES

Berglund, L., Björling, E., Oksvold, P., Fagerberg, L., Asplund, A., Szigyarto, C.A., Persson, A., Ottosson, J., Wernérus, H., Nilsson, P., et al. (2008). Mol. Cell. Proteomics *7*, 2019–2027.

Biswas, D., Milne, T.A., Basrur, V., Kim, J., Elenitoba-Johnson, K.S., Allis, C.D., and Roeder, R.G. (2011). Proc. Natl. Acad. Sci. USA *108*, 15751–15756.

Harris, W.J., Huang, X., Lynch, J.T., Spencer, G.J., Hitchin, J.R., Li, Y., Cicero, F., Blaser, J.G., Greystroke, B.F., Jordan, A.M., et al. (2012). Cancer Cell *21*, this issue, 473–487.

Hayami, S., Kelly, J.D., Cho, H.S., Yoshimatsu, M., Unoki, M., Tsunoda, T., Field, H.I., Neal, D.E., Yamaue, H., Ponder, B.A.J., et al. (2011). Int. J. Cancer *128*, 574–586.

Metzger, E., Wissmann, M., Yin, N., Müller, J.M., Schneider, R., Peters, A.H., Günther, T., Buettner, R., and Schüle, R. (2005). Nature *437*, 436–439.

Nakamura, T., Mori, T., Tada, S., Krajewski, W., Rozovskaia, T., Wassell, R., Dubois, G., Mazo, A., Croce, C.M., and Canaani, E. (2002). Mol. Cell *10*, 1119–1128.

Schenk, T., Chen, W.C., Göllner, S., Howell, L., Jin, L., Hebestreit, K., Klein, H.U., Popescu, A.C., Burnett, A., Mills, K., et al. (2012). Nature Medicine. Published online March 11, 2012. 10.1038/nm.2661.

Shi, Y., Lan, F., Matson, C., Mulligan, P., Whetstine, J.R., Cole, P.A., Casero, R.A., and Shi, Y. (2004). Cell *119*, 941–953.

Wang, J., Scully, K., Zhu, X., Cai, L., Zhang, J., Prefontaine, G.G., Krones, A., Ohgi, K.A., Zhu, P., Garcia-Bassets, I., et al. (2007). Nature *446*, 882–887.

You, A., Tong, J.K., Grozinger, C.M., and Schreiber, S.L. (2001). Proc. Natl. Acad. Sci. USA *98*, 1454–1458.

Hijacking T Cell Differentiation: New Insights in TLX Function in T-ALL

Bryan King,[1] Panagiotis Ntziachristos,[1] and Iannis Aifantis[1,*]
[1]Howard Hughes Medical Institute and Department of Pathology, NYU School of Medicine, New York, NY 10016, USA
*Correspondence: iannis.aifantis@nyumc.org
DOI 10.1016/j.ccr.2012.03.026

TLX1 and TLX3 are two closely-related homeobox transcriptional repressors frequently misexpressed and translocated in T cell acute lymphoblastic leukemia (T-ALL). In this issue of *Cancer Cell*, Dadi et al. provide new insights into how these factors are recruited by ETS-1 to the TCRα enhancer and actively repress differentiation.

In the majority of human cancers, tumor cells tend to share aspects of their identity with a corresponding cell of origin, a property that has proved useful for diagnosis in the clinic and provided researchers with a wide range of potential therapeutic targets. In particular, acute lymphoblastic leukemia (ALL) often presents as a snapshot of lymphocyte differentiation, based on surface marker expression and characteristic molecular genetic signatures (Aifantis et al., 2008). A large amount of data over the last decade has underlined the connection between physiological lymphocyte differentiation and the transformation events that lead to ALL. Whole-genome profiling and sequencing studies have suggested that some of the most common mutational targets in ALL are also key regulators of normal differentiation, including *IKZF1* and *PAX5* in B-ALL and *NOTCH1* and *GATA3* in T cell ALL (T-ALL) (Mullighan and Downing, 2009). Such findings have suggested that certain oncogenic lesions have the ability to "freeze" cellular differentiation at distinct stages. Therefore, a thorough understanding of how oncogenes halt developmental processes will provide clues toward the reinforcement of differentiation and, presumably, the desired outcomes of cell cycle exit and/or programmed cell death. In this issue of *Cancer Cell*, Dadi et al. (2012) reveal how two such oncogenes (*TLX1* and *TLX3*) manage to interfere with a critical stage of T cell differentiation, leading to development of a subset of T-ALL.

T cell differentiation and ALL are ideal models to study such oncogenic effects due to our detailed knowledge on the phenotypic and molecular programs of differentiation. T cells mature in the thymus following a highly orchestrated process, controlled by cell intrinsic (transcription factors) and cell extrinsic (antigen, cytokines, and chemokines) factors. Uncommitted, multipotent progenitors enter the thymus through the cortico-medullary junction, sense Notch ligands, and initiate commitment to the T cell lineage. At this point the T cell receptor (TCR) β, γ, and δ loci become accessible and the outcome of rearrangement leads to either the differentiation toward the γδ lineage or (as it happens with the vast majority of T cells) the expression of the pre-TCR, which helps drive cellular proliferation and leads to the $CD4^+8^+$ stage. At this stage, the TCRα locus undergoes recombination which leads to the surface expression of a TCRαβ and subsequent selection events (Sleckman et al., 1998). RAG-mediated rearrangement of the TCRα locus is a process controlled by distinct

emerging field of targeting epigenetic regulators in cancer, the results presented in these articles highlight the potential of using such therapies, not only in AML, but perhaps in other cancers that are dependent on aberrant epigenetic activity for survival.

REFERENCES

Berglund, L., Björling, E., Oksvold, P., Fagerberg, L., Asplund, A., Szigyarto, C.A., Persson, A., Ottosson, J., Wernérus, H., Nilsson, P., et al. (2008). Mol. Cell. Proteomics *7*, 2019–2027.

Biswas, D., Milne, T.A., Basrur, V., Kim, J., Elenitoba-Johnson, K.S., Allis, C.D., and Roeder, R.G. (2011). Proc. Natl. Acad. Sci. USA *108*, 15751–15756.

Harris, W.J., Huang, X., Lynch, J.T., Spencer, G.J., Hitchin, J.R., Li, Y., Cicero, F., Blaser, J.G., Greystroke, B.F., Jordan, A.M., et al. (2012). Cancer Cell *21*, this issue, 473–487.

Hayami, S., Kelly, J.D., Cho, H.S., Yoshimatsu, M., Unoki, M., Tsunoda, T., Field, H.I., Neal, D.E., Yamaue, H., Ponder, B.A.J., et al. (2011). Int. J. Cancer *128*, 574–586.

Metzger, E., Wissmann, M., Yin, N., Müller, J.M., Schneider, R., Peters, A.H., Günther, T., Buettner, R., and Schüle, R. (2005). Nature *437*, 436–439.

Nakamura, T., Mori, T., Tada, S., Krajewski, W., Rozovskaia, T., Wassell, R., Dubois, G., Mazo, A., Croce, C.M., and Canaani, E. (2002). Mol. Cell *10*, 1119–1128.

Schenk, T., Chen, W.C., Göllner, S., Howell, L., Jin, L., Hebestreit, K., Klein, H.U., Popescu, A.C., Burnett, A., Mills, K., et al. (2012). Nature Medicine. Published online March 11, 2012. 10.1038/nm.2661.

Shi, Y., Lan, F., Matson, C., Mulligan, P., Whetstine, J.R., Cole, P.A., Casero, R.A., and Shi, Y. (2004). Cell *119*, 941–953.

Wang, J., Scully, K., Zhu, X., Cai, L., Zhang, J., Prefontaine, G.G., Krones, A., Ohgi, K.A., Zhu, P., Garcia-Bassets, I., et al. (2007). Nature *446*, 882–887.

You, A., Tong, J.K., Grozinger, C.M., and Schreiber, S.L. (2001). Proc. Natl. Acad. Sci. USA *98*, 1454–1458.

Hijacking T Cell Differentiation: New Insights in TLX Function in T-ALL

Bryan King,[1] Panagiotis Ntziachristos,[1] and Iannis Aifantis[1,*]
[1]Howard Hughes Medical Institute and Department of Pathology, NYU School of Medicine, New York, NY 10016, USA
*Correspondence: iannis.aifantis@nyumc.org
DOI 10.1016/j.ccr.2012.03.026

TLX1 and TLX3 are two closely-related homeobox transcriptional repressors frequently misexpressed and translocated in T cell acute lymphoblastic leukemia (T-ALL). In this issue of *Cancer Cell*, Dadi et al. provide new insights into how these factors are recruited by ETS-1 to the TCRα enhancer and actively repress differentiation.

In the majority of human cancers, tumor cells tend to share aspects of their identity with a corresponding cell of origin, a property that has proved useful for diagnosis in the clinic and provided researchers with a wide range of potential therapeutic targets. In particular, acute lymphoblastic leukemia (ALL) often presents as a snapshot of lymphocyte differentiation, based on surface marker expression and characteristic molecular genetic signatures (Aifantis et al., 2008). A large amount of data over the last decade has underlined the connection between physiological lymphocyte differentiation and the transformation events that lead to ALL. Whole-genome profiling and sequencing studies have suggested that some of the most common mutational targets in ALL are also key regulators of normal differentiation, including *IKZF1* and *PAX5* in B-ALL and *NOTCH1* and *GATA3* in T cell ALL (T-ALL) (Mullighan and Downing, 2009). Such findings have suggested that certain oncogenic lesions have the ability to "freeze" cellular differentiation at distinct stages. Therefore, a thorough understanding of how oncogenes halt developmental processes will provide clues toward the reinforcement of differentiation and, presumably, the desired outcomes of cell cycle exit and/or programmed cell death. In this issue of *Cancer Cell*, Dadi et al. (2012) reveal how two such oncogenes (*TLX1* and *TLX3*) manage to interfere with a critical stage of T cell differentiation, leading to development of a subset of T-ALL.

T cell differentiation and ALL are ideal models to study such oncogenic effects due to our detailed knowledge on the phenotypic and molecular programs of differentiation. T cells mature in the thymus following a highly orchestrated process, controlled by cell intrinsic (transcription factors) and cell extrinsic (antigen, cytokines, and chemokines) factors. Uncommitted, multipotent progenitors enter the thymus through the cortico-medullary junction, sense Notch ligands, and initiate commitment to the T cell lineage. At this point the T cell receptor (TCR) β, γ, and δ loci become accessible and the outcome of rearrangement leads to either the differentiation toward the γδ lineage or (as it happens with the vast majority of T cells) the expression of the pre-TCR, which helps drive cellular proliferation and leads to the $CD4^+8^+$ stage. At this stage, the TCRα locus undergoes recombination which leads to the surface expression of a TCRαβ and subsequent selection events (Sleckman et al., 1998). RAG-mediated rearrangement of the TCRα locus is a process controlled by distinct

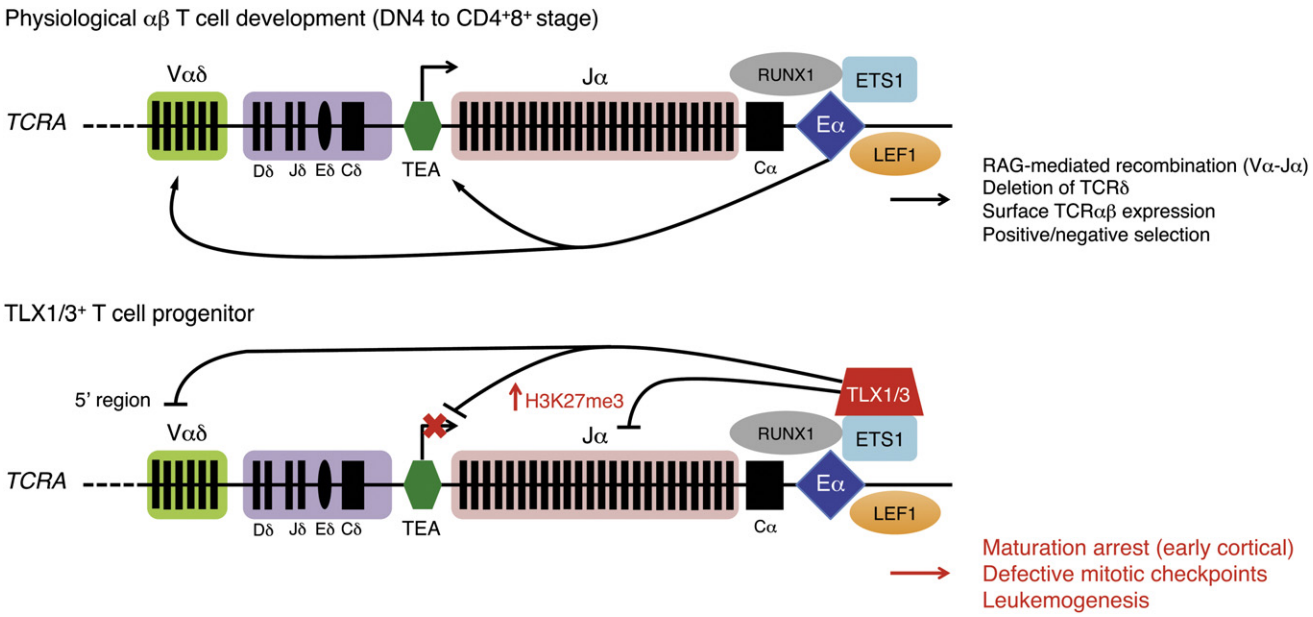

Figure 1. TLX-Mediated Repression of the TCRα Enhancer

Under normal conditions of αβ T cell development (top), transcriptional access to the TCRα locus at the late double-negative (DN) to $CD4^+8^+$ stage is imparted primarily by the function of the Eα enhancer, shown bound by its transcriptional activators ETS-1, RUNX1, and LEF1. The onset of Vα-Jα recombination begins with transcription from the TEA promoter and increased histone acetylation throughout the Jα region. In a subset of T cell leukemias where *TLX1* or *TLX3* are misexpressed (bottom), Dadi et al. (2012) found that ETS-1 can recruit TLX1/3 to Eα and that this correlates with an enrichment of repressive histone modifications and lack of *TCRA* gene expression, ultimately leading to an arrest in differentiation.

cis-regulatory regions, most notably the Eα enhancer, and a large number of factors regulating chromatin accessibility, locus contraction and gene transcription (Schatz and Swanson, 2011). Interestingly, topology is essential for normal maturation, suggesting an intimate relationship between developing progenitors and thymic microenvironments. Human and mouse T cell differentiation follow similar rules with very small differences, underlining the evolutionary conservation of such a critical process. Human T-ALL cases can be roughly separated into three categories, reminiscent of physiological developmental stages: (1) immature, early T-ALL, expressing markers and genes characteristic for pre-committed progenitors; (2) early cortical, αβ-committed thymocytes, harboring TCRβ rearrangements and (in most cases) expressing a pre-TCR; and (3) late, TCR-expressing leukemia, with full rearrangement of the TCRα locus.

In concordance with previous studies, Dadi et al. (2012) found that TLX1 and TLX3 are overexpressed in a significant fraction of T-ALL, and their expression defines a molecular signature characteristic of early cortical thymocytes. *TLX1* is overexpressed in 5%–10% of pediatric and up to 30% of adult T-ALL as a consequence of chromosomal translocations. Similarly, *TLX3* is overexpressed as a result of t(5;14)(q35;q32) in approximately 25% of pediatric and 5%–10% of adult T-ALL cases. *TLX1*, which is not expressed during physiological T cell differentiation, was first implicated in T-ALL from a t(10;14) translocation by Hatano et al. (1991). As a result of this translocation, TLX1 is ectopically expressed in thymocytes driven by cis-regulatory elements of the TCRα/δ locus. The targeting of antigen receptor loci by translocations is a frequent event in ALL, most likely caused by the function of RAG nucleases and the accessible state of the chromatin during specific differentiation stages. TLX1/3 overexpression defines a distinct subgroup of T-ALL, one that predicts an overall favorable prognosis, bears characteristic molecular and cellular phenotypes, and is enriched in *NUP12-ABL1* fusions or mutations in *WT1*, *PHF6*, and *RUNX1* (Van Vlierberghe et al., 2010). Transgenic expression of *TLX1* in the thymus of mice eventually leads to T cell neoplasms (De Keersmaecker et al., 2010). Interestingly, these $TLX1^+$ tumors are prone to aneuploidy and show marked defects in the activation of normal mitotic checkpoints, possibly due to deregulated expression of *Chek1*. Further analysis revealed that ectopic *TLX1* expression alone is likely insufficient to induce T cell leukemia but leads to aberrant T cell differentiation and sets the stage for secondary transformation events. Indeed, genetic lesions in loci encoding known regulators of lymphocytic transformation were identified, including mutations in *Notch1*, *Pten*, *Tp53* and, most notably, *Bcl11B*, a factor controlling early T cell progenitor differentiation in the thymus (Gutierrez et al., 2011). Altogether, these data suggested that TLX1 might act first and foremost as an antagonist of physiological T cell development. However, the mechanism by which TLX1/3 could exert this effect remained elusive.

Intriguingly, Dadi et al. (2012) found that $TLX1/3^+$ leukemias were significantly less likely to have TCRα rearrangements. Accordingly, increased levels of the repressive histone mark H3K27me3 was observed across the TCRα locus in these leukemias, suggesting that the unrearranged TCRα segments were epigenetically silenced in the presence of TLX1/3. However, their most critical finding is that the TLX factors could directly interfere with Eα function through

interaction with ETS1, a critical component of the complex that binds and activates Eα (Figure 1). To test the biological significance of this interaction on the enhancer element, the authors silenced TLX1/3 in human T-ALL cell lines and observed increases in differentiation and cell death, suggesting abortive differentiation and induction of apoptosis. Ectopic expression of rearranged TCRα caused identical effects. These findings therefore connect proper TCR rearrangement and expression to tumor differentiation state.

Altogether, the work of Dadi et al. (2012) presents a novel mechanism of differentiation arrest orchestrated by the TLX oncogenes in the induction and maintenance of T-ALL. To this end, it will be important to determine whether additional transcriptional targets that are potentially perturbed by TLX1/3 are also important for progression of the disease. This is an important question as the differentiation defects seen in *TLX1* transgenic mice are distinct from those caused by paucity of TCRα rearrangement in human leukemia. One such example could be the downregulation *BCL11B*, a target of TLX1 that is essential for T cell commitment. Further investigation on the potential synergistic role other factors play in the TCR recombination (Polycomb complex, the CTCF insulator protein, and others) and on the mechanisms leading to sustained expression of the TLX proteins will shed light on the intricacies of this leukemia. Ultimately, the most intriguing implication of this study is whether there are means of regulating TLX function using targeted therapies to enforce differentiation of TLX1/3$^+$ T-ALL. A similar approach of "differentiation therapy" has been extremely effective in the treatment of acute promyelocytic leukemia with all-trans retinoic acid (Kogan and Bishop, 1999). Given that their expression is normally restricted to embryonic development, TLX1/3 could prove to be ideal targets in the treatment of large fraction T cell leukemias with limited potential for adverse side effects.

REFERENCES

Aifantis, I., Raetz, E., and Buonamici, S. (2008). Nat. Rev. Immunol. *8*, 380–390.

Dadi, S., Le Noir, S., Payet-Bornet, D., Lhermitte, L., Zacarias-Cabeza, J., Bergeron, J., Villarèse, P., Vachez, E., Dik, W.A., Millien, C., et al. (2012). Cancer Cell *21*, this issue, 563–576.

De Keersmaecker, K., Real, P.J., Gatta, G.D., Palomero, T., Sulis, M.L., Tosello, V., Van Vlierberghe, P., Barnes, K., Castillo, M., Sole, X., et al. (2010). Nat. Med. *16*, 1321–1327.

Gutierrez, A., Kentsis, A., Sanda, T., Holmfeldt, L., Chen, S.C., Zhang, J., Protopopov, A., Chin, L., Dahlberg, S.E., Neuberg, D.S., et al. (2011). Blood *118*, 4169–4173.

Hatano, M., Roberts, C.W., Minden, M., Crist, W.M., and Korsmeyer, S.J. (1991). Science *253*, 79–82.

Kogan, S.C., and Bishop, J.M. (1999). Oncogene *18*, 5261–5267.

Mullighan, C.G., and Downing, J.R. (2009). Leukemia *23*, 1209–1218.

Schatz, D.G., and Swanson, P.C. (2011). Annu. Rev. Genet. *45*, 167–202.

Sleckman, B.P., Bassing, C.H., Bardon, C.G., Okada, A., Khor, B., Bories, J.C., Monroe, R., and Alt, F.W. (1998). Immunol. Rev. *165*, 121–130.

Van Vlierberghe, P., Palomero, T., Khiabanian, H., Van der Meulen, J., Castillo, M., Van Roy, N., De Moerloose, B., Philippé, J., González-García, S., Toribio, M.L., et al. (2010). Nat. Genet. *42*, 338–342.

Personalized Medicine: Patient-Predictive Panel Power

Paul Workman,[1,*] Paul A. Clarke,[1] and Bissan Al-Lazikani[2]
[1]Signal Transduction and Molecular Pharmacology Team
[2]Computational Biology and Chemogenomics Team
Cancer Research UK Cancer Therapeutics Unit, Division of Cancer Therapeutics, The Institute of Cancer Research, Haddow Laboratories, 15 Cotswold Road, Sutton SM2 5NG, UK
*Correspondence: paul.workman@icr.ac.uk
DOI 10.1016/j.ccr.2012.03.030

Two recent papers published in *Nature* demonstrate the power of systematic high-throughput pharmacologic profiling of very large, diverse, molecularly-characterized human cancer cell line panels to reveal linkages between genetic profile and targeted-drug sensitivity. Known oncogene addictions are confirmed while surprising complexities and biomarker relationships with clinical potential are revealed.

The need to identify predictive biomarkers of tumor response has intensified with the era of molecularly-targeted therapies that exploit addictions and vulnerabilities in tumors with identifiable molecular traits, in contrast to the one-size-fits-all approach that dominated cytotoxic chemotherapy (Yap and Workman, 2012). Two recent *Nature* articles describe a systematic large-scale approach to this challenge by high-throughput profiling many targeted agents against hundreds of clinically-relevant human cancer cells lines with detailed genetic annotation (Garnett et al., 2012; Barretina et al., 2012).

There are three important general take-home messages from these two studies. (1) The articles provide the most extensive

Cancer Cell
Article

Targeting Nonclassical Oncogenes for Therapy in T-ALL

Prem S. Subramaniam,[1] Dosh W. Whye,[1] Evgeni Efimenko,[1] Jianchung Chen,[1] Valeria Tosello,[3] Kim De Keersmaecker,[3] Adam Kashishian,[4,5] Mary Ann Thompson,[6] Mireia Castillo,[8] Carlos Cordon-Cardo,[8] Utpal P. Davé,[7] Adolfo Ferrando,[1,2,3] Brian J. Lannutti,[4,5] and Thomas G. Diacovo[1,2,*]
[1]Department of Pediatrics
[2]Department of Pathology and Cell Biology
Columbia University Medical Center, New York, NY 10032, USA
[3]Institute for Cancer Genetics, Columbia University, New York, NY 10032, USA
[4]Calistoga Pharmaceuticals, Seattle, WA 9810, USA
[5]Gilead Sciences, Seattle, WA 9810, USA
[6]Department of Pathology
[7]Department of Medicine and Cancer Biology
Vanderbilt University Medical Center, Nashville, TN 37232, USA
[8]Department of Genetics and Genomic Sciences, The Mount Sinai School of Medicine, New York, NY 10029, USA
*Correspondence: td2142@columbia.edu
DOI 10.1016/j.ccr.2012.02.029

SUMMARY

Constitutive phosphoinositide 3-kinase (PI3K)/Akt activation is common in T cell acute lymphoblastic leukemia (T-ALL). Although four distinct class I PI3K isoforms (α, β, γ, δ) could participate in T-ALL pathogenesis, none has been implicated in this process. We report that in the absence of PTEN phosphatase tumor suppressor function, PI3Kγ or PI3Kδ alone can support leukemogenesis, whereas inactivation of both isoforms suppressed tumor formation. The reliance of PTEN null T-ALL on the combined activities of PI3Kγ/δ was further demonstrated by the ability of a dual inhibitor to reduce disease burden and prolong survival in mice as well as prevent proliferation and promote activation of proapoptotic pathways in human tumors. These results support combined inhibition of PI3Kγ/δ as therapy for T-ALL.

INTRODUCTION

Constitutive activation of the phosphoinositide 3-kinase (PI3K)/Akt signal transduction pathway is a common event in cancer, promoting the growth, proliferation, and survival of various types of tumors including T cell acute lymphoblastic leukemia (T-ALL) (Yuan and Cantley, 2008; Zhao and Vogt, 2008; Gutierrez et al., 2009; Palomero et al., 2008; Silva et al., 2008; Larson Gedman et al., 2009). Class I PI3Ks are a family of lipid kinases that generate the potent second messenger phosphatidylinositol-3,4,5 trisphosphate (PIP_3) in response to ligation of a number of distinct cell surface receptors (Katso et al., 2001; Cantley, 2002). This results in the activation of Akt as well as numerous downstream effector molecules, which ultimately promote cell growth and survival. Class I PI3Ks are heterodimeric molecules composed of a regulatory and a catalytic subunit, the latter consisting of four unique isoforms that include p110α, p110β, p110γ, and p110δ. Each is capable of regulating distinct biological functions in normal tissues and cellular compartments. However, some overlap in activity does exist, as is the case for thymocytes where the combined activities of PI3Kγ and PI3Kδ contribute to cellular processes required for the generation and function of mature T cells (Webb et al., 2005; Swat et al., 2006; Ji et al., 2007). Although the importance of these two PI3K isoforms in T cell biology is well established (Okkenhaug and Vanhaesebroeck, 2003), what role, if any, they

Significance

Loss of PTEN function is a frequent occurrence in cancer resulting in unbridled PI3K/Akt signaling that contributes to tumor pathogenesis. Consequently, much emphasis has been placed on developing inhibitors that target this pathway. Here, we report that PI3Kγ and PI3Kδ act as a tumorigenic bottleneck in PTEN null T-ALL. We also demonstrate that it is possible to exploit the "addiction" of a hematological malignancy to specific PI3K isoforms, enabling the rational design of a PI3Kγ/δ dual inhibitor. This work represents a significant advancement in our understanding of the dynamic interplay that exists between PTEN and particular PI3K isoforms in regulating both normal and abnormal T cell development as well as in sustaining tumor cell proliferation and survival.

play in malignant transformation and tumor cell survival remains to be determined.

Previously, it has been reported that p110α is involved in oncogenesis because function-enhancing mutations in this catalytic subunit are found in many cancers of solid organs (Samuels et al., 2004; Zunder et al., 2008). In contrast, cancer-specific mutations have yet to be identified for the other p110 isoforms. That said, overexpression of p110β, p110γ, or p110δ in an in vitro culture system induces cellular transformation (Kang et al., 2006). Moreover, increased or preferential expression of p110γ and p110δ has been described in chronic and acute forms of myeloid leukemia, respectively (Hickey and Cotter, 2006; Sujobert et al., 2005). However, to our knowledge, overexpression of specific PI3K isoforms has not been reported for T-ALL, and mutations in PI3Kα are rare, suggesting that they are not a major contributor to its pathogenesis (Gutierrez et al., 2009; Lo et al., 2009).

PTEN is a nonredundant plasma-membrane phosphatase that is responsible for counteracting the potential cancer-promoting activities of class I PI3K (Sulis and Parsons, 2003; Salmena et al., 2008). It does so by limiting the levels of PIP_3 generated in response to the activation of these lipid kinases. Clinically, mutations in the *PTEN* tumor suppressor gene are common in multiple types of human cancer, resulting in unbridled PI3K/Akt signaling as well as conferring resistance to chemotherapeutic agents (Carnero et al., 2008; Huang and Hung, 2009). It has been well established that deletion of the tumor suppressor gene *PTEN* in T cell progenitors drives the malignant transformation of these cells within the thymus of mice (Suzuki et al., 2001; Hagenbeek and Spits, 2008; Liu et al., 2010). Moreover, the resulting tumors possess similar genetic and biochemical aberrations associated with a subset of patients with T-ALL including hyperactivation of the PI3K/Akt signaling pathway (Maser et al., 2007; Guo et al., 2008). In fact Gutierrez et al. (2009) have reported a loss of PTEN function due to mutations or deletions in approximately 40% of primary T-ALL samples, suggesting that hyperactivation of the PI3K/Akt signaling pathway is a common feature of this hematological malignancy. Based on these clinical observations and known reliance of thymocyte development on PI3Kγ and PI3Kδ, we set out to determine whether these nonclassical oncogenes contribute to leukemogenesis and if it is possible to exploit tumor cell "addiction" to the activity of distinct PI3K isoforms, thus permitting the rational design of a chemotherapeutic agent to treat T-ALL.

RESULTS

PI3Kγ or PI3Kδ Can Support Malignant Transformation of T Cells

We crossed mice containing both *Pten* alleles floxed by the loxP Cre excision sites with *Lck*-cre transgenic animals (*Lck/Pten*$^{fl/fl}$) alone or together with those lacking p110γ, encoded by *Pik3cg*, and/or p110δ, encoded by *Pik3cd*, catalytic subunits. Consistent with previous studies, >85% of *Lck/Pten*$^{fl/fl}$ mice develop T-ALL and eventually succumb to the disease (median survival of 140 days), which was confirmed by flow cytometric analysis (Figures 1A and 1B). In contrast to PTEN null tumors of solid organs that have been reported to rely on PI3Kβ activity (Jia et al., 2008; Wee et al., 2008), tumorigenesis in the context of a deficiency of PTEN in T cell progenitors appears to be critically dependent on PI3Kγ and PI3Kδ. This is evidenced by the marked delay in the onset of disease and increased survival of *Lck/Pten*$^{fl/fl}$*;Pik3cg*$^{-/-}$*;Pik3cd*$^{-/-}$ triple-mutant mice (TKO) because <20% of animals succumb to T-ALL by 220 days. However, the activity of either isoform alone was sufficient to promote tumor formation, yielding similar median survival times for *Lck/Pten*$^{fl/fl}$*;Pik3cg*$^{-/-}$ and *Lck/Pten*$^{fl/fl}$*;Pik3cd*$^{-/-}$ mice (175 versus 178 days, respectively). Comparable percentages of these animals developed and died of T-ALL (65% versus 64%, respectively), and tumors had evidence of activation of the PI3K/Akt signaling pathway, albeit much reduced as compared to those from *Lck/Pten*$^{fl/fl}$ animals (Figure 1C). However, there was no evidence of overexpression of any *Pik3c* isoform in thymic tumors (Figure 1D).

Further evidence demonstrating that it is the unleashed activities of PI3Kγ and PI3Kδ that provide the signals necessary for the development of T-ALL is suggested by the continued reduction in thymus size and cellularity in 6-week-old TKO mice (Figure 2A). Although absence of PTEN should permit unrestricted activity of all four class I PI3K isoforms, it appears that PI3Kα and PI3Kβ cannot adequately compensate for their γ and δ counterparts as evidenced by the persistent diminution in the total number of $CD4^+CD8^+$ double-positive thymocyte population and near-basal levels of phosphorylated Akt (Ser473) as compared to mice deficient in PTEN alone (Figures 2A and 2B). Cellular alterations associated with p110γ/δ double deficiency also persisted in the peripheral blood and in secondary lymphoid organs of TKO mice and included a paucity of $CD3^+$ T cells (Figures 2C and 2D). No active tumor was found in peripheral blood or spleen of the surviving animals at ~7 months of age as determine by absence of staining for the proliferation marker Ki67 on Thy1.2-positive cells (Figure 2E).

Effect of PI3Kγ/PI3Kδ Dual Inhibition on Thymocyte Signaling and Development

In order to ascertain whether PI3Kγ and PI3Kδ are also required for tumor maintenance and can be targeted therapeutically in T-ALL, we generated a small molecule that preferentially inhibits the function of both p110γ and p110δ catalytic domains, designated CAL-130 (Figure 3A). IC_{50} values of this compound were 1.3 and 6.1 nM for p110δ and p110γ, respectively, as compared to 115 and 56 nM for p110α and p110β. Importantly, this small molecule does not inhibit additional intracellular signaling pathways (i.e., p38 mitogen-activated protein kinase or insulin receptor tyrosine kinase) that are critical for general cell function and survival (Table 1; see Table S1 available online). To demonstrate that CAL-130 can block the activities of both PI3Kδ and PI3Kγ in thymocytes, we evaluated its ability to prevent phosphorylation of Akt (Ser473) and calcium flux in response to T cell receptor (TCR) crosslinking. Previously, we have shown that the combined activities of these two class I PI3K isoforms are necessary for phosphorylation of this protein kinase in this cell population (Swat et al., 2006). Consistent with these results, CAL-130 treatment of thymocytes harvested from 6-week-old WT animals prevented TCR-induced Akt phosphorylation and attenuated calcium flux to levels observed for their *Pik3cg*$^{-/-}$*;Pik3cd*$^{-/-}$ counterparts (Figures 3B, 3C, and S1A).

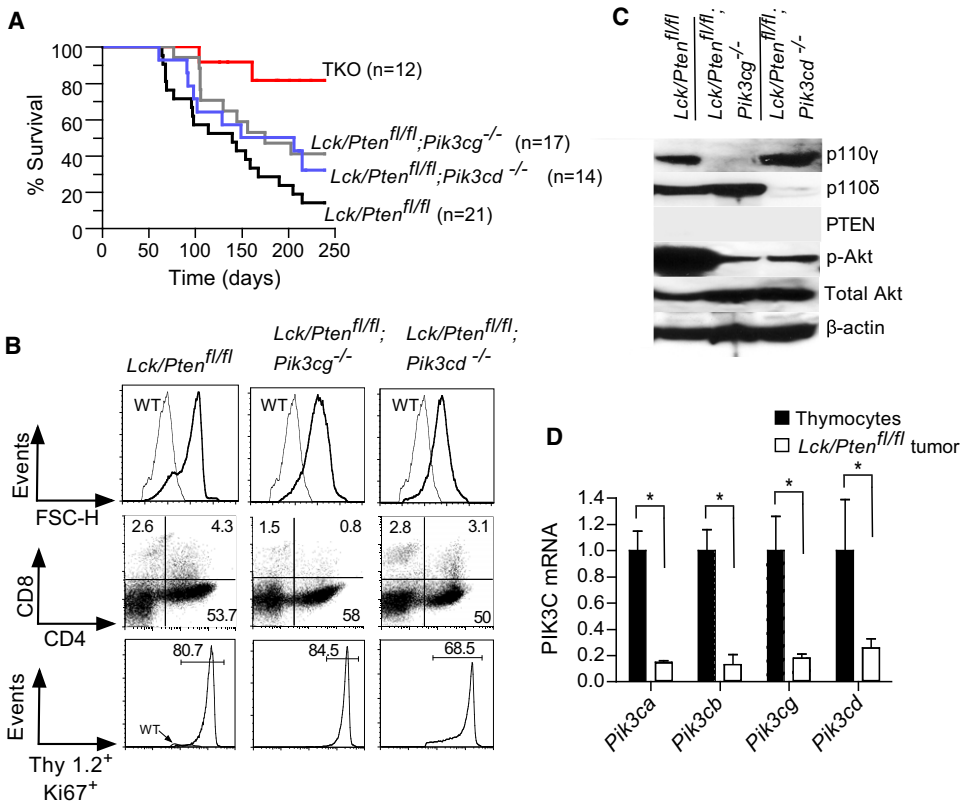

Figure 1. PI3Kγ or PI3Kδ Can Support Leukemogenesis in the Context of PTEN Deficiency

(A) Kaplan-Meyer survival curves demonstrating the requirement for PI3Kγ and PI3Kδ activity in the development of PTEN null T-ALL. All animals were followed for a period of 7 months.

(B) Representative flow cytometric profiles of peripheral blood from diseased mice lacking p110γ or p110δ in the absence of PTEN in T cell progenitors. Forward scatter (FSC) and Ki67 staining are indicators of cell size and proliferation, respectively. Thy 1.2 expression identifies T-lineage cells.

(C) Representative immunoblots depicting p110γ, p110δ, and PTEN expression as well as Akt activation state (phosphorylation of Ser473) in thymic lysates from the same animals.

(D) Quantitative reverse-transcription PCR analysis of *Pik3c (a/b/g/d)* transcript levels in WT thymocytes (n = 5) and tumors (n = 5) harvested from *Lck/Pten*$^{fl/fl}$ mice. Error bars represent ±SD. The difference in *Pik2c* expression levels between the WT thymocytes and tumor cells was statistically significant (*$p < 0.05$) using a Student's t test.

To assess the in vivo efficacy of the inhibitor, we determined its effects on thymi of 6-week-old WT mice, specifically for its ability to recapitulate the phenotype observed when both p110γ and p110δ are deficient. Animals received 10 mg kg^{-1} of the inhibitor orally, which was sufficient to maintain plasma concentrations of 0.33 ± 0.18 μM at the end of 8 hr (Figure 3D). Notably, this dose did not affect either plasma glucose or insulin levels in contrast to the metabolic perturbations associated with tissue-specific deficiencies in p110α and p110β (Figures 3E and 3F) (Jia et al., 2008; Sopasakis et al., 2010). CAL-130 was also found to have a limited ability to impair PDGF-induced activation of PI3Kα as compared to the pan-PI3K/mTOR inhibitor BEZ235 (Figure S1B). Similarly, platelets harvested from *Pik3cg*$^{-/-}$*;Pik3cd*$^{-/-}$ mice 2 hr post-administration of CAL-130 had no obvious defect in ADP-mediated platelet aggregation, a process known to rely predominantly on PI3Kβ (Figure S1C) (Jackson et al., 2005). However, CAL-130 treatment (10 mg kg^{-1} every 8 hr) for a period of 7 days markedly affected the size, cellularity, and overall architecture of the thymus faithfully reproducing the phenotype associated with *Pik3cg*$^{-/-}$*;Pik3cd*$^{-/-}$ mice (Figure 3G). In particular there was a 18-fold reduction in total thymocyte number in comparison to controls, which was primarily due to the loss of DP population (Figure 3H). These observations are consistent with the ability of CAL-130 to preferentially block the function of both PI3Kγ and PI3Kδ.

Antileukemic Effects of Pharmacological Inhibition of PI3Kγ and PI3Kδ in PTEN Null T-ALL Tumors in Mice

The clinical significance of interfering with the combined activities of PI3Kγ and PI3Kδ was determined by administering CAL-130 to *Lck/Pten*$^{fl/fl}$ mice with established T-ALL. Candidate animals for survival studies were ill appearing, had a white blood cell (WBC) count above 45,000 μl^{-1}, evidence of blasts on peripheral smear, and a majority of circulation cells (>75%) staining double positive for Thy1.2 and Ki-67. Mice received an oral dose (10 mg kg^{-1}) of the inhibitor every 8 hr for a period of 7 days and were then followed until moribund. Despite the limited duration of therapy, CAL-130 was highly effective in extending the median survival for treated animals to 45 days as compared 7.5 days for the control group (Figure 4A).

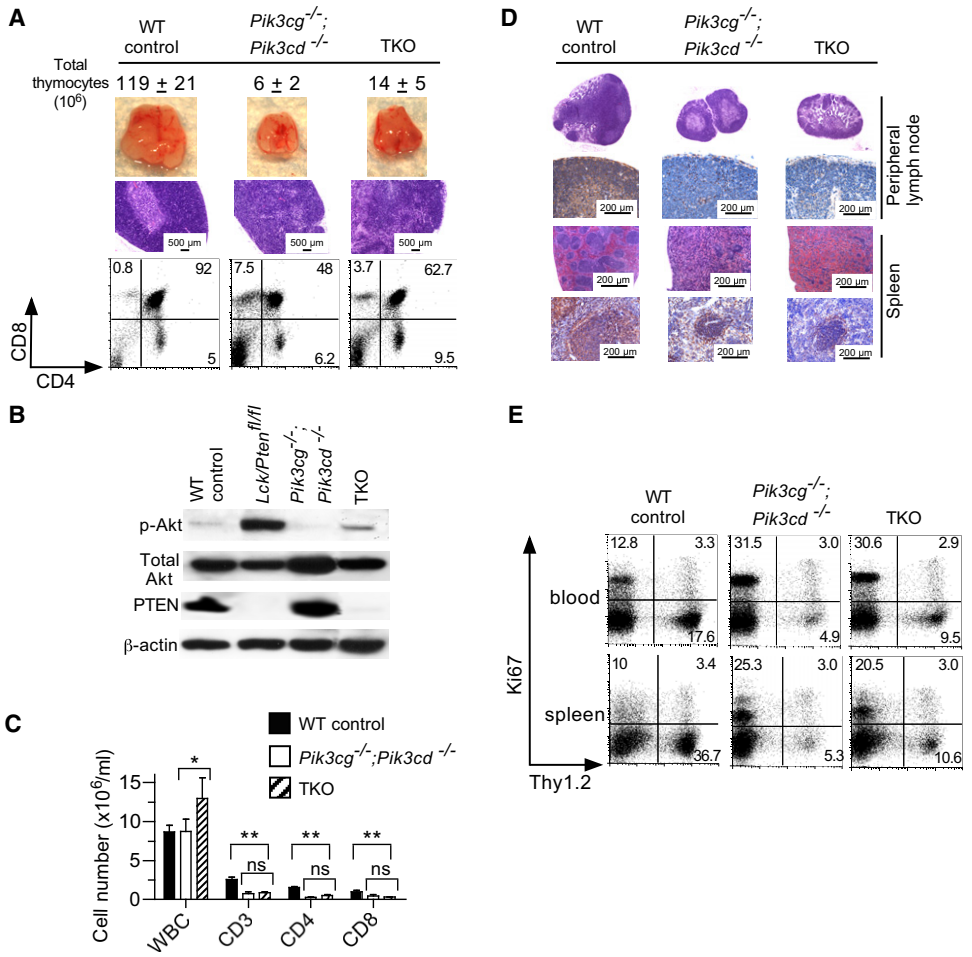

Figure 2. Persistence of Cellular and Structural Defects in Thymi Associated with a Combined Deletion of p110γ/p110δ and PTEN

(A) Hematoxylin and eosin staining (H&E) and flow cytometric analyses of thymi derived from 6-week-old mice lacking both p110γ and p110δ catalytic subunits in the presence or absence of PTEN. The panels are representative of data from five animals in each group.

(B) Immunoblots assessing for Akt phosphorylation (Ser473) and PTEN levels in thymocyte lysates.

(C) Number of WBC and T cell subsets in the peripheral blood of the same animals. *ns (not significant) for *Pik3cg*$^{-/-}$;*Pik3cd*$^{-/-}$ versus TKO; **$p < 0.01$ for WT versus TKO.

(D and E) Representative (D) micrografts of H&E peripheral lymph nodes and spleen and (E) flow cytometry plots of blood and spleen from triple mutant animals (n = 5 mice per genotype). Histological identification of T cells was by immunoperoxidase detection of CD3. Scale bars correspond to 200 μm in secondary lymphoid organs and to 500 μm in thymi. Data represent the mean ± SD.

To determine the effect of CAL-130 on disease burden, we performed sequential blood counts and peripheral smears as well as flow cytometric analyses on *Lck/Pten*$^{fl/fl}$ mice pre- and post-administration of the inhibitor (Figures 4B and S2A–S2C). All animals showed a dramatic reduction in WBC count by day 4 reflected in the loss of the highly proliferative blast population (Thy1.2/Ki-67 double positive, high FSC-H), which remained at low levels for the duration of treatment. Moreover, both CD4 single-positive and CD4/CD8 double-positive T-ALL responded to CAL-130, which corresponded with an increase in apoptosis detected as sub-G0 population after propidium iodide (PI) staining on days 4–7. Treatment of diseased *Lck/Pten*$^{fl/fl}$;*Pik3cg*$^{-/-}$ mice but not their *Lck/Pten*$^{fl/fl}$ counterparts with the PI3Kδ selective inhibitor IC87114 (10 mg kg^{-1} every 8 hr) produced similar results, confirming the critical reliance of PTEN null tumors on the combined activities of PI3Kγ and PI3Kδ (Figures 4C and S2D).

Further evidence to support the ability of CAL-130 to reduce tumor burden was obtained by bioluminescent imaging. *Pten*$^{fl/fl}$ mice were crossed with a strain in which a luciferase cDNA, preceded by a LoxP-stop-LoxP cassette, was introduced into the ubiquitously expressed *ROSA26* locus (Safran et al., 2003). Progenies were then crossed with *Lck*-cre transgenics to delete *Pten* in T cell progenitors and induce expression of luciferase (*Lck/Pten*$^{fl/fl}$;*Gt(ROSA)26Sor*$^{tm1(Luc)Kael}$/J). Imaging of T-ALL tumor-bearing animals was performed just prior to and after 4 days of treatment with CAL-130. Signals at day 4 were dramatically lower in treated animals, consistent with the reduction in the WBC count and the CD4 single-positive population of tumor cells (Figure 4D). Moreover, weights of thymi, liver, spleen, and kidneys from treated *Pten*$^{fl/fl}$ mice were significantly less than that for animals that received vehicle control for 7 days (Figure 4E).

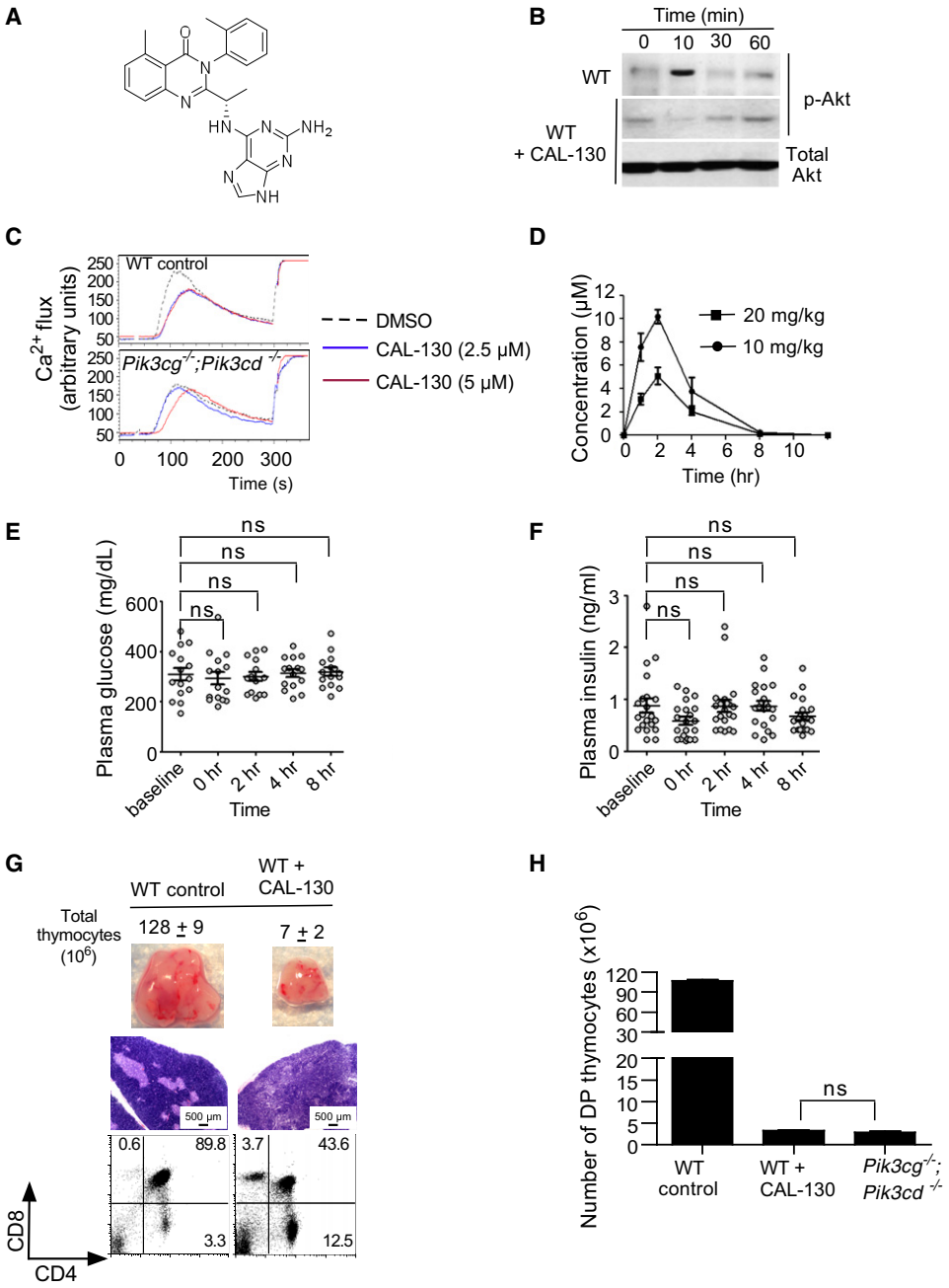

Figure 3. Inhibitory Profile of CAL-130

(A) Chemical structure of CAL-130.

(B and C) Effect of the inhibitor on (B) Akt phosphorylation (Ser473) or (C) Ca^{2+} flux in purified thymocytes from WT or *Pik3cg*$^{-/-}$;*Pik3cd*$^{-/-}$ animals in response to TCR crosslinking. Data are representative of three separate experiments.

(D) Plasma concentrations of CAL-130 in mice after a single oral dose (n = 4).

(E and F) Plasma glucose (E) and corresponding insulin levels (F) in WT mice before and after receiving a single dose of inhibitor (10 mg kg^{-1}). $p > 0.5$ for glucose and $p > 0.2$ for insulin as compared to baseline (n = 15 mice per time point; ns, not significant).

(G) Phenotypic analyses of thymi from mice treated with either CAL-130 (10 mg kg^{-1} every 8 hr) or vehicle control for 7 days. The panels are representative of data from five animals in each group.

(H) Total DP thymocyte count in the same animals in (G). Results are compared to PI3Kγ/δ double-knockout mice. Data represent the mean ± SD.

See also Figure S1.

Table 1. P110 Catalytic Domain Selectivity of CAL-130 as Assessed by Ambit KinomeScan Screening

Ambit Gene Symbol	Control Binding (%)	Ambit Gene Symbol	Control Binding (%)
PIK3CA	12	PIK3CG	3.2
PIK3CB	10	PIK3CD	0.2

CAL-130 (10 μM) was evaluated for its ability to prevent tagged kinases from interacting with immobilized "bait" ligand (Fabian et al., 2005; Karaman et al., 2008). Results are reported as percentage (%) of control binding, where lower numbers indicate stronger interactions with the tagged kinase. Values >35% are considered "no hits." PI3Kδ had the lowest percentage of control binding at 0.2% followed by PI3Kγ at 3.2%, indicating a high probability of a potent interaction. A total of 353 kinases were assessed in the screen (Table S1).

Reliance of PTEN Null Human T-ALL on PI3Kγ and PI3Kδ

To test whether CAL-130 may have similar effects on human tumors, we first analyzed the response of T-ALL cell lines to the compound. Incubation of cultured cells with CAL-130, but not inhibitors of either PI3Kγ or PI3Kδ, prevented proliferation and promoted apoptosis within 24 hr, which persisted over 4 days of treatment (Figures 5A, 5B, and S3A–S3J). To further demonstrate that the combined activities of PI3Kγ and PI3Kδ are essential for these processes, we utilized an shRNA vector that targeted the p110γ catalytic domain in CCRF-CEM cells. Western blot analysis revealed a >95% reduction in expression of p110γ with no effect on the other isoforms (Figure 5C, inset). Subsequent incubation of these cells with the PI3Kδ-specific inhibitor IC87114 prevented proliferation and promoted apoptosis as observed for nontransfected CCRF-CEM exposed to CAL-130 (Figures 5C and 5D). In contrast, IC87114 had no major effect on cells containing empty vector alone; neither did siRNA knockdown of either p110α or p110β (Figures S3K–S3N). These observations are consistent with our in vivo studies demonstrating that PI3Kγ and PI3Kδ are strictly required for the proliferation and survival of T-ALL lymphoblasts. Moreover, blockade of these two isoforms significantly enhanced the apoptotic properties of dexamethasone, a drug of considerable importance in the treatment of various lymphoid malignancies including T-ALL (Figures 5E–5H) (Beesley et al., 2009).

It is well known that PI3K/Akt signaling pathway can play a major role in cell-cycle progression and growth of tumors by regulating the activation state of the downstream targets such as glycogen synthase kinase-3β (GSK3β) and mTOR (Schmelzle and Hall, 2000; Cohen and Frame, 2001). PI3K/Akt-mediated phosphorylation suppresses the function of the former and promotes the activity of the latter. Tumor cell survival, on the other hand, is largely mediated by the ability of this pathway to inactivate proapoptotic effectors such as the BH3-only proapoptotic protein BAD and to repress the expression of BIM, both of which participate in the mitochondria-dependent cell death pathway (Strasser et al., 2000; Duronio, 2008). Therefore, we examined the ability of CAL-130 treatment to interfere with such events. Indeed, CCRF-CEM cells exposed to increasing concentration of drug exhibited a corresponding reduction and complete abrogation of Akt (Ser473) phosphorylation at 2.5 μM (Figure 6A). Downstream targets of this protein kinase were also affected as evidenced by the reduction in phosphorylation of GSK3β and mTOR. Consistent with the importance of PI3K in tumor cell survival, CAL-130 treatment resulted in a reduction in phosphorylation of BAD, as well as an enhanced expression of its counterpart BIM (including the L and S isoforms) (Figure 6B). The latter would also explain in part the synergy between CAL-130 and dexamethasone because BIM expression is required for glucocorticoid-induced apoptosis (Erlacher et al., 2005; Wang et al., 2003).

To assess the in vivo relevance of these observations, we evaluated the ability of CAL-130 to prevent the proliferation of CCRF-CEM cells implanted subcutaneously or to prolong the survival of NOD.Cg-*Prkdc*^{scid} *Il2rg*^{tm1Wjl}/Sz that received these cells intravenously. In the former, luciferase-expressing CCRF-CEM cells were injected into the flanks of immunodeficient mice and allowed to grow for 1 week before administering vehicle control or inhibitor (10 mg kg^{-1} every 8 hr) for a total of 4 days. In the latter, treatment commenced 3 days postinjection of tumor cells for a total of 7 days. Bioimaging of subcutaneous tumors revealed a 5-fold difference in luminescence in CAL-130-treated versus vehicle control-treated animals (Figure 6C). This translated into an increase in median survival time for treated animals with systemic disease of 35 versus 23 days for mice that received vehicle control alone (Figure 6D).

Because the continued passage of rapidly growing tumor lines can result in genetic alterations distinct from the cell from which it was originally derived, we also evaluated the effect of CAL-130 on primary T-ALL samples isolated from patients with active disease. Consistent with our animal studies, human tumor cells devoid of PTEN were exquisitely sensitive to dual inhibition of PI3Kγ/δ, but not single inhibition of PI3Kδ, which resulted in a reduction in tumor cell viability as well as in Akt phosphorylation in response to treatment (Figures 7A–7C; data not shown). Interestingly, one primary sample that not only expressed PTEN (T-ALL 4) but also high levels of phospho-Akt was as responsive to CAL-130 as its PTEN null counterparts. This would suggest that T-ALL sensitivity to a PI3Kγ/δ dual inhibitor might correlate better with the degree of Akt phosphorylation rather than with PTEN expression. As observed with primary mouse T-ALL, human tumors did not appear to overexpress any of the four class I *PIK3C* isoforms (Figure 7D).

DISCUSSION

Oncogenesis is a complex and multigenic process that often involves constitutive activation of the PI3K signaling pathway. Most notably are the gain-of-function mutations frequently found in *PIK3CA*, the gene that encodes for the p110α catalytic subunit, and genetic alterations that lead to the inactivation of the tumor suppressor gene *PTEN* (Samuels et al., 2004; Zunder et al., 2008; Sulis and Parsons, 2003; Salmena et al., 2008). In the latter scenario the possibility exists that the unregulated activity of any of the four class I PI3K isoforms could drive tumor development. For instance, previous reports demonstrate that PI3Kβ is essential for the induction, growth, and survival of PTEN-deficient tumors of epithelial cell origin (Jia et al., 2008; Wee et al., 2008). Moreover, it has been suggested that all class I PI3K isoforms are capable of coupling to upstream signaling pathways in which they are not normally engaged, thus compensating for inhibition/genetic deletion of a particular isoform

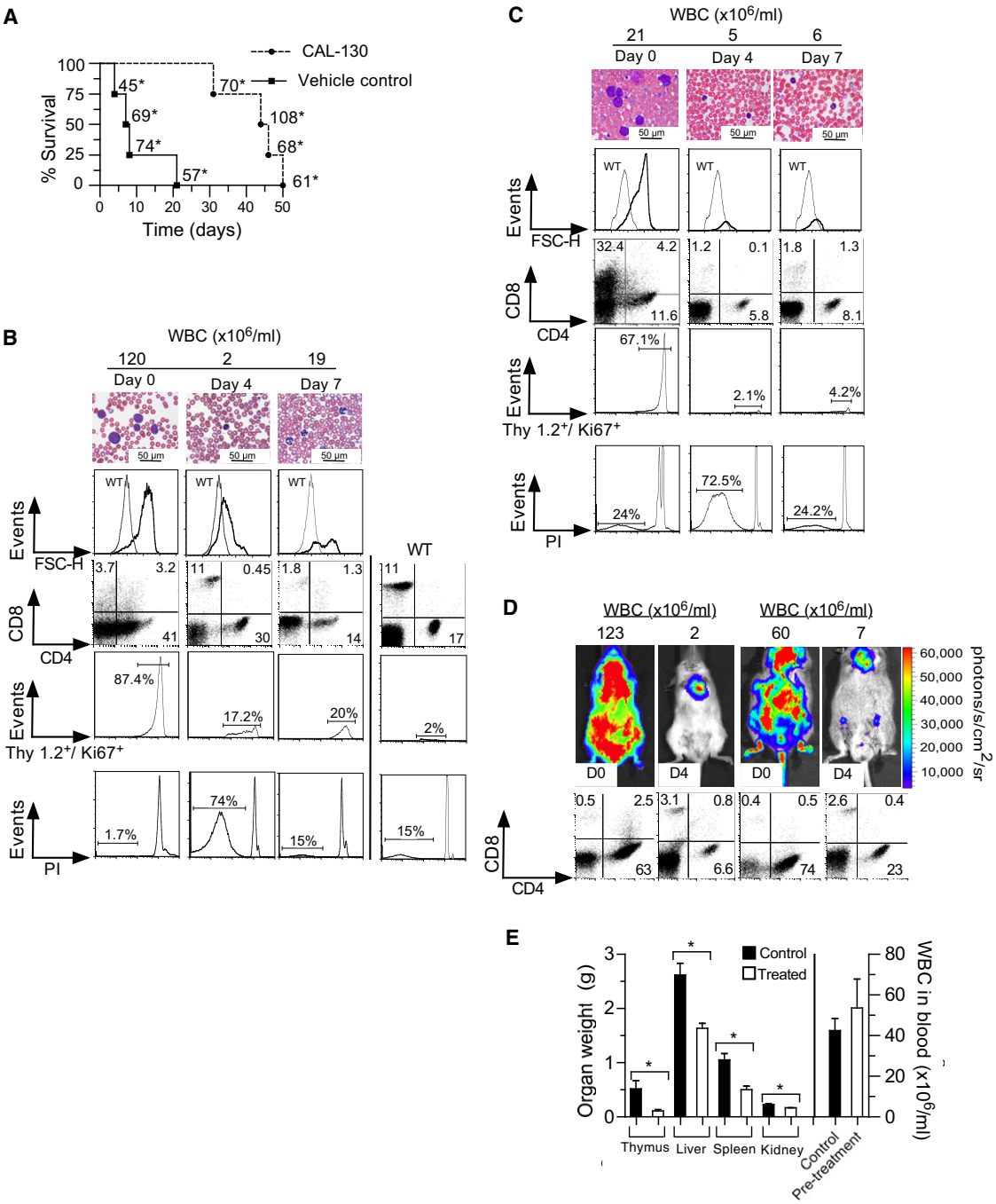

Figure 4. Combined Inhibition of p110γ and p110δ Reduces Tumor Burden and Increases Survival in Animals with PTEN Null T-ALL

(A) Kaplan-Meyer survival curve for *Lck/Pten*$^{fl/fl}$ mice diagnosed with T-ALL and immediately treated with CAL-130 for a total of 7 days. $p < 0.001$ for CAL-130 treated versus vehicle control. Numbers with an asterisk (*) represent the initial WBC count ($\times 10^6$) for each animal prior to instituting therapy.

(B and C) Peripheral blood smears and flow cytometric profiles for diseased (B) *Lck/Pten*$^{fl/fl}$ and (C) *Lck/Pten*$^{fl/fl}$;*Pik3cg*$^{-/-}$ mice just before and 4 and 7 days after initiating treatment with either CAL-130 or the PI3Kδ-specific inhibitor IC87114, respectively. The panels are representative of data from four *Lck/Pten*$^{fl/fl}$ mice and two *Lck/Pten*$^{fl/fl}$;*Pik3cg*$^{-/-}$ mice with T-ALL. Untreated WT animal is shown for comparison.

(D) Bioluminescent images and corresponding flow cytometric profiles of *Lck/Pten*$^{fl/fl}$/*Gt(ROSA)26Sor*$^{tm1(Luc)Kael}$/J animals with T-ALL immediately before and 4 days after treatment.

(E) Weights of thymi, liver, spleen, and kidneys harvested from *Lck/Pten*$^{fl/fl}$ mice with T-ALL 7 days posttreatment with either CAL-130 or vehicle control (n = 5, *$p < 0.01$ for CAL-130 treated versus vehicle control). Peripheral blood counts (WBC, right axis) represent the mean ± SD prior to treatment.

See also Figure S2.

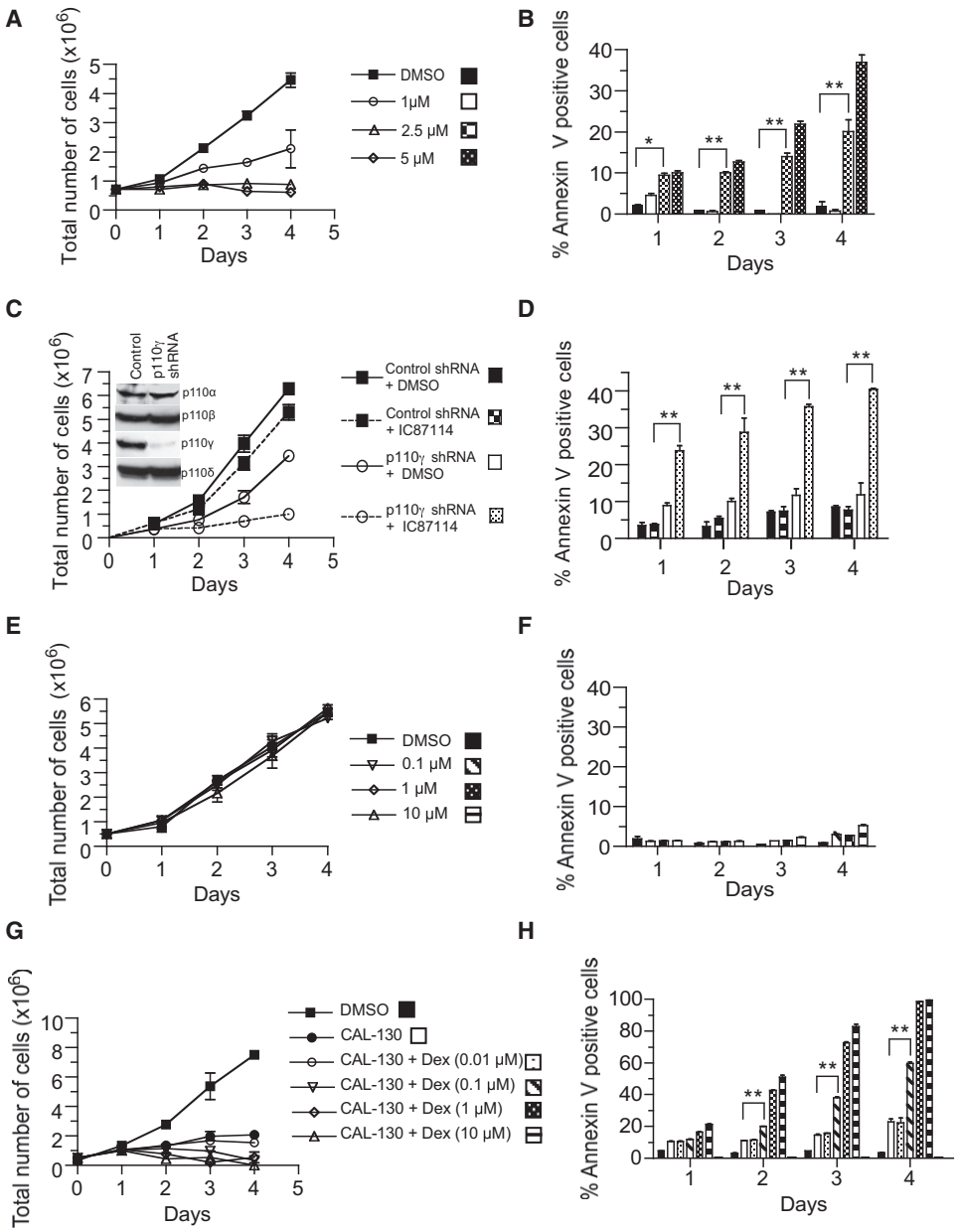

Figure 5. Contribution of PI3Kγ and PI3Kδ to the Growth and Survival of PTEN Null Human T-ALL Tumor Cell Lines

(A and B) Proliferation (A) and survival (B) of CCRF-CEM cells cultured in the presence of CAL-130 or vehicle control. *$p < 0.01$, **$p < 0.001$ for CAL-130 treated (2.5 μM) versus DMSO.

(C and D) Effect of the PI3Kδ-specific inhibitor IC87114 (10 μM) on proliferation (C) and survival (D) of CCRF-CEM cells in which p110γ expression was knocked down by shRNA transfection. **$p < 0.001$ for p110γ shRNA treated with IC87114 versus nonsilencing vector treated with IC87114. Inset in (C) depicts western blot analysis for p110 catalytic subunits.

(E–H) Proliferation and survival of CCRF-CEM cells cultured in the presence of dexamethasone alone (E and F) or in combination with 2.5 μM CAL-130 (G and H). **$p < 0.001$ for dexamethasone plus CAL-130 treated (2.5 μM) versus CAL-130 (2.5 μM) alone. Data represent the mean ± SD of experiments performed in triplicate.

See also Figure S3.

(Foukas et al., 2010). To date, to our knowledge, no conclusive evidence exists to implicate PI3Kβ or any other class I PI3K in the genesis of hematological malignancies such as T-ALL.

Our results demonstrate that in the absence of physiological regulation, the activity of either PI3Kγ or PI3Kδ is sufficient for the malignant transformation of T cell progenitors in a living animal. This is exemplified by the similar onset of disease and percent survival of mice lacking either p110γ or p110δ, and the rare incidence of tumor development in their combined absence. Moreover, pharmacological blockade of both p110γ and p110δ

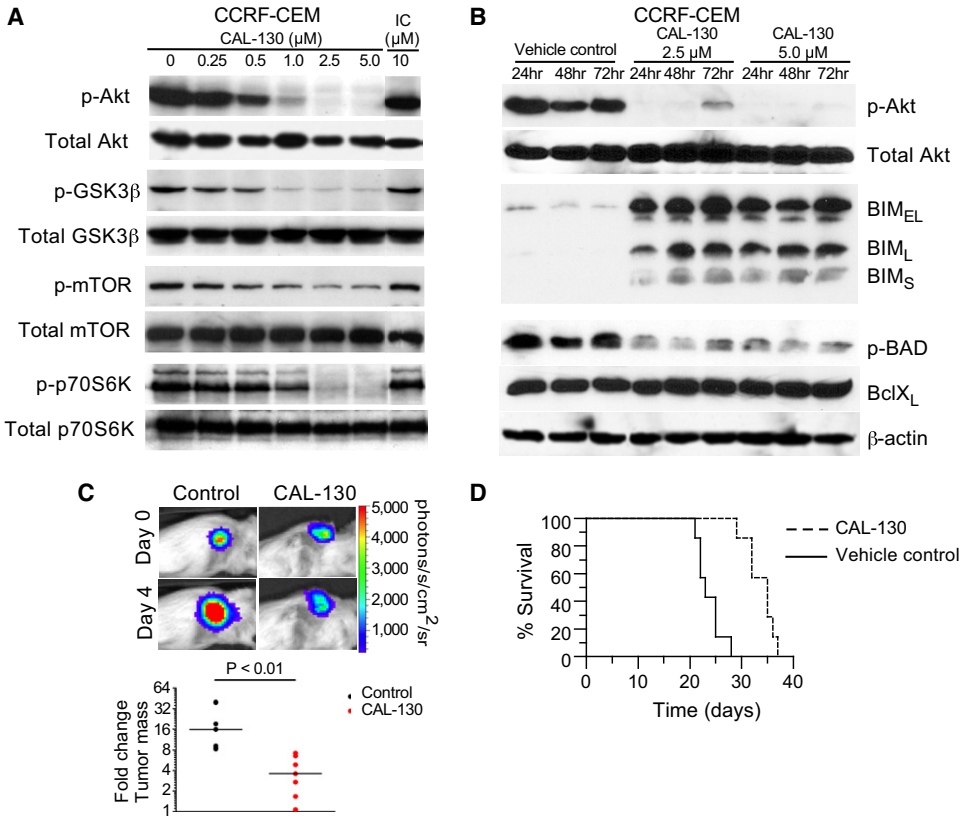

Figure 6. Effect of CAL-130 on Signaling Pathways Downstream of PI3Kγ and PI3Kδ

(A) Representative immunoblots of lysates obtained from CCRF-CEM cells treated (6 hr) with either CAL-130 or vehicle control and probed with the stated antibodies. The PI3Kδ-specific inhibitor IC87114 (IC) is shown for comparison.

(B) Representative immunoblots demonstrating activation of the proapoptotic pathway in CAL-130-treated CCRF-CEM cells.

(C) Representative bioluminescence images (upper panel) and quantification of tumor mass changes (lower panel) in mice with subcutaneous CCRF-CEM xenografts that received vehicle control or CAL-130 for 4 days (n = 7).

(D) Kaplan-Meyer analysis of overall survival of mice treated with vehicle control or CAL-130 for 7 days in a systemic CCRF-CEM xenograft model ($p < 0.01$ for CAL-130 treated versus vehicle control; n = 7 per group).

dramatically impacted on tumor cell proliferation and survival as demonstrated in CAL-130 treatment of diseased *Lck/Pten*$^{fl/fl}$ mice, IC87114 treatment of diseased *Lck/PTEN*$^{fl/fl}$;*Pik3cg*$^{-/-}$ mice, as well as CAL-130 treatment of PTEN null human T-ALL primary tumors or tumor cell lines; no such effects were observed with siRNA knockdown of either p110α or p110β, and selective blockade of PI3Kδ with IC87114 was ineffective in reducing the viability of primary human T-ALL samples. These results would suggest that propagation of upstream signaling pathways critical for the development and/or survival of PTEN null T-ALL tumors relies on PI3Kγ and PI3Kδ and that the remaining isoforms (i.e., α and β) cannot adequately compensate for their inactivity. Clearly, the same PI3K isoforms can participate in both tumorigenesis and tumor maintenance.

It has previously been established that PTEN loss is necessary but not sufficient to cause the malignant transformation of T cell progenitors (Liu et al., 2010; Guo et al., 2011). This typically requires additional genetic events such as chromosomal translocations involving the TCR α/δ locus and c-*myc* oncogene (Bernard et al., 1988; Finger et al., 1986), which are acquired during the transition from CD4$^-$CD8$^-$ DN to CD4$^+$CD8$^+$ DP development stage. Despite the presence of these strong oncogenic signals, the combined absence of PI3Kγ and PI3Kδ significantly impaired leukemogenesis, suggesting that loss of these isoforms can act as a tumorigenic bottleneck. Although it is possible that the overall reduction in CD4$^+$CD8$^+$ DP thymocyte numbers can partially account for the lower tumor incidence, we have previously shown that the transition from DN to DP thymocyte population in double-knockout mice is relatively normal (Swat et al., 2006). That is to say, there is no major deficiency in the number of early T cell progenitors that could undergo malignant transformation in the absence of PTEN activity. Yet, not only is tumorigenesis disrupted in TKO mice, but the abnormality observed in T cell development persisted as well. This is in contrast to the severe defect in thymocyte development associated with a genetic deletion of phosphoinositide-dependent kinase 1 (PDK1) (Hinton et al., 2004), a direct downstream target of class I PI3K, which can be overcome by the loss of PTEN resulting in near-normal numbers of thymocytes and peripheral T cells (Finlay et al., 2009). Similarly, PTEN deficiency can bypass a defect in either IL-7R or pre-TCR signaling, which are critical for the normal development and survival of T cells (Hagenbeek et al.,

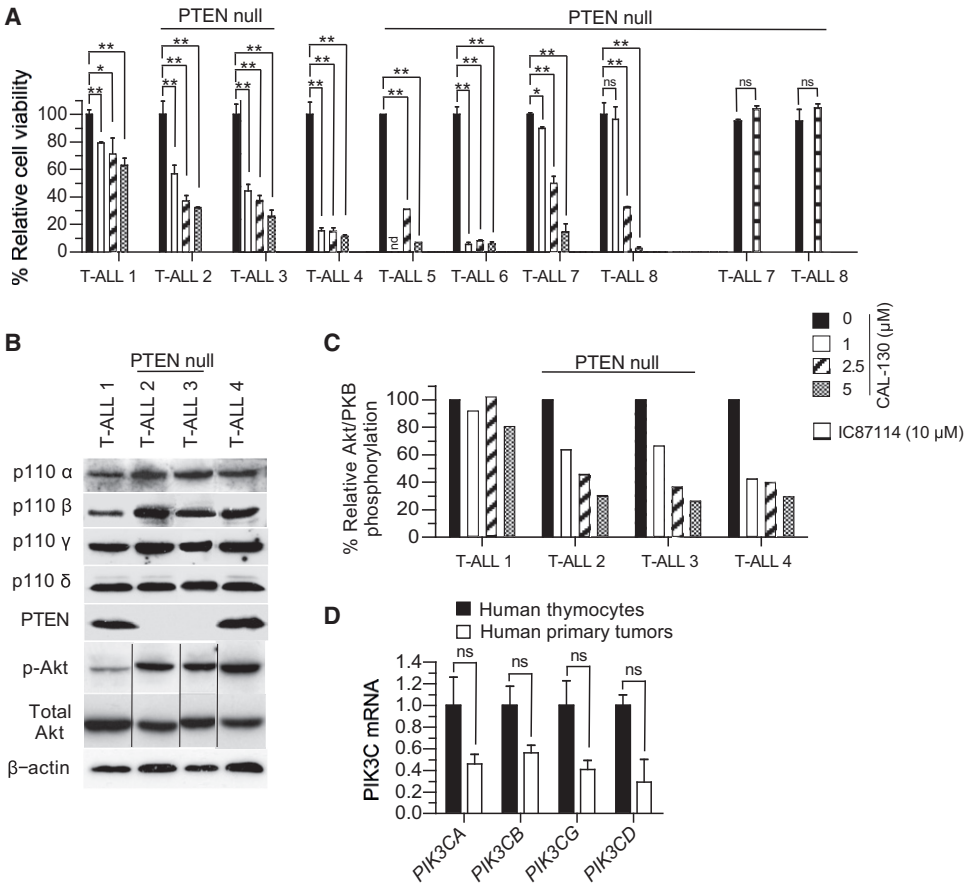

Figure 7. Susceptibility of Primary Human T-ALL Tumor Cells to Combined Inhibition of p110γ and p110δ

(A) Cell survival analyses of tumors cultured in the presence of increasing concentrations of CAL-130 for 72 hr. Percent viability indicates the proportion of live-gated cells in the treated populations relative to its vehicle control counterpart. Data represent the mean ± SD of experiments performed in duplicate or triplicate. *$p < 0.01$, **$p < 0.001$ for CAL-130 treated versus DMSO control. nd, not done; ns, not significant.

(B) Representative immunoblots of four primary human T-ALL samples to assess for expression of p110 catalytic domains and PTEN as well as phosphorylation state of Akt.

(C) Effect of CAL-130 on Akt phosphorylation on the same four representative T-ALL samples after 6 hr of treatment. Densitometry was performed on bands from immunoblots. The P-Akt signal was normalized to total Akt.

(D) Quantitative reverse-transcription PCR analysis of *PIK3C* (*A*/*B*/*G*/*D*) transcript levels in human thymocytes (n = 5) and primary human T-ALL tumors (n = 5). Error bars represent ±SD. The difference in *PIK3C* expression levels between the thymocytes and tumor cells was not statistically significant ($p > 0.05$) using a Student's t test.

2004). In stark contrast to these studies is the inability of a PTEN-deficient state to promote thymocyte proliferation and development in TKO mice. Taken together, these observations further suggest that developmental and genomic events responsible for the generation as well as the malignant transformation of T cells in the context of a PTEN-deficient state are critically reliant on proliferation and survival signals provided by PI3Kγ and PI3Kδ.

It is interesting to note that although PTEN appears to play a key role in regulating the activities of class I PI3K, it is not the only phosphatase in T cells. SHIP1 (SH2-containing inositol-5′-phosphatase) is also capable of hydrolyzing PIP3 and has been shown to play an important role in the immunoregulatory capacity and development of specific subsets of T cells (Tarasenko et al., 2007; Collazo et al., 2009). Although deletion of SHIP1 alone in T cell progenitors is not sufficient to induce leukemogenesis, low levels of this phosphatase in conjunction with PTEN inactivation have been reported in human T-ALL tumors suggesting that inactivation of both phosphatases contribute to the hyperactivation of the PI3K/Akt signaling pathway (Lo et al., 2009). Our discovery that both PI3Kγ and PI3Kδ are the engines that help drive the oncogenic process in T cell progenitors in the absence of appropriate regulation and can provide sufficient growth and survival signals necessary for tumor cell maintenance makes them attractive targets for therapy in such clinical cases. Moreover, dual inhibition of PI3Kγ and PI3Kδ in combination with conventional chemotherapies such as glucocorticoids may be of particular clinical utility in such individuals because they are more likely to fail induction chemotherapy and relapse (Gutierrez et al., 2009; Jotta et al., 2010).

It has been suggested that a complex signaling network involving PI3K exists between leukemic and supporting cells in

the tissue microenvironment that may contribute to disease progression and drug resistance (Ayala et al., 2009; Konopleva et al., 2009; Burger et al., 2009). This is exemplified by the recent observations that the PI3Kδ-specific inhibitor CAL-101 reduces levels of circulating chemokines known to contribute to tissue localization of chronic lymphocytic leukemic cells (Hoellenriegel et al., 2011). Consequently, this results in a generalized lymphocytosis during treatment of patients with this hematological malignancy. In contrast we have observed a dramatic and sustained reduction in peripheral blood T-ALL cells within hours of CAL-130 treatment of diseased *Lck/Pten*$^{fl/fl}$ mice (data not shown). That said, it is possible that paracrine and/or autocrine signaling responsible for T-ALL survival in tissues may be disrupted by simultaneously blocking the activities of PI3Kγ and PI3Kδ. Further work will be required to establish the role of these PI3K isoforms in supporting microenvironmental interactions in T-ALL.

In the broader perspective our results indicate that in the absence of PTEN-mediated regulation, distinct class I PI3K can predominate in the development and survival of tumors in a manner that is most likely to involve isoforms that normally play a critical role in the function of that particular cell type. Furthermore, we demonstrate that it is possible to target cancer cells by exploiting their "addiction" to the activity of distinct PI3K isoforms that are not themselves classical oncogenes. More generally, by identifying PI3Kγ and PI3Kδ as key therapeutic targets, it may be possible to limit toxicities that would be associated with the administration of pan-PI3K or Akt inhibitors including perturbations in insulin signaling and glucose metabolism (Crouthamel et al., 2009).

EXPERIMENTAL PROCEDURES

Cell Lines and Reagents and Antibodies

CCRF-CEM, CEM/C1, and MOLT-4 cells were obtained from ATCC and grown in RPMI-1640 medium containing 10% FBS and antibiotics. Antibodies to Akt (catalog #9272), phospho-Akt (S473, clone 193H12), phospho-mTOR (S2448, catalog #2971S), mTOR (catalog #2972), phospho-GSK3α/β (S21/9, catalog #9331S), GSK-3β (clone 27C10), phospho-p70S6K (Thr389, catalog #9205S), p70S6K (catalog #9202), and β-actin (catalog #4967S) were from Cell Signaling Technology. Antibodies to class I PI3K subunits were as follows: p110α (catalog #4255) from Cell Signaling Technology; p110β (clone Y384) from Millipore and mouse p110β from Santa Cruz Biotechnology (catalog #sc-602); p110γ (clone H1) from Jena Biosciences; and p110δ (clone H-219) from Santa Cruz Biotechnology. Antibodies to PTEN (clone 6H2.1) were from Cascade Bioscience. For flow cytometry, antibodies were obtained from BD Biosciences: CD3ε-Alexa 488 (clone 145-2C11), CD4-APC (clone RM4-5), CD8-PerCP-Cy5.5 (clone 53-6.7), CD90.2-APC (Thy-1.2, clone 53-2.1), Ki67-FITC (clone B56), and Annexin V-APC. Antibodies to Bim, phospho-Bad, Bad, and BclX_L were from Cell Signaling Technology (proapoptotic sampler kit #9942S).

The shRNA construct for p110γ in the pLKO.1 vector was obtained from Sigma-Aldrich (MISSION shRNA Plasmid DNA; clone ID: NM_002649.2-4744s1c1; TRC number: TRCN0000196870). siRNA constructs for p110α (ON-TARGET plus SMARTpool #L-003018-00) and p110β (ON-TARGET plus SMARTpool # L-003019-00) were obtained from Dharmacon (Thermo Scientific).

Primary Leukemia Samples

Cryopreserved samples were provided by collaborating institutions in the United States (Department of Pediatrics, Columbia Presbyterian Hospital and Departments of Medicine and Pathology, Vanderbilt University), The Netherlands (Erasmus MC-Sophia Children's Hospital), and Italy (Hemato-Oncology Laboratory, Department of Pediatrics, University of Padua). All samples were collected with informed consent and under the supervision of the Medical Ethics Committee of the Erasmus Medical Center, the Columbia University Medical Center Institutional Review Board, the Vanderbilt University Medical Center Institutional Review Board, and the Acute Lymphoblastic Leukemia Strategic Scientific Committee.

Cell Counts, Cell Proliferation, and Cell Viability Assay

Cell counts for mice thymi were determined as previously described by Swat et al. (2006). Cell proliferation of CCRF-CEM cells or shRNA-transfected CCRF-CEM cells, in presence or absence of appropriate drug, was followed by cell counting of samples in triplicate using a hemocytometer and trypan blue. For apoptosis determinations of untransfected or shRNA-transfected CCRF-CEMs, cells were stained with APC-conjugated Annexin-V (BD Biosciences) in Annexin Binding Buffer (Miltyeni Biotec) and analyzed by flow cytometry. For primary T-ALL samples, cell viability was assessed using the BD Cell Viability kit (BD Biosciences) coupled with the use of fluorescent-counting beads as previously described by Armstrong et al. (2009). For this, cells were plated with MS5-DL1 stroma cells, and after 72 hr following drug treatment, cells were harvested and stained with an APC-conjugated anti-human CD45 followed by a staining with the aforementioned kit according to the manufacturer's instructions.

CAL130 IC_{50}

CAL-130 is a derivative of IC87114, the synthesis of which has been previously described by Sadhu et al. (2003). IC_{50} values for CAL-130 inhibition of PI3K isoforms were determined in ex vivo PI3 kinase assays using recombinant PI3K. A ten-point kinase inhibitory profile was determined with ATP at a concentration consistent with the K_M for each enzyme (Puri et al., 2004).

Calcium Flux Measurements in Thymocytes

Ca^{2+} flux measurements in single-cell suspensions of mouse thymocytes were performed as previously described by Swat et al. (2006). Drug inhibition of Ca^{2+} flux was measured after 30 min preincubation with CAL-130 at room temperature of dye-loaded cells. Percent overall change in Ca^{2+} flux is reported as $(Ca^{2+}\ flux_{peak} - Ca^{2+}\ flux_{baseline}/Ca^{2+}flux_{ionomycin} - Ca^{2+}\ flux_{baseline}) \times 100$.

Flow Cytometry for Cell Surface Staining and Apoptosis

For cell surface staining in mouse whole blood, following incubation with appropriate antibodies, blood was processed using the BD Bioscience BD FACS Lysing Solution according to the manufacturer's instructions. For intracellular staining of Ki67, immediately after RBC lysis with the BD FACS Lysing solution, cells were permeabilized without washing with 0.025% Tween 20 in lysing solution for an additional 15 min, washed, and then incubated with Ki67 antibodies. For thymocytes, single-cell suspensions of thymocytes were isolated and stained with the appropriate antibodies as previously described by Swat et al. (2006).

Histological and Immunohistochemical Study of Tissue Samples

Formalin-fixed paraffin-embedded 5 μm tissue sections were stained with hematoxylin and eosin for histopathological diagnosis. For immunohistochemistry we performed anti-CD3 (rabbit polyclonal; Dako) staining on tissue sections after antigen retrieval by microwave heating in citrate buffer (pH 6.0). After epitope recovery, slides were incubated with antibody (anti-CD3 1:50) overnight at room temperature before antigen detection with diaminobenzidine (DAB) using a Ventana automated staining platform (Ventana).

Western Blotting

Cell lysates (from cell lines or thymocytes) were prepared on ice in M-PER Mammalian Protein Extraction reagent (Pierce) containing a cocktail of protease and phosphatase inhibitors as previously described by Swat et al. (2006). Equal amounts of total protein from lysates were subjected to SDS-PAGE, transferred to PVDF membrane (Immobilon-P; Millipore), and membranes were probed by overnight incubation with appropriate primary antibodies. Bound antibodies were visualized with HRP-conjugated secondary antibodies and ECL chemistry (SuperPico West; Pierce).

shRNA and siRNA Knockdown

CCRF-CEMs were transfected using the Amaxa Human T cell Nucleofecor kit (Lonza) according to the manufacturer's optimized protocol kit for this cell line. For shRNA knockdown of p110γ, CCRF-CEMs (2×10^6 cells) were transfected with 2 μg of purified plasmid DNA, and clones were selected by high dilution in puromycin used at a concentration predetermined by a killing curve. Expression of p110γ and p110δ was determined by western blotting.

For siRNA knockdown of p110α or p110β, CCRF-CEMs (2×10^6 cells) were transfected with 300 nM of siRNA construct. After a brief recovery period, cells were diluted to between 1 and 2×10^5/ml and grown for further 48 hr for cell counting, flow cytometry, and western blotting.

Mice and Animal Procedures

All mice were kept in a specific pathogen-free facility at Columbia University Medical Center. All mice studies and breeding were carried out under the approval of Institutional Animal Care and Use Committee of Columbia University. NOD.Cg-*Prkdc*^{scid} *Il2rg*^{tm1Wjl}/Sz mice for xenograft experiments and *Gt(ROSA)26Sor*$^{tm1(Luc)Kael}$/J for bioimaging studies were obtained from The Jackson Laboratory. Mice deficient for *Pten* in the T cell lineage were generated by crossing *Lck-cre* with floxed *Pten* (Hennet et al., 1995; Trotman et al., 2003). P110γ$^{-/-}$ and p110δ$^{-/-}$ mice have been previously described by Swat et al. (2006). These animals were intercrossed with *Lck-cre/Pten*$^{fl/fl}$ animals to generate mice homozygous mutant for either p110γ or p110δ and *Pten* or homozygous mutant for p110γ, 110δ, and *Pten*.

For subcutaneous xenograft experiments, luminescent CCRF-CEM (CEM-luc) cells were generated by lentiviral infection with FUW-luc and selection with neomycin. Luciferase expression was verified with the Dual-Luciferase Reporter Assay kit (Promega). We injected 2.5×10^6 CEM-luc cells embedded in Matrigel (BD Biosciences) in the flank of NOD.Cg-*Prkdc*^{scid} *Il2rg*^{tm1Wjl}/Sz mice. After 1 week, mice were treated by oral gavage with vehicle (0.5% methyl cellulose, 0.1% Tween 80), or CAL-130 (10 mg kg^{-1}) every 8 hr daily for 4 days, and then tumors were imaged as follows: mice anesthetized by isoflurane inhalation were injected intraperitoneally with D-luciferin (50 mg kg^{-1}; Xenogen). Photonic emission was imaged with the In Vivo Imaging System (IVIS; Xenogen). Tumor bioluminescence was quantified by integrating the photonic flux (photons per second) through a region encircling each tumor using the Living Image software package (Xenogen). Administration of D-luciferin and detection of tumor bioluminescence in *Lck/Pten*$^{fl/fl}$*/Gt(ROSA)26Sor*$^{tm1(Luc)Kael}$/J mice were performed in a similar manner.

For intravenous xenograft transplantation, 5×10^6 CCRF-CEM cells were injected intravenously in 14 NOD.Cg-*Prkdc*^{scid} *Il2rg*^{tm1Wjl}/Sz mice. After 3 days, mice were segregated into two treatment groups that received either CAL-130 or vehicle by oral gavage as described above for 7 days. Mice in both groups were then followed until moribund (and euthanized).

Plasma Levels of CAL130, Glucose, and Insulin

For CAL-130 level determinations, animals received a single oral dose (10 or 20 mg kg^{-1}) of inhibitor. Plasma was collected at 0, 2, 4, 8, and 12 hr and subjected to high-performance liquid chromatography-MS/MS (sensitivity 1 ng/ml). The concentration of CAL-130 in plasma was determined using a standard curve (analyte peak area versus concentration) generated with calibration standard pools. Values represent the mean (±SD) for four animals per group.

Plasma glucose and insulin levels were determined following a single oral dose of CAL-130 (10 mg kg^{-1}). Blood was collected into K_2EDTA tubes by cardiac puncture at baseline and 0, 2, 4, and 8 hr post-dose, and plasma samples were frozen at −80°C until analysis. The insulin and glucose levels were determined by using an Ultra Sensitive Mouse Insulin ELISA Kit (Crystal Chem) or WaveSense Presto Blood Glucose Monitoring System (Agamatrix, Boston), respectively.

Statistical Analyses

Statistical analyses were performed using Student's t test (GraphPad Prism software). Kaplan-Meier survival curves were analyzed using a log rank test (GraphPad Prism software). Values were considered significant at $p < 0.05$.

SUPPLEMENTAL INFORMATION

Supplemental Information includes three figures, one table, and Supplemental Experimental Procedures and can be found with this article online at doi:10.1016/j.ccr.2012.02.029.

ACKNOWLEDGMENTS

We thank Andrew Kung for providing the FUW luciferase vector, Jerry Evarts for supplying CAL-130, Juan Carlos Zuniga-Pflucker for providing the OP9-DL1 cells, Richard Friedman for statistical analyses, Kui Tan and Mikin Patel for genotyping and animal husbandry, and Timothy Wang for critical review of the manuscript. This work was supported by the DOD (Grant PR093714 to T.G.D. and A.F.), the Leukemia & Lymphoma Society Translational Research Program (Grant 140229 to T.G.D. and A.F.), and the Leukemia & Lymphoma Society Scholar Award (to A.F.). B.J.L. and A.K. are employees of the company (Gilead Sciences) that manufactured CAL-130.

Received: August 10, 2011
Revised: December 26, 2011
Accepted: February 24, 2012
Published: April 16, 2012

REFERENCES

Armstrong, F., Brunet de la Grange, P., Gerby, B., Rouyez, M.C., Calvo, J., Fontenay, M., Boissel, N., Dombret, H., Baruchel, A., Landman-Parker, J., et al. (2009). NOTCH is a key regulator of human T-cell acute leukemia initiating cell activity. Blood *113*, 1730–1740.

Ayala, F., Dewar, R., Kieran, M., and Kalluri, R. (2009). Contribution of bone microenvironment to leukemogenesis and leukemia progression. Leukemia *23*, 2233–2241.

Beesley, A.H., Firth, M.J., Ford, J., Weller, R.E., Freitas, J.R., Perera, K.U., and Kees, U.R. (2009). Glucocorticoid resistance in T-lineage acute lymphoblastic leukaemia is associated with a proliferative metabolism. Br. J. Cancer *100*, 1926–1936.

Bernard, O., Larsen, C.J., Hampe, A., Mauchauffé, M., Berger, R., and Mathieu-Mahul, D. (1988). Molecular mechanisms of a t(8;14)(q24;q11) translocation juxtaposing c-myc and TcR-alpha genes in a T-cell leukaemia: involvement of a V alpha internal heptamer. Oncogene *2*, 195–200.

Burger, J.A., Ghia, P., Rosenwald, A., and Caligaris-Cappio, F. (2009). The microenvironment in mature B-cell malignancies: a target for new treatment strategies. Blood *114*, 3367–3375.

Cantley, L.C. (2002). The phosphoinositide 3-kinase pathway. Science *296*, 1655–1657.

Carnero, A., Blanco-Aparicio, C., Renner, O., Link, W., and Leal, J.F. (2008). The PTEN/PI3K/AKT signalling pathway in cancer, therapeutic implications. Curr. Cancer Drug Targets *8*, 187–198.

Cohen, P., and Frame, S. (2001). The renaissance of GSK3. Nat. Rev. Mol. Cell Biol. *2*, 769–776.

Collazo, M.M., Wood, D., Paraiso, K.H., Lund, E., Engelman, R.W., Le, C.T., Stauch, D., Kotsch, K., and Kerr, W.G. (2009). SHIP limits immunoregulatory capacity in the T-cell compartment. Blood *113*, 2934–2944.

Crouthamel, M.C., Kahana, J.A., Korenchuk, S., Zhang, S.Y., Sundaresan, G., Eberwein, D.J., Brown, K.K., and Kumar, R. (2009). Mechanism and management of AKT inhibitor-induced hyperglycemia. Clin. Cancer Res. *15*, 217–225.

Duronio, V. (2008). The life of a cell: apoptosis regulation by the PI3K/PKB pathway. Biochem. J. *415*, 333–344.

Erlacher, M., Michalak, E.M., Kelly, P.N., Labi, V., Niederegger, H., Coultas, L., Adams, J.M., Strasser, A., and Villunger, A. (2005). BH3-only proteins Puma and Bim are rate-limiting for gamma-radiation- and glucocorticoid-induced apoptosis of lymphoid cells in vivo. Blood *106*, 4131–4138.

Fabian, M.A., Biggs, W.H., 3rd, Treiber, D.K., Atteridge, C.E., Azimioara, M.D., Benedetti, M.G., Carter, T.A., Ciceri, P., Edeen, P.T., Floyd, M., et al. (2005). A

small molecule-kinase interaction map for clinical kinase inhibitors. Nat. Biotechnol. *23*, 329–336.

Finger, L.R., Harvey, R.C., Moore, R.C., Showe, L.C., and Croce, C.M. (1986). A common mechanism of chromosomal translocation in T- and B-cell neoplasia. Science *234*, 982–985.

Finlay, D.K., Sinclair, L.V., Feijoo, C., Waugh, C.M., Hagenbeek, T.J., Spits, H., and Cantrell, D.A. (2009). Phosphoinositide-dependent kinase 1 controls migration and malignant transformation but not cell growth and proliferation in PTEN-null lymphocytes. J. Exp. Med. *206*, 2441–2454.

Foukas, L.C., Berenjeno, I.M., Gray, A., Khwaja, A., and Vanhaesebroeck, B. (2010). Activity of any class IA PI3K isoform can sustain cell proliferation and survival. Proc. Natl. Acad. Sci. USA *107*, 11381–11386.

Guo, W., Lasky, J.L., Chang, C.J., Mosessian, S., Lewis, X., Xiao, Y., Yeh, J.E., Chen, J.Y., Iruela-Arispe, M.L., Varella-Garcia, M., and Wu, H. (2008). Multi-genetic events collaboratively contribute to Pten-null leukaemia stem-cell formation. Nature *453*, 529–533.

Guo, W., Schubbert, S., Chen, J.Y., Valamehr, B., Mosessian, S., Shi, H., Dang, N.H., Garcia, C., Theodoro, M.F., Varella-Garcia, M., and Wu, H. (2011). Suppression of leukemia development caused by PTEN loss. Proc. Natl. Acad. Sci. USA *108*, 1409–1414.

Gutierrez, A., Sanda, T., Grebliunaite, R., Carracedo, A., Salmena, L., Ahn, Y., Dahlberg, S., Neuberg, D., Moreau, L.A., Winter, S.S., et al. (2009). High frequency of PTEN, PI3K, and AKT abnormalities in T-cell acute lymphoblastic leukemia. Blood *114*, 647–650.

Hagenbeek, T.J., and Spits, H. (2008). T-cell lymphomas in T-cell-specific Pten-deficient mice originate in the thymus. Leukemia *22*, 608–619.

Hagenbeek, T.J., Naspetti, M., Malergue, F., Garçon, F., Nunès, J.A., Cleutjens, K.B., Trapman, J., Krimpenfort, P., and Spits, H. (2004). The loss of PTEN allows TCR alphabeta lineage thymocytes to bypass IL-7 and Pre-TCR-mediated signaling. J. Exp. Med. *200*, 883–894.

Hennet, T., Hagen, F.K., Tabak, L.A., and Marth, J.D. (1995). T-cell-specific deletion of a polypeptide N-acetylgalactosaminyl-transferase gene by site-directed recombination. Proc. Natl. Acad. Sci. USA *92*, 12070–12074.

Hickey, F.B., and Cotter, T.G. (2006). BCR-ABL regulates phosphatidylinositol 3-kinase-p110gamma transcription and activation and is required for proliferation and drug resistance. J. Biol. Chem. *281*, 2441–2450.

Hinton, H.J., Alessi, D.R., and Cantrell, D.A. (2004). The serine kinase phosphoinositide-dependent kinase 1 (PDK1) regulates T cell development. Nat. Immunol. *5*, 539–545.

Hoellenriegel, J., Meadows, S.A., Sivina, M., Wierda, W.G., Kantarjian, H., Keating, M.J., Giese, N., O'Brien, S., Yu, A., Miller, L.L., et al. (2011). The phosphoinositide 3′-kinase delta inhibitor, CAL-101, inhibits B-cell receptor signaling and chemokine networks in chronic lymphocytic leukemia. Blood *118*, 3603–3612.

Huang, W.C., and Hung, M.C. (2009). Induction of Akt activity by chemotherapy confers acquired resistance. J. Formos. Med. Assoc. *108*, 180–194.

Jackson, S.P., Schoenwaelder, S.M., Goncalves, I., Nesbitt, W.S., Yap, C.L., Wright, C.E., Kenche, V., Anderson, K.E., Dopheide, S.M., Yuan, Y., et al. (2005). PI 3-kinase p110beta: a new target for antithrombotic therapy. Nat. Med. *11*, 507–514.

Ji, H., Rintelen, F., Waltzinger, C., Bertschy Meier, D., Bilancio, A., Pearce, W., Hirsch, E., Wymann, M.P., Rückle, T., Camps, M., et al. (2007). Inactivation of PI3Kgamma and PI3Kdelta distorts T-cell development and causes multiple organ inflammation. Blood *110*, 2940–2947.

Jia, S., Liu, Z., Zhang, S., Liu, P., Zhang, L., Lee, S.H., Zhang, J., Signoretti, S., Loda, M., Roberts, T.M., and Zhao, J.J. (2008). Essential roles of PI(3)K-p110beta in cell growth, metabolism and tumorigenesis. Nature *454*, 776–779.

Jotta, P.Y., Ganazza, M.A., Silva, A., Viana, M.B., da Silva, M.J., Zambaldi, L.J., Barata, J.T., Brandalise, S.R., and Yunes, J.A. (2010). Negative prognostic impact of PTEN mutation in pediatric T-cell acute lymphoblastic leukemia. Leukemia *24*, 239–242.

Kang, S., Denley, A., Vanhaesebroeck, B., and Vogt, P.K. (2006). Oncogenic transformation induced by the p110beta, -gamma, and -delta isoforms of class I phosphoinositide 3-kinase. Proc. Natl. Acad. Sci. USA *103*, 1289–1294.

Karaman, M.W., Herrgard, S., Treiber, D.K., Gallant, P., Atteridge, C.E., Campbell, B.T., Chan, K.W., Ciceri, P., Davis, M.I., Edeen, P.T., et al. (2008). A quantitative analysis of kinase inhibitor selectivity. Nat. Biotechnol. *26*, 127–132.

Katso, R., Okkenhaug, K., Ahmadi, K., White, S., Timms, J., and Waterfield, M.D. (2001). Cellular function of phosphoinositide 3-kinases: implications for development, homeostasis, and cancer. Annu. Rev. Cell Dev. Biol. *17*, 615–675.

Konopleva, M., Tabe, Y., Zeng, Z., and Andreeff, M. (2009). Therapeutic targeting of microenvironmental interactions in leukemia: mechanisms and approaches. Drug Resist. Updat. *12*, 103–113.

Larson Gedman, A., Chen, Q., Kugel Desmoulin, S., Ge, Y., LaFiura, K., Haska, C.L., Cherian, C., Devidas, M., Linda, S.B., Taub, J.W., and Matherly, L.H. (2009). The impact of NOTCH1, FBW7 and PTEN mutations on prognosis and downstream signaling in pediatric T-cell acute lymphoblastic leukemia: a report from the Children's Oncology Group. Leukemia *23*, 1417–1425.

Liu, X., Karnell, J.L., Yin, B., Zhang, R., Zhang, J., Li, P., Choi, Y., Maltzman, J.S., Pear, W.S., Bassing, C.H., and Turka, L.A. (2010). Distinct roles for PTEN in prevention of T cell lymphoma and autoimmunity in mice. J. Clin. Invest. *120*, 2497–2507.

Lo, T.C., Barnhill, L.M., Kim, Y., Nakae, E.A., Yu, A.L., and Diccianni, M.B. (2009). Inactivation of SHIP1 in T-cell acute lymphoblastic leukemia due to mutation and extensive alternative splicing. Leuk. Res. *33*, 1562–1566.

Maser, R.S., Choudhury, B., Campbell, P.J., Feng, B., Wong, K.K., Protopopov, A., O'Neil, J., Gutierrez, A., Ivanova, E., Perna, I., et al. (2007). Chromosomally unstable mouse tumours have genomic alterations similar to diverse human cancers. Nature *447*, 966–971.

Okkenhaug, K., and Vanhaesebroeck, B. (2003). PI3K in lymphocyte development, differentiation and activation. Nat. Rev. Immunol. *3*, 317–330.

Palomero, T., Dominguez, M., and Ferrando, A.A. (2008). The role of the PTEN/AKT Pathway in NOTCH1-induced leukemia. Cell Cycle *7*, 965–970.

Puri, K.D., Doggett, T.A., Douangpanya, J., Hou, Y., Tino, W.T., Wilson, T., Graf, T., Clayton, E., Turner, M., Hayflick, J.S., and Diacovo, T.G. (2004). Mechanisms and implications of phosphoinositide 3-kinase δ in promoting neutrophil trafficking into inflamed tissue. Blood *103*, 3448–3456.

Sadhu, C., Masinovsky, B., Dick, K., Sowell, C.G., and Staunton, D.E. (2003). Essential role of phosphoinositide 3-kinase δ in neutrophil directional movement. J. Immunol. *170*, 2647–2654.

Safran, M., Kim, W.Y., Kung, A.L., Horner, J.W., DePinho, R.A., and Kaelin, W.G., Jr. (2003). Mouse reporter strain for noninvasive bioluminescent imaging of cells that have undergone Cre-mediated recombination. Mol. Imaging *2*, 297–302.

Salmena, L., Carracedo, A., and Pandolfi, P.P. (2008). Tenets of PTEN tumor suppression. Cell *133*, 403–414.

Samuels, Y., Wang, Z., Bardelli, A., Silliman, N., Ptak, J., Szabo, S., Yan, H., Gazdar, A., Powell, S.M., Riggins, G.J., et al. (2004). High frequency of mutations of the PIK3CA gene in human cancers. Science *304*, 554.

Schmelzle, T., and Hall, M.N. (2000). TOR, a central controller of cell growth. Cell *103*, 253–262.

Silva, A., Yunes, J.A., Cardoso, B.A., Martins, L.R., Jotta, P.Y., Abecasis, M., Nowill, A.E., Leslie, N.R., Cardoso, A.A., and Barata, J.T. (2008). PTEN posttranslational inactivation and hyperactivation of the PI3K/Akt pathway sustain primary T cell leukemia viability. J. Clin. Invest. *118*, 3762–3774.

Sopasakis, V.R., Liu, P., Suzuki, R., Kondo, T., Winnay, J., Tran, T.T., Asano, T., Smyth, G., Sajan, M.P., Farese, R.V., et al. (2010). Specific roles of the p110alpha isoform of phosphatidylinsositol 3-kinase in hepatic insulin signaling and metabolic regulation. Cell Metab. *11*, 220–230.

Strasser, A., Puthalakath, H., Bouillet, P., Huang, D.C., O'Connor, L., O'Reilly, L.A., Cullen, L., Cory, S., and Adams, J.M. (2000). The role of bim, a proapoptotic BH3-only member of the Bcl-2 family in cell-death control. Ann. N Y Acad. Sci. *917*, 541–548.

Sujobert, P., Bardet, V., Cornillet-Lefebvre, P., Hayflick, J.S., Prie, N., Verdier, F., Vanhaesebroeck, B., Muller, O., Pesce, F., Ifrah, N., et al. (2005). Essential

role for the p110delta isoform in phosphoinositide 3-kinase activation and cell proliferation in acute myeloid leukemia. Blood *106*, 1063–1066.

Sulis, M.L., and Parsons, R. (2003). PTEN: from pathology to biology. Trends Cell Biol. *13*, 478–483.

Suzuki, A., Yamaguchi, M.T., Ohteki, T., Sasaki, T., Kaisho, T., Kimura, Y., Yoshida, R., Wakeham, A., Higuchi, T., Fukumoto, M., et al. (2001). T cell-specific loss of Pten leads to defects in central and peripheral tolerance. Immunity *14*, 523–534.

Swat, W., Montgrain, V., Doggett, T.A., Douangpanya, J., Puri, K., Vermi, W., and Diacovo, T.G. (2006). Essential role of PI3Kdelta and PI3Kgamma in thymocyte survival. Blood *107*, 2415–2422.

Tarasenko, T., Kole, H.K., Chi, A.W., Mentink-Kane, M.M., Wynn, T.A., and Bolland, S. (2007). T cell-specific deletion of the inositol phosphatase SHIP reveals its role in regulating Th1/Th2 and cytotoxic responses. Proc. Natl. Acad. Sci. USA *104*, 11382–11387.

Trotman, L.C., Niki, M., Dotan, Z.A., Koutcher, J.A., Di Cristofano, A., Xiao, A., Khoo, A.S., Roy-Burman, P., Greenberg, N.M., Van Dyke, T., et al. (2003). Pten dose dictates cancer progression in the prostate. PLoS Biol. *1*, E59.

Wang, Z., Malone, M.H., He, H., McColl, K.S., and Distelhorst, C.W. (2003). Microarray analysis uncovers the induction of the proapoptotic BH3-only protein Bim in multiple models of glucocorticoid-induced apoptosis. J. Biol. Chem. *278*, 23861–23867.

Webb, L.M., Vigorito, E., Wymann, M.P., Hirsch, E., and Turner, M.J. (2005). Cutting edge: T cell development requires the combined activities of the p110gamma and p110delta catalytic isoforms of phosphatidylinositol 3-kinase. J. Immunol. *175*, 2783–2787.

Wee, S., Wiederschain, D., Maira, S.M., Loo, A., Miller, C., deBeaumont, R., Stegmeier, F., Yao, Y.M., and Lengauer, C. (2008). PTEN-deficient cancers depend on PIK3CB. Proc. Natl. Acad. Sci. USA *105*, 13057–13062.

Yuan, T.L., and Cantley, L.C. (2008). PI3K pathway alterations in cancer: variations on a theme. Oncogene *27*, 5497–5510.

Zhao, L., and Vogt, P.K. (2008). Class I PI3K in oncogenic cellular transformation. Oncogene *27*, 5486–5496.

Zunder, E.R., Knight, Z.A., Houseman, B.T., Apsel, B., and Shokat, K.M. (2008). Discovery of drug-resistant and drug-sensitizing mutations in the oncogenic PI3K isoform p110 alpha. Cancer Cell *14*, 180–192.

Cancer Cell
Article

Chemical Genomics Identifies Small-Molecule *MCL1* Repressors and BCL-xL as a Predictor of MCL1 Dependency

Guo Wei,[1,2,5] Adam A. Margolin,[1,5,6] Leila Haery,[1] Emily Brown,[1] Lisa Cucolo,[1] Bina Julian,[1] Shyemaa Shehata,[3] Andrew L. Kung,[2] Rameen Beroukhim,[1,3] and Todd R. Golub[1,2,4,*]
[1]Cancer Program, The Broad Institute of the Massachusetts Institute of Technology and Harvard University, Cambridge, MA 02142, USA
[2]Department of Pediatric Oncology
[3]Department of Medical Oncology
[4]Howard Hughes Medical Institute
Dana-Farber Cancer Institute, Harvard Medical School, Boston, MA 02115, USA
[5]These authors contributed equally to this work
[6]Present address: Sage Bionetworks, 1100 Fairview Avenue North, Seattle, WA 98109, USA
*Correspondence: golub@broadinstitute.org
DOI 10.1016/j.ccr.2012.02.028

SUMMARY

MCL1, **which encodes the antiapoptotic protein MCL1, is among the most frequently amplified genes in human cancer. A chemical genomic screen identified compounds, including anthracyclines, that decreased *MCL1* expression. Genomic profiling indicated that these compounds were global transcriptional repressors that preferentially affect *MCL1* due to its short mRNA half-life. Transcriptional repressors and *MCL1* shRNAs induced apoptosis in the same cancer cell lines and could be rescued by physiological levels of ectopic *MCL1* expression. Repression of MCL1 released the proapoptotic protein BAK from MCL1, and *Bak* deficiency conferred resistance to transcriptional repressors. A computational model, validated in vivo, indicated that high *BCL-xL* expression confers resistance to *MCL1* repression, thereby identifying a patient-selection strategy for the clinical development of MCL1 inhibitors.**

INTRODUCTION

Inhibition of apoptosis is a critical step in the pathogenesis of cancers, and is a major barrier to effective treatment (Adams and Cory, 2007; Danial and Korsmeyer, 2004). It is now thought that one or more components of the apoptosis pathway are dysregulated in all cancers (Hanahan and Weinberg, 2011), either by genetic mutation of the genes encoding these proteins (e.g., point mutations, copy-number abnormalities, or chromosomal translocation) or by other mechanisms (e.g., epigenetic mechanisms or upstream oncogenic mutations). Despite this central importance in the development and maintenance of cancer, few apoptosis-targeted therapeutics have reached clinical evaluation.

Of particular importance is the BCL2 family of proteins. Highly conserved from worm to human, these proteins control the activation of downstream caspases, which are the major effectors of apoptosis. The BCL2 family can be divided into three main subclasses, defined in part by the homology shared within four conserved regions termed BCL2 homology (BH) domains (Adams and Cory, 2007; Danial and Korsmeyer, 2004). The "multidomain" proapoptotic members BAX and BAK possess BH1–BH3 domains, and together constitute a requisite gateway to the intrinsic apoptosis pathway (Lindsten et al., 2000; Wei et al., 2001). In contrast, the proapoptotic proteins, such as BIM, PUMA, and NOXA, share homology only within the BH3 amphipathic α-helical death domain, prompting the title "BH3-only." Antiapoptotic family members such as BCL2, BCL-xL, and MCL1 show conservation in all four BH domains. The BH1, BH2, and BH3 domains of these proteins are in close proximity, and create a hydrophobic pocket that can accommodate the BH3 domain of a

Significance

Human tumors effectively escape cell death by activating antiapoptotic mechanisms, one of which is amplification of *MCL1*. We describe here a chemical genomic approach to the discovery of repressors of *MCL1* expression. We also identify high *BCL-xL* expression as a primary resistance mechanism to MCL1 inhibition, including resistance to anthracyclines, which we show act at least in part through an MCL1-inhibitory mechanism.

proapoptotic member (Danial and Korsmeyer, 2004; Petros et al., 2004).

Despite overwhelming genetic and functional evidence implicating the BCL2-family proteins as therapeutic targets, effective therapeutic inhibitors of these proteins have been difficult to develop. Elegant NMR-based structural biology efforts led to development of the small-molecule BCL2/BCL-xL inhibitor ABT-737 (Oltersdorf et al., 2005) and its analog ABT-263, now in early clinical trials (Tse et al., 2008). Although it is expected that ABT-263 or related compounds will have clinical activity in BCL2- or BCL-xL-dependent tumors, it is clear that many tumors do not depend on these proteins but rather rely on other antiapoptotic factors such as MCL1 (Lin et al., 2007; van Delft et al., 2006).

MCL1 has only recently been recognized as an important therapeutic target in cancer. *MCL1* is highly expressed in a variety of human cancers (Krajewska et al., 1996a, 1996b). Its expression has been linked to tumor development (Zhou et al., 2001) and resistance to anticancer therapies. For example, overexpression of MCL1 is a major resistance mechanism for the experimental BCL2/BCL-xL inhibitor ABT-737 (Chen et al., 2007; Keuling et al., 2009; van Delft et al., 2006), and MCL1 has been similarly implicated in the resistance of non-BCL2-family-targeted therapy (Wei et al., 2006). Importantly, we recently reported that amplification of the *MCL1* locus is one of the most frequent somatic genetic events in human cancer, further pointing to its centrality in the pathogenesis of malignancy (Beroukhim et al., 2010). Although the development of MCL1 inhibitors has been of considerable interest, no such inhibitors have yet reached the clinic. A particularly promising strategy, however, was recently reported by Walensky and colleagues, whereby "stapled" helical MCL1 BH3 peptides function as effective MCL1 inhibitors in preclinical models (Stewart et al., 2010). Whether such stapled peptides will make for effective clinical therapeutics remains to be established. Furthermore, no biomarkers for patient selection have been discovered for MCL1 inhibitors. Therefore, we used a chemical genomic strategy to identify MCL1-downregulating small molecules and to discover biomarkers of MCL1 dependency.

RESULTS

Gene-Expression-Based High-Throughput Screen Identifies Small Molecules Repressing MCL1 Expression

MCL1 is frequently amplified in human cancers (Beroukhim et al., 2010), and is highly expressed across a panel of 729 human cancer cell lines (see Figure S1A available online). We hypothesized that it might be possible to discover small molecules that decrease *MCL1* expression, thereby activating the apoptosis cascade in *MCL1*-dependent tumors. We therefore developed an assay to profile the mRNA levels of *MCL1* and 48 other apoptosis-related genes using the Luminex bead-based method (Hieronymus et al., 2006; Peck et al., 2006) (Figure 1A; Table S1). We profiled many apoptosis-related genes in addition to *MCL1* in order to identify compounds that preferentially repress *MCL1* while preserving expression of the proapoptotic factors.

We carried out a pilot screen using MCF7 breast cancer cells treated with 2,922 small-molecule compounds, including 530 FDA-approved drugs. We used MCF7 cells, which are deficient in caspase-3, to avoid identifying compounds that repress *MCL1* expression through feedback apoptosis mechanisms. We also performed the assay at an early time point (8 hr post-treatment) for this reason. We counterscreened against compounds that caused significant cell death at 8 hr using a lactate dehydrogenase viability assay, reasoning that such compounds must not be acting by classical apoptosis-inducing mechanisms.

Twenty-four compounds (0.8%) decreased *MCL1* expression at least 2-fold (Figure 1B). All 24 compounds reduced *MCL1* expression more than any of the other 48 apoptosis-related genes assayed, suggesting at least some degree of preferential activity against *MCL1*. We selected 14 commercially available compounds for further testing. Seven of these exhibited significant dose-related repression of *MCL1* expression. The seven compounds included the natural product triptolide, the transcription inhibitors 5,6-dichlorobenzimidazole riboside (DRB) and actinomycin D, the kinase inhibitor 5-iodotubercidin, and the anthracyclines doxorubicin, daunorubicin, and epirubicin. Despite having distinct reported mechanisms of action (Table S2), treatment with these compounds resulted in decreased MCL1 expression in multiple cell lines, suggesting a common mechanism of *MCL1* repression across cancer types (Figure S1B).

Small Molecules that Repress MCL1 Share Transcriptional Profiles

We compared genome-wide expression profiles of cells following treatment with candidate compounds to determine whether they shared a common mechanism of action. We performed genome-wide gene-expression profiling in MCF7 cells following treatment with triptolide and actinomycin D. The expression changes induced by triptolide and actinomycin D were highly similar (R^2 = 0.85), suggesting that, like actinomycin D, triptolide likely functions as a transcriptional inhibitor (Figure 1C). Consistent with this observation, triptolide was recently reported to bind to XPB, a subunit of TFIIH (Titov et al., 2011), and inhibit phosphorylation of the C-terminal tail of RNA polymerase II, which results in transcriptional inhibition (Leuenroth and Crews, 2008).

Using the Connectivity Map database containing expression profiles of 1,366 compounds (http://www.broadinstitute.org/cmap) (Lamb et al., 2006), the triptolide-induced profile showed a high degree of similarity to both doxorubicin and daunorubicin (ranked 1 and 2 of 1,366, respectively, using Spearman correlation) (Figure 1D). The anticancer effect of anthracyclines has long been attributed to inhibition of DNA topoisomerase II (Desmedt et al., 2011; Moretti et al., 2009). However, the DNA topoisomerase II inhibitor etoposide induced a transcriptional profile distinct from that induced by triptolide (Figure 1D). Taken together, these results strongly suggest that the compounds that emerged from our *MCL1*-repression screen, including the anthracyclines, function as global transcriptional repressors. We therefore refer to them as transcriptional repressor (TR) compounds.

Strikingly, the TR compounds showed dramatic preferential activity against *MCL1* compared to the rest of the transcriptome. For example, *MCL1* was in the top 0.05 percentile of

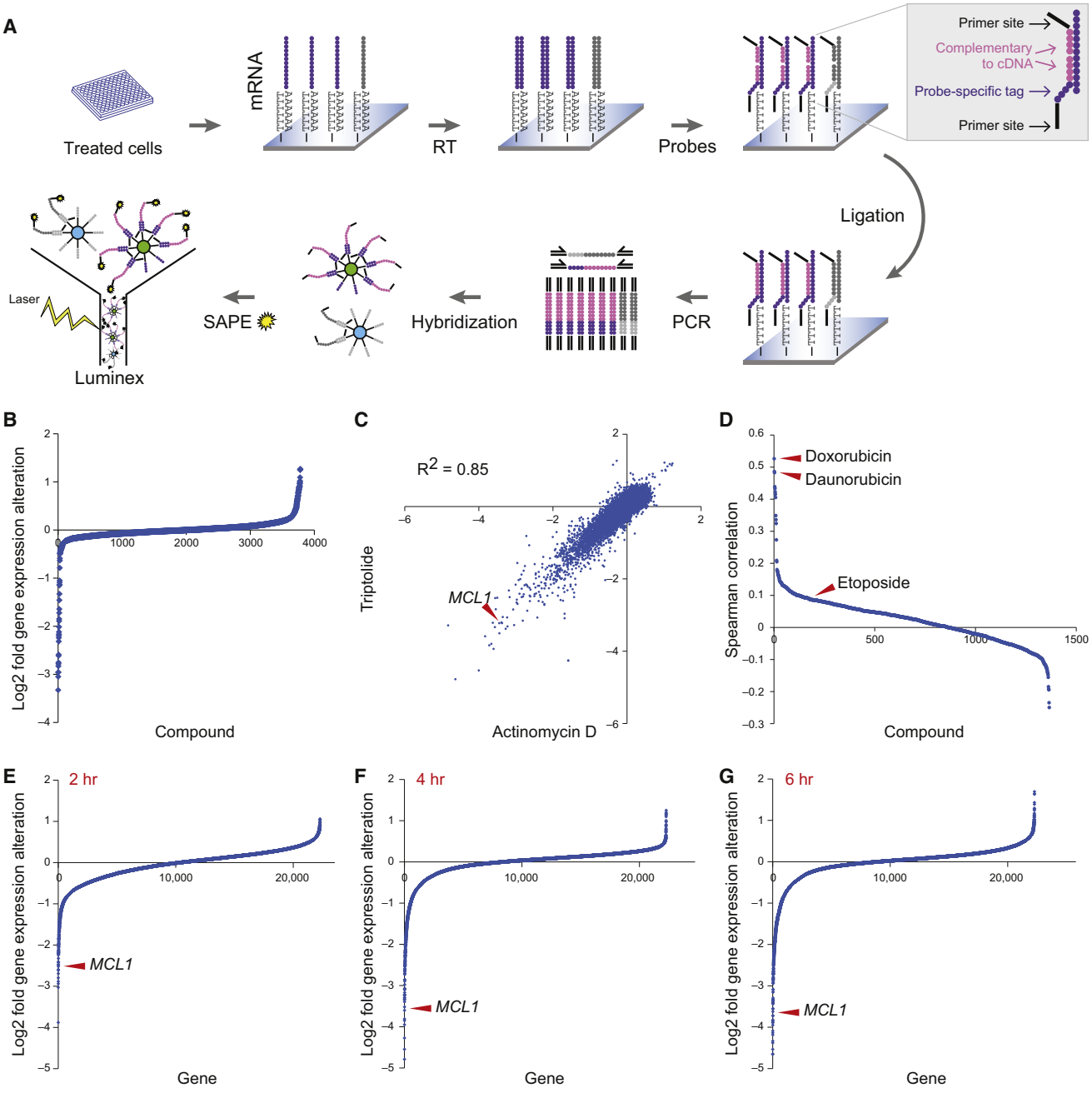

Figure 1. Bead-Based High-Throughput Gene-Expression Screening Identified *MCL1* Repression by Transcriptional Inhibitor Compounds

(A) Illustration of screening procedure. mRNA levels of *MCL1* and 48 other apoptotic genes were measured in MCF7 cells 8 hr after treatment with 2,922 small molecules.

(B) *MCL1* expression modulation by 2,922 compounds. Compounds and DMSO controls were sorted by *MCL1* expression repression. The y axis displays log2 gene-expression fold change.

(C) Gene-expression profiling by Affymetrix microarrays of MCF7 cells with triptolide (500 nM) and actinomycin D (2.5 μM) for 4 hr. Both the x and y axes display log2 gene-expression fold alteration.

(D) The 1,317 compounds used to treat MCF7 cells in the Connectivity Map are displayed in descending order of their correlation with triptolide (calculated as the Spearman rank correlation of the differential gene expression across the Affymetrix U133A chip).

(E–G) Gene-expression repression by triptolide at 2 hr (E), 4 hr (F), and 6 hr (G). The genes are ranked by the extent of repression. The y axis displays log2 gene-expression fold alteration. Arrowheads indicate *MCL1*.

See also Figure S1 and Tables S1 and S2.

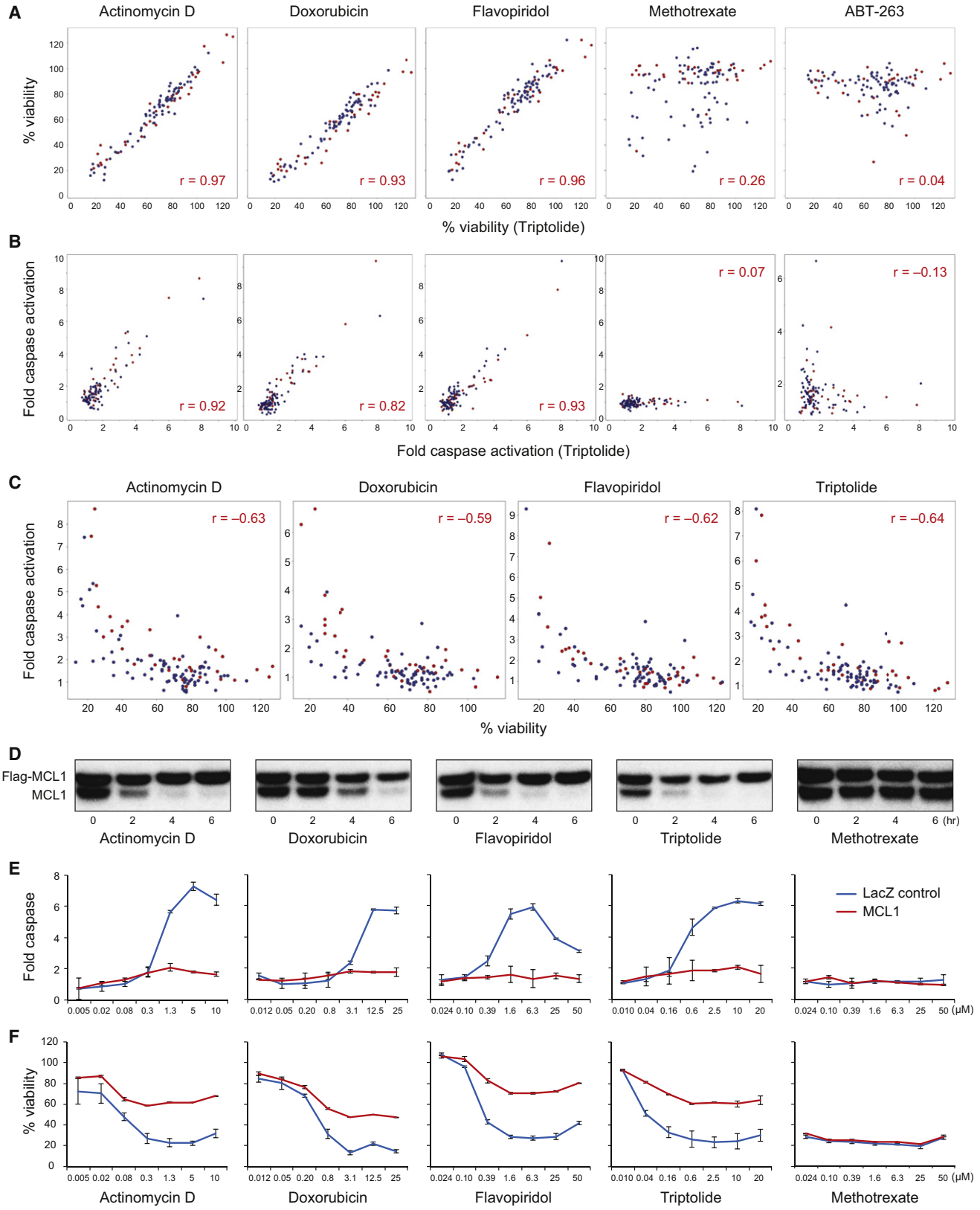
A
Actinomycin D
Doxorubicin
Flavopiridol
Methotrexate
ABT-263
% viability
r = 0.97
r = 0.93
r = 0.96
r = 0.26
r = 0.04
% viability (Triptolide)
B
Fold caspase activation
r = 0.92
r = 0.82
r = 0.93
r = 0.07
r = –0.13
Fold caspase activation (Triptolide)
C
Actinomycin D
Doxorubicin
Flavopiridol
Triptolide
Fold caspase activation
r = –0.63
r = –0.59
r = –0.62
r = –0.64
% viability
D
Flag-MCL1
MCL1
Actinomycin D
Doxorubicin
Flavopiridol
Triptolide
Methotrexate
6 (hr)
E
Fold caspase
LacZ control
MCL1
50 (μM)
F
% viability
Actinomycin D
Doxorubicin
Flavopiridol
Triptolide
Methotrexate
50 (μM)

triptolide-repressed genes (Figures 1E–1G), and the *MCL1* transcript was repressed more than 5-fold within 2 hr of treatment (Figure 1E). On the contrary, none of the other BCL2-family genes were repressed more than 2-fold. Consistent with the reported short half-life of MCL1 protein (30 min) (Adams and Cooper, 2007), inhibition of *MCL1* mRNA caused a rapid decrease in MCL1 protein levels that occurred prior to poly(ADP ribose) polymerase (PARP) cleavage, a marker for caspase activation (Figure S1C).

TR Compounds Share a Pattern of Cell Killing and Can Be Rescued by Physiologically Relevant Levels of MCL1

Based on the shared mechanisms suggested above, we hypothesized that if *MCL1* repression is a biologically relevant target of TR compounds, then these compounds should induce apoptosis in the same cancer cell lines. We therefore measured caspase activation and cell viability of 74 non-small-cell lung cancer (NSCLC) and 33 breast cancer cell lines following treatment with actinomycin D, doxorubicin, triptolide, and flavopiridol. Flavopiridol has previously been reported to repress *MCL1* expression via inhibition of CDK9 (Chen et al., 2005).

Responses to the TR compounds were highly correlated when measured both by caspase activation and cell viability (Pearson $r > 0.82$ and 0.93, respectively, when compared to triptolide) (Figures 2A and 2B). As expected, cell viability was highly correlated with caspase activation for each TR compound (Figure 2C; Pearson $r > 0.59$), indicating that the TR compounds impair cell viability via apoptosis. By contrast, compounds that kill cells via different mechanisms, such as methotrexate and etoposide, demonstrated different patterns of cytotoxicity (Figures 2A and 2B; Figure S2A). Despite the fact that TR compounds repress the expression of many genes, ectopic expression of physiological levels of MCL1 rescued cells from TR-compound treatment (Figures 2D–2F). In contrast, ectopic expression of *MCL1* had no such rescue effect for other classes of compounds, such as methotrexate (Figures 2D–2F).

If TRs block global transcription, we hypothesized that combination treatment with TR compounds would counteract the effects of compounds that kill cells by inducing the expression of proapoptotic proteins. The proteasome inhibitor bortezomib induces apoptosis through the induction of the proapoptotic protein NOXA (Gomez-Bougie et al., 2007; Voortman et al., 2007). As predicted, treatment with the TR compounds doxorubicin, actinomycin D, or triptolide rescued cells from the apoptotic effects of bortezomib, whereas treatment with the non-TR compound etoposide had no effect (Figures S2B–S2F). Similarly, the TR compounds were able to rescue cells from the histone deacetylase (HDAC) inhibitor vorinostat (Figure S2G), which kills cells via the induction of the proapoptotic proteins BMF and NOXA (Wiegmans et al., 2011).

MCL1 Knockdown Phenocopies TR Compounds

In order to determine whether *MCL1* repression explains the activity of TR compounds, we tested whether their effects could be phenocopied by knockdown of *MCL1*. We treated 17 breast cancer and 16 NSCLC cell lines representing different levels of sensitivity to TR compounds with each of the five most effective shRNAs selected from a library of 60 anti-*MCL1* shRNAs (Figure 3A). The response to the five *MCL1* shRNAs was highly correlated ($R^2 > 0.64$ for breast cell lines and $R^2 > 0.55$ for NSCLC cell lines) (Figure 3B). Ectopic expression of *MCL1* with a heterologous 3′ UTR at physiologically relevant levels was able to rescue cells from the two *MCL1* shRNAs targeting the 3′ UTR of *MCL1* but not the three *MCL1* shRNAs targeting the coding region of *MCL1* (Figure 3C), indicating that their cellular effects are most likely due to *MCL1* repression as opposed to off-target effects.

In addition, we generated shRNAs against *BCL-xL* to test whether *MCL1*-dependent cells were sensitive to knockdown of other antiapoptotic genes. The responses to the five most effective *BCL-xL* shRNAs (out of the 24 shRNAs tested) were highly correlated (Figures 3D and 3E; Figure S3A), but these responses did not correlate with the response to the *MCL1* shRNAs ($R^2 = 0.002$) (Figure 3F; Figure S3B).

Impaired viability induced by doxorubicin was strongly correlated with the effects of *MCL1* shRNAs [$R^2 = 0.80$ for breast cancer cells (Figure 3G) and $R^2 = 0.74$ for NSCLC cells]. Conversely, doxorubicin sensitivity did not correlate with the effects of shRNAs targeting *BCL-xL* ($R^2 = 0.0001$ for breast cancer cell lines) (Figure 3H). Furthermore, doxorubicin did not induce additional significant cell death after *MCL1* knockdown, consistent with *MCL1* repression being a major effector of doxorubicin action (Figures 3I and 3J). Triptolide yielded similar results, suggesting that this is a general property of TR compounds (Figure S3C). Taken together, these results further support the notion that a subset of tumor cells is dependent upon MCL1 for survival, and that TR compounds act largely via *MCL1* repression.

Discovering Predictive Biomarkers of MCL1 Essentiality

We next sought to discover biomarkers that are predictive of *MCL1* essentiality by comparing TR-compound sensitivities with genomic data. Such biomarkers would prove useful for the prediction of sensitivity to any present or future MCL1

Figure 2. TR Compounds Shared a Pattern of Cell Killing

(A and B) Seventy-four NSCLC (blue dots) and 33 breast cancer (red dots) cell lines were treated with small molecules. The effect of triptolide (x axis) is compared with the effect of other compounds (y axis), measured both by cell viability after 24 hr of treatment (A) and fold-caspase-3 activation after 6 hr of treatment (B). Concentrations of the compounds for the displayed data were actinomycin D (1.25 μM), doxorubicin (12.5 μM), flavopiridol (6.25 μM), methotrexate (6.25 μM), ABT-263 (6.25 μM), and triptolide (2.5 μM).

(C) Correlation between cell viability and caspase activation.

(D) Expression levels of endogenous MCL1 and FLAG-MCL1 in HMC-1-8 cells after treatment with the indicated compounds were evaluated by western blot. For each panel, cells were treated with the compound for 0, 2, 4, and 6 hr (left to right for each compound).

(E and F) Ectopic expression of physiological levels of FLAG-MCL1 rescued HMC-1-8 cells from TR compounds but not methotrexate, as measured by caspase activation at 6 hr (E) and cell viability at 24 hr (F). Error bars indicate standard deviation of duplicate measurements.

See also Figure S2.

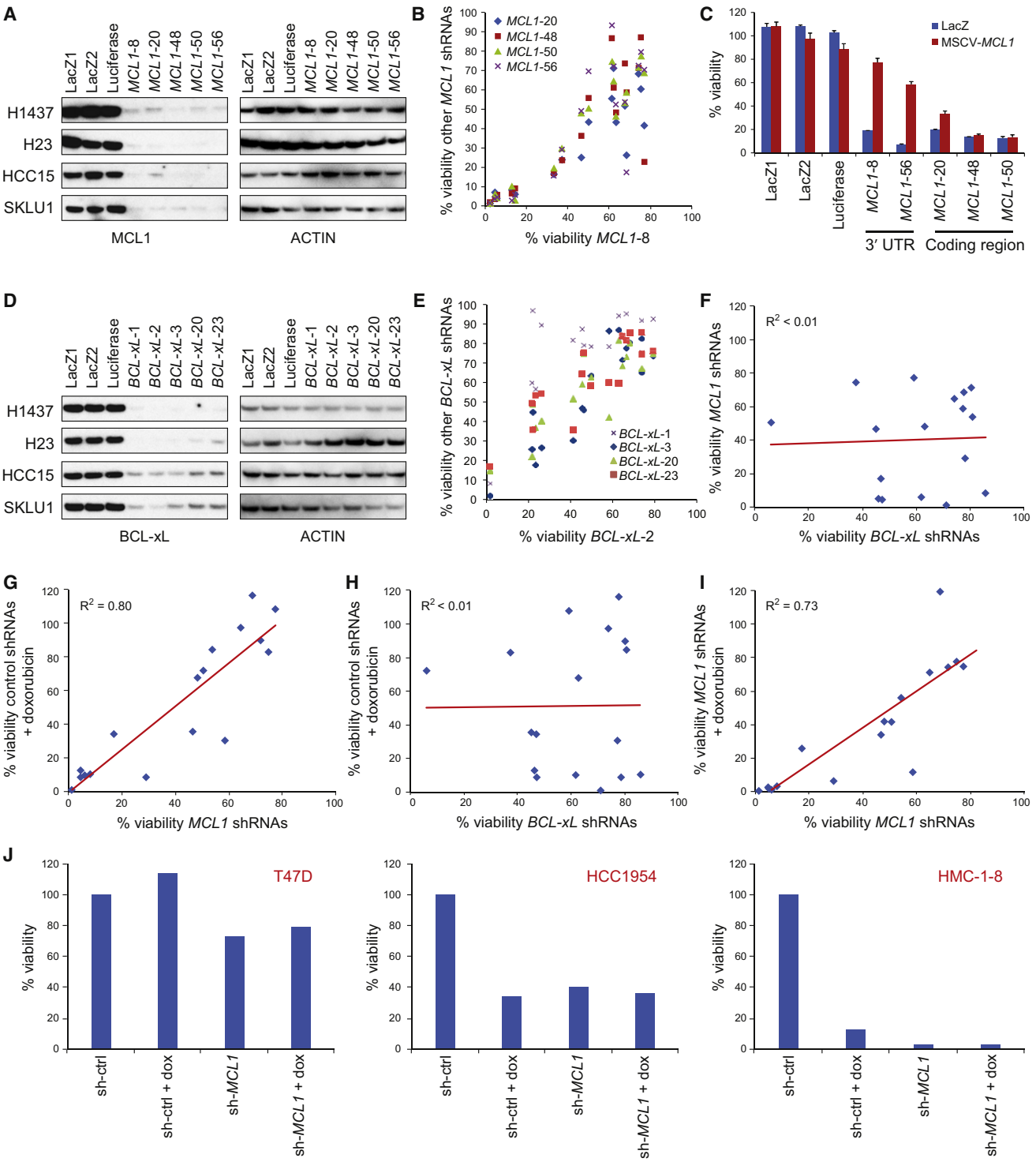

Figure 3. *MCL1* Knockdown Phenocopied TR Compounds

(A) Knockdown efficiency of the five best *MCL1* shRNAs as determined by western blot.

(B) Effects of one shRNA (*MCL1*-8) on cell viability are plotted on the x axis against the effects of the other four *MCL1* shRNAs on the y axis. Data were measured from 17 breast cancer cell lines.

(C) Effect of expressing physiological levels of FLAG-tagged MCL1 on apoptosis induced by *MCL1* shRNAs targeting the 3′ UTR of *MCL1* (*MCL1*-8 and *MCL1*-56) or targeting the coding region of *MCL1* (*MCL1*-20, *MCL1*-48, and *MCL1*-50) in HMC-1-8 cells. Error bars indicate standard deviation of duplicate measurements.

(D) Five *BCL-xL* shRNAs effectively knocked down BCL-xL expression. H1437 and H23 cells had longer exposure time than HCC15 and SKLU1 cells for western blots to show the shRNA effects.

inhibitors. We developed an analytical method to infer groups of compounds that induce sensitivity in similar cancer genetic subtypes and infer predictive biomarkers of sensitivity to each compound group. Briefly, the method uses an expectation-maximization algorithm and iterates until convergence between clustering groups of compounds based on the similarity of their response profiles, and uses an elastic net algorithm to infer a predictive model for each group based on its genetic features (Lee et al., 2009). The method further employs a bootstrapping procedure to obtain a parsimonious model containing only robustly predictive features (Figure 4A; see Supplemental Experimental Procedures for details).

We examined the genetic features (copy number and expression data for >18,000 genes, and mutation data for 34 genes) across 72 cell lines for which we had TR-compound sensitivity measurements. To ensure that our predicted biomarkers were specific to sensitivity induced by the TR compounds, we also performed dose-response measurements on 37 additional control compounds (Table S2). The algorithm identified a cluster of compounds consisting of all of the TR compounds (actinomycin D, doxorubicin, flavopiridol, and triptolide), as well as three additional compounds (puromycin, emetine, and anisomycin) that function as global repressors of protein translation (Figure 4B). Similar to *MCL1* mRNA, the extremely short half-life of MCL1 protein likely explains the selective effects of protein translation inhibitors on MCL1 activity.

The predictive model of sensitivity to the group of transcriptional and translational repressors contained only a single feature, corresponding to mRNA expression of *BCL-xL*. Specifically, low expression of *BCL-xL* was associated with sensitivity, and high expression of *BCL-xL* was associated with resistance to compounds that repress *MCL1* expression. The half-life of BCL-xL protein is much longer than that of MCL1 (Figure S1C), consistent with its ability to prevent apoptosis induced by transcriptional and translational inhibitors. Also consistent with this observation, sensitivity to *MCL1* shRNAs anticorrelated with *BCL-xL* mRNA levels in the 17 breast cancer cell lines ($R^2 = 0.57$) (Figure 4C).

We next sought to derive a computational model for the causal interactions that explain how *MCL1* and *BCL-xL* influence sensitivity to TR compounds. We applied the ARACNE reverse-engineering algorithm (Basso et al., 2005; Margolin et al., 2006), which is designed to deconvolute direct and indirect interactions among a set of covariates, and derived a network of direct interactions among variables corresponding to gene expression and copy number of *MCL1* and *BCL-xL* and sensitivity to TR compounds. We used as input to the algorithm a matrix of values across the panel of 72 cell lines, corresponding to normalized expression and copy number of *MCL1* and *BCL-xL*, as well as sensitivity to the TR compounds, computed as the average of normalized IC_{50} values across all TR compounds. This approach yielded a model in which expression of *BCL-xL* was indeed the direct predictor of sensitivity to TRs (Figure 4D). As expected, gene expression of *BCL-xL* and *MCL1* was directly influenced by the copy number of the respective genes (Figures 4E and 4F). Interestingly, the model indicated an epistatic relationship between *MCL1* copy number and *BCL-xL* expression. *MCL1* copy number was negatively correlated with *BCL-xL* expression (Figure 4G), suggesting that *MCL1* amplification may decrease the selective pressure requiring *BCL-xL* for inhibition of apoptosis.

Sequestration of Proapoptotic Proteins by MCL1 and BCL-xL

The above data suggested that breast and lung cancer cells with low expression of BCL-xL rely on MCL1 to sequester proapoptotic proteins. Upon repression of MCL1 protein levels, proapoptotic proteins might be released from MCL1 and cause downstream caspase activation and apoptosis. BIM binds to all antiapoptotic proteins (Mérino et al., 2011). In a panel of 19 NSCLC cell lines, in cells expressing low levels of BCL-xL, depletion of MCL1 by immunoprecipitation resulted in depleting nearly the entirety of BIM (Figures 5A and 5B). In contrast, in cells expressing high levels of BCL-xL, only a small fraction of BIM was sequestered by MCL1 (Figures 5A and 5B). Furthermore, when BCL-xL was overexpressed in cells that normally have low levels of BCL-xL, the fraction of BIM bound by MCL1 decreased significantly (Figure 5C). These experiments demonstrate a shuttling of BIM sequestration between MCL1 and BCL-xL, depending on their relative expression levels. To explore whether the release of BIM from MCL1 explains the apoptotic effect of MCL1-repressing TR compounds, we repeated the MCL1-BIM coimmunoprecipitation experiments under conditions of TR treatment. Surprisingly, despite the TR compounds triptolide or flavopiridol significantly reducing MCL1 levels, the majority of BIM protein remained bound to the residual MCL1 (Figures S4A and S4B). In addition, *BIM* knockdown by shRNA did not abrogate the sensitivity to TR compounds (Figures S7C–S7G), although we cannot exclude the possibility that more complete BIM knockdown might have a more dramatic effect.

Because BIM seemed unlikely to be the principal proapoptotic mediator of MCL1 repression, we considered other candidate proteins. MCL1 coimmunoprecipitation experiments showed that whereas the majority of PUMA, BAK, and BAX proteins were not bound by MCL1 (Figure 5A; Figure S4A), significant amounts of PUMA and BAK were pulled down by MCL1, and overexpression of BCL-xL disrupted this interaction (Figures 5C and 5D). MCL1-bound PUMA decreased after triptolide-mediated MCL1 repression, but this result is best explained by triptolide's concomitant repression of PUMA expression (Figure 5D). To test the possibility that BAK release from MCL1

(E) Effects of one shRNA (*BCL-xL-2*) on cell viability are plotted on the x axis against the effects of the other four *BCL-xL* shRNAs on the y axis. Data were measured from 17 breast cancer cell lines.
(F–I) Effects of *MCL1* shRNAs (G and I) or *BCL-xL* shRNAs (F and H) on cell viability plotted on the x axis against sensitivity to *MCL1* shRNAs (F), doxorubicin (G and H), or *MCL1* shRNAs + doxorubicin (I) plotted on the y axis in 17 breast cancer cell lines. Cells were infected with viruses carrying shRNAs for *MCL1* or *BCL-xL* for 3 days, or 2 days followed by treatment with 5 μM doxorubicin for an additional 24 hr (median of five *MCL1* shRNAs or *BCL-xL* shRNAs, as indicated).
(J) Examples of cell lines that were resistant (T47D), partially sensitive (HCC1954), or sensitive (HMC-1-8) to *MCL1* inhibition. Dox, doxorubicin.
See also Figure S3.

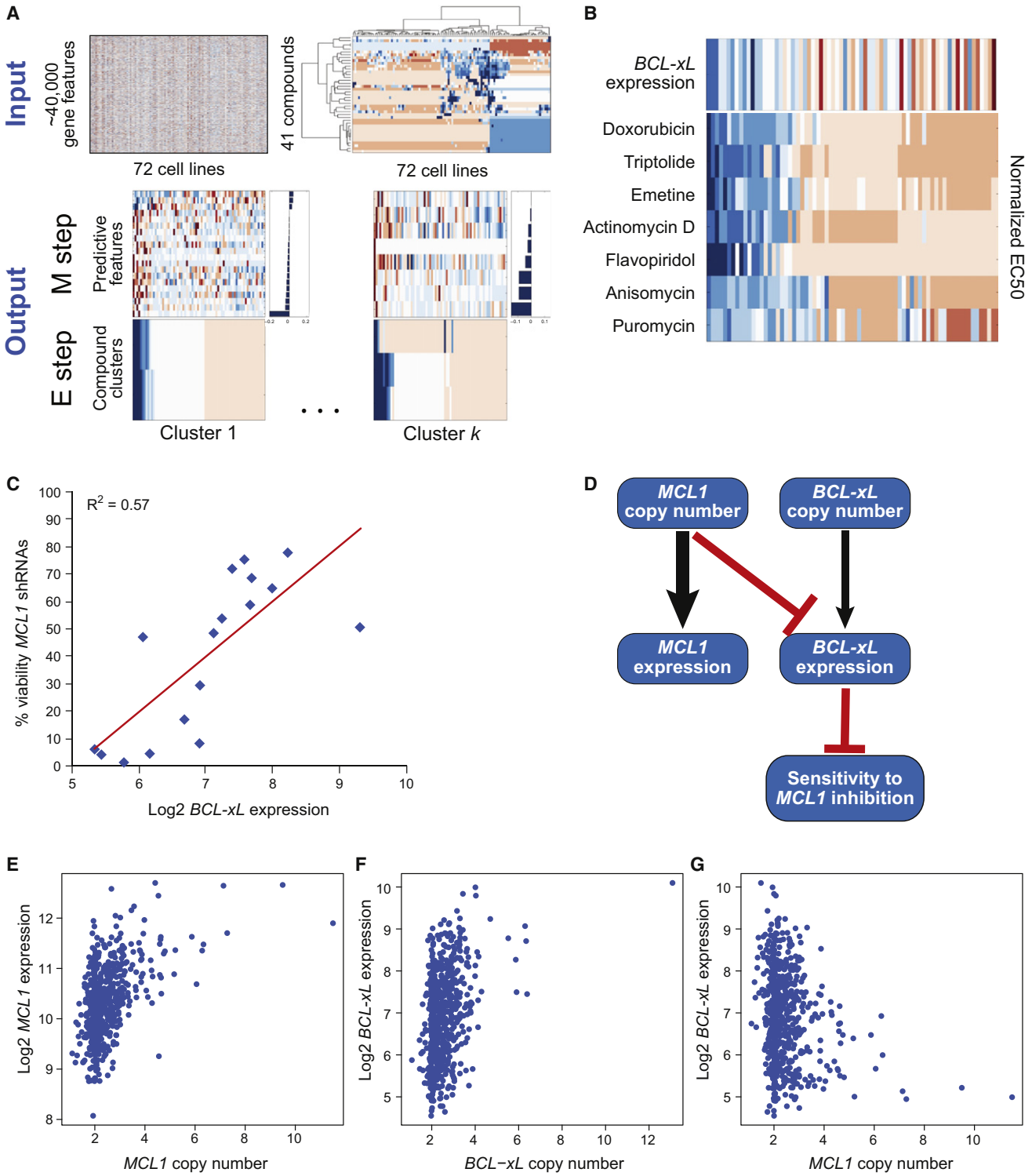

Figure 4. Unbiased Computational Analysis Identified TR Compound Sensitivity Predicted by Low Expression of *BCL-xL*

(A) Schematic of biomarker discovery algorithm (see Supplemental Experimental Procedures for details).

(B) *BCL-xL* expression as a predictive biomarker of TR-compound sensitivity. The expectation-maximization algorithm identified one cluster that contained all of the TR compounds (bottom panel; blue indicates drug sensitivity, red indicates resistance), coupled to a single predictive feature, *BCL-xL* RNA expression (top panel; blue indicates low level of expression, red indicates high expression).

(C) Correlation between expression level of *BCL-xL* (x axis) and cell viability upon *MCL1* knockdown (y axis), represented as the percent viability relative to control shRNAs, averaged over two replicates treated for 3 days with five different shRNA constructs targeting *MCL1* across a panel of 17 breast cancer cell lines.

explains the TR effect, we used *Bak*$^{-/-}$ MEFs to determine contribution of Bak in TR compound-induced apoptosis. *Bak* deletion nearly completely rescued cells from TRs but did not protect cells from the non-TR compound trichostatin A (Figures 5E–5H). BAX and BAK are both multidomain proapoptotic BCL2-family proteins. However, BAK proved unique in that we did not detect MCL1-BAX interaction in coimmunoprecipitation experiments (Figures 5C and 5D), and *Bax*$^{-/-}$ cells were not rescued from TR compounds (Figures 5E–5G). Taken together, our data suggest that MCL1 protects cells from cell death at least in part through sequestration of BAK, and this sequestration is diminished with TR compound-mediated *MCL1* repression.

BCL-xL Predicts MCL1 Dependency In Vivo

An important question in developing biomarkers of MCL1 dependency is whether resistance mechanisms observed in vitro hold in vivo, where tumor-microenvironment interactions are known to modulate apoptotic mechanisms (Bewry et al., 2008; Buggins et al., 2010). We therefore examined the in vivo response of two NSCLC cell lines grown as xenografts in NOD-SCID mice. H1437 cancer cells express low levels of *BCL-xL* and are sensitive to triptolide (as a prototype *MCL1* repressor) in vitro. HCC15 cells, in contrast, express high levels of *BCL-xL* and are triptolide resistant in vitro. This pattern of sensitivity persisted in vivo. Triptolide significantly attenuated the growth of the H1437 NSCLC cancer model (Figures 6A and 6B). By contrast, in the HCC15 xenograft model, triptolide did not significantly affect tumor volume or survival of the mice (Figures 6C and 6D). Western blotting of whole-tumor lysates demonstrated that treatment with triptolide decreased MCL1 protein abundance and increased PARP cleavage in the H1437 xenograft model (Figure 6E), indicating that triptolide repressed MCL1 expression and induced apoptosis in vivo.

Our model predicts that patients with high levels of *BCL-xL* expression are resistant to TRs. To test this hypothesis, we investigated the relationship between *BCL-xL* gene expression and clinical response to neoadjuvant treatment with the anthracycline epirubicin in 114 estrogen receptor (ER)-negative breast cancer patients for which it was determined whether a complete pathological response (pCR) was achieved (Desmedt et al., 2011). *BCL-xL* showed significant differential expression between patients who achieved pCR and those who did not (Figure 6F). As previously reported, expression of topoisomerase 2A (TOP2A) did not correlate with response to epirubicin (Figure S5), consistent with our finding that anthracyclines kill tumor cells via a transcriptional repressive mechanism rather than via a topoisomerase-inhibitory mechanism as has been generally assumed.

BCL-xL Is a Functional Determinant of MCL1 Dependency

We next investigated whether *BCL-xL* was simply a marker of MCL1 dependency or whether it was a functional determinant of response. Overexpression of *BCL-xL* in MCL1-dependent lines protected them from apoptosis induced by *MCL1* shRNAs or TR compounds (Figures 7A–7C) but not by other cytotoxic agents such as methotrexate (Figures 7B and 7C), suggesting a specific effect for TR compounds. Conversely, *BCL-xL* knockdown conferred sensitivity in cell lines otherwise resistant to TR compounds. Cell lines resistant to treatment with TR compounds (using doxorubicin as a representative example) were sensitive to combined treatment with *BCL-xL* shRNAs (Figures 7D and 7G), and cell lines resistant to treatment with *MCL1* shRNAs were sensitive to combined treatment with the BCL-xL inhibitor ABT-263 (Figures 7E and 7G). The viability of cells treated with *BCL-xL* shRNAs was highly correlated with viability after treatment with the BCL-xL inhibitor ABT-263, and combined treatment of cells with ABT-263 and *BCL-xL* shRNAs did not yield synergistic effects (Figures 7F and 7G).

The above data suggest that TR compounds would exhibit a synergistic effect when used in combination with BCL-xL inhibitors. We treated a panel of 74 NSCLC cell lines with a 42-point dose-response matrix (six concentrations of triptolide or actinomycin D, and seven concentrations of ABT-263 or ABT-737). We examined the synergy between TR compounds and BCL-xL inhibitors for each cell line by computing the excess growth inhibition over the Bliss independence model for each combination of compound concentrations (Figures 8A–8C). Cell lines that were highly sensitive to TR compounds showed no evidence of synergy when treated in combination with ABT-737. Cell lines that were resistant to TR compounds and to BCL-xL inhibitors were sensitive to the combination (Figures 8A–8C).

A synergy score was computed for each combination experiment in each of the 74 NSCLC cell lines by summing the excess over Bliss independence across all dose combinations. The synergy score was averaged over the four combination experiments, performed by pairing triptolide or actinomycin D with ABT-263 or ABT-737. This synergy score was highly correlated with expression of *BCL-xL* (Figure 8D), suggesting that high expression of *BCL-xL* determines the synergistic relationship between TR compounds and BCL-xL-inhibitory compounds, and that resistance to TR compounds, caused by high expression of *BCL-xL*, can be overcome by treating in combination with BCL-xL inhibitors. Consistent with this notion, ABT-263 released BAK from BCL-xL (Figure 8E).

DISCUSSION

At an accelerating pace, the genomic characterization of human cancer is elucidating the molecular basis of the disease. Recent large-scale analyses of gene copy number in cancer demonstrated that the genes encoding the BCL2-family proteins MCL1 and BCL-xL are frequent targets of amplification. Low-level *MCL1* amplification is particularly notable, representing one of the most common copy-number abnormalities in all of

(D) The ARACNE reverse-engineering algorithm was used to identify direct interactions between sensitivity to TR compounds and *MCL1* and *BCL-xL* gene expression and gene copy number. Arrows represent inferred direct interactions, with the weight of the edge proportional to the mutual information between the corresponding nodes. Arrows indicate the presumed direction of causality (e.g., copy number to gene expression). Black lines indicate positive correlations and red lines indicate negative correlations.
(E–G) Comparisons of gene expression and copy-number values of *MCL1* and *BCL-xL* across 643 cancer cell lines. (E) *MCL1* copy number versus *MCL1* expression. (F) *BCL-xL* copy number versus *BCL-xL* expression. (G) *MCL1* copy number versus *BCL-xL* expression.

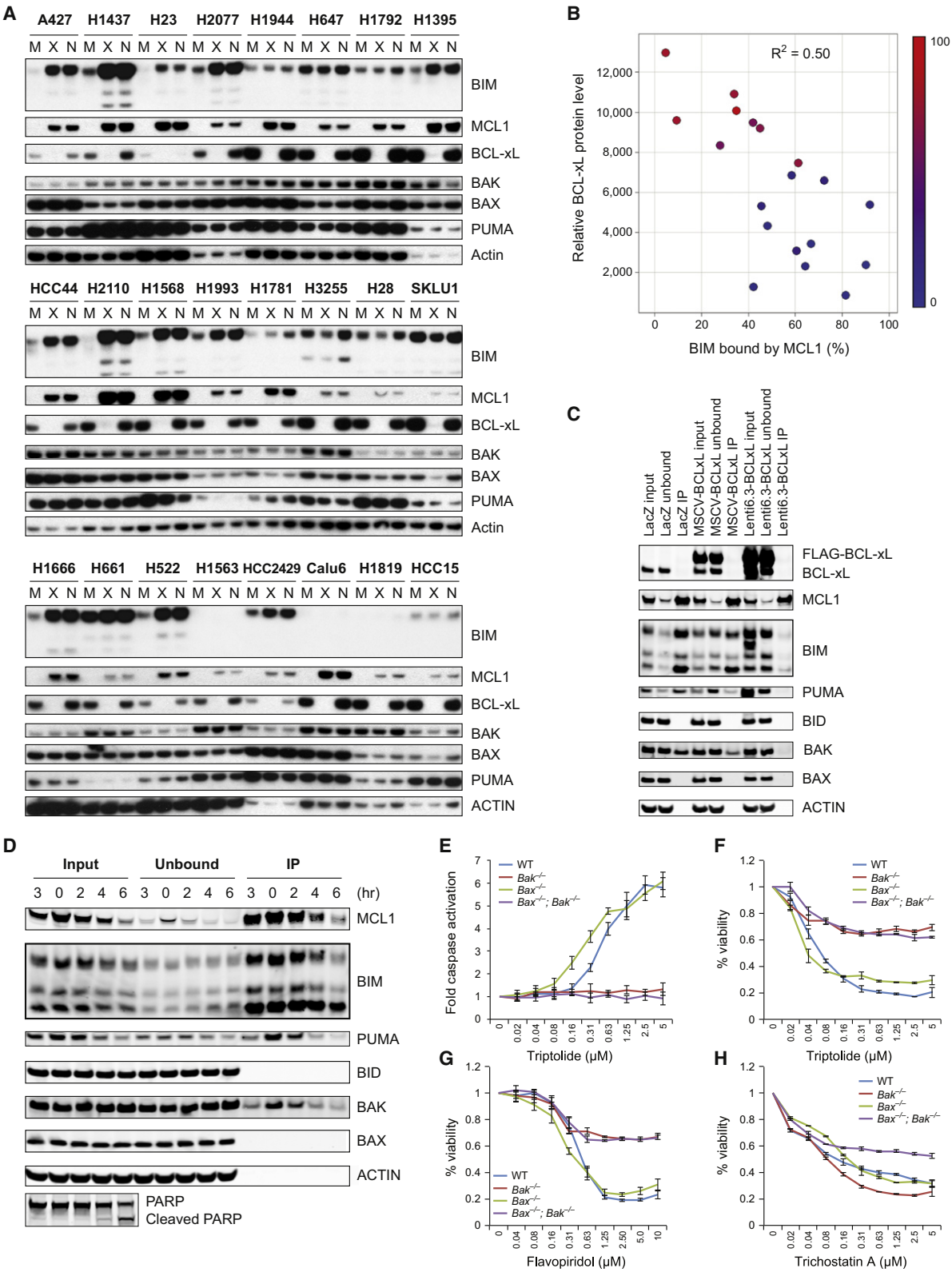

Figure 5. MCL1 Is the Major Antiapoptotic Protein in Cells with Low BCL-xL Expression

(A and B) Cell lysates of the indicated NSCLC cell lines were subjected to immunoprecipitation with an anti-MCL1 antibody (M), an anti-BCL-xL antibody (X), or no antibody control (N). The indicated proteins left in the postimmunoprecipitation fraction were detected using western blotting (A). The fraction of unbound BIM and BIM input was quantified by ImageJ software, and the color denotes cell viability after 24 hr of treatment with triptolide (B).

human cancer (Beroukhim et al., 2010). In support of a functionally important role of MCL1, numerous studies have elucidated the critical role of MCL1 in preventing tumor cell death (Warr and Shore, 2008).

Using a multiplexed Luminex bead-based assay, we screened for compounds that reduced *MCL1* expression while preserving the expression of proapoptotic genes. Although the compounds that emerged from this screen were general transcriptional repressor compounds (as opposed to specifically targeting the *MCL1* locus), they preferentially repressed *MCL1* because of the short half-life of *MCL1* mRNA and protein. Multiple lines of evidence suggest that TR compounds induce apoptosis in cancer cells primarily through repression of *MCL1* expression, including: (1) upon treatment with TR compounds, MCL1 protein levels decreased rapidly and preceded caspase activation; (2) ectopic expression of physiological levels of *MCL1* rescued cancer cells from TR compounds, despite the expression of other genes still being repressed; (3) the pattern of TR-compound sensitivity across a panel of cancer cell lines closely mirrored the pattern of sensitivity of those cell lines to *MCL1* knockdown by RNAi; (4) of over 40,000 genomic features measured, the top feature that predicted sensitivity to TR compounds was the low expression of *BCL-xL*, which shares redundant function with *MCL1*; (5) ectopic expression of *BCL-xL* rescued cancer cells from TR compounds; (6) *MCL1* repression by TR compounds resulted in the release of proapoptotic protein BAK from MCL1; and (7) *Bak* deficiency protected cells from TR compounds. These results suggest that the mechanism of cell death induced by TR compounds is best explained by *MCL1* inhibition.

This indicated that some of the widely used chemotherapeutic drugs such as anthracyclines may preferentially repress *MCL1* to induce apoptosis in tumor cells. Although the antitumor effect of anthracyclines has long been speculated to be related to the drug's inhibition of DNA topoisomerase II (Desmedt et al., 2011; Moretti et al., 2009) and an association between low TOP2A expression and anthracycline response in ER-negative breast cancer patients has been reported (Martin et al., 2011), our data suggest that their activity may be largely explained by inhibition of transcription, leading most dramatically to the repression of short-lived *MCL1* transcripts. Although it is possible that multiple mechanisms of action explain the antitumor effects of anthracyclines, at least in the experimental cancer models studied here, anthracycline gene-expression consequences most reflected transcriptional inhibition rather than DNA topoisomerase II inhibition. Furthermore, the similar pattern of sensitivity of cell lines to *MCL1* knockdown compared to anthracycline treatment is also consistent with an *MCL1*-mediated transcriptional inhibitory effect. Last, our observation that *BCL-xL* expression is predictive of resistance to *MCL1* repression both in model systems and in patients with breast cancer further strengthens the anthracycline-*MCL1* connection. We note that the concentration of doxorubicin used in our experiments approximates that observed in human tumor tissues (1.9–24.4 μM) (Rossi et al., 1987). Doxorubicin stimulates topoisomerase II-mediated DNA cleavage only at low concentrations, whereas at doses greater than ~0.4 μM, topoisomerase II-mediated DNA cleavage is lost (Tewey et al., 1984). These data therefore suggest that at clinically relevant concentrations, anthracyclines act as transcriptional repressors, as opposed to DNA-damaging agents.

The transcriptional inhibitory role of anthracyclines is also of importance when considering anthracycline-based combination therapies. The transcriptional induction of proapoptotic proteins has been reported to be crucial for the efficacy of many classes of antineoplastic agents including radiation (Jeffers et al., 2003; Villunger et al., 2003), the proteasome inhibitor bortezomib (Gomez-Bougie et al., 2007; Voortman et al., 2007), the HDAC inhibitor vorinostat (Wiegmans et al., 2011), and the kinase inhibitors imatinib (Kuroda et al., 2006) and erlotinib (Gong et al., 2007). Anthracyclines may block the induction of such proapoptotic proteins and counteract, rather than synergize with, those therapies. For example, we found that doxorubicin treatment actually rescues cancer cells from bortezomib- and vorinostat-induced killing (Figure S2). Such antagonistic actions may be preventable by adjusting the dosing schedule of combination therapies, but the results serve as a reminder that knowledge of mechanisms of action should ideally be considered in developing combination strategies.

Taken together, the results reported here elucidate a strategy for the development of MCL1 inhibitors as cancer therapeutics. The multiplexed, gene-expression-based high-throughput screening approach described here holds promise for the future discovery of specific inhibitors of *MCL1* expression and for the use of chemical genomic approaches to elucidate small-molecule mechanisms of action. The study also highlights the power of genomically characterized cell lines for the discovery of predictive biomarkers of drug response. Most immediately, the work suggests an approach to the clinical development of any MCL1 inhibitor in breast and NSCLC tumors, focusing on tumors expressing low levels of *BCL-xL* as a patient-selection strategy.

EXPERIMENTAL PROCEDURES

Cell Culture, Caspase, and Viability Assay

All human cell lines were part of the Broad-Novartis Cancer Cell Line Encyclopedia Project (http://www.broadinstitute.org/ccle/home) or gifts from

(C) HMC-1-8 cells stably expressing FLAG-BCL-xL via the MSCV retroviral vector or the Lenti6.3 lentiviral vector, or LacZ control were subjected to immunoprecipitation using an anti-MCL1 antibody. Input, unbound, and immunoprecipitation (IP) fractions were analyzed by western blotting. The IP fraction was 5-fold more concentrated than input and unbound.

(D) HMC-1-8 cells were treated with 2 μM triptolide for the indicated times and subjected to immunoprecipitation with an anti-MCL1 antibody conjugated to agarose beads, eluted with an MCL1 peptide, and western blotted for proapoptotic proteins. The IP fraction was 5-fold more concentrated than input and unbound.

(E–H) Wild-type (WT), $Bak^{-/-}$, $Bax^{-/-}$, and $Bax^{-/-}$;$Bak^{-/-}$ MEFs were treated with TR compounds triptolide (E–F) or flavopiridol (G), or non-TR compound trichostatin A (H), at the indicated concentrations for 7 hr (E, for caspase activation) or 24 hr (F–H, for viability). Error bars indicate standard deviation of duplicate measurements.

See also Figure S4.

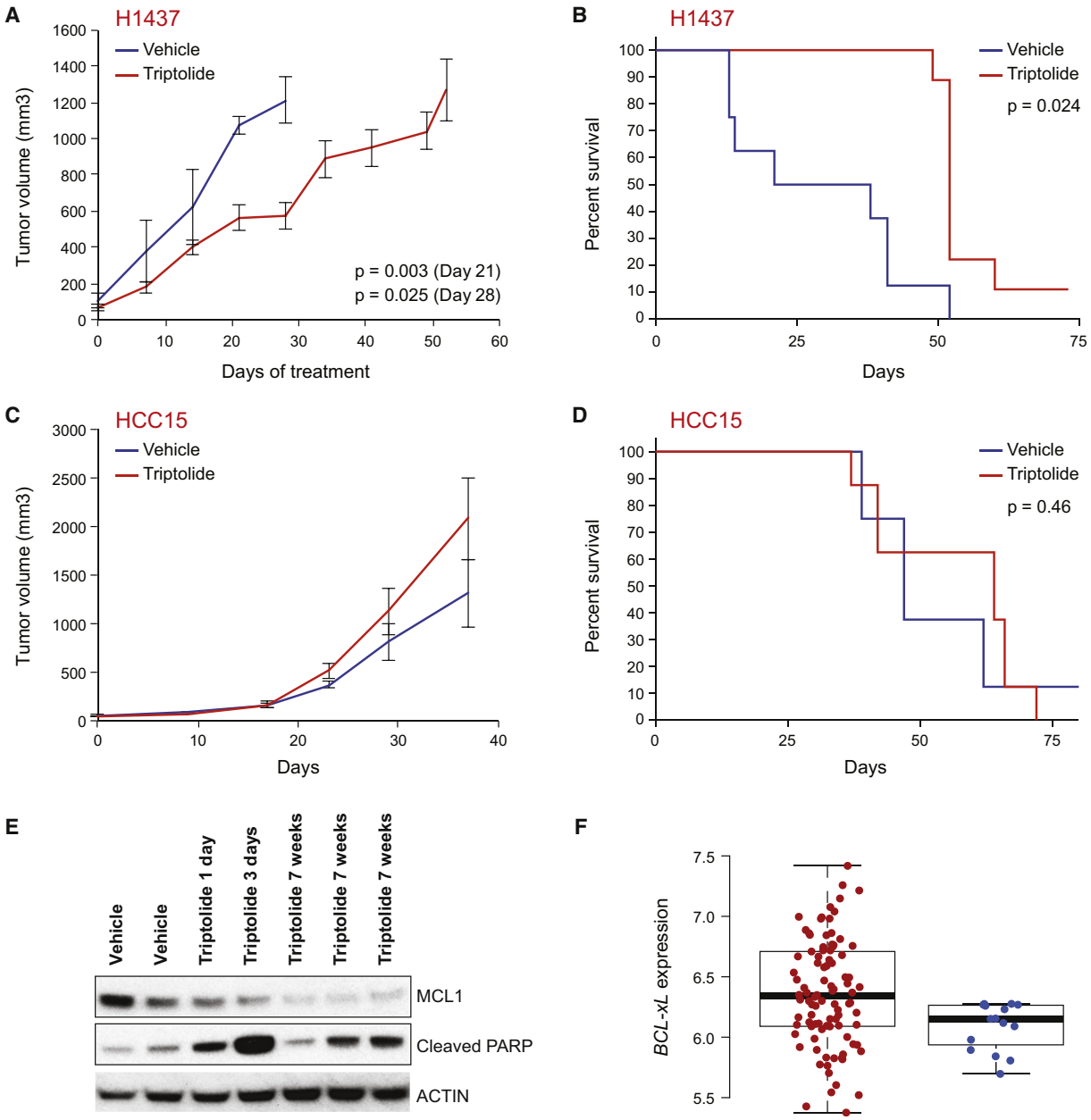

Figure 6. Cells Expressing Low Levels of *BCL-xL* Were Sensitive to Triptolide In Vivo

(A–D) H1437 (low *BCL-xL* expression; A and B) and HCC15 (high *BCL-xL* expression; C and D) NSCLC cell lines were grown as xenografts in NOD-SCID mice, and the mice were treated with triptolide or vehicle as indicated. (A and C) Tumor volume. (B and D) Survival curves. Error bars indicate standard deviation of tumor volume of eight or nine mice.

(E) Triptolide treatment in vivo reduced MCL1 expression and induced PARP cleavage, a marker of apoptosis in tumors. Mice were treated either with vehicle alone or triptolide for 7 weeks, or with vehicle for 7 weeks followed by 1 or 3 days of triptolide.

(F) Correlation between *BCL-xL* expression levels and resistance to epirubicin in ER-negative breast cancer patients (GEO accession number GSE16446). The distribution of *BCL-xL* expression levels, averaged over all *BCL-xL* probe sets on the Affymetrix U133 Plus 2 array, is displayed as a box plot for patients who obtained (n = 16, blue dots, right column) or did not obtain (n = 98, red dots, left column) pathological complete response to single-agent epirubicin treatment. Whiskers of box plots represent 5%–95% data span. Box plots present median, 25th, and 75th percentiles of data.

See also Figure S5.

Matthew Meyerson at the Broad Institute. *Bak*$^{-/-}$, *Bax*$^{-/-}$, and *Bax*$^{-/-}$;*Bak*$^{-/-}$ MEFs were gifts from Anthony Letai at the Dana-Farber Cancer Institute. Caspase activity was measured by the Caspase-Glo 3/7 kit and cell viability was measured by CellTiter-Glo (both from Promega). cDNAs for ectopic expression were from the Human ORFeome Collection by Mark Vidal at the Dana-Farber Cancer Institute. Compounds were purchased from commercial sources listed in Table S2 or were synthesized at the Broad Institute.

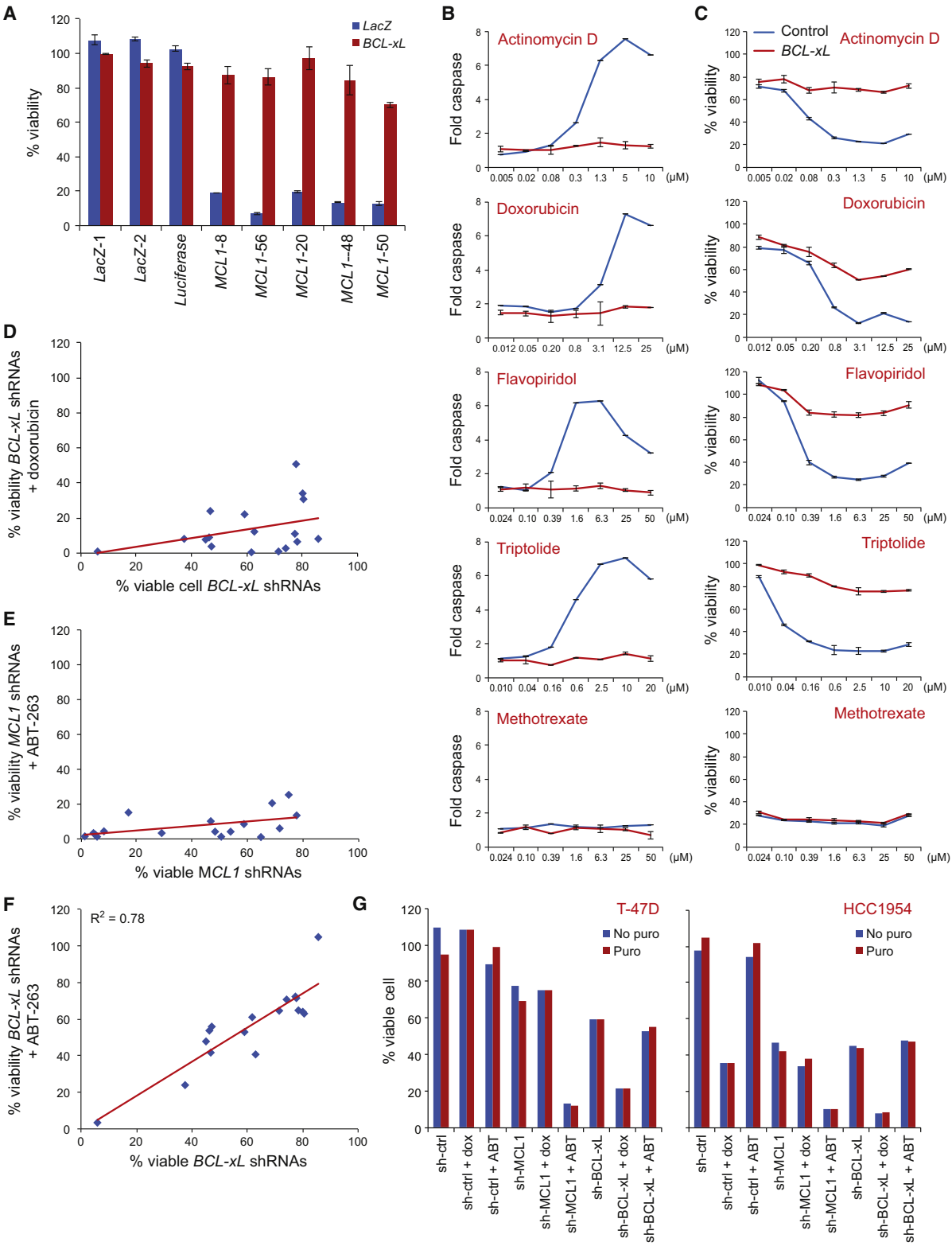

Figure 7. *BCL-xL* Expression Determined Sensitivity to TR Compounds and *MCL1* Repression

(A) Effect of ectopic expression of *BCL-xL* on apoptosis induced by *MCL1* shRNAs in HMC-1-8 cells. Error bars indicate standard deviation of duplicate measurements.

(B and C) Ectopic expression of *BCL-xL* protected sensitive HMC-1-8 cells from TR compounds but not methotrexate, as measured both by caspase activity (B) and cell viability (C). Error bars indicate standard deviation of duplicate measurements.

High-Throughput Gene-Expression Screen for Proximal Apoptosis Genes and Gene-Expression Profiling by Microarray

MCF7 cells growing in 384-well dishes were treated with 2,922 small molecules from small-molecule libraries from the Broad Institute Chemical Biology Program for 8 hr before being lysed. mRNA in cell lysates was hybridized to dT_{20}-conjugated plates (QIAGEN) and then reverse transcribed by Superscript II (Promega). The resulting covalently attached cDNA was amplified by ligation-mediated amplification. For each gene to be assayed, upstream and downstream probes with unique barcode tags and universal primer sites were annealed to targeted cDNA, and ligation by Taq DNA ligase (New England BioLabs) generated a sequence complementary to the transcript. The ligation product was PCR amplified using biotin-conjugated universal primers. The PCR products were then captured by hybridization to probes complementary to the barcodes that were linked to uniquely colored polystyrene beads (Luminex). The products were subsequently stained with streptavidin-phycoerythrin (SAPE) (Invitrogen). Each gene product was identified by the color of its capture bead and quantified using the associated SAPE fluorescence, as measured by a Luminex detector. MCF-7 cells were treated with 500 nM triptolide or 2.5 μM actinomycin D for 2, 4, or 6 hr, and gene expression was profiled using Affymetrix microarrays (Gene Expression Omnibus [GEO] accession number GSE28662).

RNAi and Ectopic Expression

shRNA viral infection was performed as previously described (Moffat et al., 2006). The targeted sequences for the best shRNAs for *MCL1* and *BCL-xL* are listed in Supplemental Experimental Procedures. Cell viability following treatment with *MCL1* or *BCL-xL* shRNAs was compared to results using three control shRNAs against luciferase or LacZ. For combination studies, cells infected with lentivirus carrying shRNAs were selected with or without puromycin (2.5 μg/ml) for 2 days before small molecules were added. Cell viability was measured 24 hr after addition of small molecules. A FLAG tag was added N-terminal of MCL1 or BCL-xL, and FLAG-MCL1 or FLAG-BCL-xL was cloned into an Entry vector (Invitrogen) followed by recombination into a murine stem cell virus (MSCV) destination vector. A *BCL-xL* Entry clone was also cloned into the pLenti6.2 destination vector (Invitrogen) for Figures 7A–7C.

Western Blot and Coimmunoprecipitation

Cells in Figure 6A were lysed in cell lysis buffer (Cell Signaling Technology). Otherwise, cells were lysed in CHAPS lysis buffer (50 mM Tris-Cl [pH 7.4], 150 mM NaCl, 1% CHAPS, 1 mM EDTA, 1 mM EGTA, protease inhibitors, PhosSTOP [Roche], and 20 μM MG132). Protein lysates were incubated with antibody for MCL1 (Santa Cruz Biotechnology) or BCL-xL (Cell Signaling Technology) overnight, and then protein A/G Plus beads (Santa Cruz Biotechnology) were added and incubated for an additional 4 hr. Agarose beads conjugated with an MCL1 antibody and an MCL1 peptide were used in Figure 5D. Anti-FLAG beads and 3X FLAG peptides (both from Sigma) were used in Figure 8E. Antibodies for MCL1 western blots were from Santa Cruz Biotechnology and BD Pharmingen. BCL-xL, BIM, PUMA, BAK, and PARP antibodies were from Cell Signaling Technology. BAX and ACTIN antibodies were from Millipore. Protein quantification was performed with ImageJ (NIH).

Animal Studies

Mice were imaged 2 weeks after subcutaneous injection of H1437-Luc-mCherry or HCC15-Luc-mCherry cells to identify mice with established tumor burden. Tumor measurements were taken twice weekly to track tumor volume. All mice had established tumors at 2 weeks and were entered into treatment groups each containing eight or nine mice, with all groups having around the same bioluminescent imaging average. Treatments were administered daily via intraperitoneal injection and mice were measured weekly for 6 weeks. The animals had tumor measurements taken twice weekly. The time to sacrifice was determined by tumor volume reaching 1,500 cm^2 or tumor ulceration. The xenograft mice were generated, housed, and bred in the Dana-Farber Cancer Institute animal facility. All animal experiments were approved by the Dana-Farber Cancer Institute Institutional Animal Care and Use Committee.

SUPPLEMENTAL INFORMATION

Supplemental Information includes five figures, two tables, and Supplemental Experimental Procedures and can be found with this article online at doi:10.1016/j.ccr.2012.02.028.

ACKNOWLEDGMENTS

This work was supported by NIH grant nos. P01 CA068484 and 5U54CA112962 (to T.R.G.). G.W. was supported by a postdoctoral fellowship from The Damon Runyon Cancer Research Foundation. R.B. was supported by a grant from the Novartis Institutes of Biomedical Research. The authors thank the Broad Institute Chemical Biology Platform for assistance in small-molecule screening; the Broad Institute Genetic Analysis Platform for Affymetrix microarray profiling; the Broad-Novartis Cancer Cell Line Encyclopedia Project for data sharing; Joshua Gould for assistance in data analysis; Jinyan Du, Xiaodong Lu, and Emily Gray for technical assistance; and Leslie Gaffney and Lauren Solomon for editorial assistance.

Received: May 10, 2011
Revised: December 12, 2011
Accepted: February 27, 2012
Published: April 16, 2012

REFERENCES

Adams, J.M., and Cory, S. (2007). The Bcl-2 apoptotic switch in cancer development and therapy. Oncogene *26*, 1324–1337.

Adams, K.W., and Cooper, G.M. (2007). Rapid turnover of mcl-1 couples translation to cell survival and apoptosis. J. Biol. Chem. *282*, 6192–6200.

Basso, K., Margolin, A.A., Stolovitzky, G., Klein, U., Dalla-Favera, R., and Califano, A. (2005). Reverse engineering of regulatory networks in human B cells. Nat. Genet. *37*, 382–390.

Beroukhim, R., Mermel, C.H., Porter, D., Wei, G., Raychaudhuri, S., Donovan, J., Barretina, J., Boehm, J.S., Dobson, J., Urashima, M., et al. (2010). The landscape of somatic copy-number alteration across human cancers. Nature *463*, 899–905.

Bewry, N.N., Nair, R.R., Emmons, M.F., Boulware, D., Pinilla-Ibarz, J., and Hazlehurst, L.A. (2008). Stat3 contributes to resistance toward BCR-ABL inhibitors in a bone marrow microenvironment model of drug resistance. Mol. Cancer Ther. *7*, 3169–3175.

Buggins, A.G., Pepper, C., Patten, P.E., Hewamana, S., Gohil, S., Moorhead, J., Folarin, N., Yallop, D., Thomas, N.S., Mufti, G.J., et al. (2010). Interaction with vascular endothelium enhances survival in primary chronic lymphocytic leukemia cells via NF-κB activation and de novo gene transcription. Cancer Res. *70*, 7523–7533.

Chen, R., Keating, M.J., Gandhi, V., and Plunkett, W. (2005). Transcription inhibition by flavopiridol: mechanism of chronic lymphocytic leukemia cell death. Blood *106*, 2513–2519.

Chen, S., Dai, Y., Harada, H., Dent, P., and Grant, S. (2007). Mcl-1 down-regulation potentiates ABT-737 lethality by cooperatively inducing Bak activation and Bax translocation. Cancer Res. *67*, 782–791.

Danial, N.N., and Korsmeyer, S.J. (2004). Cell death: critical control points. Cell *116*, 205–219.

(D–F) The effects of *BCL-xL* shRNAs (D and F) or *MCL1* shRNAs (E) on cell viability plotted on the x axis against sensitivity to the combination of *BCL-xL* shRNAs (D and F) or *MCL1* shRNAs (E) and doxorubicin (D) or ABT-263 (E and F) in 17 breast cancer cell lines. Cells were infected with viruses carrying shRNAs for *MCL1* or *BCL-xL* for 3 days, or 2 days followed by treatment with 5 μM doxorubicin or 1 μM ABT-263 for an additional 24 hr (median of five *MCL1* shRNAs or *BCL-xL* shRNAs, as indicated).
(G) Examples of combination treatment of *MCL1* or *BCL-xL* shRNAs and doxorubicin (dox) or ABT-263 (ABT). Puro, puromycin.
See also Figure S5.

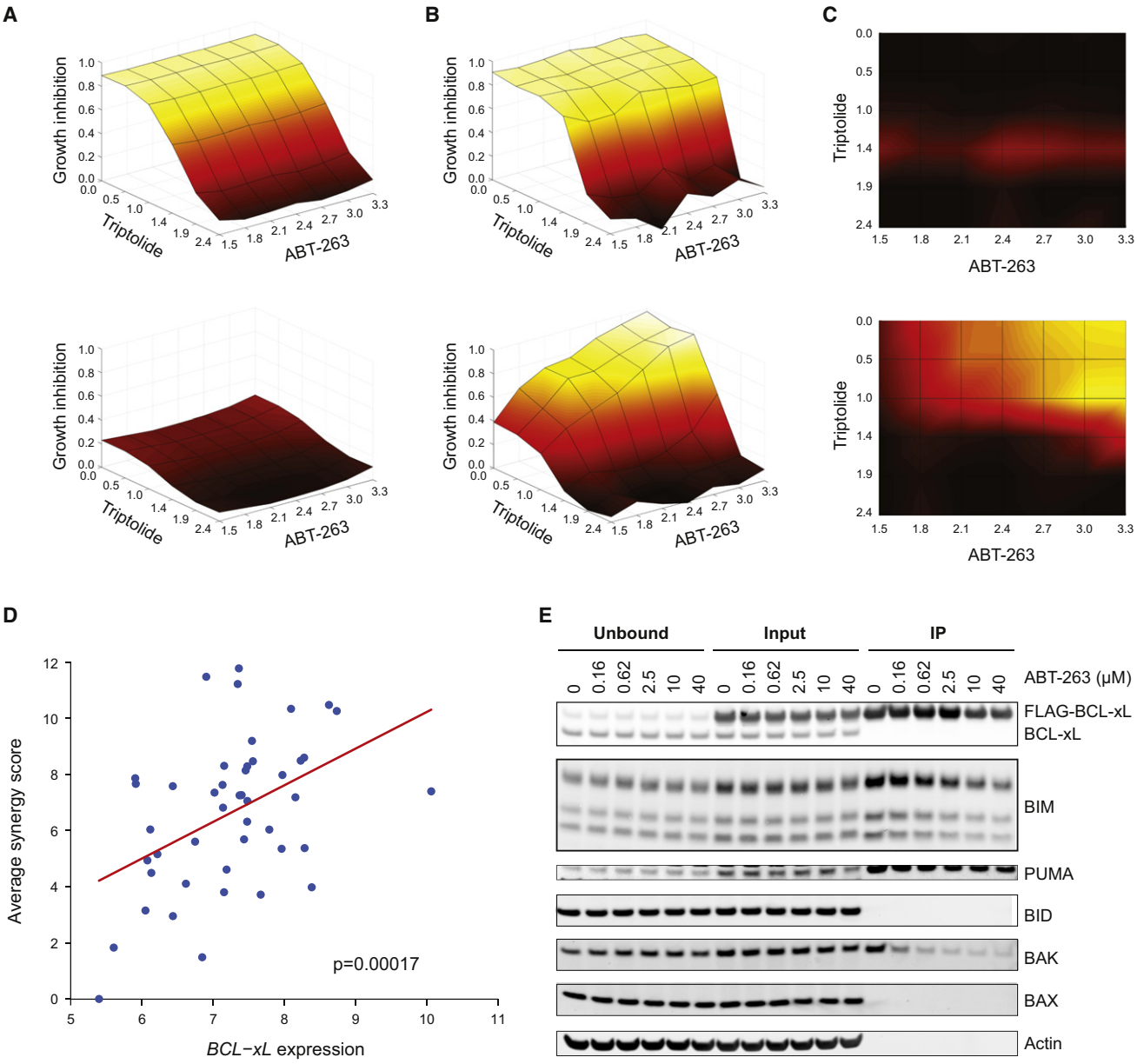

Figure 8. TR Compounds and BCL-xL Inhibitor Compounds Synergistically Killed Cells with High *BCL-xL* Expression

(A–C) Example of synergy calculation. Cell lines expressing *BCL-xL* at the lowest (NCI-H23; top panel) and highest (SKLU1; bottom panel) levels, across a panel of 74 NSCLC cell lines.

(A) Bliss independence model. Dose-response curves for single-agent treatment with ABT-263 and triptolide were used to compute the null-hypothesis surface of expected response to combination treatment with ABT-263 and triptolide using a Bliss independence model. The x and y axes represent concentrations of ABT-263 and triptolide in log10(nM), and the z axis (as well as the color scale) represents the expected percent growth inhibition for each combination of compound concentrations under the null-hypothesis model.

(B) Dose-response matrix. Observed response surfaces for the combination experiments were plotted.

(C) Excess over Bliss independence. Excess percent growth inhibition over the null-hypothesis model was computed for each combination of compound concentrations by subtracting the growth inhibition values displayed in (A) from those in (B). Black represents no excess growth inhibition and yellow represents excess growth inhibition (scale 0–1).

(D) *BCL-xL* expression level versus compound synergy across the panel of 74 cell lines. The x axis displays the log2 expression level of *BCL-xL*. The y axis displays the synergy score, computed by summing the excess over Bliss independence values (as shown in C) over all combinations of compound concentrations. The synergy scores displayed in the plot represent the average synergy score over the four combination experiments, performed by pairing triptolide or actinomycin D with ABT-263 or ABT-737.

(E) Cells stably expressing FLAG-tagged BCL-xL were treated with ABT-263 at the indicated concentrations for 3 hr, subjected to immunoprecipitation with anti-FLAG antibody beads, and eluted with 3X FLAG peptides. The IP fraction was 5-fold more concentrated than input and unbound.

Desmedt, C., Di Leo, A., de Azambuja, E., Larsimont, D., Haibe-Kains, B., Selleslags, J., Delaloge, S., Duhem, C., Kains, J.P., Carly, B., et al. (2011). Multifactorial approach to predicting resistance to anthracyclines. J. Clin. Oncol. *29*, 1578–1586.

Gomez-Bougie, P., Wuillème-Toumi, S., Ménoret, E., Trichet, V., Robillard, N., Philippe, M., Bataille, R., and Amiot, M. (2007). Noxa up-regulation and Mcl-1 cleavage are associated to apoptosis induction by bortezomib in multiple myeloma. Cancer Res. *67*, 5418–5424.

Gong, Y., Somwar, R., Politi, K., Balak, M., Chmielecki, J., Jiang, X., and Pao, W. (2007). Induction of BIM is essential for apoptosis triggered by EGFR kinase inhibitors in mutant EGFR-dependent lung adenocarcinomas. PLoS Med. *4*, e294.

Hanahan, D., and Weinberg, R.A. (2011). Hallmarks of cancer: the next generation. Cell *144*, 646–674.

Hieronymus, H., Lamb, J., Ross, K.N., Peng, X.P., Clement, C., Rodina, A., Nieto, M., Du, J., Stegmaier, K., Raj, S.M., et al. (2006). Gene expression signature-based chemical genomic prediction identifies a novel class of HSP90 pathway modulators. Cancer Cell *10*, 321–330.

Jeffers, J.R., Parganas, E., Lee, Y., Yang, C., Wang, J., Brennan, J., MacLean, K.H., Han, J., Chittenden, T., Ihle, J.N., et al. (2003). Puma is an essential mediator of p53-dependent and -independent apoptotic pathways. Cancer Cell *4*, 321–328.

Keuling, A.M., Felton, K.E., Parker, A.A., Akbari, M., Andrew, S.E., and Tron, V.A. (2009). RNA silencing of Mcl-1 enhances ABT-737-mediated apoptosis in melanoma: role for a caspase-8-dependent pathway. PLoS One *4*, e6651.

Krajewska, M., Fenoglio-Preiser, C.M., Krajewski, S., Song, K., Macdonald, J.S., Stemmerman, G., and Reed, J.C. (1996a). Immunohistochemical analysis of Bcl-2 family proteins in adenocarcinomas of the stomach. Am. J. Pathol. *149*, 1449–1457.

Krajewska, M., Krajewski, S., Epstein, J.I., Shabaik, A., Sauvageot, J., Song, K., Kitada, S., and Reed, J.C. (1996b). Immunohistochemical analysis of bcl-2, bax, bcl-X, and mcl-1 expression in prostate cancers. Am. J. Pathol. *148*, 1567–1576.

Kuroda, J., Puthalakath, H., Cragg, M.S., Kelly, P.N., Bouillet, P., Huang, D.C., Kimura, S., Ottmann, O.G., Druker, B.J., Villunger, A., et al. (2006). Bim and Bad mediate imatinib-induced killing of Bcr/Abl^{+} leukemic cells, and resistance due to their loss is overcome by a BH3 mimetic. Proc. Natl. Acad. Sci. USA *103*, 14907–14912.

Lamb, J., Crawford, E.D., Peck, D., Modell, J.W., Blat, I.C., Wrobel, M.J., Lerner, J., Brunet, J.P., Subramanian, A., Ross, K.N., et al. (2006). The Connectivity Map: using gene-expression signatures to connect small molecules, genes, and disease. Science *313*, 1929–1935.

Lee, S.I., Dudley, A.M., Drubin, D., Silver, P.A., Krogan, N.J., Pe'er, D., and Koller, D. (2009). Learning a prior on regulatory potential from eQTL data. PLoS Genet. *5*, e1000358.

Leuenroth, S.J., and Crews, C.M. (2008). Triptolide-induced transcriptional arrest is associated with changes in nuclear substructure. Cancer Res. *68*, 5257–5266.

Lin, X., Morgan-Lappe, S., Huang, X., Li, L., Zakula, D.M., Vernetti, L.A., Fesik, S.W., and Shen, Y. (2007). 'Seed' analysis of off-target siRNAs reveals an essential role of Mcl-1 in resistance to the small-molecule Bcl-2/Bcl-XL inhibitor ABT-737. Oncogene *26*, 3972–3979.

Lindsten, T., Ross, A.J., King, A., Zong, W.X., Rathmell, J.C., Shiels, H.A., Ulrich, E., Waymire, K.G., Mahar, P., Frauwirth, K., et al. (2000). The combined functions of proapoptotic Bcl-2 family members bak and bax are essential for normal development of multiple tissues. Mol. Cell *6*, 1389–1399.

Margolin, A.A., Nemenman, I., Basso, K., Wiggins, C., Stolovitzky, G., Dalla Favera, R., and Califano, A. (2006). ARACNE: an algorithm for the reconstruction of gene regulatory networks in a mammalian cellular context. BMC Bioinformatics *7* (*Suppl 1*), S7.

Martin, M., Romero, A., Cheang, M.C.U., López García-Asenjo, J.A., García-Saenz, J.A., Oliva, B., Román, J.M., He, X., Casado, A., de la Torre, J., et al. (2011). Genomic predictors of response to doxorubicin versus docetaxel in primary breast cancer. Breast Cancer Res. Treat. *128*, 127–136.

Mérino, D., Strasser, A., and Bouillet, P. (2011). Bim must be able to engage all pro-survival Bcl-2 family members for efficient tumor suppression. Oncogene, in press. Published online November 14, 2011. 10.1038/onc.2011.508.

Moffat, J., Grueneberg, D.A., Yang, X., Kim, S.Y., Kloepfer, A.M., Hinkle, G., Piqani, B., Eisenhaure, T.M., Luo, B., Grenier, J.K., et al. (2006). A lentiviral RNAi library for human and mouse genes applied to an arrayed viral high-content screen. Cell *124*, 1283–1298.

Moretti, E., Oakman, C., and Di Leo, A. (2009). Predicting anthracycline benefit: have we made any progress? Curr. Opin. Oncol. *21*, 507–515.

Oltersdorf, T., Elmore, S.W., Shoemaker, A.R., Armstrong, R.C., Augeri, D.J., Belli, B.A., Bruncko, M., Deckwerth, T.L., Dinges, J., Hajduk, P.J., et al. (2005). An inhibitor of Bcl-2 family proteins induces regression of solid tumours. Nature *435*, 677–681.

Peck, D., Crawford, E.D., Ross, K.N., Stegmaier, K., Golub, T.R., and Lamb, J. (2006). A method for high-throughput gene expression signature analysis. Genome Biol. *7*, R61.

Petros, A.M., Olejniczak, E.T., and Fesik, S.W. (2004). Structural biology of the Bcl-2 family of proteins. Biochim. Biophys. Acta *1644*, 83–94.

Rossi, C., Gasparini, G., Canobbio, L., Galligioni, E., Volpe, R., Candiani, E., Toffoli, G., and D'Incalci, M. (1987). Doxorubicin distribution in human breast cancer. Cancer Treat. Rep. *71*, 1221–1226.

Stewart, M.L., Fire, E., Keating, A.E., and Walensky, L.D. (2010). The MCL-1 BH3 helix is an exclusive MCL-1 inhibitor and apoptosis sensitizer. Nat. Chem. Biol. *6*, 595–601.

Tewey, K.M., Rowe, T.C., Yang, L., Halligan, B.D., and Liu, L.F. (1984). Adriamycin-induced DNA damage mediated by mammalian DNA topoisomerase II. Science *226*, 466–468.

Titov, D.V., Gilman, B., He, Q.L., Bhat, S., Low, W.K., Dang, Y., Smeaton, M., Demain, A.L., Miller, P.S., Kugel, J.F., et al. (2011). XPB, a subunit of TFIIH, is a target of the natural product triptolide. Nat. Chem. Biol. *7*, 182–188.

Tse, C., Shoemaker, A.R., Adickes, J., Anderson, M.G., Chen, J., Jin, S., Johnson, E.F., Marsh, K.C., Mitten, M.J., Nimmer, P., et al. (2008). ABT-263: a potent and orally bioavailable Bcl-2 family inhibitor. Cancer Res. *68*, 3421–3428.

van Delft, M.F., Wei, A.H., Mason, K.D., Vandenberg, C.J., Chen, L., Czabotar, P.E., Willis, S.N., Scott, C.L., Day, C.L., Cory, S., et al. (2006). The BH3 mimetic ABT-737 targets selective Bcl-2 proteins and efficiently induces apoptosis via Bak/Bax if Mcl-1 is neutralized. Cancer Cell *10*, 389–399.

Villunger, A., Michalak, E.M., Coultas, L., Müllauer, F., Böck, G., Ausserlechner, M.J., Adams, J.M., and Strasser, A. (2003). p53- and drug-induced apoptotic responses mediated by BH3-only proteins puma and noxa. Science *302*, 1036–1038.

Voortman, J., Checinska, A., Giaccone, G., Rodriguez, J.A., and Kruyt, F.A. (2007). Bortezomib, but not cisplatin, induces mitochondria-dependent apoptosis accompanied by up-regulation of noxa in the non-small cell lung cancer cell line NCI-H460. Mol. Cancer Ther. *6*, 1046–1053.

Warr, M.R., and Shore, G.C. (2008). Unique biology of Mcl-1: therapeutic opportunities in cancer. Curr. Mol. Med. *8*, 138–147.

Wei, G., Twomey, D., Lamb, J., Schlis, K., Agarwal, J., Stam, R.W., Opferman, J.T., Sallan, S.E., den Boer, M.L., Pieters, R., et al. (2006). Gene expression-based chemical genomics identifies rapamycin as a modulator of MCL1 and glucocorticoid resistance. Cancer Cell *10*, 331–342.

Wei, M.C., Zong, W.X., Cheng, E.H., Lindsten, T., Panoutsakopoulou, V., Ross, A.J., Roth, K.A., MacGregor, G.R., Thompson, C.B., and Korsmeyer, S.J. (2001). Proapoptotic BAX and BAK: a requisite gateway to mitochondrial dysfunction and death. Science *292*, 727–730.

Wiegmans, A.P., Alsop, A.E., Bots, M., Cluse, L.A., Williams, S.P., Banks, K.M., Ralli, R., Scott, C.L., Frenzel, A., Villunger, A., and Johnstone, R.W. (2011). Deciphering the molecular events necessary for synergistic tumor cell apoptosis mediated by the histone deacetylase inhibitor vorinostat and the BH3 mimetic ABT-737. Cancer Res. *71*, 3603–3615.

Zhou, P., Levy, N.B., Xie, H., Qian, L., Lee, C.Y., Gascoyne, R.D., and Craig, R.W. (2001). MCL1 transgenic mice exhibit a high incidence of B-cell lymphoma manifested as a spectrum of histologic subtypes. Blood *97*, 3902–3909.

Cancer Cell
Article

The Histone Demethylase KDM1A Sustains the Oncogenic Potential of MLL-AF9 Leukemia Stem Cells

William J. Harris,[1] Xu Huang,[1] James T. Lynch,[1] Gary J. Spencer,[1] James R. Hitchin,[2] Yaoyong Li,[3] Filippo Ciceri,[1] Julian G. Blaser,[1] Brigit F. Greystoke,[1] Allan M. Jordan,[2] Crispin J. Miller,[3] Donald J. Ogilvie,[2] and Tim C.P. Somervaille[1,*]
[1]Cancer Research UK Leukaemia Biology Laboratory
[2]Cancer Research UK Drug Discovery Unit
[3]Cancer Research UK Applied Computational Biology and Bioinformatics Group
Paterson Institute for Cancer Research, University of Manchester, Manchester, M20 4BX, United Kingdom
*Correspondence: tsomervaille@picr.man.ac.uk
DOI 10.1016/j.ccr.2012.03.014

SUMMARY

Using a mouse model of human MLL-AF9 leukemia, we identified the lysine-specific demethylase KDM1A (LSD1 or AOF2) as an essential regulator of leukemia stem cell (LSC) potential. KDM1A acts at genomic loci bound by MLL-AF9 to sustain expression of the associated oncogenic program, thus preventing differentiation and apoptosis. In vitro and in vivo pharmacologic targeting of KDM1A using tranylcypromine analogs active in the nanomolar range phenocopied *Kdm1a* knockdown in both murine and primary human AML cells exhibiting *MLL* translocations. By contrast, the clonogenic and repopulating potential of normal hematopoietic stem and progenitor cells was spared. Our data establish KDM1A as a key effector of the differentiation block in MLL leukemia, which may be selectively targeted to therapeutic effect.

INTRODUCTION

Epigenetic dysfunction has a central role in the pathology of myeloid malignancy. This is illustrated by the discovery of recurrently occurring mutations targeting genes that code for epigenetic regulators, such as the methylcytosine hydroxylase TET2, DNA methyltransferase DNMT3A, histone H3K27 methyltransferase EZH2, and Polycomb-related protein ASXL1. Mutations in IDH1 and IDH2 likely also affect the epigenome through neomorphic generation of 2-hydroxyglutarate, which inhibits TET2 and Jumonji-domain histone demethylases. Further, subtypes of acute myeloid leukemia (AML) exhibit distinct and abnormal patterns of DNA methylation (reviewed in Fathi and Abdel-Wahab, 2012).

Novel oncoproteins generated by recurrently occurring chromosomal translocations in myeloid leukemia also induce epigenetic dysfunction. For example, the gene coding for the H3K4 methyltransferase MLL, itself a key epigenetic regulator, is mutated by translocation in about 4% of human AML. This results in constitutive transcription at MLL target genes through aberrant recruitment by MLL fusion partners of proteins and complexes associated with transcription elongation, including pTEFb, PAFc, and DOT1L, an H3K79 methyltransferase (Yokoyama et al., 2010; Lin et al., 2010; Muntean et al., 2010).

These and other observations have led to speculation that regulators of the structure and function of chromatin, such as enzymes that regulate turnover of DNA methylation, histone methylation, or histone acetylation, might be attractive therapeutic targets in myeloid malignancy. To date, only the DNA demethylating agent azacitidine has provided a survival benefit in phase III trials in patients with high-risk myelodysplasia (Fenaux et al., 2009). Although this emphasizes that epigenetic therapies hold significant potential, it also highlights the necessity for identification and evaluation of other therapeutic targets.

Significance

Epigenetic therapies hold promise in the treatment of myeloid malignancy but few targets have been identified and evaluated. Our observations delineate the histone demethylase KDM1A as an enzymatic target to effect downregulation of the MLL-associated oncogenic program and cellular oncogenic potential. The finding that potent pharmacologic inhibitors of KDM1A abrogate clonogenic potential and induce differentiation of both murine and primary human MLL leukemia cells, both in vitro and in vivo, while sparing normal repopulating cells, provides strong evidence for a possible therapeutic window. Our data suggest that KDM1A is a candidate target for differentiation therapy in the MLL molecular subtype of human myeloid leukemia and mandate evaluation of KDM1A inhibition as a therapeutic strategy more generally in myeloid malignancy.

One such candidate is KDM1A (also known as AOF2, LSD1, KIAA0601, or BHC110), a flavin adenine dinucleotide (FAD)-dependent lysine-specific demethylase with monomethyl- and dimethyl-histone H3 lysine-4 (H3K4) and lysine-9 (H3K9) substrate specificity (Shi et al., 2004; Metzger et al., 2005). It is a component of both an MLL supercomplex (Nakamura et al., 2002), which is associated with sites of active transcription, and an ELL (elongation factor RNA polymerase II) complex, which contains pTEFb components that interact with AF9 and AF4, two common oncogenic fusion partners for MLL (Biswas et al., 2011). It is also a component of complexes associated with transcription repression, such as CoREST-HDAC, CtBP, and NuRD (reviewed in Hou and Yu, 2010). Although KDM1A expression has been correlated with poor prognosis in high-risk prostate and breast cancer and poor differentiation in neuroblastoma (Kahl et al., 2006; Schulte et al., 2009; Lim et al., 2010), there is little information to date as to its functional role in myeloid leukemia nor whether it represents a viable therapeutic target.

RESULTS

Kdm1a Is Required for the Clonogenic and LSC Potential of MLL-AF9 AML Cells

To determine whether the expression of known or candidate histone demethylases correlates with AML LSC potential, we analyzed microarray data sets from 23 murine MLL leukemias with known AML colony-forming cell (AML-CFC) frequencies, including those with high (MLL-AF9 and MLL-ENL) or low (MLL-AF10, MLL-AF1p and MLL-GAS7) frequencies (Somervaille et al., 2009). The formation of blast-like (type 1) colonies in semi-solid culture by murine MLL-AF9 AML-CFCs directly correlates with LSC potential (Somervaille and Cleary, 2006). The strongest correlation of array expression values with AML-CFC frequency was observed for *Kdm1a* (Figure S1A and Table S1 available online), and this was confirmed by quantitative PCR (Figure S1B). With the exception of MLL-AF1p AMLs, which exhibit a more myeloproliferative morphologic phenotype than do the other MLL subtypes (Somervaille et al., 2009), FACS-purified KIT^+ cell populations, which are enriched for LSCs (Somervaille and Cleary, 2006; Krivtsov et al., 2006), expressed higher levels of *Kdm1a* than did their downstream KIT^{neg} progeny (Figure S1C), suggesting downregulation of expression upon LSC differentiation. We therefore hypothesized that *Kdm1a* is a key regulator of MLL LSCs.

To address this hypothesis, we generated a cohort of mice with MLL-AF9 AML using a retroviral transduction and transplantation approach (Somervaille et al., 2009) and targeted *Kdm1a* for knockdown (KD) in AML cells from sick mice. *Kdm1a* KD AML cells formed significantly fewer colonies in semi-solid culture compared with cells infected with a nontargeting control (NTC) vector (Figure 1A). The small number of *Kdm1a* KD colonies that did form exhibited altered morphology. Compared with controls, there was a significantly higher frequency of type 3 colonies, which contain terminally differentiated macrophages, and a significantly lower frequency of type 1 colonies, which contain poorly differentiated myeloblasts (Figures 1A and 1B). Cytospin preparations of cells recovered at the end of culture confirmed these observations (Figure S1D). The extent of *Kdm1a* KD correlated significantly with loss of AML-CFC potential, both when separate targeting constructs were compared one with another (Figure 1C) and when a single targeting construct was used with GFP as a selectable marker and transduced cell populations were sorted according to GFP expression (Figures S1E–S1G). Consistent with loss of AML-CFC potential, *Kdm1a* KD cells expressed lower levels of genes associated with MLL LSC potential (Figure 1D). Annexin V binding assays also demonstrated that some *Kdm1a* KD cells underwent apoptosis, beginning at 72–96 hr (Figures S1H and S1I). Loss of AML-CFC potential was also observed with *Kdm1a* KD in murine MLL-ENL, MLL-AF10, MLL-LAF4, and MLL-AF1p leukemia cells (Figure S1J). Forced expression of human *KDM1*A, which differs by three bases to murine *Kdm1a* at the locus targeted by shRNA #4, in significant part rescued CFC potential and blocked differentiation (Figures 1E–1G). Forced expression of h*KDM1A* in leukemias with lower frequencies of LSC, such as those initiated by MLL-AF10 and MLL-AF1p, did not increase AML-CFC frequency (data not shown).

To confirm *Kdm1a* KD AML cells were unable to function as LSCs, we performed secondary transplantation of *Kdm1a* KD or control MLL-AF9 AML cells. All mice (n = 5) receiving 2,000 control AML cells died of short latency AML, as did two of five mice transplanted with 500 cells (Figure 1H). AML cells recovered from sick mice were $Mac1^+Gr1^+GFP^+$, consistent with expression of the NTC lentiviral vector (Figure S1K). By contrast, all mice receiving 500 *Kdm1a* KD AML cells survived to the termination of the experiment, as did three of five mice receiving 2,000 *Kdm1a* KD cells. Of the two mice that received *Kdm1a* KD cells that died, cells from one could not be analyzed due to putrefaction; the other died of a GFP^- leukemia, which expressed normal levels of KDM1A (Figure S1K). Two further cohorts of mice were analyzed for engraftment of GFP^+ MLL-AF9 AML cells 40 days following secondary transplant (Figure S1L). Whereas 68% ± 15% or 25% ± 17% (mean ± SEM) of bone marrow (BM) cells were GFP^+ in mice transplanted with 10^4 or 2.5×10^3 control AML cells, respectively, only 0.06% ± 0.03% or 0.04% ± 0.03% of cells were GFP^+ in mice receiving *Kdm1a* KD cells. Together, these data demonstrate that *Kdm1a* is an essential regulator of murine MLL-AF9 LSCs and sustains the LSC potential of MLL AML cells through prevention of differentiation and apoptosis.

KDM1A Is Required to Sustain Expression of the MLL-AF9 Oncogenic Program

To investigate the genetic program regulated by KDM1A in murine MLL-AF9 AML cells enriched for LSCs (Somervaille and Cleary, 2006; Krivtsov et al., 2006), we compared the transcriptome of KIT^+Gr1^+ control and *Kdm1a* KD cells using exon arrays soon after initiation of KD (Figure 2A). Three separate samples from two different animals were used. At this time there was no immunophenotypic evidence of differentiation in *Kdm1a* KD cells (Figure 2A and data not shown).

Exonic expression values were condensed into gene level expression summaries (Table S2), which represent the mean expression value of the probe sets targeting the length of a given protein coding gene. *Kdm1a* was the most consistently and extensively downregulated gene in *Kdm1a* KD AML LSCs across the three sample pairs, as demonstrated by a signal-to-noise ranking metric (Figure 2B). In conventional comparative analyses, many more genes were downregulated than were

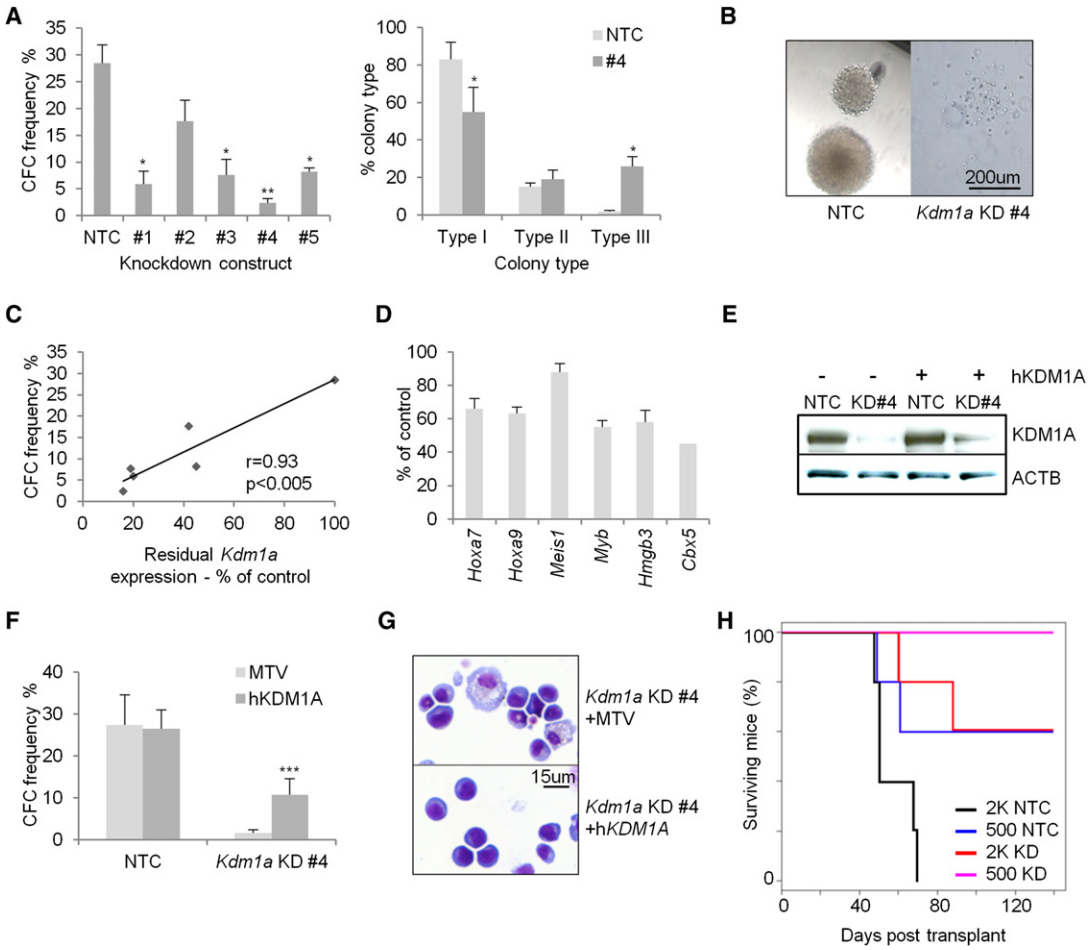

Figure 1. KDM1A Is an Essential Regulator of MLL-AF9 LSC

Murine MLL-AF9 AML BM cells were infected with lentiviruses expressing shRNAs targeting *Kdm1a* or a nontargeting control (NTC).

(A) Bar graphs show AML-CFC frequencies of control or *Kdm1a* KD cells (constructs #1–#5; left) or colony types formed by control (right) or *Kdm1a* KD (construct #4) cells, enumerated after six days of culture (mean ± SEM; n = 3; * indicates $p \leq 0.05$, ** indicates $p \leq 0.01$).

(B) Image shows typical type 1 or type 3 colonies.

(C) Graph shows correlation of *Kdm1a* KD with inhibition of CFC formation, as determined by qPCR 96 hr after KD initiation, for the five constructs tested.

(D) Relative expression of LSC-associated genes, as determined by qPCR, in *Kdm1a* KD cells (construct #4) compared with control cells after five days in semi-solid culture. Error bars refer to SEM of triplicate analyses.

(E) Western blot shows KDM1A expression in murine MLL-AF9 AML cells 48 hr following initiation of *Kdm1a* KD (construct #4) in the presence or absence of forced human KDM1A expression.

(F) Bar graph shows mean ± SEM AML-CFC frequencies of control and *Kdm1a* KD murine MLL-AF9 AML cells in the presence or absence of forced expression of human *KDM1A* (n = 8; *** indicates $p \leq 0.001$). MTV, empty pMSCV vector.

(G) Representative images of cytospin preparations of AML cells recovered at the end of semi-solid culture.

(H) Survival curves of sublethally irradiated syngeneic mice transplanted with 500 (n = 5) or 2,000 (n = 5) control or *Kdm1a* KD (construct #4) MLL-AF9 AML cells.

See also Figure S1 and Table S1.

upregulated (374 genes downregulated and 63 upregulated at $p \leq 0.05$ [paired t test] and 1.25-fold change; Figure 2C and Table S3). False discovery rates (1,000 permutations) were 12.0% and 76.2%, respectively, confirming the significance of the downregulated gene set. Genes consistently and significantly downregulated across the three sample pairs upon *Kdm1a* KD included leukemia-associated genes, such as *Ctnnb1* and *Id2*, and chromatin regulatory genes, such as Polycomb-regulatory complex 1 (PRC1) components *Bmi1*, *Pcgf1*, *Pcgf5*, and *Sfmbt1*; NuRD components *Mta3* and *Hdac2*; and ING2/HDAC complex components *Ing2*, *Arid4a*, and *Hdac2*. This initial analysis suggested that KDM1A contributes directly or indirectly to maintenance of expression of key transcription factors and chromatin regulatory genes in MLL-AF9 LSCs.

To identify gene sets whose co-ordinate expression was dependent upon KDM1A, we performed gene set enrichment analysis (GSEA; Subramanian et al., 2005). This revealed highly significant downregulation of gene sets required for, or associated with, MLL-AF9 leukemogenesis, including an MLL LSC-associated gene set (Somervaille et al., 2009; Figure 2D; NES −2.0; FDR 0%); the set of genes directly bound by MLL-AF9 in murine AML cells (Bernt et al., 2011; Figure 2E; NES −2.1;

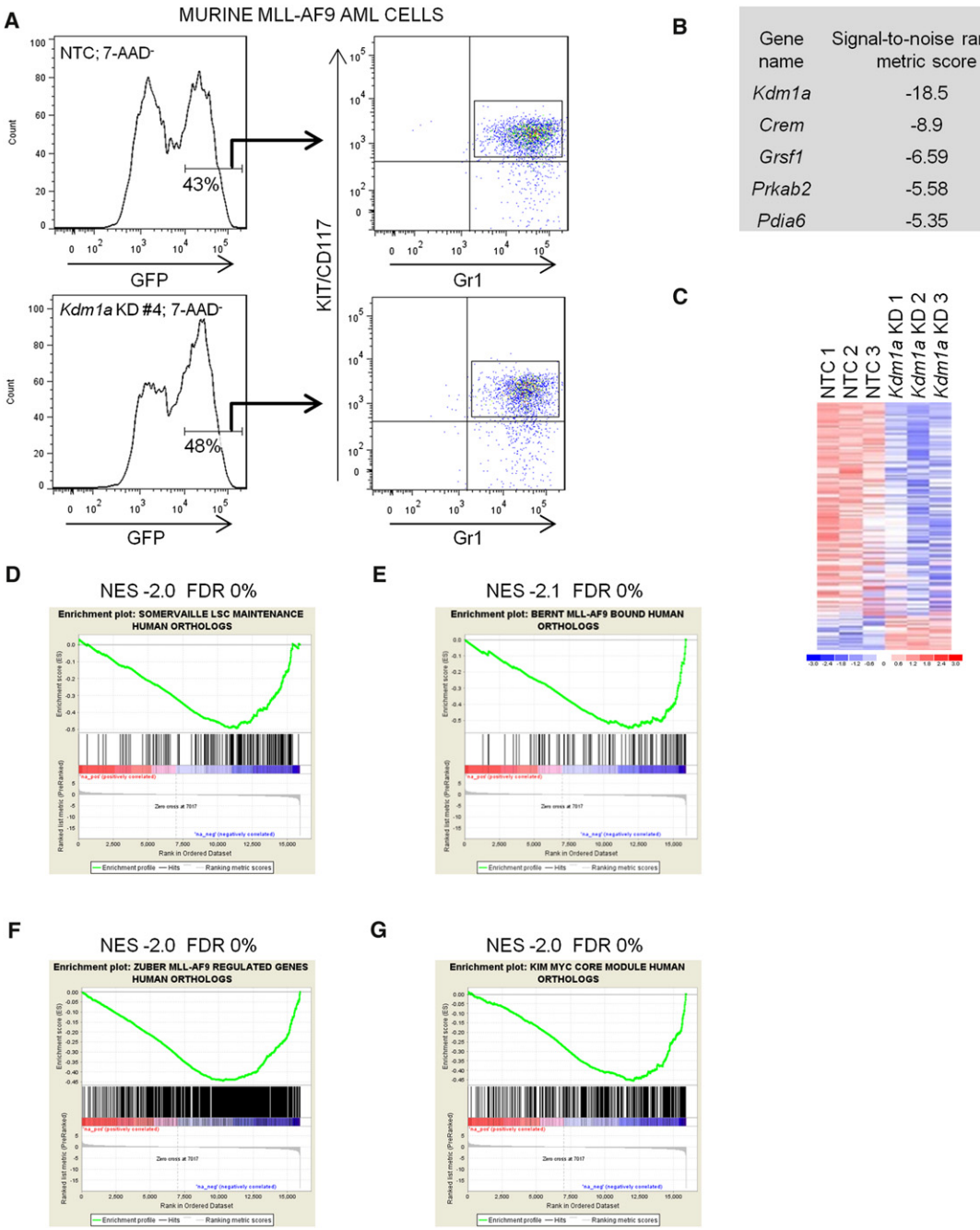

Figure 2. KDM1A Sustains Expression of an MLL-AF9-Associated Oncogenic Program

BM cells from mice with MLL-AF9 AML were infected with *Kdm1a* KD or nontargeting control lentiviruses, with GFP as a selectable marker.

(A) FACS plots show the gating strategy for sorting $GFP^+KIT^+Gr1^+$ control (NTC) or *Kdm1a* KD cells 42 hr following lentiviral infection.

(B) Table shows the five most consistently and extensively downregulated protein coding genes, according to a signal-to-noise ranking metric.

(C) Heat map represents 374 downregulated and 63 upregulated protein coding genes differentially expressed ($p \leq 0.05$; fold change ≥ 1.25) between *Kdm1a* KD and control samples (n = 3). Color scale indicates normalized expression values.

(D–G) GSEA plots show downregulation of (D) MLL LSC maintenance signature genes, (E) genes bound by MLL-AF9 in murine AML cells, (F) genes regulated by MLL-AF9 in murine MLL-AF9;$Nras^{G12D}$ AML cells, and (G) MYC "core module" genes in embryonic stem cells, in *Kdm1a* KD MLL-AF9 LSCs versus controls (for gene sets, see Table S5).

See also Tables S2–S6.

FDR 0%); the set of genes downregulated upon withdrawal of *MLL-AF9* expression in murine *MLL-AF9*;$Nras^{G12D}$ AML cells (Zuber et al., 2011a; Figure 2F; NES −2.0; FDR 0%) and MYC "core module" genes; the set of genes bound by the combination of MYC, MAX, MYCN, DMAP1, E2F1, E2F4, and ZFX in murine embryonic stem cells (ESCs; Kim et al., 2010; Figure 2G; NES

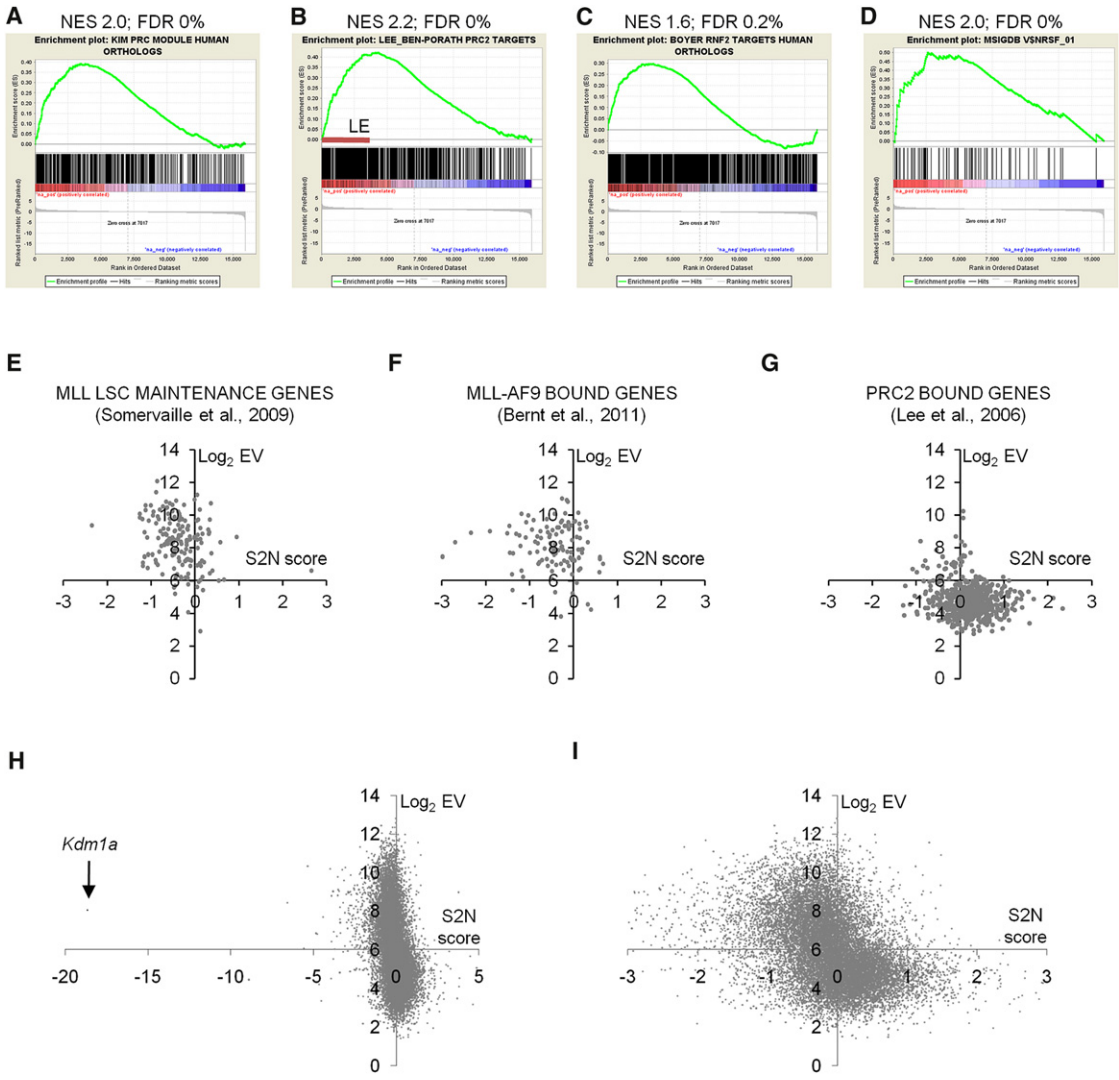

Figure 3. Derepression of Polycomb and REST Target Genes and Differential Regulation of Active versus Inactive Genes in *Kdm1a* KD MLL-AF9 AML cells

(A–D) GSEA plots show derepression of (A) Polycomb-related complex (PRC) module genes, (B) genes bound by PRC2 in ESCs, (C) genes bound by the PRC1 component RNF2 in ESCs, and (D) genes with a REST binding motif at their promoter in *Kdm1a* KD MLL-AF9 LSCs versus controls (for gene sets, see Table S5). LE, leading edge.

(E–G) Graphs show $\log_2$ gene level array expression values (Log_2 EV) versus signal-to-noise ranking metric scores (S2N score, reflecting change in expression; Table S4) for (E) MLL LSC maintenance signature genes, (F) genes bound by MLL-AF9, and (G) genes bound by PRC2 in ESCs. The x axis crosses at the median expression value for all protein coding genes.

(H and I) Graphs show Log_2 EV versus S2N score for (H) all 15,920 protein coding genes represented on the array that have annotated human orthologs or (I) those with S2N scores between −3 and 3.

−2.0; FDR 0%). These data show that KDM1A is required to sustain expression of oncogenic programs associated with MLL-AF9.

Derepression of Polycomb Targets following *Kdm1a* Knockdown

In contrast to simple comparative analysis, GSEA revealed coordinate upregulation of genes bound by Polycomb proteins in ESCs. In *Kdm1a* KD cells, there was significant enrichment in the set of upregulated genes of Polycomb-related complex (PRC) module genes (Figure 3A; NES 2.0; FDR 0%; Kim et al., 2010), which are genes co-occupied by SUZ12, EED, PHC1, and RNF2 in ESCs. Significant enrichment was also observed when genes targeted by PRC2 (Figure 3B; NES 2.2; FDR 0%; Lee et al., 2006; Ben-Porath et al., 2008; the set of genes co-occupied/marked by SUZ12, EED and H3K27Me3 in human ESCs) or the PRC1 component RNF2 (Figure 3C; NES 1.6; FDR 0.2%; Boyer et al., 2006) were considered separately. Many of the 279 genes in the PRC2 analysis "leading edge" (Figure 3B) were developmental regulators; 53 were annotated with the Swiss-Prot/Protein Information Resource keyword "Homeobox" ($p = 10^{-44}$), with roles in the development of skeletal muscle, nervous tissue, pancreas, heart, limbs, and sensory

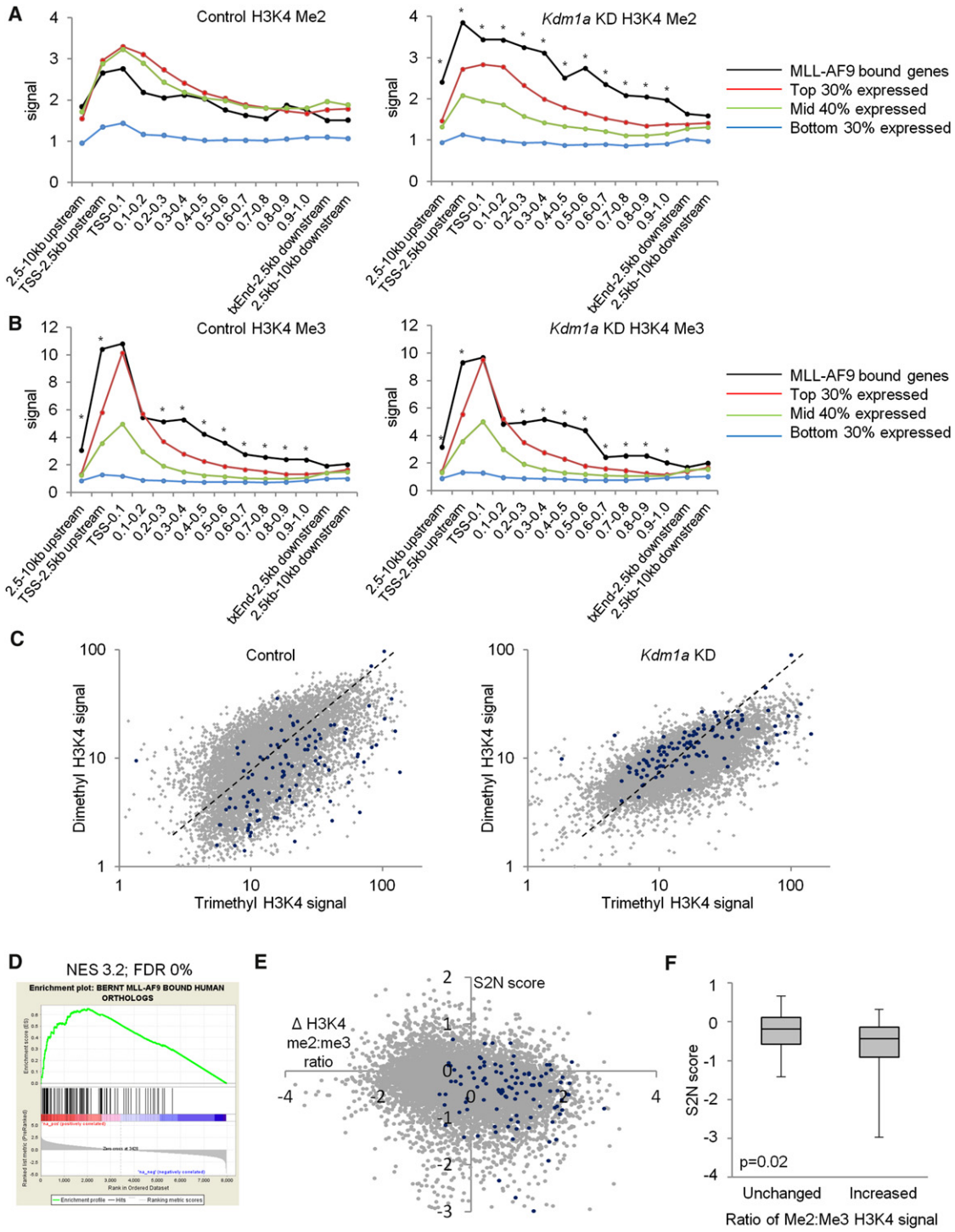

Figure 4. Selective Increase in Dimethyl-H3K4 ChIPseq Signal at MLL-AF9-Bound Genes in *Kdm1a* KD MLL-AF9 AML Cells

(A and B) *Kdm1a* KD or control murine MLL-AF9 AML cells were FACS purified 42 hr following lentiviral infection, with GFP as the selectable marker, and subjected to ChIPseq. Graphs show mean signal for (A) dimethyl-H3K4 and (B) trimethyl-H3K4 across and surrounding MLL-AF9 bound genes and non-MLL-AF9 bound genes with high, intermediate, and low level expression, in control (left panels) and KD cells (right panels). The open reading frame of each gene was divided into ten equal segments for the analysis. Signal is defined as mean uniquely mapped reads per kilobase per million reads. * indicates $p < 0.005$ for comparison of MLL-AF9 bound genes (black line) versus highly expressed non-MLL-AF9 bound genes (red line) at the same locus.

(C) Scatter plots show mean dimethyl- versus trimethyl-H3K4 signal for MLL-AF9 bound (blue dots) or non-MLL-AF9 bound (gray dots) genes with above median array expression values in control (left panel) or knockdown (right panel) cells. Dotted lines indicate median dimethyl:trimethyl H3K4 signal ratio for non-MLL-AF9 bound genes.

organs. There was also co-ordinate upregulation of genes with promoter regions containing a RE1-silencing transcription factor (REST)-binding motif (http://www.broadinstitute.org/gsea; Figure 3D; NES 2.1; FDR 0%). REST recruits KDM1A and RCOR1 (CoREST) to silence neuronal genes in nonneuronal tissues by demethylation of H3K4 (Lee et al., 2005). By contrast, there was no co-ordinate upregulation of genes associated with terminal myeloid differentiation, as demonstrated by GSEA using monocyte or neutrophil "fingerprint" gene sets or the set of genes upregulated during phorbol ester-induced macrophage differentiation of human THP1 MLL-AF9 AML cells (data not shown; for gene sets, see Table S5). Thus, while KDM1A contributes directly or indirectly to gene repression in MLL-AF9 AML LSCs, downregulation of the oncogenic program precedes upregulation of a myeloid differentiation program.

Differential Response of Active versus Less-Active/Repressed Genes

The above observations reflected more generalized, differential consequences for active versus less-active/repressed genes following *Kdm1a* KD. For example, MLL LSC maintenance signature genes (Somervaille et al., 2009) and genes bound by MLL-AF9 (Bernt et al., 2011), which were co-ordinately downregulated, almost exclusively exhibited above median array expression values (Figures 3E and 3F). By contrast, genes targeted by PRC2 in ESCs, which were co-ordinately upregulated, mostly exhibited below median expression levels (Figure 3G). Differential changes in expression of these discrete gene sets occurred in concert with a more generalized shift in gene expression, with downregulation of active genes (above median) and upregulation of less-active/repressed genes (below median; Figures 3H and 3I).

Selective Increase in Dimethyl-H3K4 ChIPseq Signal at MLL-AF9 Bound Genes following *Kdm1a* Knockdown

To investigate the effects of *Kdm1a* KD on histone modifications, we performed chromatin immunoprecipitation, followed by next-generation sequencing (ChIPseq), in control and *Kdm1a* KD MLL-AF9 AML cells for dimethyl-H3K4 and dimethyl-H3K9, as well as for trimethyl-H3K4 and trimethyl-H3K9. Dimethyl-H3K4 and dimethyl-H3K9 are targeted for demethylation by KDM1A. For each of these histone modifications, we compared the mean ChIPseq signal across and around protein-coding genes bound by the MLL-AF9 oncoprotein (Bernt et al., 2011; Table S5), with the mean signal from genes not bound by MLL-AF9 expressed at high, middle, or low levels (Table S2). As expected, in control cells the highest dimethyl- and trimethyl-H3K4 signal was observed surrounding promoter regions, with signal strength related to gene expression (Figures 4A, 4B, and S2A). Following *Kdm1a* KD, and consistent with localization of KDM1A in myeloid leukemia cells at active promoters and enhancers (Figure S2B; Ram et al., 2011), there was a highly significant increase in mean dimethyl-H3K4 signal at promoters and across bodies of genes bound by MLL-AF9 compared with other moderately or highly expressed non-MLL-AF9-bound genes (Figure 4A). By contrast, there was no significant increase in mean dimethyl-H3K4 signal when the MLL LSC-associated gene set (Somervaille et al., 2009), the set of genes downregulated upon withdrawal of *MLL-AF9* expression in murine *MLL-AF9;Nras*^{G12D} AML cells (Zuber et al., 2011a), or MYC "core module" genes (Kim et al., 2010) were considered (data not shown). Indeed, mean dimethyl-H3K4 signal decreased at moderately expressed non-MLL-AF9 bound genes (Figure 4A, green line). There was also no significant change in mean trimethyl-H3K4, dimethyl-H3K9, or trimethyl-H3K9 signal in *Kdm1a* KD versus control cells (Figures 4B, S2A–S2D), and there were only modest changes in global signals for each of the marks in western blotting analyses (Figure S2E). Thus, knockdown of the dimethyl-H3K4 demethylase KDM1A leads to a selective increase in dimethyl-H3K4 ChIPseq signal at genes bound by the MLL-AF9 oncoprotein.

The mean ratio of dimethyl-H3K4 to trimethyl-H3K4 signal was significantly lower in control cells at MLL-AF9-bound genes compared with non-MLL-AF9-bound genes expressed at above array median levels (0.54 ± 0.72 versus 0.88 ± 0.66, respectively [mean ± SD]; $p < 10^{-5}$; Figure 4C), due in large part to significantly greater trimethyl-H3K4 signal across the bodies of MLL-AF9-bound genes (Figure 4B). Following knockdown, ratios became comparable (0.84 ± 0.59 versus 0.76 ± 0.46, respectively [mean ± SD]; p = NS; Figure 4C). The significance of the selective increase in dimethyl-H3K4 signal at MLL-AF9-bound genes was further illustrated by GSEA (Figure 4D). MLL-AF9-bound genes cluster toward the top of a list of protein-coding genes ranked according to fold change in dimethyl-H3K4 marks in *Kdm1a* KD versus control cells (Table S7). Increased dimethyl:trimethyl H3K4 ratio at MLL-AF9-bound genes was associated with reduced expression (Figures 4E and 4F). Of note, we also observed a modest but significant excess of dimethyl- and trimethyl-H3K9 marks at MLL-AF9-bound genes by comparison with non-MLL-AF9-bound moderately or highly expressed genes (Figures S2C and S2D).

Together, these data are consistent with the concept of an epigenetic lesion in MLL leukemia (Guenther et al., 2008; Bernt et al., 2011) and suggest that, in this context, continued expression of MLL-AF9-bound genes may be directly dependent upon the colocalized dimethyl-H3K4 demethylase activity of KDM1A. The LSC maintenance or MYC module oncogenic programs, and other active genes, whose expression is subordinate to the set of MLL-AF9-bound genes, are likely indirectly dependent on KDM1A, downstream of MLL-AF9.

(D) GSEA plot shows enrichment of MLL-AF9-bound genes among protein coding genes ranked according to fold change in dimethyl-H3K4 ChIPseq signal in *Kdm1a* KD versus control cells (Table S7).
(E) Scatter plot shows $\log_2$ fold change in dimethyl:trimethyl H3K4 ratio (ΔH3K4 me2:me3 ratio) at MLL-AF9 bound (blue dots) and unbound (gray dots) genes in *Kdm1a* KD versus control cells plotted against their signal-to-noise metric (S2N) scores (reflecting change in expression; Table S4).
(F) Box plot shows median ± 25th percentile and range of S2N scores for MLL-AF9 bound genes with unchanged (i.e., −0.5 to 0.5) or increased (>1) $\log_2$ dimethyl:trimethyl H3K4 ratios.
See also Figure S2 and Table S7.

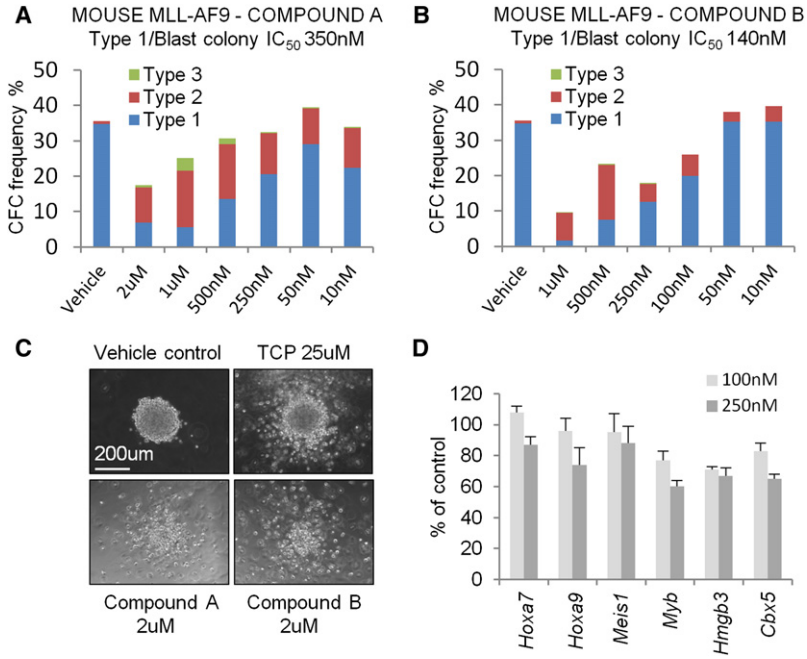

Figure 5. Tranylcypromine Analogs Phenocopy *Kdm1a* Knockdown

(A and B) Bar graphs show frequencies of colony types following treatment of AML cells with the indicated concentrations of Compounds A and B (means of three experiments and estimated biologic IC_{50} for type 1 colony formation are shown).

(C) Representative images of murine MLL-AF9 AML colonies after six days in semi-solid culture with the indicated type and concentration of inhibitor or vehicle.

(D) Relative expression of LSC-associated genes, as determined by qPCR, in murine MLL-AF9 AML cells treated with the indicated concentrations of Compound B compared with vehicle-treated cells after five days in semi-solid culture. Error bars refer to SEM of triplicate analyses.

See also Figure S3.

Pharmacologic Inhibition of KDM1A Phenocopies Knockdown in Murine and Primary Human MLL AML Cells

Given these data, *Kdm1a* represents an attractive therapeutic target in MLL leukemia. KDM1A is inhibited in vitro at an IC_{50} of ~20 μM by the monoamine oxidase inhibitor tranylcypromine (TCP) (Hou and Yu, 2010), which is used in the treatment of depression. We treated murine MLL-AF9 AML cells, human THP1 cells (which harbor a t(9;11) translocation, the cytogenetic hallmark of *MLL-AF9*), and primary human MLL leukemia cells with TCP. At a concentration close to the IC_{50} for KDM1A, TCP induced loss of clonogenic potential and induction of differentiation in murine (Figures S3A and S3B), human THP1 (Figures S3C and 3SD), and primary human MLL leukemic blasts (Figures S3E and S3F), as demonstrated by colony morphology and examination of cytospin preparations. Consistent with the depletion of type 1 myeloblast colonies by TCP treatment (Figure S3A) and our previous observation that MLL-AF9 AML-CFCs have LSC potential (Somervaille and Cleary, 2006), there was a significant delay in initiation of secondary AML by murine MLL-AF9 AML cells that had been incubated in vitro for five days with 25 μM TCP versus vehicle-treated control cells (Figure S3G).

In view of its lack of potency and selectivity, tranylcypromine is likely to be of limited use in the clinic. We therefore synthesized two analogs of tranylcypromine reported to be more potent and selective inhibitors of KDM1A (Guibourt, 2010): trans-N-((2,3-dihydrobenzo[b][1,4]dioxin-6-yl)methyl)-2-phenylcyclopropan-1-amine (hereafter Compound A) and trans-N-((2-methoxypyridin-3-yl)methyl)-2-phenylcyclopropan-1-amine (hereafter Compound B; Figure S3H). These compounds inhibited the enzymatic activity of KDM1A with IC_{50}s of 670 and 98 nM, respectively, versus 15.7 μM for tranylcypromine using the same assay (Figures S3I–3K). Treatment of murine MLL-AF9 AML cells with Compounds A and B phenocopied both *Kdm1a* KD and TCP treatment, also at concentrations close to their IC_{50}s for KDM1A (Figures 5A–5C; versus 8 μM for TCP; Figure S3A). Thus, the tested TCP analogs exhibited 23- and 57-fold greater biological potencies, respectively, than did TCP in a similar cell setting. As with *Kdm1a* KD, MLL-AF9 AML cells treated with Compound B also exhibited reduced expression of genes associated with LSC potential (Figure 5D), in particular core components of the LSC maintenance signature (Somervaille et al., 2009).

Next, we tested fresh cells from a patient newly diagnosed with high-count AML associated with a t(9;11) translocation, the hallmark of MLL-AF9 AML. As for murine MLL-AF9 cells, Compounds A and B inhibited colony formation of human MLL-AF9 AML cells and promoted differentiation in a dose-dependent manner (Figures 6A and 6B), with the effect being observed at biologic IC_{50}s of 270 and 50 nM, respectively. Following ten days of semi-solid culture, Compound B treatment induced both morphologic (Figure 6C) and immunophenotypic differentiation (Figures 6D and S4A–S4C), the latter demonstrated by reduction in the proportion of AML cells with an immature immunophenotype ($CD34^+CD14^-CD86^-CD36^-$). CD14, CD86, and CD36 are upregulated during monocyte/macrophage differentiation. A similar phenotype was observed following *Kdm1a* KD in primary AML cells from a patient with a t(6;11) translocation, the cytogenetic hallmark of *MLL-AF6* (Figures S4D and S4E). We also tested the effect of Compound B on the clonogenic potential in semi-solid culture of a panel of AML cell lines reflecting a range of molecular subtypes (Figure 6E). Whereas dose-dependent inhibition of colony formation was observed for most lines tested, the most striking inhibition was observed for MLL fusion oncogene-associated lines.

KDM1A Knockdown or Inhibition Spares the Clonogenic Potential of Normal Myeloid, but Not Erythroid, Progenitor Cells

Knockdown or inhibition of KDM1A in primary normal human $CD34^+$ hematopoietic cells significantly reduced the frequency of CFCs, predominantly due to loss of erythroid burst-forming units (BFU-E; Figures 7A–7E). The clonogenic potential of

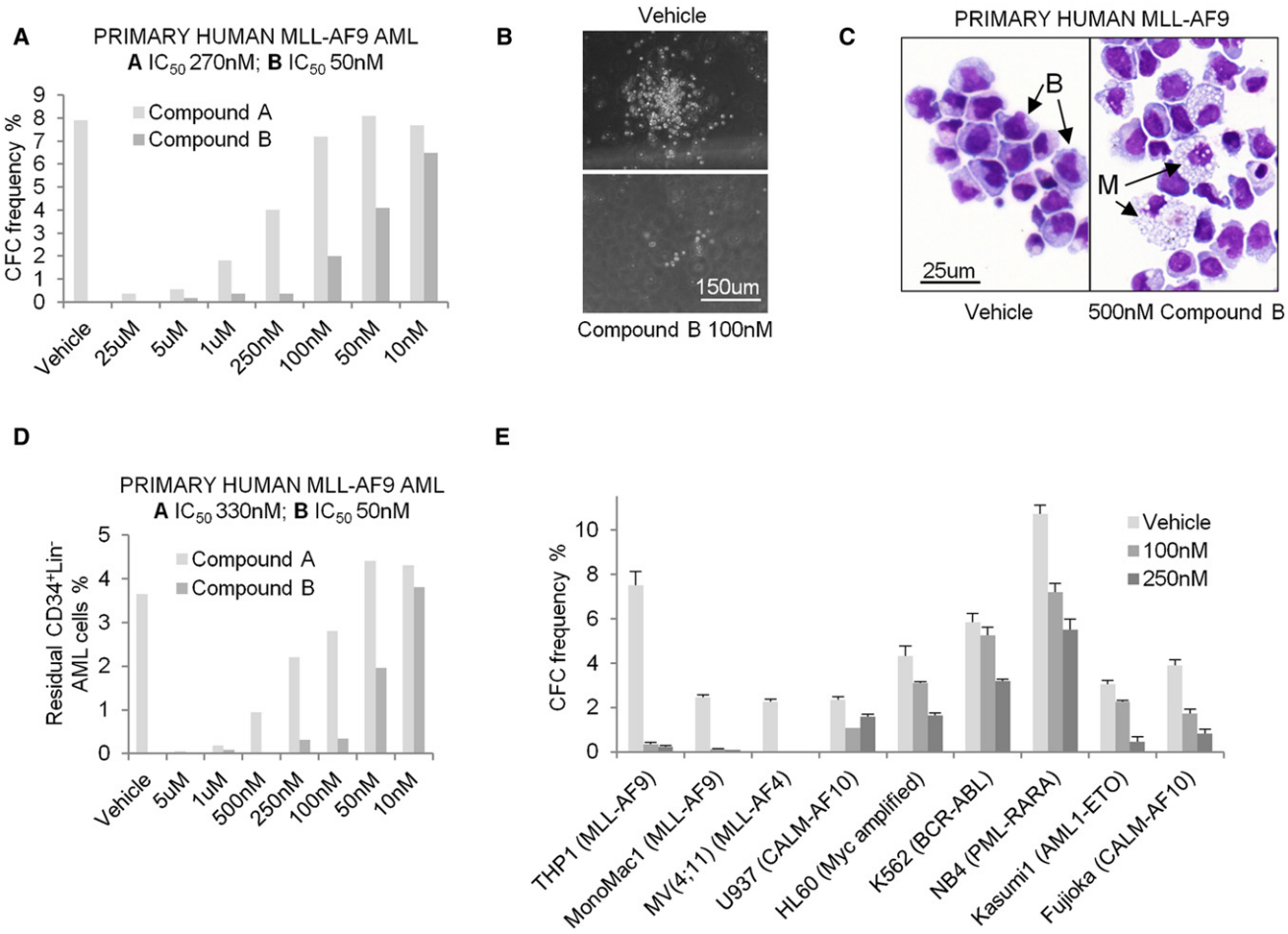

Figure 6. Tranylcypromine Analogs Phenocopy *Kdm1a* Knockdown in Human MLL Leukemia Cells

(A) Bar graph shows CFC frequencies of primary human MLL-AF9 AML cells after ten days in semi-solid culture with the indicated concentrations of Compounds A and B. Representative images show (B) primary human MLL-AF9 AML colonies (sample BB160) and (C) cytospin preparations of cells recovered at the end of semi-solid culture. B, blast; M, macrophage.

(D) Bar graph shows frequency of $CD34^+Lin^-$ ($CD14^-CD36^-CD86^-$) primary human MLL-AF9 AML cells at the end of semi-solid culture in the presence of the indicated concentration of KDM1A inhibitor, as determined by FACS analysis.

(E) Bar graph shows mean ± SEM CFC frequency in semi-solid culture of the indicated human AML cell lines following treatment with Compound B or vehicle (n = 3). See also Figure S4.

myeloid lineage colonies was preserved, although an increase in CFU-M was noted in Compound B-treated cells. For knockdown experiments, two different lentivirally expressed shRNAs, which reduced *KDM1A* expression to 31% (#1) or 38% (#2), respectively, were used. FACS analysis of TCP-treated $CD34^+$ cells after two weeks of culture revealed a significant reduction in the proportion of cells expressing high levels of glycophorin A (Figure 7F), a marker upregulated in the late stages of human erythroid differentiation. We found similar sparing of myeloid colony-forming potential in experiments using murine KIT^+ BM HSPCs cultured in conditions supporting myeloid development (data not shown).

Selective In Vivo Activity of KDM1A Inhibition versus MLL-AF9 Leukemia

To assess whether KDM1A inhibition also selectively targets MLL AML cells in vivo, we transplanted $CD45.2^+$ MLL-AF9 murine AML cells into sublethally irradiated $CD45.1^+$ congenic recipients and treated mice with DMSO vehicle, 10 mg/kg Compound B or 25 mg/kg Compound B twice daily by intraperitoneal injection according to the indicated schedule (Figure 8A). Plasma levels of Compound B measured one hour after a dose of 50 mg/kg IP were 2.0 ± 0.2 μM (n = 3), as determined by liquid chromatography-mass spectrometry. Complete blood counts and blood smears performed at the end of treatment in vehicle-treated mice demonstrated substantial leukemic leukocytosis with circulating blasts and leukemic myelomonocytic cells, modest anemia, and thrombocytopenia, consistent with incipient AML (Figures 8B and 8C). By contrast, mice treated with KDM1A inhibitor lacked evidence of circulating AML cells but were instead significantly more anemic and thrombocytopenic than were vehicle-treated controls and exhibited circulating nucleated erythroid precursors and polychromasia consistent with the degree of anemia (mean ± SEM hemoglobin

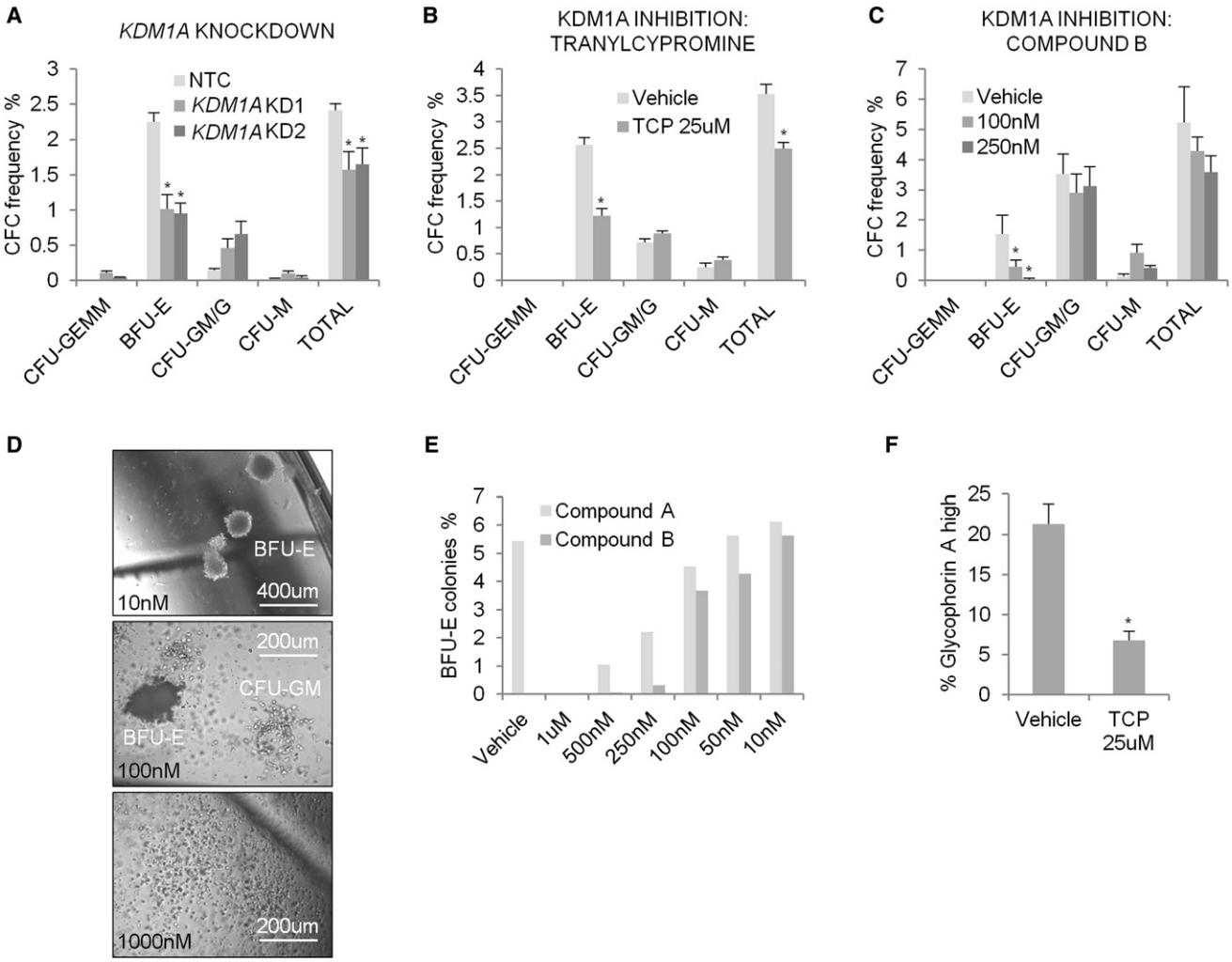

Figure 7. Preservation of Normal Myeloid, but Not Erythroid, Colonies following *KDM1A* Knockdown or Inhibition

(A and B) Bar graphs show CFC frequencies and colony types of normal human CD34$^+$ cells (A) infected with nontargeting control (NTC) or *KDM1A*-targeting (#1 and #2) lentiviruses, (B) treated with tranylcypromine 25 μM or (C) treated with the indicated concentrations of Compound B (mean ± SEM; n = 3; * indicates $p \leq 0.05$). Note sample-to-sample variability in BFU-E frequency in primary patient material.

(D) Representative images show colonies formed in the presence of the indicated concentrations of Compound B.

(E) Bar graph shows frequency of BFU-E arising from normal human CD34$^+$ HSPCs cultured in the indicated concentration of KDM1A inhibitor.

(F) Bar graph shows the percentage of glycophorin A$^+$ cells at the end of ten days in semi-solid culture of CD34$^+$ cells in the presence of tranylcypromine or vehicle (mean ± SEM; n = 3; * indicates $p \leq 0.05$). BFU-E, burst-forming unit erythroid; CFU-GM/G, colony-forming unit granulocyte/macrophage or colony-forming unit granulocyte; CFU-M, colony-forming unit macrophage.

5.0 ± 0.7 g/dl for mice receiving the 25 mg/kg dose vs. 9.0 ± 0.4 g/dl for vehicle-treated mice; $p < 0.001$; n = 6; mean ± SEM platelet count 89 ± 9 × 10^9/l for mice receiving the 25 mg/kg dose vs. 592 ± 55 × 10^9/l for vehicle-treated mice; $p < 0.001$; n = 6; Figures 8B and 8C). Thus, treatment of mice with KDM1A inhibitor completely blocked progression of MLL-AF9 leukemia into the circulation.

Consistent with this observation, analysis of AML cells aspirated from BM at the end of the treatment period showed a dose-dependent, significant reduction in both expression of KIT, which marks MLL-AF9 LSCs, and the frequency of AML-CFCs in FACS-purified CD45.2$^+$ AML cells (Figures 8D–8G). There was also a dose-dependent trend toward reduced donor:-recipient chimerism (Figure S5A). By contrast, neither KIT expression nor clonogenic potential of FACS-purified residual CD45.1$^+$ normal hematopoietic cells were impacted by treatment with KDM1A inhibitor (Figures 8E and 8H). Furthermore, FACS-purified CD45.1$^+$KIT$^+$Gr1$^-$ normal cells from KDM1A inhibitor-treated mice retained lympho-myeloid repopulating activity in secondary transplantation assays (Figures 8I–8K). Although there was a trend toward prolonged survival for leukemic mice treated with Compound B (Figure S5B), a number of mice died of drug-induced anemia rather than leukemia, thus confounding interpretation of survival as an endpoint. Finally, we treated immune-deficient mice xenografted with primary human MLL-AF6 AML cells with Compound B. By comparison, with vehicle-treated mice, a higher proportion of human AML cells in animals treated with KDM1A inhibitor expressed the

monocyte/macrophage differentiation markers CD36 and CD86, and fewer cells expressed an immature $CD34^{+}CD36^{-}CD86^{-}$ immunophenotype (Figure S5C).

Together, these in vitro and in vivo data demonstrate that different types of normal and malignant hematopoietic cells exhibit differential sensitivities to pharmacologic KDM1A inhibition. The relative sensitivity of MLL-AF9 AML cells by comparison with normal HSPCs suggests a significant therapeutic window.

Discussion

Our genetic and pharmacologic data using murine models and primary human AML cells demonstrate that KDM1A is required to sustain the expression of the MLL-AF9-associated oncogenic program, thus maintaining the oncogenic potential of MLL-AF9 LSCs. They also highlight the enzyme as a potential therapeutic target in MLL leukemias, which is of importance given the development of KDM1A inhibitors by the pharmaceutical industry (Guibourt, 2010). The progeny of individually isolated blast-like (type 1) MLL-AF9 AML colonies (Figure 1B) reliably initiate AML in secondarily transplanted recipients, demonstrating the identity of the parental CFC as a cell with LSC potential (Somervaille and Cleary, 2006). Thus, our observation that *Kdm1a* KD or inhibition resulted in loss of AML-CFCs, with induction of differentiation, was highly significant, as was the observation that *Kdm1a* KD MLL-AF9 AML cells fail to initiate leukemia in secondary transplantation experiments. Although a direct link between in vitro clonogenic potential and LSC potential in primary human MLL AML has not been proven, it is nevertheless of note that we found frequencies of clonogenic cells in patient samples ranging from 1%–9%, not dissimilar to those found in the murine model.

KDM1A Sustains Expression of the MLL-AF9 Oncogenic Program

Recent studies have associated the expression of defined gene sets with the oncogenic potential of MLL LSCs (Somervaille et al., 2009; Kim et al., 2010; Bernt et al., 2011; Zuber et al., 2011a). At an early time point following initiation of *Kdm1a* KD in murine MLL-AF9 LSCs, these gene sets were co-ordinately downregulated, and this occurred prior to upregulation of gene sets or cell surface markers associated with terminal myeloid differentiation or the onset of apoptosis in some cells. Loss of clonogenic potential with induction of differentiation and apoptosis is a phenotype very similar to that observed upon tamoxifen withdrawal from murine BM HSPCs immortalized by an MLL-ENL estrogen receptor fusion (Somervaille et al., 2009). This observation suggests the possibility that KDM1A might have a close physical or functional interaction with MLL-AF9, acting as an essential oncogenic cofactor to maintain transformation.

Two lines of evidence suggest this may be the case. First, KDM1A is a member of an ELL complex identified in 293 cells (Biswas et al., 2011), which includes pTEFb members CDK9 and CCNT1 and the MLL oncogenic fusion partners AFF1 (also known as AF4) and AFF4 (also known as AF5q). ELL, CDK9, CCNT1, AFF1, and AFF4 associate with one another either in a static "super-elongation complex" (SEC) or in a dynamic set of higher order complexes that interact with MLL oncogenic fusions, including MLL-AF9 (Lin et al., 2010; Yokoyama et al., 2010). Such interactions may serve to recruit KDM1A to genomic loci bound by MLL oncoproteins. The second piece of evidence arises from our ChIP-sequencing analyses, which suggest a "footprint" of KDM1A activity at genomic loci bound by MLL-AF9. While KDM1A binds promiscuously across the genome, especially at active promoters and enhancers (Ram et al., 2011), following *Kdm1a* KD we observed a highly significant and selective increase in dimethyl-H3K4 ChIPseq signal at genes bound by the MLL-AF9 oncoprotein (Bernt et al., 2011), which was associated with co-ordinate downregulation of the same gene set. Dimethyl-H3K4 is a demethylation target for KDM1A. Of note, global changes in ChIPseq signals were only observed for the dimethyl-H3K4 mark; a global change in the pattern of histone modifications at the gene sets analyzed was not observed for the other marks investigated, including dimethyl-H3K9, which is also a demethylation target of KDM1A. Thus, the only histone modification that exhibited significant change at MLL-AF9-bound genes following *Kdm1a* KD is an enzymatic target of KDM1A.

This observation was unexpected because the dimethyl-H3K4 mark has been considered to be associated with active transcription and its removal by KDM1A has been considered to be associated with transcription repression. Examples of the repressive function of KDM1A include its recruitment with RCOR1 (CoREST) by REST to silence neuronal genes in non-neuronal cells (Lee et al., 2005), its recruitment by ZEB1 to the *Gh* promoter to suppress *Gh* expression in pituitary lactotrophs (Wang et al., 2007), and its recruitment by GFI1 (Saleque et al., 2007) or TAL1 (Hu et al., 2009) to their respective target genes in early erythroid development. KDM1A is also an established transcription activator, although in the context of demethylation of the repression-associated dimethyl-H3K9 mark. For example, it demethylates dimethyl-H3K9 to facilitate androgen- or estrogen-dependent transcription in prostate or breast cancer cells, respectively, by opposing the activity of H3K9 methyltransferases (Metzger et al., 2005; Garcia-Bassets et al., 2007). Likewise, in development, KDM1A is required for activation of *Gh* transcription in pituitary precursor cells (Wang et al., 2007). Our observations in MLL-AF9 AML cells suggest a role for KDM1A in the context of the epigenetic lesion associated with MLL leukemia. This lesion is characterized by an abnormal extent and distribution of the elongation-associated dimethyl-H3K79 mark and the transcription initiation-associated trimethyl-H3K4 mark at genes bound by MLL oncoproteins, as well as mistargeting of elongation factors, such as MLLT1 (also known as ENL; Guenther et al., 2008; Bernt et al., 2011). In keeping with Guenther et al. (2008), we also observed an excess of trimethyl-H3K4 marks upstream of the promoter and across the bodies of genes bound by MLL-AF9.

It was of note that in control MLL-AF9 AML cells the ratio of dimethyl:trimethyl H3K4 marks at MLL-AF9-bound genes was significantly lower than that of non-MLL-AF9-bound genes expressed at similar levels, in large part due to comparatively higher levels of trimethyl-H3K4. Ratios became similar following *Kdm1a* KD. Our data are consistent with a model in which KDM1A acts at MLL-AF9-bound genes to maintain low levels of dimethyl- relative to trimethyl-H3K4, a chromatin state presumably permissive for levels of transcription required for oncogenic transformation. This raises the question as to how

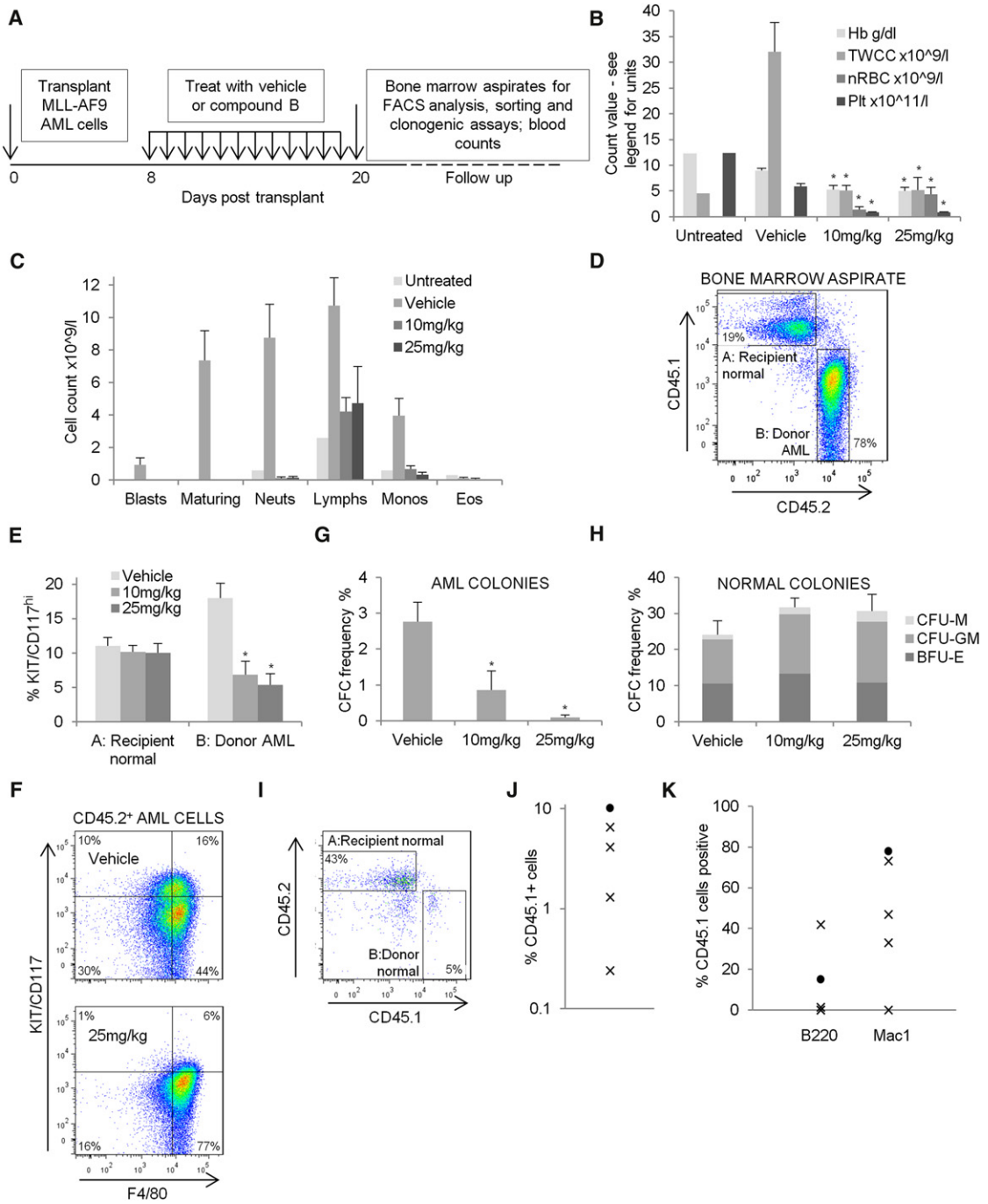

Figure 8. Selective In Vivo Efficacy of KDM1A Inhibition versus MLL-AF9 AML Cells

(A) Image shows experimental plan.

(B) Bar chart shows mean ± SEM hemoglobin (Hb), total white cell count (TWCC), nucleated red blood cell count (nRBC), and platelet count (Plt) in complete blood counts from mice after 12 days of treatment with DMSO vehicle or Compound B at the indicated dose (n = 6 for each cohort). * indicates $p < 0.01$ for values from KDM1A inhibitor-treated mice compared with vehicle-treated controls. Blood count values from an untreated normal adult C57BL/6 mouse are shown for comparison.

(C) Bar chart shows mean ± SEM leukocyte manual differential counts in blood smears from vehicle- and KDM1A inhibitor-treated mice (n = 6 for each cohort). Values from an untreated normal adult C57BL/6 mouse are shown for comparison. Maturing, maturing leukemic myelomonocytic cells; Neuts, neutrophils, including leukemic neutrophils; Lymphs, lymphocytes; Monos, monocytes; Eos, eosinophils.

(D) Representative FACS plot shows chimerism of $CD45.1^+$ normal recipient hematopoietic cells (A, Recipient normal) and $CD45.2^+$ AML cells (B, Donor AML) in a BM aspirate sample taken on day 20 post-transplant.

(E) Bar graph shows mean ± SEM percentage of $CD45.1^+$ normal recipient or $CD45.2^+$ AML cells co-expressing KIT. * indicates $p < 0.01$ for comparison of vehicle-treated versus Compound B-treated mice (n = 6).

accumulation of dimethyl-H3K4 marks might be inhibitory. It is clear from work in yeast that dimethyl-H3K4 is a functionally distinct modification and not simply a metabolic intermediate between monomethyl- and trimethyl-H3K4. It serves as a platform for recruitment of a Set3 complex that contains histone deacetylase activity, which reduces acetylation toward the 5′ end of genes to suppress transcription from cryptic internal promoters (Kim and Buratowski, 2009). Furthermore, chromatin state maps of the genome indicate that increased ratios of dimethyl:trimethyl H3K4 are observed at poised or weakly active promoters by comparison with fully activated promoters (Ernst et al., 2011). Thus, accumulation of dimethyl-H3K4 marks at MLL oncoprotein-bound genes may enable locoregional binding of complexes that repress transcription, leading to downregulation of genes bound by MLL-AF9. Reduced expression of other actively expressed genes, including subordinate oncogenic programs, such as the LSC maintenance program and MYC module, and increased expression of Polycomb-bound genes, is likely an indirect effect of *Kdm1a* KD, downstream of the set of genes bound by MLL-AF9, because we did not observe coordinate changes in histone methylation status at these genomic loci. With regard to Polycomb bound genes, for example, among those most highly downregulated upon *Kdm1a* KD were genes coding for components of PRC1, including *Bmi1*, which is required for stable maintenance of transcriptionally repressed states.

KDM1A as a Therapeutic Target in Leukemia

KDM1A has been suggested as a therapeutic target in cancer because of its high-level expression in poor-risk prostate adenocarcinoma (Kahl et al., 2006), poorly differentiated neuroblastoma (Schulte et al., 2009), and high-grade ER-negative breast cancer (Lim et al., 2010). Our data suggest a therapeutic role for KDM1A inhibition in leukemias associated with expression of MLL fusion oncoproteins. This is demonstrated by the use of potent KDM1A inhibitors selectively to induce loss of clonogenic potential and induction of differentiation in both murine and primary human MLL leukemia cells, both in vitro and in vivo. KDM1A inhibitor treatment of mice engrafted with congenic MLL-AF9 AML cells prevented progression of AML cells into the circulation, downregulated expression of the LSC marker KIT, and reduced the frequency of AML cells with clonogenic potential. Similarly, it also induced immunophenotypic differentiation of xenografted primary human MLL-AF6 cells. By contrast, normal HSPCs were spared as demonstrated by unchanged expression of KIT, unchanged clonogenic potential in semi-solid culture, and a retained capacity to provide lympho-myeloid reconstitution in secondary transplant experiments. KDM1A inhibition in congenic transplant recipients also resulted in a trend toward prolonged survival, although survival curves were confounded by treated mice dying as a result of drug-induced anemia. The effect of KDM1A inhibition on erythropoiesis was predicted by our in vitro studies, which showed a selective loss of BFU-E activity in normal human $CD34^+$ cells following both *Kdm1a* KD and inhibition. Together, these data point to a significant potential therapeutic window for the use of KDM1A inhibitors in the MLL molecular subtype of AML.

Such differential consequences for different normal and malignant hematopoietic cell types are consistent with a previous study using murine cell lines; *Kdm1a* KD impaired DMSO-induced erythroid differentiation of MEL cells and phorbol ester-induced megakaryocytic differentiation of L8057 cells but induced granulocytic differentiation of 32D.4 cells (Saleque et al., 2007). Thus, KDM1A depletion or inhibition has differing consequences for different cellular subtypes.

How might KDM1A inhibitors be used therapeutically? Induction of differentiation of leukemic blasts using all-trans retinoic acid (ATRA) is standard therapy in one subtype of AML, acute promyelocytic leukemia (APML). However, whereas ATRA alone may induce remission, it is insufficient for cure and concomitant treatment with anthracyline or arsenic trioxide is required (Sanz and Lo-Coco, 2011). Indeed single-agent therapy in AML is rarely, if ever, curative. One option may be the combination of KDM1A inhibition with chemotherapy, as has been historically effective for APML and ATRA. Alternatives might include single agent maintenance therapy or combination therapy with histone deacetylase (HDAC) inhibitors, because KDM1A inhibition sensitizes breast cancer and glioblastoma cells to HDAC inhibitor-induced cell cycle arrest or apoptosis (Singh et al., 2011; Huang et al., 2012). Anemia or thrombocytopenia associated with therapy could be managed by transfusion. KDM1A inhibitors may be also of value in certain myeloproliferative disorders.

Examination of a web-based repository of microarray data from primary human AML samples (http://www.oncomine.org) shows that *KDM1A* is expressed at comparable levels in MLL-rearranged leukemias to those in other molecular subtypes. Although our human cell line data suggest that MLL oncoprotein leukemias are selectively sensitive to KDM1A inhibition by comparison with other molecular subtypes of AML, dose-dependent inhibition of clonogenic potential was also observed for other lines, for example, NB4 cells and Kasumi1 cells (associated with *PML-RARA* and *RUNX1-RUNX1T1*, respectively). This suggests the possibility that KDM1A inhibition

(F) Representative FACS plots show expression of KIT and the monocyte/macrophage differentiation marker F4/80 in AML cells in BM aspirates from mice treated with the vehicle (upper panel) or 25 mg/kg Compound B (lower panel).
(G) Bar graph shows mean ± SEM AML-CFC frequency in $CD45.2^+$ MLL-AF9 AML cells, as determined by semi-solid culture.
(H) Bar graph shows mean ± SEM CFC frequency, and colony type, in normal $CD45.1^+$ cells FACS purified from BM aspirates, as determined by semi-solid culture (for G and H, * indicates $p < 0.01$ for comparison of vehicle-treated versus Compound B-treated mice [n = 6]). BFU-E, burst-forming unit erythroid; CFU-GM, colony-forming unit granulocyte/macrophage; CFU-M, colony-forming unit macrophage.
(I) FACS plot shows donor:recipient chimerism in a BM aspirate 21 days following transplantation of 1,000 normal $CD45.1^+KIT^+Gr1^+$ cells, FACS purified from mice treated with Compound B, into a sublethally irradiated normal $CD45.2^+$ congenic recipient.
(J) Graph shows percentage donor ($CD45.1^+$) chimerism in BM aspirates for each of the five recipients transplanted with 1,000 cells (x indicates cells were from mice receiving a 25mg/kg dose; ● indicates cells were from mice receiving a 10 mg/kg dose).
(K) Graph indicates percentage of donor engrafted cells positive for B-lineage (B220) or myeloid lineage (Mac1) markers.
See also Figure S5.

may be a useful therapeutic strategy in other types of myeloid malignancy. Consistent with this, *KDM1A* is among the 5% most highly expressed genes in microarray data sets from prospectively purified immunophenotypic LSCs from a variety of distinct AML subtypes (data extracted from Goardon et al., 2011).

In summary, our identification of KDM1A as a candidate therapeutic target in the MLL translocated subtype of AML adds to recent studies suggesting new approaches to treat this disease, including inhibition of the DOT1L H3K79 histone methyltransferase (Bernt et al., 2011) and the bromodomain protein BRD4 (Zuber et al., 2011b; Dawson et al., 2011). Our data mandate further studies of the effects of KDM1A inhibition in other subtypes of myeloid malignancy, evaluation of combination therapies and clinical trials in AML of KDM1A inhibitors in development by the pharmaceutical industry.

EXPERIMENTAL PROCEDURES

Vectors, Reagents, Cell Lines, Chemicals, and Antibodies

Details of retroviral and lentiviral vectors, cell lines, chemicals, FACS, western blotting, or chromatin immunoprecipitation antibodies are in the Supplemental Experimental Procedures. Tranylcypromine analogs trans-N-[1-(2,3-dihydro-1,4-benzodioxin-6-yl)ethyl]-2-phenylcyclopropan-1-amine (Compound A) and trans-N-[(2-methoxypyridin-3-yl)methyl]-2-phenylcyclopropan-1-amine (Compound B) were synthesized in house, as described in Guibourt (2010).

Chromatin Immunoprecipitation and Next-Generation Sequencing

Chromatin immunoprecipitation (ChIP) was performed using a Red ChIP Kit (Diagenode, Liege, Belgium) in accordance with the manufacturer's instructions. Details of shearing, ChIPseq library preparation, next-generation sequencing, and bioinformatics analysis are in the Supplemental Experimental Procedures. ChIPseq BED files and raw data files are available at http://www.ncbi.nlm.nih.gov/geo/ under the accession number GSE36348.

Flow Cytometry

FACS analyses were performed using an LSR Model II flow cytometer (BD Biosciences, Oxford, UK). Cell sorting experiments were performed using either an Influx or a FACS Aria flow cytometer (both from BD Biosciences).

Mice and Murine Experiments

Experiments were approved by the Paterson Institute's Animal Ethics Committee and performed under a project license issued by the United Kingdom Home Office, in keeping with the Home Office Animal Scientific Procedures Act, 1986. C57BL/6 ($CD45.2^+$) mice were purchased from Harlan (Shardlow, UK). B6.SJL-*Ptprc*^{a} *Pepc*^{b}/BoyJ ($CD45.1^+$) and NOD.Cg-*Prkdc*^{scid} *Il2rg*^{tm1Wjl}/SzJ mice were purchased from Jackson Laboratories (Bar Harbor, ME, USA) and bred in house. Details of experimental initiation of murine MLL-AF9 leukemia (both primary and secondary), lentiviral infection of cryopreserved AML cells, and clonogenic assays of normal and leukemic cells are in the Supplemental Experimental Procedures.

Human Tissue and Experiments

Use of human tissue was in compliance with the ethical and legal framework of the Human Tissue Act, 2004. Normal human $CD34^+$ mobilized HSPCs surplus to requirements were from patients undergoing chemotherapy and autologous transplantation for lymphoma and myeloma. Their use was authorized by the Salford and Trafford Research Ethics Committee and, where possible, following the written informed consent of donors. Primary human AML blasts were from Manchester Cancer Research Centre's Tissue Biobank (instituted with approval of the South Manchester Research Ethics Committee); their use was authorized following ethical review by the Tissue Biobank's scientific sub-committee. Written informed consent was obtained for all samples donated to the Biobank. Details of lentiviral infection protocols and clonogenic assays are in the Supplemental Experimental Procedures.

RNA Extraction, Quantitative PCR, Microarray Hybridization, and Data Analysis

Details are in the Supplemental Experimental Procedures. Exon array CEL files are available at http://www.ncbi.nlm.nih.gov/geo/ under the accession number GSE36348.

SUPPLEMENTAL INFORMATION

Supplemental Information includes five figures, Supplemental Experimental Procedures, and seven tables and can be found with this article online at doi:10.1016/j.ccr.2012.03.014.

ACKNOWLEDGMENTS

We thank Mark Wappett, Morgan Blaylock, Jeff Barry, Michael Hughes, Helen Small, Gail Bruder, Angela Cleworth, Angela Cooke, Yvonne Hey, Stuart Pepper, Jodie Whitaker, and Gillian Newton for technical support, as well as Nullin Divecha, Valerie Kouskoff, and Georges Lacaud for a critical reading of the manuscript. This work was supported by Cancer Research UK (grant numbers C480/A12328 and C480/A11411). B.F.G. was supported by a Leukaemia and Lymphoma Research Clinical Training Fellowship.

Received: October 24, 2011
Revised: January 30, 2012
Accepted: March 8, 2012
Published online: March 29, 2012

REFERENCES

Ben-Porath, I., Thomson, M.W., Carey, V.J., Ge, R., Bell, G.W., Regev, A., and Weinberg, R.A. (2008). An embryonic stem cell-like gene expression signature in poorly differentiated aggressive human tumors. Nat. Genet. *40*, 499–507.

Bernt, K.M., Zhu, N., Sinha, A.U., Vempati, S., Faber, J., Krivtsov, A.V., Feng, Z., Punt, N., Daigle, A., Bullinger, L., et al. (2011). MLL-rearranged leukemia is dependent on aberrant H3K79 methylation by DOT1L. Cancer Cell *20*, 66–78.

Biswas, D., Milne, T.A., Basrur, V., Kim, J., Elenitoba-Johnson, K.S., Allis, C.D., and Roeder, R.G. (2011). Function of leukemogenic mixed lineage leukemia 1 (MLL) fusion proteins through distinct partner protein complexes. Proc. Natl. Acad. Sci. USA *108*, 15751–15756.

Boyer, L.A., Plath, K., Zeitlinger, J., Brambrink, T., Medeiros, L.A., Lee, T.I., Levine, S.S., Wernig, M., Tajonar, A., Ray, M.K., et al. (2006). Polycomb complexes repress developmental regulators in murine embryonic stem cells. Nature *441*, 349–353.

Dawson, M.A., Prinjha, R.K., Dittmann, A., Giotopoulos, G., Bantscheff, M., Chan, W.I., Robson, S.C., Chung, C.W., Hopf, C., Savitski, M.M., et al. (2011). Inhibition of BET recruitment to chromatin as an effective treatment for MLL-fusion leukaemia. Nature *478*, 529–533.

Ernst, J., Kheradpour, P., Mikkelsen, T.S., Shoresh, N., Ward, L.D., Epstein, C.B., Zhang, X., Wang, L., Issner, R., Coyne, M., et al. (2011). Mapping and analysis of chromatin state dynamics in nine human cell types. Nature *473*, 43–49.

Fathi, A.T., and Abdel-Wahab, O. (2012). Mutations in epigenetic modifiers in myeloid malignancies and the prospect of novel epigenetic-targeted therapy. Adv. Hematol. *2012*, 469592.

Fenaux, P., Mufti, G.J., Hellstrom-Lindberg, E., Santini, V., Finelli, C., Giagounidis, A., Schoch, R., Gattermann, N., Sanz, G., List, A., et al; International Vidaza High-Risk MDS Survival Study Group. (2009). Efficacy of azacitidine compared with that of conventional care regimens in the treatment of higher-risk myelodysplastic syndromes: a randomised, open-label, phase III study. Lancet Oncol. *10*, 223–232.

Garcia-Bassets, I., Kwon, Y.S., Telese, F., Prefontaine, G.G., Hutt, K.R., Cheng, C.S., Ju, B.G., Ohgi, K.A., Wang, J., Escoubet-Lozach, L., et al. (2007). Histone methylation-dependent mechanisms impose ligand dependency for gene activation by nuclear receptors. Cell *128*, 505–518.

Goardon, N., Marchi, E., Atzberger, A., Quek, L., Schuh, A., Soneji, S., Woll, P., Mead, A., Alford, K.A., Rout, R., et al. (2011). Coexistence of LMPP-like and

GMP-like leukemia stem cells in acute myeloid leukemia. Cancer Cell *19*, 138–152.

Guenther, M.G., Lawton, L.N., Rozovskaia, T., Frampton, G.M., Levine, S.S., Volkert, T.L., Croce, C.M., Nakamura, T., Canaani, E., and Young, R.A. (2008). Aberrant chromatin at genes encoding stem cell regulators in human mixed-lineage leukemia. Genes Dev. *22*, 3403–3408.

Guibourt, N. July 2010. Phenylcyclopropylamine derivatives and their medical use. International Patent, WO2010/084160.

Hou, H., and Yu, H. (2010). Structural insights into histone lysine demethylation. Curr. Opin. Struct. Biol. *20*, 739–748.

Hu, X., Li, X., Valverde, K., Fu, X., Noguchi, C., Qiu, Y., and Huang, S. (2009). LSD1-mediated epigenetic modification is required for TAL1 function and hematopoiesis. Proc. Natl. Acad. Sci. USA *106*, 10141–10146.

Huang, Y., Vasilatos, S.N., Boric, L., Shaw, P.G., and Davidson, N.E. (2012). Inhibitors of histone demethylation and histone deacetylation cooperate in regulating gene expression and inhibiting growth in human breast cancer cells. Breast Cancer Res. Treat. *131*, 777–789.

Kahl, P., Gullotti, L., Heukamp, L.C., Wolf, S., Friedrichs, N., Vorreuther, R., Solleder, G., Bastian, P.J., Ellinger, J., Metzger, E., et al. (2006). Androgen receptor coactivators lysine-specific histone demethylase 1 and four and a half LIM domain protein 2 predict risk of prostate cancer recurrence. Cancer Res. *66*, 11341–11347.

Kim, J., Woo, A.J., Chu, J., Snow, J.W., Fujiwara, Y., Kim, C.G., Cantor, A.B., and Orkin, S.H. (2010). A Myc network accounts for similarities between embryonic stem and cancer cell transcription programs. Cell *143*, 313–324.

Kim, T., and Buratowski, S. (2009). Dimethylation of H3K4 by Set1 recruits the Set3 histone deacetylase complex to 5′ transcribed regions. Cell *137*, 259–272.

Krivtsov, A.V., Twomey, D., Feng, Z., Stubbs, M.C., Wang, Y., Faber, J., Levine, J.E., Wang, J., Hahn, W.C., Gilliland, D.G., et al. (2006). Transformation from committed progenitor to leukaemia stem cell initiated by MLL-AF9. Nature *442*, 818–822.

Lee, M.G., Wynder, C., Cooch, N., and Shiekhattar, R. (2005). An essential role for CoREST in nucleosomal histone 3 lysine 4 demethylation. Nature *437*, 432–435.

Lee, T.I., Jenner, R.G., Boyer, L.A., Guenther, M.G., Levine, S.S., Kumar, R.M., Chevalier, B., Johnstone, S.E., Cole, M.F., Isono, K., et al. (2006). Control of developmental regulators by Polycomb in human embryonic stem cells. Cell *125*, 301–313.

Lim, S., Janzer, A., Becker, A., Zimmer, A., Schüle, R., Buettner, R., and Kirfel, J. (2010). Lysine-specific demethylase 1 (LSD1) is highly expressed in ER-negative breast cancers and a biomarker predicting aggressive biology. Carcinogenesis *31*, 512–520.

Lin, C., Smith, E.R., Takahashi, H., Lai, K.C., Martin-Brown, S., Florens, L., Washburn, M.P., Conaway, J.W., Conaway, R.C., and Shilatifard, A. (2010). AFF4, a component of the ELL/P-TEFb elongation complex and a shared subunit of MLL chimeras, can link transcription elongation to leukemia. Mol. Cell *37*, 429–437.

Metzger, E., Wissmann, M., Yin, N., Müller, J.M., Schneider, R., Peters, A.H., Günther, T., Buettner, R., and Schüle, R. (2005). LSD1 demethylates repressive histone marks to promote androgen-receptor-dependent transcription. Nature *437*, 436–439.

Muntean, A.G., Tan, J., Sitwala, K., Huang, Y., Bronstein, J., Connelly, J.A., Basrur, V., Elenitoba-Johnson, K.S., and Hess, J.L. (2010). The PAF complex synergizes with MLL fusion proteins at HOX loci to promote leukemogenesis. Cancer Cell *17*, 609–621.

Nakamura, T., Mori, T., Tada, S., Krajewski, W., Rozovskaia, T., Wassell, R., Dubois, G., Mazo, A., Croce, C.M., and Canaani, E. (2002). ALL-1 is a histone methyltransferase that assembles a supercomplex of proteins involved in transcriptional regulation. Mol. Cell *10*, 1119–1128.

Ram, O., Goren, A., Amit, I., Shoresh, N., Yosef, N., Ernst, J., Kellis, M., Gymrek, M., Issner, R., Coyne, M., et al. (2011). Combinatorial patterning of chromatin regulators uncovered by genome-wide location analysis in human cells. Cell *147*, 1628–1639.

Saleque, S., Kim, J., Rooke, H.M., and Orkin, S.H. (2007). Epigenetic regulation of hematopoietic differentiation by Gfi-1 and Gfi-1b is mediated by the cofactors CoREST and LSD1. Mol. Cell *27*, 562–572.

Sanz, M.A., and Lo-Coco, F. (2011). Modern approaches to treating acute promyelocytic leukemia. J. Clin. Oncol. *29*, 495–503.

Schulte, J.H., Lim, S., Schramm, A., Friedrichs, N., Koster, J., Versteeg, R., Ora, I., Pajtler, K., Klein-Hitpass, L., Kuhfittig-Kulle, S., et al. (2009). Lysine-specific demethylase 1 is strongly expressed in poorly differentiated neuroblastoma: implications for therapy. Cancer Res. *69*, 2065–2071.

Shi, Y., Lan, F., Matson, C., Mulligan, P., Whetstine, J.R., Cole, P.A., Casero, R.A., and Shi, Y. (2004). Histone demethylation mediated by the nuclear amine oxidase homolog LSD1. Cell *119*, 941–953.

Singh, M.M., Manton, C.A., Bhat, K.P., Tsai, W.W., Aldape, K., Barton, M.C., and Chandra, J. (2011). Inhibition of LSD1 sensitizes glioblastoma cells to histone deacetylase inhibitors. Neuro-oncol. *13*, 894–903.

Somervaille, T.C., and Cleary, M.L. (2006). Identification and characterization of leukemia stem cells in murine MLL-AF9 acute myeloid leukemia. Cancer Cell *10*, 257–268.

Somervaille, T.C., Matheny, C.J., Spencer, G.J., Iwasaki, M., Rinn, J.L., Witten, D.M., Chang, H.Y., Shurtleff, S.A., Downing, J.R., and Cleary, M.L. (2009). Hierarchical maintenance of MLL myeloid leukemia stem cells employs a transcriptional program shared with embryonic rather than adult stem cells. Cell Stem Cell *4*, 129–140.

Subramanian, A., Tamayo, P., Mootha, V.K., Mukherjee, S., Ebert, B.L., Gillette, M.A., Paulovich, A., Pomeroy, S.L., Golub, T.R., Lander, E.S., and Mesirov, J.P. (2005). Gene set enrichment analysis: a knowledge-based approach for interpreting genome-wide expression profiles. Proc. Natl. Acad. Sci. USA *102*, 15545–15550.

Wang, J., Scully, K., Zhu, X., Cai, L., Zhang, J., Prefontaine, G.G., Krones, A., Ohgi, K.A., Zhu, P., Garcia-Bassets, I., et al. (2007). Opposing LSD1 complexes function in developmental gene activation and repression programmes. Nature *446*, 882–887.

Yokoyama, A., Lin, M., Naresh, A., Kitabayashi, I., and Cleary, M.L. (2010). A higher-order complex containing AF4 and ENL family proteins with P-TEFb facilitates oncogenic and physiologic MLL-dependent transcription. Cancer Cell *17*, 198–212.

Zuber, J., Rappaport, A.R., Luo, W., Wang, E., Chen, C., Vaseva, A.V., Shi, J., Weissmueller, S., Fellmann, C., Taylor, M.J., et al. (2011a). An integrated approach to dissecting oncogene addiction implicates a Myb-coordinated self-renewal program as essential for leukemia maintenance. Genes Dev. *25*, 1628–1640.

Zuber, J., Shi, J., Wang, E., Rappaport, A.R., Herrmann, H., Sison, E.A., Magoon, D., Qi, J., Blatt, K., Wunderlich, M., et al. (2011b). RNAi screen identifies Brd4 as a therapeutic target in acute myeloid leukaemia. Nature *478*, 524–528.

Cancer Cell
Special Collection
10 YEARS OF EXCITING CANCER RESEARCH SINCE 2002

Cancer Stem Cells: Impact, Heterogeneity, and Uncertainty

Jeffrey A. Magee,[1] Elena Piskounova,[1] and Sean J. Morrison[1,*]
[1]Howard Hughes Medical Institute, Children's Research Institute, and Department of Pediatrics, University of Texas Southwestern Medical Center, Dallas, TX, 75390, USA
*Correspondence: sean.morrison@utsouthwestern.edu
DOI 10.1016/j.ccr.2012.03.003

The differentiation of tumorigenic cancer stem cells into nontumorigenic cancer cells confers heterogeneity to some cancers beyond that explained by clonal evolution or environmental differences. In such cancers, functional differences between tumorigenic and nontumorigenic cells influence response to therapy and prognosis. However, it remains uncertain whether the model applies to many, or few, cancers due to questions about the robustness of cancer stem cell markers and the extent to which existing assays underestimate the frequency of tumorigenic cells. In cancers with rapid genetic change, reversible changes in cell states, or biological variability among patients, the stem cell model may not be readily testable.

Sources of Heterogeneity within Cancer

Many tumors contain phenotypically and functionally heterogeneous cancer cells (Fidler and Hart, 1982; Fidler and Kripke, 1977; Heppner, 1984; Nowell, 1986). This heterogeneity among cancer cells in the same patient can arise in multiple ways. The most well-established mechanism involves intrinsic differences among cancer cells caused by stochastic genetic (Nowell, 1976) or epigenetic (Baylin and Jones, 2011) changes (clonal evolution; Figure 1A). Differences can also arise among cancer cells through extrinsic mechanisms in which different microenvironments within a tumor confer phenotypic and functional differences upon cancer cells in different locations (Figure 1B) (Polyak et al., 2009; Bissell and Hines, 2011). Finally, some cancers follow a stem cell model in which tumorigenic cancer stem cells "differentiate" into nontumorigenic cancer cells, creating a hierarchical organization (Figure 1C; Table 1) (Dick, 2008; Reya et al., 2001; Shackleton et al., 2009). The differentiation of cancer stem cells provides a mechanism for generating phenotypic and functional heterogeneity beyond the heterogeneity that can be attributed to clonal evolution or environmental differences (Figure 1D). However, the fact that heterogeneity can arise through multiple mechanisms means that heterogeneity alone does not imply the existence of a cancer stem cell hierarchy.

The Cancer Stem Cell Model

The cancer stem cell model is not a new idea (Hamburger and Salmon, 1977). It has been clear for decades that some cancers, including some germ lineage cancers (Kleinsmith and Pierce, 1964), some neuroblastomas (Shimada et al., 1984), and some myeloid leukemias (Fearon et al., 1986; Ogawa et al., 1970), can differentiate into progeny that have limited proliferative potential despite retaining the oncogenic mutations of their malignant progenitors.

Some germ lineage cancers contain rapidly dividing cells that differentiate into postmitotic derivatives (mature teratoma elements) in a process that resembles aberrant embryogenesis (Chaganti and Houldsworth, 2000). The presence of only mature differentiated cells in residual tumor masses after chemotherapy is a favorable prognostic factor, while the presence of residual undifferentiated cells predicts disease recurrence (Stenning et al., 1998). These and other data suggest that undifferentiated cells are primarily responsible for tumor growth and disease progression, consistent with the cancer stem cell model.

Neuroblastomas also exhibit variable degrees of differentiation (Ambros et al., 2002; Shimada et al., 1999a, 1999b, 1984). Neuroblastomas with widespread differentiation have a better prognosis than those with limited differentiation (Shimada et al., 1999b). Highly differentiated neuroblastic tumors are typically focal and can often be cured with surgery (Nitschke et al., 1988). Conversely, poorly differentiated neuroblastomas are often widely disseminated and are usually fatal despite aggressive treatment (Matthay et al., 2009, 1999; Shimada et al., 1999b). Therapies that promote differentiation significantly improve survival (Matthay et al., 2009, 1999). In some infants, disseminated tumors undergo spontaneous differentiation, leading to a favorable outcome even without therapy (Baker et al., 2010). While staging of neuroblastoma is complex and involves a number of variables other than differentiation status, these clinical observations are consistent with the cancer stem cell model in suggesting that undifferentiated neuroblastoma cells sometimes drive disease progression.

While the overt differentiation in some germ lineage cancers and some neuroblastomas provided clinical evidence consistent with the cancer stem cell model, these rare and unusual malignancies are of uncertain relevance to more prevalent adult cancers. Thus, the cancer stem cell model gained increased attention when evidence emerged supporting the model in leukemia and breast cancer. The advent of flow cytometry made it possible to separate phenotypically distinct subpopulations of live cancer cells to compare their tumorigenic potential. Using this approach, some human acute myeloid leukemias (AMLs) (Bonnet and Dick, 1997; Lapidot et al., 1994) and breast cancers (Al-Hajj et al., 2003) were found to follow the cancer stem cell model, suggesting that a broad spectrum of cancers might be hierarchically organized into tumorigenic and nontumorigenic components. In each of these studies, cells capable of forming leukemias/tumors were rare when transplanted into immunocompromised mice but could be enriched by selecting

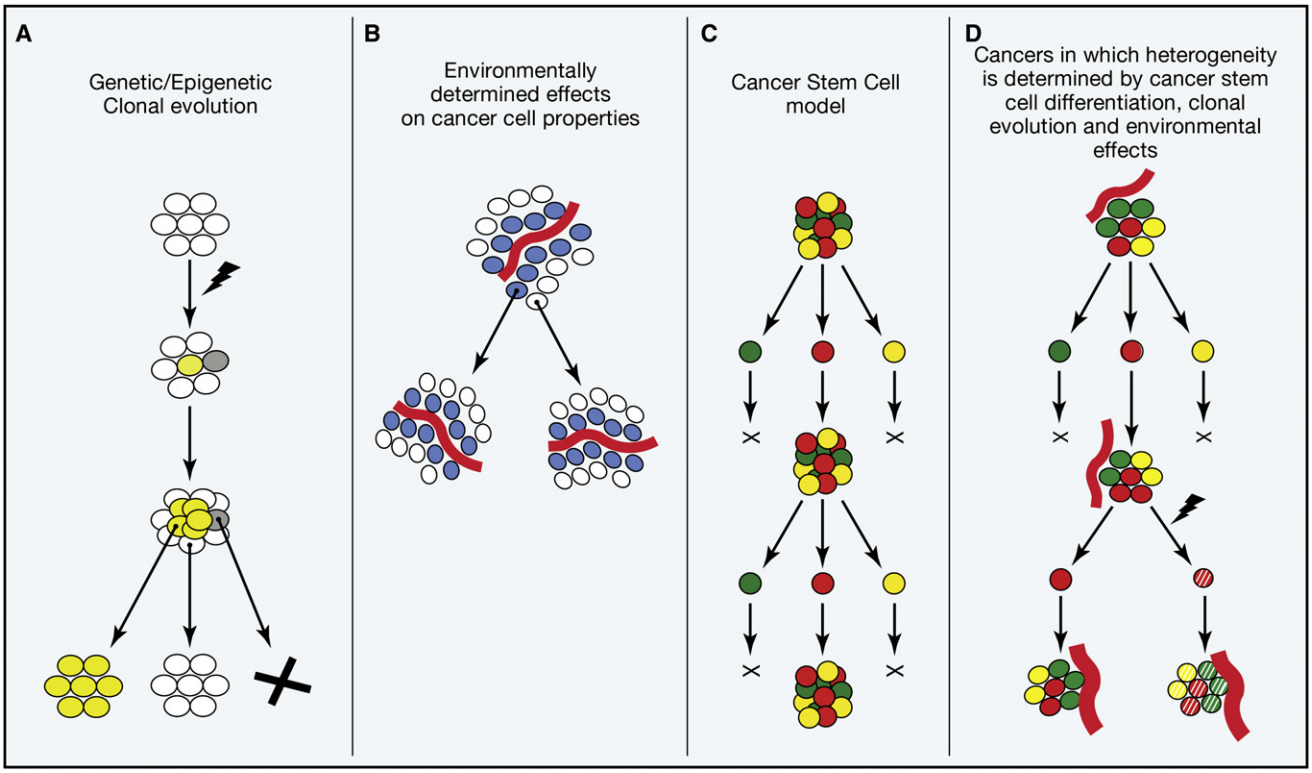

Figure 1. Sources of Heterogeneity within Cancer

(A) Heterogeneity can arise within tumors through stochastic genetic (Nowell, 1976) and epigenetic (Baylin and Jones, 2011) changes that confer heritable phenotypic and functional differences upon cancer cells. This process is known as clonal evolution because the genetic/epigenetic changes are subject to selection within tumors. This process tends to lead to more aggressive cancers over time; however, some cancer cells (gray) would be predicted to lose their tumorigenic capacity as a consequence of disadvantageous genetic changes.

(B) Heterogeneity can arise in response to extrinsic environmental differences within tumors: cancer cells (blue) adjacent to blood vessels (red) are different from cancer cells further from blood vessels (white) (Charles et al., 2010). The differences are shown as being reversible, though environmental differences could also cause irreversible changes in cancer cell properties.

(C) Cancers that follow the stem cell model contain intrinsically different subpopulations of tumorigenic (red) and nontumorigenic cells (yellow and green) organized in a hierarchy in which a minority population of tumorigenic cells gives rise to phenotypically diverse nontumorigenic cells. Nontumorigenic cells are thought to compose the bulk of tumors but have little capacity to contribute to cancer progression (Dick, 2008; Reya et al., 2001; Shackleton et al., 2009). Tumorigenic cells can be serially transplanted, re-establishing phenotypic heterogeneity with each passage.

(D) Cancers that follow the stem cell model are also subject to clonal evolution as well as heterogeneity from environmental differences within tumors. Thus, these sources of heterogeneity are not mutually exclusive and may each apply to variable extents depending on the cancer.

cells that expressed specific combinations of surface markers: leukemia-initiating cells were $CD34^{+}CD38^{-}$ (Bonnet and Dick, 1997; Lapidot et al., 1994) while breast cancer-initiating cells were $CD44^{+}CD24^{-/low}$ (Al-Hajj et al., 2003). This suggested that in some cancers only a small minority of cells can proliferate extensively and that some therapies that shrink tumors might not be curative because they fail to eliminate cancer stem cells.

Since these studies were published, other studies have taken similar approaches to provide evidence that other human cancers also follow the cancer stem cell model, including colon cancer (Dalerba et al., 2007; O'Brien et al., 2007; Ricci-Vitiani et al., 2007), pancreatic cancer (Li et al., 2007), brain tumors (Bao et al., 2006; Piccirillo et al., 2006; Singh et al., 2004) and ovarian cancer (Alvero et al., 2009; Curley et al., 2009; Stewart et al., 2011; Zhang et al., 2008b). In each case, the capacity to propagate the malignancy appeared to be restricted to a small, phenotypically distinct subpopulation of cancer cells. In tumorigenesis assays, many unfractionated cells had to be transplanted in order to transfer disease, suggesting that tumorigenic cells were rare. These studies suggested that many cancers follow the stem cell model and might be more effectively treated by targeting cancer stem cells.

Sources of Heterogeneity among Cancers

Despite these studies, the generalizability of the model remained uncertain. Does the model apply to all cancers, or only some? Do all AMLs and breast cancers follow the cancer stem cell model, or only in certain patients? Differences among cancers in driver mutations and in the cell-of-origin create great diversity in cancer biology. Sometimes these differences are reflected in the histopathology of the cancer, but in other cases they may influence the underlying biology without recognized effects on histopathology. Nonetheless, these sources of heterogeneity complicate the testing of the cancer stem cell model and mean that observations in a cancer from one patient may be true of cancers in certain other patients, but not all patients.

Some cancers, including hierarchically organized cancers that follow the stem cell model, can arise from normal stem cells

Table 1. Testing the Cancer Stem Cell Model

Properties of Cancers That Follow the Stem Cell Model	
	Experimental Evidence
Phenotypic and functional heterogeneity	Flow cytometry distinguishes phenotypically distinct subpopulations of cancer cells that are transplanted to test whether some are tumorigenic while others are nontumorigenic.
Hierarchical organization	Cancer stem cells are tumorigenic cells that give rise to a hierarchy of tumorigenic and nontumorigenic progeny. Upon transplantation, tumorigenic cells should give rise to more tumorigenic cells as well as phenotypically distinct nontumorigenic cells.
Properties Sometimes Ascribed to Cancer Stem Cells but Not Required by the Model	
	Experimental Evidence
Therapy resistance	Are tumorigenic cells more likely to survive therapy than nontumorigenic cells? Are tumorigenic cells enriched by therapy?
Rarity	Tumorigenic cells have been rare in many studies that supported the cancer stem cell model but, in principle, such cells do not have to be rare in a hierarchically organized cancer.
Quiescence	While cancer stem cells are sometimes claimed to be quiescent, little data support this assertion and the cell cycle distribution of most cancer stem cells is unknown.
Asymmetric division	Cancer stem cells are sometimes claimed to divide asymmetrically, but this has never been demonstrated in vivo and cannot be an obligate property because it would prevent the numerical expansion of cancer stem cells.
Derive from normal stem cells	Experimentally, cancer stem cells can arise from either normal stem cells or from restricted progenitors/differentiated cells. In practice, the cell-of-origin of most cancers is unknown.

through mutations that overactivate self-renewal mechanisms (Barker et al., 2009; Merlos-Suárez et al., 2011; Yang et al., 2008). Other cancers, including hierarchically organized cancers, can arise from restricted progenitors or differentiated cells as a result of mutations that ectopically activate self-renewal mechanisms in these cells (Figure 2A) (Cozzio et al., 2003; Huntly et al., 2004; Krivtsov et al., 2006; Schüller et al., 2008; Yang et al., 2008; Zhao et al., 2010). Thus, hierarchical organization in a cancer does not imply that it originated from normal stem cells, and the cancer stem cell model does not address the cell-of-origin (Wang and Dick, 2005). However, the cell-of-origin can influence the hierarchical organization of cancers as it influences the mutations that are competent to transform (Wang et al., 2010). The interaction of driver mutations with cellular context influences the frequency of leukemogenic cells and perhaps the degree of hierarchical organization (Heuser et al., 2009; Somervaille et al., 2009). Nonetheless, these inferences are all based upon experimentally induced cancers. The cell-of-origin for most cancers that spontaneously arise in patients has not been identified, at least not with precision, making it difficult to assess which biological differences among human cancers reflect differences in cell-of-origin.

Spatial differences in the cell-of-origin can also influence cancer properties. In some tissues, regional differences in cellular properties influence the driver mutations that are competent to transform. Medulloblastomas can arise either from Sonic Hedgehog pathway activation in granule neuron precursors of the cerebellum or from Wnt pathway activation in dorsal brainstem progenitors (Gibson et al., 2010; Schüller et al., 2008; Yang et al., 2008) (Figure 2B). Medulloblastomas are hierarchically organized, consistent with the cancer stem cell model (Read et al., 2009; Singh et al., 2004; Ward et al., 2009), so it is likely that the regional identity of the cell-of-origin influences cancer stem cell properties, though this has not yet been tested. Ependymomas that arise from different regions of the central nervous system have different mutations, different patterns of gene expression, and different prognoses (Johnson et al., 2010; Taylor et al., 2005). Because ependymomas appear to arise from radial glia and are hierarchically organized into tumorigenic and nontumorigenic components (Taylor et al., 2005), these results suggest that regional differences in radial glia lead to regional differences in driver mutations and cancer stem cell properties.

Temporal differences in the cell-of-origin also affect the properties of leukemogenic cells. Stem cell properties and self-renewal mechanisms change with age (He et al., 2009; Levi and Morrison, 2008). This likely alters the types of mutations that are competent to initiate cancers. Consistent with this, the mutation spectrum changes with age in human leukemias. Some driver mutations are found primarily in older patients (e.g., in FLT3, Nucleophosmin1, and Dnmt3a), whereas other mutations occur throughout life (e.g., in Ras) or more commonly in young patients (e.g., translocations involving AML1, MLL, and NUP98) (Figure 2C) (Armstrong and Look, 2005; Berman et al., 2011; Brown et al., 2007; Downing and Shannon, 2002; Falini et al., 2005; Ho et al., 2011; Kiyoi et al., 1999; Kottaridis et al., 2001; Ley et al., 2010; Meshinchi et al., 2001; Stirewalt et al., 2001; Thiede et al., 2006; Vogelstein et al., 1990; Zwaan et al., 2003). Because many AMLs are hierarchically organized (Lapidot et al., 1994; Yilmaz et al., 2006) and driver mutations influence the frequency of leukemogenic cells (Heuser et al., 2009; Somervaille et al., 2009), temporal changes in the cell-of-origin likely influence cancer stem cell properties.

Heterogeneity among Patients in Cancer Stem Cell Phenotype

Differences in driver mutations and cell-of-origin among patients raise the question of whether similar hierarchies of tumorigenic and nontumorigenic cells, with similar markers, are conserved among patients with similar cancers. Initial studies suggested that AMLs in many patients adopted a similar hierarchical organization in which rare leukemogenic cells were distinguished

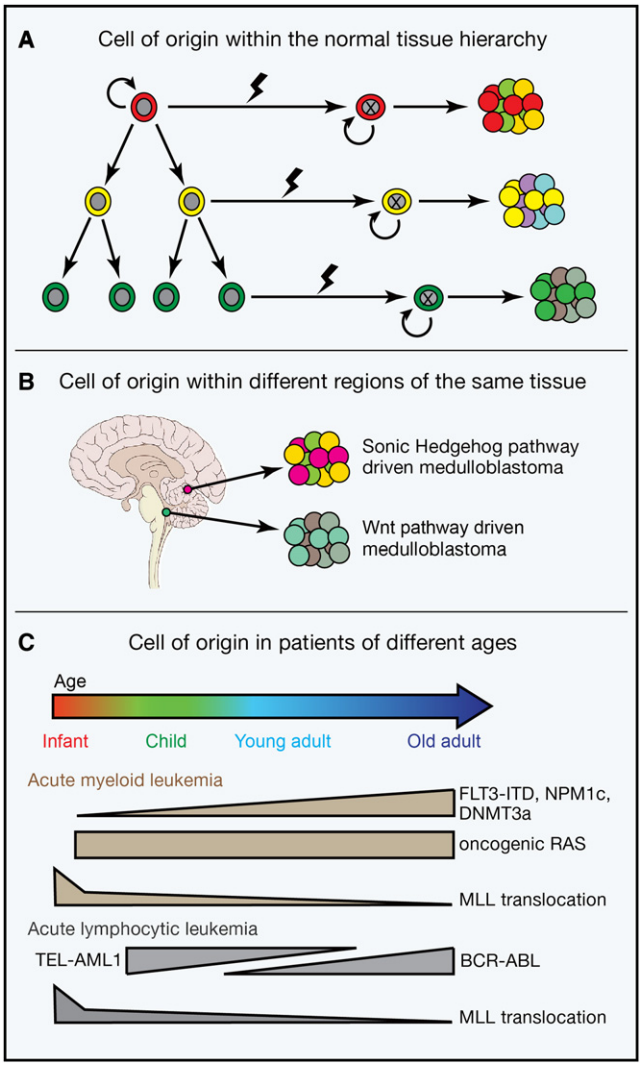

Figure 2. Sources of Heterogeneity among Cancers

Differences in the cell-of-origin can directly and indirectly influence the phenotype of tumorigenic cells and, perhaps, whether or not the cancer is hierarchically organized.

(A) Different cell types in a stem/progenitor cell hierarchy within a normal tissue may be transformed into cancer cells. The properties of the cell-of-origin influence the types of mutations that are competent to transform and the properties of the resulting cancer (Huntly et al., 2004; Wang et al., 2010).

(B) Spatial differences in the identity of the cell-of-origin within tissues influence the types of mutations that are competent to transform and the properties of the resulting cancer (Gibson et al., 2010; Johnson et al., 2010).

(C) Temporal differences in the cell-of-origin also influence the types of mutations that are competent to transform and the properties of the resulting cancer (J.A.M. and S.J.M., unpublished data), consistent with the observation that the driver mutation spectrum changes with age in patients (Downing and Shannon, 2002) (see text for references regarding age-related changes in the incidence of specific mutations).

from nonleukemogenic progeny by having a $CD34^+CD38^-$ surface marker phenotype, largely irrespective of AML subtype or blast cell maturation state (Bonnet and Dick, 1997; Lapidot et al., 1994). Many studies from other laboratories went on to characterize "leukemic stem cell" properties, such as gene expression signatures, by isolating $CD34^+CD38^-$ cells without verifying that these markers distinguished leukemogenic from nonleukemogenic cells in the patients they studied.

It was subsequently determined that there are leukemia-initiating cells among $CD34^-$ and $CD38^+$ cells in some AMLs (Sarry et al., 2011; Taussig et al., 2008, 2010). Dick and colleagues systematically addressed this issue by comparing the leukemogenic capacity of $CD34^+CD38^-$, $CD34^+CD38^+$, $CD34^-CD38^+$, and $CD34^-CD38^-$ AML cells from 16 patients (Eppert et al., 2011). In the 13 AMLs that engrafted, there was leukemogenic activity in the $CD34^+CD38^-$ fraction; however, leukemogenic cells were also detected in at least one other fraction in most patients. Most leukemogenic cells were contained in the $CD34^+CD38^-$ fraction in half of the patients and in the $CD34^+CD38^+$ fraction in the other half of patients. In one case, there were similar frequencies of leukemogenic cells in all fractions, and a second case had leukemogenic cells in 3 of 4 fractions. Leukemogenic activity is therefore not usually restricted to the $CD34^+CD38^-$ fraction and there is heterogeneity among patients in leukemogenic cell phenotype (Figure 3). Some AMLs might not follow the cancer stem cell model at all.

The frequency and phenotype of leukemogenic cells is also highly variable in mouse AMLs. Deletion of *Pten* from adult mouse hematopoietic cells leads to the development of AML upon transplantation into wild-type mice (Yilmaz et al., 2006). In these AMLs, leukemogenic activity is most highly enriched among rare cells with a surface marker phenotype similar to normal HSCs, but cells that express mature myeloid markers possess lower levels of leukemogenic activity. Mouse AMLs induced by MLL-AF9 expression appear to have much higher frequencies of leukemogenic cells than observed after *Pten* deletion (Krivtsov et al., 2006; Somervaille and Cleary, 2006; Somervaille et al., 2009). In these leukemias, cells bearing GMP-like surface markers have the highest frequency of leukemogenic cells (Krivtsov et al., 2006); however, leukemogenic activity is also found in other cell fractions (Somervaille and Cleary, 2006; Somervaille et al., 2009). Differences in oncogenic mutations can thus have profound effects on the frequency and phenotype of leukemia-initiating cells.

The same is true in solid cancers. Tumorigenic cells are enriched within the $CD44^+CD24^{-/low}$ population of some breast cancers (Al-Hajj et al., 2003). However, other breast cancers studied by Al-Hajj et al. had more phenotypically diverse breast cancer-initiating cells, demonstrating that the $CD44^+CD24^{-/low}$ surface marker phenotype does not universally distinguish tumorigenic from nontumorigenic breast cancer cells (Al-Hajj et al., 2003). In mouse models of mammary cancer, different driver mutations give rise to cancers that differ in the extent to which they follow the stem cell model (Cho et al., 2008; Vaillant et al., 2008; Zhang et al., 2008a); for example, CD61 enriched for cancer stem cell activity in mice with Wnt1 driven breast cancers but not in mice with Neu/ErbB2 driver breast cancers (Vaillant et al., 2008). Mouse models of lung cancer with different transforming mutations have tumorigenic cells with different surface marker phenotypes (Curtis et al., 2010). Thus, different oncogenic mutations give rise to cancers that differ in the extent to which they follow the cancer stem cell model and in tumorigenic cell phenotype.

These results demonstrate the importance of testing cancer stem cell markers in significant numbers of patients to

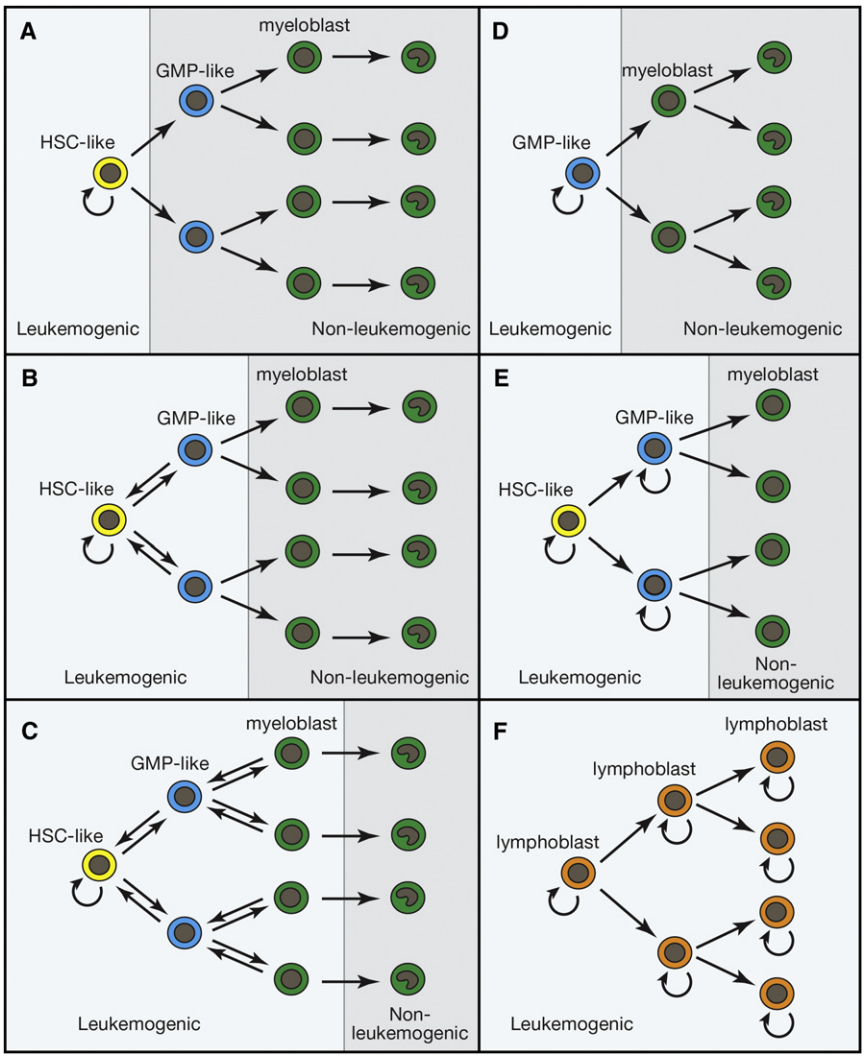

Figure 3. Variation among Leukemias in the Degree and Nature of Hierarchical Organization

Although most AMLs follow a cancer stem cell model, the surface marker phenotypes of the leukemogenic cells vary from patient to patient. (A–C) Different oncogenic mutations can transform cells at different levels within the hematopoiesis hierarchy (Wang et al., 2010), potentially influencing the frequency, spectrum, and phenotype of cells with leukemogenic potential. Interconversion between leukemogenic cell populations would allow any population to recapitulate the heterogeneity of the leukemogenic cell pool (Eppert et al., 2011; Sarry et al., 2011). (D) Some mutations, such as MLL-AF9 translocations, can confer leukemogenic activity upon restricted progenitors (Cozzio et al., 2003; Huntly et al., 2004; Krivtsov et al., 2006; Zhao et al., 2010). (E) If multiple populations have leukemogenic capacity but do not interconvert, then only the most immature cells can recapitulate the full heterogeneity of the parent leukemia, but multiple levels of the hierarchy may be able to drive disease progression (Goardon et al., 2011). (F) In some ALLs, many cells have leukemogenic activity despite heterogeneity in marker expression (le Viseur et al., 2008; Williams et al., 2007).

appreciate the heterogeneity among patients. Yet studies of cancer stem cell characteristics often assume that markers identified in one study can be applied without validation to other patients, to cell lines, or to cells transformed in culture. The conclusions in such studies may be undermined by heterogeneity among patients or by context- or oncogene-dependent effects on tumorigenic cell phenotype.

The Implications of the Cancer Stem Cell Model for Therapy

In cancers that follow the stem cell model, the functional differences between tumorigenic and nontumorigenic cells can have important implications for therapy. For example, the BCR-ABL inhibitor imatinib has been incredibly effective at restoring the health and prolonging the lives of patients with chronic myeloid leukemia (CML) (Druker et al., 2006); however, these patients must remain on imatinib indefinitely because many patients fail to completely eliminate BCR-ABL-expressing cells from their bone marrow (Bhatia et al., 2003; Chu et al., 2011) and even patients that achieve a complete molecular remission often relapse upon withdrawal of therapy (Rousselot et al., 2007).

These clinical observations appear to be explained by the persistence of rare imatinib-resistant CML stem cells (Chu et al., 2011; Graham et al., 2002; Holtz et al., 2002). A mouse model of CML-like disease driven by HIP1-PDGFR and AML1-ETO fusion proteins had leukemogenic and nonleukemogenic subpopulations of cancer cells distinguished by differences in surface marker expression (Oravecz-Wilson et al., 2009). The leukemogenic cells were rare and much more resistant to imatinib than their nonleukemogenic progeny. Imatinib treatment dramatically enriched leukemogenic cells despite reducing overall leukemia burden. Evidence has also been presented for radiation resistance in brain tumor-initiating cells (Bao et al., 2006) and breast cancer-initiating cells (Diehn et al., 2009).

While it has become fashionable to consider therapy resistance a defining feature of cancer stem cells, the sensitivity of tumorigenic and nontumorigenic cells to therapy depends upon the cancer and the therapy. Some therapies actually exploit the capacity of tumorigenic cells to differentiate into nontumorigenic cells by inducing differentiation. Acute promyelocytic leukemia is treated with arsenic trioxide and trans-retinoic acid, which induce rapid terminal differentiation, growth arrest, and apoptosis of the cancer cells (de Thé and Chen, 2010). Differentiation therapy has also been exploited experimentally in glioblastoma by treating with bone morphogenetic protein 4 (BMP4) to induce glial differentiation, reducing proliferation, tumor growth, and tumorigenic cell frequency (Piccirillo et al., 2006). BMP4 also promotes glial differentiation by normal CNS stem cells (Gross et al., 1996) suggesting tumorigenic cancer cells sometimes inherit differentiation pathways from normal

stem cells in the same tissue. Cis-retinoic acid also induces glial differentiation and improves survival in high-risk neuroblastoma patients (Matthay et al., 1999; Thiele et al., 1985). Thus, tumorigenic cells are specifically targeted by some therapies.

Therapy resistance can also arise through genetic mechanisms that are not necessarily related to cancer stem cells. While the intrinsic resistance of CML-initiating cells to imatinib allows these cells to persist in treated patients who are in remission, the ongoing administration of imatinib generally prevents relapse until the CML-initiating cells acquire an amplification of BCR-ABL or point mutations that confer imatinib resistance (Gorre et al., 2001; Roumiantsev et al., 2002). Melanomas carrying V600E BRAF mutations become resistant to the BRAF inhibitor vemurafenib through a variety of genetic mechanisms (Johannessen et al., 2010; Nazarian et al., 2010; Poulikakos et al., 2011; Poulikakos and Rosen, 2011; Villanueva et al., 2010), and we are unable to find any evidence that melanoma follows a cancer stem cell model (Quintana et al., 2010; Quintana et al., 2008). Therefore, cancer progression and therapy resistance may be influenced by the properties of cancers stem cells in cancers that follow the model, but therapy resistance and disease progression can also arise through genetic changes unrelated to the question of whether a cancer follows the stem cell model.

Tumorigenesis Assays

The xenotransplantation of human cancer cells into mice differs in a number of important respects from the growth of human cancer cells in patients. Mouse tissues differ from human tissues in terms of architecture and stromal cells (Kuperwasser et al., 2004). Mouse growth factors and adhesion molecules sometimes do not bind human receptors (Manz, 2007). Autologous immune cells are an important element of the tumor microenvironment as they can either promote or impair tumor growth (de Visser et al., 2006). Yet there are profound differences in immune regulation between the autologous and xenogeneic settings. Human cells transplanted into mice are subject to powerful xenogeneic immune responses that kill most human cells before they have an opportunity to proliferate (Auchincloss and Sachs, 1989). That is why human cancer cells must be transplanted into highly immunocompromised mice to assay tumorigenic capacity. Even NOD/SCID mice retain an attenuated xenogeneic barrier. Transplantation into more highly immunocompromised mice (such as NOD/SCID IL2Rγ^{null}) can significantly increase the frequency of tumorigenic cells that is detected in some, but not all, human cancers (Ishizawa et al., 2010; Kennedy et al., 2007; Quintana et al., 2008).

Some have speculated that less immunocompromised mice may represent ''better models'' for studying human cancers because the preservation of some immune activity makes these mice more similar to patients. However, the mechanisms by which mouse immune cells respond to transplanted human cells bear little resemblance to the mechanisms by which human immune cells sometimes respond to autologous cancer cells (Auchincloss and Sachs, 1989). No xenotransplantation assay can model the immune responses that sometimes occur in patients against their own tumors. Normal human hematopoietic stem cells (HSCs) and cancer-initiating cells are therefore more likely to be detected in more highly immunocompromised mice: NOD/SCID mice treated with anti-CD122 antibody to deplete NK cells or NOD/SCID IL2Rγ^{null} mice (Eppert et al., 2011; McDermott et al., 2010; Quintana et al., 2008).

It is also critical to recognize that transplantation assays, particularly xenotransplantation assays, test the potential of cells to form tumors, not their actual fate in the tumor in which they are born (Figure 4). There are many environmental variables in the tumor environment, such as hypoxia and immune responses, which can prevent cells that have the potential to form a tumor from actually doing so in their normal environment. Consequently, nobody knows whether many, or few, cells with tumorigenic potential actually contribute to disease progression in patients. The question of which cells are actually fated to contribute to disease progression is highly context dependent and is probably not testable in patients because of the experimental manipulations that would be required; however, this is testable by fate mapping of cells in mouse tumors. It will be interesting to compare the results of side-by-side fate-mapping experiments and transplantation assays to assess whether the cells that have the potential to form tumors upon transplantation are the same cells that drive disease progression in situ.

Tumorigenic Cells Are Abundant in Some Cancers

Not all hematopoietic malignancies contain rare cancer-initiating cells. Tumorgenic/leukemogenic cells are common in certain mouse models of B cell lymphoma, T cell lymphoma, and AML in which it is possible to transfer disease to wild-type recipients by transplanting only ten cells (Kelly et al., 2007). In a mouse model of B cell acute lymphoblastic leukemia (ALL), at least 50% of cancer cells are capable of transferring disease into wild-type recipient mice (Williams et al., 2007). In these malignancies, the abundance of tumorgenic/leukemogenic cells suggests that if there is any hierarchy it must be much more shallow than observed in many human AMLs, which so far have consistently appeared to have rare leukemogenic cells (Bonnet and Dick, 1997; Lapidot et al., 1994).

Tumorigenic cells are also common in some human cancers. When human melanomas were first transplanted into NOD/SCID mice, it was estimated that only one in a million melanoma cells were capable of forming tumors, and melanoma was proposed to follow a cancer stem cell model (Schatton et al., 2008). However, simple changes in tumorigenesis assay conditions (including the use of NOD/SCID IL2Rγ^{null} mice) increased the detected frequency of tumorigenic cells to one in four (Quintana et al., 2008). We now routinely transplant single cells directly from patients into NOD/SCID IL2Rγ^{null} mice and on average 30% of single cells form tumors (Quintana et al., 2010). We have quantified the frequency of tumorigenic cells from more than 30 patients with diverse stages and sites of disease, and in every case, the frequency of tumorigenic cells has been high, even in primary cutaneous melanomas obtained directly from patients (Quintana et al., 2010). Similar results have been published with mouse models of melanoma (Held et al., 2010). Thus, xenotransplantation assays sometimes dramatically underestimate the frequency of human cancer cells with tumorigenic potential.

Is melanoma unique among solid cancers in having common tumorigenic cells? We addressed this question in mouse models of malignant peripheral nerve sheath tumors (MPNSTs)

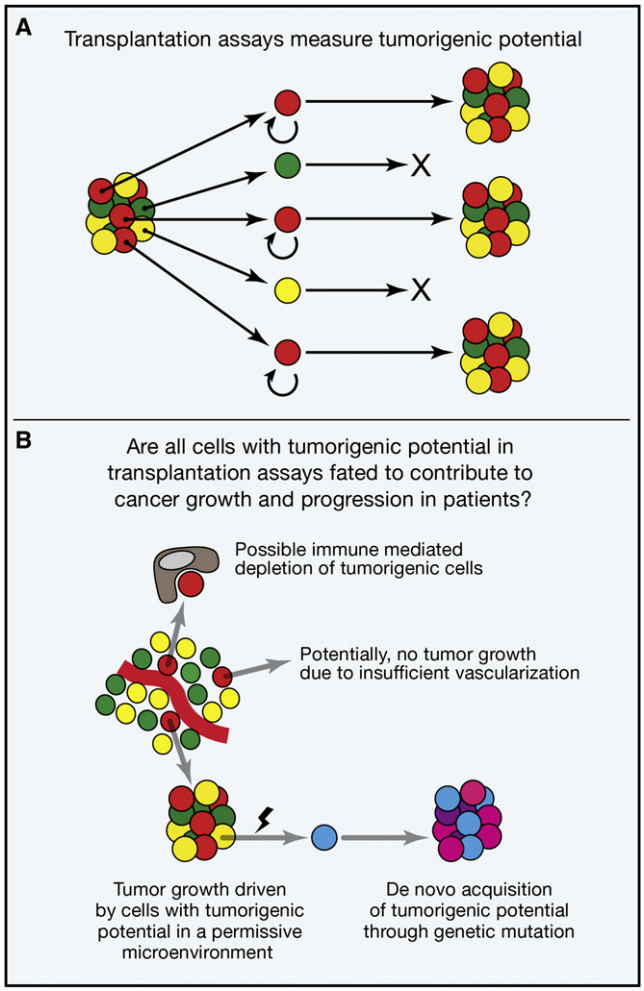

Figure 4. Fate versus Potential in Cancer

(A) Potential describes what cells can do in a permissive environment. The cancer stem cell model, and the transplantation assays (black arrows) on which it is largely based, address the potential of cancer cells to form tumors. (B) Fate reflects what cells actually do in a specific environment. In the context of cancer, the question is which cells are fated to contribute to tumor growth and disease progression in their actual environment in the patient. Many of the cells that have the potential to form tumors upon transplantation may not be fated to contribute to disease progression in a particular patient because they are not in a permissive environment. For example, some cancer cells undergo cell death due to hypoxia or immune effector activity. Some of these cells might have the potential to form a tumor if transplanted into another environment, but are fated to undergo cell death in the tumor environment in which they actually reside in the patient. There may also be cells that lack the ability to form a tumor upon transplantation but that are nonetheless fated to contribute to disease progression in the patient, such as if they acquire a new mutation that increases their proliferation. Transplantation assays only assess potential, not fate, in a patient and therefore should attempt to detect the full range of cells with the potential to form tumors. No transplantation assay mimics the environment within patient tissues and such assays are neither designed nor capable of assessing cell fate in patients. Consequently, very little is known about the spectrum of cells fated to contribute to tumor growth and disease progression in patients or the extent to which it overlaps with the spectrum of cells that can form a tumor upon transplantation.

(Buchstaller et al., 2012). We found that approximately 20% of mouse MPNST cells have the potential to form tumors, even when transplanted into fully immunocompetent mice. This suggests that tumorigenic cells may be common in a number of solid cancers, though it is important to note that we have not tested whether MPNSTs are hierarchically organized, and therefore, it is unknown whether this cancer has a shallow hierarchical organization.

An important question is whether we have systematically underestimated the frequency of tumorigenic cells by using transplantation assays that have not been optimized to detect the full range of cells with the potential to form tumors. Work on human HSCs and AML has identified numerous assay improvements that increased estimates of stem cell frequency by orders of magnitude (Eppert et al., 2011; Kennedy et al., 2007; McDermott et al., 2010; McKenzie et al., 2005; Notta et al., 2010), but assays for tumorigenic cells from solid cancers generally have not been studied to the same extent. Enzymatic dissociation conditions, sorting conditions, transplantation site, the extracellular matrix environment, and the recipient mouse (sex and strain) all affect the ability to detect tumorigenic cells. Other undiscovered assay parameters may also be important. Estimates of tumorigenic cell frequencies may continue to increase in many cancers as assays improve, though tumorigenic cells will likely remain rare in some cancers despite such improvements (Eppert et al., 2011; Ishizawa et al., 2010).

Do Tumorigenesis Assays Test the Ability to Recapitulate Tumor Heterogeneity?

A fundamental element of the stem cell model is that cancer stem cells give rise to phenotypically diverse progeny that recapitulate the heterogeneity of the tumor from which they derive (Figure 1C). This is presumed to occur through epigenetic mechanisms akin to the differentiation of normal stem cells; however, nobody has experimentally confirmed that epigenetic differences distinguish tumorigenic from nontumorigenic cells. The differentiation of cancer stem cells into nontumorigenic progeny is commonly assumed to be the major driver of heterogeneity in cancers that follow the stem cell model; however, the degree of genetic heterogeneity in such cancers is unknown. Therefore, some of the phenotypic and functional differences among cancer cells that have been attributed to the differentiation of cancer stem cells might derive from genetic differences that arise through clonal evolution (Figure 5A).

Since genetic changes are irreversible and stochastic, no tumorigenic cell can recapitulate the genetic heterogeneity of the tumor from which it derives. If the degree of genetic heterogeneity within a tumor is low, then cancer stem cells may be able to largely recapitulate the heterogeneity of the tumors from which they derive by differentiating into nontumorigenic cells (Figure 5B). However, if there is extensive genetic heterogeneity, then every tumorigenic cell may form a genetically distinct tumor and no tumorigenic cell will recapitulate the heterogeneity of the primary tumor (Figure 5C). Increasing evidence suggests that there is more genetic heterogeneity within tumors than previously thought (Navin et al., 2011; Yachida et al., 2010). However, driver mutations are rare among the genetic changes observed in cancer, so the degree of genetic heterogeneity that influences cancer cell function may be more modest. Nonetheless, if there is widespread genetic heterogeneity, functional and phenotypic differences among cancer cells cannot be assumed to be driven by epigenetic hierarchies rather than genetic differences (Campbell et al., 2010; Ding et al., 2010).

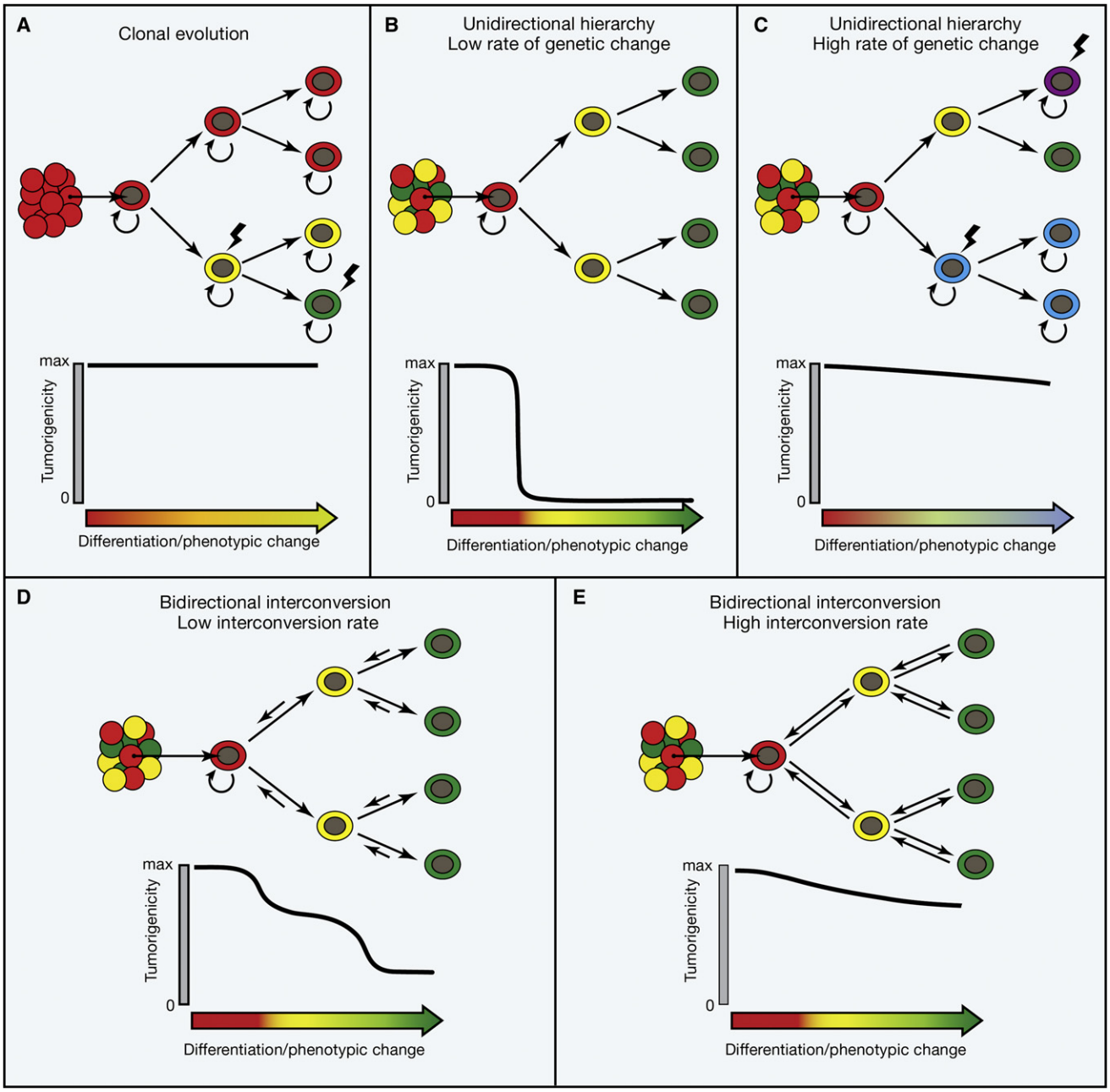

Figure 5. The Influences of Genetic Change and Reversible Transitions in Cell States on Hierarchical Organization in Cancer

(A) According to the clonal evolution model, many cancer cells have tumorigenic potential (circular self-renewal arrows) and heterogeneity arises through stochastic genetic/epigenetic changes (lightning bolt). Changes in cell phenotype are not necessarily associated with changes in tumorigenic potential.

(B) For cancers that follow a stem cell model in which only the cells at the top of the hierarchy retain tumorigenic capacity, the differentiation of these cells into nontumorigenic progeny creates tumor heterogeneity. Differentiation is associated with a loss of tumorigenic potential.

(C) For cancers with a high rate of genetic change, clones of cells within the hierarchy depicted in (B) may acquire tumorigenic potential as a consequence of new mutations. Phenotypic changes are sometimes associated with changes in tumorigenic potential and sometimes not. Note that it would be difficult to experimentally distinguish this model from the model in (A).

(D) A cancer that is hierarchically organized according to the cancer stem cell model but in which nontumorigenic cells can inefficiently revert to higher levels of the hierarchy. In this case, tumorigenic cells could be enriched or depleted using markers but "nontumorigenic" cells from the bottom of the hierarchy would always retain some tumorigenic capacity due to their ability to revert to tumorigenic states.

(E) A hierarchically organized cancer in which cells readily and reversibly interconvert between tumorigenic (red) and nontumorigenic (yellow and green) states. Note that it would be difficult to experimentally distinguish case (E) from case (C). In cancers that are genetically unstable or subject to efficient reversible cell transitions, the cancer stem cell model may be untestable, because it may be difficult to experimentally distinguish from cancers in which there is no hierarchy but where heterogeneity arises through clonal evolution.

In cancers that follow the stem cell model, cancer stem cells would be expected to undergo genetic change over time. Consistent with this, leukemia-initiating cells in B-ALLs undergo clonal evolution (Anderson et al., 2011; Notta et al., 2011), though these studies did not test whether the B-ALLs were hierarchically organized according to the cancer stem cell model. In cancers that do not follow the cancer stem cell model, genetic change would also occur over time and would be predicted to introduce phenotypic and functional heterogeneity. Thus, the cancer stem cell and clonal evolution models can be interacting, or independent, sources of heterogeneity depending on the cancer.

Another issue concerns the extent to which existing assays reliably test phenotypic heterogeneity. Some have suggested that melanomas have intrinsically different populations of tumorigenic and nontumorigenic cells that can be distinguished based on ABCB5 (Schatton et al., 2008) or CD271 (Civenni et al., 2011; Boiko et al., 2010) expression. However, neither of these markers correlate with the frequency of tumorigenic cells, and in our hands, small numbers of cells that are positive or negative for ABCB5 or CD271 have a similar capacity to form tumors and to recapitulate the phenotypic heterogeneity of the tumors from which they derive (Quintana et al., 2010). We also identified 20 other markers that are heterogeneously expressed by human melanoma cells and transplanted just 10 cells that were either positive or negative for each of these markers into NOD/SCID IL2Rγ^{null} mice (Quintana et al., 2010). All subpopulations exhibited a similar capacity to form phenotypically heterogeneous tumors. Thus, we have subdivided melanomas from many patients into almost 50 subpopulations of cells based on differences in marker expression and have not found any subpopulation that lacks the ability to form a phenotypically heterogeneous tumor.

The simplest interpretation of our data (Quintana et al., 2010) and other data (Pinner et al., 2009; Roesch et al., 2010) is that melanoma cells are phenotypically plastic, reversibly turning on and off markers. In contrast, Civenni et al. reported that both CD271$^+$ and CD271$^-$ melanoma cells formed tumors in NOD/SCID IL2Rγ^{null} mice but that the tumors formed by CD271$^-$ cells were not heterogeneous for CD271 expression and that only CD271$^+$ cells formed tumors in NOD/SCID mice (Civenni et al., 2011). They speculated that the difference relative to our results reflected different dissociation conditions. In our hands, both dissociation methods yield similar results with CD271$^+$ and CD271$^-$ melanoma cells each forming heterogeneous tumors that can be serially passaged, irrespective of whether they are transplanted in to NOD/SCID or NOD/SCID IL2Rγ^{null} mice (E. Quintana, U. Eskiocak, and S.J.M., unpublished data); however, if differences in enzymatic dissociation methods in solid cancers can sometimes generate reproducible differences in the phenotype of tumorigenic cells, this would illustrate the complexity of reproducing ''cancer stem cell'' markers.

If there are certain cells that reproducibly form tumors in NOD/SCID IL2Rγ^{null} mice and reproducibly fail to form tumors in NOD/SCID mice, what would this mean? Are some human cells more able to evade rejection by mouse immune cells? If so, does this have any physiological relevance for these cells in humans? If some tumorigenic cells are more able to generate phenotypically heterogeneous progeny than others, what does this mean? Could this reflect genetic differences among the cells (Campbell et al., 2010; Ding et al., 2010) rather than hierarchical epigenetic differences? Ultimately, a cell that has the potential to form a tumor in any assay has the potential to contribute to disease progression in a patient and cannot be ignored during therapy.

Uncertainty in Cancer Stem Cell Markers

In some cases, it has proven difficult to confirm markers that originally appeared to robustly distinguish tumorigenic from nontumorigenic cells; for example, CD133 was reported as a marker of tumorigenic brain cancer cells, and even large numbers of CD133-negative brain tumor cells were reported to lack the ability to form tumors (Bao et al., 2006; Singh et al., 2004). On this basis, gliomas and medulloblastomas were concluded to follow a cancer stem cell model. Yet subsequent studies found tumorigenic activity among both CD133$^+$ and CD133$^-$ brain tumor cells (Beier et al., 2007; Chen et al., 2010; Joo et al., 2008; Wang et al., 2008). These discrepancies could reflect differences among patients, methodological differences among laboratories, or ascertainment/tumor selection bias that led early studies to overestimate the robustness of markers. Work with other markers continues to support the conclusion that gliomas and medulloblastomas follow a cancer stem cell model (Read et al., 2009; Son et al., 2009; Ward et al., 2009); however, to confirm the existence and identity of cancer stem cells, it is necessary to identify markers that reproducibly distinguish tumorigenic and nontumorigenic cells, at least in specific subsets of patients.

Tumorigenic ovarian cancer cells have been reported to be enriched in the CD44$^+$ (Alvero et al., 2009), CD44$^+$CD117$^+$ (Zhang et al., 2008b), and CD133$^+$ (Curley et al., 2009) subpopulations of ovarian cancer cells. However, when Stewart et al. evaluated a large cohort of ovarian cancers, they were unable to find CD44$^+$CD117$^+$ cells in most ovarian cancers and the CD44$^+$CD117$^+$ cells they did find were depleted for tumorigenic activity (Stewart et al., 2011). CD133 enriched tumorigenic ovarian cancer cells in some cases and not in other cases. CD133 expression changed on some tumorigenic cells during passaging (Stewart et al., 2011). This suggests that CD133 only marks ovarian cancer stem cells under defined conditions in some patients and that the hierarchical organization of some ovarian cancers is not stable. It remains uncertain what fraction of ovarian cancers follow the stem cell model.

Cancer stem cell markers have proven difficult to broadly confirm in a number of solid cancers, raising questions about whether we have overestimated the number of cancers that follow this model and making it difficult to study the biology of these cells. Alternatively, it is possible that many cancers are hierarchically organized but that there is considerable diversity among patients in terms of the markers that distinguish tumorigenic from nontumorigenic cells. This is a key issue that must be resolved and which may require approaches other than the traditional dependence upon cell surface markers. For example, the separation of live cancer cells based on functional measures, such as signaling pathway activation (Vermeulen et al., 2010), might reduce phenotypic variability among tumorigenic cells. Unfortunately, the genetic approaches currently required to do this are only possible in mice where the use of inbred genetic

backgrounds and targeted mutations already reduce variability in cancer models relative to what is observed in patients.

Do Nontumorigenic Cells Sometimes Form Tumorigenic Cells?

Recent studies have suggested that the differentiation of cancer stem cells into nontumorigenic cells may be reversible (Chaffer et al., 2011; Gupta et al., 2011). In culture, immortalized human mammary epithelial cells (HMECs) undergo an epithelial-to-mesenchymal transition (EMT) following sustained expression of the transcription factors Snail or Twist, silencing of E-cadherin, or exposure to TGF-β (Mani et al., 2008; Morel et al., 2008; Scheel et al., 2011). This EMT was interpreted as conferring stem cell properties upon normal or transformed epithelial cells in culture, partly because the cells acquired a $CD44^+CD24^-$ phenotype, similar to breast cancer stem cells. The idea that cancer cells might reversibly transition between epigenetically defined tumorigenic and nontumorigenic states is appealing, partly because mechanisms that generate reversible heterogeneity can confer therapy resistance (Roesch et al., 2010; Sharma et al., 2010). However, it is not clear whether CD44 and CD24 consistently distinguish tumorigenic from nontumorigenic cells in cultured cell lines or whether nontumorigenic cells acquire tumorigenic potential by EMT in breast cancers in vivo.

The idea that nontumorigenic cancer cells could sometimes revert to having tumorigenic capacity is plausible given that restricted progenitors dedifferentiate into stem cells in certain normal tissues. In the *Drosophila* testis and ovary, spermatogonia and cytocytes dedifferentiate into germline stem cells under certain circumstances (Brawley and Matunis, 2004; Kai and Spradling, 2004). In mouse testis, spermatogonial progenitors can also dedifferentiate into spermatogonial stem cells (Barroca et al., 2009). So far this dedifferentiation has only been observed in normal tissues at low frequencies or under restricted circumstances. Nonetheless, if nontumorigenic cancer cells revert to a tumorigenic state at an appreciable rate in certain cancers, then this would undermine the ability to distinguish tumorigenic from nontumorigenic cells as even the ''nontumorigenic'' cells would be expected to form tumors at some level.

It is not clear whether the cancer stem cell model would effectively describe cancers in which there are tumorigenic and nontumorigenic states that can reversibly interconvert. If cells in the nontumorigenic state only convert to the tumorigenic state under restricted circumstances or with low efficiency, then it may still be possible to identify markers that distinguish populations that are enriched or depleted for tumorigenic capacity (Figure 5D). However, if cells in the nontumorigenic state convert to the tumorigenic state with high efficiency, it should not be possible to distinguish tumorigenic from nontumorigenic cells, potentially rendering the cancer stem cell model untestable in such cancers (Figure 5E). New models may be required to describe the heterogeneity in such cancers.

Cancer Stem Cells and Metastasis

Metastasis requires cells from a primary tumor to detach, invade the vascular or lymphatic system, migrate to distant sites, extravasate, then proliferate extensively and recruit new vasculature (Nguyen et al., 2009). There is much discussion regarding the metastasis of cancer stem cells, though nobody has actually tested whether the cells that are enriched for tumorigenic activity in transplantation assays are also enriched for the capacity to metastasize under physiological conditions. A fundamental question is whether metastatic potential is confined to a single population of tumorigenic cells or whether it arises stochastically through genetic or epigenetic changes that occur in many cancer cells without regard to their competence to form tumors prior to the stochastic change.

Some studies have suggested that subpopulations of tumorigenic pancreatic cancer (Hermann et al., 2007) and colon cancer (Pang et al., 2010) cells are enriched for the capacity to metastasize. However, the relationship between tumorigenic cells and metastasis has not yet been addressed systematically by examining all of the cancer cells that can be found in circulation and their tumorigenic capacity. Therefore, it remains uncertain whether nontumorigenic cancer cells have a similar capacity to disseminate as tumorigenic cells, or whether nontumorigenic cells from a primary tumor can sometimes acquire tumorigenic capacity after migrating to a new environment.

It has been proposed that cancer cells acquire metastatic potential by undergoing an EMT (Kalluri and Weinberg, 2009). As cancer cells lose their epithelial characteristics, they lose intracellular adhesions and polarity while acquiring more mesenchymal features such as the ability to migrate, invade, and resist apoptosis (Thiery et al., 2009). EMT has been proposed as a requisite step for breast cancer metastasis (Yang et al., 2004) and induction of an EMT also confers upon cultured cells a surface marker phenotype ($CD44^+CD24^-$) similar to tumorigenic breast cancer cells (Mani et al., 2008; Scheel et al., 2011). If cancer cells that have no tumorigenic capacity in transplantation assays can acquire this potential by undergoing an EMT, then any cancer cell could acquire metastatic potential.

Although the cancer stem cell model and work on EMTs focus on epigenetic differences between tumorigenic and nontumorigenic cells, there is good evidence that irreversible genetic mutations also confer metastatic potential (Vogelstein et al., 1988). In pancreatic cancer and medulloblastoma, genetically distinct subclones initiate metastatic disease (Campbell et al., 2010; Wu et al., 2012; Yachida et al., 2010). This raises the question of whether only cancer stem cells are competent to acquire genetic changes that confer metastatic potential or whether nontumorigenic cells can acquire genetic changes that confer both tumorigenic and metastatic potential. These fundamental questions remain to be studied in primary tumors in vivo, so the implications of the cancer stem cell model for metastasis are unresolved.

Conclusions and Future Directions

- Some cancers are hierarchically organized into undifferentiated cells that can drive disease progression and differentiated cells with less capacity to drive disease progression, consistent with the cancer stem cell model.
- Cancers that exhibit this kind of hierarchical organization have functional differences among undifferentiated and differentiated cancer cells that affect response to therapy and prognosis.

- There remain a number of uncertainties that make it difficult to assess whether many, or few, cancers follow the stem cell model. Some "cancer stem cell" markers have proven difficult to confirm, and tumorigenic cell frequencies can sometimes increase dramatically as a result of changes in assay conditions.
- Many studies have assumed that markers discovered in earlier studies were universally able to distinguish tumorigenic from nontumorigenic cells, even in independent patient cohorts or in cultured cell lines. Given the heterogeneity that is evident among patients and the context dependence of some markers, "cancer stem cell" markers should be confirmed in functional assays in each patient or under each experimental circumstance in which they are used.
- It remains unclear to what extent we have systematically underestimated tumorigenic cell frequencies by using assays that are not optimized for the engraftment of transplanted cells. In some cases, the underestimates may be modest and may not affect conclusions. In other cases, cancers thought to have only rare tumorigenic cells may actually have common tumorigenic cells.
- It will be necessary to systematically assess the degree to which changes in assay conditions affect the spectrum of cancer cells that can form tumors. If a cancer cell has the potential to proliferate extensively in any assay, then it has the potential to contribute to disease progression, and it is perilous to ignore that cell during therapy.
- It will be important to fate map cells within tumors thought to follow the cancer stem cell model to test whether only small populations of phenotypically distinct cells actually promote tumor growth and disease progression.
- Few studies have assessed the degree of genetic heterogeneity among cancer cells within the same tumor or the extent to which this causes phenotypic and functional differences. In some cancers, genetic heterogeneity may confound the assumption that heterogeneity arises from hierarchical epigenetic differences, rendering the cancer stem cell model difficult to test.
- It will be important to test whether primary tumors in vivo contain cells that reversibly transition between tumorigenic and nontumorigenic states. The cancer stem cell model may not effectively describe cancers in which the efficiency of interconversion is high.
- It will be necessary to distinguish cancers that follow the stem cell model from those that do not to avoid testing agents that target specific subpopulations of cancer cells in patients who have no chance of benefitting from them.

ACKNOWLEDGMENTS

This work was supported by the Howard Hughes Medical Institute and the Cancer Prevention and Research Institute of Texas. J.A.M. is supported by a grant from the National Institute of Child Health and Human Development to the University of Texas Southwestern Medical Center (K12 HD 068369-02).

REFERENCES

Al-Hajj, M., Wicha, M.S., Benito-Hernandez, A., Morrison, S.J., and Clarke, M.F. (2003). Proc. Natl. Acad. Sci. USA *100*, 3983–3988.

Alvero, A.B., Chen, R., Fu, H.H., Montagna, M., Schwartz, P.E., Rutherford, T., Silasi, D.A., Steffensen, K.D., Waldstrom, M., Visintin, I., et al. (2009). Cell Cycle *8*, 158–166.

Ambros, I.M., Hata, J., Joshi, V.V., Roald, B., Dehner, L.P., Tuchler, H., Potschger, U., and Shimada, H. (2002). Cancer *94*, 1574–1583.

Anderson, K., Lutz, C., van Delft, F.W., Bateman, C.M., Guo, Y., Colman, S.M., Kempski, H., Moorman, A.V., Titley, I., Swansbury, J., et al. (2011). Nature *469*, 356–361.

Armstrong, S.A., and Look, A.T. (2005). J. Clin. Oncol. *23*, 6306–6315.

Auchincloss, H., and Sachs, D.H. (1989). Transplantation and Graft Rejection. In Fundamental Immunology, W.E. Paul, ed. (New York: Raven Press), pp. 889–922.

Baker, D.L., Schmidt, M.L., Cohn, S.L., Maris, J.M., London, W.B., Buxton, A., Stram, D., Castleberry, R.P., Shimada, H., Sandler, A., et al. (2010). N. Engl. J. Med. *363*, 1313–1323.

Bao, S., Wu, Q., McLendon, R.E., Hao, Y., Shi, Q., Hjelmeland, A.B., Dewhirst, M.W., Bigner, D.D., and Rich, J.N. (2006). Nature *444*, 756–760.

Barker, N., Ridgway, R.A., van Es, J.H., van de Wetering, M., Begthel, H., van den Born, M., Danenberg, E., Clarke, A.R., Sansom, O.J., and Clevers, H. (2009). Nature *457*, 608–611.

Barroca, V., Lassalle, B., Coureuil, M., Louis, J.P., Le Page, F., Testart, J., Allemand, I., Riou, L., and Fouchet, P. (2009). Nat. Cell Biol. *11*, 190–196.

Baylin, S.B., and Jones, P.A. (2011). Nat. Rev. Cancer *11*, 726–734.

Beier, D., Hau, P., Proescholdt, M., Lohmeier, A., Wischhusen, J., Oefner, P.J., Aigner, L., Brawanski, A., Bogdahn, U., and Beier, C.P. (2007). Cancer Res. *67*, 4010–4015.

Berman, J.N., Gerbing, R.B., Alonzo, T.A., Ho, P.A., Miller, K., Hurwitz, C., Heerema, N.A., Hirsch, B., Raimondi, S.C., Lange, B., et al. (2011). Leukemia *25*, 1039–1042.

Bhatia, R., Holtz, M., Niu, N., Gray, R., Snyder, D.S., Sawyers, C.L., Arber, D.A., Slovak, M.L., and Forman, S.J. (2003). Blood *101*, 4701–4707.

Bissell, M.J., and Hines, W.C. (2011). Nat. Med. *17*, 320–329.

Boiko, A.D., Razorenova, O.V., van de Rijn, M., Swetter, S.M., Johnson, D.L., Ly, D.P., Butler, P.D., Yang, G.P., Joshua, B., Kaplan, M.J., et al. (2010). Nature *466*, 133–137.

Bonnet, D., and Dick, J.E. (1997). Nat. Med. *3*, 730–737.

Brawley, C., and Matunis, E. (2004). Science *304*, 1331–1334.

Brown, P., McIntyre, E., Rau, R., Meshinchi, S., Lacayo, N., Dahl, G., Alonzo, T.A., Chang, M., Arceci, R.J., and Small, D. (2007). Blood *110*, 979–985.

Buchstaller, J., McKeever, P.E., and Morrison, S.J. (2012). Cancer Cell *21*, 240–252.

Campbell, P.J., Yachida, S., Mudie, L.J., Stephens, P.J., Pleasance, E.D., Stebbings, L.A., Morsberger, L.A., Latimer, C., McLaren, S., Lin, M.L., et al. (2010). Nature *467*, 1109–1113.

Chaffer, C.L., Brueckmann, I., Scheel, C., Kaestli, A.J., Wiggins, P.A., Rodrigues, L.O., Brooks, M., Reinhardt, F., Su, Y., Polyak, K., et al. (2011). Proc. Natl. Acad. Sci. USA *108*, 7950–7955.

Chaganti, R.S., and Houldsworth, J. (2000). Cancer Res. *60*, 1475–1482.

Charles, N., Ozawa, T., Squatrito, M., Bleau, A.M., Brennan, C.W., Hambardzumyan, D., and Holland, E.C. (2010). Cell Stem Cell *6*, 141–152.

Chen, R., Nishimura, M.C., Bumbaca, S.M., Kharbanda, S., Forrest, W.F., Kasman, I.M., Greve, J.M., Soriano, R.H., Gilmour, L.L., Rivers, C.S., et al. (2010). Cancer Cell *17*, 362–375.

Cho, R.W., Wang, X., Diehn, M., Shedden, K., Chen, G.Y., Sherlock, G., Gurney, A., Lewicki, J., and Clarke, M.F. (2008). Stem Cells *26*, 364–371.

Chu, S., McDonald, T., Lin, A., Chakraborty, S., Huang, Q., Snyder, D.S., and Bhatia, R. (2011). Blood *118*, 5565–5572.

Civenni, G., Walter, A., Kobert, N., Mihic-Probst, D., Zipser, M., Belloni, B., Seifert, B., Moch, H., Dummer, R., van den Broek, M., et al. (2011). Cancer Res. *71*, 3098–3109.

Cozzio, A., Passegue, E., Ayton, P.M., Karsunky, H., Cleary, M.L., and Weissman, I.L. (2003). Genes Dev. *17*, 3029–3035.

Curley, M.D., Therrien, V.A., Cummings, C.L., Sergent, P.A., Koulouris, C.R., Friel, A.M., Roberts, D.J., Seiden, M.V., Scadden, D.T., Rueda, B.R., et al. (2009). Stem Cells *27*, 2875–2883.

Curtis, S.J., Sinkevicius, K.W., Li, D., Lau, A.N., Roach, R.R., Zamponi, R., Woolfenden, A.E., Kirsch, D.G., Wong, K.K., and Kim, C.F. (2010). Cell Stem Cell *7*, 127–133.

Dalerba, P., Dylla, S.J., Park, I.K., Liu, R., Wang, X., Cho, R.W., Hoey, T., Gurney, A., Huang, E.H., Simeone, D.M., et al. (2007). Proc. Natl. Acad. Sci. USA *104*, 10158–10163.

de Thé, H., and Chen, Z. (2010). Nat. Rev. Cancer *10*, 775–783.

de Visser, K.E., Eichten, A., and Coussens, L.M. (2006). Nat. Rev. Cancer *6*, 24–37.

Dick, J.E. (2008). Blood *112*, 4793–4807.

Diehn, M., Cho, R.W., Lobo, N.A., Kalisky, T., Dorie, M.J., Kulp, A.N., Qian, D., Lam, J.S., Ailles, L.E., Wong, M., et al. (2009). Nature *458*, 780–783.

Ding, L., Ellis, M.J., Li, S., Larson, D.E., Chen, K., Wallis, J.W., Harris, C.C., McLellan, M.D., Fulton, R.S., Fulton, L.L., et al. (2010). Nature *464*, 999–1005.

Downing, J.R., and Shannon, K.M. (2002). Cancer Cell *2*, 437–445.

Druker, B.J., Guilhot, F., O'Brien, S.G., Gathmann, I., Kantarjian, H., Gattermann, N., Deininger, M.W., Silver, R.T., Goldman, J.M., Stone, R.M., et al. (2006). N. Engl. J. Med. *355*, 2408–2417.

Eppert, K., Takenaka, K., Lechman, E.R., Waldron, L., Nilsson, B., van Galen, P., Metzeler, K.H., Poeppl, A., Ling, V., Beyene, J., et al. (2011). Nat. Med. *17*, 1086–1093.

Falini, B., Mecucci, C., Tiacci, E., Alcalay, M., Rosati, R., Pasqualucci, L., La Starza, R., Diverio, D., Colombo, E., Santucci, A., et al. (2005). N. Engl. J. Med. *352*, 254–266.

Fearon, E.R., Burke, P.J., Schiffer, C.A., Zehnbauer, B.A., and Vogelstein, B. (1986). N. Engl. J. Med. *315*, 15–24.

Fidler, I.J., and Kripke, M.L. (1977). Science *197*, 893–895.

Fidler, I.J., and Hart, I.R. (1982). Science *217*, 998–1003.

Gibson, P., Tong, Y., Robinson, G., Thompson, M.C., Currle, D.S., Eden, C., Kranenburg, T.A., Hogg, T., Poppleton, H., Martin, J., et al. (2010). Nature *468*, 1095–1099.

Goardon, N., Marchi, E., Atzberger, A., Quek, L., Schuh, A., Soneji, S., Woll, P., Mead, A., Alford, K.A., Rout, R., et al. (2011). Cancer Cell *19*, 138–152.

Gorre, M.E., Mohammed, M., Ellwood, K., Hsu, N., Paquette, R., Rao, P.N., and Sawyers, C.L. (2001). Science *293*, 876–880.

Graham, S.M., Jorgensen, H.G., Allan, E., Pearson, C., Alcorn, M.J., Richmond, L., and Holyoake, T.L. (2002). Blood *99*, 319–325.

Gross, R.E., Mehler, M.F., Mabie, P.C., Zang, Z., Santschi, L., and Kessler, J.A. (1996). Neuron *17*, 595–606.

Gupta, P.B., Fillmore, C.M., Jiang, G., Shapira, S.D., Tao, K., Kuperwasser, C., and Lander, E.S. (2011). Cell *146*, 633–644.

Hamburger, A.W., and Salmon, S.E. (1977). Science *197*, 461–463.

He, S., Nakada, D., and Morrison, S.J. (2009). Annu. Rev. Cell Dev. Biol. *25*, 377–406.

Held, M.A., Curley, D.P., Dankort, D., McMahon, M., Muthusamy, V., and Bosenberg, M.W. (2010). Cancer Res. *70*, 388–397.

Heppner, G.H. (1984). Cancer Res. *44*, 2259–2265.

Hermann, P.C., Huber, S.L., Herrler, T., Aicher, A., Ellwart, J.W., Guba, M., Bruns, C.J., and Heeschen, C. (2007). Cell Stem Cell *1*, 313–323.

Heuser, M., Sly, L.M., Argiropoulos, B., Kuchenbauer, F., Lai, C., Weng, A., Leung, M., Lin, G., Brookes, C., Fung, S., et al. (2009). Blood *114*, 3983–3993.

Ho, P.A., Kutny, M.A., Alonzo, T.A., Gerbing, R.B., Joaquin, J., Raimondi, S.C., Gamis, A.S., and Meshinchi, S. (2011). Pediatr. Blood Cancer *57*, 204–209.

Holtz, M.S., Slovak, M.L., Zhang, F., Sawyers, C.L., Forman, S.J., and Bhatia, R. (2002). Blood *99*, 3792–3800.

Huntly, B.J., Shigematsu, H., Deguchi, K., Lee, B.H., Mizuno, S., Duclos, N., Rowan, R., Amaral, S., Curley, D., Williams, I.R., et al. (2004). Cancer Cell *6*, 587–596.

Ishizawa, K., Rasheed, Z.A., Karisch, R., Wang, Q., Kowalski, J., Susky, E., Pereira, K., Karamboulas, C., Moghal, N., Rajeshkumar, N.V., et al. (2010). Cell Stem Cell *7*, 279–282.

Johannessen, C.M., Boehm, J.S., Kim, S.Y., Thomas, S.R., Wardwell, L., Johnson, L.A., Emery, C.M., Stransky, N., Cogdill, A.P., Barretina, J., et al. (2010). Nature *468*, 968–972.

Johnson, R.A., Wright, K.D., Poppleton, H., Mohankumar, K.M., Finkelstein, D., Pounds, S.B., Rand, V., Leary, S.E., White, E., Eden, C., et al. (2010). Nature *466*, 632–636.

Joo, K.M., Kim, S.Y., Jin, X., Song, S.Y., Kong, D.S., Lee, J.I., Jeon, J.W., Kim, M.H., Kang, B.G., Jung, Y., et al. (2008). Lab. Invest. *88*, 808–815.

Kai, T., and Spradling, A. (2004). Nature *428*, 564–569.

Kalluri, R., and Weinberg, R.A. (2009). J. Clin. Invest. *119*, 1420–1428.

Kelly, P.N., Dakic, A., Adams, J.M., Nutt, S.L., and Strasser, A. (2007). Science *317*, 337.

Kennedy, J.A., Barabe, F., Poeppl, A.G., Wang, J.C., and Dick, J.E. (2007). Science *318*, 1722.

Kiyoi, H., Naoe, T., Nakano, Y., Yokota, S., Minami, S., Miyawaki, S., Asou, N., Kuriyama, K., Jinnai, I., Shimazaki, C., et al. (1999). Blood *93*, 3074–3080.

Kleinsmith, L.J., and Pierce, G.B. (1964). Cancer Res. *24*, 1544–1551.

Kottaridis, P.D., Gale, R.E., Frew, M.E., Harrison, G., Langabeer, S.E., Belton, A.A., Walker, H., Wheatley, K., Bowen, D.T., Burnett, A.K., et al. (2001). Blood *98*, 1752–1759.

Krivtsov, A.V., Twomey, D., Feng, Z., Stubbs, M.C., Wang, Y., Faber, J., Levine, J.E., Wang, J., Hahn, W.C., Gilliland, D.G., et al. (2006). Nature *442*, 818–822.

Kuperwasser, C., Chavarria, T., Wu, M., Magrane, G., Gray, J.W., Carey, L., Richardson, A., and Weinberg, R.A. (2004). Proc. Natl. Acad. Sci. USA *101*, 4966–4971.

Lapidot, T., Sirard, C., Vormoor, J., Murdoch, B., Hoang, T., Caceres-Cortes, J., Minden, M., Paterson, B., Caligiuri, M.A., and Dick, J.E. (1994). Nature *17*, 645–648.

le Viseur, C., Hotfilder, M., Bomken, S., Wilson, K., Rottgers, S., Schrauder, A., Rosemann, A., Irving, J., Stam, R.W., Shultz, L.D., et al. (2008). Cancer Cell *14*, 47–58.

Levi, B.P., and Morrison, S.J. (2008). Cold Spring Harb. Symp. Quant. Biol. *73*, 539–553.

Ley, T.J., Ding, L., Walter, M.J., McLellan, M.D., Lamprecht, T., Larson, D.E., Kandoth, C., Payton, J.E., Baty, J., Welch, J., et al. (2010). N. Engl. J. Med. *363*, 2424–2433.

Li, C., Heidt, D.G., Dalerba, P., Burant, C.F., Zhang, L., Adsay, V., Wicha, M., Clarke, M.F., and Simeone, D.M. (2007). Cancer Res. *67*, 1030–1037.

Mani, S.A., Guo, W., Liao, M.J., Eaton, E.N., Ayyanan, A., Zhou, A.Y., Brooks, M., Reinhard, F., Zhang, C.C., Shipitsin, M., et al. (2008). Cell *133*, 704–715.

Manz, M.G. (2007). Immunity *26*, 537–541.

Matthay, K.K., Villablanca, J.G., Seeger, R.C., Stram, D.O., Harris, R.E., Ramsay, N.K., Swift, P., Shimada, H., Black, C.T., Brodeur, G.M., et al. (1999). N. Engl. J. Med. *341*, 1165–1173.

Matthay, K.K., Reynolds, C.P., Seeger, R.C., Shimada, H., Adkins, E.S., Haas-Kogan, D., Gerbing, R.B., London, W.B., and Villablanca, J.G. (2009). J. Clin. Oncol. *27*, 1007–1013.

McDermott, S.P., Eppert, K., Lechman, E.R., Doedens, M., and Dick, J.E. (2010). Blood *116*, 193–200.

McKenzie, J.L., Gan, O.I., Doedens, M., and Dick, J.E. (2005). Blood *106*, 1259–1261.

Merlos-Suárez, A., Barriga, F.M., Jung, P., Iglesias, M., Cespedes, M.V., Rossell, D., Sevillano, M., Hernando-Momblona, X., da Silva-Diz, V., Munoz, P., et al. (2011). Cell Stem Cell *8*, 511–524.

Meshinchi, S., Woods, W.G., Stirewalt, D.L., Sweetser, D.A., Buckley, J.D., Tjoa, T.K., Bernstein, I.D., and Radich, J.P. (2001). Blood *97*, 89–94.

Morel, A.P., Lievre, M., Thomas, C., Hinkal, G., Ansieau, S., and Puisieux, A. (2008). PLoS ONE *3*, e2888.

Navin, N., Kendall, J., Troge, J., Andrews, P., Rodgers, L., McIndoo, J., Cook, K., Stepansky, A., Levy, D., Esposito, D., et al. (2011). Nature *472*, 90–94.

Nazarian, R., Shi, H., Wang, Q., Kong, X., Koya, R.C., Lee, H., Chen, Z., Lee, M.K., Attar, N., Sazegar, H., et al. (2010). Nature *468*, 973–977.

Nguyen, D.X., Bos, P.D., and Massague, J. (2009). Nat. Rev. Cancer *9*, 274–284.

Nitschke, R., Smith, E.I., Shochat, S., Altshuler, G., Travers, H., Shuster, J.J., Hayes, F.A., Patterson, R., and McWilliams, N. (1988). J. Clin. Oncol. *6*, 1271–1279.

Notta, F., Doulatov, S., and Dick, J.E. (2010). Blood *115*, 3704–3707.

Notta, F., Mullighan, C.G., Wang, J.C., Poeppl, A., Doulatov, S., Phillips, L.A., Ma, J., Minden, M.D., Downing, J.R., and Dick, J.E. (2011). Nature *469*, 362–367.

Nowell, P.C. (1976). Science *194*, 23–28.

Nowell, P.C. (1986). Cancer Res. *46*, 2203–2207.

O'Brien, C.A., Pollett, A., Gallinger, S., and Dick, J.E. (2007). Nature *445*, 106–110.

Ogawa, M., Fried, J., Sakai, Y., Strife, A., and Clarkson, B.D. (1970). Cancer *25*, 1031–1049.

Oravecz-Wilson, K.I., Philips, S.T., Yilmaz, O.H., Ames, H.M., Li, L., Crawford, B.D., Gauvin, A.M., Lucas, P.C., Sitwala, K., Downing, J.R., et al. (2009). Cancer Cell *16*, 137–148.

Pang, R., Law, W.L., Chu, A.C., Poon, J.T., Lam, C.S., Chow, A.K., Ng, L., Cheung, L.W., Lan, X.R., Lan, H.Y., et al. (2010). Cell Stem Cell *6*, 603–615.

Piccirillo, S.G., Reynolds, B.A., Zanetti, N., Lamorte, G., Binda, E., Broggi, G., Brem, H., Olivi, A., Dimeco, F., and Vescovi, A.L. (2006). Nature *444*, 761–765.

Pinner, S., Jordan, P., Sharrock, K., Bazley, L., Collinson, L., Marais, R., Bonvin, E., Goding, C., and Sahai, E. (2009). Cancer Res. *69*, 7969–7977.

Polyak, K., Haviv, I., and Campbell, I.G. (2009). Trends Genet. *25*, 30–38.

Poulikakos, P.I., and Rosen, N. (2011). Cancer Cell *19*, 11–15.

Poulikakos, P.I., Persaud, Y., Janakiraman, M., Kong, X., Ng, C., Moriceau, G., Shi, H., Atefi, M., Titz, B., Gabay, M.T., et al. (2011). Nature *480*, 387–390.

Quintana, E., Shackleton, M., Sabel, M.S., Fullen, D.R., Johnson, T.M., and Morrison, S.J. (2008). Nature *456*, 593–598.

Quintana, E., Shackleton, M., Foster, H.R., Fullen, D.R., Sabel, M.S., Johnson, T.M., and Morrison, S.J. (2010). Cancer Cell *18*, 510–523.

Read, T.A., Fogarty, M.P., Markant, S.L., McLendon, R.E., Wei, Z., Ellison, D.W., Febbo, P.G., and Wechsler-Reya, R.J. (2009). Cancer Cell *15*, 135–147.

Reya, T., Morrison, S.J., Clarke, M.F., and Weissman, I.L. (2001). Nature *414*, 105–111.

Ricci-Vitiani, L., Lombardi, D.G., Pilozzi, E., Biffoni, M., Todaro, M., Peschle, C., and De Maria, R. (2007). Nature *445*, 111–115.

Roesch, A., Fukunaga-Kalabis, M., Schmidt, E.C., Zabierowski, S.E., Brafford, P.A., Vultur, A., Basu, D., Gimotty, P., Vogt, T., and Herlyn, M. (2010). Cell *141*, 583–594.

Roumiantsev, S., Shah, N.P., Gorre, M.E., Nicoll, J., Brasher, B.B., Sawyers, C.L., and Van Etten, R.A. (2002). Proc. Natl. Acad. Sci. USA *99*, 10700–10705.

Rousselot, P., Huguet, F., Rea, D., Legros, L., Cayuela, J.M., Maarek, O., Blanchet, O., Marit, G., Gluckman, E., Reiffers, J., et al. (2007). Blood *109*, 58–60.

Sarry, J.E., Murphy, K., Perry, R., Sanchez, P.V., Secreto, A., Keefer, C., Swider, C.R., Strzelecki, A.C., Cavelier, C., Recher, C., et al. (2011). J. Clin. Invest. *121*, 384–395.

Schatton, T., Murphy, G.F., Frank, N.Y., Yamaura, K., Waaga-Gasser, A.M., Gasser, M., Zhan, Q., Jordan, S., Duncan, L.M., Weishaupt, C., et al. (2008). Nature *451*, 345–349.

Scheel, C., Eaton, E.N., Li, S.H., Chaffer, C.L., Reinhardt, F., Kah, K.J., Bell, G., Guo, W., Rubin, J., Richardson, A.L., et al. (2011). Cell *145*, 926–940.

Schüller, U., Heine, V.M., Mao, J., Kho, A.T., Dillon, A.K., Han, Y.G., Huillard, E., Sun, T., Ligon, A.H., Qian, Y., et al. (2008). Cancer Cell *14*, 123–134.

Shackleton, M., Quintana, E., Fearon, E.R., and Morrison, S.J. (2009). Cell *138*, 822–829.

Sharma, S.V., Lee, D.Y., Li, B., Quinlan, M.P., Takahashi, F., Maheswaran, S., McDermott, U., Azizian, N., Zou, L., Fischbach, M.A., et al. (2010). Cell *141*, 69–80.

Shimada, H., Chatten, J., Newton, W.A., Jr., Sachs, N., Hamoudi, A.B., Chiba, T., Marsden, H.B., and Misugi, K. (1984). J. Natl. Cancer Inst. *73*, 405–416.

Shimada, H., Ambros, I.M., Dehner, L.P., Hata, J., Joshi, V.V., and Roald, B. (1999a). Cancer *86*, 349–363.

Shimada, H., Ambros, I.M., Dehner, L.P., Hata, J., Joshi, V.V., Roald, B., Stram, D.O., Gerbing, R.B., Lukens, J.N., Matthay, K.K., et al. (1999b). Cancer *86*, 364–372.

Singh, S.K., Hawkins, C., Clarke, I.D., Squire, J.A., Bayani, J., Hide, T., Henkelman, R.M., Cusimano, M.D., and Dirks, P.B. (2004). Nature *432*, 396–401.

Somervaille, T.C., and Cleary, M.L. (2006). Cancer Cell *10*, 257–268.

Somervaille, T.C., Matheny, C.J., Spencer, G.J., Iwasaki, M., Rinn, J.L., Witten, D.M., Chang, H.Y., Shurtleff, S.A., Downing, J.R., and Cleary, M.L. (2009). Cell Stem Cell *4*, 129–140.

Son, M.J., Woolard, K., Nam, D.H., Lee, J., and Fine, H.A. (2009). Cell Stem Cell *4*, 440–452.

Stenning, S.P., Parkinson, M.C., Fisher, C., Mead, G.M., Cook, P.A., Fossa, S.D., Horwich, A., Jones, W.G., Newlands, E.S., Oliver, R.T., et al. (1998). Cancer *83*, 1409–1419.

Stewart, J.M., Shaw, P.A., Gedye, C., Bernardini, M.Q., Neel, B.G., and Ailles, L.E. (2011). Proc. Natl. Acad. Sci. USA *108*, 6468–6473.

Stirewalt, D.L., Kopecky, K.J., Meshinchi, S., Appelbaum, F.R., Slovak, M.L., Willman, C.L., and Radich, J.P. (2001). Blood *97*, 3589–3595.

Taussig, D.C., Miraki-Moud, F., Anjos-Afonso, F., Pearce, D.J., Allen, K., Ridler, C., Lillington, D., Oakervee, H., Cavenagh, J., Agrawal, S.G., et al. (2008). Blood *112*, 568–575.

Taussig, D.C., Vargaftig, J., Miraki-Moud, F., Griessinger, E., Sharrock, K., Luke, T., Lillington, D., Oakervee, H., Cavenagh, J., Agrawal, S.G., et al. (2010). Blood *115*, 1976–1984.

Taylor, M.D., Poppleton, H., Fuller, C., Su, X., Liu, Y., Jensen, P., Magdaleno, S., Dalton, J., Calabrese, C., Board, J., et al. (2005). Cancer Cell *8*, 323–335.

Thiede, C., Koch, S., Creutzig, E., Steudel, C., Illmer, T., Schaich, M., and Ehninger, G. (2006). Blood *107*, 4011–4020.

Thiele, C.J., Reynolds, C.P., and Israel, M.A. (1985). Nature *313*, 404–406.

Thiery, J.P., Acloque, H., Huang, R.Y., and Nieto, M.A. (2009). Cell *139*, 871–890.

Vaillant, F., Asselin-Labat, M.L., Shackleton, M., Forrest, N.C., Lindeman, G.J., and Visvader, J.E. (2008). Cancer Res. *68*, 7711–7717.

Vermeulen, L., De Sousa, E.M.F., van der Heijden, M., Cameron, K., de Jong, J.H., Borovski, T., Tuynman, J.B., Todaro, M., Merz, C., Rodermond, H., et al. (2010). Nat. Cell Biol. *12*, 468–476.

Villanueva, J., Vultur, A., Lee, J.T., Somasundaram, R., Fukunaga-Kalabis, M., Cipolla, A.K., Wubbenhorst, B., Xu, X., Gimotty, P.A., Kee, D., et al. (2010). Cancer Cell *18*, 683–695.

Vogelstein, B., Fearon, E.R., Hamilton, S.R., Kern, S.E., Preisinger, A.C., Leppert, M., Nakamura, Y., White, R., Smits, A.M., and Bos, J.L. (1988). N. Engl. J. Med. *319*, 525–532.

Vogelstein, B., Civin, C.I., Preisinger, A.C., Krischer, J.P., Steuber, P., Ravindranath, Y., Weinstein, H., Elfferich, P., and Bos, J. (1990). Genes Chromosomes Cancer *2*, 159–162.

Wang, J.C., and Dick, J.E. (2005). Trends Cell Biol. *15*, 494–501.

Wang, J., Sakariassen, P.O., Tsinkalovsky, O., Immervoll, H., Boe, S.O., Svendsen, A., Prestegarden, L., Rosland, G., Thorsen, F., Stuhr, L., et al. (2008). Int. J. Cancer *122*, 761–768.

Wang, Y., Krivtsov, A.V., Sinha, A.U., North, T.E., Goessling, W., Feng, Z., Zon, L.I., and Armstrong, S.A. (2010). Science *327*, 1650–1653.

Ward, R.J., Lee, L., Graham, K., Satkunendran, T., Yoshikawa, K., Ling, E., Harper, L., Austin, R., Nieuwenhuis, E., Clarke, I.D., et al. (2009). Cancer Res. *69*, 4682–4690.

Williams, R.T., den Besten, W., and Sherr, C.J. (2007). Genes Dev. *21*, 2283–2287.

Wu, X., Northcott, P.A., Dubuc, A., Dupuy, A.J., Shih, D.J., Witt, H., Croul, S., Bouffet, E., Fults, D.W., Eberhart, C.G., et al. (2012). Nature *482*, 529–533.

Yachida, S., Jones, S., Bozic, I., Antal, T., Leary, R., Fu, B., Kamiyama, M., Hruban, R.H., Eshleman, J.R., Nowak, M.A., et al. (2010). Nature *467*, 1114–1117.

Yang, J., Mani, S.A., Donaher, J.L., Ramaswamy, S., Itzykson, R.A., Come, C., Savagner, P., Gitelman, I., Richardson, A., and Weinberg, R.A. (2004). Cell *117*, 927–939.

Yang, Z.J., Ellis, T., Markant, S.L., Read, T.A., Kessler, J.D., Bourboulas, M., Schuller, U., Machold, R., Fishell, G., Rowitch, D.H., et al. (2008). Cancer Cell *14*, 135–145.

Yilmaz, O.H., Valdez, R., Theisen, B.K., Guo, W., Ferguson, D.O., Wu, H., and Morrison, S.J. (2006). Nature *441*, 475–482.

Zhang, M., Behbod, F., Atkinson, R.L., Landis, M.D., Kittrell, F., Edwards, D., Medina, D., Tsimelzon, A., Hilsenbeck, S., Green, J.E., et al. (2008a). Cancer Res. *68*, 4674–4682.

Zhang, S., Balch, C., Chan, M.W., Lai, H.C., Matei, D., Schilder, J.M., Yan, P.S., Huang, T.H., and Nephew, K.P. (2008b). Cancer Res. *68*, 4311–4320.

Zhao, Z., Zuber, J., Diaz-Flores, E., Lintault, L., Kogan, S.C., Shannon, K., and Lowe, S.W. (2010). Genes Dev. *24*, 1389–1402.

Zwaan, C.M., Meshinchi, S., Radich, J.P., Veerman, A.J., Huismans, D.R., Munske, L., Podleschny, M., Hahlen, K., Pieters, R., Zimmermann, M., et al. (2003). Blood *102*, 2387–2394.

Cancer Cell
Article

VHL-Regulated MiR-204 Suppresses Tumor Growth through Inhibition of LC3B-Mediated Autophagy in Renal Clear Cell Carcinoma

Olga Mikhaylova,[1,5] Yiwen Stratton,[1,5] Daniel Hall,[1] Emily Kellner,[1] Birgit Ehmer,[1] Angela F. Drew,[1] Catherine A. Gallo,[1] David R. Plas,[1] Jacek Biesiada,[3] Jarek Meller,[2,3] and Maria F. Czyzyk-Krzeska[1,4,*]
[1]Department of Cancer and Cell Biology
[2]Department of Environmental Health
University of Cincinnati College of Medicine, Cincinnati, OH 45267-0056, USA
[3]Division of Biomedical Informatics, Cincinnati Children's Hospital Medical Center, Cincinnati, OH 45229, USA
[4]Department of Veterans Affairs, VA Research Service, Cincinnati, OH 45220, USA
[5]These authors contributed equally to this work
*Correspondence: maria.czyzykkrzeska@uc.edu
DOI 10.1016/j.ccr.2012.02.019

SUMMARY

The von Hippel-Lindau tumor-suppressor gene (*VHL*) is lost in most clear cell renal cell carcinomas (ccRCC). Here, using human ccRCC specimens, VHL-deficient cells, and xenograft models, we show that miR-204 is a VHL-regulated tumor suppressor acting by inhibiting macroautophagy, with MAP1LC3B (LC3B) as a direct and functional target. Of note, higher tumor grade of human ccRCC was correlated with a concomitant decrease in miR-204 and increase in LC3B levels, indicating that LC3B-mediated macroautophagy is necessary for RCC progression. VHL, in addition to inducing endogenous miR-204, triggered the expression of LC3C, an HIF-regulated LC3B paralog, that suppressed tumor growth. These data reveal a function of VHL as a tumor-suppressing regulator of autophagic programs.

INTRODUCTION

Clear cell renal cell carcinoma (ccRCC), the most frequent and malignant type of renal cancer, is characterized by early loss of the von Hippel-Lindau tumor-suppressor gene (*VHL*) in a majority (60%–80%) of tumors. One well-recognized oncogenic effect of *VHL* loss is induction of the hypoxia inducible factor (HIF) and HIF-regulated genes, which stimulate angiogenesis and thus provide nutrients necessary for tumor growth (Gossage and Eisen, 2010). Discovery of this pathway laid the groundwork for the development of several antiangiogenic therapeutic approaches for treatment of ccRCC (Heng and Bukowski, 2008). However, antiangiogenic therapies have not lived up to their initial promise, which suggests that tumor growth and survival might be supported by alternative sources of nutrients such as autophagy.

Autophagy is a complex and tightly regulated homeostatic process that allows a cell to eliminate defective organelles and molecules and to recycle nutrients for survival under deprived conditions. Dependence of cancer cells on such oncogenic autophagy has been demonstrated (Degenhardt et al., 2006; Jin et al., 2007). Conversely, changes in the rate of autophagy may result in metabolic imbalance and cell death (Mathew et al., 2007; White and DiPaola, 2009). Classic macroautophagy involves a process utilizing ubiquitin-like cascades of ATG proteins leading to the formation of double-membrane autophagosomes containing cytoplasm, ribosomes, and other organelles. Autophagosomes ultimately fuse with lysosomes targeting the cargo for proteolytic degradation (He and Klionsky, 2009). The initial step includes formation of an isolation membrane (phagophore), which can originate from the endoplasmic

Significance

ccRCC tumor growth depends on abundant angiogenesis and activation of glycolytic metabolic pathways that result from *VHL* loss and induction of hypoxia-inducible factor (HIF) and HIF targets. Here we show that loss of VHL also promotes, in an HIF-independent manner, access to nutrients from intracellular sources through activation of LC3B-mediated autophagy. This autophagic program is necessary for tumor growth. In addition, VHL, by repressing HIF, induces expression of LC3C, which exercises tumor-suppressing activity. These findings support a role for VHL as a tumor suppressor in the control of different autophagic programs. Addiction of cancer cells to oncogenic autophagy creates the possibility that miR-204 could be used in ccRCC therapy with minimal effects on normal renal cells.

reticulum (Axe et al., 2008), outer mitochondrial membrane (Hailey et al., 2010), or plasma membrane (Ravikumar et al., 2010). The diverse origins of membranes for autophagic vacuoles create the possibility for adaptive and alternative autophagic programs that can be activated during different types or durations of starvation in a cell-type-specific manner. Phagophores interact with several regulatory multiprotein complexes, including mTOR and AMPK-regulated ULK complexes and the Beclin 1/class III PI3K complex. Further processing of the phagophore to the mature autophagosome requires covalent conjugation of ATG12 to ATG5 via a mechanism involving the E1-like enzyme ATG7 and the E2-like enzyme ATG10. The ATG12-ATG5 conjugate forms a complex with ATG16L and carries the final E3-like conjugation of the microtubule-associated protein light chain (MAP1LC3, here referred to as LC3) on an exposed C-terminal glycine to phosphatidylethanolamine (PE) initiated by the ubiquitinylation-like cascade processed by ATG7(E1) and ATG3 (E2) factors (Tanida et al., 2004). The appearance of the lipidated form of LC3 (LC3-II) in the autophagosome membrane is a commonly used marker of ongoing autophagy and can be quantified by endpoint flux analysis in the presence of lysosomal inhibitors (Rubinsztein et al., 2009; Klionsky et al., 2008).

In contrast to a single LC3 (ATG8) in yeast, mammalian cells have six different orthologs of ATG8 (LC3A, LC3B, LC3C, GABARAP, GABARAPL1, and GATE16/GABARAPL2) (Tanida et al., 2004). While tissue-specific patterns of expression and intracellular localization have been reported (Tanida et al., 2004), the precise functions of the individual orthologs are not well understood. Specific involvement of the different orthologs at different stages of autophagosome formation was observed in HeLa cells, with the LC3 family participating in earlier stages of autophagosome membrane elongation, and the GABARAP family involved in later stages of maturation (Weidberg et al., 2010). At least some functional redundancy among orthologs is expected based on similarities in sequence and structure (Wu et al., 2006) and the overlapping partner-protein binding patterns (Behrends et al., 2010). It is interesting that an alternative ATG5-/ATG7-/LC3B-independent pathway of autophagy has been described, wherein autophagosomes are derived from trans-Golgi and late endosomes in a RAB9-dependent manner (Nishida et al., 2009). The existence of multiple autophagic programs suggests differential functions dependent on the cellular context. Therapeutic manipulations of autophagy may provide anticancer treatments alternative to or supporting of antiangiogenic therapies. In that respect, the small-molecule STF-62247 has been identified as a stimulator of autophagy leading to cell death and inhibition of RCC growth in xenograft models (Turcotte et al., 2008). On the other hand, inhibition of autophagy by chloroquine appears to cause robust tumor regression in the case of pancreatic cancer (Yang et al., 2011). Thus, autophagy represents a therapeutic target in need of further investigation.

MicroRNAs (miRs) are small noncoding RNAs that modulate gene expression (Selbach et al., 2008). There is ample evidence that miRs have regulatory functions in cancer initiation, progression, and metastasis (Lu et al., 2005; Calin and Croce, 2006). Introduction of stabilized miRs may restore lost tumor suppressor activity (Czech, 2006; Negrini et al., 2007; Tong and Nemunaitis, 2008; Kota et al., 2009). Conversely, the use of antagomirs may allow for a decrease in the level and activity of miRs that promote oncogenesis (Krützfeldt et al., 2005). MiR-204 is expressed from the large intron 6 of *TRPM3*, which is located on chromosome 9q21.12 and encodes a transient receptor potential, Ca^{2+}-permeable, nonselective cation channel (Oberwinkler and Phillipp, 2007) (Figure 1A). Both miR-204 and TRPM3 are expressed at higher levels in human kidney as compared with other organ tested (Lu et al., 2005).

Here, we investigate the role of VHL and miR-204 in the regulation of autophagic programs in ccRCC.

RESULTS

MiR-204 Acts as a Tumor Suppressor in RCC

We analyzed the expression of miR-204 in 128 human ccRCC with known *VHL* status and, in 114 cases, a matched normal kidney specimen. The miR-204 level was significantly decreased in ccRCC as compared with matched normal kidney tissue in both paired (Figure 1B) and unpaired (data not shown) analyses. MiR-211 (Figure S1A available online), is a miR-204 paralog expressed from intron 6 of *TRPM1* on chromosome 15q13.3. Steady-state levels of miR-211 were also reduced in tumors as compared to normal kidneys, but the absolute expression levels of this miR were about 100-fold lower than that of miR-204 (Figure 1B). In contrast, HIF-inducible miR-210 (Kulshreshtha et al., 2007) was uniformly induced in ccRCC as compared with normal kidney, as reported by others (Figure 1B) (Nakada et al., 2008; Jung et al., 2009; Juan et al., 2010).

MiR-204 inhibited the growth of RCC in two different xenograft models. In the first model, intratumoral injections of lentivirus particles containing wild-type pre-miR-204 arrested subcutaneous tumor growth, as compared with tumors injected with the same titer (10^7) of miR-204 carrying a 3-nucleotide mutation of its seed sequence (Figures 1C and S1A), which does not have miR-204 activity (see Figure 3Bb). The levels of wild-type miR-204 were in the range of miR-204 levels in normal kidneys (Figure S1B). Inhibition of tumor growth was accompanied by areas of focal necrosis, which stained positively for the necrosis marker C9, in the tumor regions directly exposed to injections (Figure 1D). Such necrosis was not observed in tumors injected with mutated miR-204 (Figure 1D). In an independent series of experiments, 786-O VHL(−) cells were transduced with lentiviral particles containing wild-type or mutated pre-miR-204 and then injected under the kidney capsules of nude mice. In each case, initial transduction efficiency was determined to be above 95% based on the number of cells expressing green fluorescent protein (Figure S1C), and the expression levels of miR-204 were also in the range of that measured in normal kidneys (Figure S1B). While the effect of miR-204 expression on tumor incidence was relatively small, there was a large decrease in the growth of tumors upon expression of miR-204 (Figure 1Ea). Moreover, tumors formed by 786-O cells expressing miR-204 were confined to the injection site under the capsule, with no infiltration of the kidney parenchyma (Figures 1Eb and 1Ec). In contrast, cells transduced with inactive mutant miR-204 formed highly invasive tumors that extensively infiltrated the kidney (Figure 1Ed). Taken together, these results indicate that miR-204 has tumor-suppressing activity.

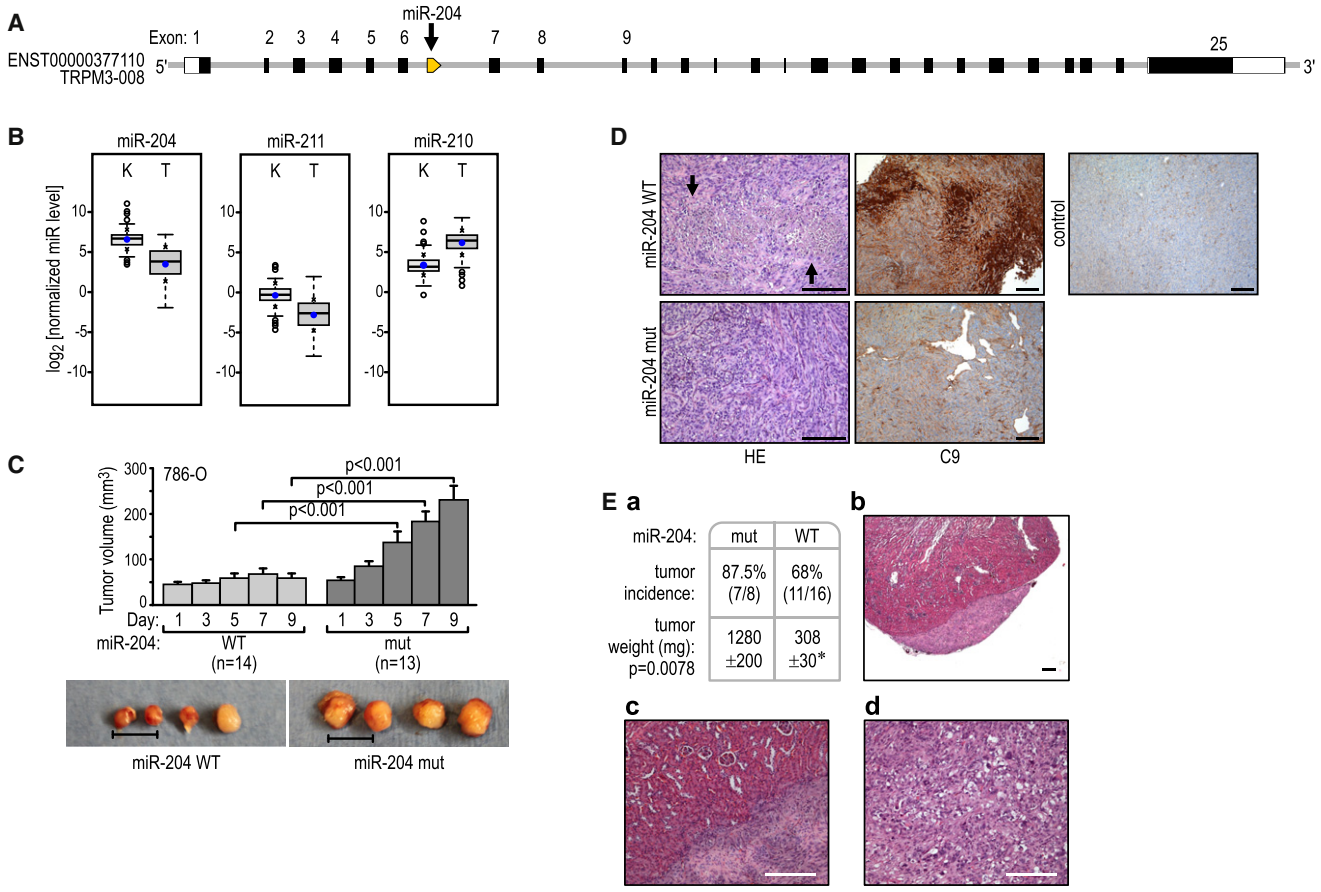

Figure 1. MiR-204 Has Tumor-Suppressing Activity in Renal Clear Cell Carcinoma

(A) Localization of miR-204 at the 5′ end of intron 6 of the host gene, *TRPM3*.

(B) Expression of miR-204, its paralog miR-211, and miR-210 in human ccRCC as compared with normal kidney tissue. Quantification of the indicated normalized miR levels (log_2) of the total unpaired kidney (K; n = 114) and tumor (T; n = 128) samples are shown. The boxes represent lower and upper quartiles separated by the median (thick horizontal line), and the whiskers extend up to the minimum and maximum values, excluding points that are outside the 1.5 interquartile range from the box (marked as circles). Means ± SD of each distribution are indicated by closed dots and crosses on the whiskers, respectively. All differences were statistically significant at $p < 0.001$.

(C) Growth of preformed 786-O VHL(−) tumors in subcutaneous xenografts injected every other day over a period of 9 days with lentiviral particles of wild-type pre-miR-204 (WT) or pre-miR-204 with the 3 bp mutation (mut). The data are cumulative over two independent series of injections. Representative samples from each group of tumors are shown. Scale bar, 1 cm.

(D) Representative images of H&E-stained or C9 antibody-probed sections from tumors injected with wild-type (top) or mutant (bottom) pre-miR-204. A section from a noninjected tumor stained for C9 is shown as a control. Scale bars, 200 μm.

(E) (a) Incidence and size of RCC tumors resulting from transduced cells injected under the kidney capsules of nude mice. (b and c) Examples of H&E-stained sections of tumors formed by cells transduced with wild-type pre-miR-204 or (d) with mutant pre-miR-204. Scale bar, 200 μm.

See also Figure S1.

MiR-204 Is Regulated by VHL

Consistent with the ccRCC tumor data, miR-204 levels in VHL(−) 786-O and A498 RCC cells were very low. Expression of miR-204, but not miR-211, was induced by reconstitution of wild-type VHL in 786-O and A498 cells, while expression of miR-210 was repressed under the same conditions, as expected (Figure 2A). Conversely, VHL knockdown in the VHL-positive Caki-1 cell line led to decreased expression of miR-204 (Figure 2B). Moreover, there was a positive and significant correlation between normalized miR-204 levels and VHL protein levels in normal human kidneys (Figures 2C and 2D). We also found that VHL-induced expression of miR-204 correlated with expression of two short transcripts from *TRPM3*, TRPM3-005 and -010, but not with expression of the large transcript encoding the full-length protein (Figures S2A and S2B). A transcriptional module with a putative promoter was identified upstream from the first exon of these short transcripts, suggesting that miR-204 is coexpressed with transcripts that do not encode the full-length protein. We have also determined that expression of miR-204 was not regulated by hypoxia lasting from 8 to 48 hr (Figure S2C), treatment with the prolyl hydroxylase inhibitor DMOG (Figure S2D), or inhibition of HIF-2α by siRNAs (Figure S2E), while all these treatments altered expression of HIF-regulated miR-210 as predicted. These data establish that VHL positively

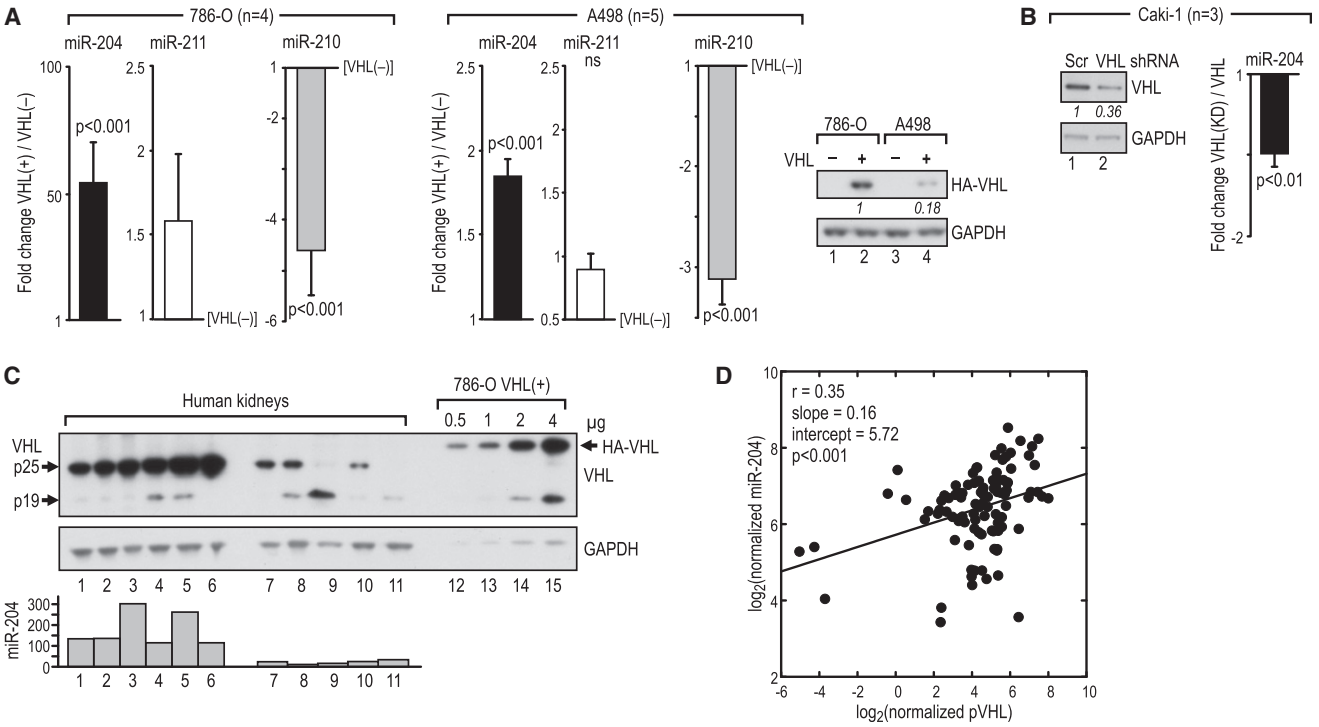

Figure 2. VHL Positively Regulates Expression of MiR-204

(A) Change in the level of miR-204, -211, and -210 in 786-O and A498 cells with reconstituted wild-type VHL as compared with the level of these miRs in VHL(−) cells. Reconstitution of human VHL (HA-VHL) is shown in a western blot.

(B) Change in miR-204 in Caki-1 with VHL knockdown as compared with cells transduced with scramble control shRNA. The western blot demonstrates knockdown of the endogenous VHL.

(C) Western blot of protein extracts from six human kidneys with high (lanes 1–6) and five human kidneys with low (lanes 7–11) levels of endogenous VHL. The indicated amounts of protein in extracts from 786-O cells with reconstituted VHL were blotted for comparison. Values for the normalized levels of miR-204 in each kidney are shown in a graph under the blot.

(D) Regression analysis of normalized miR-204 levels as a function of normalized VHL levels in kidneys (n = 99). Data are $\log_2$-transformed. Each dot represents a sample, and the solid line represents the linear regression fit, with the Pearson correlation coefficient (r) as well as the slope and intercept of the fitted line shown in the upper left corner of the box.

See also Figure S2.

regulates expression of miR-204 in a manner most likely coordinate with some of the TRPM3 transcripts but independent of HIF activity.

MiR-204 Is Cytotoxic to VHL(–) but Not VHL(+) Cells

In our search for the tumor-suppressing mechanism of miR-204, we found that expression of exogenous miR-204 in VHL(−) cells was cytotoxic if cells were cultured in starvation conditions (Figures 3A and 3B). It is important to note that the same dose of exogenous miR-204 was not cytotoxic to 786-O or A498 RCC cells reconstituted with wild-type VHL, which show several features of normal epithelial cells and are characterized by suppressed ability to form tumors in xenograft models, or to HK-2-immortalized renal epithelial cells (Figure 3Ba). The levels of exogenous miR-204 measured in VHL(−) or VHL(+) RCC cells or HK2 cells a were very similar. The effect required miR-204 targeting activity, as mutation of three nucleotides within the core binding site of miR-204 abolished this cytotoxic effect (Figure 3Bb). Figure 3C shows an example of dying VHL(−) cells with extensive cytoplasmic vacuolization, in contrast to healthy VHL(+) cells. The cytotoxic effect of miR-204 was significantly attenuated when cells were continuously grown in 10% serum (Figure 3Bb). Similarly, if VHL(−) RCC cells starved for 48 hr were treated with fresh medium containing 10% fetal calf serum for 6 hr before miR-204 was applied, the cytotoxic effect of miR-204 was greatly diminished (Figure 3D). Moreover, when cells were treated with 10 mM glucose 16 hr after addition of miR-204 (before the beginning of massive cell death), cell death was greatly reduced (Figure 3E), suggesting that cell death resulted from starvation.

By using different approaches, we excluded a role for caspase-mediated apoptosis (Figures S3A and S3B), necroptosis (Figure S3C), or cathepsin-mediated cell death as causes of the cell death (Figure S3D). Moreover, at the cell densities used in these experiments, all VHL(−) and VHL(+) cells proliferated at similar rates and no differences in their cell cycle kinetics were observed, despite starvation (data not shown).

MiR-204 Inhibits Macroautophagy Downstream of Autophagosome Initiation

The aforementioned findings prompted us to investigate the role of miR-204 in the regulation of starvation-induced autophagy.

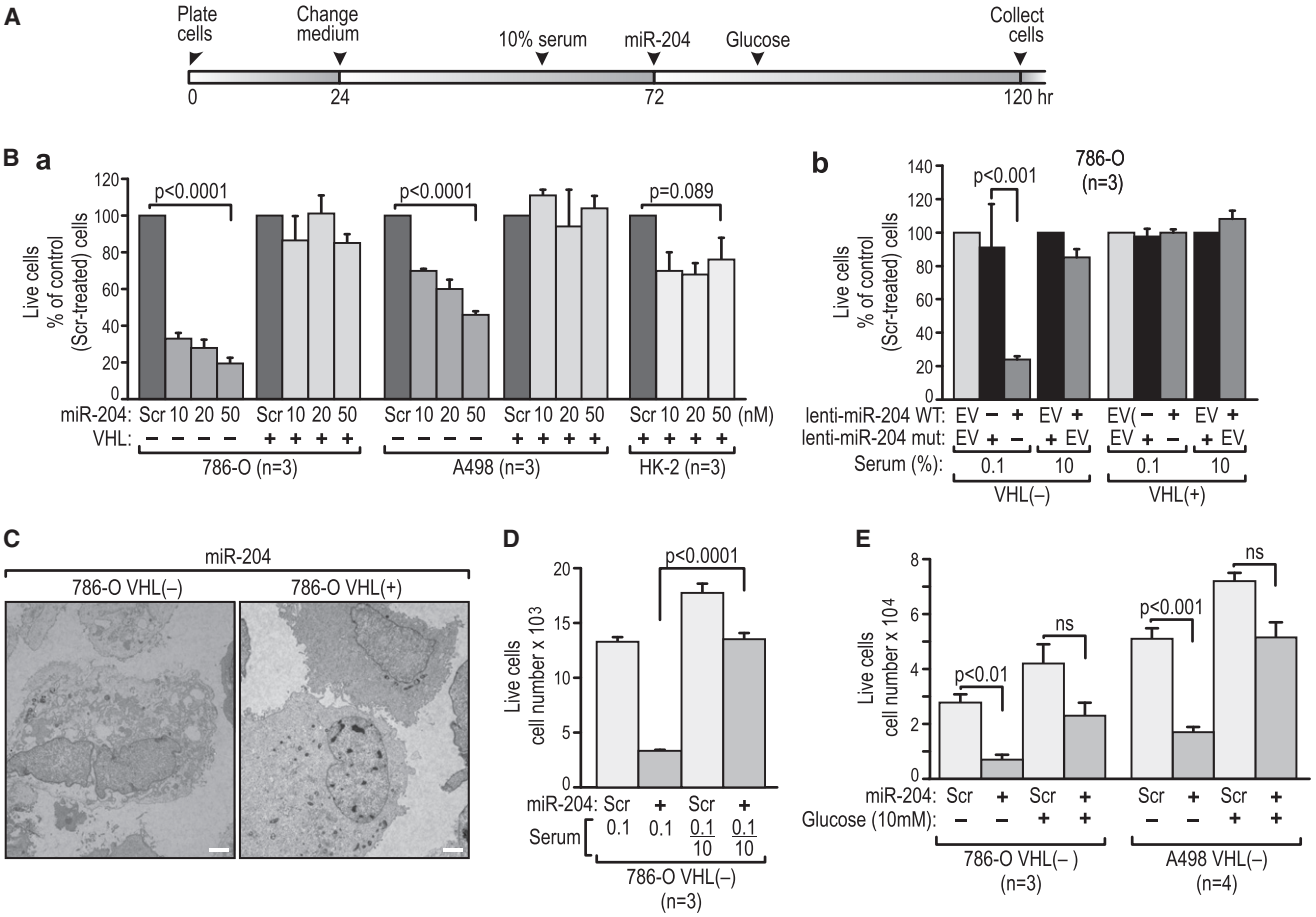

Figure 3. Cytotoxic Effects of MiR-204 in VHL(–) RCC Cells Are Eliminated by Reconstituted Wild-Type VHL

(A) Time line of the procedures performed during the course of experiments shown in (B)–(E). In all experiments, cells were plated at a density of 3,000 per well and the number of live cells treated with the scramble controls was between 10,000 and 20,000 at the time of collection (also see Figure 3C). Treatments were repeated at least three times in triplicate.

(B) Percentages of live cells determined by trypan blue exclusion 48 hr after administration of (a) short pre-miR-204 at the indicated concentrations as compared with the same cells treated with scramble control (Scr) at the same concentrations or (b) lentiviral miR-204 particles administered to the indicated cells as compared with the same cells treated with mutated miR-204 or empty virus (EV) in the presence of 0.1% or 10% serum. In (a), all experiments were performed in the presence of 0.1% serum.

(C) Example of a TEM microphotograph of VHL(–) cells dying from miR-204 cytotoxicity (left) and of live VHL(+) cells (right) under the same conditions. Scale bars, 2 μm.

(D) Numbers of live cells when fresh medium containing 10% serum was given 6 hr before administration of miR-204; see also (A).

(E) Numbers of live cells when medium was supplemented with 10 mM glucose after treatment with miR-204 (see panel A).

See also Figure S3.

Treatment with miR-204 did not cause additional cell death after autophagy was inhibited with an upstream inhibitor of macroautophagy, 3-methyladenine (Figure S4A). Moreover, similar to the effects of miR-204, inhibition of autophagy by knockdown of the upstream regulator, ATG5, resulted in significantly higher death of VHL(–) cells as compared to VHL(+) cells (Figure S4B), supporting the idea that VHL(–) cells are more dependent on autophagy and therefore more sensitive to its inhibition.

Using transmission electron microscopy (TEM) to quantify the number of autophagic vesicles, we found that treatment with miR-204 significantly reduced the number of autophagic vesicles in VHL(–) but not in VHL(+) cells, an effect measured in both the presence and absence of the autophagy inhibitor, chloroquine (Figure 4A). Moreover the vesicles present in VHL(–) cells treated with miR-204 were smaller and less developed as compared with those in the untreated cells. This indicates that miR-204 inhibits the formation of autophagic vesicles.

Next we determined whether miR-204 exerted its effect during autophagosome initiation or maturation. MiR-204 did not alter mTORC1 pathway activity (Figure S4C), indicating that the effects of miR-204 were not mediated by inhibition of this pathway. Recently, Weidberg et al. (2010) reported that inhibition of autophagy by knocking down subfamilies of LC3s or GABARAPs, which function at the level of autophagosome maturation, resulted in the accumulation of upstream regulators that participate in forming the initial membranes, such as ATG12-ATG5 and ATG16L punctate structures. Treatment with miR-204 alone significantly increased the number of cells

expressing both ATG5-ATG12 and ATG16L punctate structures and induced an increase in the number of ATG16L puncta per cell in VHL(−) cells, but not in VHL(+) cells, grown in 0.1% serum (Figures 4B, 4C, and S4D). Inhibition of autophagy by chloroquine alone also resulted in increased numbers of VHL(−) 786-O and A498 cells expressing ATG5-ATG12 puncta, with the effects significantly weaker in VHL(+) cells (Figure 4B). Chloroquine alone had a stronger effect in VHL(−) cells than miR-204 alone, and simultaneous treatment with both agents resulted in an accumulation of a similar magnitude to that induced by chloroquine alone. In the case of ATG16L puncta, chloroquine and miR-204 had similar effects on the number of cells with these puncta, particularly in 786-O cells (Figures 4C and S4D). Taken together, these data suggest that miR-204 exerts its effect downstream of the formation of the initial phagophore membranes and, possibly, at the level of autophagosome maturation.

The presence of the lipidated form of LC3 (LC3-II) in the autophagosome membrane is a marker of effective autophagy; we therefore measured accumulation of the lipidated forms of the LC3s and GABARAPs. The accumulation of LC3B-II was inhibited in VHL(−) cells by miR-204 in the absence of chloroquine (Figure 5A, lanes 6 and 5 in each panel). Treatment with chloroquine, as expected, induced accumulation of LC3B-II (Figure 5A; cf. lanes 7 and 5), but miR-204 inhibited this accumulation by two- to threefold as well (Figure 5A; cf. lanes 7 and 8). In contrast, while LC3B-II accumulated in response to chloroquine in VHL(+) cells, this response was not affected by miR-204 (Figure 5A, lanes 1–4). Similarly, while increased accumulation of LC3B-II was observed in HK-2 cells in response to chloroquine, levels of LC3B-II were not affected by miR-204 (Figure S5A). Treatment with miR-204 had no effect on the expression of LC3B mRNA in either cell line (Figure S5B). The accumulation of LC3A-II was not affected by VHL or miR-204 in any consistent manner. Surprisingly, LC3C-II was expressed only in VHL(+) RCC cells. Among the GABARAP-like proteins, only GABARAPL2-II showed slightly decreased expression in response to miR-204 (Figure 5A), and the dependence of its overall expression on VHL varied depending on the cell line. GABARP-II was predominantly expressed in 786-O VHL(+) cells and barely detectable in A498 cells. We were unable to detect expression of GABARAPL1 protein. Immunofluorescence staining confirmed the effects of miR-204 on the endogenous LC3B in VHL(−) and VHL(+) RCC cells (Figure S5C), and the results were consistent with the accumulation of LC3B-II as measured by western blot (Figure 5A). Overall, these data indicate that miR-204 inhibits starvation-induced macroautophagy in VHL(−), but not VHL(+) RCC cells, at the stages of autophagosome maturation and not at initiation.

Knockdown of LC3B resulted in a significantly higher rate of cell death in VHL(−) cells as compared with VHL(+) cells in both 786-O and A498 cells (Figures 5B and S5D). This result further supports the concept of a specific dependence of VHL(−) cells on an ATG5/LC3B/miR-204–regulated autophagic program.

LC3B Is a Direct Target of MiR-204 and It Is Necessary for MiR-204 Cytotoxic Activity

To identify specific miR-204 targets with potential relevance in the regulation of autophagy, we used several miR target-prediction algorithms (Pictar, TargetScan, Miranda, and Sanger) and found conserved miR-204 sites in the 3′UTRs of two direct regulators of autophagy, LC3B and LC3B2. Because LC3B2 is not expressed in 786-O cells, we concentrated our further analysis on LC3B.

The miR-204 binding site in LC3B mRNA is a broadly conserved element located between 55 and 61 base pairs (bp) of the LC3B 3′UTR (Figure 6Aa). The 3′UTR of LC3B with the wild-type, but not with a mutant, miR-204–binding site conferred repression by miR-204 to a luciferase reporter (Figure 6Ab). Furthermore, as expected, inhibition of miR-204 activity by using miRZip anti-204 (Mavrakis et al., 2010; Veronese et al., 2010; Lovén et al., 2010) or siRNA (80%–90% knockdown) upregulated LC3B protein expression in VHL(+) RCC cells (Figure 6B), indicating that LC3B is under constitutive repression by endogenous miR-204. This observation was further supported by a significant negative correlation between levels of miR-204 and LC3B protein in the subpopulation of human ccRCC tumors with the wild-type *VHL* (Figures 6C and 6D). It is important to note that the increased accumulation of LC3B-II in the presence of chloroquine in VHL(+) 786-O cells with miR-204 knocked down, as compared with control VHL(+) cells, indicates an induction of macroautophagy (Figure 6E, lanes 3 and 4). Moreover, levels of endogenous LC3B were higher in VHL(−) as compared with VHL(+) RCC cells (Figure 5A), consistent with higher levels of endogenous miR-204 in VHL(+) cells.

It is most important to note that reexpression of LC3B lacking the 3′UTR, and therefore insensitive to miR-204, protected VHL(−) 786-O cells from miR-204 cytotoxicity (Figure 6F). Cells from the same transfection that had lost LC3B-RFP (RFP-negative cells) or cells transfected with red fluorescent protein (RFP) alone demonstrated significant miR-204–induced cytotoxicity (Figure 6F). This rescue from cell death by expression of RFP-LC3B was accompanied by a reduction in the accumulation of ATG16L-positive puncta in response to miR-204 in RFP-LC3B–transfected cells (Figures 6G, S6A, and S6B) as compared to the effect of miR-204 on nontransfected cells (RFP-negative cells) or cells transfected with RFP alone (Figures 6G, S6C, and S6D).

Next, we asked if miR-204 was cytotoxic to cells with LC3B knocked down. In the first approach, we used 786-O and A498 pools of cells with LC3B stably knocked down (Figure S6E). Because all cells with stable LC3B knockdown grew very slowly and progressively died in medium containing 0.1% serum, they were initially seeded in higher numbers to assure a similar degree of confluence for cells in the control and LC3B knockdown pools at the time of treatment with miR-204. Under these conditions, miR-204 did not have a cytotoxic effect on 786-O or A498 cells with LC3B knockdown but remained cytotoxic to the control cells (Figure 6H). We also performed another experiment where VHL(−) cells were plated at the same densities, starved as in Figure 3A, and then transiently transfected with miR-204, siRNA for LC3B, or both, along with the respective negative controls (Figure S6F). The effects of miR-204 and LC3B siRNA on cell death were similar, and there was no additional effect when miR-204 and LC3B siRNA were applied together (Figure S6F).

LC3C Protects VHL(+) RCC Cells from Loss of LC3B-Mediated Autophagy

The presence of VHL protected RCC cells from the cytotoxic effects of miR-204 and LC3B knockdown. We found that VHL

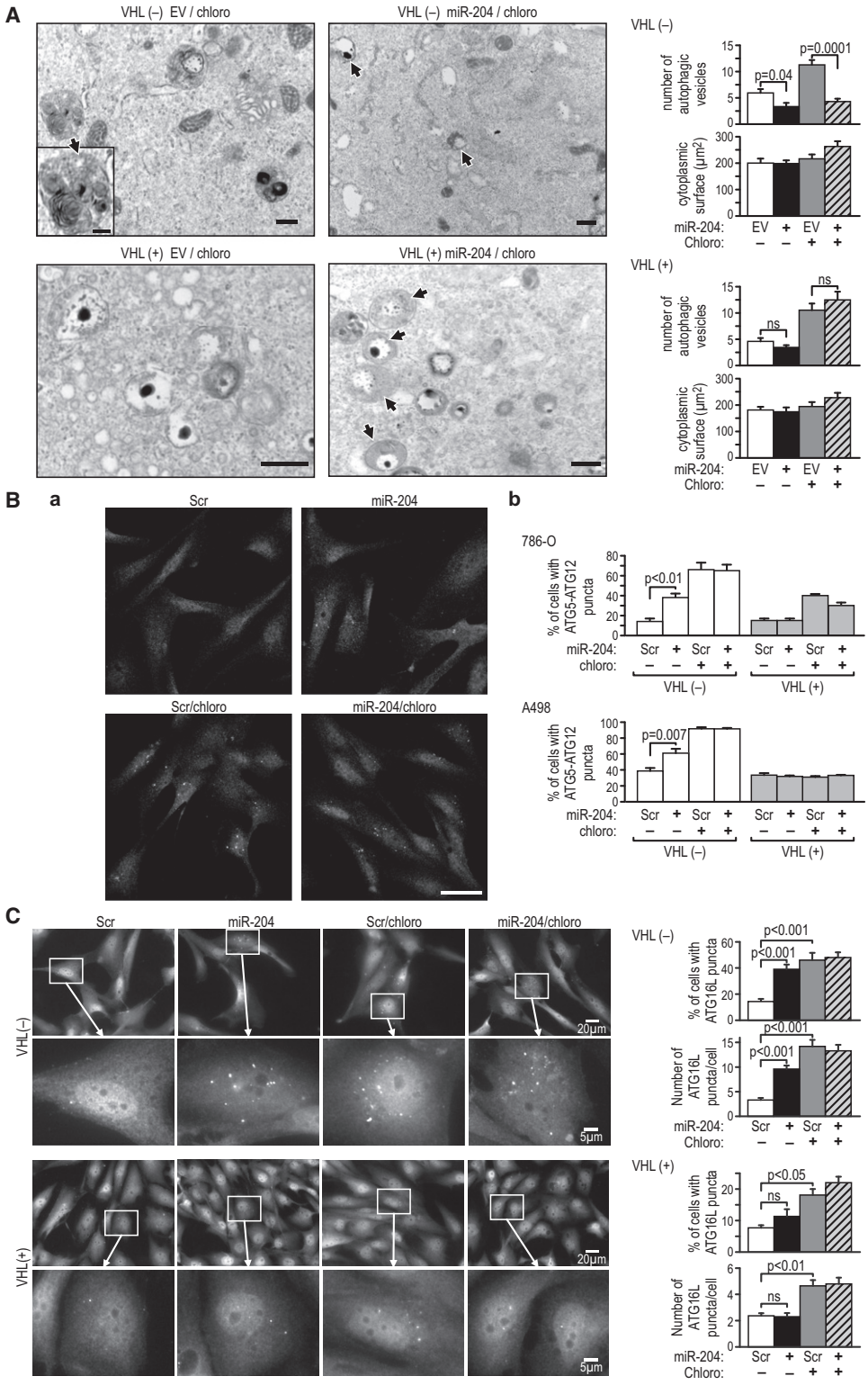

Figure 4. MiR-204 Inhibits Macroautophagy in VHL(–) Cells but Not VHL(+) Cells

(A) TEM microphotographs with quantification of the number of autophagic vesicles (AV) (top) and the cytoplasmic area (bottom) in 20 cells under the indicated conditions in 786-O VHL(−) and VHL(+) cells. Controls were treated with the same empty lentiviral constructs (EV). The arrows indicate AV. Scale bars, 1 μm. (B) Representative image of immunofluorescence staining for the endogenous ATG5-ATG12 complex in the indicated conditions in VHL(−) 786-O cells (a). (b) Quantification of the percent of cells with puncta versus total number of cells in five independent fields containing on average 50 to 150 cells per field in each condition in 786-O and A498 cells. Controls were transfected with scramble construct. Scale bar, 50 μm.

is a strong inducer of a largely uncharacterized LC3B paralog, LC3C (Figures 5A, 7A, and S7A). Reconstitution of VHL in RCC cells induced (Figures 5A and 7A), while knockdown of VHL in Caki-1 cells (Figure S7A) reduced, expression of LC3C-II. This regulation occurred at the level of mRNA (Figure 7B) and was responsive to HIF-2α. Knockdown of HIF-2α induced LC3C mRNA (Figure 7C), while activation of HIF-2α using DMOG repressed LC3C mRNA (Figure 7D). The high levels of LC3C in VHL(+) cells suggested that LC3C may protect VHL(+) cells from inhibition of LC3B-mediated autophagy. Testing this possibility, we found that the effect of a single LC3C knockdown (Figure S7B) on the survival of VHL(+) cells during serum starvation was comparable to that caused by a single knockdown of LC3B, and this effect was relatively minor. In contrast, double LC3B/LC3C knockdown (Figure S7B) reduced the viability of VHL(+) cells to the levels measured in VHL(−) cells (Figure 7E).

LC3B-Dependent Autophagy Is Necessary for RCC Tumor Growth

We then tested the hypothesis that LC3B-mediated autophagy is necessary for tumor growth. Injection of preformed subcutaneous tumors with lentiviral particles containing shRNAs against LC3B or ATG5 every other day for 9 days resulted in significant inhibition of tumor growth, as compared with tumors injected with scrambled shRNA (Figure 8A). A similar result was obtained when cell lines with stable expression of shRNA targeting LC3B or ATG5 were injected into the kidneys of nude mice, and growth of orthotopic tumors was determined after 10 weeks. 786-O VHL(−) cells formed tumors in 83% of mice, which was a reproducible incidence in at least five independent experimental series performed in our laboratory over the past 2 years (see also Yi et al., 2010). In contrast, injection of cells with knockdown of LC3B or ATG5 resulted in reduced tumor growth (Figure 8B). Similar results were obtained using A498 cells, where the formation of tumors was completely inhibited by the knockdown of either LC3B or ATG5 (Figure 8C). These data indicate that ATG5/LC3B-mediated macroautophagy is necessary for the growth of VHL(−) RCC tumors in nude mice.

Next, we determined the status of LC3B and ATG5 in 102 human kidney-ccRCC tumor pairs by using quantitative immunoblotting with a set of reference standards to normalize results from multiple blots (Yi et al., 2010). We found a significant correlation between tumor-kidney ratios of the normalized protein levels for LC3B (all three forms) and ATG5 (Figure S8A). It is important to note that we found that LC3B levels positively correlated with tumor grade, while miR-204 levels showed a negative correlation (Figure 8D), suggesting that loss of miR-204 and activation of autophagy are critical regulators of cancer progression in sporadic human ccRCC.

Finally, we tested the role of LC3C in the tumor-suppressing activity of VHL. Knockdown of LC3C in VHL(+) 786-O and A498 cells (Figure S7B) increased the incidence of small tumor formation by both cell lines when injected into the kidneys of nude mice (Figure 8E). Moreover, analysis of the human ccRCC kidney-tumor pairs revealed decrease in LC3C protein expression in majority of tumors (Figure S8B). These results support the role of LC3C as a regulator of an autophagic program involved in tumor suppression.

DISCUSSION

A large majority of human ccRCC is characterized by early loss of *VHL*. Here, we identify two pathways that are regulated by VHL and contribute significantly, although in opposite directions, to ccRCC tumor growth (Figure 8F). The data clearly demonstrate that formation of RCC tumors by VHL(−) RCC cells in nude mice requires active LC3B/ATG5-dependent autophagy. Consistent with this, progression of human ccRCC is associated with increasing levels of LC3B protein. We propose that the crucial event leading to activation of this protumorigenic autophagic program is the loss of miR-204 and derepression of LC3B, which in turn, stimulates and/or maintains autophagy. It is also likely that miR-204 regulates a network of targets that influence macroautophagy through mechanisms and pathways converging at the level of LC3B and maturation of the autophagosome without affecting phagophore initiation. This renders cancer cells addicted to macroautophagic activity, and, thus, subject to synthetic lethality when macroautophagy is inhibited by exogenous miR-204, with necrotic cell death caused by starvation.

We have also discovered that VHL, through inhibition of HIF, induces LC3C. LC3C, thus far uncharacterized, contributes to basic autophagic activity in VHL(+) cells at a level similar to LC3B, but it also mediates an antitumorigenic autophagic activity as its knockdown increased the incidence of small tumors in VHL(+) cells. At present, the biochemical activity of such a program is not understood, but there is growing evidence for autophagic programs that are not mediated by ATG5/LC3B (Nishida et al., 2009) or ULK1/2 (Cheong et al., 2011). Thus, LC3C could be a part of such yet unidentified pathway or could participate in a nonautophagic tumor-suppressing pathway. Moreover, an LC3C-specific autophagic program could have selectivity toward specific pro-oncogenic targets. It is interesting that the potential functional differences between LC3C and LC3B/LC3A could be related to the fact that LC3C contains an unstructured C terminus domain that is not present in other family members. The mechanism by which HIF represses expression of LC3C remains to be investigated, but the LC3C proximal promoter contains E2-boxes, similar to those that mediate HIF-dependent inhibition of E-cadherin mRNA by ZFHX1B and SNAI1 (Esteban et al., 2006; Evans et al., 2007).

The requirement for macroautophagy in RCC cells, and the protective activity of LC3C in normal cells, creates a unique opportunity for the use of miR-204 or miR-204-like approaches

(C) Representative image of immunofluorescence staining for endogenous ATG16L puncta in 786-O VHL(−) and VHL(+) cells under the indicated conditions. Percentage of cells expressing puncta under the indicated conditions was calculated as in (B). 100 cells expressing puncta were analyzed for each condition, with the exception of nontreated controls where the number of cells with puncta was small and only 30 to 50 cells were counted. Control cells were treated with scramble construct. Scale bars are as indicated in the figure. All measurements shown in this figure were performed on cells grown in 0.1% serum and 24–30 hr after treatment with miR-204. This was approximately 24 hr before cell death was observed as shown in Figure 3B.
See also Figure S4.

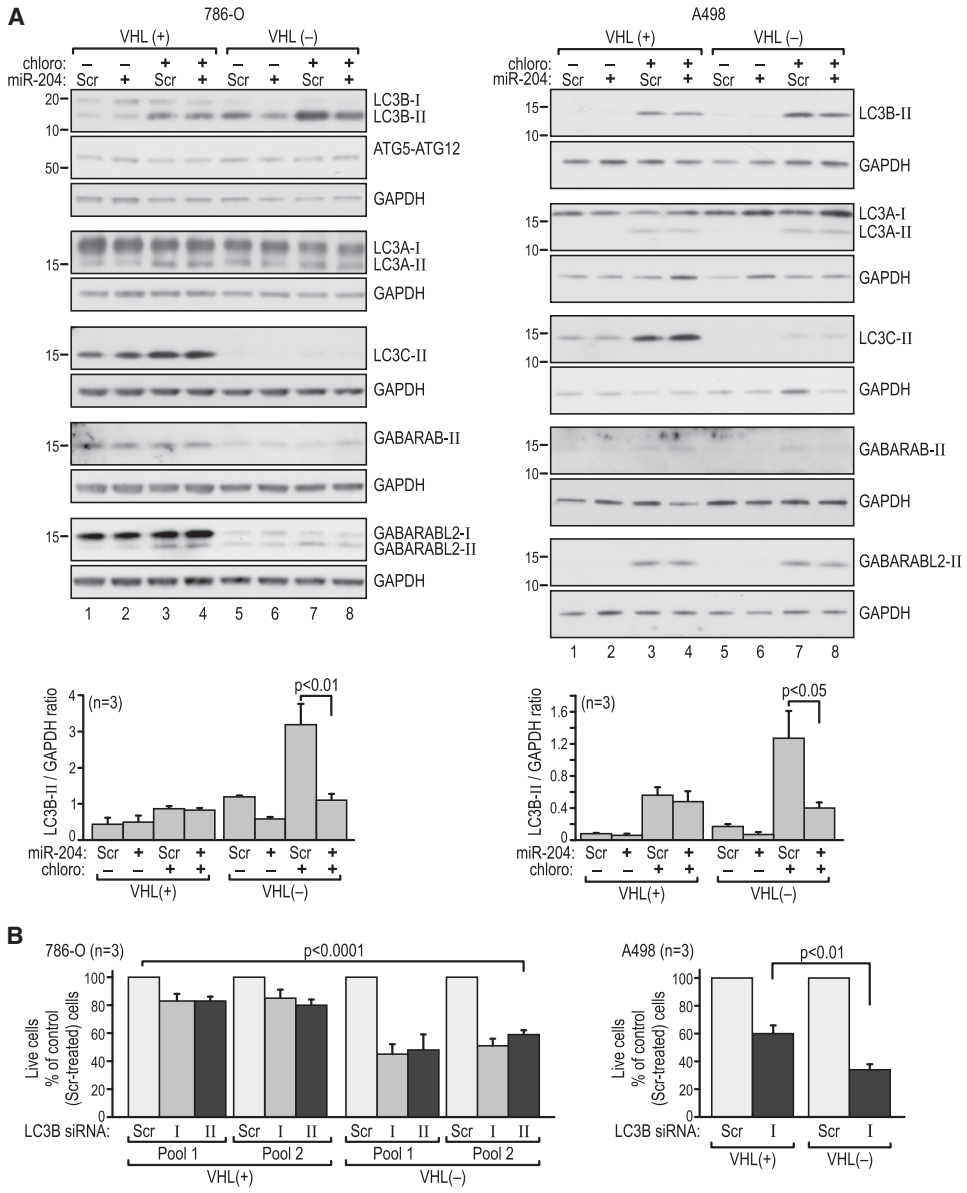

Figure 5. MiR-204 Specifically Represses Accumulation of LC3B-II in the Flux Experiment

(A) Western blot analysis of LC3 paralogs in extracts from 786-O and A498 cells grown in 0.1% serum conditions. The experiment follows the same treatment sequence as shown in Figure 3A, with 100 μM chloroquine applied 24 hr after treatment with short pre-miR-204 or scramble control. The cells were collected after 1.5 hr in the case of 786-O cells and after 3 hr in the case of A498 cells, when saturating effects of chloroquine were observed based on the time course experiments. This was approximately 24 hr before cell death was observed as shown in Figure 3B. Quantification of three independent experiments is shown at the bottom.

(B) Percentage of live cells measured using trypan blue analysis in 786-O and A498 VHL(+) and VHL(–) cells transfected with LC3B siRNAs, where 100% corresponds to live cells counted after transfection with scramble control construct.

Time line is as shown in Figure S4A.

See also Figure S5.

in the treatment of RCC. Such strategies would spare normal epithelial cells while killing malignant tumor cells. In particular, a therapeutic approach inducing cytotoxic, rather than cytostatic, effects is desirable, as the currently used antiangiogenic treatments are only cytostatic. Of note, treatments for pancreatic cancer involving general inhibitors of autophagy, such as chloroquine, are currently in clinical trials (Yang et al., 2011).

While VHL is a positive regulator of miR-204 expression in normal tissues, it is likely that factors additional to the loss of VHL could trigger decreased miR-204 expression, particularly during cancer progression. In that respect, miR-204 is expressed from locus 9q21.12, and published data indicate that chromosome 9 is the second most frequently lost chromosome, after 3p, in ccRCC (20%–30% of tumors) and decreased

expression of genes from this region was reported (Fukunaga et al., 2002; Yoshimoto et al., 2007; Toma et al., 2008). Our initial evidence points toward coordinated expression of miR-204 with short, but not full-size, TRPM3 transcripts, which could represent a more general mechanism for expression of intronic miRs from long genes.

Taken together, our findings indicate that VHL regulates at least two autophagic programs through an HIF-independent pathway activating miR-204 and an HIF-regulated pathway activating LC3C.

EXPERIMENTAL PROCEDURES

Human RCC Tumors

Fresh-frozen samples of renal clear cell carcinomas (n = 128) and matched normal kidneys (n = 114) were obtained and analyzed for *VHL* gene sequence and protein expression as described earlier (Yi et al., 2010). Specimens were also analyzed for expression of miR-204, miR-211, and miR-210. All human samples were anonymous and exempted from institutional review board protocol.

Cell Culture Methods and Treatments

Pools of human VHL(−) and VHL(+) 786-O and Caki-1 cells were described by us before (Mikhaylova et al., 2008; Yi et al., 2010); A498 cells were obtained from Dr. W. G. Kaelin Jr., (Dana-Farber Institute, Harvard Medical School). HK-2 cells were purchased from ATCC. All cells were authenticated (Genetica, Cincinnati, OH). For miR-204 treatments, cells were plated in 12-well cell culture dishes at 3,000 per well in normal medium. Twenty-four hours later, the medium was replaced with fresh medium containing 10% or 0.1% serum. After the next 48 hr, cells were transduced with lentiviral particles containing wild-type or mutated pri-miR-204 or transfected with the respective short pre-miR-204, in each case with the appropriate negative controls. Cell viability was determined 48 hr after miR-204 treatment by trypan blue exclusion. For the LC3-II flux experiments, cells were plated and treated as described earlier, and 24 hr after miR-204 treatment, cells were treated with 100 μM chloroquine to inhibit lysosomal function. Cells were collected at the indicated times and analyzed by PAGE for the proteins of interest.

Quantitative Real-Time PCR

Total RNA was extracted using the mirVana miRNA Isolation kit (Ambion). For microRNA analysis, the samples were first reverse transcribed using the TaqMan microRNA Reverse Transcription kit and miR-specific primers and probes (TaqMan microRNA Assays, Applied Biosystems) and were quantified with real-time PCR on an Applied Biosystems 7900HT Fast Real-Time PCR System. The small nucleolar RNA (snoRNA) RNU44 was used as the internal control for the $-\Delta Ct$ calculation. Data are presented normalized to snoRNU44 or as ratios of the normalized values between paired cell lines differing in the status of VHL or tumor/kidney pairs. For mRNA, qRT-PCR was performed as described before (Yi et al., 2010), and the sequence of primers is provided in the Supplemental Experimental Procedures.

Constructs and Plasmids

The following miR-204 reagents were used: Pre-miR-204 precursor and Pre-miR negative control were purchased from Ambion (Pre-miR-204 miRNA Precursor Molecules and negative control Pre-miR miRNA Precursor Molecules). Anti-miR-204 and the corresponding negative control were purchased from Dharmacon (miRIDIAN Hairpin Inhibitor: human hsa-miR-204, and miRIDIAN microRNA Hairpin Inhibitor Negative Control #1). HIV-based lenti-miR pri-micro RNA-204 construct and control lentivector were from System Biosciences (microRNA Expression Construct Lenti-miR-204 MI0000284 and corresponding lentivector negative control). To alter the miR-204 core sequence, we performed site-directed mutagenesis on PMIRH204 to replace the core CCC sequence with a GGG sequence (GenScript). The mutation was verified by sequencing. A list of siRNA and shRNA constructs is provided in the Supplemental Experimental Procedures. All lentiviral DNA constructs were VSV-G envelope packaged (Cincinnati Children's Hospital Medical Center Viral Vector Core) and infected into cells followed by plasmid-appropriate selection. The LC3B-RFP construct contained human LC3B-myc fused to RFP from pDsRed1-N1 in the PRK5 vector and was a gift from Drs. P. Dennis and C. Mercer (University of Cincinnati). The Luciferase-LC3B-3′UTR construct was based on pLightSwitch_3′UTR vector and purchased from Switchgear Genomics.

Transfections and Transduction Experiments

Transient transfections of microRNA constructs or pools of siRNAs were performed using Lipofectamine 2000 according to the manufacturer's protocol. Transductions with lentiviral particles were performed using 2 μg/ml of polybrene.

Western Blot Analysis

Total cellular lysates were obtained by lysing cells in RIPA buffer containing proteinase and phosphatase inhibitors. A total of 5 to 30 μg of extracts were separated on 12% polyacrylamide gels and transferred on to polyvinylidene fluoride membrane. Blots were probed with relevant antibodies described in the Supplemental Experimental Procedures. Quantitative immunoblotting for human RCC tumors and matched kidneys was performed as described in (Yi et al., 2010).

Mouse Xenograft Experiments

All experiments on mice were performed in accordance with University of Cincinnati Institutional Animal Care and Use Committee-approved protocol. For the intrakidney injections, 30,000 cells were resuspended in Matrigel to a final volume of 30 μl and then slowly injected into the parenchyma of the kidneys of 4- to 5-week-old athymic nude mice, and tumors were collected after 10–12 weeks. For the subcutaneous injections, 1×10^6 cells in cell culture medium were injected subcutaneously into the flanks of the same strain of nude mice. After 6 weeks, these tumors reached an approximate average volume of 50 mm^3, and mice were randomly assigned to groups in which the tumors would be injected with specific viral particles containing constructs encoding mutant miR-204, wild-type miR-204, or specific shRNAs. For each control and experimental condition, the same titer of viral particles was used. Injections were performed with 25 μl of supernatant every other day for a period of 9 days. Before injections, three standard dimensions of the tumor were measured with a protractor, and the volume of the tumor was calculated using the equation $d1 \times d2 \times d3 \times \pi/6$. At the end of the experiments, mice were sacrificed and tumors were fixed in 4% paraformaldehyde, paraffin embedded, and hematoxylin and eosin (H&E) stained or processed for immunocytochemistry using a monoclonal antibody against Complement Component 9 (Vector Laboratories).

Immunofluorescence Staining

Cells were plated on coverslips and treated with miR-204. At the end of the experiment, cells were fixed in 4% paraformaldehyde, permeabilized in 0.3% Triton, blocked in 0.1% Triton with 3% bovine serum albumin, and incubated with primary antibody for 1 hr at 37°C. Cells were then washed and incubated with the Alexa 488-labeled secondary antibody for 1 hr at room temperature. Confocal images were acquired on a Zeiss LSM510 confocal or by using a Zeiss Axioplan 2 microscope with the appropriate filter cubes and a Zeiss Axiocam MRm to record the images. The number of cells expressing puncta and the number of puncta per cell were counted manually.

Preparation of Samples and TEM

Samples were processed in the Electron Microscopy Core at Cincinnati Children's Hospital Medical Center. Briefly, cells were washed with PBS and resuspended in 0.2 M cacodylate buffer with 3% glutaraldehyde. Cells were postfixed with 1% osmium tetroxide (Electron Microscopy Sciences, Fort Washington, PA) with 0.2 M sodium cacodylate buffer for 1 hr at 4°C. After three washes with 0.2 M sodium cacodylate buffer, cells were resuspended in 1% agarose (type IX, Sigma), centrifuged for 5 min at 3,000 rpm, and left for 24 hr at 4°C. The following day, samples were dehydrated and embedded in LX-112 embedding medium (Ladd Research Industries, Burlington, VT). Samples were then polymerized for 48 hr at 60°C, cut into 100-nm-thick sections on a USA Reichert-Jung UltraCut E microtome, positioned on 200 mesh grids, and stained with uranyl acetate and lead citrate. TEM was

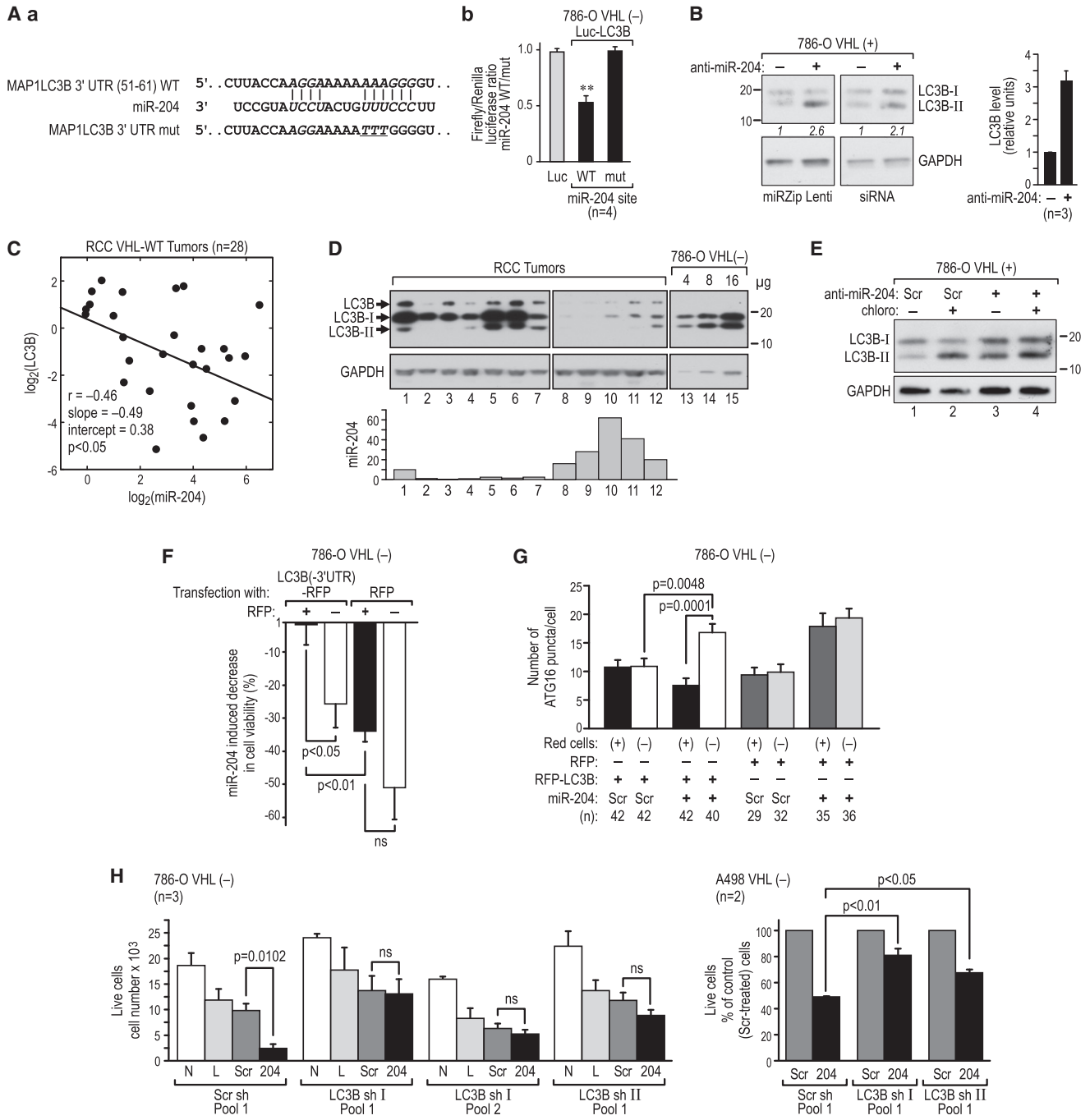

Figure 6. MAP1LC3B Is a Direct Target of MiR-204

(A) (a)Sequence of the wild-type (WT) miR-204 site in the 3′UTR of LC3B and mutation (mut) of the core binding site. (b) The 3′UTR of LC3B with the wild-type but not mutant miR-204 site confers regulation by miR-204 to the luciferase reporter construct.

(B) Effects of an anti-miR-204 lentiviral Zip or siRNAs on LC3B protein expression in 786-O VHL(+) RCC cells shown by western blot and quantification of three independent experiments.

(C) Regression analysis showing negative correlation between normalized miR-204 level and normalized LC3B protein level in human ccRCC tumors with the wild-type *VHL*, performed as described in Figure 2D.

(D) Representative western blot showing tumors with high and low levels of LC3B. Normalized values of miR-204 levels for each tumor are shown in a graph below the blot. Expression of LC3B in 786-O cells is shown as reference.

(E) Western blot showing accumulation of LC3B-II in 786-O VHL(+) cells treated with anti-miR-204 in the absence or presence of 100 μM chloroquine.

(F) 786-O VHL(–) cells transfected with RFP-LC3B or RFP were sorted, plated, and maintained for 48 hr in medium containing 0.1% serum. Cells were then treated with 25 nM short pre-miR-204 or scramble control construct and, 48 hr later, stained by DAPI. Fraction of live cells was determined among the stained and unstained cells in both conditions.

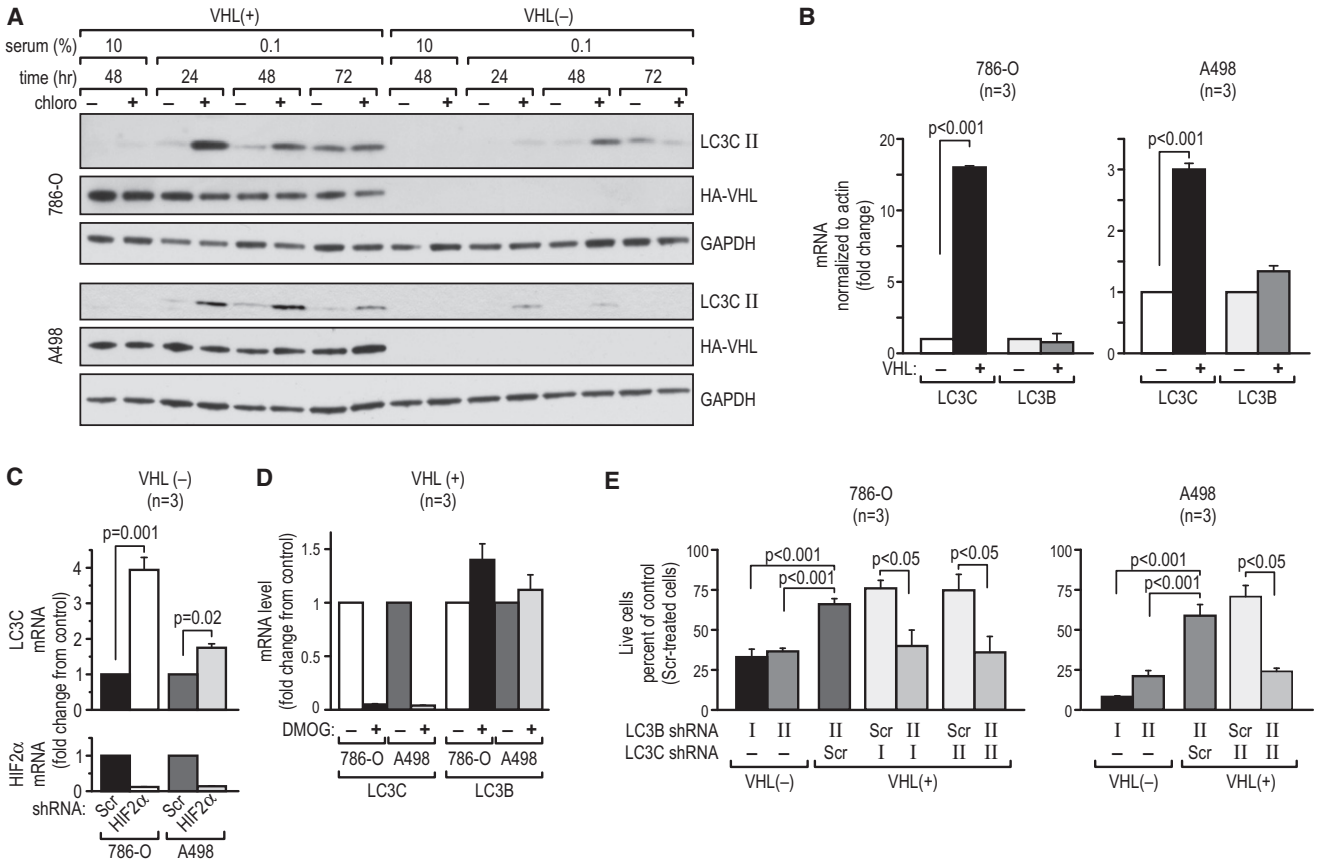

Figure 7. VHL-Induced Expression of LC3C Protects RCC Cells from Inhibition of LC3B-Dependent Autophagy

(A) Western blot showing time course of LC3C-II induction in VHL(+) and VHL(–) 786-O and A498 cells in response to serum starvation.

(B) Quantitative RT-PCR for LC3C and LC3B mRNAs (48 hr of starvation) in VHL(+) as compared with VHL(–) cells.

(C) Quantitative RT-PCR for LC3C mRNA in VHL(–) cells where HIF-2α was knocked down by using siRNA.

(D) Quantitative RT-PCR for LC3C mRNA in VHL(+) cells where HIF was stimulated with DMOG (1 mM) for 16 hr.

(E) Effect of single LC3C or LC3B knockdown or of double LC3C/LC3B knockdown on the viability of indicated cells, as compared with scramble-treated cells. The timeline followed was the same as that shown in Figure 3A.

See also Figure S7.

performed on a JEOL 1230 TEM at an accelerating voltage of 80 kV. Images were acquired with an AMT Advantage Plus 2K × 2K digital camera connected to the TEM.

LC3B Rescue Experiments

Cells were plated at 85,000 cells per 60 mm plate in regular medium containing 10% fetal bovine serum (FBS). Transfections with LC3B-RFP or RFP construct were performed 24 hr later using Lipofectamine LTX and PLUS reagent (Invitrogen) according to the manufacturer's protocol. Expression of RFP was clearly visible by 24 hr to 30 hr after transfection. Cells were then collected and sorted using a BD FACSAria. Sorted cells were plated at a density of 5,000 per well in 12-well plates in normal medium with 10% FBS with added antibiotics and antimycotics. Twenty-four hours after plating, the medium was replaced with medium containing 0.1% serum. After 48 hr of starvation, cells were transfected with 25 nM of pre-miR-204 precursor or a negative control construct (Ambion) by using Lipofectamine 2000. On the last day, cells were collected, stained with DAPI to distinguish live cells, and the percentage of RFP+ cells was determined, among both viable and dead cell populations, by flow cytometry.

Statistical Analysis

For descriptive statistics, data are expressed as mean ± SEM unless indicated otherwise. Analysis of differential expression was performed using one-way analysis of variance, followed by Tukey-Kramer multiple comparison tests.

(G) Quantification of endogenous ATG16L puncta per cell in 786-O VHL(–) cells transfected with LC3B-RFP or RFP alone and treated with miR-204 as in (F). For red cells, a plus sign indicates cells expressing RFP fluorescence from either construct, and a minus sign indicates cells that did not express RFP fluorescence. Numbers of cells (n) in which puncta were counted are shown below the graph.

(H) Effect of LC3B knockdown on cell death induced by miR-204. 786-O or A498 VHL(–) cells stably transfected with two different LC3B shRNAs or scramble construct were additionally transfected with miR-204 or scramble control. Two independent pools of 786-O cells expressing LC3B sh I RNA were used (Pool 1 and Pool 2). N, nontreated cells; L, cells transfected with Lipofectamine only; Scr, cells transfected with scramble pre-miR-204 control; 204, cells transfected with 50 nM of pre-miR-204.

See also Figure S6.

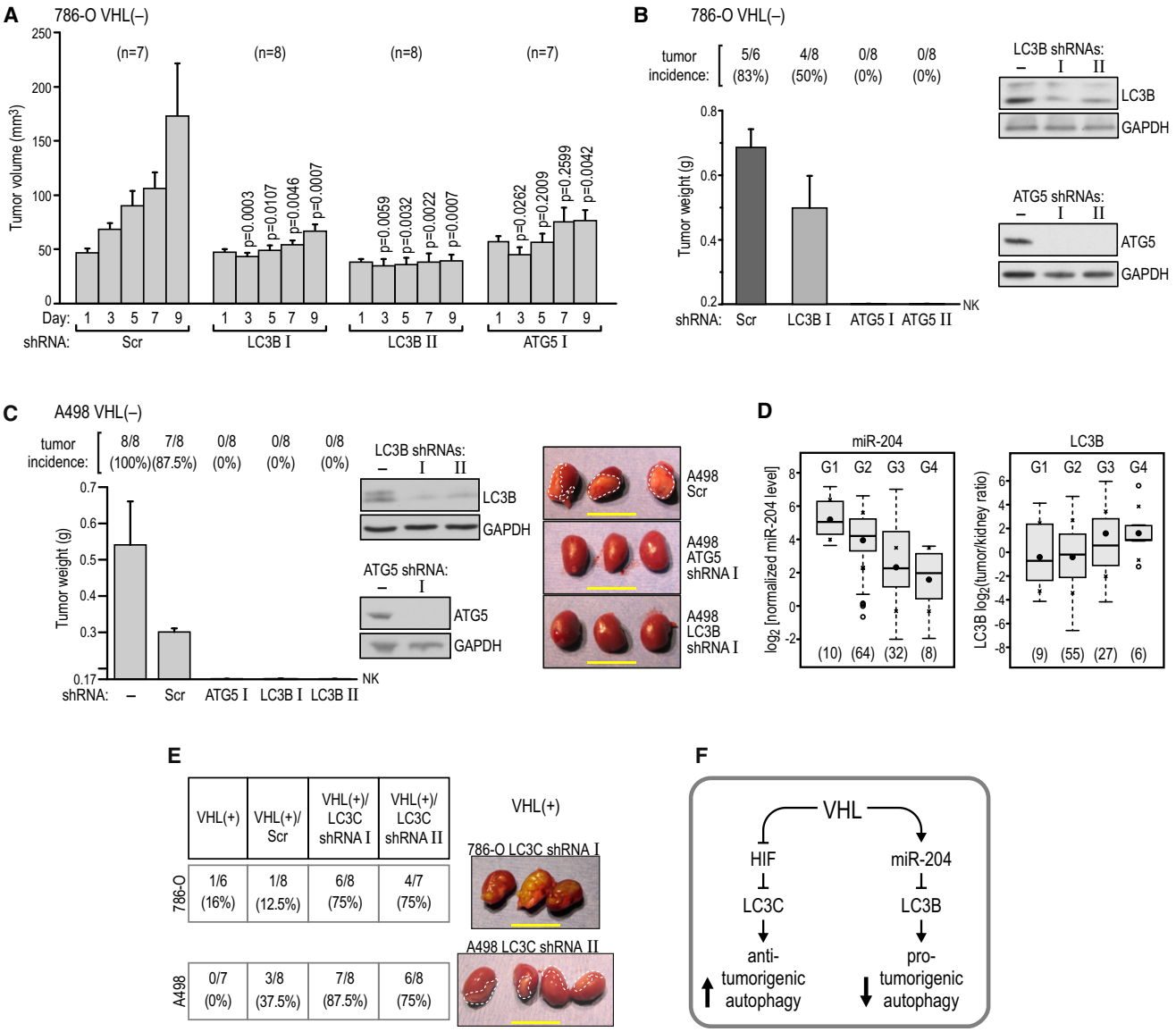

Figure 8. LC3B-Dependent Macroautophagy Is Necessary for RCC Tumor Growth

(A) Growth of tumors formed by 786-O VHL(−) cells in subcutaneous xenografts injected with packaged lentiviruses containing two different shRNAs against LC3B, or one against ATG5, as compared with the growth of control tumors injected with scramble sequence-containing virus. The number of mice in each experiment is shown in parentheses above the graph.

(B) Growth of tumors formed by pools of 786-O VHL(−) cells stably transfected with two different shRNAs against ATG5 or one against LC3B, and injected under the kidney capsule in nude mice. Western blots show levels of protein knockdown in stable pools of cells under conditions of 10% serum starvation. Cells were plated and grown for 48 hr in medium containing 10% serum before injection.

(C) Growth of tumors formed by pools of A498 VHL(−) cells stably transfected with two different shRNAs against LC3B and one against ATG5 and injected under the kidney capsule in nude mice. Western blots show levels of protein knockdown in stable pools of cells. Cells were treated as in (B). Photographs of representative tumors are shown with dashed lines drawn to help visualize the tumors.

(D) There is a significant decrease in the level of miR-204 ($p < 0.001$) and a significant increase in the level of LC3B ($p < 0.05$) correlating with tumor grade in human ccRCC tumors. Because of the small number of tumors classified as Grades 1 and 4, the statistical comparison was made between combined subpopulations of G1+G2 versus G3+G4 tumors. The number of tumors of each grade is provided in parentheses at the bottom. Statistics were calculated as in Figure 1B. Means ± SD are shown.

(E) Formation of tumors in orthotopic xenografts by VHL(+) 786-O and A498 with stable knockdowns of LC3C using two different LC3C shRNAs in each cell line. The table lists numbers of mice analyzed and photographs of representative tumors are shown. Dashed lines help visualize tumorigenic infiltrate of A498 cells. All scale bars, 1 cm.

(F) Schematic representation of the role of VHL in the regulation of autophagy in RCC tumor growth.

See also Figure S8.

Differences where $p < 0.05$ were considered to be statistically significant. In quantitative immunoblotting experiments, we used $\log_2$-transformed normalized values to facilitate robust and outlier-insensitive analyses. Standard box-and-whisker plots were used to compare distributions of the normalized abundance measure for individual proteins. Correlations between variables were assessed by means of regression analysis and by Pearson and Spearman rank correlation coefficients.

SUPPLEMENTAL INFORMATION

Supplemental Information includes eight figures and Supplemental Experimental Procedures and can be found with this article online at doi:10.1016/j.ccr.2012.02.019.

ACKNOWLEDGMENTS

This work was supported in part by the following grants: NCI CA122346, DoD W81XWH-07-02-0026, BLR&D VA Merit Award to M.F.C.-K., and UC P30-ES006096 CEG; D.R.P. and C.A.G. were supported by NCI Grant CA133164. We thank Drs. P. Dennis and C. Mercer for LC3B-RFP constructs, K. Winstead for the collection of human ccRCC tumors, Z. Shan for the histological preparation of tumor sections, G. Ciraolo for processing tissues for TEM, J. Neumann for injection of mice, G. Doerman for preparing the figures, Dr. M. Daston for editorial assistance, and undergraduate students P. Bastola and P.J. Krzeski for technical assistance.

Received: October 5, 2010
Revised: January 6, 2012
Accepted: February 15, 2012
Published: April 16, 2012

REFERENCES

Axe, E.L., Walker, S.A., Manifava, M., Chandra, P., Roderick, H.L., Habermann, A., Griffiths, G., and Ktistakis, N.T. (2008). Autophagosome formation from membrane compartments enriched in phosphatidylinositol 3-phosphate and dynamically connected to the endoplasmic reticulum. J. Cell Biol. *182*, 685–701.

Behrends, C., Sowa, M.E., Gygi, S.P., and Harper, J.W. (2010). Network organization of the human autophagy system. Nature *466*, 68–76.

Calin, G.A., and Croce, C.M. (2006). MicroRNA signatures in human cancers. Nat. Rev. Cancer *6*, 857–866.

Cheong, H., Lindsten, T., Wu, J., Lu, C., and Thompson, C.B. (2011). Ammonia-induced autophagy is independent of ULK1/ULK2 kinases. Proc. Natl. Acad. Sci. USA *108*, 11121–11126.

Czech, M.P. (2006). MicroRNAs as therapeutic targets. N. Engl. J. Med. *354*, 1194–1195.

Degenhardt, K., Mathew, R., Beaudoin, B., Bray, K., Anderson, D., Chen, G., Mukherjee, C., Shi, Y., Gélinas, C., Fan, Y., et al. (2006). Autophagy promotes tumor cell survival and restricts necrosis, inflammation, and tumorigenesis. Cancer Cell *10*, 51–64.

Esteban, M.A., Tran, M.G., Harten, S.K., Hill, P., Castellanos, M.C., Chandra, A., Raval, R., O'brien, T.S., and Maxwell, P.H. (2006). Regulation of E-cadherin expression by VHL and hypoxia-inducible factor. Cancer Res. *66*, 3567–3575.

Evans, A.J., Russell, R.C., Roche, O., Burry, T.N., Fish, J.E., Chow, V.W., Kim, W.Y., Saravanan, A., Maynard, M.A., Gervais, M.L., et al. (2007). VHL promotes E2 box-dependent E-cadherin transcription by HIF-mediated regulation of SIP1 and snail. Mol. Cell. Biol. *27*, 157–169.

Fukunaga, K., Wada, T., Matsumoto, H., Yoshihiro, S., Matsuyama, H., and Naito, K. (2002). Renal cell carcinoma: allelic loss at chromosome 9 using the fluorescent multiplex-polymerase chain reaction technique. Hum. Pathol. *33*, 910–914.

Gossage, L., and Eisen, T. (2010). Alterations in VHL as potential biomarkers in renal-cell carcinoma. Nat. Rev. Clin. Oncol. *7*, 277–288.

Hailey, D.W., Rambold, A.S., Satpute-Krishnan, P., Mitra, K., Sougrat, R., Kim, P.K., and Lippincott-Schwartz, J. (2010). Mitochondria supply membranes for autophagosome biogenesis during starvation. Cell *141*, 656–667.

He, C., and Klionsky, D.J. (2009). Regulation mechanisms and signaling pathways of autophagy. Annu. Rev. Genet. *43*, 67–93.

Heng, D.Y., and Bukowski, R.M. (2008). Anti-angiogenic targets in the treatment of advanced renal cell carcinoma. Curr. Cancer Drug Targets *8*, 676–682.

Jin, S., DiPaola, R.S., Mathew, R., and White, E. (2007). Metabolic catastrophe as a means to cancer cell death. J. Cell Sci. *120*, 379–383.

Juan, D., Alexe, G., Antes, T., Liu, H., Madabhushi, A., Delisi, C., Ganesan, S., Bhanot, G., and Liou, L.S. (2010). Identification of a microRNA panel for clear-cell kidney cancer. Urology *75*, 835–841.

Jung, M., Mollenkopf, H.J., Grimm, C., Wagner, I., Albrecht, M., Waller, T., Pilarsky, C., Johannsen, M., Stephan, C., Lehrach, H., et al. (2009). MicroRNA profiling of clear cell renal cell cancer identifies a robust signature to define renal malignancy. J. Cell. Mol. Med. *13* (9B), 3918–3928.

Klionsky, D.J., Abeliovich, H., Agostinis, P., Agrawal, D.K., Aliev, G., Askew, D.S., Baba, M., Baehrecke, E.H., Bahr, B.A., Ballabio, A., et al. (2008). Guidelines for the use and interpretation of assays for monitoring autophagy in higher eukaryotes. Autophagy *4*, 151–175.

Kota, J., Chivukula, R.R., O'Donnell, K.A., Wentzel, E.A., Montgomery, C.L., Hwang, H.W., Chang, T.C., Vivekanandan, P., Torbenson, M., Clark, K.R., et al. (2009). Therapeutic microRNA delivery suppresses tumorigenesis in a murine liver cancer model. Cell *137*, 1005–1017.

Krützfeldt, J., Rajewsky, N., Braich, R., Rajeev, K.G., Tuschl, T., Manoharan, M., and Stoffel, M. (2005). Silencing of microRNAs in vivo with 'antagomirs'. Nature *438*, 685–689.

Kulshreshtha, R., Ferracin, M., Wojcik, S.E., Garzon, R., Alder, H., Agosto-Perez, F.J., Davuluri, R., Liu, C.G., Croce, C.M., Negrini, M., et al. (2007). A microRNA signature of hypoxia. Mol. Cell. Biol. *27*, 1859–1867.

Lovén, J., Zinin, N., Wahlström, T., Müller, I., Brodin, P., Fredlund, E., Ribacke, U., Pivarcsi, A., Påhlman, S., and Henriksson, M. (2010). MYCN-regulated microRNAs repress estrogen receptor-alpha (ESR1) expression and neuronal differentiation in human neuroblastoma. Proc. Natl. Acad. Sci. USA *107*, 1553–1558.

Lu, J., Getz, G., Miska, E.A., Alvarez-Saavedra, E., Lamb, J., Peck, D., Sweet-Cordero, A., Ebert, B.L., Mak, R.H., Ferrando, A.A., et al. (2005). MicroRNA expression profiles classify human cancers. Nature *435*, 834–838.

Mathew, R., Karantza-Wadsworth, V., and White, E. (2007). Role of autophagy in cancer. Nat. Rev. Cancer *7*, 961–967.

Mavrakis, K.J., Wolfe, A.L., Oricchio, E., Palomero, T., de Keersmaecker, K., McJunkin, K., Zuber, J., James, T., Khan, A.A., Leslie, C.S., et al. (2010). Genome-wide RNA-mediated interference screen identifies miR-19 targets in Notch-induced T-cell acute lymphoblastic leukaemia. Nat. Cell Biol. *12*, 372–379.

Mikhaylova, O., Ignacak, M.L., Barankiewicz, T.J., Harbaugh, S.V., Yi, Y., Maxwell, P.H., Schneider, M., Van Geyte, K., Carmeliet, P., Revelo, M.P., et al. (2008). The von Hippel-Lindau tumor suppressor protein and Egl-9-Type proline hydroxylases regulate the large subunit of RNA polymerase II in response to oxidative stress. Mol. Cell. Biol. *28*, 2701–2717.

Nakada, C., Matsuura, K., Tsukamoto, Y., Tanigawa, M., Yoshimoto, T., Narimatsu, T., Nguyen, L.T., Hijiya, N., Uchida, T., Sato, F., et al. (2008). Genome-wide microRNA expression profiling in renal cell carcinoma: significant down-regulation of miR-141 and miR-200c. J. Pathol. *216*, 418–427.

Negrini, M., Ferracin, M., Sabbioni, S., and Croce, C.M. (2007). MicroRNAs in human cancer: from research to therapy. J. Cell Sci. *120*, 1833–1840.

Nishida, Y., Arakawa, S., Fujitani, K., Yamaguchi, H., Mizuta, T., Kanaseki, T., Komatsu, M., Otsu, K., Tsujimoto, Y., and Shimizu, S. (2009). Discovery of Atg5/Atg7-independent alternative macroautophagy. Nature *461*, 654–658.

Oberwinkler, J., and Phillipp, S.E. (2007). TRPM3. Handb. Exp. Pharmacol. *179*, 253–267.

Ravikumar, B., Moreau, K., Jahreiss, L., Puri, C., and Rubinsztein, D.C. (2010). Plasma membrane contributes to the formation of pre-autophagosomal structures. Nat. Cell Biol. *12*, 747–757.

Rubinsztein, D.C., Cuervo, A.M., Ravikumar, B., Sarkar, S., Korolchuk, V., Kaushik, S., and Klionsky, D.J. (2009). In search of an "autophagomometer". Autophagy *5*, 585–589.

Selbach, M., Schwanhäusser, B., Thierfelder, N., Fang, Z., Khanin, R., and Rajewsky, N. (2008). Widespread changes in protein synthesis induced by microRNAs. Nature *455*, 58–63.

Tanida, I., Ueno, T., and Kominami, E. (2004). LC3 conjugation system in mammalian autophagy. Int. J. Biochem. Cell Biol. *36*, 2503–2518.

Toma, M.I., Grosser, M., Herr, A., Aust, D.E., Meye, A., Hoefling, C., Fuessel, S., Wuttig, D., Wirth, M.P., and Baretton, G.B. (2008). Loss of heterozygosity and copy number abnormality in clear cell renal cell carcinoma discovered by high-density affymetrix 10K single nucleotide polymorphism mapping array. Neoplasia *10*, 634–642.

Tong, A.W., and Nemunaitis, J. (2008). Modulation of miRNA activity in human cancer: a new paradigm for cancer gene therapy? Cancer Gene Ther. *15*, 341–355.

Turcotte, S., Chan, D.A., Sutphin, P.D., Hay, M.P., Denny, W.A., and Giaccia, A.J. (2008). A molecule targeting VHL-deficient renal cell carcinoma that induces autophagy. Cancer Cell *14*, 90–102.

Veronese, A., Lupini, L., Consiglio, J., Visone, R., Ferracin, M., Fornari, F., Zanesi, N., Alder, H., D'Elia, G., Gramantieri, L., et al. (2010). Oncogenic role of miR-483-3p at the IGF2/483 locus. Cancer Res. *70*, 3140–3149.

Weidberg, H., Shvets, E., Shpilka, T., Shimron, F., Shinder, V., and Elazar, Z. (2010). LC3 and GATE-16/GABARAP subfamilies are both essential yet act differently in autophagosome biogenesis. EMBO J. *29*, 1792–1802.

White, E., and DiPaola, R.S. (2009). The double-edged sword of autophagy modulation in cancer. Clin. Cancer Res. *15*, 5308–5316.

Wu, J., Dang, Y., Su, W., Liu, C., Ma, H., Shan, Y., Pei, Y., Wan, B., Guo, J., and Yu, L. (2006). Molecular cloning and characterization of rat LC3A and LC3B—two novel markers of autophagosome. Biochem. Biophys. Res. Commun. *339*, 437–442.

Yang, S., Wang, X., Contino, G., Liesa, M., Sahin, E., Ying, H., Bause, A., Li, Y., Stommel, J.M., Dell'antonio, G., et al. (2011). Pancreatic cancers require autophagy for tumor growth. Genes Dev. *25*, 717–729.

Yi, Y., Mikhaylova, O., Mamedova, A., Bastola, P., Biesiada, J., Alshaikh, E., Levin, L., Sheridan, R.M., Meller, J., and Czyzyk-Krzeska, M.F. (2010). von Hippel-Lindau-dependent patterns of RNA polymerase II hydroxylation in human renal clear cell carcinomas. Clin. Cancer Res. *16*, 5142–5152.

Yoshimoto, T., Matsuura, K., Karnan, S., Tagawa, H., Nakada, C., Tanigawa, M., Tsukamoto, Y., Uchida, T., Kashima, K., Akizuki, S., et al. (2007). High-resolution analysis of DNA copy number alterations and gene expression in renal clear cell carcinoma. J. Pathol. *213*, 392–401.

Cancer Cell
Article

Altered Microenvironmental Regulation of Leukemic and Normal Stem Cells in Chronic Myelogenous Leukemia

Bin Zhang,[1] Yin Wei Ho,[1] Qin Huang,[2] Takahiro Maeda,[1] Allen Lin,[1] Sung-uk Lee,[1] Alan Hair,[3] Tessa L. Holyoake,[3] Claudia Huettner,[4] and Ravi Bhatia[1,*]
[1]Division of Hematopoietic Stem Cell and Leukemia Research
[2]Department of Pathology
City of Hope National Medical Center, Duarte, CA 91010, USA
[3]College of Medical, Veterinary & Life Sciences, Institute of Cancer Sciences, University of Glasgow, Glasgow, G61 1BD, Scotland, UK
[4]Beffer Institute of Applied Cancer Science, Dana-Farber Cancer Institute, Boston, MA 02215, USA
*Correspondence: rbhatia@coh.org
DOI 10.1016/j.ccr.2012.02.018

SUMMARY

We characterized leukemia stem cells (LSC) in chronic phase chronic myelogenous leukemia (CML) using a transgenic mouse model. LSC were restricted to cells with long-term hematopoietic stem cell (LTHSC) phenotype. CML LTHSC demonstrated reduced homing and retention in the bone marrow (BM), related to decreased CXCL12 expression in CML BM, resulting from increased G-CSF production by leukemia cells. Altered cytokine expression in CML BM was associated with selective impairment of normal LTHSC growth and a growth advantage to CML LTHSC. Imatinib (IM) treatment partially corrected abnormalities in cytokine levels and LTHSC growth. These results were validated using human CML samples and provide improved understanding of microenvironmental regulation of normal and leukemic LTHSC and their response to IM in CML.

INTRODUCTION

Chronic myelogenous leukemia (CML) is a lethal hematological malignancy resulting from the transformation of a primitive hematopoietic cell by the *BCR-ABL* oncogene (Sawyers, 1999). CML leukemia stem cells (LSCs) retain the ability to regenerate multilineage hematopoiesis (Fialkow et al., 1977) and generate a vast expansion of malignant myeloid cells, which retain differentiating capacity and displace residual normal hematopoiesis. CML cells also demonstrate altered trafficking resulting in increased numbers of circulating progenitors, extramedullary hematopoiesis, and massive splenomegaly (Petzer et al., 1996). Leukemic cells acquire additional genetic abnormalities over time, leading to disease progression from an initial chronic phase (CP) to advanced accelerated phase (AP) and blast crisis (BC; Perrotti et al., 2010).

BCR-ABL tyrosine kinase inhibitors (TKI) are effective in inducing remission and prolonging survival in CP CML patients (Druker et al., 2006; Kantarjian et al., 2010; Saglio et al., 2010). However, TKI are less effective in targeting CML stem cells compared to more mature leukemia cells (Corbin et al., 2011; Graham et al., 2002; Holtz et al., 2002). As a result, LSC persist despite TKI treatment (Chomel et al., 2011), and there is a high frequency of leukemia relapse upon discontinuation of treatment. Although a small subset of patients can discontinue TKI treatment without disease recurrence, most patients need to take TKIs indefinitely to prevent relapse (Mahon et al., 2010; Michor et al., 2005), with associated risk of noncompliance, toxicity, and considerable expense (Cortes et al., 2011). Improved characterization of LSC is critical to a better understanding of CML pathogenesis and development of effective therapeutic strategies.

Significance

Chronic myelogenous leukemia (CML) results from stem cell transformation by the *BCR-ABL* oncogene. BCR-ABL tyrosine kinase inhibitors (TKI) induce remission in CML patients but do not eliminate leukemia stem cells (LSC), which can regenerate leukemia on drug discontinuation. Improved understanding of LSC regulation is critical to understanding CML pathogenesis and developing curative therapies. We show here that leukemia-induced decrease in CXCL12 expression results in reduced retention of LSC in CML bone marrow (BM). Furthermore, leukemia-induced abnormalities in cytokine expression in CML BM result in selective suppression of normal stem cell growth and enhanced growth of LSC. These changes were partially corrected by TKI treatment. These results improve our understanding of LSC regulation in CML and could guide strategies for targeting this resistant population.

In vitro analysis of progenitor cells from CML patients has revealed enhanced proliferation, reduced apoptosis, and increased differentiation in culture compared to normal progenitors. However, in vivo characterization of LSC from CP CML patients in immunodeficient mouse hosts is limited by low levels of engraftment and lack of leukemia development. Expression of BCR-ABL in murine cells using retroviral vectors followed by transplantation into irradiated hosts results in development of a myeloproliferative disorder (Li et al., 1999; Pear et al., 1998). This model has been useful in studying molecular mechanisms contributing to leukemia development. However, leukemia in this model is quite fulminant, associated with pulmonary hemorrhage and death within four weeks, and may be more representative of advanced phase CML. In addition, although LSC are known to be present within $Lin^-Sca\text{-}1^+c\text{-}Kit^+$ (LSK) cells in this model, they have not been characterized with a higher degree of resolution.

An inducible transgenic mouse model of CML in which the *BCR-ABL* gene is expressed under control of a Tet-regulated 3′ enhancer of the murine stem cell leukemia (SCL) gene allows targeted BCR-ABL expression in stem and progenitor cells (Koschmieder et al., 2005; Schemionek et al., 2010). Induction of BCR-ABL expression by tetracycline withdrawal results in a chronic myeloproliferative disorder with neutrophilic leukocytosis and splenomegaly that resembles CP CML. Leukemia is reversed on re-introduction of tetracycline. This model allows for the study of leukemogenesis in vivo under steady-state conditions. In the current study, we used the transgenic BCR-ABL model to study leukemia-induced alterations in the BM microenvironment and their contributions to normal and CML LTHSC cell growth and localization and to determine the effect of TKI treatment on these alterations.

RESULTS

Development of CP CML-like Myeloproliferative Disease in BCR-ABL Mice

Induction of BCR-ABL expression in SCL-tTA/BCR-ABL transgenic mice (FVB/N background) by tetracycline withdrawal resulted in 4 to 6 weeks in development of a CML-like myeloproliferative disorder characterized by neutrophilic leukocytosis (Figure 1A), splenomegaly (Figure 1B), BM hypercellularity (Figure 1C), and spleen infiltration with myeloid cells (Figure 1D). A subset of mice developed BM fibrosis after eight or more weeks (Figure 1E). Approximately 20% of mice developed lymph node enlargement, with infiltration of lymph nodes, BM and spleen with pro-B lymphoblastic cells ($B220^+CD43^+CD19^+IgM^-$; Figure 1F). The median survival after induction of BCR-ABL expression was 56 days (Figure 1G). These observations suggest that the BCR-ABL mouse model is representative of CP CML and develops features of advanced phase CML with prolonged BCR-ABL expression.

Changes in Stem and Progenitor Cell Populations in BCR-ABL Mice

Changes in distribution of stem and progenitor populations in the BM and spleen were observed within two weeks after induction of BCR-ABL expression and were more prominent after eight weeks. Primitive LSK cells and granulocyte-macrophage progenitors (GMP) were increased in the BM of BCR-ABL mice compared to controls, whereas megakaryocyte-erythrocyte progenitors (MEP) and common myeloid progenitors (CMP) were decreased (Figures S1A–S1C). In normal hematopoiesis, LTHSC capacity is restricted to the $Flt3^-CD150^+CD48^-LSK$ subpopulation, whereas $Flt3^-CD150^-CD48^-$, $Flt3^-CD150^+CD48^+$, and $Flt3^-CD150^-CD48^+$ LSK cells represent multipotent progenitors (MPP) lacking extensive self-renewal and long-term engrafting capacity (Figure 2A; Akala et al., 2008; Kiel et al., 2005). Although total LSK cell numbers were increased, LTHSC numbers were markedly reduced in the BM of BCR-ABL mice (Figures 2B and 2C). $CD150^-CD48^-$ MPP were also reduced in the BM of BCR-ABL mice. Increased LSK cells represented mainly $Flt3^-CD48^+$ MPP and $Flt3^+$ LSK cells representing lymphoid-primed MPP (LMPP; Månsson et al., 2007). IL-7Rα-expressing common lymphoid progenitors (CLP; Kondo et al., 1997) were reduced in BCR-ABL mice. In summary, reduction in LTHSC is associated with an increase in $CD48^+$ MPP, LMPP, and GMP in the BM of BCR-ABL mice. BCR-ABL mice demonstrated increased LTHSC numbers in the spleen compared with controls (Figures 2D and 2E), together with a vast increase in MPP, LMPP, CMP, and GMP, consistent with increased extramedullary hematopoiesis (Figures 2D and 2E; Figures S1D and S1E available online). Reduced BM and increased splenic LTHSC in BCR-ABL mice suggest altered LTHSC trafficking and/or niche requirements.

Long-Term Engrafting and Leukemia-Initiating Capacity Is Restricted to BCR-ABL+ LTHSC

SCL-tTA/BCR-ABL mice were crossed with transgenic GFP-expressing mice to facilitate detection of donor cells after transplantation. BCR-ABL expression was induced for four weeks and GFP^+ BM cells selected by flow cytometry and transplanted into irradiated congenic recipient mice. We observed robust engraftment of GFP^+ donor cells and development of myeloproliferative disease in recipient mice (Figure S2A). Leukemia usually developed within eight weeks posttransplant. Leukemia developing in recipient mice had a similar phenotype to that in donor mice and was transplantable to secondary (Figure S2B) and tertiary recipients (not shown). To identify subpopulations of cells capable of long-term engraftment and leukemia-initiation, GFP^+ GMP, CMP, and LSK cells from BM of leukemic mice were transplanted into irradiated congenic recipients. Transplantation of LSK cells, but not CMP and GMP, resulted in long-term engraftment and leukemia development in recipient mice (Figure S2C). LSK cells from the spleen also engrafted and generated leukemia in recipient mice (Figure S2D). The frequency of functional long-term engrafting cells within the BM LSK population measured using limiting dilution analysis was significantly reduced in BCR-ABL compared to control mice (Figure S2E), consistent with reduced numbers of cells with LTHSC phenotype. Cells with the LTHSC phenotype generated robust long-term engraftment with predominantly myeloid cells and development of CML-like myeloproliferative disease (Figure 3A). In contrast, $CD48^+$ MPP generated short-term engraftment with predominantly myeloid cells for up to eight weeks but did not sustain long-term engraftment. Sufficient numbers of $CD150^-CD48^-$ MPP were not obtained from CML mice for transplantation experiments. Transplantation of $Flt3^+$

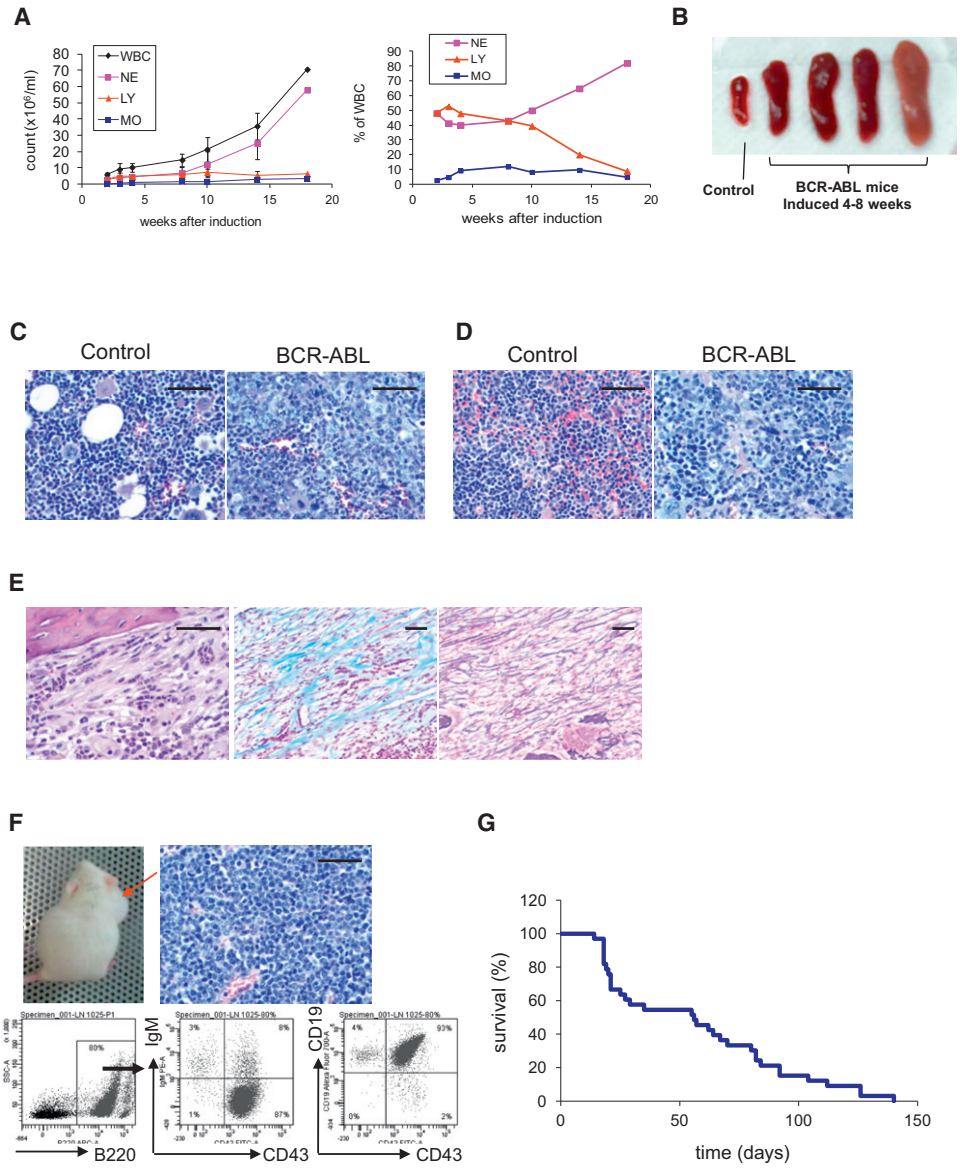

Figure 1. Development of CML-like Myeloproliferative Disorder in SCL-tTA/BCR-ABL Transgenic Mice

(A–D) Development of a myeloproliferative disorder in SCL-tTA/BCR-ABL transgenic mice within 4–6 weeks after induction of BCR-ABL expression by withdrawal of tetracycline, characterized by (A) neutrophilic leukocytosis and (B) splenomegaly (n = 20). Histopathological evaluation of (C) BM and (D) spleen tissue obtained four weeks after induction of BCR-ABL expression showing leukocytic infiltration.

(E) Development of BM fibrosis ten weeks after induction of BCR-ABL expression as seen with hematoxylin and eosin (left), Trichrome (center), and reticulin (right) staining.

(F) Development of pro-B lymphoblastic leukemia/lymphoma with lymph node enlargement (upper left panel), lymphoblastic infiltration of lymph nodes (upper right panel), and expression of pro-B cell markers on flow cytometry (lower panel).

(G) Survival curve of SCL-tTA/BCR-ABL mice after BCR-ABL induction (n = 33). All scale bars represent a size of 100 μm.

LMPP frequently resulted in the development of lymphoid tumors (not shown). Tumor cells did not engraft after transplantation into secondary recipient mice. In mice that did not develop tumors, Flt3$^+$LMPP generated short-term engraftment of lymphoblastic and myeloid cells, which was lost after 12 weeks. These observations suggest a hierarchical organization of leukemic LTHSC, MPP, and LMPP within LSK cells in BCR-ABL mice, as with normal hematopoiesis, with self-renewal and long-term engraftment capacity restricted to LTHSC, which was lost after differentiation to MPP. Despite having both myeloid and lymphoid capacity, leukemic LTHSC generated predominantly myeloid lineage cells. Interestingly, transplantation of limiting numbers of CML LTHSC often resulted in long-term engraftment with BCR-ABL$^+$ cells without development of leukemia (Figures 3B and 3C). One in six BM cells with LTHSC phenotype possessed long-term repopulation activity, whereas

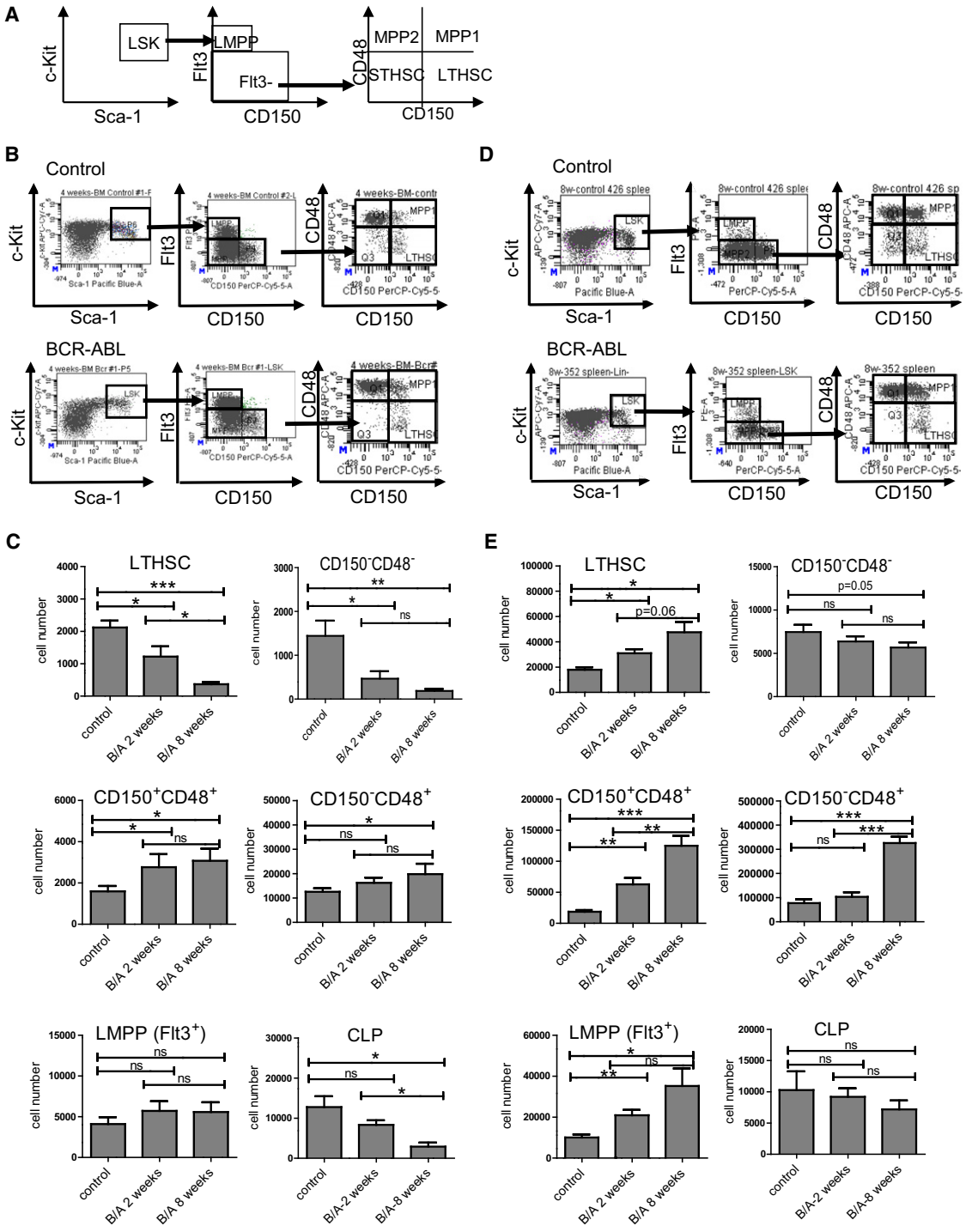

Figure 2. Changes in Stem and Progenitor Cell Populations in BCR-ABL-Expressing Mice

(A) The populations analyzed are shown and included Lin$^-$Sca-1$^+$c-Kit$^+$ (LSK) cells, which were further subdivided into Flt3$^-$CD150$^+$CD48$^-$ (LTHSC); Flt3$^-$CD150$^-$CD48$^-$, Flt3$^-$CD150$^+$CD48$^+$, and Flt3$^-$CD150$^-$CD48$^+$ (MPP); and Flt3$^+$CD150$^-$ cells (LMPP).

(B) Representative flow cytometry plots of LTHSC, MPP, and LMPP populations in the BM of control and BCR-ABL-expressing mice.

(C) Total numbers of LTHSC, CD150$^-$CD48$^-$, CD150$^+$CD48$^-$, CD150$^-$CD48$^+$ MPP, LMPP, and CLP (common lymphoid progenitor, Lin$^-$Sca-1^{Low}c-Kit^{Low}Flt3^{High}IL-7Rα^{High}) in the BM (per femur) of control and SCL-tTA/BCR-ABL mice at two and eight weeks after BCR-ABL induction (n = 6–8).

(D) Representative flow cytometry plots of LTHSC, MPP, and LMPP in the spleen of control mice and BCR-ABL-expressing mice.

(E) Total numbers of LTHSC, CD150$^-$CD48$^-$, CD150$^+$CD48$^-$, CD150$^-$CD48$^+$ MPP, LMPP, and CLP in the spleen of control mice and SCL-tTA/BCR-ABL mice at two and eight weeks after BCR-ABL induction. Results represent mean ± SEM. Significance values: *p < 0.05; **p < 0.01; ***p < 0.001; ns, not significant, n = 6–8. See also Figure S1.

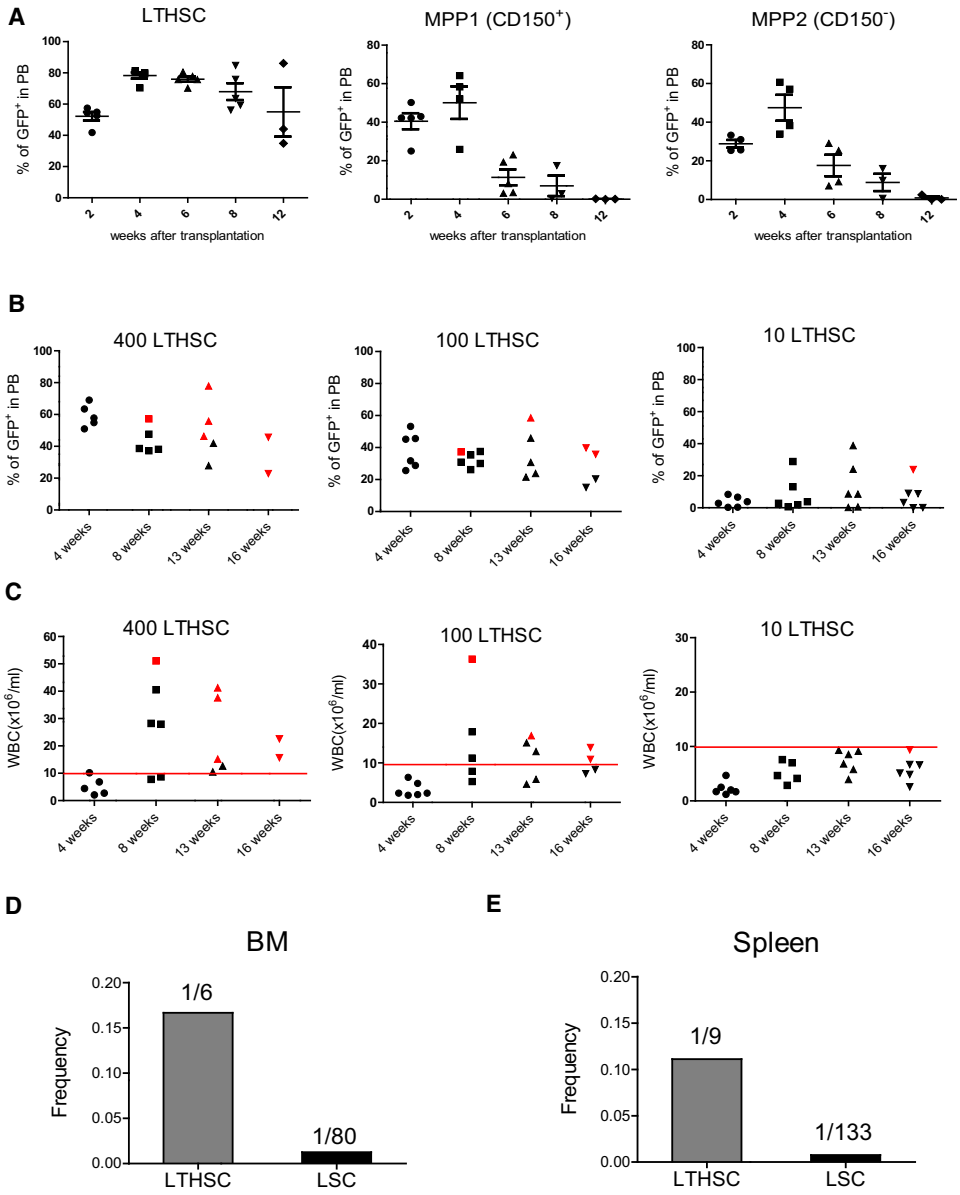

Figure 3. Long-Term Engraftment and Leukemia Induction by BCR-ABL-Expressing LTHSC

(A) Levels of donor GFP$^+$ cells in peripheral blood after transplantation of BCR-ABL-expressing LTHSC (500 cells/mouse), MPP1 (CD150$^+$CD48$^-$;2,000 cells/mouse), and MPP2 (CD150$^-$CD48$^+$; 2,000 cells/mouse) into irradiated recipients. Mice were followed for 16 weeks. The mean ± SEM is shown. (B) Engraftment of GFP$^+$ cells in peripheral blood and (C) peripheral blood WBC counts in recipient mice after transplantation of BCR-ABL-expressing LTHSC in limiting dilutions. Red spots indicate mice that died of leukemia within 20 weeks. The calculated frequency of functional long-term engrafting and leukemia-initiating cells within cells with LTHSC (Lin$^-$Sca-1$^+$Kit$^+$Flt3$^-$CD150$^+$CD48$^-$) phenotype in the (D) BM and (E) spleen of BCR-ABL mice is shown. The 95% confidence interval for LTHSC and LSC in the BM is 1/15-1/2 and 1/198-1/34, respectively. The 95% confidence interval for LTHSC and LSC in the spleen is 1/21-1/4 and 1/286-1/62, respectively.

See also Figure S2.

1 in 80 BM LTHSC were capable of initiating leukemia (defined as development of leukocytosis) within 20 weeks (Figure 3D), suggesting heterogeneity in leukemia-initiating capacity of individual BCR-ABL$^+$ LTHSC. The frequency of functional, long-term engrafting stem cells and leukemia-inducing cells within phenotypically defined LTHSC in the spleen was similar to BM LTHSC (Figure 3E).

BCR-ABL Expression and Cell Cycle Status of LTHSC

Expression of BCR-ABL mRNA levels was higher in LSK cells compared with CMP, GMP, and MEP cells (Figure S3A). Within LSK cells, BCR-ABL expression was higher in MPP compared with LTHSC but was reduced in LMPP (Figure S3B). Although the BCR-ABL transgene expression through the SCL promoter in transgenic mice may differ from expression driven by the

endogenous human promoter, the patterns of BCR-ABL expression in murine cells are in general consistent with previous reports for human CML subpopulations (Jamieson et al., 2004). Cell cycle status of stem and progenitor populations was evaluated by administration of 5-ethynyl-2′-deoxyuridine (EdU). EdU labeling of BM LTHSC was significantly reduced compared to total LSK cells in both normal and CML mice (Figure S3C). However, cycling of BCR-ABL$^+$ LTHSC was increased compared to control mice, both in vivo (Figure 4A) and in vitro (data not shown). Ki-67 and 4′, 6-diamidino-2-phenylindole (DAPI) labeling showed a modest increase in the proportion of BM LTHSC from BCR-ABL mice in S/G_2/M phase compared to control mice (Figure 4B). LTHSC from the spleen of BCR-ABL mice showed significantly increased S/G_2/M phase cells and reduced G_0 cells compared to splenic LTHSC from control mice. These results demonstrate modest increase in cycling of LTHSC in the BM and greater increase in cycling of LTHSC in the spleen of BCR-ABL mice.

Reduced Homing and Retention of BCR-ABL Expressing LTHSC in BM and Increased Egress to Spleen

We evaluated whether altered LTHSC localization, with reduced BM LTHSC and increased splenic LTHSC, was related to impaired LTHSC homing and/or reduced retention in BM. To evaluate homing, CFSE-labeled LTHSC were injected intravenously into irradiated recipients and CFSE-labeled cells in the BM and spleen of recipient mice evaluated after 4 hr (Figure 4C). There was reduced homing of BCR-ABL$^+$ LTHSC to the BM of recipient mice compared to controls ($p = 0.04$), with similar levels of homing to spleen (Figure 4D). To study retention of LTHSC in the BM, BCR-ABL$^+$ and control LTHSC were injected directly into the femur of irradiated congenic mice (Figure 4E). We observed significantly increased numbers of BCR-ABL$^+$ LTHSC in the spleen and decreased numbers of BCR-ABL$^+$ LTHSC in the injected and contralateral femur of recipient mice at four weeks postinjection (Figure S3D). In contrast, control LTHSC were present in increased numbers in the BM and lower numbers in the spleen of recipient mice, after both intrafemoral and intravenous transplantation (Figure 4F). Increased egress of BCR-ABL$^+$ LTHSC was not related to increased BM cellularity since total BM cell counts were not increased in CML mice compared to normal mice (Figure 4G). These results indicate that both reduced homing to the BM and enhanced egress from the BM to the spleen contribute to altered LTHSC localization in BCR-ABL mice.

Altered Chemokine and Cytokine Expression in BCR-ABL Mice

The chemokine CXCL12 mediates hematopoietic cell localization to the BM through interactions with the CXCR4 receptor on hematopoietic cells (Peled et al., 1999). Enzyme-linked immunosorbent assay (ELISA) analysis demonstrated significantly reduced CXCL12 levels in the BM and a marginal increase of CXCL12 levels in the spleen of BCR-ABL mice compared to control mice (Figure 5A). We also observed reduced CXCL12 mRNA levels in BM cells from BCR-ABL mice compared to controls (Figure 5B). CXCL12 mRNA was expressed at higher levels in CD45$^-$Ter119$^-$ nonhematopoietic stromal cells compared with CD45$^+$ hematopoietic cells (Figure 5C). CXCL12 mRNA levels were significantly lower in BM stromal cells from BCR-ABL mice compared to controls. Reduced CXCL12 expression may contribute to reduced retention of LTHSC in the BM of BCR-ABL mice. In the spleen, CXCL12 was mainly expressed in CD45$^-$Ter119$^-$CD31$^-$ nonhematopoietic, nonendothelial stromal cells, and levels were increased in CML compared to control mice (Figure 5D).

We evaluated the levels of additional chemokines and cytokines in BCR-ABL and control mice using Luminex xMAP technology. In contrast to reduced CXCL12 levels, several chemokines, including MIP-1α and MIP-1β, and cytokines, including IL-1α, IL-1β, IL-6, G-CSF, TNF-α, and LIF, showed increased expression in BM of BCR-ABL mice (Figures 5E and S4A–S4M). Expression of mRNA for MIP-1α, MIP-1β, IL-1α, IL-1β, IL-4, MIP-2, and IL-6 was significantly higher in both hematopoietic cells and, to a lesser extent, nonhematopoietic cells from the BM of BCR-ABL compared to control mice (Figures S4N–S4T). Levels of several chemokines/cytokines were also increased in the spleen of BCR-ABL mice compared with control mice (Figures 5E and S4A–S4M). An additional subset of chemokines and cytokines, including VEGF, IL-9, and MIG, were selectively enhanced in the spleen but not BM of BCR-ABL compared to control mice. These observations indicate complex alterations of cytokine and chemokine production by leukemic and stromal cells in the BM and splenic microenvironment of BCR-ABL mice.

Coculture with BM cells and BM plasma from BCR-ABL mice resulted in reduced CXCL12 mRNA levels in murine BM stromal cells (M2-10B4), compared to BM cells (Figure 5F) and BM plasma (Figure 5G) from control mice, indicating that reduced CXCL12 expression is related to diffusible factors produced by leukemia cells. Culture of stromal cells with MIP-1α, MIP-1β, IL-1α, IL-1β, TNF-α, G-CSF, or IL6 (at concentrations similar to those measured in BCR-ABL BM plasma) indicated that CXCL12 mRNA levels are reduced in stromal cells cultured with G-CSF and, to a lesser extent, MIP-1β and IL-6 (Figure 5H). The addition of a function-blocking anti-G-CSF antibody increased CXCL12 levels in stromal cells exposed to CML BM plasma (Figure 5I). Finally, BCR-ABL mice treated with function-blocking anti-mouse G-CSF antibody or isotype control antibody demonstrated enhanced CXCL12 levels in BM cells and enhanced numbers of BM and reduced numbers of splenic LTHSC (Figure 5J). These results support an important role for G-CSF-mediated reduction in CXCL12 levels in altered LTHSC localization in BCR-ABL mice.

Differential Regulation of Normal and Leukemic LTHSC Growth by the CML BM Microenvironment

In view of the observed abnormalities of chemokine and cytokine expression, we investigated whether BCR-ABL mice demonstrated altered capacity to support LTHSC engraftment. LTHSC from control or BCR-ABL mice were transplanted into irradiated BCR-ABL mice (induced for four weeks) or control recipient mice by tail vein injection (Figure 6A). BCR-ABL mice showed mild to modest elevation in WBC count; most of them had not developed leukemia and were not sick. Since it was not clear how long leukemia-induced microenvironmental alterations could be sustained after myeloablative treatment, mice were followed for up to four weeks after transplantation. We observed

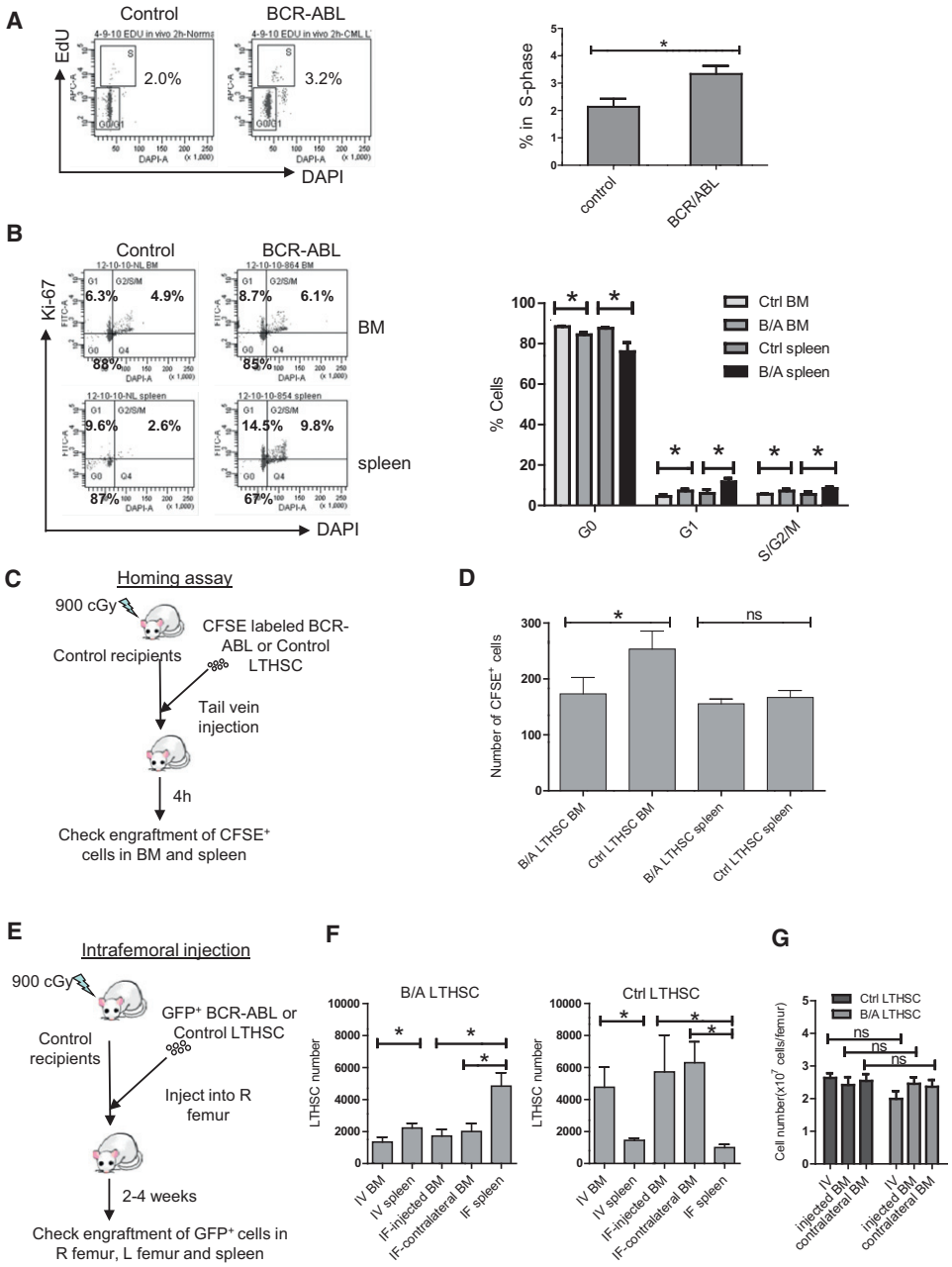

Figure 4. Alterations in Cell Cycle, Homing, and Trafficking of BCR-ABL-Expressing LTHSC

(A) Percentage of cycling LTHSC in the BM of BCR-ABL and control mice evaluated 2 hr after in vivo administration of EdU. Representative flow cytometry plots (left) and combined results (right) are shown (n = 3).

(B) The proportion of LTHSC from the BM and spleen of BCR-ABL and control mice in G0, G1, and S/G2/M phase evaluated by labeling with Ki-67 and DAPI. Representative flow cytometry plots (left) and combined results (right) are shown (n = 3).

(C) CFSE-labeled LTHSC were transplanted by tail vein injection into irradiated congenic recipient mice and the number of CFSE-expressing cells in the BM and spleen of recipient mice were evaluated 4 hr after injection.

(D) Homing of BCR-ABL and control LTHSC to the marrow and spleen of recipient mice after IV injection is shown (n = 8).

(E) GFP^+ BCR-ABL or control LTHSC (1,000 cells/mouse) were injected directly into the right femur of irradiated congenic mice. Donor GFP^+ LTHSC numbers in the injected femur; contralateral femur and spleen were analyzed two weeks and four weeks after transplantation.

(F) Mice receiving control and $BCR\text{-}ABL^+$ LTHSC administered intrafemorally or IV were analyzed after four weeks (n = 8 for both). The number of donor GFP^+ LTHSC in the injected femur, contralateral femur, and the spleen were analyzed following intrafemoral transplantation, and the number of LTHSC per femur and in the spleen were analyzed following IV transplantation.

(G) The BM cellularity at four weeks after transplantation is shown. Results represent mean ± SEM. Significance values: *$p < 0.05$; ns, not significant, compared with controls, or as indicated.

See also Figure S3.

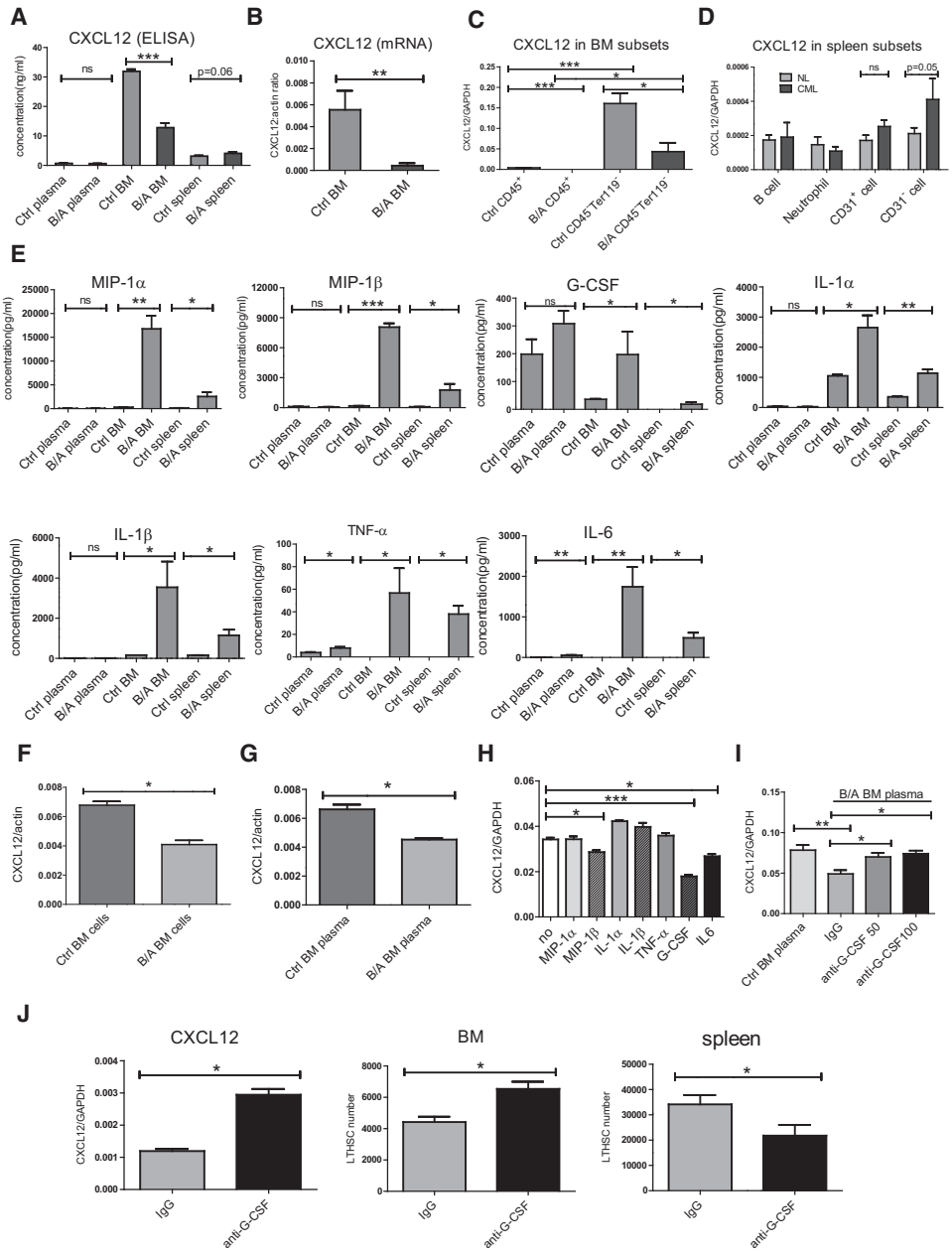

Figure 5. Altered Chemokine and Cytokine Expression in BCR-ABL Mice

(A–D) CXCL12 levels (A) measured by ELISA in peripheral blood and BM plasma and spleen supernatants from control and BCR-ABL mice. CXCL12 mRNA levels measured by qRT-PCR in (B) total BM cells; (C) BM hematopoietic cells ($CD45^+$) and BM stromal cells ($CD45^-Ter119^-$); and (D) splenic B cells ($CD45^+B220^+$), neutrophils ($CD45^+Gr\text{-}1^+$), endothelial cells ($CD45^-Ter119^-CD31^+$), and nonendothelial stromal cells ($CD45^-Ter119^-CD31^-$) cells from control and BCR-ABL mice.

(E–G) Expression of cytokines and chemokines (E) in peripheral blood and BM plasma and spleen supernatants from BCR-ABL-expressing and control mice measured by ELISA using Luminex xMAP technology. CXCL12 mRNA levels in M2-10B4 murine stromal cells cocultured for 48 hr with (F) BM cells and (G) BM plasma from BCR-ABL and control mice.

(H) CXCL12 mRNA levels in M2-10B4 murine stromal cells cultured for 24 hr in serum-free medium without addition of cytokines or with MIP-1α (16 ng/ml), MIP-1β (8 ng/ml), IL-1α (2.5 ng/ml), IL-1β (3.5 ng/ml), TNF-α (0.05 ng/ml), G-CSF (0.2 ng/ml), or IL-6 (2 ng/ml).

(I) CXCL12 mRNA levels in M2-10B4 murine stromal cells following culture for 24 hr with BM plasma from control and BCR-ABL mice, together with a function blocking anti-mouse G-CSF antibody (50 and 100 ng/ml) or isotype control antibody.

(J) BCR-ABL mice were induced for one week and then were treated with function-blocking anti-mouse G-CSF antibody (10 μg/mouse, IV, once per day) or isotype control antibody for an additional two weeks. CXCL12 mRNA levels in the BM and the numbers of LTHSC cells in the BM and spleen were measured. Results represent mean ± SEM. Significance values: *$p < 0.05$; **$p < 0.01$; ***$p < 0.001$; ns, not significant.

See also Figure S4.

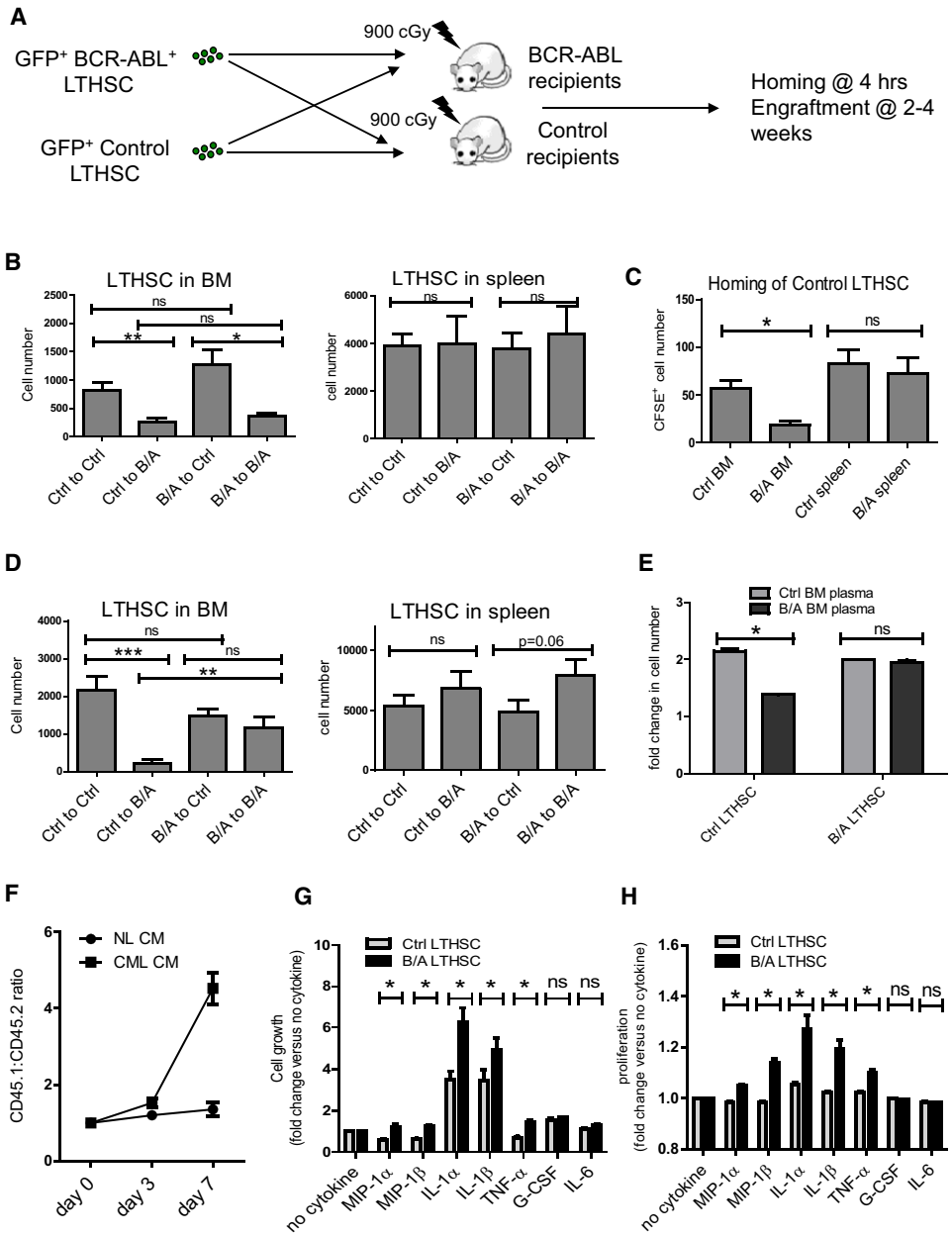

Figure 6. Differential Regulation of Normal and Leukemic LTHSC Growth by the CML BM Microenvironment

(A) GFP$^+$ LTHSC (1,000 cells/mouse) from control or BCR-ABL mice were transplanted into irradiated BCR-ABL or control mice by tail vein injection (n = 16 for each group, with a total of 64 mice at two weeks and 64 mice at four weeks).

(B) The numbers of GFP$^+$ LTHSC in the BM and spleen of irradiated control and BCR-ABL recipient mice at two weeks posttransplant.

(C) Homing of CFSE-labeled control LTHSC transplanted by tail vein injection into irradiated control and BCR-ABL recipient mice evaluated 4 hr after injection (n = 8).

(D) The numbers of GFP$^+$ LTHSC in the BM and spleen of irradiated control and BCR-ABL recipient mice at four weeks posttransplant.

(E) Control LTHSC and BCR-ABL$^+$ LTHSC were cultured with BM plasma obtained from control and BCR-ABL mice. Results shown represent fold-change in cell numbers after two days of culture (n = 3).

(F–H) BCR-ABL$^+$ LTHSC (CD45.1) and control LTHSC (CD45.2) (F) were mixed in a 1:1 ratio and cultured with CML or control BM conditioned medium (CM). The proportion of input cells was checked using flow cytometry. The ratio of CD45.1:CD45.2 cells at different times is shown (n = 3). CFSE$^+$ LTHSC from control and BCR-ABL-expressing mice were cultured with serum-free medium without cytokine or supplemented with MIP-1α (16 ng/ml), MIP-1β (8 ng/ml), IL-1α (2.5 ng/ml), IL-1β (3.5 ng/ml), TNF-α (0.05 ng/ml), G-CSF (0.2 ng/ml), or IL-6 (2 ng/ml) for 72 hr and cell growth (G) and proliferation (H) were measured. Results represent mean ± SEM. Significance values: *p < 0.05; **p < 0.01; ***p < 0.001; ns, not significant.

See also Figure S5.

reduced engraftment of both control and BCR-ABL$^+$ LTHSC in the BM of BCR-ABL recipients compared with control recipients two weeks after transplantation (Figure 6B), associated with reduced homing of control LTHSC (Figure 6C) and BCR-ABL$^+$ LTHSC (Figure 4D) to the BM of BCR-ABL compared to control mice, possibly related to low BM CXCL12 levels (Figures 5A and 5B). The numbers of control LTHSC in the BM of BCR-ABL recipient mice remained low, whereas BCR-ABL$^+$ LTHSC were increased four weeks after transplant and were similar to the numbers seen in the BM of control recipients (Figure 6D). Similar results were seen for CD48$^+$MPP, committed progenitors, and total GFP$^+$ leukemic cells (Figures S5A and S5C). There was no difference in the number of engrafted LTHSC or progenitor cells in the spleen of BCR-ABL and control mice at two weeks (Figures 6B and S5B), but there was a modest increase in LTHSC but not progenitor engraftment in the spleen of BCR-ABL mice at four weeks after transplantation (Figures 6D and S5D). These results suggest that increased splenic CXCL12 expression may not be sufficient to increase LTHSC homing but may contribute to increased relocalization of LTHSC to the spleen at later times. Lack of increased homing of normal LTHSC to CML spleen despite increased CXCL12 levels may reflect the involvement of additional factors besides CXCL12 in the homing process.

In vitro exposure to BM plasma from CML mice resulted in impaired growth of control LTHSC compared to BM plasma from control mice. In contrast, growth of BCR-ABL$^+$ LTHSC was similar after exposure to CML and control BM plasma (Figure 6E), suggesting that diffusible factors produced by leukemia cells contribute to reduced growth of normal compared to BCR-ABL$^+$ LTHSC in the BM microenvironment of BCR-ABL mice, resulting in a growth advantage for the leukemic clone. To directly test the hypothesis, we performed a competitive in vitro assay in which BCR-ABL$^+$ LTHSC (CD45.1) and control LTHSC (CD45.2) were mixed in a 1:1 ratio and cultured with CML or control BM-conditioned medium (CM). The proportion of the input cells was checked every three days using flow cytometry. We observed a markedly enhanced proportion of BCR-ABL$^+$ compared with control cells following culture with CML CM, whereas the proportion of BCR-ABL$^+$ and control cells was similar following culture with control CM (Figure 6F). These results indicate that factors produced by CML BM cells confer a competitive growth advantage to BCR-ABL$^+$ LTHSC over control LTHSC. We further show that the growth of control LTHSC was reduced compared to BCR-ABL$^+$ LTHSC in the presence of MIP-1α, MIP-1β, IL-1α, IL-1β, and TNF-α (at concentrations similar to those in BM plasma from BCR-ABL mice; Figure 6G). Reduced growth was related to reduced proliferation of control compared to BCR-ABL$^+$ LTHSC (Figure 6H), without significant changes in apoptosis (Figure S5E).

We examined the effect of IM treatment on BM microenvironmental function in BCR-ABL mice. LTHSC from control mice were transplanted into irradiated control or BCR-ABL mice that had been treated or not treated with IM for two weeks (Figure 7A). LTHSC engraftment was increased in IM-treated BCR-ABL mice, indicating at least partial correction of the microenvironmental defect (Figure 7B). We observed increased expression of CXCL12 and reduced expression of G-CSF, IL-6, IL-1β, MIP-1α, and MIP-1β in BM cells from IM-treated compared to untreated BCR-ABL mice (Figure 7C). Levels of IL-1α, IL-4, and MIP-2 were not significantly changed. Enhanced growth of normal LTHSC in the BM of BCR-ABL mice pretreated with IM was associated with enhanced CXCL12 and reduced cytokine levels.

Cytokine and Chemokine Expression in Human CML BM Cells

We analyzed cytokine and chemokine expression in BM cells from newly diagnosed CML CP patients, CML CP patients in complete cytogenetic remission (CCR) on IM treatment, and from healthy controls. CML BM cells demonstrated reduced expression of CXCL12 and increased expression of G-CSF, IL-1α, MIP-1β, and MIP-2, compared to normal BM cells. BM cells from patients in CCR showed increased CXCL12 and reduced G-CSF, TNF-α, and MIP-2 expression without significant change in other factors (Figures 8A and S6A). However, CXCL12 levels in CML patients in CCR remained significantly lower than in normal BM. Immunohistochemical analysis of BM sections from newly diagnosed CML CP patients showed reduced CXCL12 labeling compared to untreated lymphoma patients without BM involvement as controls. BM sections from the same CML patients after six months or more of IM treatment showed increased CXCL12 staining (Figures 8B and S6B). CXCL12 expression was seen in stromal cells and in a subset of mature hematopoietic cells. In contrast, G-CSF expression was increased in hematopoietic cells in BM sections from CML patients compared to controls and was reduced after IM treatment (Figures 8C and S6B). Primary human stromal cells immortalized with hTERT (Mihara et al., 2003) were exposed to conditioned medium (CM) made with BM cells from control and CML CP patients. Exposure to CML CM resulted in reduced CXCL12 in stromal cells compared to control CM (Figure 8D). CXCL12 expression was partially restored by the addition of an anti-G-CSF blocking antibody. These results support a role for increased G-CSF expression by CML hematopoietic cells in reduced CXCL12 production by human stromal cells, validating the results obtained with the murine model.

Primitive CD34$^+$CD38$^-$ cells from newly diagnosed CML CP patients and control healthy individuals were cultured with CP CML and normal BM CM. Culture with CML CM reduced growth of normal but not CML CD34$^+$CD38$^-$ cells in luminescent cell viability (Figure 8E) and CFC assays (Figure 8F). Human CML and normal CD34$^+$CD38$^-$ cells were also cultured without cytokines or with MIP-1β, MIP-2, IL-1α, and G-CSF—the four cytokines significantly increased in the BM cells from CML CP patients. IL-1α and G-CSF treatment resulted in significantly less expansion of normal compared to CML CD34$^+$CD38$^-$ cells, compared to controls cultured without cytokines in luminescent cell viability (Figure 8G) and CFC assays (Figure 8H), related to reduced proliferation of normal compared to CML CD34$^+$CD38$^-$ cells (Figure S6C), consistent with results obtained with the mouse model.

DISCUSSION

The transgenic BCR-ABL mouse demonstrates gradual development of a myeloproliferative disorder with neutrophilic leukocytosis, extramedullary hematopoiesis, and splenomegaly and

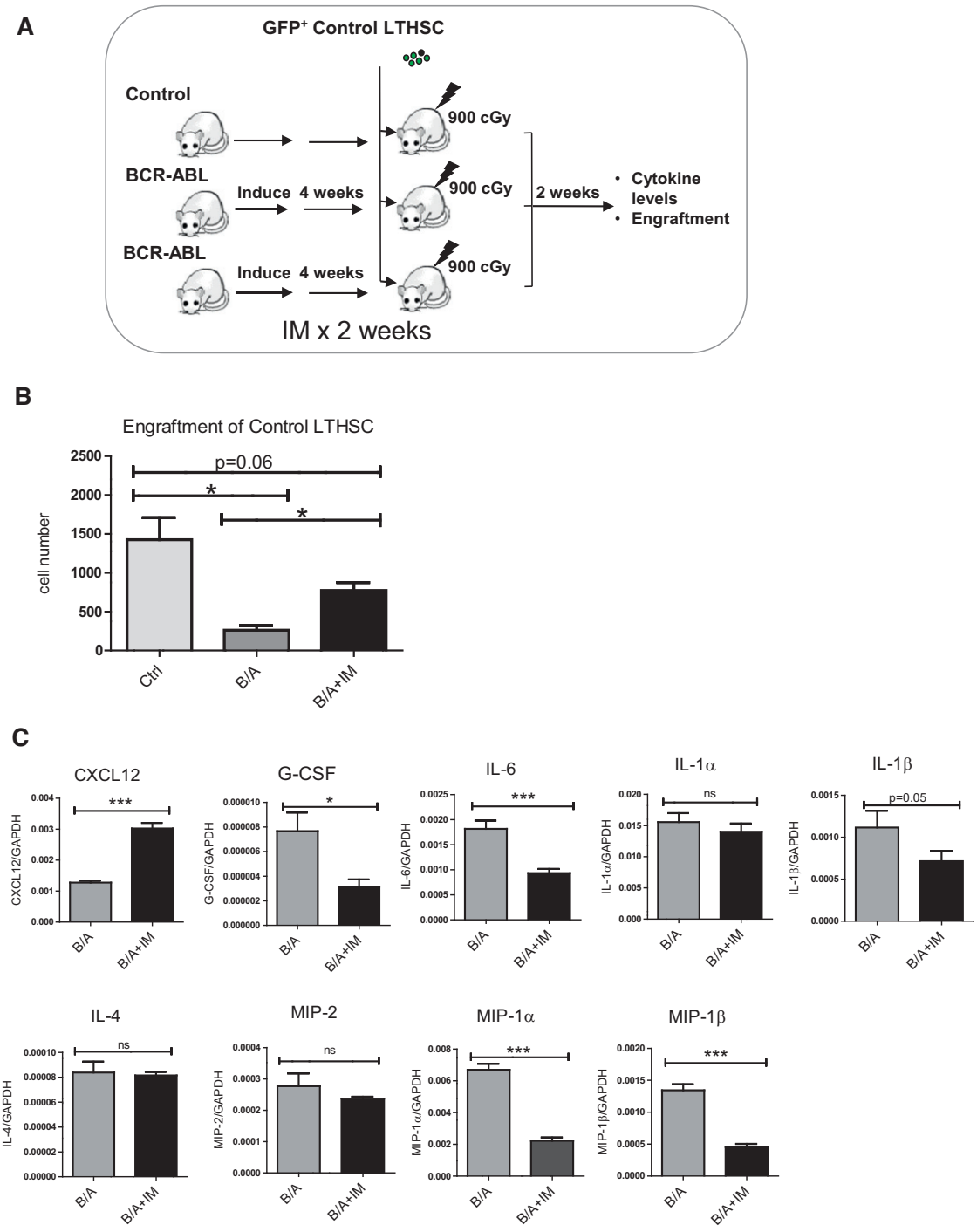

Figure 7. Effect of IM Treatment on Cytokine Levels on CML BM Microenvironmental Function

(A) One thousand GFP$^+$ control LTHSC/mouse were sorted and transplanted into irradiated control mice, BCR-ABL mice (induced four weeks), and BCR-ABL mice treated with IM for the last two weeks of the induction period (n = 8 each).

(B) Engraftment of control LTHSC in the BM of irradiated control, BCR-ABL, and IM-treated BCR-ABL mice.

(C) Cytokine and chemokine mRNA levels in the BM of BCR-ABL mice treated with or without IM were measured. Results represent mean ± SEM. Significance values: *$p < 0.05$; **$p < 0.01$, n = 8.

provides a representative model of human CP CML. We used the transgenic BCR-ABL mouse model to identify LSC with a high degree of resolution and to characterize their microenvironmental regulation. Long-term engraftment and leukemia-initiating capacity was restricted to a small subfraction of LSK cells that had the LTHSC (Flt3$^-$CD150$^+$CD48$^-$) phenotype.

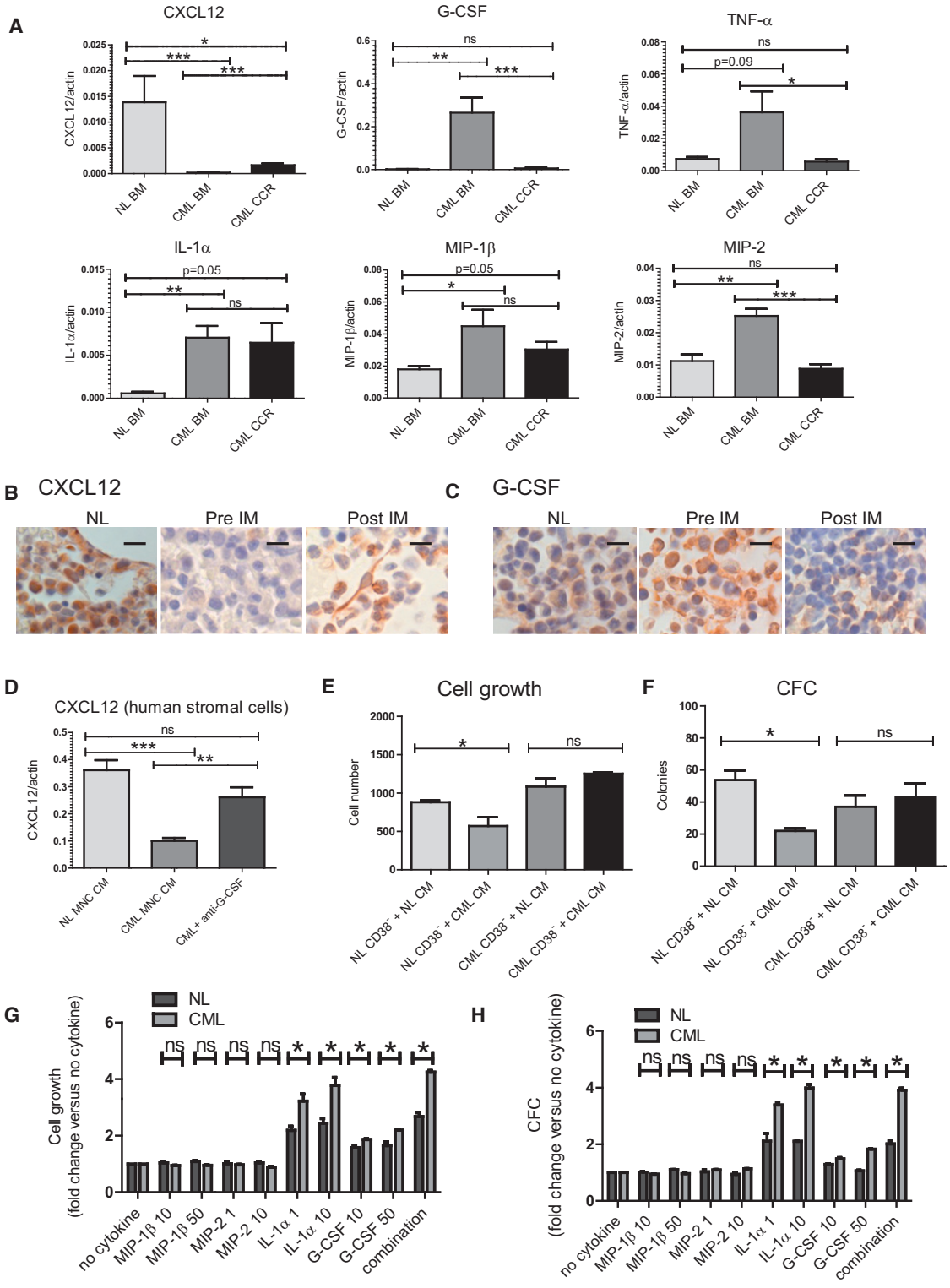

Figure 8. Cytokine and Chemokine Expression in Human CML BM Cells

(A) Cytokine and chemokine mRNA levels in BM MNC from control, newly diagnosed CML CP patients and CML CP patients in complete cytogenetic remission (CCR) on IM treatment were measured by qRT-PCR and results were normalized to actin expression.

(B and C) CXCL12 (B) and G-CSF (C) expression in BM sections obtained from untreated lymphoma patients without BM involvement by disease (NL), newly diagnosed CML CP patients prior to starting IM treatment (pre-IM), and the same patients after six months or more of IM treatment (post-IM) were analyzed by immunohistochemistry (n = 3). Scale bars represent a size of 10 μm.

In contrast, LSK cells with MPP or LMPP phenotypes generated only short-term engraftment. These results indicate that CML originates from transformation at the level of the LTHSC rather than more differentiated MPP or LMPP and that leukemic hematopoiesis follows a hierarchical differentiation pattern as seen in normal hematopoiesis. These results are consistent with a recent report in which SCL-tTA/BCR-ABL mice in the C57BL/6 background were studied (Reynaud et al., 2011). In contrast to the FVB/N strain, leukemia developing in C57BL/6 background mice is more aggressive with a higher incidence of BM fibrosis and hypocellularity, and secondary lymphoid disorders are not seen, suggesting that strain-specific factors modulate the phenotype and course of leukemia. Our results contrast with observations made in BC CML and acute myeloid leukemia, where more mature LMPP or GMP progenitors may acquire self-renewal and leukemia-initiating capacity (Jamieson et al., 2004; Sarry et al., 2011).

LTHSC numbers were reduced in the BM of CML mice, with a concomitant increase in MPP, suggesting enhanced LTHSC differentiation and enhanced proliferation and expansion of MPP. CML MPP generated short-term engraftment with predominantly myeloid cells after transplantation, whereas CML LMPP generated expanded populations of immature pro-B cells after transplantation. Although CML LTHSC can generate progeny with both myeloid and lymphoid potential, selective expansion of the myeloid population is seen following the transplantation of purified LTHSC and lymphoid cells are suppressed. The recent report that IL-6 produced by leukemic cells inhibits lymphoid and promotes myeloid differentiation and expansion of the leukemic clone could provide an explanation for these findings (Reynaud et al., 2011).

We observed reduced BM and increased splenic LTHSC in BCR-ABL mice related to decreased LTHSC homing to the BM, reduced retention in the BM and increased egress to the spleen, and enhanced proliferation in the spleen. The abnormal trafficking and growth of BCR-ABL$^+$ LTHSC indicates alterations in microenvironmental interactions compared to normal LTHSC. Intrinsic defects in adhesion receptors, including β1 integrins (Verfaillie et al., 1992) and CD44 (Krause et al., 2006), may be seen in CML progenitor cells. In addition, migration of CML progenitors to CXCL12 is reported to be reduced compared to normal progenitors (Jin et al., 2008; Peled et al., 2002). We identified reduction in BM CXCL12 levels as a mechanism underlying impaired LTHSC homing and retention in CML BM. CXCL12 expression in BM stromal cells was reduced in both BCR-ABL mice and CML patients. Since CXCL12 regulates LTHSC quiescence, reduced CXCL12 levels could directly contribute to increased cycling of LTHSC in the BM of BCR-ABL mice (Cashman et al., 2002). In addition, reduced CXCL12 expression could contribute to abnormal regulation of LTHSC proliferation and differentiation indirectly by altering their niche localization.

Growth of normal LTHSC was reduced in the BM of BCR-ABL mice compared to control mice, whereas BCR-ABL$^+$ LTHSC demonstrated similar growth in the BM of BCR-ABL and normal mice, related to diffusible factors produced by CML BM cells. These results are consistent with our previous observations that normal human progenitors demonstrate impaired in vitro growth on stromal layers derived from human CML BM but that growth of human CML progenitors is similar on normal and CML BM-derived stromal layers (Bhatia et al., 1995) and suggest that altered BM microenvironmental function contributes to suppression of normal LTHSC and provides a selective advantage to LSC in CML. Expression of several other chemokines and cytokines was significantly increased in the BM of BCR-ABL mice. These cytokines were produced mainly by leukemic hematopoietic cells. We identified the chemokines MIP-1α and β and the cytokines IL-1α and β and TNF-α as supporting reduced proliferation and growth of normal compared to CML LTHSC. Relevant to these findings it has been previously reported that certain chemokines selectively inhibit the proliferation of normal progenitors while sparing CML progenitors (Cashman et al., 1998; Eaves et al., 1993) and that CML LTHSC have enhanced expression of proteins affecting IL-1 signaling (Järås et al., 2010). Additional as yet unidentified inhibitory factors could also contribute to selective inhibition of normal LTHSC in the CML BM microenvironment. Growth of normal LTHSC was enhanced in the BM micro-environment of IM-treated, compared to untreated BCR-ABL, mice in association with reduced levels of several of the abnormally expressed cytokines. These results support a role for specific cytokines produced by leukemic cells within the CML BM microenvironment in conferring a growth advantage to CML compared with normal LTHSC.

Cytokine alterations, in addition to direct effects on LTHSC, may also indirectly affect LTHSC by altering the function of stromal cells (Bonig et al., 2006). The cytokines G-CSF, IL-1, and TNF-α can suppress expression of CXCL12 in osteoblasts or fibroblastic cells (Peng et al., 2006; Zhang et al., 2008). We identified an important role for G-CSF produced by leukemic cells in reducing CXCL12 expression in CML BM stromal cells. Inhibition of G-CSF activity increased CXCL12 levels in BM stromal cells in vitro and in vivo, leading to increased retention of LTHSC in the BM and reduced LTHSC in the spleen of BCR-ABL mice. CXCL12 expression was increased and G-CSF expression was reduced in the BM of IM-treated BCR-ABL mice and in the BM of CML patients in remission following IM treatment. Restoration of normal niche interactions could play a role in leukemia control in a physiological setting.

(D) Primary human stromal cells immortalized with hTERT expression were exposed to CM made with BM MNC from healthy controls and CML CP patients for 24 hr. The effect of addition of a blocking anti-human G-CSF (10 μg/ml) antibody or isotype control antibody on CXCL12 mRNA levels was evaluated.
(E–H) CD34$^+$CD38$^-$ cells (E) from control and newly diagnosed CML CP patients were cultured for 48 hr with CM made with BM MNC from healthy controls and newly diagnosed CML CP patients and cell growth measured using a luminescent cell viability assay and (F) in CFC assays. CD34$^+$ cells from normal and newly diagnosed CML CP patients were labeled with CFSE. CFSE$^+$ Lin$^-$CD34$^+$CD38$^-$ cells were sorted and cultured for 72 hr in serum-free medium either without cytokines or supplemented with MIP-1β (10 and 50 ng/ml), MIP-2 (1 and 10 ng/ml), IL-1α (1 and 10 ng/ml), G-CSF (10 and 50 ng/ml), or a combination (10 ng/ml MIP-1β, 1 ng/ml MIP2, 1 ng/ml IL-1α, and 50 ng/ml G-CSF). Cell growth was measured using a (G) luminescent viability assay and (H) in CFC assay. Results represent mean ± SEM. Significance values: *$p < 0.05$; **$p < 0.01$; ***$p < 0.001$; ns, not significant.
See also Figure S6.

However, CXCL12 levels in CML BM after IM treatment remained lower than in normal BM, indicating that recovery of CXCL12 expression is incomplete. Although our studies demonstrate reduced CXCL12 mRNA expression by stromal cells in CML, we recognize that additional mechanisms, such as increased CXCL12 cleavage by proteolytic enzymes, could also be active (Cho et al., 2010).

These studies support important, new concepts regarding the contribution of leukemia-induced alterations in the BM microenvironment to a selective growth advantage to leukemic compared with normal LTHSC and have relevance to our understanding of the response and resistance to TKI at the organismal level. Although IM treatment corrects several abnormalities in cytokine and chemokine expression in CML cells and reduces normal LTHSC inhibition by leukemic cells and facilitates their regrowth, it does not completely reverse leukemia-associated changes in the microenvironment. It will be important to determine the mechanisms underlying these persistent changes and how leukemia-related alterations in the hematopoietic microenvironment affect LSC response to TKI treatment, regrowth of normal LTHSC, and persistence of LSC in CML patients on prolonged TKI treatment. These insights could lead to improved strategies to eliminate resistant LSC populations in TKI-treated patients.

EXPERIMENTAL PROCEDURES

Mice

Inducible, transgenic SCL-tTa/BCR-ABL mice in the FVB/N background (Koschmieder et al., 2005) were maintained with administration of tetracycline in the drinking water (0.5 g/l) and were crossed with transgenic GFP-expressing mice (FVB.Cg-Tg [ACTB-EGFP] B5Nagy/J; Jackson Laboratories, Bar Harbor, ME) for transplantation experiments to facilitate tracking of donor cells. If not indicated, BCR-ABL expression was induced for three weeks by tetracycline withdrawal. Mouse care and experimental procedures were performed in accordance with federal guidelines and protocols approved by the Institutional Animal Care and Use Committee at the City of Hope.

Samples

Aliquots of normal peripheral blood and BM mononuclear cells (MNC) were obtained from allogeneic transplant donors. CML samples were obtained from patients in CP who had not received prior IM treatment from City of Hope and the University of Glasgow. Sample acquisition was approved by the Institutional Review Boards (IRB) at City of Hope, and the North Glasgow University Hospital Division of NHS Greater Glasgow and Clyde in accordance with the Declaration of Helsinki. All donors signed informed consent forms. BM sections from NHL patients were obtained from the City of Hope Biospecimen Repository, as anonymized specimens, using an IRB-approved protocol which exempted consent requirements. MNC were isolated using Ficol separation. $CD34^+$ cells were isolated using a positive magnetic bead selection protocol (Miltenyi, Auburn, CA, USA).

Flow Cytometry

Cells were obtained from BM (both tibias and femurs), lymph nodes, or spleen. All analyses were performed on an LSRII flow cytometer (Becton Dickinson, Franklin Lakes, NJ, USA). Myeloid progenitors were identified as $Lin^-Sca\text{-}1^-c\text{-}Kit^+CD34^+Fc\gamma RII/III^{lo}$ (CMP), $Lin^-Sca\text{-}1^-c\text{-}Kit^+CD34^+Fc\gamma RII/III^{hi}$ (GMP), or $Lin^-Sca\text{-}1^-c\text{-}Kit^+CD34^-Fc\gamma RII/III^{lo}$ (MEP; Akashi et al., 2000). Stem and multipotent progenitor populations were identified as LSK cells ($Lin^-Sca\text{-}1^{hi}c\text{-}Kit^{hi}$), LTHSC (LSK $Flt3^-CD150^+CD48^-$), MPP (LSK $Flt3^-CD150^-CD48^-$, LSK $Flt3^-CD150^+CD48^+$, LSK $Flt3^-CD150^-CD48^+$) and LMPP (LSK $Flt3^+CD150^-$; Kiel et al., 2005). Human stem cells/primitive progenitors were isolated by sorting $CD34^+CD38^-$ cells. For cell cycle analysis EdU (Invitrogen, Grand Island, NY, USA) was administered intraperitoneally (1 mg/mouse), BM cells were obtained 2 hr postinjection and EdU incorporation into stem cell populations analyzed (Cappella et al., 2008). Cell cycle was also analyzed by Ki-67 (BD) and DAPI labeling as previously described (Jordan et al., 1996). Details are provided in the Supplemental Experimental Procedures.

Transplantation

GFP^+ BM cells or purified progenitor populations from BCR-ABL/GFP transgenic mice and control mice were injected into 8-week-old FVB/N or BCR-ABL mice irradiated at 900 cGy. To evaluate homing, LTHSC were labeled with 1.25 μM CFSE (Molecular Probes, Eugene, OR, USA) and injected intravenously, and the percentage of $CFSE^+$ cells in the BM and spleen was analyzed after 4 hr. To evaluate egress of cells from the BM to the spleen, GFP^+ LTHSC cells were injected into the right femur of FVB/N mice irradiated at 900 cGy, and the number of GFP^+ LTHSC in the right femur, left femur, and spleen of mice was analyzed after two and four weeks. For some experiments, mice were treated with IM for two weeks pretransplantation. Details are provided in the Supplemental Experimental Procedures.

Measurement of Cytokine Levels

BM, peripheral blood, and spleen cell suspensions were centrifuged and supernatants were aliquoted and frozen. ELISA assays for CXCL12 (R&D Systems, Minneapolis, MN, USA; MCX120) and Luminex xMAP assays for a panel of murine cytokines and chemokines (MILLIPLEX MAP Mouse Cytokine/Chemokine Panel from Millipore, Billerica, MA, USA; MPXMCYTO-70K) were performed. Expression of mRNA for different cytokines and chemokines in human and murine BM and spleen cells were analyzed using quantitative reverse transcriptase-polymerase chain reaction (qRT-PCR). CXCL12 and G-CSF expression in BM sections from CML patients and controls were analyzed by immunohistochemistry. Details are provided in the Supplemental Experimental Procedures.

Statistics

Results are expressed as means ± standard error of means. Significance was estimated using Student's t test.

SUPPLEMENTAL INFORMATION

Supplemental Information includes six figures and Supplemental Experimental Procedures and can be found with this article online at doi:10.1016/j.ccr.2012.02.018.

ACKNOWLEDGMENTS

This work was supported by the National Institutes of Health grants (R01 HL77847 and R01 CA95684 to R.B.) and CR-UK grant (C11074/A11008 to T.H.). We acknowledge the excellent technical support of the COHNMC Analytical Cytometry core, the Clinical Immunobiology Correlative Studies laboratory, and the Animal Resources Center. Procurement of biospecimens was facilitated by the City of Hope Biospecimen Repository Protocol. This study was supported by the Glasgow Experimental Cancer Medicine Centre (ECMC), which is funded by Cancer Research UK and the Chief Scientist's Office (Scotland).

Received: March 2, 2011
Revised: November 24, 2011
Accepted: February 17, 2012
Published: April 16, 2012

REFERENCES

Akala, O.O., Park, I.K., Qian, D., Pihalja, M., Becker, M.W., and Clarke, M.F. (2008). Long-term haematopoietic reconstitution by Trp53-/-p16Ink4a-/-p19Arf-/- multipotent progenitors. Nature *453*, 228–232.

Akashi, K., Traver, D., Miyamoto, T., and Weissman, I.L. (2000). A clonogenic common myeloid progenitor that gives rise to all myeloid lineages. Nature *404*, 193–197.

Bhatia, R., McGlave, P.B., Dewald, G.W., Blazar, B.R., and Verfaillie, C.M. (1995). Abnormal function of the bone marrow microenvironment in chronic myelogenous leukemia: role of malignant stromal macrophages. Blood *85*, 3636–3645.

Bonig, H., Priestley, G.V., and Papayannopoulou, T. (2006). Hierarchy of molecular-pathway usage in bone marrow homing and its shift by cytokines. Blood *107*, 79–86.

Cappella, P., Gasparri, F., Pulici, M., and Moll, J. (2008). Cell proliferation method: click chemistry based on BrdU coupling for multiplex antibody staining. Curr. Protoc. Cytom., Chapter 7:Unit7.34.

Cashman, J.D., Eaves, C.J., Sarris, A.H., and Eaves, A.C. (1998). MCP-1, not MIP-1alpha, is the endogenous chemokine that cooperates with TGF-beta to inhibit the cycling of primitive normal but not leukemic (CML) progenitors in long-term human marrow cultures. Blood *92*, 2338–2344.

Cashman, J., Clark-Lewis, I., Eaves, A., and Eaves, C. (2002). Stromal-derived factor 1 inhibits the cycling of very primitive human hematopoietic cells in vitro and in NOD/SCID mice. Blood *99*, 792–799.

Cho, S.Y., Xu, M., Roboz, J., Lu, M., Mascarenhas, J., and Hoffman, R. (2010). The effect of CXCL12 processing on CD34+ cell migration in myeloproliferative neoplasms. Cancer Res. *70*, 3402–3410.

Chomel, J.C., Bonnet, M.L., Sorel, N., Bertrand, A., Meunier, M.C., Fichelson, S., Melkus, M., Bennaceur-Griscelli, A., Guilhot, F., and Turhan, A.G. (2011). Leukemic stem cell persistence in chronic myeloid leukemia patients with sustained undetectable molecular residual disease. Blood *118*, 3657–3660.

Corbin, A.S., Agarwal, A., Loriaux, M., Cortes, J., Deininger, M.W., and Druker, B.J. (2011). Human chronic myeloid leukemia stem cells are insensitive to imatinib despite inhibition of BCR-ABL activity. J. Clin. Invest. *121*, 396–409.

Cortes, J., Hochhaus, A., Hughes, T., and Kantarjian, H. (2011). Front-line and salvage therapies with tyrosine kinase inhibitors and other treatments in chronic myeloid leukemia. J. Clin. Oncol. *29*, 524–531.

Druker, B.J., Guilhot, F., O'Brien, S.G., Gathmann, I., Kantarjian, H., Gattermann, N., Deininger, M.W., Silver, R.T., Goldman, J.M., Stone, R.M., et al; IRIS Investigators. (2006). Five-year follow-up of patients receiving imatinib for chronic myeloid leukemia. N. Engl. J. Med. *355*, 2408–2417.

Eaves, C.J., Cashman, J.D., Wolpe, S.D., and Eaves, A.C. (1993). Unresponsiveness of primitive chronic myeloid leukemia cells to macrophage inflammatory protein 1 alpha, an inhibitor of primitive normal hematopoietic cells. Proc. Natl. Acad. Sci. USA *90*, 12015–12019.

Fialkow, P.J., Jacobson, R.J., and Papayannopoulou, T. (1977). Chronic myelocytic leukemia: clonal origin in a stem cell common to the granulocyte, erythrocyte, platelet and monocyte/macrophage. Am. J. Med. *63*, 125–130.

Graham, S.M., Jørgensen, H.G., Allan, E., Pearson, C., Alcorn, M.J., Richmond, L., and Holyoake, T.L. (2002). Primitive, quiescent, Philadelphia-positive stem cells from patients with chronic myeloid leukemia are insensitive to STI571 in vitro. Blood *99*, 319–325.

Holtz, M.S., Slovak, M.L., Zhang, F., Sawyers, C.L., Forman, S.J., and Bhatia, R. (2002). Imatinib mesylate (STI571) inhibits growth of primitive malignant progenitors in chronic myelogenous leukemia through reversal of abnormally increased proliferation. Blood *99*, 3792–3800.

Jamieson, C.H., Ailles, L.E., Dylla, S.J., Muijtjens, M., Jones, C., Zehnder, J.L., Gotlib, J., Li, K., Manz, M.G., Keating, A., et al. (2004). Granulocyte-macrophage progenitors as candidate leukemic stem cells in blast-crisis CML. N. Engl. J. Med. *351*, 657–667.

Järås, M., Johnels, P., Hansen, N., Agerstam, H., Tsapogas, P., Rissler, M., Lassen, C., Olofsson, T., Bjerrum, O.W., Richter, J., and Fioretos, T. (2010). Isolation and killing of candidate chronic myeloid leukemia stem cells by antibody targeting of IL-1 receptor accessory protein. Proc. Natl. Acad. Sci. USA *107*, 16280–16285.

Jin, L., Tabe, Y., Konoplev, S., Xu, Y., Leysath, C.E., Lu, H., Kimura, S., Ohsaka, A., Rios, M.B., Calvert, L., et al. (2008). CXCR4 up-regulation by imatinib induces chronic myelogenous leukemia (CML) cell migration to bone marrow stroma and promotes survival of quiescent CML cells. Mol. Cancer Ther. *7*, 48–58.

Jordan, C.T., Yamasaki, G., and Minamoto, D. (1996). High-resolution cell cycle analysis of defined phenotypic subsets within primitive human hematopoietic cell populations. Exp. Hematol. *24*, 1347–1355.

Kantarjian, H., Shah, N.P., Hochhaus, A., Cortes, J., Shah, S., Ayala, M., Moiraghi, B., Shen, Z., Mayer, J., Pasquini, R., et al. (2010). Dasatinib versus imatinib in newly diagnosed chronic-phase chronic myeloid leukemia. N. Engl. J. Med. *362*, 2260–2270.

Kiel, M.J., Yilmaz, O.H., Iwashita, T., Yilmaz, O.H., Terhorst, C., and Morrison, S.J. (2005). SLAM family receptors distinguish hematopoietic stem and progenitor cells and reveal endothelial niches for stem cells. Cell *121*, 1109–1121.

Kondo, M., Weissman, I.L., and Akashi, K. (1997). Identification of clonogenic common lymphoid progenitors in mouse bone marrow. Cell *91*, 661–672.

Koschmieder, S., Göttgens, B., Zhang, P., Iwasaki-Arai, J., Akashi, K., Kutok, J.L., Dayaram, T., Geary, K., Green, A.R., Tenen, D.G., and Huettner, C.S. (2005). Inducible chronic phase of myeloid leukemia with expansion of hematopoietic stem cells in a transgenic model of BCR-ABL leukemogenesis. Blood *105*, 324–334.

Krause, D.S., Lazarides, K., von Andrian, U.H., and Van Etten, R.A. (2006). Requirement for CD44 in homing and engraftment of BCR-ABL-expressing leukemic stem cells. Nat. Med. *12*, 1175–1180.

Li, S., Ilaria, R.L., Jr., Million, R.P., Daley, G.Q., and Van Etten, R.A. (1999). The P190, P210, and P230 forms of the BCR/ABL oncogene induce a similar chronic myeloid leukemia-like syndrome in mice but have different lymphoid leukemogenic activity. J. Exp. Med. *189*, 1399–1412.

Mahon, F.X., Réa, D., Guilhot, J., Guilhot, F., Huguet, F., Nicolini, F., Legros, L., Charbonnier, A., Guerci, A., Varet, B., et al; Intergroupe Français des Leucémies Myéloïdes Chroniques. (2010). Discontinuation of imatinib in patients with chronic myeloid leukaemia who have maintained complete molecular remission for at least 2 years: the prospective, multicentre Stop Imatinib (STIM) trial. Lancet Oncol. *11*, 1029–1035.

Månsson, R., Hultquist, A., Luc, S., Yang, L., Anderson, K., Kharazi, S., Al-Hashmi, S., Liuba, K., Thorén, L., Adolfsson, J., et al. (2007). Molecular evidence for hierarchical transcriptional lineage priming in fetal and adult stem cells and multipotent progenitors. Immunity *26*, 407–419.

Michor, F., Hughes, T.P., Iwasa, Y., Branford, S., Shah, N.P., Sawyers, C.L., and Nowak, M.A. (2005). Dynamics of chronic myeloid leukaemia. Nature *435*, 1267–1270.

Mihara, K., Imai, C., Coustan-Smith, E., Dome, J.S., Dominici, M., Vanin, E., and Campana, D. (2003). Development and functional characterization of human bone marrow mesenchymal cells immortalized by enforced expression of telomerase. Br. J. Haematol. *120*, 846–849.

Pear, W.S., Miller, J.P., Xu, L., Pui, J.C., Soffer, B., Quackenbush, R.C., Pendergast, A.M., Bronson, R., Aster, J.C., Scott, M.L., and Baltimore, D. (1998). Efficient and rapid induction of a chronic myelogenous leukemia-like myeloproliferative disease in mice receiving P210 bcr/abl-transduced bone marrow. Blood *92*, 3780–3792.

Peled, A., Petit, I., Kollet, O., Magid, M., Ponomaryov, T., Byk, T., Nagler, A., Ben-Hur, H., Many, A., Shultz, L., et al. (1999). Dependence of human stem cell engraftment and repopulation of NOD/SCID mice on CXCR4. Science *283*, 845–848.

Peled, A., Hardan, I., Trakhtenbrot, L., Gur, E., Magid, M., Darash-Yahana, M., Cohen, N., Grabovsky, V., Franitza, S., Kollet, O., et al. (2002). Immature leukemic CD34+CXCR4+ cells from CML patients have lower integrin-dependent migration and adhesion in response to the chemokine SDF-1. Stem Cells *20*, 259–266.

Peng, H., Erdmann, N., Whitney, N., Dou, H., Gorantla, S., Gendelman, H.E., Ghorpade, A., and Zheng, J. (2006). HIV-1-infected and/or immune activated macrophages regulate astrocyte SDF-1 production through IL-1beta. Glia *54*, 619–629.

Perrotti, D., Jamieson, C., Goldman, J., and Skorski, T. (2010). Chronic myeloid leukemia: mechanisms of blastic transformation. J. Clin. Invest. *120*, 2254–2264.

Petzer, A.L., Eaves, C.J., Lansdorp, P.M., Ponchio, L., Barnett, M.J., and Eaves, A.C. (1996). Characterization of primitive subpopulations of normal and leukemic cells present in the blood of patients with newly diagnosed as well as established chronic myeloid leukemia. Blood *88*, 2162–2171.

Reynaud, D., Pietras, E., Barry-Holson, K., Mir, A., Binnewies, M., Jeanne, M., Sala-Torra, O., Radich, J.P., and Passegué, E. (2011). IL-6 controls leukemic multipotent progenitor cell fate and contributes to chronic myelogenous leukemia development. Cancer Cell *20*, 661–673.

Saglio, G., Kim, D.W., Issaragrisil, S., le Coutre, P., Etienne, G., Lobo, C., Pasquini, R., Clark, R.E., Hochhaus, A., Hughes, T.P., et al; ENESTnd Investigators. (2010). Nilotinib versus imatinib for newly diagnosed chronic myeloid leukemia. N. Engl. J. Med. *362*, 2251–2259.

Sarry, J.E., Murphy, K., Perry, R., Sanchez, P.V., Secreto, A., Keefer, C., Swider, C.R., Strzelecki, A.C., Cavelier, C., Récher, C., et al. (2011). Human acute myelogenous leukemia stem cells are rare and heterogeneous when assayed in NOD/SCID/IL2Rγc-deficient mice. J. Clin. Invest. *121*, 384–395.

Sawyers, C.L. (1999). Chronic myeloid leukemia. N. Engl. J. Med. *340*, 1330–1340.

Schemionek, M., Elling, C., Steidl, U., Bäumer, N., Hamilton, A., Spieker, T., Göthert, J.R., Stehling, M., Wagers, A., Huettner, C.S., et al. (2010). BCR-ABL enhances differentiation of long-term repopulating hematopoietic stem cells. Blood *115*, 3185–3195.

Verfaillie, C.M., McCarthy, J.B., and McGlave, P.B. (1992). Mechanisms underlying abnormal trafficking of malignant progenitors in chronic myelogenous leukemia. Decreased adhesion to stroma and fibronectin but increased adhesion to the basement membrane components laminin and collagen type IV. J. Clin. Invest. *90*, 1232–1241.

Zhang, Q., Guo, R., Schwarz, E.M., Boyce, B.F., and Xing, L. (2008). TNF inhibits production of stromal cell-derived factor 1 by bone stromal cells and increases osteoclast precursor mobilization from bone marrow to peripheral blood. Arthritis Res. Ther. *10*, R37.

Cancer Cell
Article

Imaging Tumor-Stroma Interactions during Chemotherapy Reveals Contributions of the Microenvironment to Resistance

Elizabeth S. Nakasone,[1,2,10] Hanne A. Askautrud,[1,3,4,5,10] Tim Kees,[1] Jae-Hyun Park,[1] Vicki Plaks,[3] Andrew J. Ewald,[3,6] Miriam Fein,[1,7] Morten G. Rasch,[1,8] Ying-Xim Tan,[3] Jing Qiu,[1] Juwon Park,[1] Pranay Sinha,[1] Mina J. Bissell,[9] Eirik Frengen,[4,5] Zena Werb,[3,11] and Mikala Egeblad[1,3,11,*]
[1]Cold Spring Harbor Laboratory
[2]Watson School of Biological Sciences
Cold Spring Harbor, NY 11724, USA
[3]Department of Anatomy, University of California, San Francisco, San Francisco, CA 94143, USA
[4]Department of Medical Genetics, Institute of Clinical Medicine, University of Oslo, N-0315 Oslo, Norway
[5]Department of Medical Genetics, Oslo University Hospital, N-0424 Oslo, Norway
[6]Departments of Cell Biology and Oncology, Center for Cell Dynamics, Johns Hopkins School of Medicine, Baltimore, MD, 21205, USA
[7]Graduate Program in Genetics, Stony Brook University, Stony Brook, New York 11794, USA
[8]Finsen Laboratory, Copenhagen University Hospital, DK-1165 Copenhagen, Denmark
[9]Life Sciences Division, Lawrence Berkeley National Laboratory, Berkeley, CA 94720, USA
[10]These authors contributed equally to this work
[11]These authors contributed equally to this work
*Correspondence: egeblad@cshl.edu
DOI 10.1016/j.ccr.2012.02.017

SUMMARY

Little is known about the dynamics of cancer cell death in response to therapy in the tumor microenvironment. Intravital microscopy of chemotherapy-treated mouse mammary carcinomas allowed us to follow drug distribution, cell death, and tumor-stroma interactions. We observed associations between vascular leakage and response to doxorubicin, including improved response in matrix metalloproteinase-9 null mice that had increased vascular leakage. Furthermore, we observed CCR2-dependent infiltration of myeloid cells after treatment and that *Ccr2* null host mice responded better to treatment with doxorubicin or cisplatin. These data show that the microenvironment contributes critically to drug response via regulation of vascular permeability and innate immune cell infiltration. Thus, live imaging can be used to gain insights into drug responses in situ.

INTRODUCTION

One of the major challenges in treating cancer is resistance to therapy. It is well appreciated that cancer cell intrinsic factors, such as genetic or epigenetic changes, can cause development of therapy resistance (Dean et al., 2005). Extrinsic factors in the microenvironment of certain organs, such as the bone marrow and thymus, can also confer resistance (Gilbert and Hemann, 2010; Meads et al., 2009). In these cases, resistance is mediated by factors secreted from stromal cells, such as IL-6. In addition, impaired drug penetration through the extracellular matrix (ECM) influences drug response in primary solid tumors (Loeffler et al., 2006; Olive et al., 2009).

Surprisingly little is known about how cells in intact tumors respond to classical chemotherapies (Minchinton and Tannock, 2006; Rottenberg et al., 2010). Most of the knowledge about these responses has been obtained from cell culture or xenograft experiments, where cancer cells grow under conditions very different from the microenvironment of human tumors. Indeed, such experiments are often not predictive of drug

Significance

It is well appreciated that intrinsic factors regulate chemoresponsiveness. Using in vivo microscopy of tumors, we show that extrinsic factors within the microenvironment support the development of chemoresistance by regulating drug distribution and the inflammatory response. These results have clinical implications, as myeloid cell infiltration is increased in human breast tumors after chemotherapy and the cellular composition of the immune infiltrate is a strong predictor of overall survival. Our data suggest that the response to classical chemotherapeutic drugs can be improved by changing the tumor microenvironment with agents that modify matrix metalloproteinase activity and chemokine signaling. Our study shows that observing the tumor response in real-time at cellular resolution can yield insights into the biology of chemoresistance.

responses in patients (Johnson et al., 2001; Minchinton and Tannock, 2006).

To investigate the role of the microenvironment in chemoresponsiveness, we chose a well-documented mouse model, the mammary tumor virus (MMTV) promoter-driven polyoma middle T oncogene (PyMT) model, that displays progressive stages of tumorigenesis similar to human luminal type B breast cancer (Herschkowitz et al., 2007; Lin et al., 2003). As MMTV-PyMT tumors progress, cancer cells undergo molecular changes, including increased expression of ErbB receptor family members (Lin et al., 2003). In parallel, the stromal microenvironment undergoes changes in blood vessel architecture, ECM composition, and immune cell infiltration (Egeblad et al., 2008, 2010).

RESULTS

Doxorubicin Induces Necrotic Cell Death In Vivo

Doxorubicin (Adriamycin) is a cytotoxic drug used to treat advanced breast cancer (Rouzier et al., 2005). To investigate the acute, cellular response to doxorubicin treatment in the context of the tumor microenvironment, we monitored mammary carcinomas in live mice using spinning disk confocal microscopy (Egeblad et al., 2008). MMTV-PyMT mice were crossbred with the ACTB-ECFP and c-fms-EGFP reporter mice to enable visualization of different tumor stages and tracking of the most abundant stromal cell type, myeloid cells (Egeblad et al., 2008). Dead cells were labeled with propidium iodide (PI) administered intraperitoneally (i.p.). Cell death became apparent 24–30 hr after doxorubicin administration and increased as imaging continued, whereas there was limited cell death in untreated control mice (Figure 1A; Figure S1A available online; see Figure 2 for quantification). The death of individual cells was readily observed as the appearance of PI staining (Figure 1B; Movie S1). In addition to cell death in the tumor mass, we observed stromal cell death (Figure 1A).

Necrosis is a major pathway of cell death after doxorubicin treatment in vitro (Obeid et al., 2007). Cell death by apoptosis and necrosis are characterized by specific changes in nuclear morphology and plasma membrane integrity (Dive et al., 1992). We next determined the nature of doxorubicin-induced cell death in vivo by imaging changes in nuclear morphology in MMTV-PyMT;ACTB-ECFP mice crossbred with mice expressing histone H2B conjugated to EGFP (Hadjantonakis and Papaioannou, 2004). The majority of the nuclei became positive for PI before their morphology changed, indicating early loss of plasma membrane integrity and necrosis-like cell death. A small percentage of cells died with breakdown of chromatin into condensed bodies followed by acquisition of PI labeling, indicating late loss of plasma membrane integrity and apoptosis-like cell death (Figures 1C and 1D; Movie S2). By histology, we observed only a minor increase in the number of cells with the condensed chromatin that is typical of apoptosis after doxorubicin treatment (Figure S1B). Thus, doxorubicin predominantly induces necrosis in vivo.

Doxorubicin Sensitivity Changes with Tumor Stage

At the macroscopic level, doxorubicin treatment reduced tumor volume in MMTV-PyMT mice bearing multiple tumors (Figures 2A and S2A). However, the smallest or largest tumors tended to be resistant (Figure S2B), suggesting that resistance was associated with tumor progression.

MMTV-PyMT tumors have been classified into four pathological stages, based on cellular morphology, lack of basement membrane, and infiltration of immune cells (Lin et al., 2003). We adapted this classification to allow a simplified assessment of tumor stage in live animals: ''hyperplasia,'' small lesions showing increased accumulation of cells as compared to normal epithelium; ''early carcinoma,'' lesions with evidence of myeloid cell infiltration and/or cancer cell invasion; and ''late carcinoma,'' large lesions with densely packed cancer cells (Egeblad et al., 2008). MMTV-PyMT mammary glands have multiple tumors, which are often at different stages of progression. This allowed us to image doxorubicin response at different stages in the same mouse (Figures 2B and S2C). Cell death increased after doxorubicin-treatment in early carcinomas (Figure 2C); on average, 10% of the fields of view (FOV) were positive for PI at 31 hr after doxorubicin-treatment compared to 2% of the FOV in the controls (Figure S2D). In contrast, cell death did not increase in hyperplasias and late carcinomas after treatment (Figures 2B, 2C, S2C, and S2D; Movie S3), suggesting marked differences in drug sensitivity between tumor stages. Cancer cells in early carcinomas also accumulated more DNA damage after doxorubicin treatment than those in hyperplasias or late carcinomas, as determined by immunostaining for histone γ-H2AX (Figure 2D). Thus, doxorubicin sensitivity changes with tumor stage but not in a linear manner.

Cancer Cell Proliferation Does Not Correspond to Doxorubicin Sensitivity In Vivo

Doxorubicin intercalates into DNA, inhibiting topoisomerase II. Hence, proliferating cells are predicted to be more sensitive than resting cells (Campiglio et al., 2003). Yet, cancer cell proliferation differed insignificantly between tumor stages (Figure 2E). Furthermore, in pulse-chase experiments, the percentage of dead cells that were $BrdU^+$ was similar in doxorubicin- and phosphate buffered saline (PBS)-treated tumors (Figure 2F). These data suggest that differences in cellular proliferation between tumor stages are not the main cause of differences in doxorubicin sensitivity in vivo.

Primary Cancer Cells from Different Tumor Stages Do Not Exhibit Intrinsic Differences in Doxorubicin Sensitivity in Culture

As tumors progress, cancer cells acquire mutations and silence or activate genes. These changes can give rise to differences in sensitivity between tumor stages. To distinguish the contribution of cancer cell intrinsic changes from those of the tissue microenvironment, we isolated cancer cells from MMTV-PyMT; ACTB-ECFP mice using a fluorescent dissection microscope. This allowed us to visualize the cancer epithelium during tissue removal, ensuring that tumors were representative of the different stages (Figure S2E). Indeed, in vitro sensitivity to the ErbB1/ErbB2 inhibitor lapatinib was highest for cells isolated from late carcinomas (Figure 2G), as predicted from the increased expression of the ErbB2/Neu oncoprotein in late-stage tumors (Lin et al., 2003). In contrast, cells from hyperplasia,

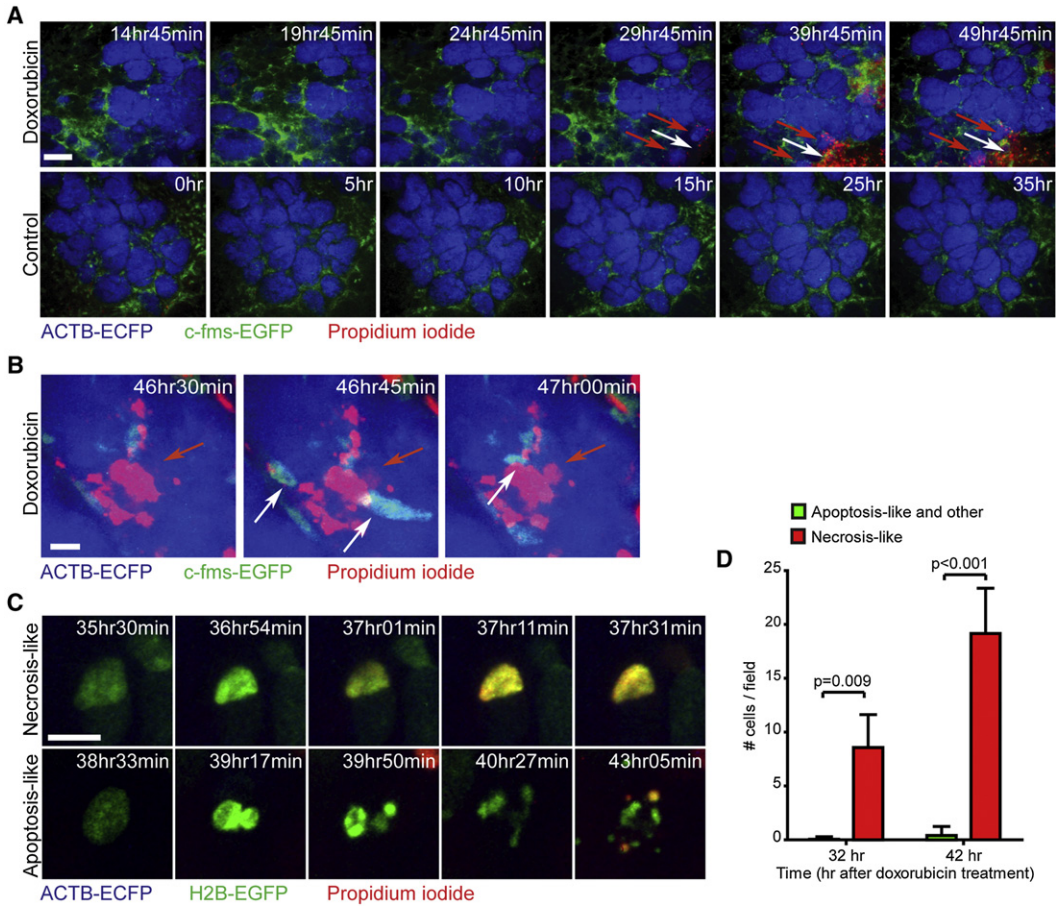

Figure 1. Visualizing Cellular Responses to Chemotherapy In Vivo

(A) Doxorubicin-induced cell death in tumors of live MMTV-PyMT;ACTB-ECFP;c-fms-EGFP mice. Induction of cell death (red), visualized by propidium iodide (PI) uptake, can be seen in a tumor lesion (blue) infiltrated with myeloid cells (green). Red arrows point to cell death in the tumor, and white arrows point to cell death in the stroma. Time after treatment (doxorubicin) or initiation of imaging (control) is indicated. Scale bar: 100 μm.

(B) Dynamics of cell death in situ. Single cell death was observed as the appearance of PI staining (red arrow). This was followed by myeloid cell infiltration (white arrows). Time after doxorubicin treatment is indicated. Scale bar: 10 μm.

(C) Dynamics and types of nuclear structural changes after doxorubicin treatment in MMTV-PyMT;ACTB-ECFP;H2B-EGFP mice. Examples of necrosis-like (nucleus becomes PI^+ without major structural changes) and apoptosis-like (nuclear structure breakdown before PI uptake) cell death. Time after treatment is indicated. Scale bar: 10 μm.

(D) Doxorubicin induces necrosis-like cell death (mean ± SEM; 18 fields of view [FOV] from three mice were counted; $p = 0.009$ at 32 hr, $p < 0.001$ at 42 hr, Student's t test).

Also see Figure S1 and Movies S1 and S2.

early carcinoma, and late carcinoma stages had similar sensitivity to doxorubicin in both two- and three-dimensional cultures (Figures 2H, 2I, and S2F). Primary macrophages and the macrophage cell line RAW 264.7 were also sensitive to doxorubicin (Figure S2G), in accordance with the stromal cell death observed by imaging. Taken together, the in vitro data indicated that cancer cell intrinsic mechanisms are unlikely to be responsible for the differences in doxorubicin sensitivity that were observed between tumor stages and that extrinsic mechanisms are operative in vivo.

Visualization of Drug Distribution in Real-Time Reveals Its Association with Drug Response

Interstitial fluid pressure is one extrinsic factor that increases in late-stage tumors as compared to early stages and it hinders drug penetration into tumors (Hagendoorn et al., 2006; Netti et al., 1999). Therefore, we hypothesized that differences in drug response between tumor stages might be related to differences in drug accessibility. Doxorubicin is naturally fluorescent, allowing for imaging of its distribution. However, its broad emission and excitation spectra overlap with those of our fluorescent reporters. It was therefore not possible to image doxorubicin distribution in MMTV-PyMT;ACTB-ECFP mice in which tumor stage could be determined. Instead, we imaged unlabeled MMTV-PyMT mice and identified tumor areas by palpation and abnormal tumor vasculature, visualized using intravenously (i.v.) injected fluorescent nanoparticles (AngioSPARK 680).

We imaged small (just palpable), medium (~160 mm^3), and large (~845 mm^3) tumors (Figure 3A; Movies S4 and S5).

Doxorubicin rapidly leaked out into the tissue and accumulated in the nuclei of cells near blood vessels (Figure 3A). This resulted in an intravascular half-life of 9.5 min (range, 7.9–11.8 min; Figure 3B), consistent with the initial plasma half-life of 8.5 min (range, 7.2–9.8 min) reported in human patients (Greene et al., 1983). Doxorubicin distribution varied among tumors of different sizes (Figures 3A and 3C), with the most leakage in larger tumors and the least leakage in those that were just palpable. Furthermore, significantly more doxorubicin was extractable from small tumors (13–81 mm^3) than from hyperplastic MMTV-PyMT tissues or normal mammary glands (Figure 3D). Solid tumors tend to have progressed further than softer ones, and when tumors were analyzed based on consistency, as well as size, the highest levels of doxorubicin were found in soft tumors, although the values were not significantly higher than in solid tumors of similar size (Figure 3E).

Tumor size and consistency is not an accurate indicator of tumor stage. Thus, to quantify vascular leakage in tumors of different stages, we co-injected i.v. fluorescent 10 kD (low) and 2 MD (high) molecular mass dextrans into MMTV-PyMT;ACTB-ECFP mice (Figures 4A and S3A; Movie S6). The intravascular half-lives of dextrans were similar in tumor microenvironments at different stages (Figures S3B and S3C), with a higher intravascular half-life for 2 MD dextran (41 [range, 32–58] min) than for 10 kD dextran (15 [range, 14–16] min; Figure S3D).

In contrast to intravascular half-life, leakage of dextrans into the extravascular space and their retention in tissues were clearly influenced by tumor stage (Figures 4A and 4B). Regions with hyperplasias showed limited leakage into the extravascular space, whereas early carcinomas and the tumor-stroma borders of late carcinomas exhibited substantially more leakage. Extravasated 10 kD dextran reached a larger area of the tissue than did extravasated 2 MD dextran (Figures 4A and 4B). Following extravasation, the dextrans accumulated in stromal cells, which we have previously shown are c-$fms^+CD68^+CD206^+$ macrophages (Egeblad et al., 2008). Leakage in normal mammary glands was minimal and below detection limits when the settings used for tumor-bearing mice were applied (not shown).

Finally, we co-injected i.v. doxorubicin-treated mice with 10 kD dextran and *Ricinus communis* agglutinin I, a lectin that binds to basement membrane exposed to the vascular lumen, marking leaky vasculature (Thurston et al., 1999). We observed that only tumor areas in close proximity to these two markers contained cells with nuclear uptake of doxorubicin (Figure S3E). Interestingly, some of the cells with doxorubicin-positive nuclei had also taken up dextran, suggesting that they were macrophages (Figure S3E).

Absence of MMP9 Results in Increased Vascular Leakage and Sensitizes Tumors to Doxorubicin Treatment

Tumor-associated macrophages promote vascular changes (Egeblad et al., 2010). We found that the extent of local c-fms-$EGFP^+$ myeloid cell infiltration correlated significantly with the degree of local 10 kD dextran leakage, regardless of tumor stage (Figures 4C and 4D). Myeloid cells can regulate vessel stability via secretion of vascular endothelial growth factor (VEGF) and transforming growth factor (TGF)-β, both of which are sequestered in the ECM and released by matrix metalloproteinases (MMPs; Yu and Stamenkovic, 2000; Ebrahem et al., 2010). Nevertheless, MMPs may also negatively regulate vascular permeability (Sounni et al., 2010). Several MMPs, including MMP9, are expressed at high levels by tumor-infiltrating myeloid cells (Figure 5A). To determine if host-derived MMP9 affects vascular stability and doxorubicin response, we transplanted MMTV-PyMT cancer cells to wild-type FVB/n and $Mmp9^{-/-}$ hosts and treated them with doxorubicin. Although MMP9 does not influence primary tumor growth in the transgenic MMTV-PyMT model (Martin et al., 2008), we found that the growth of grafted tumors was reduced in $Mmp9^{-/-}$ hosts compared to FVB/n hosts (Figure S4A). Interestingly, tumors in $Mmp9^{-/-}$ hosts responded better to doxorubicin than those in FVB/n hosts (Figure S4B).

Since transplanted MMTV-PyMT tumors grew slower in $Mmp9^{-/-}$ hosts, we could not rule out that the influence of MMP9 on doxorubicin response was related to its effects on cancer cell proliferation. Therefore, we tested if MMP9 influenced the response in the MMTV-Neu model, another doxorubicin-sensitive, luminal breast cancer model, in which the absence of MMP9 does not affect cancer cell proliferation or tumor growth (Figures S4C and S4D; data not shown). Vascular volume, determined by i.v. tomato lectin staining, was not affected by MMP9 status, but tumor vessels were leakier in the absence of MMP9, as determined by i.v. staining with *Ricinus communis* agglutinin I (Figures 5B–5D). In the absence of MMP9, the endothelial cell adhesion molecule VE-cadherin showed increased phosphorylation (Figures 5E and 5F), which results in loose adherence junctions (Gavard, 2009). Vascular coverage with pericytes, which support endothelial cells, was also decreased (Figures 5G and S4E). In keeping with the increased permeability of the vasculature, MMTV-Neu;$Mmp9^{-/-}$ tumors treated with doxorubicin responded better than did MMTV-Neu;$Mmp9^{+/+}$ tumors (Figure 5H). In contrast, C3(1)-Tag tumors, a basal-like mammary carcinoma model that is largely doxorubicin-resistant (Figure S4F), did not respond better in the absence of MMP9 (Figure S4G).

Doxorubicin Treatment Leads to Recruitment of Myeloid Cells to Tumors

We observed that vascular leakage was associated with higher infiltration of macrophages (Figure 4D), so we sought to determine the effect of MMP9 on macrophage infiltration. There were increased numbers of cells expressing the F4/80 and CD206 macrophage markers in untreated tumors of $Mmp9^{-/-}$ hosts compared to those of FVB/n hosts (Figures 6A and 6B). Interestingly, doxorubicin treatment significantly reduced the number of macrophages in $Mmp9^{-/-}$ hosts, suggesting that macrophages were killed.

Despite the reduction in macrophage numbers observed after doxorubicin-treatment of $Mmp9^{-/-}$ hosts, imaging consistently showed recruitment of myeloid cells to doxorubicin-treated tumors in wild-type mice (Figures 6C and 6D; Movie S7). These myeloid cells often formed granuloma-like structures in areas with cell death (Movie S7). Rarely, we observed myeloid cell recruitment prior to cancer cell death (Figure S5A).

Myeloid cells are a diverse family of innate immune cells, including neutrophils, monocytes, and macrophages, that are

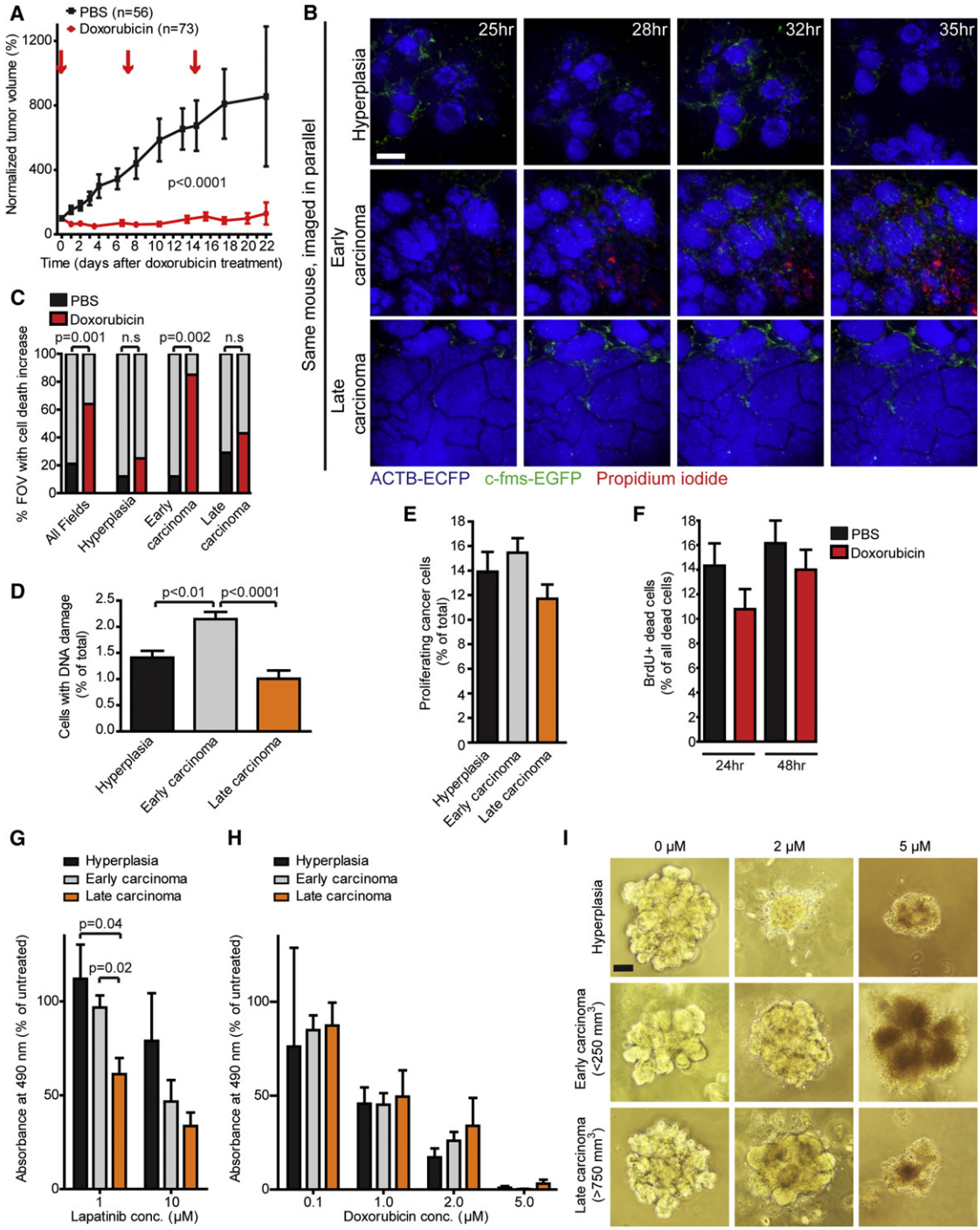

Figure 2. Doxorubicin Sensitivity Changes with Tumor Stage In Vivo but Not In Vitro

(A) Doxorubicin treatment reduces tumor volume in MMTV-PyMT mice. Mice were given doxorubicin or PBS at days 0, 7, and 14 (indicated by arrows). Analysis includes 73 tumors from eleven doxorubicin-treated mice and 56 tumors from 12 PBS-treated mice (mean ± SEM, $p < 0.0001$ for all time-points, Student's t test).

(B) Doxorubicin-induced cell death preferentially occurs in early carcinomas and not in hyperplasias and late carcinomas. Different microenvironments imaged in the same MMTV-PyMT;ACTB-ECFP;c-fms-EGFP mouse after doxorubicin treatment. Time after treatment is indicated. Scale bar: 100 μm.

(C) Cell death increases between 24 and 36 hr after doxorubicin treatment (n = 25 fields of view [FOV]) as compared to control mice imaged for similar time frames (n = 23 FOV; Fisher's exact test; $p = 0.001$). Cell death increases in early carcinomas (12 of 14 doxorubicin-treated versus 1 of 8 control-treated FOV, Fisher's exact test, $p = 0.002$) but not in hyperplasias (1 of 4 versus 1 of 8 fields) or late carcinomas (3 of 7 versus 2 of 7). Four control- and four doxorubicin-treated mice were imaged.

(D) DNA damage response measured by γ-H2AX immunostaining differs between tumor stages (mean ± SEM, analysis of variance [ANOVA], $p < 0.0001$) and is higher in early carcinomas than in hyperplasia ($p < 0.01$, Bonferroni posttest) or late carcinomas ($p < 0.0001$; Bonferroni posttest; 21 hyperplasia, 25 early carcinoma, and 24 late carcinoma FOV were evaluated in five tumors from five mice).

all recruited to areas of cell death (Murdoch et al., 2004). To determine a basis for myeloid cell infiltration, we injected necrotic cell debris into mammary glands of non-tumor-bearing mice and imaged the response. In this model, the results are independent of any direct effects of doxorubicin on myeloid cells, such as induction of cell death. Myeloid cell infiltration increased in areas injected with necrotic debris as compared to areas injected with only saline and dextran (Figure S5B). Once a myeloid cell recognized the cell debris, other myeloid cells were rapidly recruited and a granuloma-like structure was formed (Figure S5B; Movie S8). Myeloid cell recruitment is often mediated by G_i-protein-coupled chemokine receptors (Sadik et al., 2011). Mice pretreated with pertussis toxin, a G_i-protein inhibitor, showed reduced myeloid cell recruitment to cell debris, suggesting the involvement of chemokine receptors in this process (Figure S5C; Movie S9).

Myeloid Cells Are Recruited to Doxorubicin-Treated Tumors through a Stromal CCL2/CCR2 Chemokine/Chemokine Receptor Axis

To screen for candidate chemokines involved in the recruitment of myeloid cells, we used a protein array. Tumor lysates isolated 48 hr after doxorubicin treatment showed increased protein levels for CCL2 and CCL12 (Figure 7A). Both of these chemokines are ligands for the CCR2 receptor, which is expressed on monocytes and is responsible for their recruitment to sites of inflammation (Tsou et al., 2007). We also observed small increases in macrophage colony-stimulating factor (M-CSF/CSF1) and tissue inhibitor of metalloproteinase 1 (TIMP1; Figure 7A). We confirmed the increases in CCL2 and CCL12 by enzyme-linked immunosorbent assay and immunostaining (Figures 7B, S6A, and S6B). CCL2-expressing cells were large cells located in the stroma that did not express markers of fibroblasts and pericytes (Figure 7C) or endothelial cells (Figure 7D).

Next, we investigated the types of myeloid cells recruited after doxorubicin treatment. Infiltration of cells expressing a neutrophil/monocyte marker, the 7/4 antigen (Ly6B.2), was significantly increased (Figure 7E). This increase was exclusively found among cells that also expressed the CCL2 receptor, CCR2, and had a monocytic nuclear morphology (Figures 7E and S6C). The number of $7/4^+CCR2^-$ cells did not increase but rather decreased, after doxorubicin treatment (Figure 7E). A small number of $CCR2^+$ cells did not express the 7/4 antigen, but their numbers did not change after doxorubicin treatment (Figure 7E). In contrast to the acute increase in the infiltration of $7/4^+CCR2^+$ cells, overall macrophage infiltration, as determined by the F4/80 marker, was not changed 48 hr after doxorubicin treatment (Figure S6D). However, a small increase was seen in the number of cells within the tumor mass that expressed CD206, a marker of alternatively activated macrophages (Figure S6E).

We next tested whether CCR2 mediates the myeloid cell infiltration seen after doxorubicin treatment. We transplanted primary cancer cells isolated from MMTV-PyMT mice to *Ccr2*$^{-/-}$ or C57BL/6 hosts and characterized the myeloid cell population after doxorubicin treatment. In C57BL/6 hosts, the fraction of cells co-expressing the myeloid cell marker CD11b with the monocyte/neutrophil markers Gr1 and 7/4 increased significantly after doxorubicin treatment (Figures 7F and 7G). The total proportion of cells in the tumors that expressed the myeloid CD11b marker did not increase (Figure S6F). Tumors of *Ccr2*$^{-/-}$ hosts had a higher fraction of $CD11b^+7/4^+Gr1^+$ cells than did C57BL/6 hosts (Figures 7F and 7G), consistent with previous reports (Pahler et al., 2008). However, there was no significant increase in this cell population after doxorubicin treatment in *Ccr2*$^{-/-}$ hosts (Figures 7F and 7G). Doxorubicin treatment did not affect the subpopulations of $CD11b^+$ cells that expressed F4/80 or CXCR4 in either genotype (Figures S6G—S6I). Together, our results suggest that doxorubicin treatment leads to a specific, acute recruitment of CCR2-expressing myeloid cells of the monocytic lineage through stromally expressed CCL2.

Host CCR2 Influences Tumor Response to Chemotherapy

To determine if CCR2-mediated recruitment of myeloid cells influenced the response to doxorubicin, we generated cohorts of MMTV-PyMT;*Ccr2*$^{+/-}$ and MMTV-PyMT;*Ccr2*$^{-/-}$ mice. For doxorubicin-sensitive tumors (250–750 mm^3), the absence of CCR2 was associated with a significantly better response, although tumors in both cohorts ultimately relapsed (Figure 8A). In contrast, tumors below 250 mm^3, which respond poorly to doxorubicin, did not show a better response to treatment when mice were deficient for CCR2 (Figure S7A).

CCL2 has been proposed to promote cancer cell survival through CCR2 receptors on cancer cells (Zhang et al., 2010). To rule out the involvement of CCR2 signaling in cancer cells, we transplanted primary cancer cells from MMTV-PyMT mice to *Ccr2*$^{-/-}$ or C57BL/6 hosts. When treated with doxorubicin or cisplatin, a different class of chemotherapeutic drug with efficacy against MMTV-PyMT tumors (Figure S7B), tumors in *Ccr2*$^{-/-}$ hosts relapsed later than those in C57BL/6 hosts (Figures 8B and 8C). Tumor growth before treatment was not significantly different between *Ccr2*$^{-/-}$ and C57BL/6 hosts (Figure 8B). Myeloid cells can secrete factors that increase cancer

(E) Cancer cell proliferation determined by BrdU labeling does not differ between tumor stages in MMTV-PyMT mice (mean ± SEM, not significant, n.s., ANOVA; 13 hyperplasia, 19 early carcinoma, and 28 late carcinoma FOV were evaluated in six tumors from three mice).
(F) Proliferating ($BrdU^+$) cells are not preferentially killed by doxorubicin treatment. The fraction of $BrdU^+$ cells with cell death-associated nuclear changes was scored (mean ± SEM, n.s., Student's t test; for each condition, 58–60 FOV were analyzed in six tumors from three mice).
(G) Sensitivity to the ErbB1/ErbB2 inhibitor lapatinib is highest for cancer cells from late-stage tumors in culture (mean ± SEM, p = 0.04 or 0.02 as indicated, Student's t test; values represent the averages of four experiments, each done in triplicate with primary cells from independent mice).
(H) Sensitivity to doxorubicin is not affected by tumor stage in culture (mean ± SEM, n.s., ANOVA; values represent the averages of four experiments, each done in triplicate with primary cells from independent mice).
(I) Morphology of organoids generated from tumors at different stages after treatment with the indicated concentrations of doxorubicin. Scale bar: 50 μm.
Also see Figure S2 and Movie S3.

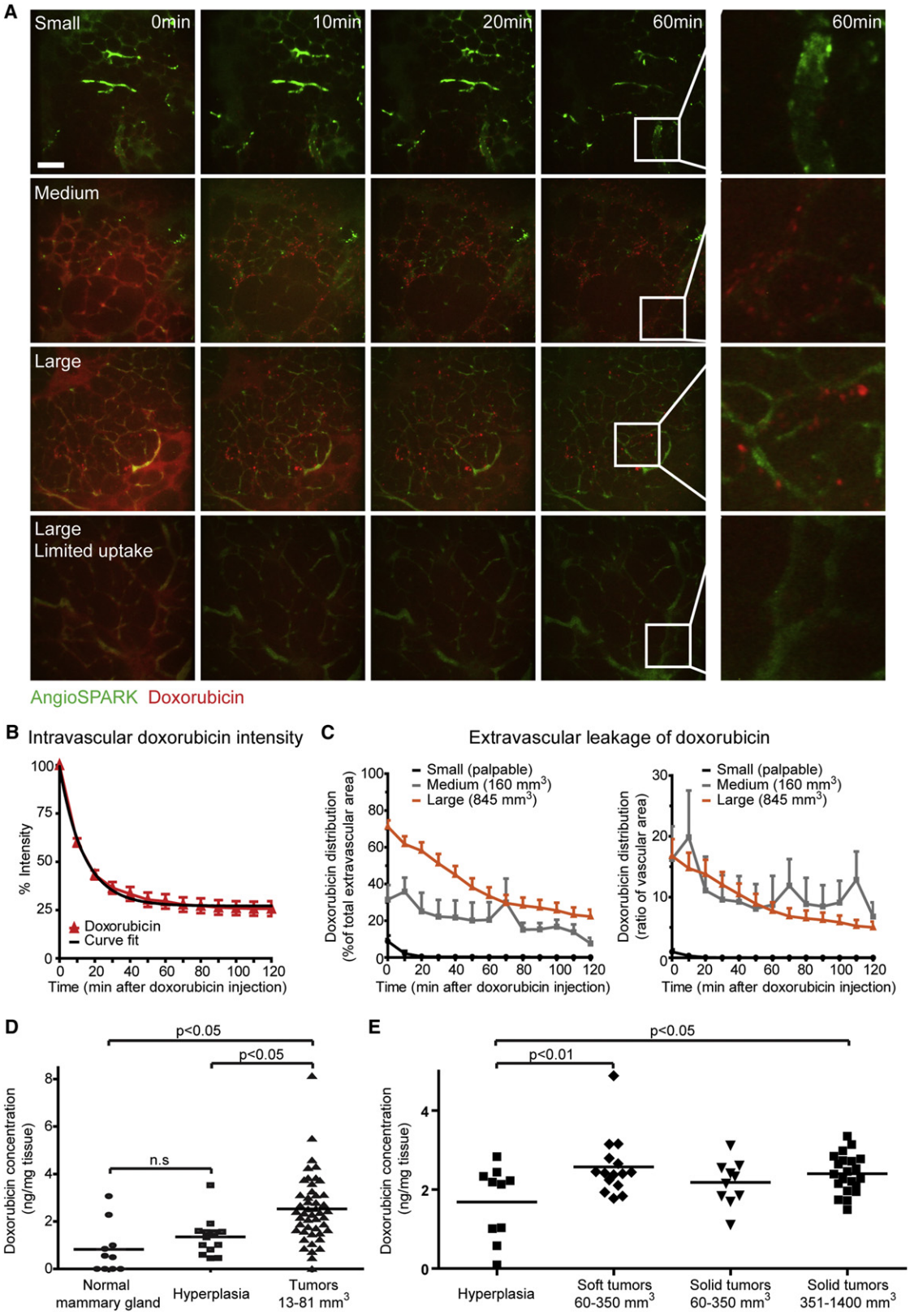

Figure 3. Distribution and Uptake of Doxorubicin in Different Tumor Sizes

(A) Doxorubicin leakage and uptake vary with tumor size. MMTV-PyMT mice with small (just palpable tumors), medium (~160 mm^3), or large tumors (~845 mm^3) were injected intravenously with AngioSPARK 680 (green) and doxorubicin (red). Minimal leakage and uptake were seen in small tumors. Leakage was high in

cell survival (Shree et al., 2011). However, we detected no lasting survival benefit on primary cancer cells when they were cultured with primary macrophages (Figures S7C and S7D).

Although tumors in *Ccr2*$^{-/-}$ hosts relapsed, they were of a strikingly lower histological grade than the high-grade relapsed tumors of C57BL/6 hosts (Figure 8D). Histological differences were already evident 48 hr after doxorubicin treatment as tumors in *Ccr2*$^{-/-}$ hosts were more cystic than those in C57BL/6 hosts (Figure 8D). Taken together, our data suggest that infiltration of CCR2-expressing myeloid cells into chemotherapy-treated tumors contributes to tumor regrowth after treatment.

Like CCR2, MMP9 can also influence myeloid cell recruitment (Gong et al., 2008). We therefore tested whether the effects of MMP9 on doxorubicin response could be explained by effects on the acute recruitment of myeloid cells to treated tumors. However, adaptively transferred bone marrow cells from c-fms-EGFP;*Mmp9*$^{+/+}$ and c-fms-EGFP;*Mmp9*$^{-/-}$ mice were recruited equally well to tumors of MMTV-PyMT mice after treatment with doxorubicin (Figure S7E). Next, we tested whether the changed myeloid cell environment in *Ccr2*$^{-/-}$ mice correlated with vascular changes, akin to the effects of loss of *Mmp9* (Figure 8E). Whereas the vascular volume was higher in tumors of *Ccr2*$^{-/-}$ mice (Figure 8F), the percentage that was leaky was significantly lower, with the net result being no change in the total volume of leaky vasculature (Figures 8G and 8H). Furthermore, pericyte coverage of the vasculature was increased in *Ccr2*$^{-/-}$ hosts, whereas VE-cadherin phosphorylation levels were unaffected (Figures S7F–S7I). Thus, although the response to doxorubicin is improved in both *Mmp9*$^{-/-}$ and *Ccr2*$^{-/-}$ microenvironments, the effects on vascular structure and myeloid cell recruitment after treatment are different.

DISCUSSION

We imaged the dynamics of doxorubicin responses in a progressive cancer model and revealed that chemosensitivity in vivo is influenced by the tumor microenvironment. The highest sensitivity to doxorubicin was not observed in the earliest or latest tumor stages but rather in the intermediate stage. These differences in drug response between stages were associated with parallel differences in vascular leakage. We therefore tested doxorubicin response in *Mmp9* null tumor microenvironments with increased vascular permeability and found an improved response. Doxorubicin treatment led to the recruitment of CCR2^{+} monocytic cells to tumors. In *Ccr2* null microenvironments, recruitment was inhibited and the response to chemotherapy better. These results have clinical implications, as myeloid cell infiltration is increased in human breast tumors after chemotherapy and the composition of the immune infiltrate is a predictor of survival (Denardo et al., 2011).

Stromal Regulation of Vascular Leakage

Primary cancer cells from different stages responded similarly to doxorubicin in vitro, whereas doxorubicin sensitivity, tumor stage, and vascular leakage were related in vivo. This suggests that stage-specific changes in vascular leakage contributed to doxorubicin response although we cannot exclude contributions from stromal cells. Strikingly, increased leakage of the tumor vasculature in *Mmp9*$^{-/-}$ mice corresponded to a better response to doxorubicin. The increased vascular permeability in *Mmp9*$^{-/-}$ mice was associated with decreased pericyte-coverage of the vasculature and increased phosphorylation of VE-cadherin, which affect endothelial cell-cell adhesions (Gavard, 2009; Goel et al., 2011). Although MMP inhibitors have failed in clinical trials (Coussens et al., 2002), our data suggest that these, or other drugs that affect vascular permeability, could be used to achieve better responses to chemotherapies.

MMP9 may regulate vascular structure by acting on a substrate in the tumor microenvironment. Indeed, a reduction of infiltrating MMP9^{+} myeloid cells through inhibition of the CSF-1 receptor results in a better response to anti-VEGFR2 treatment (Priceman et al., 2010). However, MMP9 may also regulate vascular permeability indirectly through its effects on macrophage infiltration. Macrophages can secrete VEGF (also known as vascular permeability factor), which induces VE-cadherin phosphorylation in endothelial cells (Gavard, 2009).

Myeloid cells are not the only stromal cells capable of regulating drug delivery in tumors. By decreasing the fibroblast pool, and thus the ECM, drugs better enter the tissue (Loeffler et al., 2006; Olive et al., 2009). Interestingly, the improved drug delivery in these cases is achieved by increased vascular density and "vascular normalization," which involves better pericyte coverage and reduced permeability (Goel et al., 2011). Since vascular volume and pericyte coverage increased in tumors of *Ccr2*$^{-/-}$ compared to C57BL/6 hosts, such vascular changes could play a role in the MMTV-PyMT model. Untangling the roles of MMP9 and CCR2 on vasculature, myeloid cell infiltration, and drug response will require the ability to temporally and conditionally manipulate these genes.

medium and some large tumors, with variable nuclear retention. Time after doxorubicin injection is indicated. The last column shows nuclear uptake of doxorubicin (higher magnification of the areas outlined in the fourth column). Scale bar: 100 μm.

(B) Decay of intravascular doxorubicin levels determined by imaging is modeled as one-phase exponential decay (black line; mean ± SEM; eight FOV from two mice were analyzed).

(C) Kinetics of doxorubicin leakage from vessels in tumors of different sizes. Quantification of the percentage of extravascular pixels with doxorubicin signal above intensity threshold (150% of background) and as a ratio of extravascular doxorubicin to vascular area (mean ± SEM; eight small, four medium, and eleven large FOV were analyzed in six mice).

(D) Doxorubicin concentration is higher in tumors than hyperplasias and normal mammary glands (means are shown; $p < 0.0001$, ANOVA, and Bonferroni posttests for comparison of groups; $p < 0.05$ or n.s. as indicated; ten normal mammary glands from five FVB/n mice and 14 hyperplastic and 47 tumors [13–81 mm^3] from five MMTV-PyMT were analyzed).

(E) Doxorubicin concentration is higher in tumors that were soft upon dissection than in hyperplastic tissue or solid tumors of similar size (means are shown, $p = 0.01$, ANOVA, and Bonferroni posttests for comparison of groups, $p < 0.01$ or 0.05 as indicated). Ten hyperplastic, 15 soft and medium-sized (60–350 mm^3), ten solid and medium-sized (60–350 mm^3), and 21 solid and large tumors (351–1,400 mm^3) from five MMTV-PyMT mice were analyzed.

Also see Movies S4 and S5.

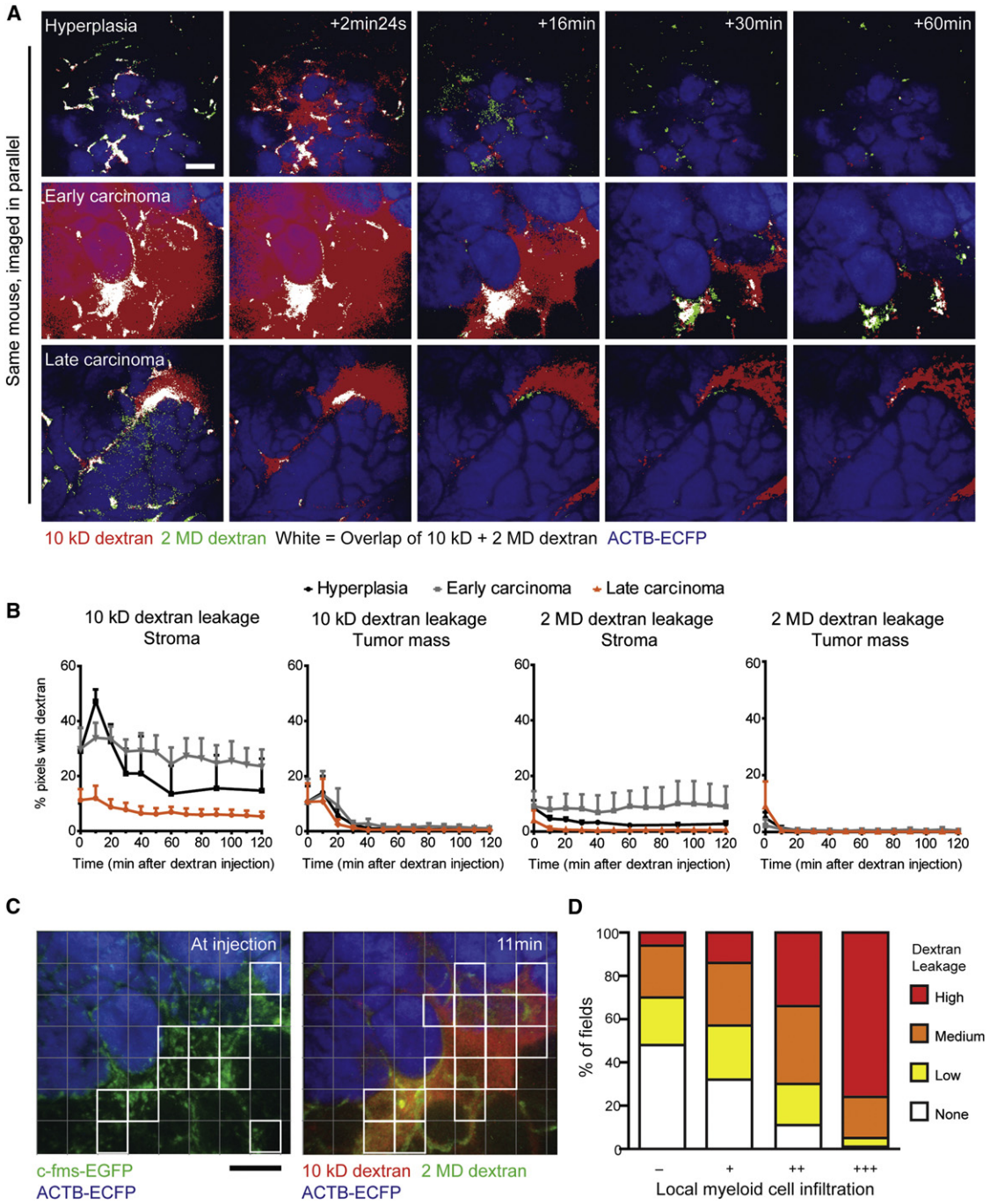

Figure 4. Leakage and Distribution of Intravenously Injected Dextran Varies with Tumor Stage

(A) Early carcinomas exhibit a higher degree of dextran leakage than do hyperplasias and late carcinomas. More extensive leakage of 10 kD than 2 MD dextran is shown for all tumor stages. Kinetics of 10 kD (red) and 2 MD dextran (green) leakage from vessels in three different tumor stages from the same MMTV-PyMT; ACTB-ECFP mouse are shown. Regions with leakage of both dextrans are depicted in white and the epithelium in blue (ACTB-ECFP). Time after dextran injection is indicated. Scale bar: 100 μm.

(B) Quantification of the percentage of pixels above intensity threshold (150% of background) for the two dextrans in the epithelial and stromal compartments (mean ± SEM; four hyperplasias from two mice, five early carcinomas from four mice, and five late carcinomas from four mice were analyzed).

(C) The extent of c-fms-EGFP^{+} myeloid cell infiltration in MMTV-PyMT;ACTB-ECFP;c-fms-EGFP mice and the degree of 10 kD dextran leakage were scored independently using the indicated pixel grid. Co-injected 2 MD dextran was used to differentiate between intra- and extravascular 10 kD dextran. Examples of pixel fields scored as maximal infiltration and leakage are indicated by the white boxes. Scale bar: 100 μm.

(D) Myeloid cell infiltration correlates with dextran leakage ($r = 0.56$ and $r = 0.47$, for observer A and B, respectively, $p < 0.0001$, Spearman's rank correlation coefficient; 720 FOV from two mice were scored).

Also see Figure S3 and Movie S6.

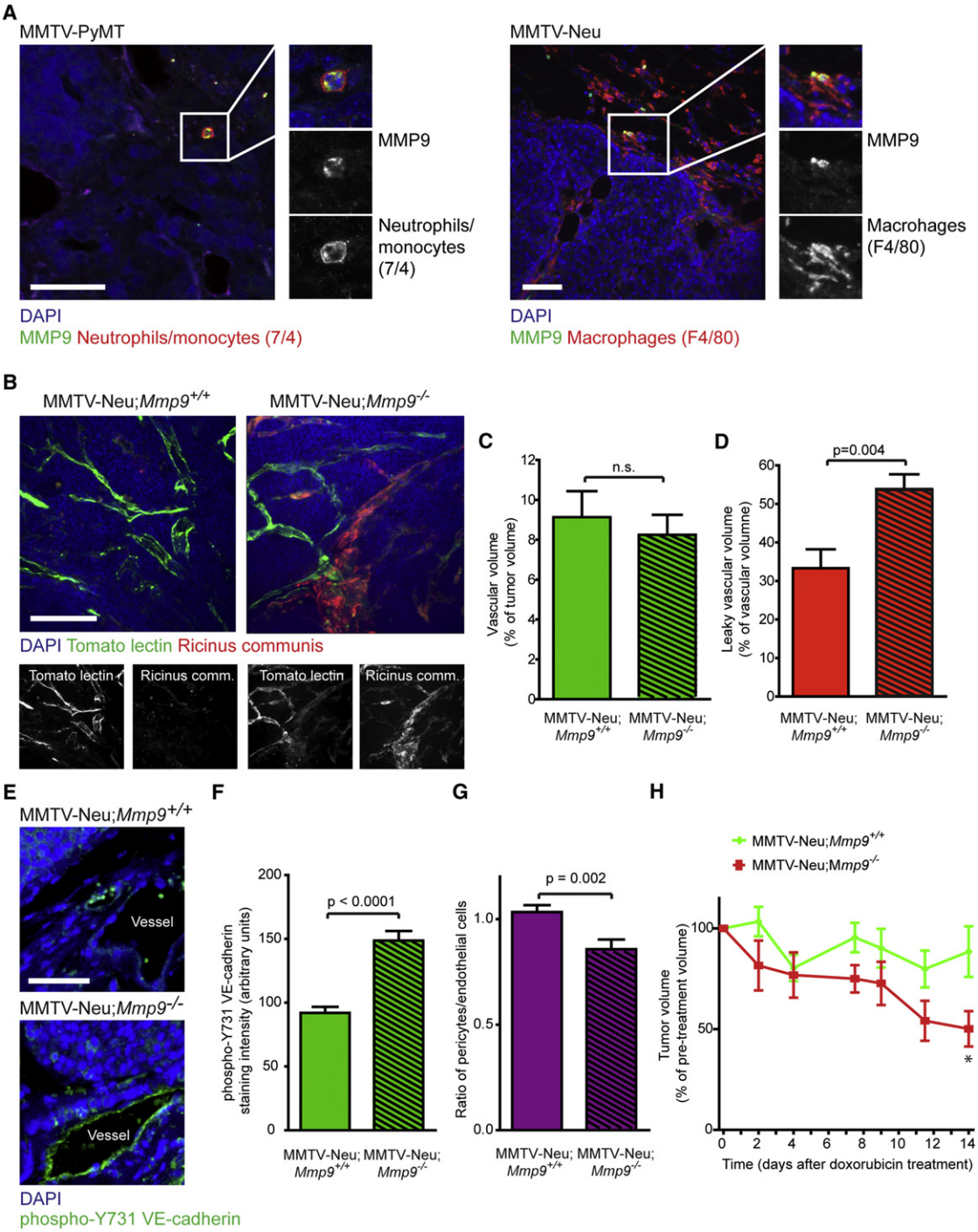

Figure 5. Matrix Metalloproteinase-9 Is Expressed by Myeloid Cells and Influences Vascular Leakage and Response to Doxorubicin

(A) MMP9 is expressed by tumor-infiltrating myeloid cells, including those marked by 7/4 (neutrophils/monocytes) and F4/80 (macrophages). Scale bars: 50 μm.

(B) Vascular structure of tumors in MMTV-Neu;*Mmp9*$^{+/+}$ and MMTV-Neu;*Mmp9*$^{-/-}$ mice analyzed by perfusion with FITC-conjugated tomato lectin (green, labels all blood vessels) and rhodamine-conjugated *Ricinus communis* agglutinin I (red, labels basement membrane exposed to the vascular lumen in leaky vessels). Scale bar: 100 μm.

(C) Vascular volume as determined by perfusion with tomato lectin does not differ between MMTV-Neu;*Mmp9*$^{+/+}$ and MMTV-Neu;*Mmp9*$^{-/-}$ mice (mean ± SEM, n.s., Student's t test, 33 FOV in ten tumors from five MMTV-Neu;*Mmp9*$^{+/+}$ mice and 29 FOV in eight tumors from three MMTV-Neu;*Mmp9*$^{-/-}$ mice were analyzed).

(D) Blood vessels are leakier in MMTV-Neu;*Mmp9*$^{-/-}$ tumors. The percentage of the vasculature that is positive for *Ricinus communis* agglutinin I is shown (mean ± SEM, p = 0.004, Student's t test, 33 FOV in ten tumors from five MMTV-Neu;*Mmp9*$^{+/+}$ mice and 29 FOV in eight tumors from three MMTV-Neu;*Mmp9*$^{-/-}$ mice were analyzed).

(E) Immunostaining for phospho-Y731 VE-cadherin. Scale bar: 100 μm.

The Role of Myeloid Cell Recruitment in Chemotherapy Responses

Recruitment of CCR2$^+$ monocytes after doxorubicin treatment correlated with tumor relapse. Similarly, an increased number of macrophages is found after treatment of tumors with chemotherapy and is associated with poor drug response (Denardo et al., 2011; Shree et al., 2011). Such macrophages can promote cancer cell survival through the secretion of cysteine cathepsins (Shree et al., 2011). CCR2$^+$ monocytes could be the source of tumor-associated macrophages in the posttreatment microenvironment. Indeed, we did not observe increased numbers of macrophages 48 hr after treatment, whereas they have been observed 7–12 days after the first dose of chemotherapy in the MMTV-PyMT model (Denardo et al., 2011; Shree et al., 2011). However, macrophage infiltration depends on CSF-1 (Denardo et al., 2011). Furthermore, macrophages do not promote survival of cancer cells in a cathepsin-dependent manner after treatment with the cisplatin-related drug carboplatin (Shree et al., 2011), whereas the response to cisplatin was better in *Ccr2*$^{-/-}$ hosts. Thus, it is possible that CCR2$^+$ monocytes and tumor-associated macrophages are recruited through independent pathways and influence drug responses through independent mechanisms. Several such mechanisms likely exist. For example, Tie-2-expressing macrophages are recruited after hypoxic tissue injury through a CXCL12/CXCR4 chemokine axis (Welford et al., 2011).

Our results, as well as those of others (Ahn et al., 2010; Denardo et al., 2011; Shree et al., 2011; Welford et al., 2011), indicate that the myeloid cell infiltration that occurs after chemotherapy, radiation, or tissue injury impedes the response to therapy. However, myeloid cell recruitment can also lead to the direct killing of cancer cells (Guerriero et al., 2011), thereby increasing the response to chemotherapy. These differences in the effects of recruited myeloid cells are likely due to the recruitment of different subpopulations of myeloid cells. Indeed, infiltration of CD206$^+$ macrophages was associated with increased vascular leakage and better doxorubicin response, whereas reduced CCR2-dependent recruitment of monocytic cells was associated with delayed tumor relapse.

Interestingly, stromal cells expressed CCL2 after doxorubicin treatment. This offers a possible explanation for the observation that stromally derived, but not cancer cell-derived, CCL2 is associated with decreased relapse-free survival in breast cancer patients (Fujimoto et al., 2009). Furthermore, administration of antibodies specific for mouse CCL2 enhances the response to docetaxol in a xenograft model of prostate cancer (Loberg et al., 2007).

Conclusions

In vivo imaging of tumors shows that different components of the microenvironment participate in the development of chemoresistance. Disruption of these microenvironments is beneficial for the response to doxorubicin and cisplatin. Our data suggest that existing drugs that inhibit MMPs or chemokine signaling may be effective when combined with traditional chemotherapies. However, the order and timing of administration of such combination therapies could be critical because of the complexity of the interactions between myeloid cells and vasculature in chemotherapy responses. Future studies combining imaging with molecular approaches hold promise for gaining further insights into the targeting of tumors in the context of its microenvironment.

EXPERIMENTAL PROCEDURES

Animals

MMTV-PyMT (FVB/n), MMTV-Neu (FVB/n), ACTB-ECFP (FVB/n), ACTB-H2B-EGFP (obtained on mixed background and backcrossed to FVB/n for six generations), and *Ccr2*$^{-/-}$ (C57BL/6) mice were from Jackson Laboratory. MMTV-PyMT (C57BL/6) mice were provided by Dr. Kasper Almholt, and c-fms-EGFP mice were provided by Dr. Jeffrey Pollard and backcrossed to FVB/n mice for six generations. *Mmp9*$^{-/-}$ mice (FVB/n) were previously described (Vu et al., 1998). All animal experiments were conducted in accordance with procedures approved by the IACUC at Cold Spring Harbor Laboratory or the University of California, San Francisco.

Tumor Transplantation Experiments

Virgin females of 6–16 weeks of age were used as hosts for transplantation. Cancer cells were isolated from 2–3 tumors at 8–10 mm diameter from MMTV-PyMT mice. Tumors were mechanically dissociated and digested with collagenase (0.2% w/v), trypsin (0.2% w/v), and DNase I (8 U/ml) in RPMI-1640 medium. Single cells and debris were removed from the resulting carcinoma organoid preparation by differential centrifugation. Purified carcinoma organoids were dissociated into single cell suspension in 0.25% trypsin with 0.1% ethylene diaminetetraacetic acid (EDTA) and washed in PBS. Cells (4×10^5 in 20 μl PBS) were injected into the inguinal mammary glands of host mice.

Tumor Response to Doxorubicin and Cisplatin

Mice received 8 mg/kg doxorubicin hydrochloride (in PBS; Sigma-Aldrich, St. Louis, MO, USA) or 10 mg/kg cisplatin (in 10% dimethyl sulfoxide in PBS; MBL International, Woburn, MA, USA) i.p. on days 0, 7, and 14. Control mice were injected with sterile PBS. Tumors were measured 2–3 times a week by caliper, and tumor volumes were calculated as length × width^2/2.

Spinning Disk Confocal Imaging of Live Mice

Details of the microscope design and imaging procedure were previously described (Egeblad et al., 2008). To track cell death, mice were injected i.p. with 50 μl/h propidium iodide (PI; 0.05–0.1 mg/ml; Invitrogen, Grand Island, NY, USA) in sterile PBS. To determine doxorubicin distribution, MMTV-PyMT mice were injected i.v. with AngioSPARK 680 (100 μl of stock solution; PerkinElmer, Waltham, MA, USA) and doxorubicin (8 mg/kg body weight in 200 μl PBS). To determine vascular leakage, mice were injected i.v. with 100 μl sterile PBS containing 1 mg/ml 10 kD Alexa-Fluor-647-conjugated dextran and 1 mg/ml 2 MD rhodamine-conjugated dextran (Invitrogen).

(F) Depletion of MMP9 increases phosphorylation of VE-cadherin in endothelial cells (mean ± SEM, $p < 0.0001$, Student's t test, 113 vessels from tumors of nine MMTV-Neu;*Mmp9*$^{+/+}$ mice and 101 vessels from tumors of nine MMTV-Neu;*Mmp9*$^{-/-}$ mice were examined).
(G) Pericyte coverage is decreased in the absence of MMP9. Double immunofluorescence was used to determine the ratio of αSMA-positive pericytes to CD31-positive endothelial cells (mean ± SEM, $p = 0.002$, Student's t test, 87 vessels from tumors of ten MMTV-Neu;*Mmp9*$^{+/+}$ mice and 71 vessels from tumors of nine MMTV-Neu;*Mmp9*$^{-/-}$ mice were examined).
(H) MMTV-Neu;*Mmp9*$^{-/-}$ (n = 7 tumors from five mice) tumors respond better to treatment with doxorubicin than do MMTV-Neu;*Mmp9*$^{+/+}$ tumors (n = 11 tumors from six mice; mean ± SEM, * indicates $p < 0.05$; Student's t test). Tumors below 256 mm^3 at the beginning of treatment were excluded from the analysis.
Also see Figure S4.

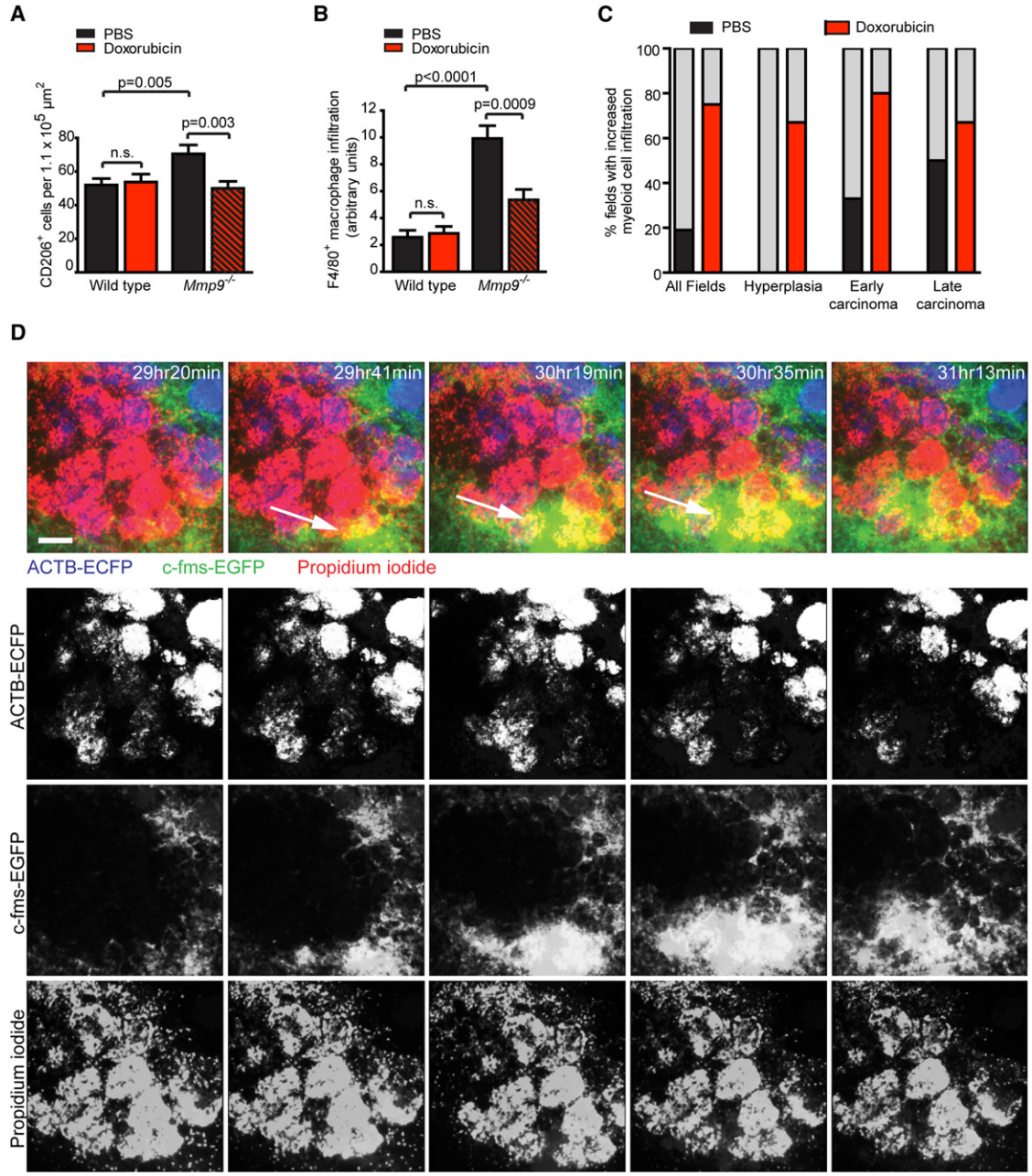

Figure 6. Myeloid Cells Are Recruited to Areas of Tumor Necrosis

(A and B) The infiltration of (A) alternatively activated macrophages (n = 40 FOV from tumors of four mice per condition) and (B) the total macrophage population (n = 22–30 FOV from 4–5 mice per condition) is increased in *Mmp9*$^{-/-}$ host mice transplanted with MMTV-PyMT tumor cells. The infiltration of these cells decreases 48 hr after doxorubicin treatment (mean ± SEM, n.s. or significant as indicated, Student's t test).

(C) Myeloid cells are recruited to tumors after doxorubicin treatment (12 of 16 movies) as compared to tumors of PBS-treated control mice (3 of 16 movies, p = 0.004, Fisher's exact test; three mice were analyzed per condition).

(D) Dynamics of myeloid cell infiltration (arrow) into an area of necrosis in a doxorubicin-treated MMTV-PyMT;ACTB-ECFP;c-fms-EGFP mouse. Time after treatment is indicated. Scale bar: 100 µm.

Also see Figure S5 and Movies S7, S8, and S9.

Histology and Immunostaining

Paraformaldehyde-fixed, paraffin-embedded sections were stained with Mayer's hematoxylin and eosin. Immunostaining was done with primary antibodies against 7/4 (Cedarlane, Burlington, NC, USA), BrdU and MECA-32 (Developmental Studies Hybridoma Bank, University of Iowa, Iowa City, IA, USA), CCL2, CD206, and F4/80 (AbD Serotec, Raleigh, NC, USA), CCR2 (Novus Biologicals, Littleton, CO, USA), phospho-histone H2AX and phospho-histone H3 (Cell Signaling, Danvers, MA, USA), αSMA (Sigma-Aldrich), CD31 and phospho-VE-cadherin (Abcam, Cambridge, MA, USA), and MMP9 (Rasch et al., 2010). Immunostained slides were quantified by counting

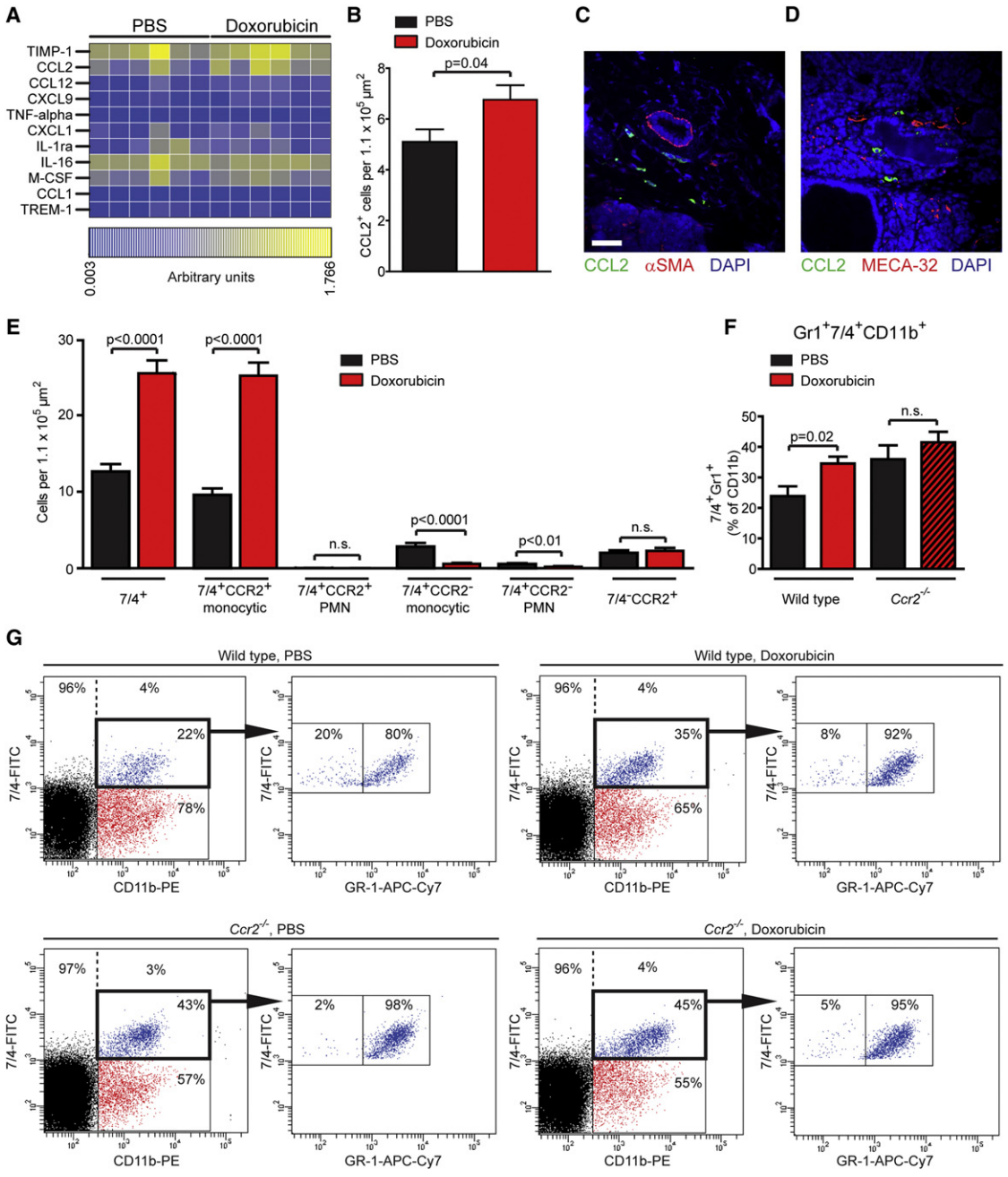

Figure 7. Myeloid Cells Are Recruited to Doxorubicin-treated Tumors through a Stromal CCL2/CCR2 Chemokine/Chemokine Receptor Axis

(A) Protein array identifies CCL2 as the most upregulated chemokine in tumor lysates 48 hr after doxorubicin treatment ($p = 0.09$ for CCL2 and $p = 0.03$ for CCL12, Student's t test). Each column represents a tumor from a different mouse.

(B) The number of CCL2-expressing cells increases 48 hr after treatment with doxorubicin (mean ± SEM, $p = 0.04$, Student's t test; 80 FOV from six PBS-treated and 66 FOV from six doxorubicin-treated mice were analyzed).

(C and D) Endothelial cells, pericytes, and fibroblasts do not express CCL2. Tumor tissue from MTMV-PyMT mice isolated 48 hr after treatment with doxorubicin was immunostained for CCL2 and (C) α-smooth muscle actin (αSMA, a pericyte, and fibroblast marker) or (D) MECA-32 (an endothelial cell marker). More than 300 αSMA or MECA-32 positive cells from PBS and doxorubicin-treated tumors were observed, and none were positive for CCL2. Scale bar: 50 µm.

(E) Doxorubicin treatment results in infiltration of $7/4^+CCR2^+$ cells with monocytic but not polymorphonuclear (PMN) morphology. Double immunostaining for CCR2 and 7/4 with scoring of nuclear morphology (mean ± SEM, Student's t test, significance levels as indicted; 104 FOV from four PBS-treated and 113 FOV from five doxorubicin-treated mice).

(F) Doxorubicin results in CCR2-dependent myeloid cell infiltration. The percentage of $Gr1^+7/4^+$ of all $CD11b^+$ myeloid cells in tumors was determined by flow cytometry (mean ± SEM, significance levels as indicated, Student's t test, n = 10–11 mice).

(G) FACS plots with indication of the percentages of the gated cell populations from representative tumors.

Also see Figure S6.

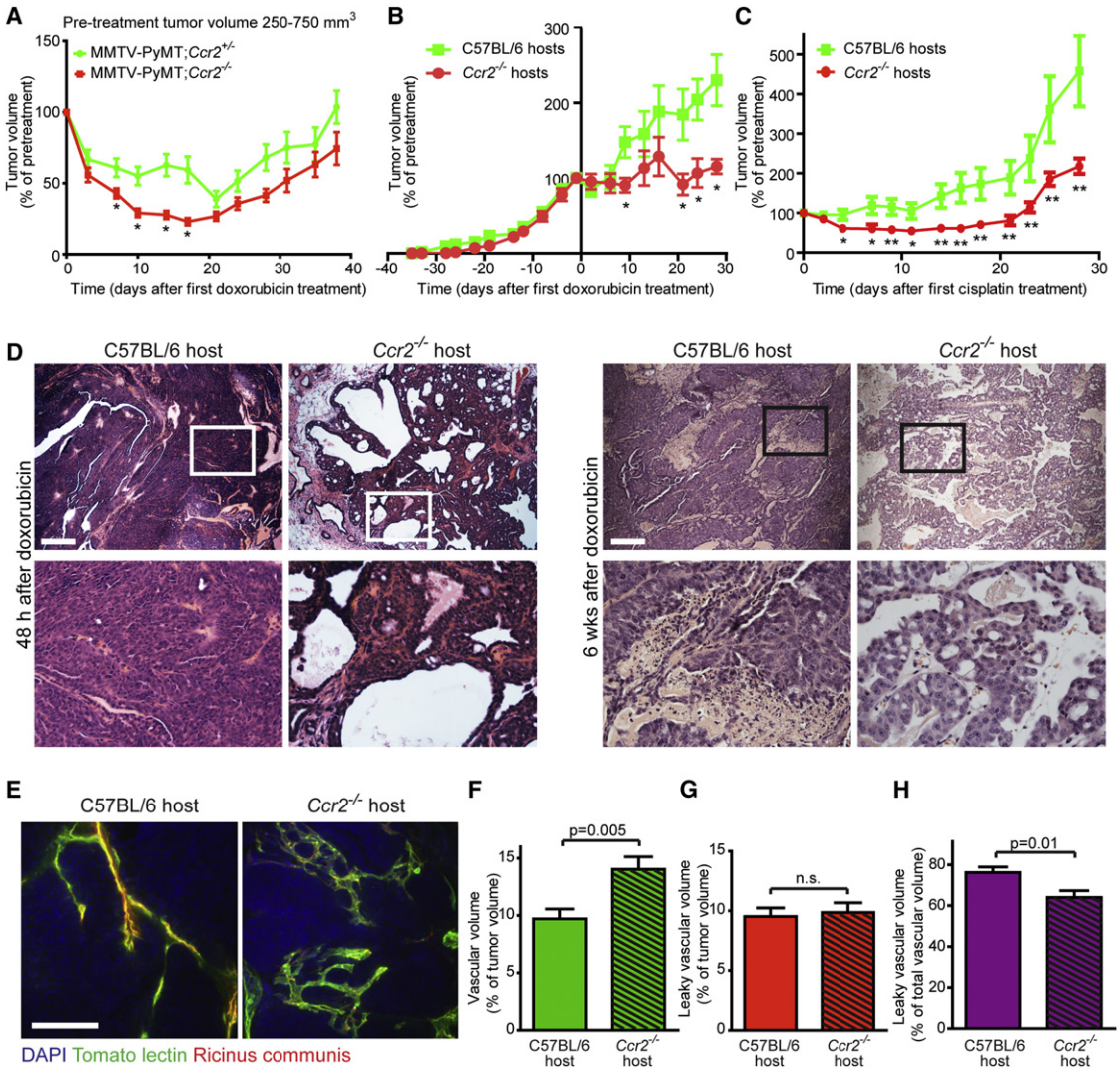

Figure 8. Host CCR2 Regulates Response to Doxorubicin

(A) Tumors in MMTV-PyMT;*Ccr2*$^{-/-}$ (26 tumors from ten mice) respond better to doxorubicin than those in MMTV-PyMT;*Ccr2*$^{+/-}$ (15 tumors from eight mice). Results for tumors with a pretreatment volume of 250–750 mm^3 (mean ± SEM, * indicates $p < 0.05$, Student's t test).

(B) Tumors in *Ccr2*$^{-/-}$ host mice respond better to doxorubicin than those in C57BL/6 hosts. Two cohorts were treated with doxorubicin and showed similar results. The results of one cohort are shown (mean ± SEM, * indicates $p < 0.05$, Student's t test; eight tumors in 6–8 hosts were analyzed per condition; one *Ccr2*$^{-/-}$ and two C57BL/6 hosts were euthanized on days 13–16 due to poor health).

(C) Tumors in *Ccr2*$^{-/-}$ hosts respond better to cisplatin than those in C57BL/6 hosts (mean ± SEM, * indicates $p < 0.05$, ** indicates $p < 0.01$, Student's t test, n = 22–24 tumors in 11–12 hosts).

(D) Tumors in *Ccr2*$^{-/-}$ hosts are more cystic and contain fewer cancer cells acutely (48 hr) after doxorubicin treatment. Relapsed tumors (six weeks after treatment) in *Ccr2*$^{-/-}$ hosts are low-grade with decreased cellularity and necrosis ($p = 0.005$, Fisher's exact test; ten low-grade and five high-grade tumors in *Ccr2*$^{-/-}$ hosts versus one low-grade and eleven high-grade tumors in C57BL/6 hosts). Scale bar: 100 μm.

(E) Vascular structure of tumors in *Ccr2*$^{-/-}$ and C57BL/6 hosts analyzed by perfusion with FITC-conjugated tomato lectin (green) and rhodamine-conjugated *Ricinus communis* agglutinin I (red). Nuclei are stained with 4′,6-diamidino-2-phenylindole (DAPI). Scale bar: 100 μm.

(F) Vascular volume is increased in tumors in *Ccr2*$^{-/-}$hosts compared to C57BL/6 wild-type hosts as determined by perfusion with tomato lectin (mean ± SEM, $p = 0.005$, Student's t test; analysis of 12 tumors from six mice per genotype and 5–10 fields of view per tumor).

(G) The total volume of leaky vasculature does not differ between tumors in *Ccr2*$^{-/-}$ and C57BL/6 hosts (mean ± SEM; n.s., Student's t test; analysis of 12 tumors from six mice per genotype and 5–10 FOV per tumor).

(H) Relative leaky vasculature is decreased in tumors of *Ccr2*$^{-/-}$hosts compared to C57BL/6 hosts as determined by the percentage of the vasculature that is positive for *Ricinus communis* agglutinin I (mean ± SEM, $p = 0.01$, Student's t test; analysis of 12 tumors from six mice per genotype and 5–10 FOV per tumor). Also see Figure S7.

(for 7/4, BrdU, CCL2, CCR2, CD206, phospho-histone H2AX, and phospho-histone H3) or by fluorescence intensity with Volocity software (PerkinElmer; for F4/80, phospho-VE-cadherin, αSMA, and CD31).

In Vitro Drug Sensitivity

Tumor lesions were isolated from MMTV-PyMT;ACTB-ECFP mice using a fluorescent dissection microscope, and primary mammary organoids were

isolated from different tumor stages and cultured in Growth Factor Reduced Matrigel (BD Biosciences, San Diego, CA, USA). To determine doxorubicin sensitivity, treatment of tumor organoids was started 72 hr after isolation. To determine lapatinib sensitivity, single cell suspensions were generated from tumor organoids, isolated as described previously, grown to subconfluence, re-seeded, and treated with lapatinib (Selleck Chemicals, LLC, Houston, TX, USA). Cell viability was measured 48 hr after the addition of drugs using the CellTiter 96 Aqueous One Solution Cell Proliferation Assay (Promega, Madison, WI, USA).

For further experimental details, see Supplemental Experimental Procedures.

SUPPLEMENTAL INFORMATION

Supplemental Information includes seven figures, nine movies, and Supplemental Experimental Procedures and can be found with this article online at doi:10.1016/j.ccr.2012.02.017.

ACKNOWLEDGMENTS

We thank E. Atamaniuc, Y. Yu, H. Capili, J. Cappellani, G. DiMino, M.B. Ebert, J. Waage, J. Paterek, and the Shared Resources at CSHL for technical support. Dr. Claire Lewis is thanked for helpful comments on the manuscript. Antibodies against BrdU and MECA-32 were obtained from the Developmental Studies Hybridoma Bank maintained by the University of Iowa. This work was supported by funds from the National Cancer Institute (U01 CA141451 to M.E.; R01 CA057621 to Z.W. and M.J.B.; and P50 CA088843 to A.J.E.), the Starr Cancer Consortium, the Breast Cancer Alliance, Susan G. Komen for the Cure, Long Island 2 Day Walk to Fight Breast Cancer and Manhasset Women's Coalition Against Breast Cancer to M.E., the Stand Up to Cancer-American Association for Cancer Research Dream Team Translational Cancer Research Grant (SU2C-AACR-DT0409 to Z.W.), a predoctoral fellowship from the Congressionally Directed Breast Cancer Research Program, U.S. (E.S.N.), the Research Council of Norway (160698/V40 and 151882 [FUGE] to E.F.), and Southeastern Regional Health Authorities (2007060 to E.F.). E.S.N. is the recipient of the Leslie C. Quick and William Randolph Hearst Foundation Fellowships from the Watson School of Biological Sciences. E.F. and H.A.A. were supported by "University of Oslo Research Fund (UNIFOR)" and Ullevål University Hospital Research Fund (VIRUUS).

Received: May 4, 2011
Revised: December 18, 2011
Accepted: February 17, 2012
Published: April 16, 2012

REFERENCES

Ahn, G.O., Tseng, D., Liao, C.H., Dorie, M.J., Czechowicz, A., and Brown, J.M. (2010). Inhibition of Mac-1 (CD11b/CD18) enhances tumor response to radiation by reducing myeloid cell recruitment. Proc. Natl. Acad. Sci. USA *107*, 8363–8368.

Campiglio, M., Somenzi, G., Olgiati, C., Beretta, G., Balsari, A., Zaffaroni, N., Valagussa, P., and Ménard, S. (2003). Role of proliferation in HER2 status predicted response to doxorubicin. Int. J. Cancer *105*, 568–573.

Coussens, L.M., Fingleton, B., and Matrisian, L.M. (2002). Matrix metalloproteinase inhibitors and cancer: trials and tribulations. Science *295*, 2387–2392.

Dean, M., Fojo, T., and Bates, S. (2005). Tumour stem cells and drug resistance. Nat. Rev. Cancer *5*, 275–284.

Denardo, D.G., Brennan, D.J., Rexhepaj, E., Ruffell, B., Shiao, S.L., Madden, S.F., Gallagher, W.M., Wadhwani, N., Keil, S.D., Junaid, S.A., et al. (2011). Leukocyte complexity predicts breast cancer survival and functionally regulates response to chemotherapy. Cancer Discov. *1*, 54–67.

Dive, C., Gregory, C.D., Phipps, D.J., Evans, D.L., Milner, A.E., and Wyllie, A.H. (1992). Analysis and discrimination of necrosis and apoptosis (programmed cell death) by multiparameter flow cytometry. Biochim. Biophys. Acta *1133*, 275–285.

Ebrahem, Q., Chaurasia, S.S., Vasanji, A., Qi, J.H., Klenotic, P.A., Cutler, A., Asosingh, K., Erzurum, S., and Anand-Apte, B. (2010). Cross-talk between vascular endothelial growth factor and matrix metalloproteinases in the induction of neovascularization in vivo. Am. J. Pathol. *176*, 496–503.

Egeblad, M., Ewald, A.J., Askautrud, H.A., Truitt, M.L., Welm, B.E., Bainbridge, E., Peeters, G., Krummel, M.F., and Werb, Z. (2008). Visualizing stromal cell dynamics in different tumor microenvironments by spinning disk confocal microscopy. Dis. Model Mech. *1*, 155–167.

Egeblad, M., Nakasone, E.S., and Werb, Z. (2010). Tumors as organs: complex tissues that interface with the entire organism. Dev. Cell *18*, 884–901.

Fujimoto, H., Sangai, T., Ishii, G., Ikehara, A., Nagashima, T., Miyazaki, M., and Ochiai, A. (2009). Stromal MCP-1 in mammary tumors induces tumor-associated macrophage infiltration and contributes to tumor progression. Int. J. Cancer *125*, 1276–1284.

Gavard, J. (2009). Breaking the VE-cadherin bonds. FEBS Lett. *583*, 1–6.

Gilbert, L.A., and Hemann, M.T. (2010). DNA damage-mediated induction of a chemoresistant niche. Cell *143*, 355–366.

Goel, S., Duda, D.G., Xu, L., Munn, L.L., Boucher, Y., Fukumura, D., and Jain, R.K. (2011). Normalization of the vasculature for treatment of cancer and other diseases. Physiol. Rev. *91*, 1071–1121.

Gong, Y., Hart, E., Shchurin, A., and Hoover-Plow, J. (2008). Inflammatory macrophage migration requires MMP-9 activation by plasminogen in mice. J. Clin. Invest. *118*, 3012–3024.

Greene, R.F., Collins, J.M., Jenkins, J.F., Speyer, J.L., and Myers, C.E. (1983). Plasma pharmacokinetics of adriamycin and adriamycinol: implications for the design of in vitro experiments and treatment protocols. Cancer Res. *43*, 3417–3421.

Guerriero, J.L., Ditsworth, D., Catanzaro, J.M., Sabino, G., Furie, M.B., Kew, R.R., Crawford, H.C., and Zong, W.X. (2011). DNA alkylating therapy induces tumor regression through an HMGB1-mediated activation of innate immunity. J. Immunol. *186*, 3517–3526.

Hadjantonakis, A.K., and Papaioannou, V.E. (2004). Dynamic in vivo imaging and cell tracking using a histone fluorescent protein fusion in mice. BMC Biotechnol. *4*, 33.

Hagendoorn, J., Tong, R., Fukumura, D., Lin, Q., Lobo, J., Padera, T.P., Xu, L., Kucherlapati, R., and Jain, R.K. (2006). Onset of abnormal blood and lymphatic vessel function and interstitial hypertension in early stages of carcinogenesis. Cancer Res. *66*, 3360–3364.

Herschkowitz, J.I., Simin, K., Weigman, V.J., Mikaelian, I., Usary, J., Hu, Z., Rasmussen, K.E., Jones, L.P., Assefnia, S., Chandrasekharan, S., et al. (2007). Identification of conserved gene expression features between murine mammary carcinoma models and human breast tumors. Genome Biol. *8*, R76.

Johnson, J.I., Decker, S., Zaharevitz, D., Rubinstein, L.V., Venditti, J.M., Schepartz, S., Kalyandrug, S., Christian, M., Arbuck, S., Hollingshead, M., and Sausville, E.A. (2001). Relationships between drug activity in NCI preclinical in vitro and in vivo models and early clinical trials. Br. J. Cancer *84*, 1424–1431.

Lin, E.Y., Jones, J.G., Li, P., Zhu, L., Whitney, K.D., Muller, W.J., and Pollard, J.W. (2003). Progression to malignancy in the polyoma middle T oncoprotein mouse breast cancer model provides a reliable model for human diseases. Am. J. Pathol. *163*, 2113–2126.

Loberg, R.D., Ying, C., Craig, M., Day, L.L., Sargent, E., Neeley, C., Wojno, K., Snyder, L.A., Yan, L., and Pienta, K.J. (2007). Targeting CCL2 with systemic delivery of neutralizing antibodies induces prostate cancer tumor regression in vivo. Cancer Res. *67*, 9417–9424.

Loeffler, M., Krüger, J.A., Niethammer, A.G., and Reisfeld, R.A. (2006). Targeting tumor-associated fibroblasts improves cancer chemotherapy by increasing intratumoral drug uptake. J. Clin. Invest. *116*, 1955–1962.

Martin, M.D., Carter, K.J., Jean-Philippe, S.R., Chang, M., Mobashery, S., Thiolloy, S., Lynch, C.C., Matrisian, L.M., and Fingleton, B. (2008). Effect of ablation or inhibition of stromal matrix metalloproteinase-9 on lung metastasis in a breast cancer model is dependent on genetic background. Cancer Res. *68*, 6251–6259.

Meads, M.B., Gatenby, R.A., and Dalton, W.S. (2009). Environment-mediated drug resistance: a major contributor to minimal residual disease. Nat. Rev. Cancer *9*, 665–674.

Minchinton, A.I., and Tannock, I.F. (2006). Drug penetration in solid tumours. Nat. Rev. Cancer *6*, 583–592.

Murdoch, C., Giannoudis, A., and Lewis, C.E. (2004). Mechanisms regulating the recruitment of macrophages into hypoxic areas of tumors and other ischemic tissues. Blood *104*, 2224–2234.

Netti, P.A., Hamberg, L.M., Babich, J.W., Kierstead, D., Graham, W., Hunter, G.J., Wolf, G.L., Fischman, A., Boucher, Y., and Jain, R.K. (1999). Enhancement of fluid filtration across tumor vessels: implication for delivery of macromolecules. Proc. Natl. Acad. Sci. USA *96*, 3137–3142.

Obeid, M., Tesniere, A., Ghiringhelli, F., Fimia, G.M., Apetoh, L., Perfettini, J.L., Castedo, M., Mignot, G., Panaretakis, T., Casares, N., et al. (2007). Calreticulin exposure dictates the immunogenicity of cancer cell death. Nat. Med. *13*, 54–61.

Olive, K.P., Jacobetz, M.A., Davidson, C.J., Gopinathan, A., McIntyre, D., Honess, D., Madhu, B., Goldgraben, M.A., Caldwell, M.E., Allard, D., et al. (2009). Inhibition of Hedgehog signaling enhances delivery of chemotherapy in a mouse model of pancreatic cancer. Science *324*, 1457–1461.

Pahler, J.C., Tazzyman, S., Erez, N., Chen, Y.Y., Murdoch, C., Nozawa, H., Lewis, C.E., and Hanahan, D. (2008). Plasticity in tumor-promoting inflammation: impairment of macrophage recruitment evokes a compensatory neutrophil response. Neoplasia *10*, 329–340.

Priceman, S.J., Sung, J.L., Shaposhnik, Z., Burton, J.B., Torres-Collado, A.X., Moughon, D.L., Johnson, M., Lusis, A.J., Cohen, D.A., Iruela-Arispe, M.L., and Wu, L. (2010). Targeting distinct tumor-infiltrating myeloid cells by inhibiting CSF-1 receptor: combating tumor evasion of antiangiogenic therapy. Blood *115*, 1461–1471.

Rasch, M.G., Lund, I.K., Illemann, M., Høyer-Hansen, G., and Gårdsvoll, H. (2010). Purification and characterization of recombinant full-length and protease domain of murine MMP-9 expressed in Drosophila S2 cells. Protein Expr. Purif. *72*, 87–94.

Rottenberg, S., Pajic, M., and Jonkers, J. (2010). Studying drug resistance using genetically engineered mouse models for breast cancer. Methods Mol. Biol. *596*, 33–45.

Rouzier, R., Perou, C.M., Symmans, W.F., Ibrahim, N., Cristofanilli, M., Anderson, K., Hess, K.R., Stec, J., Ayers, M., Wagner, P., et al. (2005). Breast cancer molecular subtypes respond differently to preoperative chemotherapy. Clin. Cancer Res. *11*, 5678–5685.

Sadik, C.D., Kim, N.D., and Luster, A.D. (2011). Neutrophils cascading their way to inflammation. Trends Immunol. *32*, 452–460.

Shree, T., Olson, O.C., Elie, B.T., Kester, J.C., Garfall, A.L., Simpson, K., Bell-McGuinn, K.M., Zabor, E.C., Brogi, E., and Joyce, J.A. (2011). Macrophages and cathepsin proteases blunt chemotherapeutic response in breast cancer. Genes Dev. *25*, 2465–2479.

Sounni, N.E., Dehne, K., van Kempen, L., Egeblad, M., Affara, N.I., Cuevas, I., Wiesen, J., Junankar, S., Korets, L., Lee, J., et al. (2010). Stromal regulation of vessel stability by MMP14 and TGFbeta. Dis. Model Mech. *3*, 317–332.

Thurston, G., Suri, C., Smith, K., McClain, J., Sato, T.N., Yancopoulos, G.D., and McDonald, D.M. (1999). Leakage-resistant blood vessels in mice transgenically overexpressing angiopoietin-1. Science *286*, 2511–2514.

Tsou, C.L., Peters, W., Si, Y., Slaymaker, S., Aslanian, A.M., Weisberg, S.P., Mack, M., and Charo, I.F. (2007). Critical roles for CCR2 and MCP-3 in monocyte mobilization from bone marrow and recruitment to inflammatory sites. J. Clin. Invest. *117*, 902–909.

Vu, T.H., Shipley, J.M., Bergers, G., Berger, J.E., Helms, J.A., Hanahan, D., Shapiro, S.D., Senior, R.M., and Werb, Z. (1998). MMP-9/gelatinase B is a key regulator of growth plate angiogenesis and apoptosis of hypertrophic chondrocytes. Cell *93*, 411–422.

Welford, A.F., Biziato, D., Coffelt, S.B., Nucera, S., Fisher, M., Pucci, F., Di Serio, C., Naldini, L., De Palma, M., Tozer, G.M., and Lewis, C.E. (2011). TIE2-expressing macrophages limit the therapeutic efficacy of the vascular-disrupting agent combretastatin A4 phosphate in mice. J. Clin. Invest. *121*, 1969–1973.

Yu, Q., and Stamenkovic, I. (2000). Cell surface-localized matrix metalloproteinase-9 proteolytically activates TGF-beta and promotes tumor invasion and angiogenesis. Genes Dev. *14*, 163–176.

Zhang, J., Lu, Y., and Pienta, K.J. (2010). Multiple roles of chemokine (C-C motif) ligand 2 in promoting prostate cancer growth. J. Natl. Cancer Inst. *102*, 522–528.

Cancer Cell
Article

TLX Homeodomain Oncogenes Mediate T Cell Maturation Arrest in T-ALL via Interaction with ETS1 and Suppression of TCRα Gene Expression

Saïda Dadi,[1,3,9] Sandrine Le Noir,[1,9] Dominique Payet-Bornet,[3,9] Ludovic Lhermitte,[1] Joaquin Zacarias-Cabeza,[3] Julie Bergeron,[1] Patrick Villarèse,[1] Elodie Vachez,[3] Willem A. Dik,[4] Corinne Millien,[1] Isabelle Radford,[2] Els Verhoeyen,[5] François-Loïc Cosset,[5] Arnaud Petit,[6] Norbert Ifrah,[7] Hervé Dombret,[8] Olivier Hermine,[1] Salvatore Spicuglia,[3] Anton W. Langerak,[4] Elizabeth A. Macintyre,[1,10] Bertrand Nadel,[3,10] Pierre Ferrier,[3,10,*] and Vahid Asnafi[1,10,*]

[1]Department of Hematologye, Université de Médecine Paris Descartes Sorbonne Cité, Centre National de la Recherche Scientifique (CNRS) UMR8147

[2]Department of Cytogenetics, Université Paris 5-Descartes
Assistance Publique-Hôpitaux de Paris, Hôpital Necker-Enfants-Malades, Paris, 75015, France

[3]Centre d'Immunologie de Marseille-Luminy (CIML), Institut National de la Santé et de la Recherche Médicale (Inserm U1104), CNRS UMR7280, Université de la Méditerranée, 13009 Marseille, France

[4]Department of Immunology, Erasmus MC, University Medical Center, 3016 Rotterdam, Netherlands

[5]Université de Lyon, F69000; Inserm, EVIR, U758, Human Virology Department, F-69007; Ecole Normale Supérieure de Lyon, F-69007; Université Lyon 1, F-69007, Lyon, France

[6]Department of Hematology, AP-HP Hôpital Armand Trousseau, Paris 75012, France

[7]Department of Hematology, Centre Hospitalier, Angers 49933, France

[8]Department of Hematology, AP-HP Hôpital St-Louis, Paris 75010, France

[9]These authors contributed equally to this work

[10]These authors contributed equally to this work

*Correspondence: vahid.asnafi@nck.aphp.fr (V.A.), ferrier@ciml.univ-mrs.fr (P.F.)

DOI 10.1016/j.ccr.2012.02.013

SUMMARY

Acute lymphoblastic leukemias (ALLs) are characterized by multistep oncogenic processes leading to cell-differentiation arrest and proliferation. Specific abrogation of maturation blockage constitutes a promising therapeutic option in cancer, which requires precise understanding of the underlying molecular mechanisms. We show that the cortical thymic maturation arrest in T-lineage ALLs that overexpress TLX1 or TLX3 is due to binding of TLX1/TLX3 to ETS1, leading to repression of T cell receptor (TCR) α enhanceosome activity and blocked TCR-Jα rearrangement. TLX1/TLX3 abrogation or enforced TCRαβ expression leads to TCRα rearrangement and apoptosis. Importantly, the autoextinction of clones carrying TCRα-driven TLX1 expression supports TLX "addiction" in TLX-positive leukemias and provides further rationale for targeted therapy based on disruption of TLX1/TLX3.

INTRODUCTION

Acute leukemias are characterized by a multistep oncogenic process leading to the maturation arrest and malignant transformation of a hematopoietic precursor (Pui et al., 2004). Understanding of the molecular mechanisms leading to this block in maturation is a prerequisite for the development of therapeutic approaches aiming to unblock differentiation of leukemic blasts (Look, 1997). Transcription factors (TFs) that are involved in the control of cell differentiation or proliferation of normal

Significance

Targeted therapy, including abrogation of a block to cell maturation, is a promising therapeutic approach in leukemias but has so far proved difficult to implement, partly due to their multioncogenic nature, especially in T-ALL where few oncogenes/tumor suppressors have emerged as tangible candidates. Among T-ALL patients, aberrant expression of TLX1/TLX3 defines a large subgroup of leukemias with a cortical thymic developmental arrest. Our data show that this differentiation block is due to failure to rearrange TCRα and that sustained TLX expression is required for leukemic maintenance despite the acquisition of a variety of additional genetic abnormalities. Taken together, our results provide further rationale for targeted therapy based on disruption of TLX1/TLX3 in this T-ALL subset.

hematopoietic progenitors and are deregulated in acute leukemias could represent promising therapeutic targets, as described for the treatment of PML-RARA$^+$ acute promyelocytic leukemia (Degos, 1992).

Human T-lymphocyte ontogeny is a hierarchical process occurring in the thymus in which the ordered somatic recombination of V, D, and J gene segments at the TCRδ, TCRγ, TCRβ, or TCRα loci determine the development into either γδ or αβ T cell lineages (Dik et al., 2005; Spits, 2002) (Figure S1 available online). Progressive lineage restriction and acquisition of T cell potential following migration from the bone marrow to the thymus involve successive differentiation steps defined by the acquisition of a number of surface molecules, including CD5, CD1a, CD34, CD3, CD4, and CD8. TCRδ rearrangement is the first to occur, at the CD5$^+$, CD1a$^-$ CD4/8 double-negative (DN) stage, followed by concurrent TCRγ and TCRβ rearrangements coinciding with CD1a expression (Dik et al., 2005). While the occurrence of productive TCRγ and TCRδ rearrangements will determine the assembly of a γδ receptor, a complete productive TCRβ gene rearrangement will first allow surface expression of a pre-TCR complex formed by the assembly of the TCRβ chain with a pre-Tα (pTα) invariant chain. Pre-TCR surface expression, referred to as the β-selection process, is marked by arrest of TCRβ gene rearrangements and extensive cellular expansion. It is mandatory to the progression of αβ T cell precursors to the CD4/CD8 double-positive (DP) cortical thymic cell stage, and to the initiation of Vα-Jα rearrangements (von Boehmer et al., 1998). The TCRδ locus being interspersed between the Vα and Jα segments, it is deleted out during Vα-Jα recombination, marking definitive engagement to the TCRαβ lineage. The "frontiers" of the TCRδ locus may be regarded as being defined by the 5′δRec and 3′ψJα elements, as all 5′V and 3′Jα gene segments located outside these segments contribute to the functional repertoire of αβ T cells, including a few Vα/Vδ gene segments that occasionally recombine with Jδ gene segments (Krangel et al., 1998). The TCRα rearrangement is a highly regulated process, in which the TCRα enhancer (Eα) plays a primary role (Bassing et al., 2003; Sleckman et al., 1997). The molecular regulation of Eα has been intensively studied (Hawwari and Krangel, 2005; Ho et al., 1989, 1990; McMurry and Krangel, 2000). The minimal Eα core contains binding sites for three TFs, LEF-1, RUNX1/AML1, and ETS1, which have been demonstrated to be crucial for the transcriptional and *cis*-chromatin opening activities of the so-called Eα enhanceosome (Giese et al., 1995; Ho et al., 1989, 1990; Roberts et al., 1997).

T-ALL is a heterogeneous group of acute leukemias that are arrested at various stages of normal thymic-cell differentiation (Asnafi et al., 2003; Ferrando et al., 2002). Recognized T-ALL oncogenic events include transcriptional activation of proto-oncogenes, submicroscopic deletion of tumor suppressor genes, and activation of the Notch1 pathway by *NOTCH1* or *FBXW7* mutations (Aifantis et al., 2008). Among the various T-ALL oncogenic alterations reported to date, TCR chromosomal translocations represent a recurrent oncogenic hallmark of T-ALL (Cauwelier et al., 2006). Such translocations are generally believed to result from illegitimate V(D)J recombination events that lead to the ectopic activation of oncogenes owing to their relocation to the vicinity of potent *cis*-activating elements within the involved TCR locus.

Overexpression of the orphan homeobox (HOX) proteins TLX1 and TLX3 represents the most frequent oncogenic event due to chromosomal translocation in human T-ALL. TLX1 and TLX3 belong to the NKL subtype of HOX proteins. They contain a highly conserved homeodomain (HD) that is known to be involved in DNA and protein-protein interactions (Holland et al., 2007). In T-ALL, both proteins are associated with specific gene expression profiles, a variety of additional genetic mutations, and differentiation arrest at an early cortical stage of thymocyte maturation (Asnafi et al., 2004; Ferrando et al., 2002; Soulier et al., 2005). Physiological expression of *TLX1* and *TLX3* is restricted to embryonic development (Roberts et al., 1994; Shirasawa et al., 2000), and no specific function of these genes in the T cell lineage has been reported. Transgenic expression of human *TLX1* in mice induces an initial DN2 thymic block followed by development of aneuploid T-ALL, mitotic checkpoint defects, clonal TCRβ rearrangements, a mostly cortical phenotype, and a transcriptional profile similar to that observed in human TLX1$^+$ T-ALLs (De Keersmaecker et al., 2010). Corresponding data are not yet available for TLX3, and the molecular mechanisms underlying the observed developmental arrest in TLX1$^+$ and TLX3$^+$ T-ALLs remain elusive. We therefore undertook to determine if and how TLX oncoproteins were linked to the cortical thymic maturation arrest and what the impact of this specific oncogenic function was on the initiation, development, and maintenance of TLX$^+$ T-ALLs.

RESULTS

TLX-Expressing T-ALLs Undergo VβDJβ Rearrangements but Display a Strong Bias against Vα-Jα Joints

A series of 230 T-ALLs were analyzed by real-time quantitative PCR (RT-qPCR) for *TLX1* and *TLX3* expression. Applying a TCR-based classification (Asnafi et al., 2003), 52 cases were immature/uncommitted (surface (s) and cytoplasmic (c) TCRβ negative) and comprised IM0, IMδ, and IMγ subtypes (i.e., harboring, respectively, a germline configuration of all three TCRβ, δ, and γ loci, or a TCRδ- or TCRγ-rearranged locus, and in some cases with an incompletely rearranged DJβ locus); 103 cases were early cortical IMβ/pre-αβ and included IMβ and pre-αβ subtypes (displaying VβDJβ rearrangement and, respectively, either a cTCRβ$^-$ or sTCR$^-$/cTCRβ$^+$ phenotype); 39 cases were sTCRαβ$^+$; and 36 were sTCRγδ$^+$ (of which 20 also harbored a VβDJβ-rearranged locus) (Table S1). Sixty-five cases (28%) demonstrated *TLX1* or *TLX3* overexpression in a mutually exclusive manner, and were henceforth referred to as TLX$^+$. Among TLX$^+$ T-ALLs, all but one demonstrated at least one VβDJβ rearrangement; this included all TCRγδ-expressing cases ($p < 0.001$). Strikingly, none of the TLX$^+$ samples displayed a sTCRαβ$^+$ phenotype, implying a uniform arrest in maturation at an early cortical cell stage, prior to TCRα chain expression.

To determine whether the lack of TCRαβ expression in TLX$^+$ T-ALLs was due to a defect in TCRα gene rearrangement or TCRα chain expression, we analyzed, by Southern blotting and DNA PCR, the status of the TCRδ locus (which is deleted during Vα-to-Jα rearrangement) in 52 phenotypically matched IMβ/pre-αβ T-ALLs (Asnafi et al., 2003), including 26 TLX$^+$ (13 each of TLX1 and TLX3) and 26 TLX$^-$ T-ALLs (Table 1). Remarkably,

Table 1. TCRδ Allele Rearrangement Status in IMβ/Pre-αβ TLX$^+$ (n = 26) and TLX$^-$ (n = 26) T-ALL

IMβ/Pre-αβ T-ALL TCRδ Allelic Status	TLX$^+$ (n = 52)	TLX$^-$ (n = 52)	p Value
GL, D-D, D-J or V-D	6 (11%)	5 (10%)	ns
VDJ	37[a] (71%)	10[b] (19%)	< 0.001
Deletion	3 (6%)	31 (60%)	< 0.001
Translocated alleles	6 (11%)	6 (11%)	ns

See also Table S1 and Figures S1 and S2.
[a]Includes 15 atypical rearrangements (seven Vα-Jδ, three Vδ8-Jδ1, one Vδ6-Jδ2, and one Vδ7-Jδ1) and 20 typical rearrangements using conventional Vδ1–3 segments.
[b]Only one atypical rearrangement (Vδ5-Jδ1).

49 of 52 (94%) TCRδ alleles were readily detected (i.e., were not deleted) in TLX$^+$ T-ALLs compared with 21 of 52 (40%) TCRδ alleles in TLX$^-$ controls ($p < 0.001$). The TCRδ locus may be regarded as defined by the 5′δRec and 3′ψJα elements (Figure S1), as all functional 5′V and 3′Jα gene segments located outside these limits were found to potentially undergo rearrangement in αβT cells, including a few Vα/Vδ gene segments that occasionally recombine with Jδ gene segments (Krangel et al., 1998). Thorough analysis of TCRδ rearrangements in TLX$^+$ versus TLX$^-$ samples by PCR cloning and sequencing demonstrated that the majority of the former samples harbored complete VδDJδ joints with, intriguingly, a high proportion involving TCRδ-specific, distal 5′ Vδ gene segments (Vδ4–6), dual TCRδ/α (Vδ7, Vδ8), or even TCRα-specific (Vα) gene segments, accounting for a total of 41% of the VDJ rearranged alleles compared to only 10% in TLX$^-$ cases (Table 1). Overall, TLX1$^+$ and TLX3$^+$ T-ALL samples displayed no significant difference in their profiles of TCRδ locus rearrangement (data not shown). These results, coupled with the lower level of TCRδ locus deletion and absence of TCRαβ expression, strongly argue for a block in V-to-Jα rearrangement in TLX$^+$ versus TLX$^-$ T-ALL samples. As Eα is required for optimal Vα-to-Jα recombination (Bassing et al., 2003; Sleckman et al., 1997), we hypothesized that Eα activity could be compromised during the course of TLX$^+$ T-ALL leukemic transformation in humans.

TLX$^+$ T-ALL Show Reduced Accessibility of the TCRα Locus

In the mouse, Eα is occupied by dedicated TFs from the CD44^{lo}CD25$^+$ (DN3) stage of thymocyte development onward, well before transcriptional and recombinational activation of—and, indeed, establishment of chromosomal accessibility at—the TCR-Jα/Cα locus, arguing that Eα binding by TFs is dissociated from its functional activity (Hernández-Munain et al., 1999; Mauvieux et al., 2003; Spicuglia et al., 2000). In order to assess the chromosomal status of the 3′ part of the TCRα locus, including Eα, in human TLX$^+$ T-ALL, we used the formaldehyde-assisted isolation of regulatory elements (FAIRE) assay, which allows the isolation of nucleosome-depleted (hence, mainly accessible) genomic DNA regions (Giresi et al., 2007). Using two primary TLX$^+$ T-ALLs, we recovered large amounts of Eα-overlapping chromosomal DNA, but the recovery of upstream DNA sequences containing the TEA promoter or the Jα58 or Jα28 segments was within the range observed for the unrelated T-ALL repressed genes PCDHGA12 and RPIB9 (Figure 1A and data not shown). In addition, quantification of the expression by RT-qPCR demonstrated a drastic decrease (~100-fold on average) of Cα transcripts in TLX$^+$ T-ALL compared with TLX$^-$ T-ALL (Figure 1B), corroborating microarray data on gene-expression analysis of similar leukemia samples (Ferrando et al., 2002). Finally, using chromatin-immunoprecipitation (ChIP)-on-chip assays we found that the H3K27me3 mark, a hallmark of silent chromatin, is significantly enriched in the TCR-Jα/Cα genomic region in TLX$^+$ T-ALL compared to TLX$^-$ T-ALL (Figures 1C and S2). In contrast, similar H3K27me3 profiles were observed in all T-ALL samples in the repressed (*GATA1*; H3K27me3-enriched) or activated (*GAPDH*; H3K27me3-depleted) control loci. Consistent with the FAIRE data of nucleosomal depletion along Eα-containing sequences, H3K27me3 enrichment in TLX$^+$ T-ALL closely surrounded but spared this discrete region. Overall, these findings imply that the unrearranged TCR-Jα/Cα alleles typically found in TLX$^+$ T-ALL blasts are poorly transcribed and most likely embedded within repressive chromatin, despite localized accessibility of Eα DNA. They further suggest that in the presence of TLX, Eα is unable to confer chromosomal accessibility to the adjacent genomic regions, notably the TCR TEA/Jα-containing region.

TLX1 and TLX3 Repress Eα Activity via Their Homeodomain

To further test the possibility that the TLX1 and TLX3 proteins interfere with Eα transcriptional activity, we used an Eα-dependent reporter that expressed chloramphenicol acetyl transferase (Eα-CAT). We found that ectopic expression of either GFP-TLX1 or GFP-TLX3 repressed Eα-CAT expression by approximately 6-fold, and that this expression was partly rescued by the co-expression of TLX1 or TLX3 siRNA, respectively (Figure 2A). We therefore evaluated the level of Eα-CAT repression exerted by TLX1 and TLX3 mutants with or without their HD (HD$^+$ and HD^{del}, respectively), in reference to that of the corresponding full-length (FL) proteins. As shown in Figure 2B, both TLX1 HD^{del} and TLX3 HD^{del} exerted a reduced repressive activity compared with their respective full-length (FL) proteins. Conversely, TLX1 HD$^+$ exerted an activity roughly equivalent to FL TLX1, whereas TLX3 HD$^+$ retained about half the repressive effect of FL TLX3. We exclude the possibility that the reduced repression activity by TLX1 HD^{del} and TLX3 HD^{del} was due to their lack of nuclear localization by demonstrating that both predominantly localized to the nucleus (Figures 2C and 2D). We conclude that TLX1 and TLX3 repress Eα transcriptional activity primarily in an HD-dependent manner.

TLX1 and TLX3 Exert Their Eα Repressive Activity by Interacting with ETS1

The Eα-mediated transcriptional activity depends on the cooperative binding of the ETS1 and RUNX1 TFs to Eα, together with the lymphoid-specific HMG domain protein LEF1. To test whether TLX1/TLX3-mediated Eα repression is ETS1, RUNX1, or LEF1 dependent, we repeated the reporter assays and removed each TF individually. The fact that Eα-CAT expression was not totally abolished in the absence of any one of these TFs (Giese et al., 1995) makes it possible to quantify repression of the residual activity after individual TF removal. In these conditions,

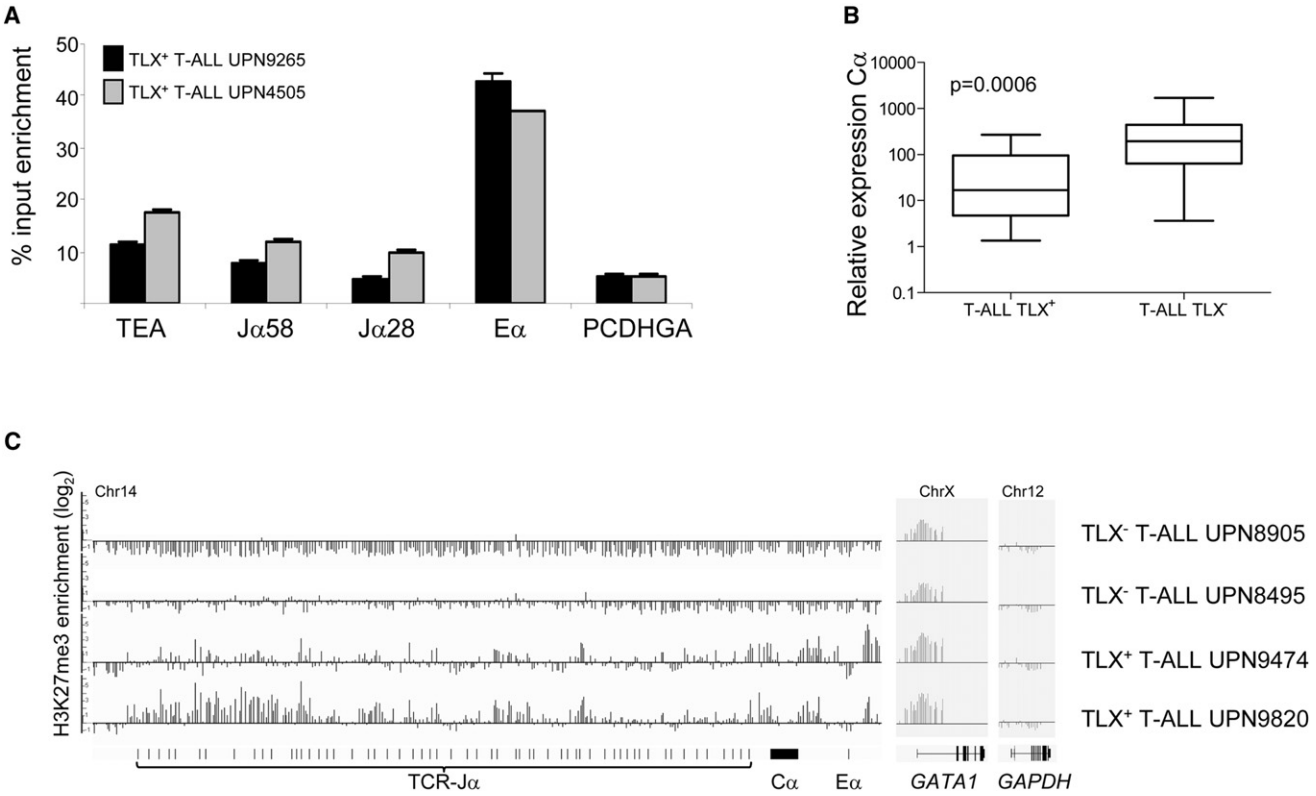

Figure 1. TLX+ T-ALLs Show Reduced Accessibility of the TCRα Locus

(A) Graph showing formaldehyde-assisted isolation of regulatory elements (FAIRE) signals on two TLX+ T-ALL primary cell samples (UPN, unique patient number), as assessed in using RT-qPCR and TEA, Jα58-, Jα28-, Eα-, or PCDHGA (a gene not expressed in T cells)-specific primers. Data represent means of duplicate measurements whereby amplification signals were normalized to those of the corresponding input DNA with error bars to represent ±SD.

(B) Box plots for relative TCR-Cα gene expression normalized to housekeeping gene Abelson1 (ABL) in phenotypically matched TLX+ (n = 23) and TLX− (n = 18) T-ALLs, as assessed by RT-qPCR.

(C) Plots of ChIP-on-chip signals for H3K27me3 relative enrichment in two TLX+ and two TLX− T-ALL cell samples. Black horizontal lines represent the no-change lines. Black vertical bars indicate H3K27me3 peaks. The positions of the TCR-Jα, Cα, and Eα genomic regions, as well as those of exons and upstream promoter sequences in the silent (*GATA1*) and expressed (*GAPDH*) control genes are indicated (exons depicted as vertical traits or black boxes). All four T-ALL samples harbor at least one unrearranged TCRα allele (not shown).

See also Figure S2.

the omission of ETS1 and, to a lesser extent, RUNX1, but not LEF1, diminished TLX1/TLX3-mediated Eα-CAT repression (Figure 2E). We also found that serial diminution of transfected ETS1-expression vector led to a progressive decrease of TLX/TLX3-mediated repression (Figure 2F). Altogether, our data imply that TLX1/TLX3-mediated repression occurs mostly via ETS1.

We therefore carried out in vitro GST-pull-down assays and found that immobilized TLX1 and TLX3 retained the ETS1 FL protein but not LEF1 (Figure 3A). The ETS1 DNA binding domain (DBD) and the TLX1 and TLX3 HD-containing regions appeared to be most important for this interaction (Figure 3A). We further performed streptavidin precipitation experiments using HeLa cells transfected with expressing vectors encoding ETS1-HA-His, LEF1-HA, and TLX1- or TLX3-Flag-SBP tagged proteins. Precipitation of TLX1/TLX3 only retained ETS1 but not LEF1 (Figure 3B). To confirm an interaction between endogenous proteins, we carried out co-immunoprecipitation (Co-IP) using TLX1+ ALL-SIL and TLX3+ DND41 cell lines and anti-TLX1 or TLX3 monoclonal antibody (mAbs), which recovered both ETS1 and the corresponding TLX in the precipitated material (Figure 3C). Finally, we investigated the subcellular localization of TLX1, TLX3, and ETS1 in TLX+ T-ALL clinical samples by cell fractionation and immunostaining. Both analyses demonstrated that TLX1, TLX3, and ETS1 localize in the nucleus (Figures 4A and 4B). Moreover, both TLX+ and TLX− T-ALL expressed similar amounts of ETS1 protein and RNA (Figure 4A and data not shown). Strikingly, the nuclear distribution of ETS1 was diffuse in TLX− patient leukemic cells and cell lines (Figure 4B) but was irregular in TLX+ nuclei and overlapped significantly with that of the TLX proteins (Figure 4C; see figure legend for statistical information). Using ALL-SIL, we showed that, as anticipated, the nuclear distribution of ETS1 became more diffuse following TLX1 downmodulation (Figure 4D).

ETS1 Mediates TLX1 and TLX3 Recruitment to Eα-Associated DNA Sequences

Given the data above in favor of an interaction between TLX1/TLX3 and ETS1 proteins impinging upon Eα activity, we next tested whether TLX1/TLX3 directly interacts with the ETS1

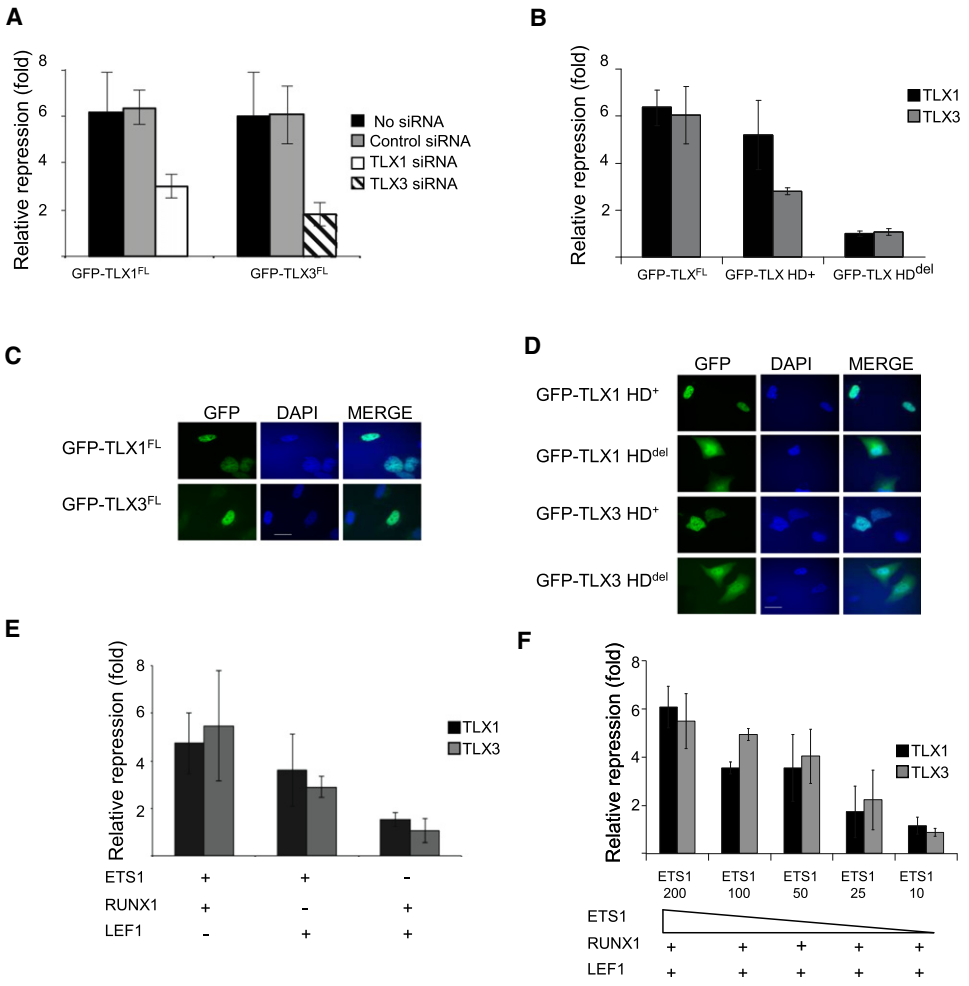

Figure 2. TLX1 and TLX3 Repress Eα-CAT Activity via Their Homeodomain

(A) Graph showing Eα-CAT fold repression in HeLa cells following transfection with GFP-TLX1^{FL} or GFP-TLX3^{FL} encoding vectors, with or without cotransfection of the indicated small interfering (si) RNAs. Data represent means of triplicate measurements whereby Eα-CAT signals were normalized to those of control cells transfected with a GFP vector, with error bars to represent ±SD.

(B) As in (A), but with HeLa cells transfected with GFP-TLX^{FL} vectors alone, or with similar vectors carrying or lacking the corresponding TLX homeodomain (GFP-TLX HD^{+} and GFP-TLX HD^{del}, respectively).

(C and D) Examples of fluorescence microscopic analysis of GFP-TLX expression in transfected HeLa cells depicted in (A) and (B). White scale bar is 10 μm.

(E) As in (A), but with HeLa cells transfected with GFP-TLX^{FL} vectors, plus (+) or minus (−) additional vectors encoding the indicated ETS1, RUNX1, or LEF1 TFs.

(F) As in (E), but using decreasing amounts (200–10 ng) of ETS1-expression vector.

binding sequences (EBS) of human Eα. Using electrophoretic mobility shift assays (EMSA) we observed no significant shift of the EBS probe when incubated with TLX1/TLX3 alone (Figure 5A, lanes 2–7). As expected, incubation with purified recombinant ETS1 led to a major shift of the labeled probe (Figure 5B, lane 1). Strikingly, the addition of TLX1 (lanes 2–4) or TLX3 (lanes 5–7) to ETS1 and EBS produced a dose-dependent super-shifted complex.

To ascertain Eα occupancy by endogenous TLX1 and TLX3 in vivo, we performed ChIP assays using ALL-SIL (TLX1^{+}), DND41 (TLX3^{+}), and, as a control, RPMI-8412 (TLX^{-}) cell lines. The ChIPed DNA was RT-qPCR amplified using Eα-specific oligonucleotide primers and primers specific for the unrelated Actin gene promoter (not bound by either ETS1 or TLX TF; data not shown), used here as a mock control for data normalization. As expected, anti-ETS1 enriched Eα-associated sequences from all three cell lines (Figure 5C). In contrast, anti-TLX1 and anti-TLX3 enriched Eα-associated sequences from only ALL-SIL and DND41, respectively, demonstrating in vivo recruitment of TLX1 and TLX3 onto Eα. Using the DND41 and ALL-SIL cell lines, we verified that knockdown of ETS1 reduced Eα-binding by both ETS1 and TLX1/TLX3 (Figure 5D). Taken together, these data indicate that TLX1 and TLX3 were recruited to Eα via their interaction with ETS1 in TLX^{+} leukemic cells.

TLX Downmodulation and Enforced TCRαβ Expression Both Lead to Redifferentiation Linked with Massive Cell Apoptosis

Our results suggest that one of the major oncogenic functions of TLX1/TLX3 in T-ALL would be to block αβ T cell development by

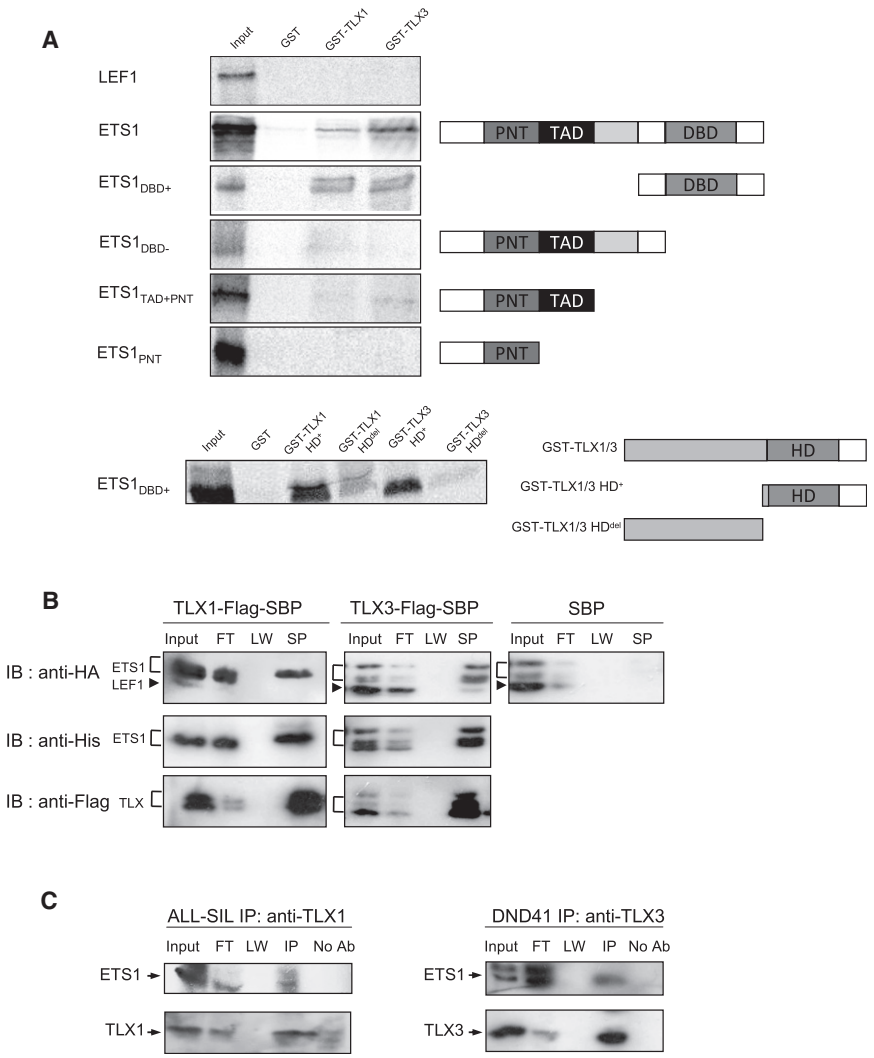

Figure 3. TLX1 and TLX3 Interact with ETS1

(A) GST, GST-TLX1, and GST-TLX3 pull-down of ^{35}S-labeled in vitro translated LEF1, ETS1, or truncated versions of ETS1: ETS1$_{DBD+}$, ETS1$_{DBD-}$, ETS1$_{TAD+PNT}$, and ETS1$_{PNT}$. The various versions of ETS1 are depicted on the right: PNT, pointed domain; TAD, transactivation domain; DBD, DNA binding domain. (Bottom) GST, GST-TLX HD^{+}, and GST-TLX HD^{del} pull-down of ^{35}S-labeled ETS1$_{DBD+}$. TLX and its truncated forms are depicted on the right: HD, homeodomain. The "Input" lanes correspond to 5% of the ^{35}S-labeled protein used for a pull-down experiment.

(B) Cell lysates from HeLa cells cotransfected with vectors expressing ETS1-HA-His, LEF1-HA, and TLX1-(or TLX3-) Flag-SBP were precipitated with streptavidin (SP) beads and then immunoblotted (IB) with either an anti-HA antibody (to reveal the fusion proteins ETS1-HA-His and LEF1-HA), an anti-His antibody (to reveal the ETS1-HA-His), or an anti-Flag antibody (to reveal TLX and to evaluate SP efficiency). Input represents 10% of cell lysate used for SP. FT, flow-through; LW, last wash.

(C) Cell lysates from ALL-SIL and DND41 cells were immunoprecipitated (IP) using anti-TLX1 (left) or anti-TLX3 (right) antibody followed by immunoblotting with indicated antibodies. The "Input" lanes correspond to 10% of cell extracts used in the Co-IP. No Ab, control IP experiment performed without antibody; FT, flow-through; LW, last wash.

inhibiting Eα activity. To further explore this possibility, we knocked down TLX1 and TLX3 expression in ALL-SIL and DND41 cell lines, respectively. While the control cells grew normally, the knockdown TLX1/ALL-SIL and TLX3/DND41 cells demonstrated massive apoptosis (Figure 6A and 6B). Strikingly, both Cα and TEA-Cα transcripts, as markers of TCR-Jα locus activation (Hernández-Munain et al., 1999; Monroe et al., 1999), were upregulated in the TLX knockdown cells (Figure 6C). Moreover, unlike transduced mock controls, the two TLX knockdown cells harbored Vα-Jα rearrangements, although with a restricted polyclonal pattern, as expected (Figure 6D). The knockdown cells further demonstrated a maturation shift, as shown by increased cell size and CD5 expression (Figure 6E). Most important, a small proportion of these cells became sTCRαβ^{+} (Figure 6F).

We then assessed whether such a redifferentiation process, including the triggering of cell death, could be induced by forced expression of sTCRαβ, thus bypassing TLX/ETS1-mediated suppression of Vα-Jα rearrangement, in a TLX^{+}/TCR^{-} T-ALL cell line. TLX1^{+} ALL-SIL cells were transduced using lentiviral multicistronic vectors enabling expression of GFP with or without TCRβ and TCRα (Figure 6G, top). GFP^{+} sTCRαβ^{+} ALL-SIL cells exhibited reduced viability and cell growth compared to GFP^{+} sTCRαβ^{-} controls when cultured in the OP9-DL1 stromal-cell system (Figure 6G, bottom). This correlated with increased apoptosis of the sTCRαβ^{+} cells, as evidenced by propidium iodide (PI)/annexin V dual staining (Figure 6H; note that Jurkat cells carrying an identical sTCRαβ were not affected). It is important to note that massive apoptosis was not observed when transduced cells were cultured in a stromal-cell-free standard culture system (Figures 6G and 6H). These data demonstrate the key role of TCR expression in mediating cell death in TLX^{+} T-ALLs and strongly suggest that the apoptosis observed upon TLX inhibition is a consequence of redifferentiation.

Overall, ectopic expression of TLX1/TLX3 in cortical thymocytes appears to be required to maintain leukemic proliferation, survival, and failure to differentiate; and defect in TCRαβ expression—via ETS1-mediated TLX recruitment onto Eα—is a major mediator in oncogenic addiction, even after acquisition of a variety of additional genetic abnormalities.

TCRα/δ Translocations Occur 5′ to TLX1 Leading to Eα-Independent TLX1 Expression

While chromosomal translocations that lead to *TLX3* deregulation in T-ALLs virtually always involve genomic partners other than *TCRα/δ* (Bernard et al., 2001; Soulier et al., 2005), those leading to *TLX1* deregulation predominantly involve *TCRα/δ*.

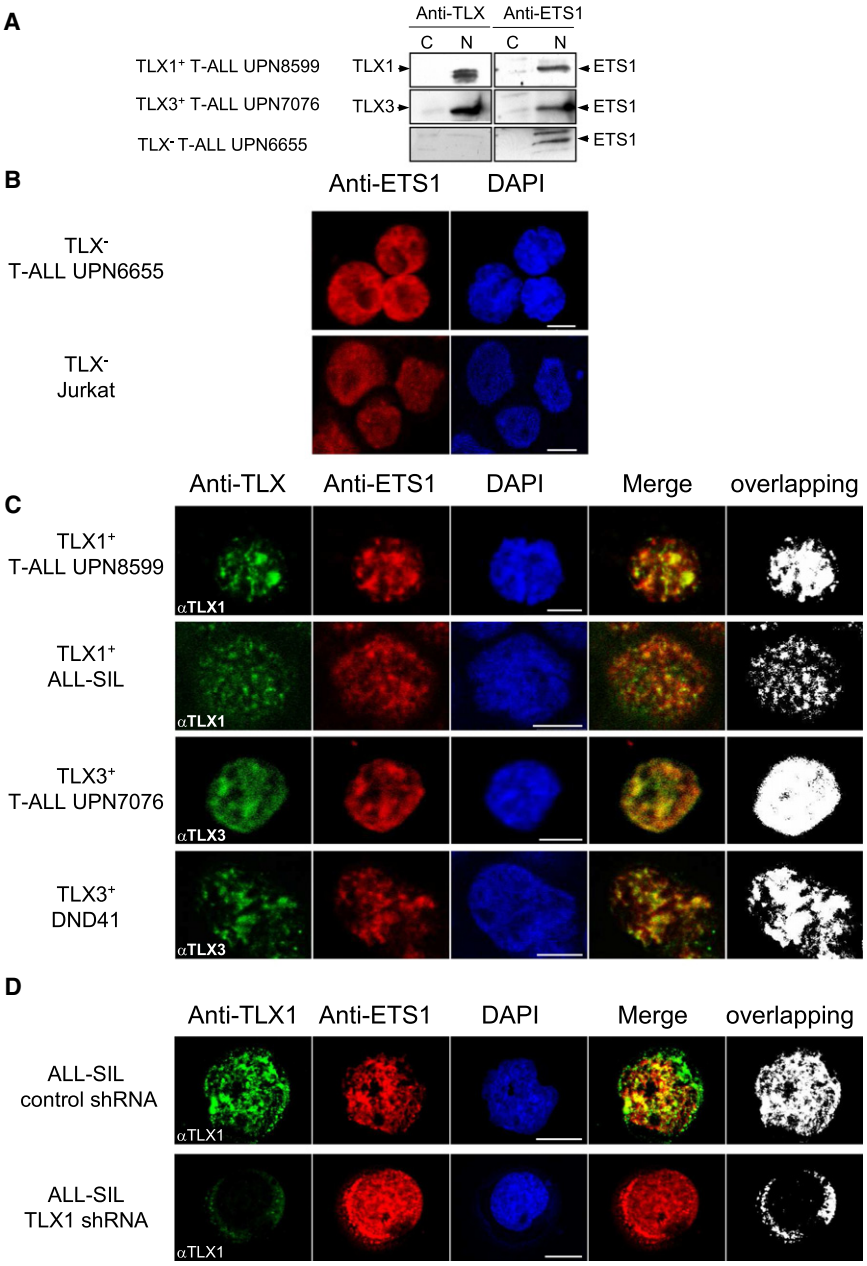

Figure 4. TLX1, TLX3 and ETS1 Colocalize in TLX$^+$ T-ALL Blast Nuclei

(A) Western blot analysis of cytoplasmic (C) and nuclear (N) extracts from TLX1$^+$, TLX1$^+$, and TLX$^-$ T-ALL cells. Blots were probed with anti-TLX and anti-ETS1 antibodies as indicated.

(B) Confocal microscopy analysis of TLX$^-$ T-ALL and cell line (Jurkat) labeled with the indicated fluorescent anti-ETS1 mAb (Alexa 647, red) or stained by DAPI.

(C) Confocal microscopy analysis of the TLX$^+$ T-ALL and cell lines ALL-SIL (TLX1$^+$) and DND41 (TLX3$^+$) labeled with the indicated fluorescent anti-TLX mAb (Alexa 488, green) and anti-ETS1 mAb (Alexa 647, red), or stained by DAPI. The merged images and overlapping areas (determined using ImageJ software) are also shown. Pearson's coefficients for the overlapping areas were as follows: $r = 0{,}851$ (UPN480); $r = 0{,}608$ (ALL-SIL); $r = 0{,}929$ (UPN364); and $r = 0{,}816$ (DND41).White scale bars are 5 μm.

(D) As in (C), but the ALL-SIL cells were transduced with TLX1-specific (TLX1 small-hairpin [sh]RNA) or nonspecific (control shRNA) RNAs as indicated. White scale bars are 5 μm.

However, if a critical oncogenic function of TLX1 is to repress Eα activity, as supported by the data above, how could Eα possibly provide sustained TLX1 expression if it is juxtaposed to and drives TLX1 expression? To get further insight into the mechanism of *TLX1* transcriptional activation, we first analyzed its expression by RT-qPCR in 526 adult and pediatric T-ALLs and identified 61 cases as TLX1$^+$. We then identified *TLX1* translocation into either the *TCRδ* locus (35 cases) or the *TCRβ* locus (12 cases) in the 47 TLX1$^+$ cases with enough material for carrying out FISH- and/or ligation-mediated (LM) PCR analysis. All informative cases tested for allelic transcripts (12 *TCRδ-TLX1* and 2 *TCRβ-TLX1*) demonstrated monoallelic *TLX1* expression, in line with a "standard" regulatory element substitution mechanism of oncogene deregulation in *cis*. We mapped the breakpoints from 8 out of 12 TCRβ-TLX1 alleles and 30 out of 35 *TCRδ-TLX1* alleles (Figure S3). While all 8 breaks from *TCRβ-TLX1* translocations mapped 3′ to *TLX1*, all 30 breaks from TCRδ-TLX1 translocations mapped 5′ to *TLX1* (Figure 7A, top lane). Consequently, whereas *TLX1* activation in *TCRβ-TLX1* fusions was consistent with a classical scenario of TCR-gene-enhancer-mediated activation (in this case, the TCRβ gene enhancer Eβ; Figure 7A, middle lanes), the *TCRδ-TLX1* translocations separated the *TLX1* gene and Eα element on the two derivative chromosomes (Figure 7A, bottom lanes), implying Eα-independent activation and/or maintenance of *TLX1* oncogenic expression.

To investigate whether *TLX1* overexpression resulted from its juxtaposition to a *cis*-regulatory element(s) within and/or upstream to the TCRδ promoter, we performed clonospecific RT-PCR across the breakpoints of both *TCRδ-TLX1* and *TCRβ-TLX1* translocations. Given the structure of these translocations, the detection of fusion transcripts in all the *TCRδ-TLX1* samples, but not in the *TCRβ-TLX1* samples (Figure 7B), was consistent with the presence of a positive regulatory element(s) within and/or upstream to the TCRδ locus that drives *TLX1* overexpression.

Eα Repression Results in a TLX1 Feed-Forward Repression Loop

Despite the obvious difference in the origin of *TLX1* transcriptional activation in *TCRβ* versus *TCRδ* translocations, we observed no significant disparity in their levels of *TLX1* expression

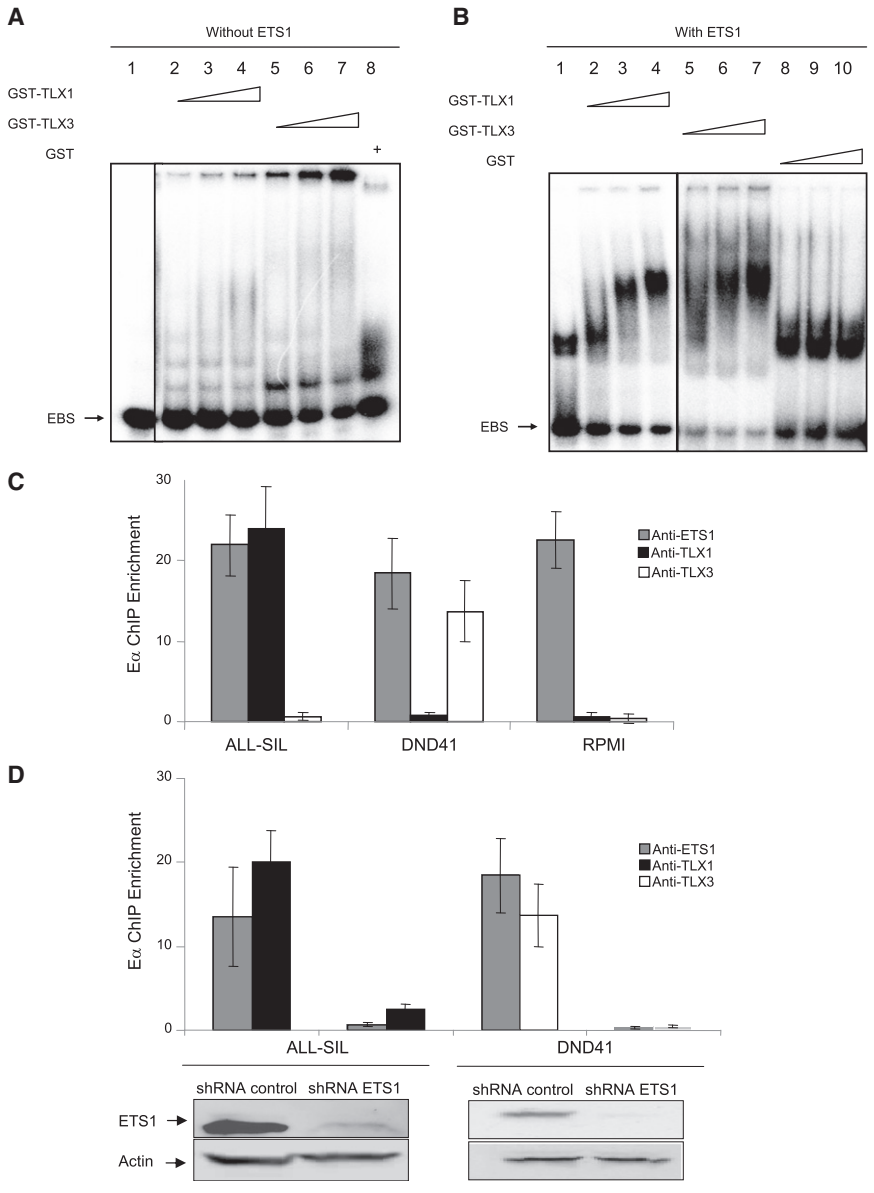

Figure 5. ETS1 Mediates TLX1 and TLX3 Recruitment to Eα-Associated DNA Sequences

(A) EMSA of the ^{32}P-labeled EBS oligonucleotide probe comprising core Eα nucleotide sequences (Giese et al., 1995) with purified recombinant GST-TLX1 and GST-TLX3 proteins. Lane 1, free EBS probe; lanes 2–4 and lanes 5–7 EBS incubated with increasing amounts (10, 50, and 100 ng) of GST-TLX1 or GST-TLX3, respectively; lane 8, EBS incubated with 100 ng of GST.

(B) As in (A), but with the presence of 20 ng of purified recombinant ETS1 protein (lanes 1–7) and ETS1 with increasing amounts (10, 50, and 100 ng) of GST (lanes 8–10).

(C) Graphs of ChIP signals for Eα from the ALL-SIL (TLX1$^+$), DND41 (TLX3$^+$), and RPMI (TLX$^-$) cell lines using anti-ETS1, anti-TLX1, and anti-TLX3 antibodies, as indicated. ChIPed DNA was qPCR amplified using Eα and actin (negative-control)-specific oligonucleotide primers. Enrichment level was determined by comparison to a standard curve from input DNA. ChIPed signal enrichments correspond to the ratios between the Eα signal and actin signal. IgG isotype control was performed to assess absence of nonspecific Eα ChIP enrichment (not shown). Data represent means of triplicate measurements with error bars to represent ±SD.

(D) As in (C), but with the ALL-SIL and DND41cells transduced with ETS1-specific or nonspecific shRNAs. Shown beneath the graph are western blots for ETS1 or actin expression from mock transduced (shRNA control) and knockdown (shRNA ETS1) cells.

(data not shown). This may reflect oncogenic selection of only those rearrangements with sufficient/optimal *TLX1* expression. We also searched for possible differences in the stage of maturation arrest and/or kinetics of *TLX1* activation. TLX1$^+$ T-ALLs are commonly arrested at a cortical TCRαβ negative stage of maturation (Ferrando et al., 2002). In keeping with this, all TLX1$^+$ T-ALL cases (whether *TCRδ* or *TCRβ* translocated) display a uniform cortical CD1a$^+$/CD34^{neg} phenotype (Asnafi et al., 2003; Ferrando et al., 2002). Furthermore, sequence analysis demonstrated that both TCRδ and TCRβ translocations occurred at a similar stage of early thymic-cell differentiation with respect to rearrangement events, since all *TCRδ*- and *TCRβ-TLX1* junctions resulted from repair mistakes introduced during, respectively, a Dδ2-Dδ3 (or Dδ3-Jδ1) rearrangement, or a Dβ-Jβ rearrangement (Figure S3). These data further implied that *TLX1* oncogenic activation uniformly took place at an immature DN/CD1a$^-$/CD34$^+$ stage of thymic cell development, while cell maturation arrest occurred at a later (cortical) stage.

We therefore hypothesized that 3′ *TCRδ-TLX1* translocations do not undergo oncogenic selection because of a feed-forward inhibitory effect exerted by TLX1 itself, inducing autorepression of Eα transcriptional activity. This would infer that TCRα/δ driven translocations with 3′ *TLX1* breakpoints could occur but would fail to be selected within an oncogenic context. As several examples of potentially oncogenic TCR translocations have previously been reported in healthy thymi (Dik et al., 2007; Marculescu et al., 2003, 2006), we searched normal thymus for putative TCRδ-TLX1 translocations with breakpoints involving either side of *TLX1* (Figure 7C, top lanes). We set up a highly sensitive double-nested qPCR allowing the recovery of rare translocation events (10^{-8}–10^{-9}) and applied this assay to screen the DNA equivalent of 10^9 thymocytes from 10 healthy postnatal thymi. Even though no *5′ type* junction was observed, two *3′ type* junctions were reliably detected (Figure 7C, bottom lanes). This demonstrates that *3′ type* TCRδ-TLX1 translocations do occur in the normal thymus and are at least no less common than *5′* translocations. The main difference between the 3′ *TCRβ-TLX1* translocations observed in T cell

leukemias and the 3′ *TCRδ-TLX1* exclusively found in nonleukemic thymi consists in their association with the Eβ or Eα element, respectively. Given the aforementioned inhibition of Eα activity by TLX1, these data support the intriguing possibility that deregulation of *TLX1*, when driven by Eα, will lead not to oncogenic selection but rather to autonomous counterselection of the chromosomal translocation due to feed-forward repression (Figure 7D).

DISCUSSION

HOX proteins in general, and TLX in particular, exert a repressive activity on transcriptional events during embryonic development (Mann et al., 2009; Merabet et al., 2005; Owens et al., 2003; Shen et al., 2001). Our study identifies TCR Eα as a target for such a repressive activity upon ectopic expression in T cell development, offering molecular insight into the stage of maturation arrest and oncogenesis of TLX$^+$ T-ALLs.

The onset of V(D)J recombination is primarily regulated at the level of chromatin and access of the RAG1/RAG2 recombinase apparatus to its DNA targets, a process that depends on the activity of transcriptional enhancers in TCR and Ig loci, including Eα and Eδ in the TCRα/δ locus (Krangel et al., 1998). Our data pinpoint a suppressive chromatin configuration around Eα and a molecular explanation to the strong bias against Vα-to-Jα rearrangement observed in TLX$^+$ T-ALLs. The TCRα repressed structure appears to specifically affect the TEA/Jα-containing region, since in cases where unrearranged TCRα/δ alleles could be analyzed for H3K27me3, the proximal, 3′ part of the TCR-Vα locus behaved similarly in TLX$^+$ and TLX$^-$ blasts (Figure S2). Although proximal Vα segments lie within the range of long-distance chromatin regulation by Eα, an active, derepressed chromatin configuration would be expected at these sequences in early cortical thymocytes due to the activity of the nearby Eδ (Hawwari and Krangel, 2005). In short, the aberrant TCRα/δ recombination patterns seen in TLX$^+$ T-ALL faithfully mirror the chromatin opening function that exclusively relies on Eα.

We have identified the ETS1 TF as a mediator, via protein-protein interaction, of this Eα-suppressing function of TLX1/TLX3. There is precedent for inhibition of a cell-developmental pathway by ETS1, MafB-ETS1 interaction having been reported to result in a block to erythroid differentiation (Sieweke et al., 1996). The precise mechanisms for the repression by TLX remain to be elucidated, but our current data provide interesting clues. Recruitment of both TLX and ETS1 onto Eα render unlikely a basic model whereby TLX sequesters ETS1 away from the enhanceosome; however, more complex, locally induced, opposing molecular switches dependent on the nature of ETS1-interacting TF partners could not be excluded (Sieweke et al., 1996). Likewise, our unpublished findings that TLX1/TLX3 still suppresses transcription on cell treatment with a histone deacetylase (HDAC) inhibitor suggest that HDAC is not involved. The creation of a distinct heterochromatin-promoting complex is plausible, since HOX proteins have been shown to fix polycomb (PcG) repressive components (Papp and Müller, 2006). Our finding of H3K27me3 enrichment along Eα-flanking genomic regions in TLX$^+$ T-ALL supports this, as H3K27me3, in addition to being a marker of repressive chromatin, is associated with activity of the PcG complex PRC2 (Sauvageau and Sauvageau, 2008). This suppressive function for TLX on Eα activity via ETS1 does not exclude protein-protein interaction with and mediation of a suppressive effect by, other TFs, such as RUNX1 (Hollenhorst et al., 2009).

ETS1 plays an important role in cell developmental controls and neoplastic processes (Dittmer, 2003). TLX1/TLX3 overexpression would therefore be expected to deregulate multiple biological networks via its interaction with ETS1. The TLX1/TLX3-ETS1-mediated Eα inhibition described here unlikely would explain the whole T-ALL oncogenic program induced by TLX1/TLX3, since Eα deletion in mice has not been associated with the development of T cell leukemia (Sleckman et al., 1997) and transgenic TLX1-driven murine leukemias demonstrate a variety of somatic genetic abnormalities (De Keersmaecker et al., 2010). TLX1/TLX3-ETS1-mediated Eα inhibition, however, likely accounts for the early cortical block in cell maturation around β-selection characteristic of these leukemias.

Inactivation of ETS1 impairs, but does not abolish, the development of DN3 thymic cell differentiation into DP cells and the defect appears to be specific to the αβ T cell lineage, as γδ T cells mature normally (Eyquem et al., 2004). In line with this, TLX$^+$ T-ALLs often express a TCRγδ, albeit in conjunction with the cytoplasmic TCRβ chain. In this context, it is noteworthy that, despite the presence of ETS1 and RUNX binding sites within Eβ, ETS1 deficiency did not affect Eβ activity (Eyquem et al., 2004), pointing to different requirements for the activity of Eβ and of Eα. As mentioned, an alternative and non-mutually-exclusive candidate for mediation of the maturation arrest might be BCL11b, recently reported to be a direct target downregulated by TLX1 (De Keersmaecker et al., 2010). Loss of BCL11b, a transcriptional repressor required for T lymphoid specification, leads, however, to a much earlier DN1/2 block (Ikawa et al., 2010; Li et al., 2000, 2004). Our data would suggest that abrogation of ETS1 activity on Eα is more likely than loss of BCL11b to explain the cortical arrest seen in human T-ALLs. As in vivo confirmation of the capacity of TLX1 to inhibit Eα-enhanceosome-driven transcription, we also show here that *TCRδ-TLX1* genomic products resulting from a t(10;14) translocation will lead to either a cell-maturation arrest and leukemogenesis or autoextinction of translocated clones, depending on the configuration of the translocation breakpoints. One interesting aspect of the autoextinction model is that in order to efficiently repress its own sustained expression *in-cis*, the TLX1 protein has to be produced prior to disrupting activity of the Eα enhanceosome on the *TLX1-TCRδ*/Eα translocated allele (Figure 7C). If so, it seems reasonable to assume that the same repression also occurs *in-trans* on the normal (nontranslocated) *TCRα* allele, leading to inhibition of *TCRα* rearrangement and a block in thymocyte differentiation. The fact that these cells do not undergo malignant transformation implies that sustained (and/or higher-level) TLX1 expression is required for leukemic transformation. Such a TLX1 "oncogene addiction" argues in favor of TLX1 being the initiating and causative oncogenic event in TLX1$^+$ T-ALL cases. This model obviously does not exclude oncogenic synergy with other abnormalities.

In line with a major role of ETS1/TLX-mediated repression of Eα in this TLX-induced oncogenic addiction, knockdown of TLX1/TLX3 led to apoptosis, concomitant TCRα transcription and rearrangement, cell-maturation, and sTCRαβ$^+$ expression

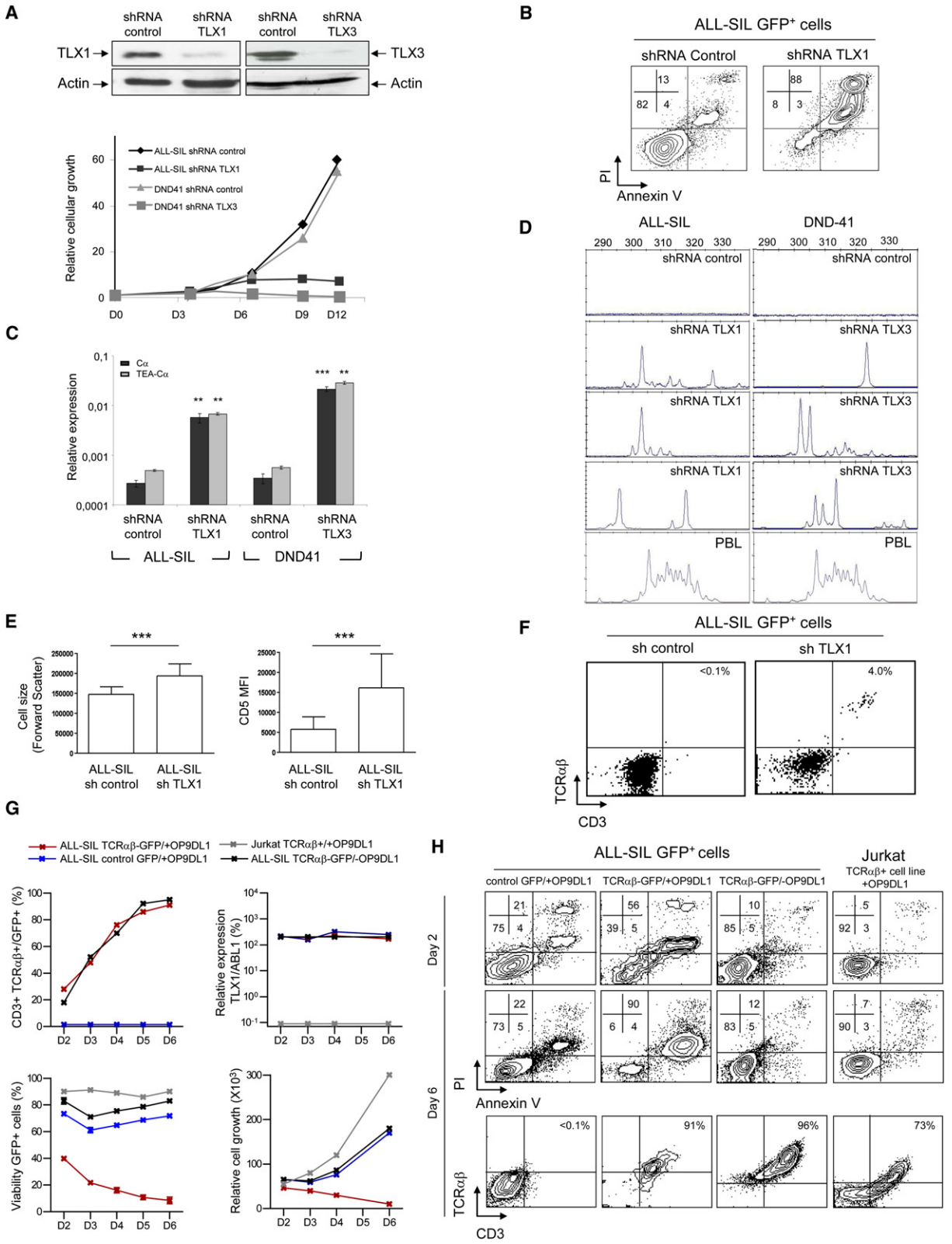

Figure 6. Abrogation of the T Cell Maturation Block Induces Cell Death

(A) Western blots for expression of TLX1 (top left), TLX3 (top right), and the actin control (bottom) in ALL-SIL and DND41 cells transduced with specific or nonspecific (control) shRNA. The graph shows cellular growth at days (D) 3, 6, 9, and 12 of cell culture.

in a significant proportion of cells. This implies that continuous TLX expression is required for maintenance of leukemic cell survival and blocked differentiation, and that both may be intricately linked. The fact that the apoptotic effect of TLX1 abrogation was mimicked by transducing a TCRαβ transgene in TLX1/ALL-SIL cells in the presence, but not in the absence, of stroma supports these conclusions. Thus, as predicted from a bypass of the ETS1/TLX-mediated Eα inhibitory control, both enforced sTCRαβ expression leading to exit from β-selection and TLX abrogation lead to a similar outcome (i.e., apoptosis). Different outcomes (cell death versus proliferation) depending on the presence or absence of OP9-DL1 stroma are likely to reflect a role for stromal (or other ligand) interaction in cell death following TCRαβ expression and differentiation. In general, T cell responses require costimulation-engagement of the clonotypic TCR together with that of distinct coreceptors and cognate ligands. Our current findings offer a unique opportunity to explore such a partnership in TLX$^+$ T-ALL tumorigenesis in prospective studies.

Taken together, our results demonstrate that the maturation block observed in TLX$^+$ T-ALLs is in large part due to ETS1-mediated TLX recruitment to the Eα core, leading to repression of Eα and blocked Vα-Jα rearrangement. Failure to express a TCRα gene arrests development of αβ-committed thymocytes around β-selection, when a variety of cell-proliferation signals are likely to be maintained, hence contributing to oncogenesis. This blockage can be overcome by TLX1/3 abrogation or by downstream TCRαβ expression within an appropriate cellular context. These observations have fundamental consequences both for targeted therapy in TLX$^+$ T-ALLs and for the role of aberrant TCR expression in T lymphoid oncogenesis.

EXPERIMENTAL PROCEDURES

Full Experimental Procedures and any associated references are available in the Supplemental Experimental Procedures.

Patient Analysis and Clinical Diagnosis

Diagnostic samples of peripheral blood or bone marrow from T-ALL patients included in the GRAALL or FRALLE protocols were investigated. Approval was obtained from institutional review boards of institutions participating in this study; the full list of participating centers is given in Supplemental Experimental Procedures. The age cut-off between pediatric and adult cases was 18 years. All samples contained ≥80% blasts. Informed consent was obtained according to the declaration of Helsinki. DNA and RNA extraction and identification of TCRδ, TCRγ, and TCRβ clonal rearrangement were identified as described (Asnafi et al., 2003).

CAT-Reporter Assays

CAT-transactivation assays were performed as described (Giese et al., 1995).

Streptavidin Precipitations and Immunoprecipitations

HeLa cells were cotransfected using expression vectors for ETS1-*HA*-*His*, LEF1-*HA*, and either TLX1-SBP-Flagx3 or TLX3-SBP-Flagx3, or the empty expression vector SBP-Flagx3 as a control. ALL-SIL (TLX1$^+$) and DND41 SIL (TLX3$^+$) cells were used for protein IPs. Nuclear extracts were prepared and incubated with streptavidin agarose beads or with anti-TLX1 (16F6) or anti-TLX3 (10A5) mAbs, respectively, covalently linked to protein G agarose beads. After washes, precipitated proteins were detected by western blot analysis.

Fluorescence and Immunofluorescence Analyses

For EGFP fluorescence analysis, HeLa cells plated on coverslips were transiently transfected with EGFP-fusion constructs and further cultured for 48 hr. Imaging was performed using a Zeiss (LSM-510) confocal microscope. For immunofluorescence analysis, cell lines or primary blast cells (1×10^5) were cytospun onto glass slides. Images were obtained on a Leica TCS SP5 confocal laser scanning microscope and merged using Leica LAS AF software.

Chromatin Immunoprecipitation

ChIPs from the ALL-SIL, DND41, and RPMI cell lines or from T-ALL samples were performed according to the Agilent protocol version 10.0 (http://www.chem.agilent.com), using anti-TLX1 (16F6), anti-TLX3 (10A5), anti-H3K27me3 (05851, Abcam), and anti-ETS1 (sc-350, C-20X, Santa Cruz) mAbs.

TLX1 and TLX3 Knockdown

MISSION TRC shRNA Target Set vectors for TLX1 (TRCN0000014995), TLX3 (TRCN0000018030), and ETS1 (TRCN0000231917) were purchased from Sigma. Knockdown of the corresponding endogenous RNA transcripts was performed by transduction of the ALL-SIL and DND41 cell lines.

Screening for TCR-TLX1 junctions

Screening for 3′ *type* t(10;14)(q24;q11) translocations was performed using pooled thymocytes from 10 healthy children undergoing cardiac surgery.

ACCESSION NUMBER

The ChIP-on-chip data have been deposited at ArrayExpress (http://www.ebi.ac.uk/arrayexpress/) with the accession number E-MEXP-3527.

SUPPLEMENTAL INFORMATION

Supplemental Information includes one table, three figures, and Supplemental Experimental Procedures and can be found with this article online at doi:10.1016/j.ccr.2012.02.013.

(B) Flow cytometric analysis of TLX1$^+$ ALL-SIL cells following transduction with retroviruses encoding the GFP protein and either control (nonspecific) or TLX1-specific shRNAs. GFP$^+$-transduced cells were gated for analysis of AnnexinV/PI staining.
(C) RT-qPCR quantification of Cα and TEA-Cα transcripts in ALL-SIL/DND41 following shRNA (TLX-specific versus mock control) transduction. Cα and TEA-Cα transcript levels are shown relative to those of ABL control transcripts (**p value ≤ 0.01; ***p value ≤ 0.001), with error bars to represent ±SD.
(D) Multiplex RT-PCR analysis of Vα-Jα-Cα rearrangements from ALL-SIL (left) and DND41 (right) cDNA, following mock control (top) or TLX-specific (second to fourth panel pairs) shRNA transduction and 9 days of cell culture. Normal TCRαβ rearranged repertoires give a Gaussian distribution of variable length Vα-Jα-rearranged PCR fluorescent products, as found in normal PBLs (bottom). Abrogation of TLX1/TLX3 allows a variety of Vα-Jα rearrangements.
(E) Histograms of forward scatter and CD5 mean of fluorescence of GFP$^+$ ALL-SIL cells assessed by flow cytometry, following shRNA transduction. Error bars represent ±SD. ***p ≤ 0.001, Student test.
(F) Flow cytometric analysis of GFP$^+$ ALL-SIL cells for CD3 and TCRαβ surface expression.
(G) Kinetics of CD3 and TCRαβ surface expression (top left), and cell viability and growth (bottom), analyzed for GFP$^+$ cells in the indicated cell lines, with or without transduction of TCRαβ cDNAs and with or without OP9-DL1 stromal culture conditions. RT-qPCR analysis for TLX1 transcription in Jurkat and ALL-SIL cells is also shown (top right).
(H) Top and middle cytographs are as in (B), but with the ALL-SIL cells treated as in (G). Bottom cytographs are as in (F), but with the ALL-SIL cells treated as in (G). Jurkat cells are shown as TCRαβ$^+$ TLX1$^-$ controls cultured in identical conditions.

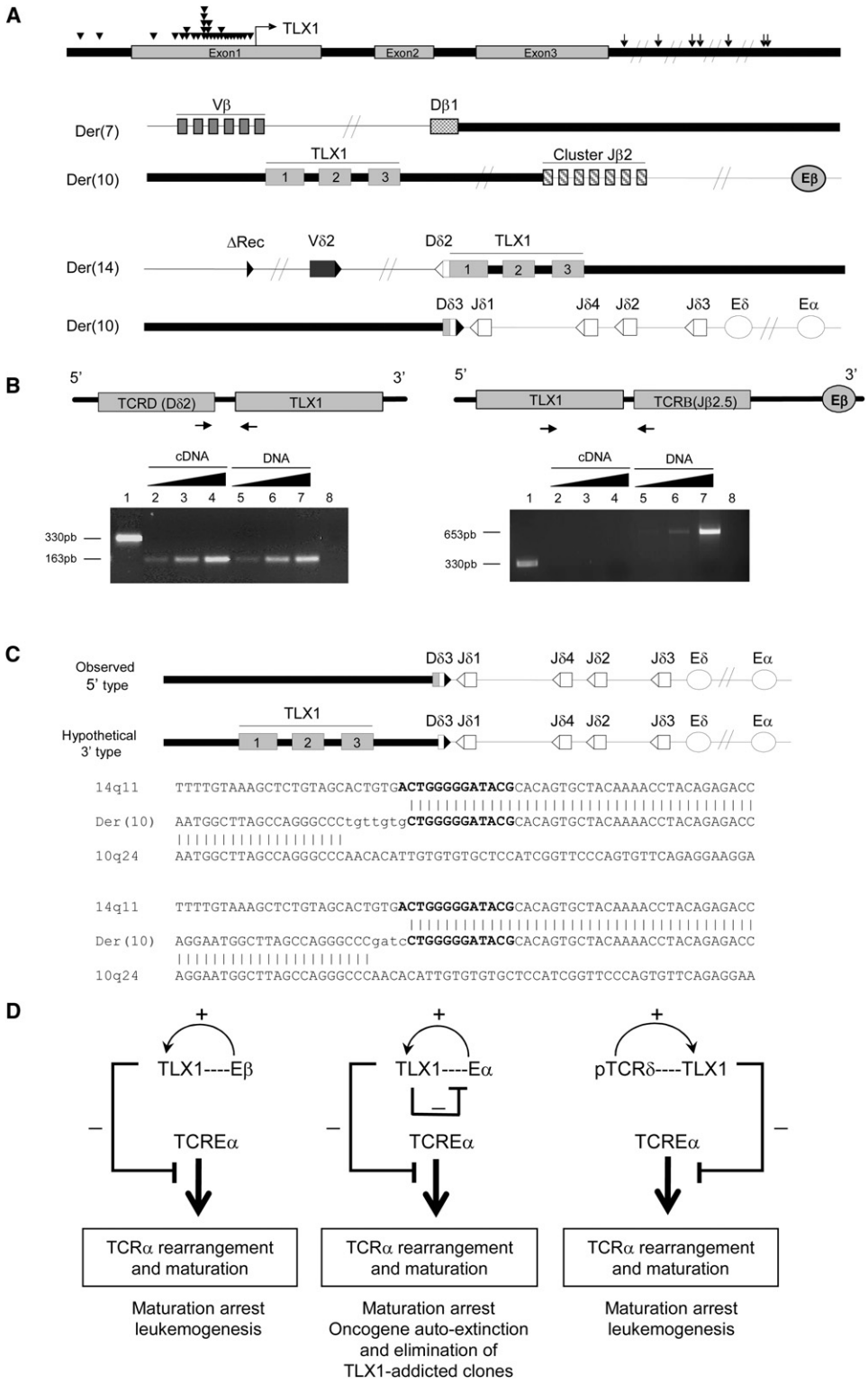

Figure 7. Molecular Analysis of *TCRβ-TLX1* and *TCRδ-TLX1* Translocations

(A) Top lane, schematic representation of the *TLX1* locus (10q24). Arrowheads and arrows indicate the relative positions of breakpoints in *TCRβ*- and *TCRδ-TLX1* translocations, respectively; middle and bottom lanes, representations of *TCRβ*- and *TCRδ-TLX1* typical translocations. Thick and thin lines depict the 10q24 and 7q34 chromosomal regions, respectively (sequences of the *TCR-TLX* breakpoint junctions are reported in Figure S3).

(B) *TCRδ-TLX1* translocations, but not *TCRβ-TLX1* translocations, generate TCR-TLX fusion transcripts. Fusion sequences resulting from *TCRδ-TLX1* translocations (left) or *TCRβ-TLX1* translocations (right) are depicted and PCR primers indicated for 150 ng of cDNA amplified using TLX1-specific primers (lane 1), 15,

ACKNOWLEDGMENTS

We thank participants in the LALA-94, GRAALL-2003/05, FRAALLE-93/2000, Dutch Childhood Oncology Group (DCOG) (project OC2001/003), and COG ALL (project #2002-09) study groups for collecting and providing biological samples and data sets. Samples were collected and processed by the AP-HP "Direction de Recherche Clinique" Tumor Bank at Necker-Enfants Malades. We are grateful to: V. Lheritier for her help in collecting clinical samples; Dr. M. Pierres (CIML) for the generation of anti-TLX1/3 mAbs; the Paris-Descartes Institute for Research at Necker-Enfants Malades (IRNEM) Cell Imaging and Cell sorting plateforms; Dr. R. Grosschedl (University of Munich, Germany) for the gift of materials for TCRαenhCAT reporter assays; and Dr. Emmanuelle Six for cell culture assistance.

S.D. was supported by grants from the Ministère de l'Enseignement Supérieur et de la Recherche, the Fondation pour la Recherche Médicale (FRM), and the Société Française d'Hématologie (SFH). J.Z.-C. was supported by a fellowship from the Agence Nationale de la Recherche (ANR). J.B. was supported by the National Cancer Institute of Canada (NCIC), Terry Fox Foundation (TFF) award. A.W.L. and W.A.D. were supported by the Dutch Cancer Society, Grant EMCR 2002-2707. S.L.N. was supported by the Institut National du Cancer (INCa-DHOS) and a grant from the Association pour la Recherche sur le Cancer (ARC). This work was supported by grants from ARC, the Fondation de France/Comité Leucémie and Enfants et Santé, in association with the Société Française de Lutte contre les Cancers et Leucémies de l'Enfant et de l'Adolescent (SFCE). Work in the P.F. laboratory is supported by institutional grants from Inserm and CNRS, and by grants from the Commission of the European Communities, the ANR, INCa, and the Fondation Princesse Grace de Monaco. Work in the BN laboratory is supported by institutional grants from Inserm and CNRS, and grants from INCa and the Fondation de France.

S.D., S.L.N., D.P.B., L.L., E.Va., J.C.Z., P.V., and S.S. performed cellular and molecular biology experiments; W.A.D. and A.W.L. provided material and data; E.Ve. and F.L.C. provided lentiviral shRNAs; J.B., C.M., and I.R. contributed to LM-PCR and FISH analysis; A.P., N.I., H.D., and O.H. provided clinical materials and data; S.D., S.L.N., D.P.B., B.N., E.A.M., P.F., and V.A. analyzed data and wrote the manuscript; D.P.B., B.N., E.A.M., P.F., and V.A. oversaw conceptual development of the project, analyzed data, and wrote the manuscript.

Received: April 2, 2010
Revised: January 3, 2012
Accepted: February 13, 2012
Published: April 16, 2012

REFERENCES

Aifantis, I., Raetz, E., and Buonamici, S. (2008). Molecular pathogenesis of T-cell leukaemia and lymphoma. Nat. Rev. Immunol. *8*, 380–390.

Asnafi, V., Beldjord, K., Boulanger, E., Comba, B., Le Tutour, P., Estienne, M.H., Davi, F., Landman-Parker, J., Quartier, P., Buzyn, A., et al. (2003). Analysis of TCR, pT α, and RAG-1 in T-acute lymphoblastic leukemias improves understanding of early human T-lymphoid lineage commitment. Blood *101*, 2693–2703.

Asnafi, V., Beldjord, K., Libura, M., Villarese, P., Millien, C., Ballerini, P., Kuhlein, E., Lafage-Pochitaloff, M., Delabesse, E., Bernard, O., and Macintyre, E. (2004). Age-related phenotypic and oncogenic differences in T-cell acute lymphoblastic leukemias may reflect thymic atrophy. Blood *104*, 4173–4180.

Bassing, C.H., Tillman, R.E., Woodman, B.B., Canty, D., Monroe, R.J., Sleckman, B.P., and Alt, F.W. (2003). T cell receptor (TCR) α/δ locus enhancer identity and position are critical for the assembly of TCR δ and α variable region genes. Proc. Natl. Acad. Sci. USA *100*, 2598–2603.

Bernard, O.A., Busson-LeConiat, M., Ballerini, P., Mauchauffé, M., Della Valle, V., Monni, R., Nguyen Khac, F., Mercher, T., Penard-Lacronique, V., Pasturaud, P., et al. (2001). A new recurrent and specific cryptic translocation, t(5;14)(q35;q32), is associated with expression of the Hox11L2 gene in T acute lymphoblastic leukemia. Leukemia *15*, 1495–1504.

Cauwelier, B., Dastugue, N., Cools, J., Poppe, B., Herens, C., De Paepe, A., Hagemeijer, A., and Speleman, F. (2006). Molecular cytogenetic study of 126 unselected T-ALL cases reveals high incidence of TCRbeta locus rearrangements and putative new T-cell oncogenes. Leukemia *20*, 1238–1244.

De Keersmaecker, K., Real, P.J., Gatta, G.D., Palomero, T., Sulis, M.L., Tosello, V., Van Vlierberghe, P., Barnes, K., Castillo, M., Sole, X., et al. (2010). The TLX1 oncogene drives aneuploidy in T cell transformation. Nat. Med. *16*, 1321–1327.

Degos, L. (1992). All-trans-retinoic acid treatment and retinoic acid receptor α gene rearrangement in acute promyelocytic leukemia: a model for differentiation therapy. Int. J. Cell Cloning *10*, 63–69.

Dik, W.A., Pike-Overzet, K., Weerkamp, F., de Ridder, D., de Haas, E.F., Baert, M.R., van der Spek, P., Koster, E.E., Reinders, M.J., van Dongen, J.J., et al. (2005). New insights on human T cell development by quantitative T cell receptor gene rearrangement studies and gene expression profiling. J. Exp. Med. *201*, 1715–1723.

Dik, W.A., Nadel, B., Przybylski, G.K., Asnafi, V., Grabarczyk, P., Navarro, J.M., Verhaaf, B., Schmidt, C.A., Macintyre, E.A., van Dongen, J.J., and Langerak, A.W. (2007). Different chromosomal breakpoints impact the level of LMO2 expression in T-ALL. Blood *110*, 388–392.

Dittmer, J. (2003). The biology of the Ets1 proto-oncogene. Mol. Cancer *2*, 29.

Eyquem, S., Chemin, K., Fasseu, M., and Bories, J.C. (2004). The Ets-1 transcription factor is required for complete pre-T cell receptor function and allelic exclusion at the T cell receptor β locus. Proc. Natl. Acad. Sci. USA *101*, 15712–15717.

Ferrando, A.A., Neuberg, D.S., Staunton, J., Loh, M.L., Huard, C., Raimondi, S.C., Behm, F.G., Pui, C.H., Downing, J.R., Gilliland, D.G., et al. (2002). Gene expression signatures define novel oncogenic pathways in T cell acute lymphoblastic leukemia. Cancer Cell *1*, 75–87.

Giese, K., Kingsley, C., Kirshner, J.R., and Grosschedl, R. (1995). Assembly and function of a TCR α enhancer complex is dependent on LEF-1-induced DNA bending and multiple protein-protein interactions. Genes Dev. *9*, 995–1008.

Giresi, P.G., Kim, J., McDaniell, R.M., Iyer, V.R., and Lieb, J.D. (2007). FAIRE (Formaldehyde-Assisted Isolation of Regulatory Elements) isolates active regulatory elements from human chromatin. Genome Res. *17*, 877–885.

75, or 150 ng of cDNA (lanes 2–4, respectively) and 1, 10, or 100 ng of genomic DNA (lanes 5–7, respectively) amplified using *TCR-TLX1* hybrid primers. The absence of genomic DNA contamination in the cDNA fractions was tested by qPCR using albumin-specific primers (lane 8).

(C) Schematic representations of the observed 5′ (Der[14]) and hypothetical 3′ (Der[10]) types of *TCRδ-TLX1* translocations. The nucleotide sequences of two 3′ *type TCRδ-TLX1* junctions amplified from healthy thymi are shown; N regions and Dδ3-specific nucleotides are indicated in bold and lowercase letters, respectively.

(D) Model of how TLX1 addiction may drive autoselection of chromosomal translocations via *trans* repression of the Eα enhanceosome. (Left) In t(7;10) translocation, TLX1 ectopic expression is driven by the TCRβ gene enhancer (Eβ), leading to Eα repression and inhibition of *TCRα* gene rearrangement. (Right) An identical scenario occurs when TLX1 ectopic expression is driven by TCRδ regulatory elements, i.e., in a subset of t(10;14) in which TLX1 and Eα are segregated on different derivative chromosomes. (Middle) In a distinct subset of t(10;14), TLX1 segregates on der(10) and is linked to Eα. Eα-driven TLX1 expression leads to Eα repression and the extinction of its own expression. This form of t(10;14) can be found in the thymus from hematologically healthy individuals, but not in T-ALL samples, implying that the resulting unsustained/cyclic TLX1 expression may not be sufficient for full leukemic transformation.

See also Figure S3.

Hawwari, A., and Krangel, M.S. (2005). Regulation of TCR δ and α repertoires by local and long-distance control of variable gene segment chromatin structure. J. Exp. Med. *202*, 467–472.

Hernández-Munain, C., Sleckman, B.P., and Krangel, M.S. (1999). A developmental switch from TCR delta enhancer to TCR α enhancer function during thymocyte maturation. Immunity *10*, 723–733.

Ho, I.C., Yang, L.H., Morle, G., and Leiden, J.M. (1989). A T-cell-specific transcriptional enhancer element 3′ of C α in the human T-cell receptor α locus. Proc. Natl. Acad. Sci. USA *86*, 6714–6718.

Ho, I.C., Bhat, N.K., Gottschalk, L.R., Lindsten, T., Thompson, C.B., Papas, T.S., and Leiden, J.M. (1990). Sequence-specific binding of human Ets-1 to the T cell receptor α gene enhancer. Science *250*, 814–818.

Holland, P.W., Booth, H.A., and Bruford, E.A. (2007). Classification and nomenclature of all human homeobox genes. BMC Biol. *5*, 47.

Hollenhorst, P.C., Chandler, K.J., Poulsen, R.L., Johnson, W.E., Speck, N.A., and Graves, B.J. (2009). DNA specificity determinants associate with distinct transcription factor functions. PLoS Genet. *5*, e1000778.

Ikawa, T., Hirose, S., Masuda, K., Kakugawa, K., Satoh, R., Shibano-Satoh, A., Kominami, R., Katsura, Y., and Kawamoto, H. (2010). An essential developmental checkpoint for production of the T cell lineage. Science *329*, 93–96.

Krangel, M.S., Hernandez-Munain, C., Lauzurica, P., McMurry, M., Roberts, J.L., and Zhong, X.P. (1998). Developmental regulation of V(D)J recombination at the TCR α/δ locus. Immunol. Rev. *165*, 131–147.

Li, A., Rue, M., Zhou, J., Wang, H., Goldwasser, M.A., Neuberg, D., Dalton, V., Zuckerman, D., Lyons, C., Silverman, L.B., et al; Dana-Farber Cancer Institute ALL Consortium. (2004). Utilization of Ig heavy chain variable, diversity, and joining gene segments in children with B-lineage acute lymphoblastic leukemia: implications for the mechanisms of VDJ recombination and for pathogenesis. Blood *103*, 4602–4609.

Li, R., Pei, H., and Watson, D.K. (2000). Regulation of Ets function by protein-protein interactions. Oncogene *19*, 6514–6523.

Look, A.T. (1997). Oncogenic transcription factors in the human acute leukemias. Science *278*, 1059–1064.

Mann, R.S., Lelli, K.M., and Joshi, R. (2009). Hox specificity unique roles for cofactors and collaborators. Curr. Top. Dev. Biol. *88*, 63–101.

Marculescu, R., Vanura, K., Le, T., Simon, P., Jäger, U., and Nadel, B. (2003). Distinct t(7;9)(q34;q32) breakpoints in healthy individuals and individuals with T-ALL. Nat. Genet. *33*, 342–344.

Marculescu, R., Vanura, K., Montpellier, B., Roulland, S., Le, T., Navarro, J.M., Jäger, U., McBlane, F., and Nadel, B. (2006). Recombinase, chromosomal translocations and lymphoid neoplasia: targeting mistakes and repair failures. DNA Repair (Amst.) *5*, 1246–1258.

Mauvieux, L., Villey, I., and de Villartay, J.P. (2003). TEA regulates local TCR-Jalpha accessibility through histone acetylation. Eur. J. Immunol. *33*, 2216–2222.

McMurry, M.T., and Krangel, M.S. (2000). A role for histone acetylation in the developmental regulation of VDJ recombination. Science *287*, 495–498.

Merabet, S., Pradel, J., and Graba, Y. (2005). Getting a molecular grasp on Hox contextual activity. Trends Genet. *21*, 477–480.

Monroe, R.J., Sleckman, B.P., Monroe, B.C., Khor, B., Claypool, S., Ferrini, R., Davidson, L., and Alt, F.W. (1999). Developmental regulation of TCR δ locus accessibility and expression by the TCR δ enhancer. Immunity *10*, 503–513.

Owens, B.M., Zhu, Y.X., Suen, T.C., Wang, P.X., Greenblatt, J.F., Goss, P.E., and Hawley, R.G. (2003). Specific homeodomain-DNA interactions are required for HOX11-mediated transformation. Blood *101*, 4966–4974.

Papp, B., and Müller, J. (2006). Histone trimethylation and the maintenance of transcriptional ON and OFF states by trxG and PcG proteins. Genes Dev. *20*, 2041–2054.

Pui, C.H., Relling, M.V., and Downing, J.R. (2004). Acute lymphoblastic leukemia. N. Engl. J. Med. *350*, 1535–1548.

Roberts, C.W., Shutter, J.R., and Korsmeyer, S.J. (1994). Hox11 controls the genesis of the spleen. Nature *368*, 747–749.

Roberts, J.L., Lauzurica, P., and Krangel, M.S. (1997). Developmental regulation of VDJ recombination by the core fragment of the T cell receptor α enhancer. J. Exp. Med. *185*, 131–140.

Sauvageau, M., and Sauvageau, G. (2008). Polycomb group genes: keeping stem cell activity in balance. PLoS Biol. *6*, e113.

Shen, W.F., Krishnan, K., Lawrence, H.J., and Largman, C. (2001). The HOX homeodomain proteins block CBP histone acetyltransferase activity. Mol. Cell. Biol. *21*, 7509–7522.

Shirasawa, S., Arata, A., Onimaru, H., Roth, K.A., Brown, G.A., Horning, S., Arata, S., Okumura, K., Sasazuki, T., and Korsmeyer, S.J. (2000). Rnx deficiency results in congenital central hypoventilation. Nat. Genet. *24*, 287–290.

Sieweke, M.H., Tekotte, H., Frampton, J., and Graf, T. (1996). MafB is an interaction partner and repressor of Ets-1 that inhibits erythroid differentiation. Cell *85*, 49–60.

Sleckman, B.P., Bardon, C.G., Ferrini, R., Davidson, L., and Alt, F.W. (1997). Function of the TCR α enhancer in αβ and γδT cells. Immunity *7*, 505–515.

Soulier, J., Clappier, E., Cayuela, J.M., Regnault, A., Garcia-Peydro, M., Dombret, H., Baruchel, A., Toribio, M.L., and Sigaux, F. (2005). HOXA genes are included in genetic and biologic networks defining human acute T-cell leukemia (T-ALL). Blood *106*, 274–286.

Spicuglia, S., Payet, D., Tripathi, R.K., Rameil, P., Verthuy, C., Imbert, J., Ferrier, P., and Hempel, W.M. (2000). TCRalpha enhancer activation occurs via a conformational change of a pre-assembled nucleo-protein complex. EMBO J. *19*, 2034–2045.

Spits, H. (2002). Development of αβ T cells in the human thymus. Nat. Rev. Immunol. *2*, 760–772.

von Boehmer, H., Aifantis, I., Azogui, O., Feinberg, J., Saint-Ruf, C., Zober, C., Garcia, C., and Buer, J. (1998). Crucial function of the pre-T-cell receptor (TCR) in TCR β selection, TCR β allelic exclusion and αβ versus γδ lineage commitment. Immunol. Rev. *165*, 111–119.

Cancer Cell
Article

DNA Damage Response and Inflammatory Signaling Limit the MLL-ENL-Induced Leukemogenesis In Vivo

Sylvia Takacova,[1] Robert Slany,[4] Jirina Bartkova,[5] Viktor Stranecky,[6] Petr Dolezel,[1] Pavla Luzna,[1,2] Jiri Bartek,[3,5,*] and Vladimir Divoky[1,*]
[1]Department of Biology
[2]Department of Histology and Embryology
[3]Institute of Molecular and Translational Medicine
Faculty of Medicine and Dentistry, Palacky University, 77515 Olomouc, Czech Republic
[4]Department of Genetics, University Erlangen, D-91058 Erlangen, Germany
[5]Danish Cancer Society Research Center, DK-2100 Copenhagen, Denmark
[6]Institute of Inherited Metabolic Disorders, Charles University in Prague, First Faculty of Medicine, 12808 Prague, Czech Republic
*Correspondence: jb@cancer.dk (J.B.), divoky@tunw.upol.cz (V.D.)
DOI 10.1016/j.ccr.2012.01.021

SUMMARY

Activation of the MLL-ENL-ERtm oncogene initiates aberrant proliferation of myeloid progenitors. Here, we show induction of a fail-safe mechanism mediated by the DNA damage response (DDR) machinery that results in activation of the ATR/ATM-Chk1/Chk2-p53/p21^{CIP1} checkpoint and cellular senescence at early stages of cellular transformation caused by a regulatable MLL-ENL-ERtm in mice. Furthermore, we identified the transcription program underlying this intrinsic anticancer barrier, and DDR-induced inflammatory regulators that fine-tune the signaling toward senescence, thereby modulating the fate of MLL-ENL-immortalized cells in a tissue-environment-dependent manner. Our results indicate that DDR is a rate-limiting event for acquisition of stem cell-like properties in MLL-ENL-ERtm-mediated transformation, as experimental inhibition of the barrier accelerated the transition to immature cell states and acute leukemia development.

INTRODUCTION

During the multistep pathogenesis of leukemia, a pool of leukemia stem cells (LSCs) emerges, capable of limitless self-renewal and disease maintenance. LSCs can originate from hematopoietic cells at different developmental stages. Mixed-lineage leukemia (MLL) fusion oncogenes can transform committed progenitors to LSCs by reactivation of a self-renewal-associated transcription program (Cozzio et al., 2003; Krivtsov et al., 2006). Several mouse models showed that *Mll* fusions expressed at physiological levels cause myeloproliferation without the capacity to propagate the disease in transplanted animals (Dobson et al., 1999; Wang et al., 2005). *Mll* fusions initiate the preleukemia stem cell (pre-LSC) state, and acquisition of further mutations or high dosage of oncogene expression is necessary for full transformation and development of acute leukemia (Wang et al., 2005; Chen et al., 2008).

Research on solid tumors has identified a DDR barrier at early pre-invasive stages of tumorigenesis. Oncogene-induced hyperproliferation and DNA replication stress trigger the cell-intrinsic DDR machinery that induces senescence or cell death and delays progression to full malignancy (Bartkova et al., 2005, 2006; Gorgoulis et al., 2005; Di Micco et al., 2006; Halazonetis et al., 2008). Recent studies have suggested that DDR cooperates with secreted cytokines in balancing the signaling thresholds and cell-fate decisions between cell proliferation, senescence and death (Bartek et al., 2008; Rodier et al., 2009; Acosta et al., 2008). However, an authentic model to assess

Significance

DNA damage response (DDR) signaling and senescence may pose a biological barrier to progression of diverse types of solid tumors, in part by an ill-defined interplay with inflammatory cytokines. Demonstrating the existence, and understanding the role of analogous phenomena in leukemia may provide novel insights into the molecular pathogenesis and biological complexity of hematological malignancies. Using a mouse model with long latency of mixed-lineage leukemia (MLL) development, we identify DDR as a critical mechanism rate-limiting for malignant transformation by the MLL-ENL oncogene, synergizing with inflammatory factors in checkpoint signaling and senescence, thereby counteracting leukemogenesis. This in vivo model of DDR and inflammatory barriers cooperating in their natural settings has implications for understanding cancer stem cell evolution and multistep tumorigenesis.

such candidate DDR and cytokine barriers during the long-latency development of any malignancy in vivo is still missing.

Inspired by these recent developments, we wished to examine whether a DDR- and/or cytokine-related barrier analogous to solid tumors and oncogene-transformed fibroblasts might also impact leukemogenesis. In addition, we wished to test the potential significance of the barrier concept in an adequate animal model. To address these issues, we generated a conditional mouse model, in which the *Mll-ENL* fusion oncogene is expressed in the physiological context of the endogenous *Mll locus* and its activity is regulatable with tamoxifen in vivo.

RESULTS

Generation of a Regulatable *Mll-ENL-ERtm* Knock-In Mouse

We created a mouse model wherein the protein function of the *Mll-ENL* oncogene depends on tamoxifen (TAM) or 4-hydroxytamoxifen (4-oht) due to fusion with the mutated estrogen-binding domain of the estrogen receptor (ERtm) (Littlewood et al., 1995). The *Mll-ENL-ERtm* fusion gene was used to engineer the mouse knock-in allele in the v6.5 mouse embryonic stem cells (ESCs) (Figure 1A; Figures S1A and S1B available online). We confirmed the expression of the *Mll-ENL-ERtm* allele in c-Kit$^+$ hematopoietic progenitors isolated from the BM of the knock-in mice (Figure S1C). The transcriptional transactivation activity of the fusion gene and serial replating ability of the Mll-ENL-ERtm c-Kit$^+$ BM cells were strictly dependent on 4-oht (Figures S1D and S1E).

Activated MLL-ENL-ERtm Induces Myeloproliferation in Both BM and Spleen with Different Hematopoietic Characteristics

After 7 months of TAM administration, the Mll-ENL-ERtm mice developed a myeloproliferative disease with a 100% penetrance, which progressed into the terminal stage in five of ten animals after a long period (mean survival: 592 ± 112 days) of continuous TAM provision. To study early and late phenotypic characteristics of the MLL-ENL-ERtm-mediated disease in vivo, we monitored hematopoiesis in the Mll-ENL-ERtm/TAM mice at the early (7 months) and terminal stage of disease. Time-matched TAM-treated wild-type mice served as controls for both stages. Early changes in the BM were characterized by hypercellularity with expansion of mature myeloid elements (band neutrophils) (Figures 1B and S2A), consistent with fluorescence-activated cell sorting (FACS) analysis showing an increase in Mac-1$^+$/Gr-1$^+$ cell population and emergence of a c-Kit$^+$/Mac-1$^+$ subpopulation in some animals (Figure 1C). At this time point, a left shift in granulopoiesis occurred with an increase of band neutrophils and monocytes at the expense of lymphocytes in the spleen (Figure S2B). The myeloid expansion in the spleen progressed at the terminal stage of disease (Figure 1D, right). This was associated with a gradual increase of Mac-1$^+$/Gr-1$^+$ myeloid cells and a decrease of B220$^+$/CD19$^+$ and CD19$^+$/IgM$^+$ B-lymphoid cells. Notably, there was an expansion of the c-Kit$^+$/Mac-1$^+$ subpopulation (Figure 1E). The terminal stage was also associated with high numbers of white blood cells, large numbers of mature segmented neutrophils, less mature band neutrophils and only a few percent of myeloblasts in the peripheral blood. There was occasionally a left shift in granulopoiesis and elevated monocytes (Figure 1F), and myeloid infiltration into the liver and kidney (Figure S2C). Some mice developed solid tumors in the mesenterium, formed by Mll-ENL-ERtm positive myeloid cells (data not shown), indicating the invasive and angiogenic nature of the MLL-ENL-ERtm-transformed cells. The initial expansion of the granulocytic lineage in the BM eventually culminated in a virtual depletion of the tissue over time. Thus, activation of the MLL-ENL-ERtm oncogene leads to abnormal expansion of the granulocytic lineage in the BM and granulo-monocytic lineages in the spleen with a potential to progress into a malignant phenotype.

Mll-ENL-ERtm hematopoietic progenitors derived from both tissues at the early stage showed increased 4-oht-dependent myeloid colony forming ability in methylcellulose cultures. In the absence of 4-oht, both CFU-GM and CFU-G colonies were lower in numbers, size, and cellularity (Figures 2A and 2B, top and bottom right panels). Besides the typical CFU-GM and CFU-G colonies, we often found colonies that were hypercellular and appeared more immature (Figure 2B, top left panel). These results suggest that the active MLL-ENL-ERtm oncogene enhances proliferation and increases survival of committed myeloid progenitors, features that could be reverted after deactivation of the oncogene. Colonies did not grow in the absence of growth factors and cytokines (with or without 4-oht) suggesting that MLL-ENL-ERtm does not confer growth factor-independent properties to immortalized progenitors.

MLL-ENL-ERtm-Induced Proliferation/Self-Renewal of Myeloid Cells Leads to Activation of a Fail-Safe Mechanism

Given the observed distinct patterns of disease in the two tissues, we next examined the proliferation rates of the expanded Mac-1$^+$ cell population in the BM and spleen of the Mll-ENL-ERtm/TAM mice by estimating bromodeoxyuridine-(BrdU) incorporation at four time points: 7, 8, 9, and 10 months. There was a striking difference in cell proliferation between the two sites. The vast majority (90%) of Mac-1$^+$ cells in the BM showed BrdU-positivity at 7 months of TAM treatment, followed by a dramatic loss of their long-term proliferative potential, as evidenced at the 8-month time point by the lack (below 1%) of BrdU incorporation. In contrast, the initial hyperproliferation of Mac-1$^+$ cells was more moderate in the spleen (40.4% of BrdU$^+$ at 7 months) and importantly, proliferating Mac-1$^+$ cells were reduced yet remained clearly detectable also during disease progression at the 9- and 10-month time points (23.8% BrdU$^+$ among Mac-1$^+$ cells) (Figures 3A, 3C, left, and 3E).

These findings prompted us to test whether the proliferation phenotypes could reflect induction of a fail-safe mechanism, possibly differentially in the BM versus spleen. To address this question, we examined total BM cells and spleen sections (from the Mll-ENL-ERtm/TAM mice that were used for the BrdU-incorporation assay) for the senescence-associated beta-galactosidase (SA-β-gal) (Dimri et al., 1995). In the BM, SA-β-gal was induced in neutrophils (Figure 3B) in parallel with the loss of their proliferative potential by 8 months of TAM treatment (Figure 3E, left). Consistent with reduced proliferation of Mac-1$^+$ cells in the spleen, we detected an accumulation of SA-β-gal above the physiological level in the Mll-ENL-ERtm/TAM mice (9–10 months of TAM) compared to wild-type/TAM

controls (Figure 3C, right). Compared to early stage (7 months of TAM treatment), spleen displayed decreased proliferation and appearance of SA-β-gal$^+$ cells at the 9- to 10-month time points (Figures 3C and 3E, right). These results suggest a balanced state of proliferation and senescence in the expanding myeloid cell population in the spleen. Collectively, these findings indicate that the MLL-ENL-ERtm-initiated hyperproliferation is followed by induction of cellular senescence that counteracts the aberrant proliferation of Mac-1$^+$ cells, a process that is more robust in the BM compared with the spleen.

The ATR-Chk1 DDR Pathway Is Activated in the Mac-1$^+$ Population

The MLL-ENL-ERtm-induced hyperproliferation and senescence prompted us to search for potential activation of DNA damage signaling, a response to oncogene-evoked replication stress reported for human cells and solid tumors (Halazonetis et al., 2008). Indeed, phosphorylation of the ataxia telangiectasia mutated and RAD3-related kinase at serine 428 (pATRS428), which is induced in response to replication-associated DNA damage, was detected in the majority of Mac-1$^+$ cells both in the BM and spleen, coincident with the early MLL-ENL-ERtm-induced hyperproliferation (7 months of TAM treatment), in contrast to absence of pATRS428 in Mac-1$^+$ cells of either organ in wild-type/TAM control mice (Figure S3A). Importantly, data very similar to pATRS428 were obtained by both immunohistochemistry and immunofluorescence using a recently published antibody against ATR autophosphorylated at threonine 1989 (T1989) (Figures 3D and S3A), a site crucial for ATR activation (Liu et al., 2011; Nam et al., 2011). The specificity of the two antibodies to phosphorylated ATR was validated using a number of tests and models including ATR-deficient control cells (Figure S3B; and data not shown). Given the consistent results seen with both antibodies, we refer to both markers collectively as pATR. Consistently, pATR was accompanied by downstream markers of ATR signaling, including histone H2AX phosphorylated at serine 139 (γH2AX) and checkpoint kinase 1 (Chk1) phosphorylated at serine 345 (pChk1S345) in Mac-1$^+$ cells in both BM and spleen (Figure 3D).

To examine whether DDR signaling persists across disease stages, we followed the level of pATR and the γH2AX signal at the time points assessed for proliferation and senescence. Analogous to proliferation and senescence phenotypes, there was a striking difference in the ATR-linked signaling between BM and spleen. In the BM, there was an increase both in the nuclear γH2AX signal intensity (data not shown) and number of Mac-1$^+$/γH2AX$^+$ cells that correlated inversely with the number of Mac-1$^+$/BrdU$^+$ cells in the transition period to senescence between 7 and 8 months of TAM treatment (Figure 3E, left). Interestingly, pATR became undetectable and the intensity of γH2AX was decreased (but not eliminated) in the senescent cells (Figure S3C). In contrast to BM, pATR was present both during the early (proliferative) and progression stages concomitant even with the partial senescence phenotype in the spleen (Figure S3D), a scenario that is consistent with partly ongoing proliferation and less pronounced γH2AX compared to BM (Figure 3E, right).

Collectively, these results indicate that in response to MLL-ENL, DDR is indeed activated in vivo, and to a higher degree in BM compared to spleen. Increased signaling of the ATR pathway and decrease in proliferation are gradual processes that precede senescence in the BM. The extent of DDR signaling correlates well with the efficiency of senescence induction in BM versus spleen, suggesting the signaling threshold may be influenced by the local tissue microenvironment.

ATM Is Required for an Effective Activation of the p53/p21^{CIP1} Pathway

The differences in γH2AX patterns between BM and spleen, and partial persistence of γH2AX in the BM even after loss of pATR led us to test whether the ataxia telangiectasia-mutated (ATM) kinase might be activated in response to MLL-ENL, particularly in the BM. Indeed, the early proliferation disease stage in the BM was associated with moderate levels of activated ATM phosphorylated at serine 1981 (pATMS1981 and pATM) seen as one to two nuclear foci in about 12% of cells. The level of pATM gradually increased to 43% of cells, and five to ten foci in most nuclei, during the transition toward senescence (Figures 4A, top, and 4B). Furthermore, active p53 (phosphorylated at serine 18, p-p53Ser18) and enhanced expression of its transcriptional target *p21^{CIP1}* (Figures 4A, bottom, and 4C) became apparent, in parallel with high levels of pATM. pATM was detectable in ~90% of myeloid cells in the senescent state of the MII-ENL-ERtm/TAM BM (Figure 4D) consistent with the high proportion of γH2AX$^+$/Mac-1$^+$ cells. Notably, ATM was not activated in the spleen (data not shown), consistent with the overall lower extent, and gradual elimination of DDR in this tissue. In contrast to the activated DDR signaling, we did not detect any increase of *p16^{INK4A}* mRNA or protein expression in the senescent BM (data not shown).

These results indicate that gradually increasing MLL-ENL-induced DDR, through combined ATR and ATM signaling, may lead to preferential activation of p53/p21^{CIP1} and more robust proliferation arrest and cellular senescence in the BM, compared to overall milder phenotypes and lack of ATM activation in the spleen.

Gene Expression Signatures of the Transition from Proliferation to Senescence

To better understand the MLL-ENL-induced dynamic cellular phenotypes and identify potential regulators of the observed cell states, we next profiled gene expression at three time points: 1), the early high proliferation with low DDR signaling; 2), the transition period of lower proliferation and high DDR activity; and 3), the senescence in the BM. Compared to BM from matched wild-type/TAM controls at each time point, gene ontology (GO) annotations of upregulated transcripts revealed enrichment of genes related to innate and adaptive immune response across the entire time course analyzed (Figure 5A). Using a pairwise analysis, we then determined unique and shared expression patterns among the three time points (Figure 5B). The shared immune response genes included those implicated in cell migration and localization, such as *Cx3cr1*, *Ccr1*, *Ccl9*, and *Vav3*, leukocyte activation, such as *Nfam1* or *Slc11a1*, and G protein coupled receptor pathways (*Emr1*, *Emr4*). Furthermore, toll-like receptor (*Tlr*) genes, implicated in cancer and in innate and adaptive immune responses through activation of cytokine and chemokine production (Rakoff-Nahoum and Medzhitov, 2009), were upregulated uniquely in the early proliferation (*Tlr5*), or

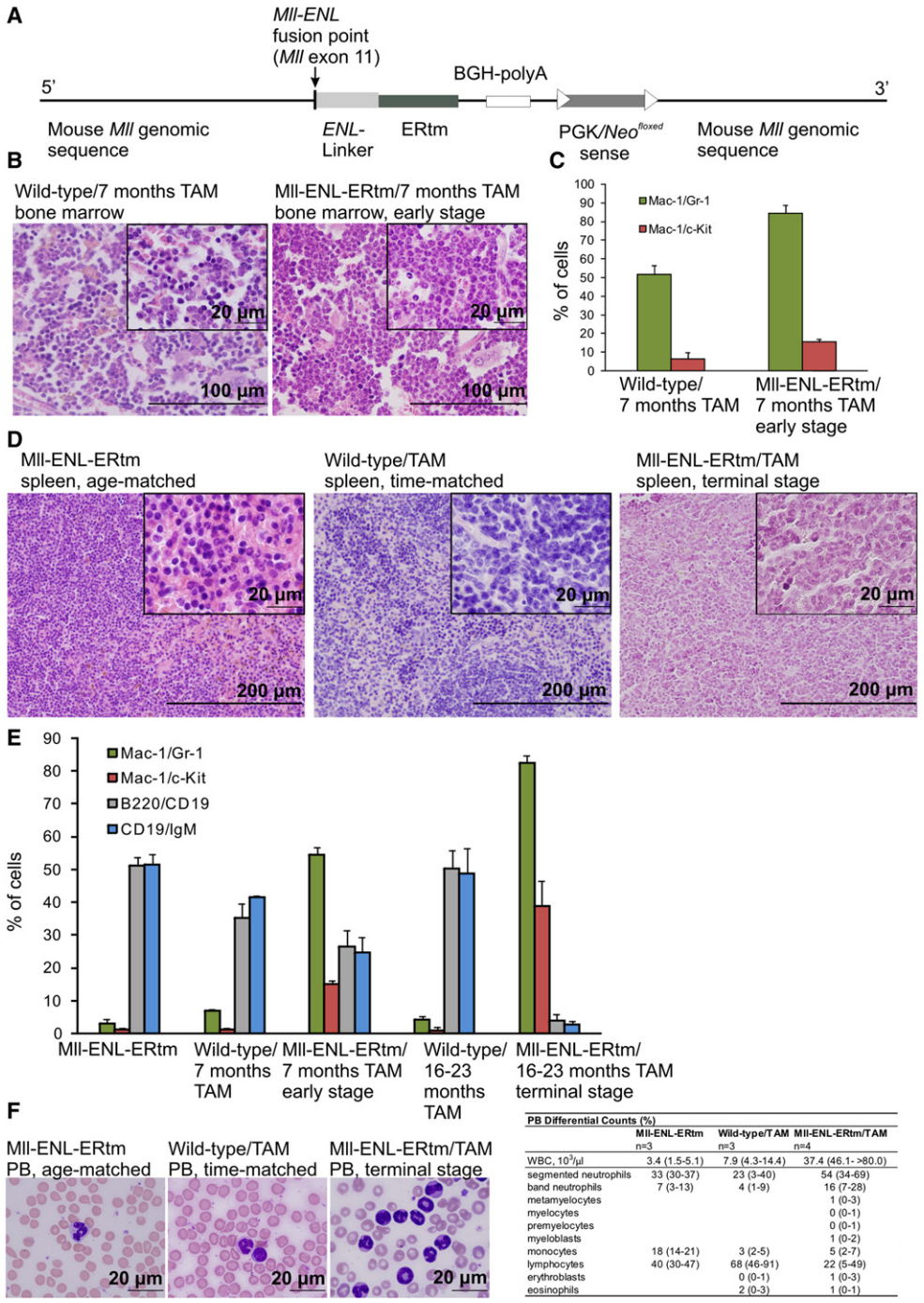

PB Differential Counts (%)	Mll-ENL-ERtm n=3	Wild-type/TAM n=3	Mll-ENL-ERtm/TAM n=4
WBC, 10^3/μl	3.4 (1.5-5.1)	7.9 (4.3-14.4)	37.4 (46.1- >80.0)
segmented neutrophils	33 (30-37)	23 (3-40)	54 (34-69)
band neutrophils	7 (3-13)	4 (1-9)	16 (7-28)
metamyelocytes			1 (0-3)
myelocytes			0 (0-1)
premyelocytes			0 (0-1)
myeloblasts			1 (0-2)
monocytes	18 (14-21)	3 (2-5)	5 (2-7)
lymphocytes	40 (30-47)	68 (46-91)	22 (5-49)
erythroblasts		0 (0-1)	1 (0-3)
eosinophils		2 (0-3)	1 (0-1)

Figure 1. Myeloproliferation in the Mll-ENL-ERtm Mice

(A) Schematic representation of the *Mll-ENL-ERtm/Neo^{floxed}* knock-in allele. The *Mll-ENL* fusion point, the estrogen receptor binding domain (ERtm), polyadenylation site (BGH-polyA), and neomycin resistance gene under the phosphoglycerate kinase promoter (PGK/*Neo^{floxed}*) are shown.

(B) Histopathology images: hypercellularity and expansion of mature myeloid cells in the BM of the Mll-ENL-ERtm mice at the early stage of disease compared to wild-type/TAM control. Scale bars represent 100 μm and 20 μm (inset).

(C) FACS determined an increase in Mac-1$^+$/Gr-1$^+$ and Mac-1$^+$/c-Kit$^+$ cells in the BM of early disease stage Mll-ENL-ERtm/TAM mice compared to wild-type/TAM animals. Data represent average cell percentages counted from three mice ± SD.

(D) Spleen histology, expansion of extramedullary hematopoiesis and disruption of the splenic architecture at the terminal stage of disease (right). Scale bars represent 200 μm and 20 μm (inset).

(E) Time course of indicated marker expression at 7 and 16–23 months of TAM treatment in the spleen of the Mll-ENL-ERtm/TAM mice compared to wild-type/TAM mice shows expansion of Mac-1$^+$/Gr-1$^+$ and Mac-1$^+$/c-Kit$^+$ myeloid cells, and decrease in B220$^+$CD19$^+$, CD19$^+$IgM$^+$ B lymphoid cells. Data represent average cell percentages measured by FACS, counted from three mice ± SD.

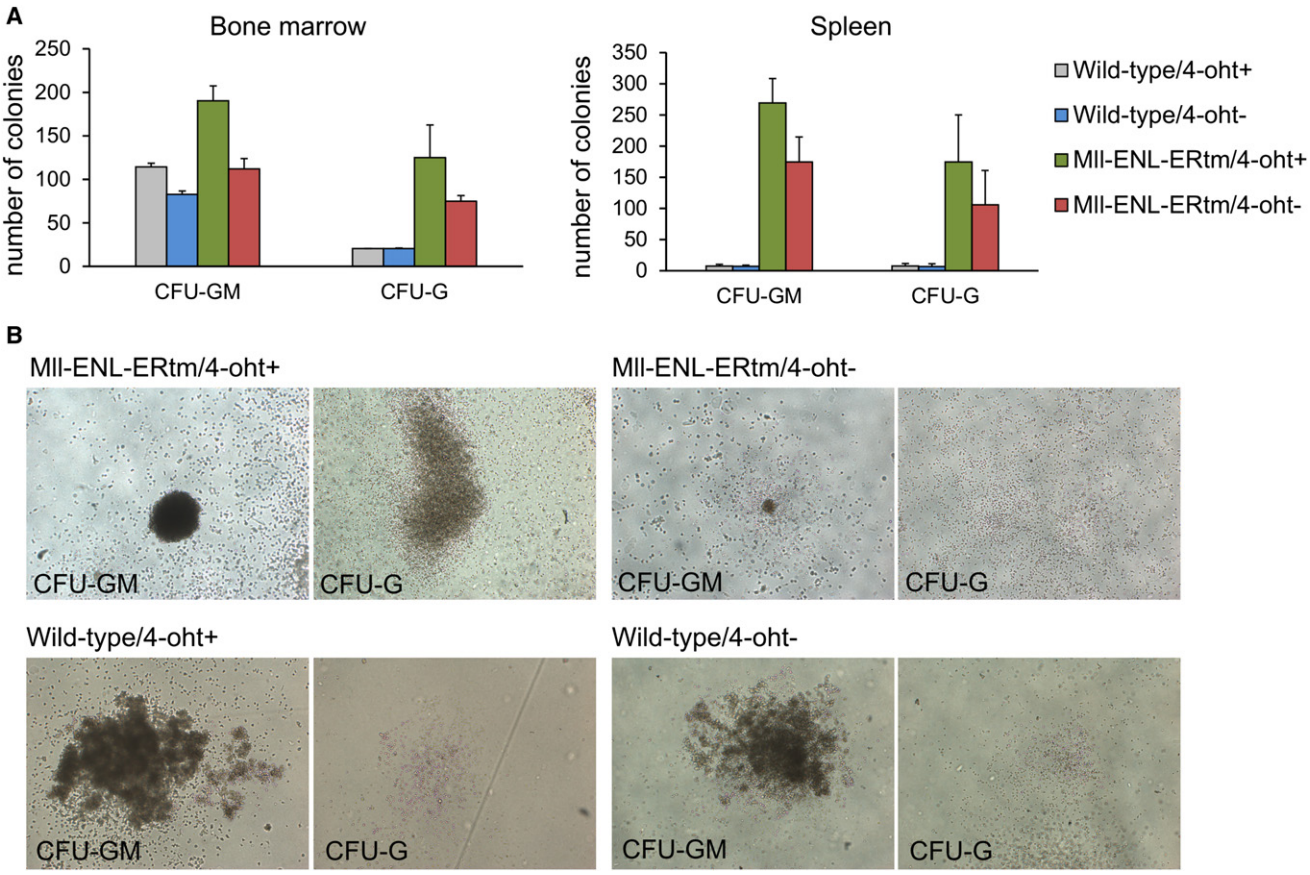

Figure 2. MLL-ENL-ERtm-Dependent Proliferation and Survival of Committed Myeloid Progenitors

(A) Increased myeloid colony formation of the Mll-ENL-ERtm BM (left) and spleen (right) cells derived from TAM-treated mice at early disease stage compared to wild-type/TAM controls. Note lower colony numbers in the absence of 4-oht (experiments performed in duplicates, data represent average colony numbers from two mice ± SD). The same color coding was used for both graphs.

(B) Mll-ENL-ERtm CFU-GM and CFU-G colonies show an immature phenotype in the presence of 4-oht: CFU-GM colonies with compact centers without the halo of single cells and hypercellular, dense CFU-G colonies (top left). Note reversion of the immortalized phenotype and loss of colony formation capacity of the Mll-ENL-ERtm CFU-GMs and CFU-Gs in the absence of 4-oht (top right).

See also Figure S2.

during both the proliferation and transition periods (*Tlr6*). Downstream mediators of TLR signaling, such as *Tnfsf14* (linked to NF-κB signaling), and MAPK and JNK kinase pathway genes such as *Map3k5* and *Fgd4*, were upregulated in the proliferation state. A set of inflammatory response genes such as *Il1f9*, *Nfkbiz*, *Stat6*, *Il1rn*, and *Tnfrsf1b* were upregulated during the proliferation and transition states, and so were two pattern recognition receptors, *Clec7a* and *Clec2i*, implicated in cytokine production.

Another set of genes was strongly yet transiently upregulated only during the transition period of high DDR signaling, followed by a drop to basal levels in senescence. These included immediate early genes such as *Jun*, *Junb*, *Egr1*, *Egr2*, *Zfp36*, *Ier2* and *Ier3*, and *Cebpb*, a candidate key regulator of inflammatory cytokine and chemokine production in oncogene-induced senescence (Acosta et al., 2008). Regulators of inflammation, including chemokine genes *Cxcl2*, *Ccl3*, and *Ccl4*, two key cytokine genes *Tnfa* and *Il1b*, and *Ptgs2*, associated with tumor-promoting inflammation (Wang and Dubois, 2010), were also upregulated (Figure 5C).

For the spleen, differential gene expression profiles were determined for three stages: 1), early (proliferation, induced DDR); 2), progression (partial senescence, DDR maintained); and 3) terminal (proliferation, low or absent DDR, no senescence). By pairwise analysis, we found a set of genes differentially expressed at the early stage and maintained their pattern during disease progression. The upregulated genes were enriched in cell cycle regulators. Interestingly, downregulated genes were enriched in innate immunity genes, acute phase

(F) Representative PB smear with abundant mature myeloid cells (scale bar represents 20 μm) and PB differential counts with a left shift in granulopoiesis at the terminal disease stage. Data are average (data range) from three to four mice, respectively. Data from untreated Mll-ENL-ERtm mice age-matched to leukemic mice at the terminal disease stage are also shown in (D–F).

See also Figure S1.

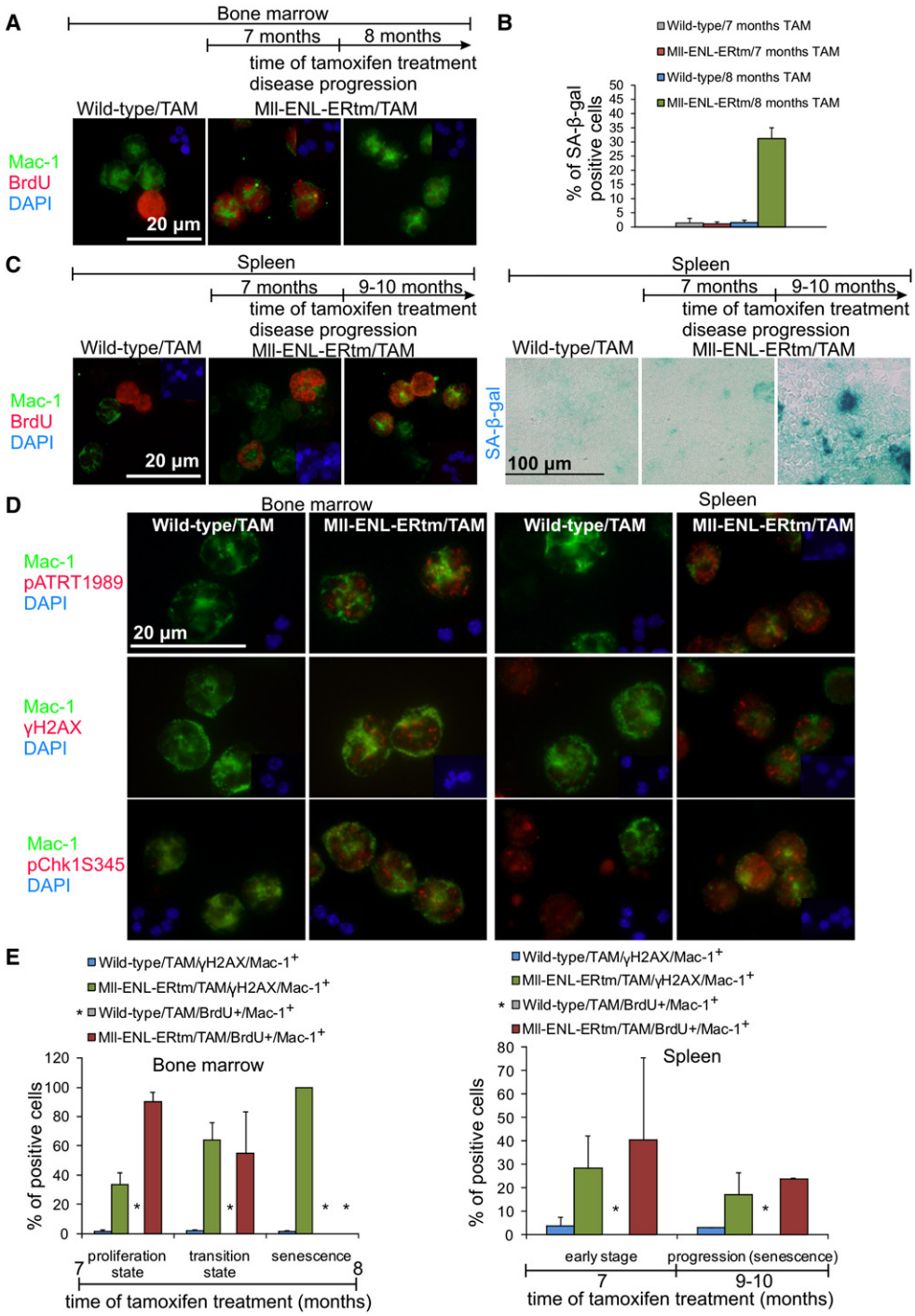

Figure 3. Tissue Specificity of Association between Proliferation Rate, Senescence, and DDR Activation in Mac-1$^+$ Cells during Disease Progression

(A) BrdU-positivity (red) of Mac-1$^+$ (green) cells indicates aberrant proliferation at 7 months of TAM treatment, and BrdU-negativity of Mac-1$^+$ cells shows loss of proliferation by 8 months of TAM treatment in the Mll-ENL-ERtm/TAM BM. Nuclei stained with DAPI (blue). Scale bar represents 20 μm.

(B) Quantification of SA-β-gal assay at 7 and 8 months of TAM treatment in the BM of Mll-ENL-ERtm/TAM mice compared to wild-type controls TAM-treated for 7 months. Average percentages of SA-β-gal positive cells from two to three mice per time point ± SD.

(C) Aberrant proliferation of Mac-1$^+$ cells during disease progression at 7 and 9–10 months of TAM treatment; cytospin preparations, scale bar represents 20 μm (left panel). SA-β-gal staining of spleen sections (right panel) performed at the same time points as the BrdU assay. Scale bar represents 100 μm.

(D) Activation of the ATR/Chk1/γH2AX pathway (red signals) in Mac-1$^+$ (green) cells in both tissues at 7 months of TAM treatment. Nuclei stained with DAPI (blue). Scale bar represents 20 μm.

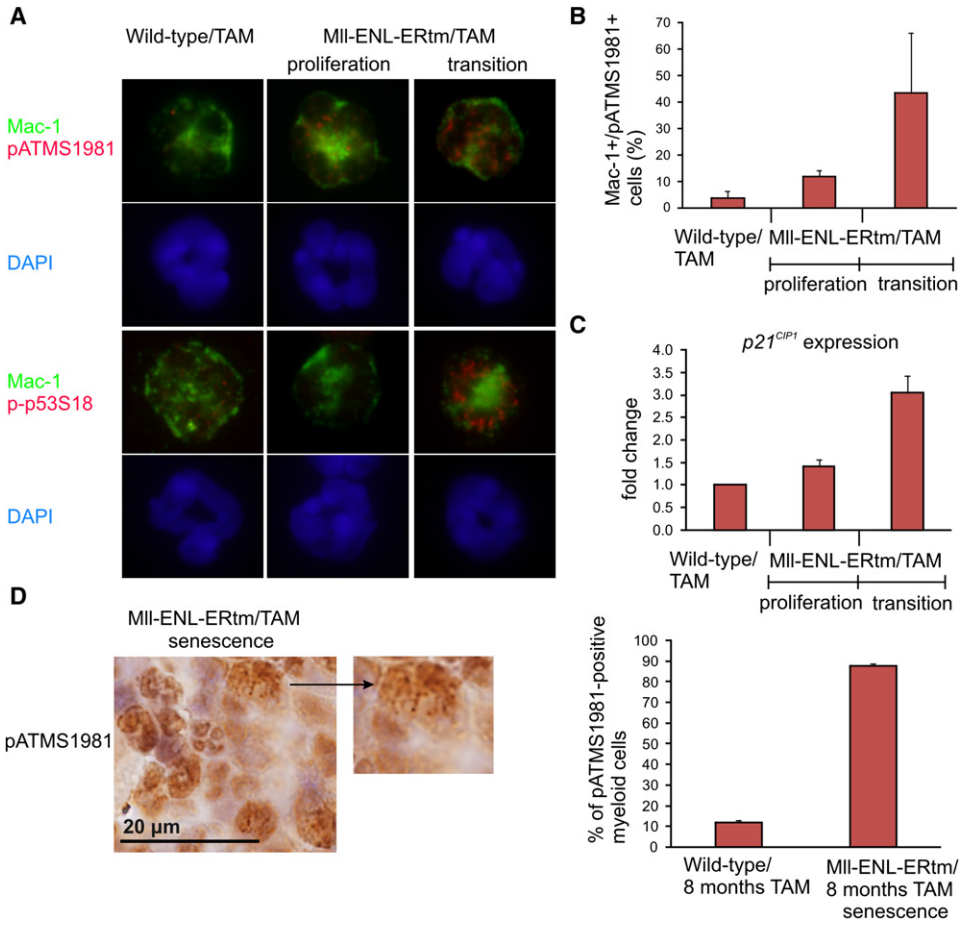

Figure 4. The ATM/p53/p21^{CIP1} Checkpoint Signaling in the Transition Cell State in the Mll-ENL-ERtm/TAM BM

(A) Activation of ATM during transition from proliferation to senescence in the Mac-1$^+$ cell population in the Mll-ENL-ERtm/TAM BM compared to wild-type/TAM mice correlated with phosphorylated p53 (p-p53S18, bottom panel).

(B) Quantification of pATMS1981 in the proliferation and transition cell states compared to wild-type/TAM mice. Data are averages from two mice per genotype and cell state ± SD.

(C) Expression level of *p21^{CIP1}* in the proliferation and transition states in the Mll-ENL-ERtm/TAM BM compared to wild-type/TAM mice. Data are averages from three mice per genotype and cell state ± SD. Each measurement performed in triplicate.

(D) Immunoperoxidase staining (left), and quantification of pATMS1981 in myeloid cells in the Mll-ENL-ERtm/8 months TAM BM associated with senescence (right). pATMS1981 quantified in granulocytes in the BM of wild-type/8 months TAM mice was used as control. Scale bar represents 20 μm. Data are averages from two mice per genotype ± SD.

genes, and those involved in cell activation and migration (Figure 5D). The genes transiently upregulated in the BM during the high-DDR transition period, were not differentially expressed in the spleen (data not shown).

These data suggest that MLL-ENL-ERtm-induced cellular transformation is associated with altered innate and adaptive immune response, manifested as inflammation with characteristic gene expression profiles and phenotypic features that differ in the tissue environments of BM and spleen, respectively. These findings raise questions about the potential interplay and/or hierarchical order of the MLL-ENL-induced DDR activation, senescence, and the inflammatory responses.

CXCL2 and CCL3 Promote DDR Signaling and Cooperate with TNF-α to Induce Senescence in MLL-ENL-ERtm-Immortalized BM Cells

As *Cxcl2* was present in the MLL-ENL-ERtm-induced inflammatory gene set (Figure 5C), and previously implicated in RAS-evoked senescence (Acosta et al., 2008), we hypothesized that CXCL2 may contribute to the MLL-ENL-ERtm-induced DNA damage and senescence in our model. We therefore derived total BM cells from the Mll-ENL-ERtm/TAM mice in the proliferation state and cultured them in the presence of GM-CSF, G-CSF, and 4-oht. Reminiscent of BM in vivo, the DDR markers pATR and γH2AX were present in such cultured cells. Notably,

(E) Inverse correlation between proliferation and DDR in the BM over time (left). Correlation of the proliferation rate of the Mac-1$^+$ spleen cells with DDR across disease stages (right). Average percentages of Mac-1$^+$/BrdU$^+$ and Mac-1$^+$/γH2AX$^+$ cells among total Mac-1$^+$ cells, calculated from three mice per time point ± SD. Asterisks indicate the average value = 0 for wild-type/TAM/BrdU$^+$/Mac-1$^+$ and Mll-ENL-ERtm/TAM/BrdU$^+$/Mac-1$^+$ in the senescence state in the BM. See also Figure S3.

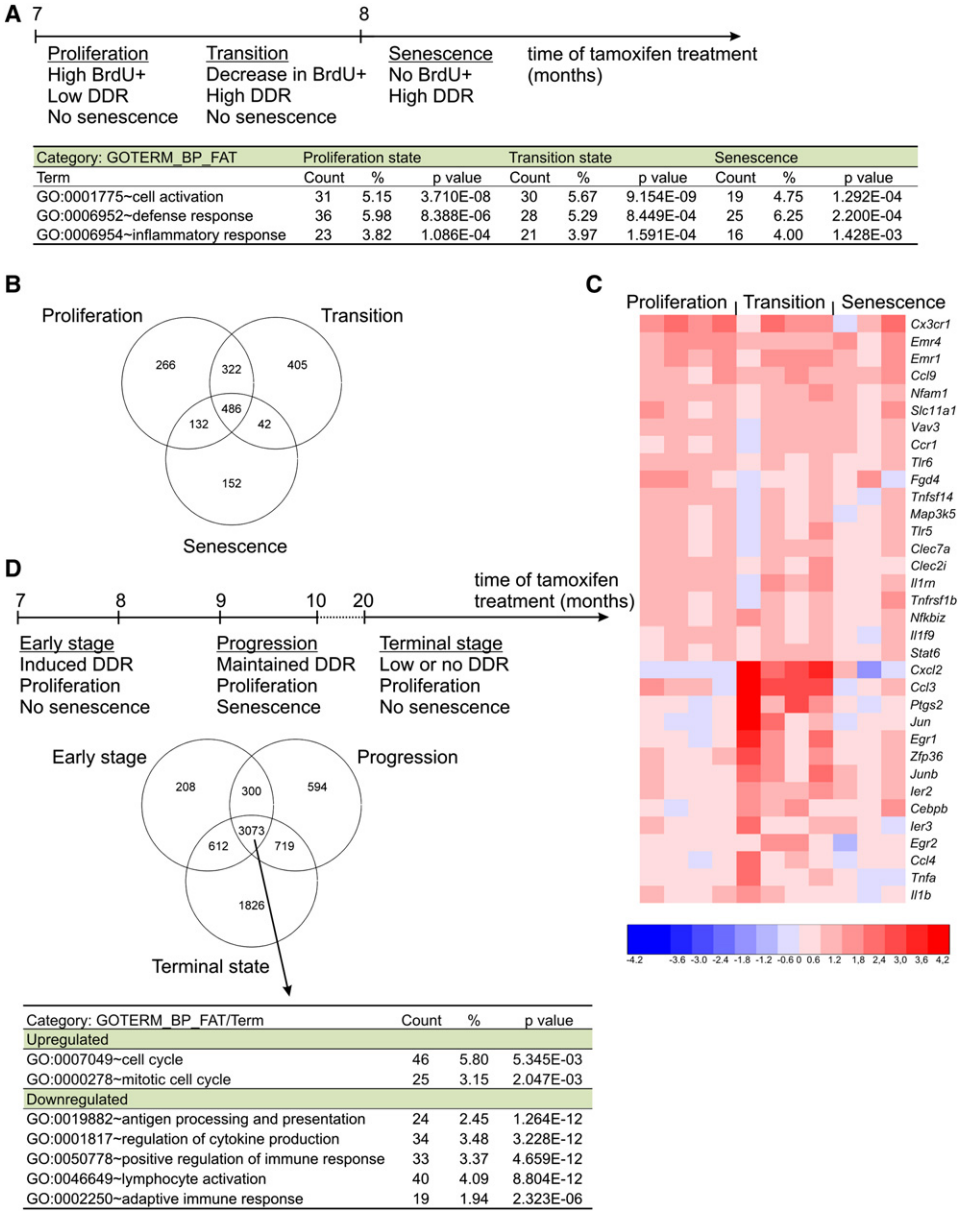

Category: GOTERM_BP_FAT	Proliferation state			Transition state			Senescence		
Term	Count	%	p value	Count	%	p value	Count	%	p value
GO:0001775~cell activation	31	5.15	3.710E-08	30	5.67	9.154E-09	19	4.75	1.292E-04
GO:0006952~defense response	36	5.98	8.388E-06	28	5.29	8.449E-04	25	6.25	2.200E-04
GO:0006954~inflammatory response	23	3.82	1.086E-04	21	3.97	1.591E-04	16	4.00	1.428E-03

Category: GOTERM_BP_FAT/Term	Count	%	p value
Upregulated			
GO:0007049~cell cycle	46	5.80	5.345E-03
GO:0000278~mitotic cell cycle	25	3.15	2.047E-03
Downregulated			
GO:0019882~antigen processing and presentation	24	2.45	1.264E-12
GO:0001817~regulation of cytokine production	34	3.48	3.228E-12
GO:0050778~positive regulation of immune response	33	3.37	4.659E-12
GO:0046649~lymphocyte activation	40	4.09	8.804E-12
GO:0002250~adaptive immune response	19	1.94	2.323E-06

Figure 5. Gene Expression Profiling across Disease Stages and Cellular States

(A) Overrepresented GO terms in indicated cellular states in the Mll-ENL-ERtm/TAM BM. GO analysis was performed on upregulated genes (5% p value cut-off, 1.5-fold change cut-off) in each cell state compared to wild-type/TAM controls.

(B) Venn diagram of differential gene expression in the BM of Mll-ENL-ERtm/TAM mice across different cellular states. Differentially expressed genes (5% p value cut-off, 1.5-fold change cut-off) in each cell state were used for pairwise comparison to identify unique and shared genes. Numbers represent the up- or downregulated genes in unique sections or shared genes in each intersection.

(C) Heatmap representation of differential expression of selected genes across cell states in the Mll-ENL-ERtm/TAM BM. Rows represent individual genes and columns represent individual mice. Values are indicated as log2 ratios.

(D) Venn diagram of differential gene expression in the spleen of Mll-ENL-ERtm/TAM mice across disease stages. Overrepresented GO terms in upregulated and downregulated gene sets shared between the three disease stages. The same approach and selection criteria were used as for the BM.

pATR declined upon 4-oht withdrawal indicating that ATR phosphorylation depends on continuous activity of MLL-ENL-ERtm (Figure S4A). Next, we exposed this BM culture to CXCL2, CCL3, TNF-α, and IL-1β (each alone or in various combinations) that were part of the inflammatory expression profile during the transition period to senescence. Cells were grown for 4 days under these conditions and assayed for γH2AX at day 2 and SA-β-gal at day 4. The highest level of γH2AX was observed in cultures exposed individually to chemokines CXCL2 or CCL3. Addition of TNF-α or IL-1β alone did not significantly enhance γH2AX (Figure 6A, left). The highest level of senescence was induced in the presence of CXCL2/TNF-α/IL-1β,

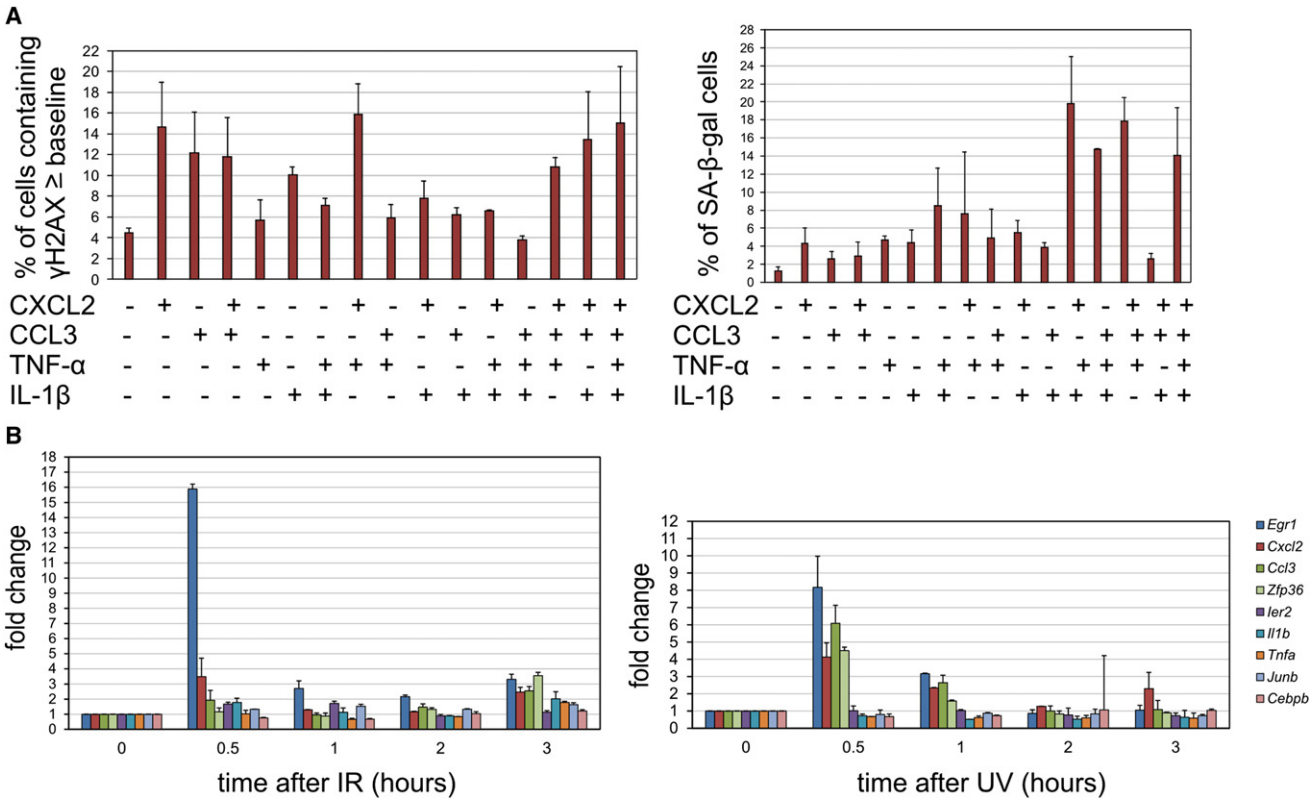

Figure 6. Cooperation of DDR and Inflammation in MLL-ENL-ERtm-Induced Senescence

(A) Effects of selected inflammatory factors on DDR in a MII-ENL-ERtm BM cell line assessed by γH2AX staining at 48 hr of treatment. The highest level of γH2AX in individual cells in untreated control culture (10–20 foci/nuclei) was estimated, and the relative number of these cells was counted. This level was used as a baseline threshold, and the relative number of cells containing γH2AX foci on the baseline level or above (≥20–30 foci/nuclei or an intense homogenous signal pattern) was estimated in each culture condition. Data are averages from two experiments ± SD (left). The effect of selected inflammatory factors on senescence induction in a MII-ENL-ERtm BM cell line. The graph shows the percentage of SA-β-gal positive cells relative to total number of cells calculated in each tested conditions at day 4. Data are averages from two experiments ± SD (right).

(B) Time course expression of selected genes from the inflammatory signature after IR in a MII-ENL-ERtm BM cell line. Data are averages from two experiments ± SD (left). Time course of expression of selected genes from the defined inflammatory signature after UV in a MII-ENL-ERtm BM cell line. Data are averages from two experiments ± SD (right). The same color coding was used for both graphs.

See also Figure S4.

CCL3/TNF-α/IL-1β, CXCL2/CCL3/TNF-α, and CXCL2/CCL3/TNF-α/IL-1β (Figure 6A, right). DDR was not increased (Figure S4B) and senescence was not induced in the control 32Dcl3 BM cells. Thus, although CXCL2 and CCL3 signaling pathways enhance the DDR in MLL-ENL-ERtm-immortalized cells, additional factors, such as TNF-α are required for MLL-ENL-ERtm-induced senescence in vitro. IL-1β may contribute to senescence induction; however, it is ineffective on its own.

DDR Activates a Subset of the Inflammatory Signature Genes

To examine whether some genes from the defined inflammatory signature in our model might selectively respond to genotoxic insults that trigger ATR and/or ATM kinase signaling, the cultured MII-ENL-ERtm BM cells were subjected to ionizing radiation (IR) and ultraviolet light (UV) exposure, and mRNA expression was measured at 0.5, 1, 2, 3, and 6 hr after irradiation. The most upregulated genes were *Egr1*, *Cxcl2*, and *Ccl3*, which rapidly responded to both IR and UV at the 0.5-hr time point. The *Zfp36* gene was highly upregulated only in response to UV, whereas three genes, *Ier2*, *Il1b* (at the 0.5-hr time point), and *Tnfa* (at the 3-hr time point), were upregulated only in response to IR (dominant ATM signaling). The expression levels of *Cebpb* and *Junb* did not change in response to either radiation treatment (Figure 6B). We conclude that *Cxcl2* and *Ccl3* are expressed very early upon DNA damage and may be coregulated with *Egr1*; furthermore *Cxcl2* has been recognized as a direct target of EGR-1 (Ramana et al., 2009). ATM-mediated signaling may contribute to the maintenance of expression levels of *Ier2*, *Il1b*, and *Tnfa*.

The DDR-Mediated Senescence Barrier Is Eliminated during Leukemia Progression

Having established the interplay between DDR and inflammatory signaling as a candidate senescence-inducing barrier in the MII-ENL-ERtm mice, we argued that elimination or bypass of such antileukemia barrier by natural selection would be predictable for those animals that have developed the terminal disease.

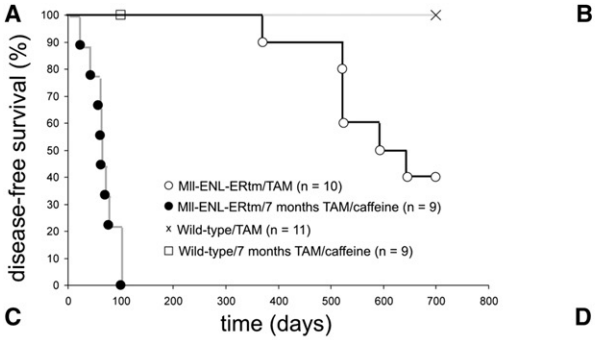

B

PB Differential Counts (%)	Wild-type/TAM/ caffeine, n= 3	Mll-ENL-ERtm/TAM/ caffeine, n= 3
WBC, 10^3/µl	5.9 (4.5-7.7)	59.5 (31.9->80.0)
segmented neutrophils	40 (30-51)	30 (21-47)
band neutrophils	9 (7-11)	28 (23-35)
metamyelocytes		5 (3-7)
myelocytes		4 (2-5)
premyelocytes		1 (0-2)
myeloblasts		3 (1-8)
monocytes	7 (5-11)	16 (9-21)
lymphocytes	43 (30-53)	12 (3-19)
erythroblasts		2 (0-3)

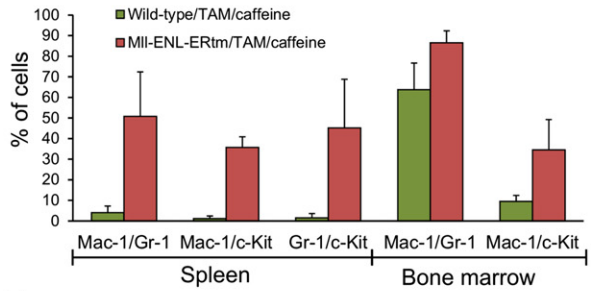

D

Spleen Differential Counts (%)	Wild-type/TAM/ caffeine, n = 4	Mll-ENL-ERtm/TAM/ caffeine, n = 4
granulocytes	4 (2-7)	53 (50-58)
myeloblasts		20 (8-29)
promyelocytes		13 (3-25)
myelocytes		3 (1-6)
metamyelocytes		2 (0-6)
band neutrophils	2 (0-5)	11 (6-14)
segmented neutrophils	2(1-3)	4 (2-5)
red cells		13 (7-22)
normo-basophilic		1 (0-1)
normo-polychromatic		9 (5-14)
normo-oxyphilic		3 (1-6)
lymphocytes	93 (90-96)	23 (9-30)
monocytes	1 (1-2)	10 (7-17)

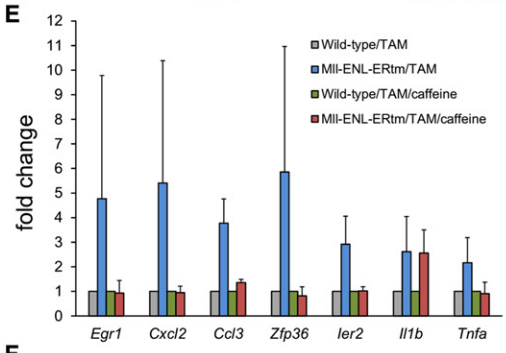

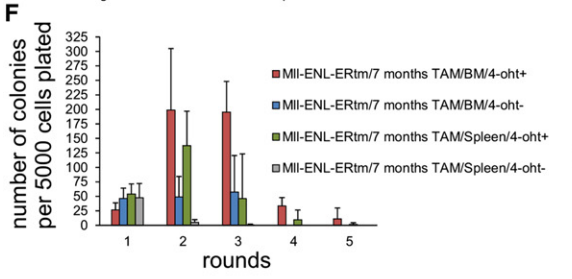

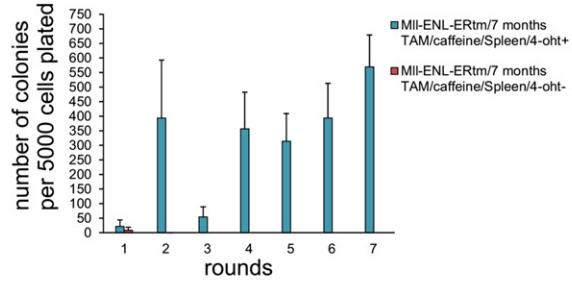

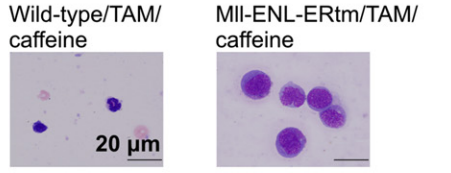

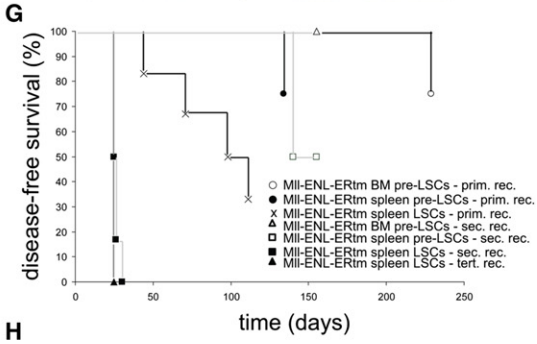

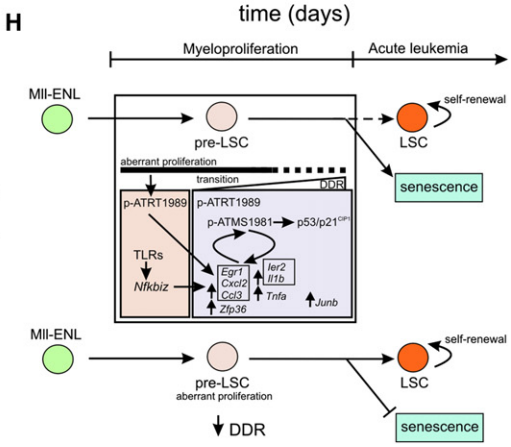

Figure 7. Caffeine Treatment Facilitates AML Development

(A) Caffeine treatment of Mll-ENL-ERtm/TAM mice at the early disease stage significantly (log rank test, $p < 0.001$) reduces disease latency in vivo.

(B) PB differential counts and WBC counts of caffeine-treated Mll-ENL-ERtm/TAM and wild-type/TAM mice. Data are averages from three mice (data range).

(C) FACS analysis shows an increase in c-Kit$^+$/Mac-1$^+$/Gr-1$^+$ cells in the BM and spleen of caffeine-treated Mll-ENL-ERtm/TAM mice compared to the early disease stage (see Figures 1C and 1E). Data are average percentages counted from three mice ± SD.

Analyses of DDR signaling and senescence in the spleen of such mice showed sustained pATR, however, the number of γH2AX-positive cells was decreased compared to earlier disease stages. Notably, features of senescence were either completely absent or only residual (Figure S5A). These results suggest that development to a more advanced stage of MLL-ENL-ERtm-driven leukemia is associated with reduced DDR signaling itself (lower γH2AX) and/or elimination/bypass of the downstream impact of DDR signaling, below the threshold required for senescence. Such a scenario is also consistent with an overall increase in the Mac-1$^+$/c-Kit$^+$ cell population in the spleen throughout disease progression (Figure 1E) indicating that this population gains selective advantage of limitless growth.

Barrier Inhibition Accelerates Cellular Transformation toward a More Immature Cell State

To test our concept of DDR as a driving force of cytokine expression and senescence induction that may delay or prevent the MLL-ENL-ERtm-mediated transformation in vivo, we assessed whether chemical silencing of DDR could impact the kinetics of disease progression in our model. To inhibit DDR in vivo, the Mll-ENL-ERtm/TAM mice at the early disease stage and wild-type/TAM controls (7 months of TAM treatment) were subjected to continuous treatment by caffeine, a commonly used inhibitor of both ATM and ATR kinases. Striking acceleration of the disease was observed in the Mll-ENL-ERtm mice that showed signs of disease with a mean survival of 62 ± 23 days of caffeine treatment (Figure 7A). PB differential counts showed high numbers of band neutrophils and monocytes (Figure 7B). Notably, FACS profiling revealed increased c-Kit$^+$/Mac-1$^+$/Gr-1$^+$ cell populations in the spleen and the BM (Figure 7C) compared to the early stage phenotype (Figures 1C and 1E). Differential counts showed a marked shift to immature myeloid elements in the spleen such as promyelocytes and myeloblasts (Figure 7D), and severe hepato-splenomegaly was apparent due to invasion of leukemia cells into tissues (Figure S5B). DDR markers were decreased in Mac-1$^+$ cells both in the BM and spleen confirming the inhibition of ATR/ATM activity, and senescence was not detected in either BM or spleen. The immunofluorescence data on tissue sections were corroborated by a sensitive immunoperoxidase staining that showed only weak to undetectable DDR markers in tissues from caffeine-treated mice, in contrast to variable and often strong nuclear focal staining in caffeine-free Mll-ENL-ERtm/TAM mice (Figure S5C and data not shown).

Given that some of the inflammatory signature genes upregulated in the high-DDR Mll-ENL-ERtm/TAM BM (validated with quantitative RT-PCR, Figure 7E) were responsive to DDR, we determined the expression level of these inflammatory genes (*Egr1*, *Cxcl2*, *Ccl3*, *Zfp36*, *Ier2*, *Il1b*, and *Tnfa*) in the BM of the caffeine-treated Mll-ENL-ERtm/TAM mice in vivo. Under such conditions, only *Il1b* became upregulated (compared to wild-type/TAM/caffeine mice) whereas all other genes evaluated were expressed at the basal level despite the active MLL-ENL oncogene (Figure 7E).

We conclude that caffeine treatment is sufficient to overcome the barrier to MLL-ENL-ERtm-induced malignancy, leading to accelerated transition of committed progenitors to immature cell states during leukemia development. Caffeine treatment also prevents activation and/or leads to reversion of a large subset of the transient inflammatory gene signature, consistent with our present data that these genes are regulated in response to DDR induction.

Caffeine Treatment Promotes Acquisition of Self-Renewal Capacity and Enables Development of LSCs

We next analyzed the impact of the dual ATM/ATR inhibitor caffeine on self-renewal potential of Mll-ENL-ERtm myeloid progenitors. BM and spleen cells isolated from Mll-ENL-ERtm/TAM myeloproliferative mice (early stage, 7 months TAM) and spleen cells from caffeine-treated Mll-ENL-ERtm/TAM AML mice were tested for their colony formation and serial replating ability in methylcellulose culture with or without 4-oht. Early stage Mll-ENL-ERtm BM and spleen myeloid progenitors exhausted their ability to form colonies during the fifth round of replating in the presence of 4-oht. In contrast, Mll-ENL-ERtm

(D) Differential counts from the spleen of caffeine-treated Mll-ENL-ERtm/TAM show a marked shift to immature cell types compared to caffeine-treated wild-type/TAM mice. Data are averages from four mice (data range). Representative spleen smear from the caffeine-treated Mll-ENL-ERtm/TAM mouse shows the morphology of promyelocytes and myeloblasts (bottom). Scale bar represents 20 μm.

(E) Quantitative RT-PCR analysis of inflammatory gene expression in the BM of caffeine-treated Mll-ENL-ERtm/TAM mice compared to caffeine-treated wild-type/TAM controls. The expression level of tested genes measured by quantitative RT-PCR in the Mll-ENL-ERtm/TAM BM (transition state) compared to time-matched wild-type/TAM mice is also indicated. The results are fold changes between average expression levels measured in two to three mice per genotype ± SD. Each measurement was performed in triplicate.

(F) Quantification of colony formation of BM and spleen cells harvested from Mll-ENL-ERtm mice of indicated disease stages and treatment-conditions over five and seven rounds of replating, respectively. Data are averages from four experiments (cells derived from individual mice) ± SD. Each experiment performed in triplicate.

(G) The Mll-ENL-ERtm spleen LSC-enriched cells initiate a rapid onset of leukemia in serial transplantations (log rank tests, primary versus secondary transplants $p = 0.001$, primary versus tertiary transplants $p = 0.003$). The in vivo leukemogenic potential of the Mll-ENL-ERtm spleen LSCs is significantly higher compared to Mll-ENL-ERtm BM pre-LSCs (log rank, $p = 0.025$) and spleen pre-LSCs (log rank, $p = 0.025$) in secondary recipients. Prim. rec., primary recipients; sec. rec., secondary recipients; tert. rec., tertiary recipients.

(H) Model summarizing the mechanistic basis of the barrier that delays MLL-ENL-induced acute leukemia development. Top scheme: MLL-ENL initiates aberrant proliferation of myeloid cells leading to development of a pre-LSC state manifested as a myeloproliferative disorder. Cell intrinsic (ATR) and extrinsic (TLRs) signaling pathways activate a complex fail-safe program consisting of antiproliferative and inflammatory signals. Inflammatory factors fine-tune the DDR signaling toward activation of p53 that modulates the fate of pre-LSCs. A critical cell-fate decision occurs between senescence and acquisition of LSC properties such as self-renewal, a prerequisite of development to a more transformed cell state. Bottom scheme: inhibition of DDR prevents senescence and accelerates progression to AML. For detailed explanation see Discussion. Lines (arrow, activation; blunted, inhibition) represent regulatory impact. Pink square, proliferation state; violet square, transition state. Upregulated expression of inflammatory regulators is highlighted by arrows.

See also Figure S5 and Tables S1 and S2.

AML cells showed enhanced cloning efficiency and continued to form numerous colonies through all seven rounds of replating evaluated. Reversion of MLL-ENL-ERtm activity by 4-oht withdrawal both in early stage and AML cells led to formation of only mature colony types in the first and second rounds of replating (Figure 7F). We therefore identify the early stage Mll-ENL-ERtm progenitors as a pre-LSC population with limited proliferation and self-renewal capacity, whereas AML cells derived from the caffeine-treated Mll-ENL-ERtm mice represent a LSC-enriched population with acquired unlimited self-renewal potential.

To further assess the leukemia-initiating potential of Mll-ENL-ERtm pre-LSCs and LSCs, we performed serial transplantations into TAM-treated SCID recipients. Consistent with the results from the in vitro replating assay, the Mll-ENL-ERtm BM pre-LSCs induced myelomonocytic proliferation with a long latency (229 days) in one of four primary recipients and all secondary recipients remained disease-free until 165 days after transplantation. The Mll-ENL-ERtm spleen pre-LSCs induced leukemia in one of four primary transplanted mice with a latency of 134 days, and in one secondary transplant with a similar latency (140 days, n = 2). Importantly, Mll-ENL-ERtm LSC-enriched spleen cells induced leukemia with a short latency (mean: 81 ± 30 days) in four of six primary recipient mice, and in both secondary and tertiary transplants with a complete penetrance in 26 ± 2 days and 25 ± 0 days after transplantation, respectively (Figure 7G). Importantly, spleen LSC-initiated AMLs exhibited a more severe phenotype, higher numbers of myeloblasts in the analyzed tissues and higher frequency of c-Kit$^+$ cells in the spleen compared with pre-LSC-induced AML in the primary transplantations (Table S1). In addition, the degree of phenotypic maturity negatively correlated with the level of DDR activation in the primary transplanted animals. We detected high level of γH2AX in the majority of spleen cells in mice with a pre-LSC-induced myelomonocytic proliferation and leukemia. In contrast, the majority of the LSC-induced AML spleen cells were negative or weakly positive for γH2AX. Thus, the high self-renewal activity correlates with perturbation of DDR signaling in the spleen of primary recipients (Figure S5D). Together, these results suggest that inhibition of DDR enables Mll-ENL-ERtm pre-LSCs to gain self-renewal property and establish a LSC population with a long-term ability to propagate leukemia in mice.

Relevance of the DDR Pathway to Human *MLL*-Rearranged Leukemia

Based on the results obtained with the mouse model, two predictions could be made for *MLL*-rearranged human leukemia at the clinically manifest, malignant stage: 1), the upstream DDR signaling could be constitutively activated, reflecting the continuous stress caused by the *MLL* fusion oncogene; and 2), downstream DDR signaling and/or effector pathways would likely be disabled during the progression to advanced leukemia. To test these predictions, we analyzed BM biopsies from three patients with confirmed *MLL*-rearranged AML (obtained at the time of diagnosis, Table S2) and from five healthy BM donors. Paraffin sections were stained for pATR, pATM, γH2AX, and p21^{CIP1} by immunohistochemistry. Interestingly, the majority of *MLL* BM cells showed strong positivity for pATM and pATR in most leukemia cells, in contrast to the largely negative staining in the normal control samples. These findings indicate that activation of the DDR pathway does occur also during human MLL leukemogenesis, thereby supporting the relevance of our mouse model. Although the upstream signaling kinases ATM and ATR were still activated in leukemia blasts, the downstream effector events, documented here by attenuated γH2AX and the lack of the p53 target p21^{CIP1} (Figure S5E), were consistent with the need to neutralize the DDR barrier to allow progression to full malignancy.

DISCUSSION

This study contributes to better understanding of multistep tumorigenesis and the basis for long latency of cancer development in vivo. Our data provide insights into the mechanism of transformation by *Mll* fusion oncogenes with emphasis on cellular antitumor barriers to emergence of a LSC population in a mouse model in vivo.

Using our Mll-ENL-ERtm mouse model, we show that MLL-ENL triggers myeloproliferation with a potential to transform to acute leukemia. Although the aberrantly proliferating myeloid cells display differentiated morphology, a subpopulation of cells coexpressing both lineage (Mac-1) and stem cell (c-Kit) surface markers emerges at the early stage of transformation. These findings argue for a previous suggestion that *MLL* fusion oncogenes can reactivate stem cell properties in a context of more differentiated progenitors (Krivtsov et al., 2006). Furthermore, we show that such aberrantly reactivated proliferation/self-renewal triggers DDR and cellular senescence, reminiscent of intrinsic antitumor barrier mechanisms suggested to operate in solid tumors (Halazonetis et al., 2008). Our model also allows to study the interplay of DDR and inflammatory antitumor barriers (Campisi and d'Adda di Fagagna, 2007; Bartek et al., 2008) in response to MLL-ENL in a disease stage-specific manner and natural settings in vivo. In addition, we found tissue-dependent properties of the leukemogenesis barrier mechanisms in BM versus spleen, indicating that such fail-safe mechanisms are influenced by factors provided by the local tissue microenvironment.

Our results implicate the DDR checkpoint machinery as a crucial fail-safe mechanism that guards against progression of MLL-ENL-immortalized myeloid cells into AML. In the early, proliferative phase of the disease, we found the ATR-Chk1 kinase module as the activated upstream signaling cascade (monitored by three markers: pATRT1989, pATRS428, and pChk1S345), consistent with hyperproliferation and ensuing replication-associated stress. This was evident in both spleen and BM; however, the latter tissue showed a greater extent of hyperproliferation and also activation of ATM, the kinase that responds to DNA DSBs (Kastan and Bartek, 2004) and is activated in early lesions among diverse human solid tumors (Halazonetis et al., 2008). The more prominent overall DDR activation, including the active ATM-p53-p21^{CIP1} pathway, correlated with more robust senescence phenotype at the later stages of the MLL-ENL-induced disease in the BM, compared to milder DDR response and only moderate senescence in the spleen. Thus, it appears that the exclusive ATR signaling as seen in the spleen can result in a balanced state of concomitant partial proliferation and limited degree of senescence, whereas the combined ATR/ATM-mediated robust DDR can lead to

pronounced proliferation arrest and senescence phenotype in the BM. Notably, the weaker DDR and senescence in the spleen apparently provides less protection against leukemia, because the features of terminal malignancy, if developed, were primarily manifested in the spleen.

The observed gradual increase in DDR activation associated with enhanced activation of the ATM kinase as the Mll-ENL-ERtm BM cells transit from proliferation to senescence correlated with a transcription response involving immediate early response genes (*Egr1*, *Ier2*, *Junb*, *Zfp36*) and inflammatory factor genes (*Cxcl2*, *Ccl3*, *Il1b*, *Tnfa*). We propose that ATM-mediated signaling reflects a higher, suprathreshold level of DNA damage in aberrantly proliferating BM cells, and plays a critical role in the amplification and maintenance of the DDR signaling with impact on transcription of a set of inflammatory genes. This interpretation is consistent with our result that *Egr1*, *Cxcl2*, and *Ccl3* are induced rapidly upon DNA-damaging treatments. In turn, both CXCL2- and CCL3-mediated signaling enhances DDR in cultured MLL-ENL-ERtm-immortalized cells, and we suggest that these factors might play the same role in vivo. Consistently with recent studies implicating the feedback loop signals from DDR to cytokine and cytokine receptor genes (Bartek et al., 2008), our data indicate that ATM-mediated DDR may act in a self-autonomous regulatory loop with CXCL2 and CCL3 to boost the p53/p21^{CIP1} checkpoint response and impose cell cycle arrest in damaged cells. Indeed, *Egr1*, *Cxcl2*, and *Ccl3* are induced promptly in response to DNA damage in MLL-ENL-ERtm-immortalized cells, at a time preceding p53 activation suggesting a possible coregulation of these genes in a p53-independent, DDR-dependent manner. This is consistent with previous reports that EGR-1 is required for p53-mediated apoptosis under stress conditions and in replicative senescence, and activates inflammatory cytokines (Krones-Herzig et al., 2003; Yan et al., 2000). We propose that EGR-1 might be a point of convergence between DDR and activation of chemokines *Cxcl2* and *Ccl3* (see model Figure 7H).

Our results document that in vivo treatment with caffeine, a dual ATM/ATR inhibitor prevented induction of the MLL-ENL-induced senescence in premalignant state and promoted acquisition of self-renewal capacity, establishment of LSCs and development of aggressive AML with a short latency. This is consistent with a recent report that p53 deficiency promotes transformation of committed myeloid progenitors into LSCs, by allowing acquisition of self-renewal (Zhao et al., 2010). Reduced expression of DDR markers in the tissues of caffeine-treated mice suggests that caffeine-mediated inhibition of ATM/ATR-signaling and prevention of p53 activation might be the decisive event that allows the shift to a malignant phenotype. In other words, DDR emerges as a signaling pathway that modulates the balance between senescence and acquisition of stem cell properties in immortalized pre-LSCs in the context of the MLL-ENL-ERtm-driven oncogenesis in vivo. Although we cannot exclude that some additional caffeine-targeted mechanism(s) might be involved in leukemia development, the natural selection process in our mouse model leading to AML in association with attenuation or loss of downstream DDR events supports our conclusion that inhibition of ATM/ATR-signaling plays a major role in caffeine-mediated acceleration of leukemogenesis.

Our data also point to a crucial role of the local tissue microenvironment in modulation of cell-fate choices in Mll-ENL-ERtm pre-LSCs. Inflammatory factors and their feedback loop with DDR help to fine tune such a choice toward senescence (Figure 7H). Our study provides a valuable link between inflammation and the kinetics of LSC development. In this context, it is noteworthy, that p53 loss apparently did not accelerate leukemogenesis when *MLL-ENL* was expressed from a retroviral promoter (Zuber et al., 2009). This difference could be attributable to high level of the oncogene that might override cellular checkpoints and increase the malignant potential regardless of p53 status.

We also speculate that upregulation of crucial homeostatic regulators such as *Egr1*, *Junb*, and *Zfp36* could potentially add an additional layer of regulation to the complexity of activated fail-safe mechanisms against leukemic transformation by MLL-ENL. Interestingly, EGR-1 regulates the cell cycle machinery in HSC to maintain quiescence, thereby preventing self-renewal and migration (Min et al., 2008). JUNB limits HSC proliferation and counteracts LSC properties (Santaguida et al., 2009; Steidl et al., 2006). In the hematopoietic system, *Zfp36* is upregulated during commitment from HSC to MPP, and thus correlates negatively with self-renewal, while promoting differentiation (Forsberg et al., 2010). Considered with our present data, we hypothesize that these transcription regulators might play a role in balancing the acquisition of LSC properties (self-renewal and migration) in lineage-committed progenitors.

In conclusion, our study extends the emerging concept of DDR activation as an inducible barrier against activated oncogenes and tumor progression, from solid tumors to hematological malignancies (Bartkova et al., 2005; Gorgoulis et al., 2005; Wajapeyee et al., 2010; Boehrer et al., 2009) under in vivo conditions in mice. Furthermore, our present results have important implications for understanding the tumor-suppressive role of DDR and cell-microenvironment regulatory interactions that modulate the fate of pre-LSCs and multistep development of MLL. We also report activation of DDR in clinical samples of human MLL blasts, accompanied by attenuated effector pathway(s) in such fully developed leukemia. Taken together with our mouse model, these results are consistent with a potential biological role of the DDR machinery in preventing the transition of the initiating pre-LSC population into a fully transformed population with LSC properties. These findings support the notion that uncoupling of DDR signaling from downstream checkpoint responses may allow preleukemia cells to acquire the pathological capacity for self-renewal. Selection for cells that avoid the full impact of DDR signaling during leukemia development is relevant both conceptually, and with respect to clinical responses to standard-of-care genotoxic therapy.

EXPERIMENTAL PROCEDURES

Generation of the *Mll-ENL-ERtm* Knock-In ESC Clone

The creation of the mouse *Mll-ENL-ERtm* knock-in allele by gene targeting in mouse ESCs, Southern blot analyses, and generation of mice were performed as described in Supplemental Experimental Procedures.

Tissue Culture

Mouse ESCs were cultured as described in Supplemental Experimental Procedures. Mll-ENL-ERtm BM cells were cultured in RPMI (high glucose,

glutamax, sodium pyruvate) supplemented with 10% FBS (GIBCO), 10 ng/ml GM-CSF (Biosource), 10 ng/ml G-CSF (Biosource), and 100 nM 4-oht (Sigma). 32Dcl3 mouse BM cell line was cultured in RPMI (high glucose, glutamax, sodium pyruvate) supplemented with 10% FBS (GIBCO) and 10 ng/ml IL-3 (Biosource). Recombinant mouse CXCL2, CCL3, TNF-α, and IL-1β were purchased from R&D Systems and used at a final concentration of 50 ng/ml. Cells were irradiated with a single dose of 4 Gy IR or 20 Jm^{-2} UV.

Mice

All mice were housed and treated at the Animal Research Facility at Faculty of Medicine and Dentistry, Palacky University in Olomouc. Animal experiments were approved by the institutional care and use committees for animal research. Mice were treated with TAM (Sigma) in concentration of 300 mg/kg chow. Mice were treated with caffeine (Sigma) in concentration of 0.4 mg/ml drinking water (Bartkova et al., 2006; Lu et al., 2008). BrdU (Sigma) was dissolved in sterile water and injected intraperitoneally in a dose of 100 mg/kg. Mice were analyzed 2 hr after injection.

Transplantation Assay

A total of 1–2 × 10^7 spleen cells were injected intravenously into SCID recipients treated with TAM in concentration of 100 mg/kg chow. Mice were monitored for disease development. Kaplan-Meier statistical analysis with log rank test was used to compare survival curves.

Methylcellulose Culture

Colony forming and replating assays were performed as described in Supplemental Experimental Procedures.

FACS Analysis

Labeling of cells for FACS was performed on ice in phosphate-buffered saline (PBS) supplemented with 0.5% bovine serum albumin (BSA) (Sigma) using conjugated antibodies purchased from BD Pharmingen. Details of the antibodies used can be found in Supplemental Experimental Procedures.

RT-PCR

RT-PCR was performed with the Stratagene Brilliant II SYBR Master Mix. Each sample was analyzed in triplicate using cDNA corresponding to 10 ng of total RNA reverse transcribed with Superscript III (Invitrogen) according to the manufacturer's recommendations.

Quantitative RT-PCR

Total tissue RNA was isolated using the RNeasy kit (QIAGEN). Reverse transcription was performed using the First Strand cDNA Transcriptor Synthesis kit (Roche). RT-PCR detection was performed using the Universal ProbeLibrary probe/primers sets in triplicate for each sample and reactions were run on the LightCycler 480 system (Roche). *Ywhaz* and *Gapdh* were used as a reference for all reactions. Relative expression was calculated by the 2DDCT method.

Gene Expression Microarray and Bioinformatics Analyses

Total tissue RNA was isolated as described above. RNA was amplified, labeled, and hybridized to Mouse 430A 2.0 genomic arrays (Affymetrix). Differential expression analysis and normalization of chip data was performed in the R statistical environment (The R Project for Statistical Computing, version 2.9.2) using the Limma and Affy packages from Bioconductor project (http://www.bioconductor.org). Differentially expressed genes were identified using lmFit function (moderated t statistics) and Benjamini-Hochberg corrected ($p < 0.05$). GO analysis were conducted using Database for Annotation, Visualization and Integrated Discovery (DAVID) (http://david.abcc.ncifcrf.gov/). For GO and heatmap, only genes with at least 1.5-fold difference between averages of the Mll-ENL-ERtm and the corresponding wild-type sample group were selected.

Immunofluorescence Analysis

Cells were fixed on glass slides in 3% paraformaldehyde at room temperature (RT) for 15 min, permeabilized in methanol at –20°C for 10 min and air-dried, incubated in 1% or 10% BSA (optional) in PBS for 1 hr at RT, followed by primary antibodies at 4°C overnight. Alexa Fluor-conjugated secondary antibodies were incubated at RT for 1 hr. Antibodies used are listed in Supplemental Experimental Procedures. For Mac-1/BrdU double staining, cells were first stained for Mac-1 as described above, fixed again in 3% paraformaldehyde and then DNA was denatured in 2 M HCl for 30 min at 37°C. After neutralization in PBS, samples were blocked with 1% BSA in PBS and incubated with the anti-BrdU antibody conjugated with Alexa594 dye (Invitrogen) for 1 hr at RT. Images were acquired using an Olympus BX51 inverted microscope equipped a ColorViewIII digital CCD camera. Validation of antibodies to pATRS428 and pATRT1989 is shown in Figure S3B.

Immunohistochemistry

Formalin-fixed tissues were paraffin embedded, sectioned at 3–5 μm, and H&E stained. Immunohistochemical analyses were performed as described in detail in the Supplemental Experimental Procedures.

Senescence Assay

Cytospin preparations of BM cells and cryostat spleen sections were used. SA-β-gal was detected by the Senescence detection kit (Calbiochem) according to manufacturer's instructions.

Human Samples

Human BM samples were obtained from the Department of Clinical and Molecular Pathology, University Hospital Olomouc (UHOL), Olomouc, Czech Republic. Diagnostic data related to patient samples were provided by the Department of Hemato-Oncology, UHOL. The original examinations were obtained with the approval of the IRB committee of the UHOL and according to the Declaration of Helsinki. Additional information on patient samples is available in Table S2.

ACCESSION NUMBERS

Microarray data have been deposited at the Gene Expression Omnibus (GSE35038).

SUPPLEMENTAL INFORMATION

Supplemental Information includes five figures, two tables, and Supplemental Experimental Procedures and can be found with this article online at doi:10.1016/j.ccr.2012.01.021.

ACKNOWLEDGMENTS

We thank Dalibor Dolezal and the Animal facility, Faculty of Medicine and Dentistry, Palacky University, Olomouc (FMD-PUO) for assistance; the transgenic facility of the University Erlangen, Erlangen, Germany for ESC injection and animal husbandry; Jan Honetschlager (Institute of Molecular Genetics, Prague) for animal husbandry; Lucie Piterkova (FMD-PUO) for assistance with mouse analyses; the members of the Department of Histology and Embryology, FMD-PUO for some of the immunohistochemical staining; the members of the Department of Hemato-Oncology, UHOL, Olomouc for blood and tissue differential counts; and Jiri Zavadil and the NYU Cancer Institute Genomics Facility, New York, USA for performing and analyzing some of the gene expression arrays. Grant support from: the Czech Ministry of Education (NPV2B06077, MSM6198959205) to V.D., (MSM6198959216) to J.B., the Czech Grant Agency (GA301/01/0489) to V.D., the German research council (DFG grant SL27/7-1) to R.S., the Grant Agency of the Czech Academy of Sciences (IAA501370902), the Czech Ministry of Health (NS10282-3/2009), the Danish National Research Foundation, the Danish Cancer Society, the European Commission (projects Infla-Care, Biomedreg: CZ.1.05/2.1.00/01.0030, DDResponse) to J.B.

Received: October 26, 2010
Revised: June 10, 2011
Accepted: January 25, 2012
Published: April 16, 2012

REFERENCES

Acosta, J.C., O'Loghlen, A., Banito, A., Guijarro, M.V., Augert, A., Raguz, S., Fumagalli, M., Da Costa, M., Brown, C., Popov, N., et al. (2008). Chemokine signaling via the CXCR2 receptor reinforces senescence. Cell *133*, 1006–1018.

Bartkova, J., Horejsí, Z., Koed, K., Krämer, A., Tort, F., Zieger, K., Guldberg, P., Sehested, M., Nesland, J.M., Lukas, C., et al. (2005). DNA damage response as a candidate anti-cancer barrier in early human tumorigenesis. Nature *434*, 864–870.

Bartkova, J., Rezaei, N., Liontos, M., Karakaidos, P., Kletsas, D., Issaeva, N., Vassiliou, L.V., Kolettas, E., Niforou, K., Zoumpourlis, V.C., et al. (2006). Oncogene-induced senescence is part of the tumorigenesis barrier imposed by DNA damage checkpoints. Nature *444*, 633–637.

Bartek, J., Hodny, Z., and Lukas, J. (2008). Cytokine loops driving senescence. Nat. Cell Biol. *10*, 887–889.

Boehrer, S., Adès, L., Tajeddine, N., Hofmann, W.K., Kriener, S., Bug, G., Ottmann, O.G., Ruthardt, M., Galluzzi, L., Fouassier, C., et al. (2009). Suppression of the DNA damage response in acute myeloid leukemia versus myelodysplastic syndrome. Oncogene *28*, 2205–2218.

Campisi, J., and d'Adda di Fagagna, F. (2007). Cellular senescence: when bad things happen to good cells. Nat. Rev. Mol. Cell Biol. *8*, 729–740.

Chen, W., Kumar, A.R., Hudson, W.A., Li, Q., Wu, B., Staggs, R.A., Lund, E.A., Sam, T.N., and Kersey, J.H. (2008). Malignant transformation initiated by Mll-AF9: gene dosage and critical target cells. Cancer Cell *13*, 432–440.

Cozzio, A., Passegué, E., Ayton, P.M., Karsunky, H., Cleary, M.L., and Weissman, I.L. (2003). Similar MLL-associated leukemias arising from self-renewing stem cells and short-lived myeloid progenitors. Genes Dev. *17*, 3029–3035.

Di Micco, R., Fumagalli, M., Cicalese, A., Piccinin, S., Gasparini, P., Luise, C., Schurra, C., Garre', M., Nuciforo, P.G., Bensimon, A., et al. (2006). Oncogene-induced senescence is a DNA damage response triggered by DNA hyper-replication. Nature *444*, 638–642.

Dimri, G.P., Lee, X., Basile, G., Acosta, M., Scott, G., Roskelley, C., Medrano, E.E., Linskens, M., Rubelj, I., Pereira-Smith, O., et al. (1995). A biomarker that identifies senescent human cells in culture and in aging skin in vivo. Proc. Natl. Acad. Sci. USA *92*, 9363–9367.

Dobson, C.L., Warren, A.J., Pannell, R., Forster, A., Lavenir, I., Corral, J., Smith, A.J.H., and Rabbitts, T.H. (1999). The mll-AF9 gene fusion in mice controls myeloproliferation and specifies acute myeloid leukaemogenesis. EMBO J. *18*, 3564–3574.

Forsberg, E.C., Passegué, E., Prohaska, S.S., Wagers, A.J., Koeva, M., Stuart, J.M., and Weissman, I.L. (2010). Molecular signatures of quiescent, mobilized and leukemia-initiating hematopoietic stem cells. PLoS ONE *5*, e8785.

Gorgoulis, V.G., Vassiliou, L.V., Karakaidos, P., Zacharatos, P., Kotsinas, A., Liloglou, T., Venere, M., Ditullio, R.A., Jr., Kastrinakis, N.G., Levy, B., et al. (2005). Activation of the DNA damage checkpoint and genomic instability in human precancerous lesions. Nature *434*, 907–913.

Halazonetis, T.D., Gorgoulis, V.G., and Bartek, J. (2008). An oncogene-induced DNA damage model for cancer development. Science *319*, 1352–1355.

Kastan, M.B., and Bartek, J. (2004). Cell-cycle checkpoints and cancer. Nature *432*, 316–323.

Krivtsov, A.V., Twomey, D., Feng, Z., Stubbs, M.C., Wang, Y., Faber, J., Levine, J.E., Wang, J., Hahn, W.C., Gilliland, D.G., et al. (2006). Transformation from committed progenitor to leukaemia stem cell initiated by MLL-AF9. Nature *442*, 818–822.

Krones-Herzig, A., Adamson, E., and Mercola, D. (2003). Early growth response 1 protein, an upstream gatekeeper of the p53 tumor suppressor, controls replicative senescence. Proc. Natl. Acad. Sci. USA *100*, 3233–3238.

Littlewood, T.D., Hancock, D.C., Danielian, P.S., Parker, M.G., and Evan, G.I. (1995). A modified oestrogen receptor ligand-binding domain as an improved switch for the regulation of heterologous proteins. Nucleic Acids Res. *23*, 1686–1690.

Liu, S., Shiotani, B., Lahiri, M., Maréchal, A., Tse, A., Leung, C.C., Glover, J.N., Yang, X.H., and Zou, L. (2011). ATR autophosphorylation as a molecular switch for checkpoint activation. Mol. Cell *43*, 192–202.

Lu, Y.P., Lou, Y.R., Peng, Q.Y., Xie, J.G., Nghiem, P., and Conney, A.H. (2008). Effect of caffeine on the ATR/Chk1 pathway in the epidermis of UVB-irradiated mice. Cancer Res. *68*, 2523–2529.

Min, I.M., Pietramaggiori, G., Kim, F.S., Passegué, E., Stevenson, K.E., and Wagers, A.J. (2008). The transcription factor EGR1 controls both the proliferation and localization of hematopoietic stem cells. Cell Stem Cell *2*, 380–391.

Nam, E.A., Zhao, R., Glick, G.G., Bansbach, C.E., Friedman, D.B., and Cortez, D. (2011). Thr-1989 phosphorylation is a marker of active ataxia telangiectasia-mutated and Rad3-related (ATR) kinase. J. Biol. Chem. *286*, 28707–28714.

Rakoff-Nahoum, S., and Medzhitov, R. (2009). Toll-like receptors and cancer. Nat. Rev. Cancer *9*, 57–63.

Ramana, C.V., Cheng, G.-S., Kumar, A., Kwon, H.-J., and Enelow, R.I. (2009). Role of alveolar epithelial early growth response-1 (Egr-1) in CD8+ T cell-mediated lung injury. Mol. Immunol. *47*, 623–631.

Rodier, F., Coppé, J.-P., Patil, C.K., Hoeijmakers, W.A.M., Muñoz, D.P., Raza, S.R., Freund, A., Campeau, E., Davalos, A.R., and Campisi, J. (2009). Persistent DNA damage signalling triggers senescence-associated inflammatory cytokine secretion. Nat. Cell Biol. *11*, 973–979.

Santaguida, M., Schepers, K., King, B., Sabnis, A.J., Forsberg, E.C., Attema, J.L., Braun, B.S., and Passegué, E. (2009). JunB protects against myeloid malignancies by limiting hematopoietic stem cell proliferation and differentiation without affecting self-renewal. Cancer Cell *15*, 341–352.

Steidl, U., Rosenbauer, F., Verhaak, R.G., Gu, X., Ebralidze, A., Otu, H.H., Klippel, S., Steidl, C., Bruns, I., Costa, D.B., et al. (2006). Essential role of Jun family transcription factors in PU.1 knockdown-induced leukemic stem cells. Nat. Genet. *38*, 1269–1277.

Yan, S.-F., Fujita, T., Lu, J., Okada, K., Shan Zou, Y., Mackman, N., Pinsky, D.J., and Stern, D.M. (2000). Egr-1, a master switch coordinating upregulation of divergent gene families underlying ischemic stress. Nat. Med. *6*, 1355–1361.

Wajapeyee, N., Wang, S.Z., Serra, R.W., Solomon, P.D., Nagarajan, A., Zhu, X., and Green, M.R. (2010). Senescence induction in human fibroblasts and hematopoietic progenitors by leukemogenic fusion proteins. Blood *115*, 5057–5060.

Wang, D., and Dubois, R.N. (2010). The role of COX-2 in intestinal inflammation and colorectal cancer. Oncogene *29*, 781–788.

Wang, J., Iwasaki, H., Krivtsov, A., Febbo, P.G., Thorner, A.R., Ernst, P., Anastasiadou, E., Kutok, J.L., Kogan, S.C., Zinkel, S.S., et al. (2005). Conditional MLL-CBP targets GMP and models therapy-related myeloproliferative disease. EMBO J. *24*, 368–381.

Zhao, Z., Zuber, J., Diaz-Flores, E., Lintault, L., Kogan, S.C., Shannon, K., and Lowe, S.W. (2010). p53 loss promotes acute myeloid leukemia by enabling aberrant self-renewal. Genes Dev. *24*, 1389–1402.

Zuber, J., Radtke, I., Pardee, T.S., Zhao, Z., Rappaport, A.R., Luo, W., McCurrach, M.E., Yang, M.M., Dolan, M.E., Kogan, S.C., et al. (2009). Mouse models of human AML accurately predict chemotherapy response. Genes Dev. *23*, 877–889.

Cancer Cell
Article

Promotion of Hepatocellular Carcinoma by the Intestinal Microbiota and TLR4

Dianne H. Dapito,[1,2,10] Ali Mencin,[3,10] Geum-Youn Gwak,[1,7,10] Jean-Philippe Pradere,[1,10] Myoung-Kuk Jang,[1] Ingmar Mederacke,[1] Jorge M. Caviglia,[1] Hossein Khiabanian,[4,5] Adebowale Adeyemi,[3] Ramon Bataller,[8] Jay H. Lefkowitch,[6] Maureen Bower,[9] Richard Friedman,[4,5] R. Balfour Sartor,[9] Raul Rabadan,[4,5] and Robert F. Schwabe[1,2,4,*]

[1]Department of Medicine, Columbia University, College of Physicians and Surgeons, New York, NY 10032, USA
[2]Institute of Human Nutrition
[3]Department of Pediatrics
[4]Herbert Irving Cancer Center
[5]Center for Computational Biology and Bioinformatics
[6]Department of Pathology
Columbia University, New York, NY 10032, USA
[7]Department of Medicine, Samsung Medical Center, Sungkyunkwan University School of Medicine, Seoul 135-710, Korea
[8]Liver Unit, Hospital Clinic, Institut d'Investigacions Biomediques August Pi i Sunyer, Barcelona 08036, Spain
[9]Department of Medicine, Division of Gastroenterology and Hepatology, University of North Carolina, Chapel Hill, NC 25799, USA
[10]These authors contributed equally to this work
*Correspondence: rfs2102@columbia.edu
DOI 10.1016/j.ccr.2012.02.007

SUMMARY

Increased translocation of intestinal bacteria is a hallmark of chronic liver disease and contributes to hepatic inflammation and fibrosis. Here we tested the hypothesis that the intestinal microbiota and Toll-like receptors (TLRs) promote hepatocellular carcinoma (HCC), a long-term consequence of chronic liver injury, inflammation, and fibrosis. Hepatocarcinogenesis in chronically injured livers depended on the intestinal microbiota and TLR4 activation in non-bone-marrow-derived resident liver cells. TLR4 and the intestinal microbiota were not required for HCC initiation but for HCC promotion, mediating increased proliferation, expression of the hepatomitogen epiregulin, and prevention of apoptosis. Gut sterilization restricted to late stages of hepatocarcinogenesis reduced HCC, suggesting that the intestinal microbiota and TLR4 represent therapeutic targets for HCC prevention in advanced liver disease.

INTRODUCTION

Increased translocation of intestinal bacteria is common in patients with chronic liver disease and causes characteristic infectious complications in advanced disease stages (Cirera et al., 2001; Schuppan and Afdhal, 2008; Tandon and Garcia-Tsao, 2008). In addition, translocation of bacterial components termed pathogen-associated molecular patterns (PAMPs) triggers inflammatory responses through Toll-like receptors (TLRs) in both early and late disease stages (Dolganiuc et al., 2007; Fukui et al., 1991; Nolan and Leibowitz, 1978; Seki et al., 2007; Wiest and Garcia-Tsao, 2005). Moreover, PAMPs from the intestinal microbiota and TLR4 contribute to liver fibrosis and cirrhosis (Broitman et al., 1964; Rutenburg et al., 1957; Seki et al., 2007). Notably, 80% of hepatocellular carcinomas (HCCs) develop in fibrotic or cirrhotic livers as a consequence of chronic liver injury (Fattovich et al., 2004; Luedde and Schwabe, 2011), with HCC being the leading cause of death in patients with compensated liver cirrhosis (Fattovich et al., 2004). However, pathways that are responsible for the high rate of HCC development in the chronically injured and fibrotic liver remain largely unknown. Here, we hypothesize that inflammatory and fibrogenic

Significance

Hepatocellular carcinoma (HCC) typically develops in chronically injured livers, but mediators that promote HCC in this setting are not well characterized. Our study demonstrates that TLR4 activation by lipopolysaccharide from the intestinal microbiota contributes to injury- and inflammation-driven tumor promotion but not to tumor initiation. Different from most previous studies that focused on inflammatory pathways in bone marrow-derived cells, our study finds that the LPS-TLR4 pathway promotes HCC by increasing proliferative and antiapoptotic signals in non-bone marrow-derived resident liver cells. Our finding that gut sterilization efficiently prevents HCC even at very late stages may provide a basis for clinically applicable HCC prevention strategies in patients with chronic liver injury.

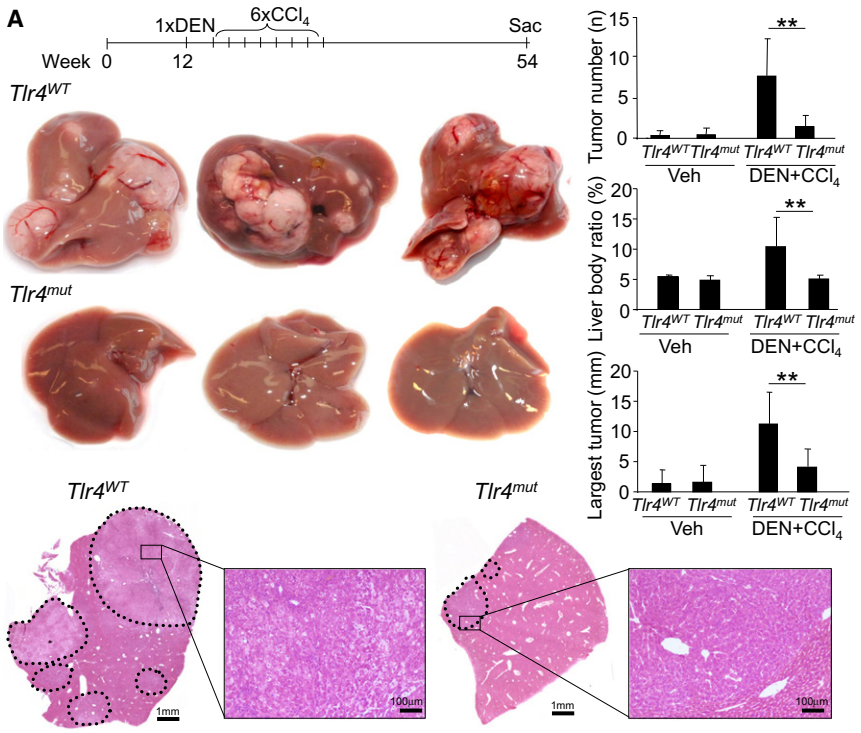

Figure 1. TLR4 Contributes to Hepatocarcinogenesis

(A) $Tlr4^{WT}$ mice (n = 10) and $Tlr4^{mut}$ (n = 9) were injected with DEN (100 mg/kg i.p.) at the age of 12 weeks followed by six injections of CCl_4 (0.5 ml/kg i.p.) and sacrificed 10.5 months after DEN. Shown are tumor number, largest tumor size, liver:body weight ratio, H&E sections, and representative images.

(B) $Tlr4^{WT}$ (n = 14) and $Tlr4^{mut}$ mice (n = 15) were treated with DEN followed by two injections of CCl_4. Gene expression and ALT and AST levels were determined 48 hr after the second CCl_4 injection. Fold induction in comparison to untreated livers. Data are represented as means ± SD. *p < 0.05. **p < 0.01.

See also Figure S1.

responses induced by the gut microbiota and TLRs contribute to hepatocarcinogenesis and might represent targets for HCC prevention or treatment.

RESULTS

TLR4 Is Required for Hepatocarcinogenesis in the Chronically-Injured Liver

To determine whether the known contribution of TLRs to hepatic inflammation and fibrosis may set the stage for HCC development, we subjected C3H/HeJ and C3H/HeOuJ mice, which carry a nonfunctional and the wild-type *Tlr4*, respectively, to a combination of diethylnitrosamine (DEN) and the hepatotoxin carbon tetrachloride (CCl_4). This model incorporates chronic injury, inflammation, fibrogenesis, and CCl_4-mediated increases of endotoxin levels (Seki et al., 2007) and thus shares several features with the microenvironment in which the majority of human HCCs arise. Tumors developing by this regimen showed typical features of HCC, and microarray analysis revealed a characteristic HCC expression profile with *Afp*, *Gpc3*, and *Cdkn2b* among the most upregulated genes with greater than 90-fold increase in comparison to normal liver (data not shown). TLR4-wild-type ($Tlr4^{WT}$) and TLR4-inactivated mutant ($Tlr4^{mut}$) mice had a similar tumor incidence (100% in $Tlr4^{WT}$ mice and 78% in $Tlr4^{mut}$ mice, p = 0.2105), but $Tlr4^{mut}$ mice displayed a profound reduction of tumor number and size and an almost normal liver:body weight ratio 10.5 months after the initial DEN injection (Figure 1A).

Taking advantage of the separate initiation and promotion stages in this model, we further analyzed the contribution of TLR4 at these stages. Following DEN injection, we observed no differences in the induction of inflammatory genes *Il6* and *Ccl2* and p53-dependent genes *Cdkn1a* and *Bax* between $Tlr4^{WT}$ and $Tlr4^{mut}$ mice (Figure S1A available online). DEN-induced liver injury, as determined by serum ALT and AST levels, was exacerbated in $Tlr4^{mut}$ mice (Figure S1A). However, the increased liver injury is unlikely to cause decreased hepatocarcinogenesis in $Tlr4^{mut}$ mice, as liver injury after DEN is thought to promote hepatocarcinogenesis by inducing regenerative responses (Maeda et al., 2005; Naugler et al., 2007). Moreover, despite a small trend toward decreased HCC development, all $Tlr4^{mut}$ mice subjected to a purely genotoxic hepatocarcinogenesis protocol developed numerous large tumors (Figure S1B). Thus, TLR4 status exerts no major effect on genotoxic tumor initiation apart from an increased susceptibility of $Tlr4^{mut}$ mice to liver injury. In contrast, we observed a significant impact of TLR4 status on tumor promotion by CCl_4, with proliferation markers *mKi67*, *Pcna*, *Ccnb1*, and *Ccnb2*; hepatic fibrogenesis markers *Col1a1* and *Acta2*; and inflammatory markers *Il6*, *Il1b*, *Tnf*, and *Ccl2* strongly reduced in $Tlr4^{mut}$ mice, as evidenced by microarray (data not shown) and qPCR analysis, despite increased liver

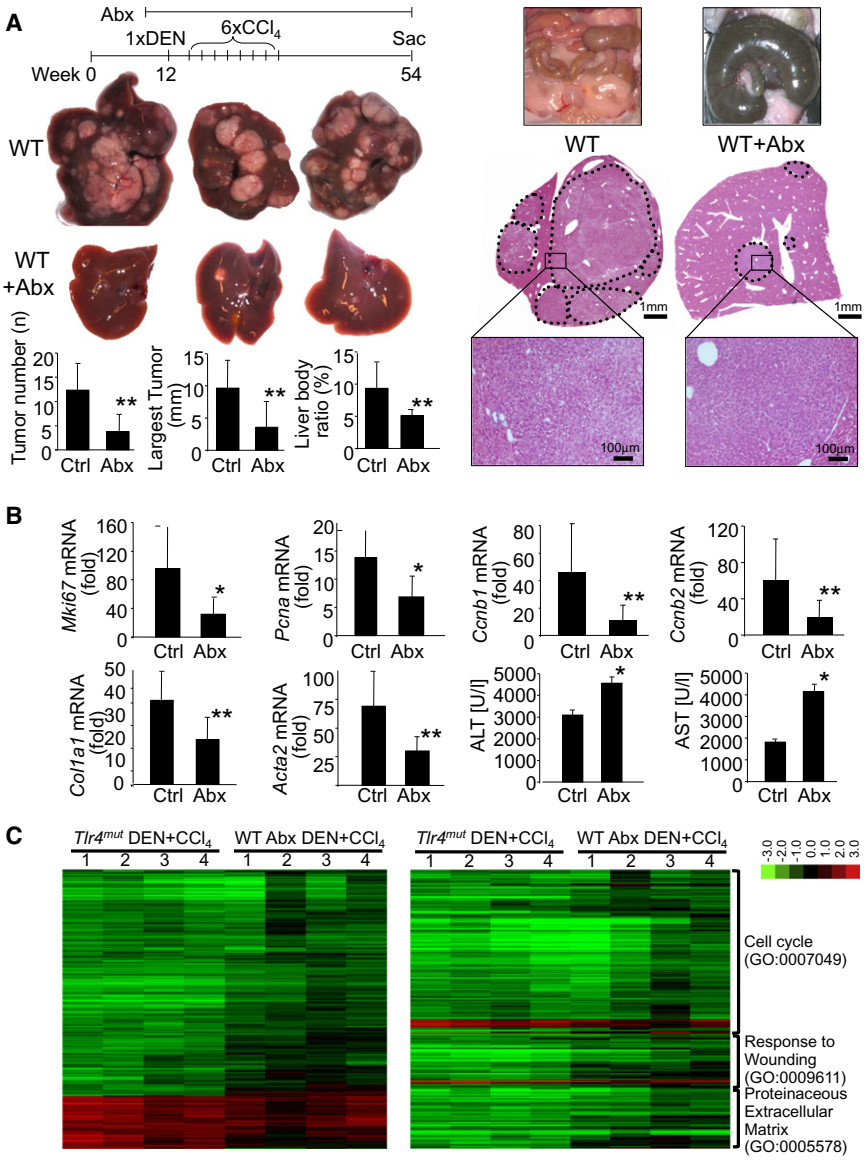

Figure 2. The Intestinal Microbiota Promotes Hepatocarcinogenesis

(A) Wild-type (WT) mice (C3H/HeOuJ) were treated with DEN plus six injections of CCl_4 and either did (n = 11) or did not (n = 7) receive antibiotics (ampicillin, neomycin, metronidazole, and vancomycin) in their drinking water starting 2 weeks before and throughout the entire period. Shown are representative images of ceca, tumors, and H&E sections.

(B) Wild-type (WT) mice were treated with DEN plus two injections of CCl_4 and either did (Abx, n = 14) or did not (Ctrl, n = 9) receive the antibiotics cocktail described in (A) 2 weeks before DEN injection until they were sacrificed 48 hr after the last CCl_4 injection. Gene expression is expressed as fold induction in comparison to untreated liver. Liver injury was assessed by ALT and AST measurements.

(C) $Tlr4^{WT}$, $Tlr4^{mut}$, and $Tlr4^{WT}$ mice treated with antibiotics were injected with DEN and two subsequent injections of CCl_4 and sacrificed 48 hr later. RNA of livers from untreated $Tlr4^{WT}$ mice (n = 3), DEN plus CCl_4-treated $Tlr4^{WT}$ (n = 4), DEN plus CCl_4-treated $Tlr4^{mut}$ mice (n = 4), and antibiotics plus DEN plus CCl_4-treated $Tlr4^{WT}$ mice (n = 4) were used for microarray analysis. The left heatmap shows changes of 1,752 genes in the $Tlr4^{mut}$ and antibiotics-treated mice that were (a) at least 1.8-fold up- or downregulated by DEN plus CCl_4 treatment in $Tlr4^{WT}$ mice in comparison to untreated mice and (b) 1.8-fold up- or downregulated in DEN plus CCl_4-treated $Tlr4^{mut}$ mice in comparison to DEN plus CCl_4-treated $Tlr4^{WT}$ mice. The right heatmap shows genes fulfilling the same conditions as described earlier restricted to the GO categories 0007049, 0009611, and 0005578. Data are represented as means ± SD. *p < 0.05. **p < 0.01.

See also Figure S2.

injury (Figure 1B; Figures S1C and S1D). Similar differences were observed after DEN plus four CCl_4 injections, suggesting a lasting effect of absent TLR4 signaling (Figure S1D). While CCl_4 plus DEN-induced liver injury was increased in $Tlr4^{mut}$ mice 48 hr after the last CCl_4 injection, it was similar to $Tlr4^{WT}$ at earlier time points (Figure S1E), suggesting that the $Tlr4^{mut}$ mice have a defect in DEN plus CCl_4-induced injury resolution and wound healing rather than a higher susceptibility to the initial injury. As chronic regeneration contributes to replication-induced mutagenesis and HCC, we confirmed the reduction of proliferation using *Tlr4 knockout* ($Tlr4^{KO}$) mice in C57Bl/6 background and Ki-67 immunohistochemistry (Figures S1F and S1G).

To exclude that our findings reflect a particular role for TLR4 in the response to CCl_4, we tested two additional models in which DEN was combined with thioacetamide or a choline-deficient diet and found essentially the same results with decreased proliferation and fibrogenesis (Figures S1H–S1J). We also tested whether TLR2, which recognizes PAMPs from the gram-positive bacterial microbiota, contributes to hepatocarcinogenesis. However, we did not find a role for TLR2 in DEN plus CCl_4-induced proliferation or HCC development (Figures S1K and S1L).

The Intestinal Microbiota and Lipopolysaccharide Promote Hepatocarcinogenesis

Next, we examined whether ligands from the bacterial intestinal microbiota are triggers for the observed TLR4-dependent tumor promotion. For this purpose, we gut-sterilized mice with a well-established cocktail of oral antibiotics that eliminates commensal bacteria (Rakoff-Nahoum et al., 2004) and reduces systemic lipopolysaccaride (LPS) levels (Seki et al., 2007). This treatment resulted in not only a >99.5% reduction of 16s levels in the cecum (Figure S2A) and an enlargement of the cecum commonly observed in germfree (GF) mice (Figure 2A) but also a highly significant reduction of tumor number, size, and the liver:body weight ratio in our DEN plus CCl_4 HCC model

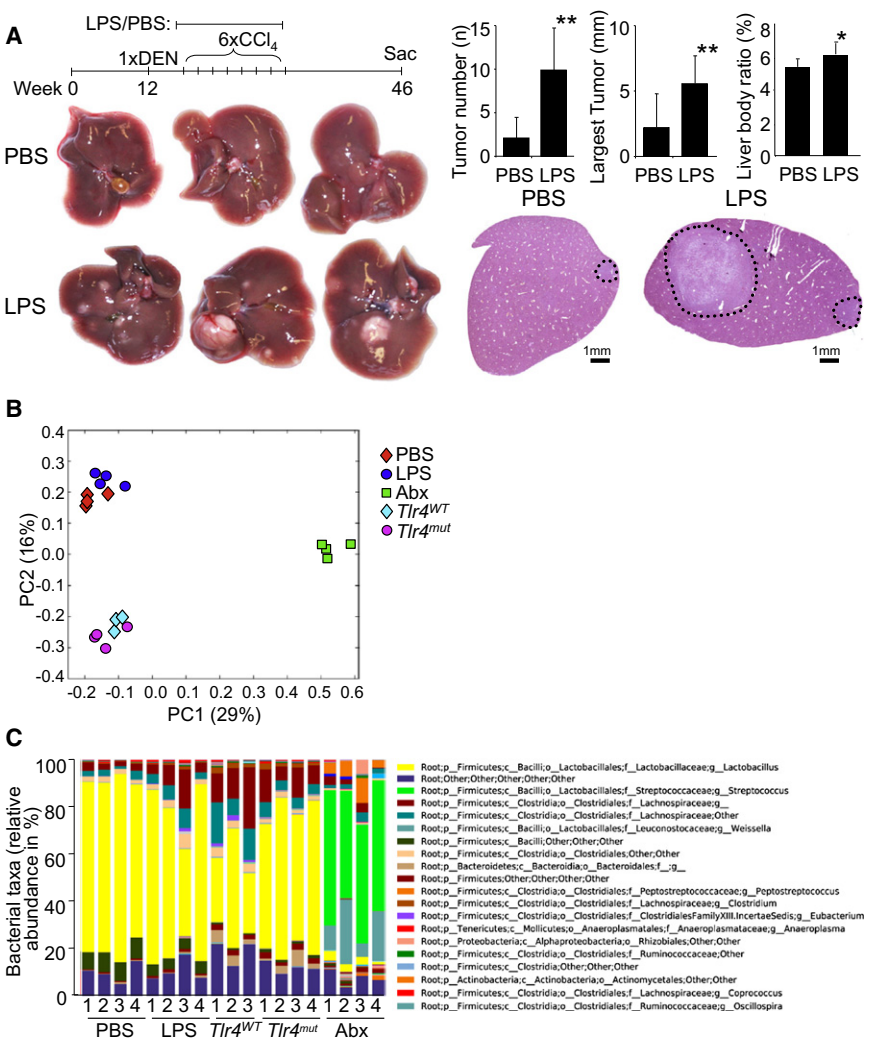

Figure 3. LPS Promotes Hepatocarcinogenesis but Does Not Change the Intestinal Bacterial Microbiota

(A) *Tlr4*^{WT} (C3H/HeOuJ) mice were treated with DEN plus six injections of CCl_4 and either received LPS (300 μg/kg/d, n = 9) or PBS (n = 10) via subcutaneous pumps starting 1 week before the first CCl_4 injection for 12 weeks. Mice were sacrificed 8.5 months after DEN injection to determine tumor number, size, and liver:body weight ratio. *p < 0.05. **p < 0.01.

(B) Unifrac analysis of 16s sequencing results of the cecal microbiome in *Tlr4*^{WT} (n = 3) and *Tlr4*^{mut} (n = 4) mice, *Tlr4*^{WT} mice treated with subcutaneous PBS (n = 4) or LPS (n = 4) pumps for 2 weeks, or *Tlr4*^{WT} mice receiving antibiotics (n = 4) for 2 weeks.

(C) Taxonomic distribution of the cecal microbiome in *Tlr4*^{WT} and *Tlr4*^{mut} mice, *Tlr4*^{WT} mice treated with subcutaneous PBS or LPS pumps for 2 weeks, or mice receiving antibiotics for 2 weeks. The chart contains a total of 118 taxa at the genus level, and the top 20 taxa are annotated on the left with most abundant taxa listed on top. Data are represented as means ± SD. *p < 0.05. **p < 0.01. See also Figure S3.

(Figure 2A). Similar to data in the *Tlr4*^{mut} mice, tumor incidence was not affected by gut sterilization (100% in gut-sterilized vs. 100% in control mice). In addition to the similar degree of HCC reduction, gut sterilization markedly phenocopied events observed in the *Tlr4*^{mut} mice such as reduced expression of cell cycle, fibrosis, and inflammatory genes and increased liver injury (Figure 2B; Figure S2B). Accordingly, the great majority of 1,752 genes that were significantly up- or downregulated by DEN plus CCl_4 and significantly up- or downregulated by TLR4 inactivation were concordantly regulated in DEN plus CCl_4-treated liver from gut-sterilized mice (r = 0.794, p < 0.0001), suggesting that TLR4 inactivation and gut sterilization exert highly similar biological effects on the liver during hepatocarcinogenesis (Figure 2C). Like *Tlr4*^{mut} mice, gut-sterilized mice also did not show differences in inflammatory and p53-dependent gene expression in response to acute DEN treatment but displayed increased liver injury (Figure S2C).

As a third approach in addition to TLR4 inactivation and gut sterilization, we treated mice with a low, nontoxic dose of LPS via subcutaneous osmotic pumps for 12 weeks during DEN plus CCl_4-induced hepatocarcinogenesis. This low-dose LPS treatment led to a significant increase in inflammatory gene expression, tumor number, tumor size and liver:body weight ratio (Figure 3A; Figure S3), further confirming our hypothesis that the LPS-TLR4 pathway promotes hepatocarcinogenesis. As *Tlr5*-deficient mice have an altered gut microbiome (Vijay-Kumar et al., 2010), it is conceivable that TLR4 might also affect the composition of the gut microbiome and thereby influence HCC development rather than exerting direct effects in the liver. To address this possibility, we first performed 16s-based pyrosequencing of the cecal gut microbiota of wild-type and *Tlr4*^{mut} mice as well as mice treated with PBS or LPS. Unifrac analysis revealed no significant differences between *Tlr4*^{WT} and *Tlr4*^{mut} mice, or between PBS- and LPS-treated mice, but showed distinct clustering of the gut-sterilized mice (Figure 3B). It is interesting that differences between these two independent experiments were larger in the Unifrac analysis than differences between *Tlr4*^{WT} and *Tlr4*^{mut} mice, or PBS- and LPS-treated mice, again underlining that LPS and TLR4 status exert no significant influence on the composition of the gut microbiome. Moreover, the taxonomic distribution of the cecal gut microbiome was similar between *Tlr4*^{WT} and *Tlr4*^{mut} mice, and PBS- and LPS-treated mice (Figure 3C); among the 118 detected taxa at the genus level, we found no significant differences between *Tlr4*^{WT} and *Tlr4*^{mut} mice and only one taxon (firmicutes;bacilli;other;other;other) with a significant but modest difference between PBS-treated mice (8.1% abundance) and LPS-treated mice (4.7% abundance). However, as there was no difference in this taxon between *Tlr4*^{WT} and *Tlr4*^{mut} mice, it is extremely unlikely that

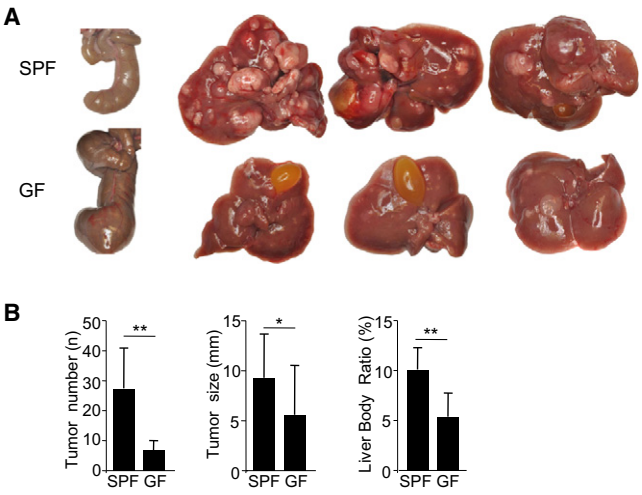

Figure 4. GF Status Decreases Hepatocarcinogenesis

GF C57Bl/6 mice were subjected to DEN (25 mg/kg i.p.) injection, split into SPF and GF groups, and then received 10 CCl_4 (0.5 ml/kg i.p.) injections.

(A) Ceca of GF and SPF mice are shown on the far left, and representative livers with tumors are shown on the right.

(B) Tumor number, size, and liver:body weight ratio was determined in SPF mice (n = 9) and GF mice (n = 10). Data are represented as means ± SD. *p < 0.05. **p < 0.01.

the different abundance of this taxon is responsible for differences in hepatocarcinogenesis.

As a fourth approach, we investigated DEN plus CCl_4-induced hepatocarcinogenesis in GF and littermate controls that had been transferred to a specific-pathogen-free (SPF) environment after the initial DEN injection. GF mice displayed the typical enlargement of the cecum and had a significantly reduced tumor number, tumor size, and liver:body weight ratio in comparison to SPF mice (Figures 4A and 4B), thus confirming results in mice gut-sterilized by antibiotics and excluding that effects of antibiotics on the liver were responsible for HCC reduction.

Non-Bone-Marrow-Derived Resident Hepatic Cells Mediate the Tumor-Promoting Effect of TLR4

To determine the hepatic cell that promotes HCC in response to TLR4 activation, we generated TLR4-chimeric mice using a combination of irradiation, bone marrow transplantation (BMT), and liposomal clodronate-mediated macrophage depletion (Seki et al., 2009; Seki et al., 2007). This protocol achieved >97% suppression of LPS responses after transplantation of $Tlr4^{mut}$ bone marrow into $Tlr4^{WT}$ mice, almost complete restoration of LPS responses after transplantation of $Tlr4^{WT}$ bone marrow into $Tlr4^{mut}$ mice, and substitution of F4/80-positive hepatic macrophages (Figure S4A). DEN plus CCl_4-induced hepatocarcinogenesis in TLR4-chimeric mice revealed no significant reduction of HCC number, size, and liver:body weight ratio in mice transplanted with $Tlr4^{mut}$ bone marrow, whereas TLR4 inactivation in resident (defined hereby as non-bone-marrow-derived) liver cells significantly reduced HCC number, size, and liver:body weight ratio (Figure 5A). Similarly, the induction of *mKi67* and *Pcna* mRNA in response to acute DEN plus CCl_4 treatment was significantly reduced in $Tlr4^{mut}$ mice with $Tlr4^{WT}$ bone marrow in comparison to $Tlr4^{WT}$ mice with $Tlr4^{WT}$ bone marrow (Figure 5B). Moreover, the depletion of hepatic macrophages by liposomal clodronate did not affect the response to DEN plus CCl_4, as evident by *mKi67* and *Pcna* mRNA levels (Figure S4B). To determine the resident liver cell that was responsive to LPS, we injected a sublethal dose of LPS into healthy mice and mice that had undergone DEN plus eight CCl_4 treatments, followed by determination of NF-κB p65 translocation. To avoid the known rapid release of tumor necrosis factor (TNF) and subsequent TNF-mediated NF-κB activation as a cofounding factor, we used either (a) TLR4-chimeric mice with $Tlr4^{mut}$ bone marrow, (b) macrophage-depleted mice, or (c) mice deficient for both TNFR1 and IL-1R1 for this experiment. In uninjured liver, we observed strong NF-κB p65 nuclear translocation in desmin-positive hepatic stellate cells and Kupffer cells but no translocation in hepatocytes after LPS injection (Figure S4C). In mice that had undergone DEN plus CCl_4 treatment, we confirmed p65 nuclear translocation in hepatic stellate cells but also observed p65 translocation in a large percentage of hepatocytes (Figure 5C; Figure S4D), suggesting that both hepatocytes and hepatic stellate are candidates for TLR4-dependent tumor promotion in the chronically injured liver.

Epiregulin Is a TLR4-Regulated Hepatomitogen that Promotes Hepatocarcinogenesis

Microarray analysis demonstrated cell cycle-related genes as most significantly affected by TLR4 status or gut sterilization (Figure 2C). Our microarray and subsequent qPCR analysis revealed reduced expression of two hepatomitogens, HGF and epiregulin (Toyoda et al., 1995), in livers from DEN plus CCl_4-treated $Tlr4^{mut}$ and gut-sterilized mice as well as from TLR4-chimeric mice with $Tlr4^{mut}$ in resident liver and $Tlr4^{WT}$ bone marrow (Figures 6A and 6C). Both HGF mRNA (data not shown) and epiregulin mRNA were expressed much higher in hepatic stellate cells than in whole liver, hepatocytes, or hepatic macrophages (Figure 6D). As the role of HGF in hepatocarcinogenesis remains controversial (Sakata et al., 1996; Santoni-Rugiu et al., 1996; Takami et al., 2007), we focused our attention on epiregulin. Hepatic stellate cells isolated from fibrotic livers secreted significantly more epiregulin than quiescent hepatic stellate cells (Figure 6D), and stimulation of hepatic stellate cells with LPS significantly upregulated epiregulin mRNA and protein in an NF-κB dependent manner (Figure 6E). Moreover, LPS injection into mice either as a bolus or via the aforementioned chronic subcutaneous infusion also significantly increased epiregulin expression in the liver (Figure 6D; Figure S3). Epiregulin mRNA expression was also induced by LPS in human hepatic stellate cells and upregulated in livers of patients with alcoholic hepatitis, a group of patients with typically very high LPS levels (Fukui et al., 1991) (Figure 6F).

To elucidate the contribution of epiregulin to hepatocarcinogenesis, we subjected wild-type and epiregulin-deficient ($Ereg^{KO}$) mice to DEN plus CCl_4-mediated hepatocarcinogenesis. Due to the much lower propensity of C57Bl/6 mice to develop HCC, we used an altered protocol in which mice were subjected to DEN at Day 15 postpartum, followed by multiple CCl_4 injections. $Ereg^{KO}$ mice displayed a significant reduction of tumor number, size, and the liver:body weight ratio, albeit to a much lesser degree than $Tlr4^{mut}$ mice (Figure 6G). Moreover,

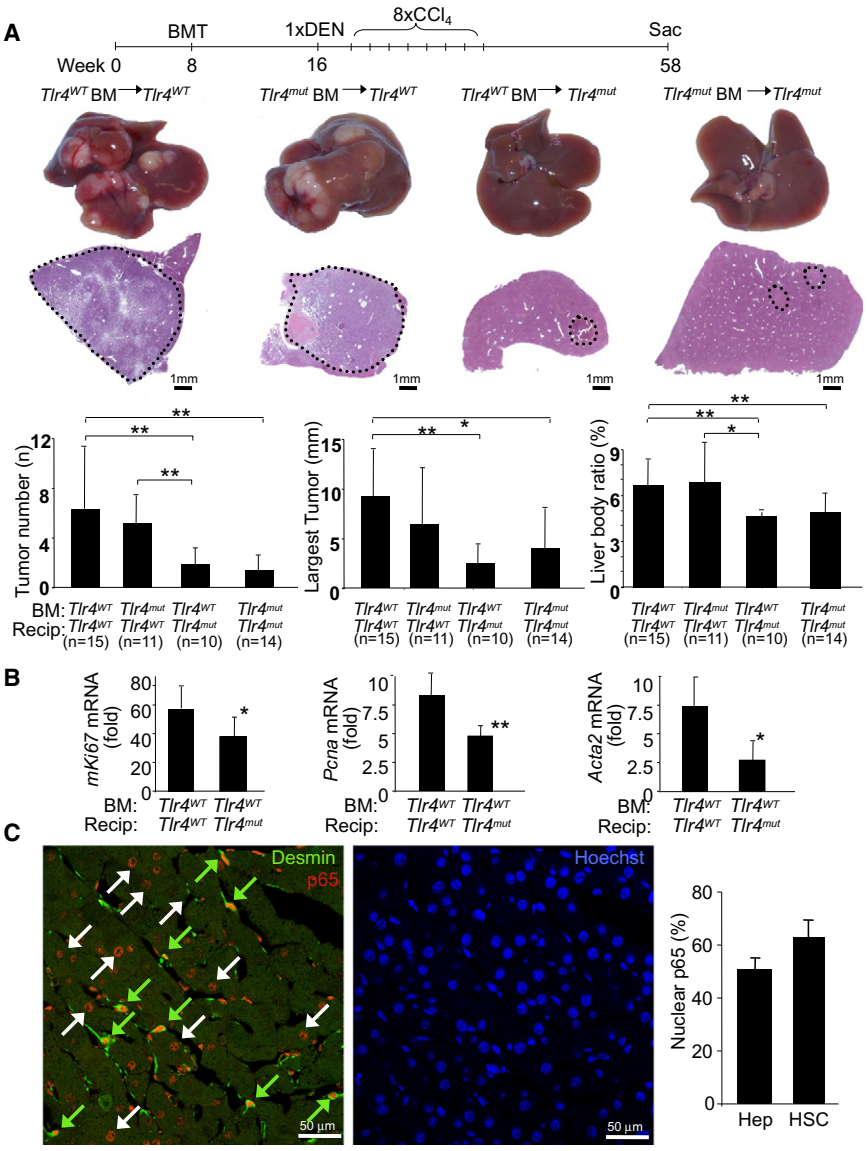

Figure 5. Resident Liver Cells Mediate TLR4-Dependent Tumor Promotion

(A) *Tlr4*^{WT} and *Tlr4*^{mut} mice were subjected to BMT ($n \geq 10$ per group) at 8 weeks followed by treatment with DEN plus eight injections of CCl_4. Mice were sacrificed 10.5 months after DEN. Shown are representative images of tumors and H&E sections, as well as tumor number, size, and liver:body weight ratio.

(B) *Tlr4*^{WT} (n = 7) and *Tlr4*^{mut} mice (n = 6) were transplanted with wild-type bone marrow and treated with DEN plus two injections of CCl_4 at the age of 8 weeks. Proliferation markers were evaluated by qPCR and shown as fold induction in comparison to untreated mice.

(C) TLR4 chimeric mice with *Tlr4*^{WT} resident cells and *Tlr4*^{mut} bone marrow (n = 3) were treated with DEN plus CCl_4 as described earlier. At 10.5 months after DEN, LPS (10 mg/kg i.v.) was injected and NF-κB p65 nuclear translocation was determined by immunohistochemistry and confocal microscopy in nontumor liver areas. Hepatic stellate cells were visualized by desmin staining, and nuclei were visualized by Hoechst staining. Green and white arrows indicate NF-κB translocation in hepatic stellate cells and hepatocytes, respectively. The percentage of hepatic stellate cells (HSC) and hepatocytes (Hep) with positive nuclear p65 was determined. Data are represented as means ± SD. *p < 0.05. **p < 0.01. See also Figure S4.

epiregulin was not upregulated at late stages in our hepatocarcinogenesis model and did not differ between wild-type, *Tlr4*^{mut}, and gut-sterilized mice at these stages of hepatocarcinogenesis (Figure 6H). Thus, additional factors must be responsible for the striking reduction of hepatocarcinogenesis in *Tlr4*^{mut} and gut-sterilized mice.

The Intestinal Microbiota and TLR4 Suppress Apoptosis in Late Stage of Hepatocarcinogenesis

Next, we attempted to establish the time frame during which bacterial PAMPs exert the most profound effects on hepatocarcinogenesis. Surprisingly, gut sterilization during the first 4.5 months of hepatocarcinogenesis showed only a moderate decrease of hepatocarcinogenesis (Figure 7A). In contrast, gut sterilization during the last 4 months of hepatocarcinogenesis reduced tumor number and size by 90% and 70%, respectively, and almost normalized the liver:body weight ratio (Figure 7A). At this point, mice had not yet developed macroscopically or microscopically visible tumors (Figure 7B), suggesting that gut sterilization prevented tumor development rather than leading to the regression of already established tumors. We additionally tested whether more selective gut decontamination with rifaximin, a widely used nonabsorbable antibiotic for the prevention of hepatic encephalopathy in patients with endstage liver disease (Bass et al., 2010), could influence hepatocarcinogenesis at late stages. We observed a borderline significant reduction of tumor numbers but saw no significant reduction in tumor size (data not shown), suggesting only moderate efficacy of rifaximin monotherapy on hepatocarcinogenesis at late stages (Figure S5).

To determine whether gut sterilization might affect already established tumors, we treated wild-type mice at a time point where tumors were already present with the quadruple antibiotics cocktail for 6 weeks. However, we found no significant change of tumor size, number, or liver:body weight ratio in comparison to control mice (Figure 7C). When following single tumors by weekly ultrasound monitoring, we also saw no change in tumor size in antibiotics-treated mice (data not shown).

To further determine the mechanism by which the intestinal microbiota and TLR4 promote hepatocarcinogenesis, we analyzed gene expression, proliferation, and apoptosis in gut-sterilized and *Tlr4*^{mut} mice. Due to the lower tumor number

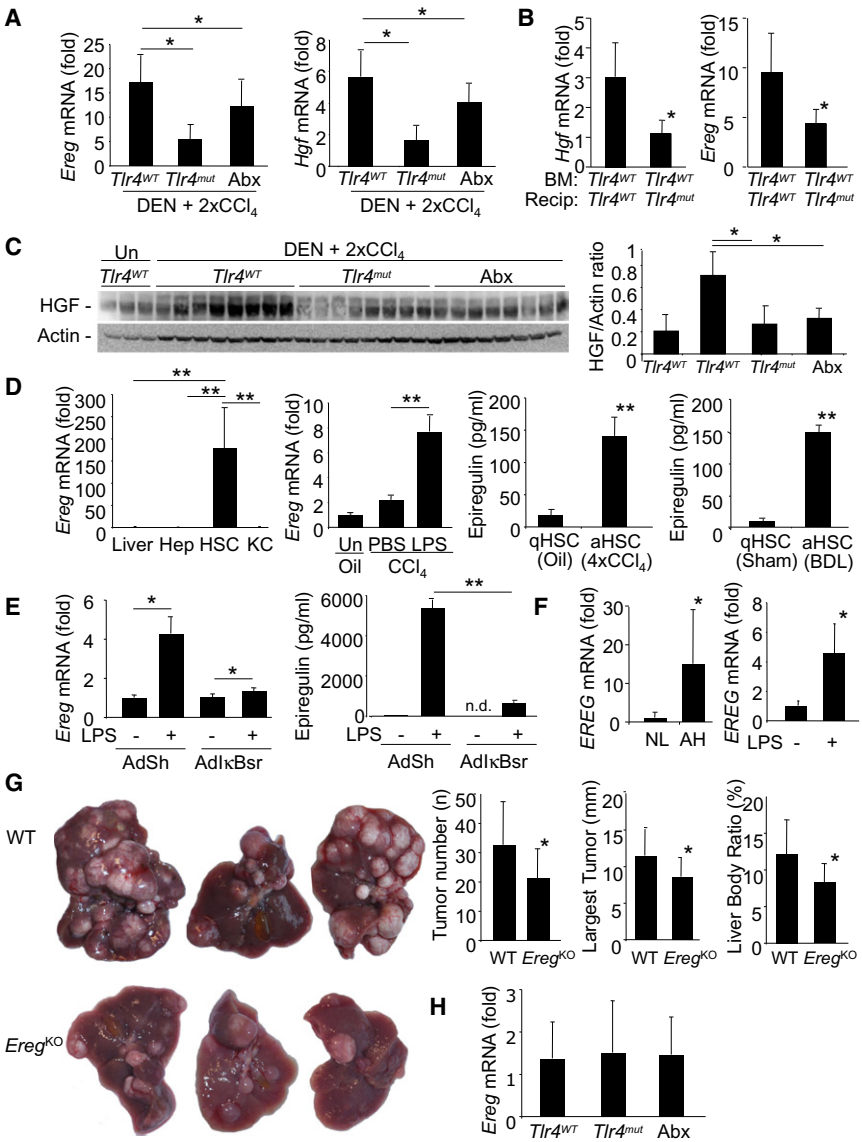

Figure 6. Epiregulin Is an LPS-Inducible Promoter of Hepatocarcinogenesis

(A) *Ereg* and *Hgf* mRNA were determined in $Tlr4^{mut}$ mice (n = 14), $Tlr4^{mut}$ (n = 15) and antibiotics-treated $Tlr4^{WT}$ (n = 9) after DEN and 2× CCl_4 injections. Fold induction versus untreated livers.

(B) *Ereg* and *Hgf* mRNA were determined in TLR4-chimeric mice with $Tlr4^{WT}$ resident cells and $Tlr4^{WT}$ bone marrow (n = 6) or $Tlr4^{mut}$ resident cells and $Tlr4^{WT}$ bone marrow (n = 6) after treatment with DEN and two CCl_4 injections. Fold induction versus untreated livers.

(C) Western blot of HGF from $Tlr4^{WT}$ mice, $Tlr4^{mut}$ mice, and antibiotics-treated mice after DEN and 2× CCl_4 injections.

(D) Hepatocytes (Hep), Kupffer cells (KC), and hepatic stellate cells (HSC) were isolated from liver treated with DEN and two injections of CCl_4 followed by analysis of *Ereg* mRNA expression by qPCR (left panel). Shown is a fold induction versus whole liver. *Ereg* mRNA was isolated in liver extracts from CCl_4-treated mice injected with LPS (10 mg/kg i.v.) or PBS 4 days after the last CCl_4 injection (second panel from left). Activated hepatic stellate cells were isolated from CCl_4-treated and bile duct-ligated livers. Epiregulin was determined by ELISA 24 hr after plating.

(E) Hepatic stellate cells from DEN plus 2× CCl_4 treated mice were stimulated with LPS (100 ng/ml) in the presence of either an adenoviral IκB super-repressor (AdIκBsr) or empty shuttle virus (AdSh) by qPCR (left panel) or ELISA (right panel).

(F) *EREG* expression was determined in normal liver (NL, n = 4) and livers of patients with alcoholic hepatitis (AH, n = 10, left panel) and in activated human hepatic stellate cells stimulated with LPS (100 ng/ml, right panel).

(G) Wild-type (WT, n = 11) and $Ereg^{KO}$ mice (n = 14) were treated with DEN plus 22 injections of CCl_4. Mice were sacrificed 6.5 months after DEN. Shown are representative images of tumors as well as tumor number, size of the largest tumor, and liver:body weight ratio.

(H) *Ereg* expression was analyzed in nontumorous regions of DEN plus CCl_4-treated $Tlr4^{WT}$ (n = 12), $Tlr4^{mut}$ (n = 9), and antibiotics-treated $Tlr4^{WT}$ (n = 6) mice 10.5 months after DEN. Fold induction versus untreated liver. Data are represented as means ± SD. *p < 0.05. **p < 0.01. nd, nondetectable.

and size, the overall amount of Ki-67 staining in $Tlr4^{mut}$ and gut-sterilized mice was expectedly lower (data not shown). Microarray comparison showed a highly similar gene expression pattern in HCC from wild-type, $Tlr4^{mut}$, and gut-sterilized mice (Figure S6A), and HCCs from these groups did not cluster separately as shown by dendrogram and Unifrac analysis (Figures S6B-S6C). There was a small but nonsignificant trend toward lower AFP and Ki-67 in HCCs from gut-sterilized mice and $Tlr4^{mut}$ mice, which was most likely due to the smaller size of the tumors in these groups. There were no genes that showed significant changes, as defined by a corrected p value of < 0.05, in the $Tlr4^{mut}$ or gut-sterilized HCC group when compared to the $Tlr4^{WT}$ HCC group (data not shown). Moreover, there were no differences in tumor grade (Figure S6D), and there was a similar loss of collagen IV staining in HCCs from all groups (Figure S6E). Microarray analysis showed no differences in expression of the cancer stem cell marker prominin 1/CD133 (data not shown), and we found only small and very rare clusters of cells positive for the progenitor marker A6 (Engelhardt et al., 1990), with mostly low A6 expression and morphology of intermediate hepatobiliary cells (Figure S6F). Similarly, there were only few cells with strong pan-cytokeratin signal typical for oval cells in tumors of all treatment groups and a larger but highly variable amount of cells with weak pan-cytokeratin expression typical of intermediate hepatobiliary cells in all groups (Figures S6G-S6H). Altogether, the microarray and immunohistochemical data suggest that TLR4 signaling is unlikely to promote hepatocarcinogenesis via progenitor cells. There was also no significant difference in Ki-67 positive cells in nontumor liver between these groups, suggesting that TLR4 and the intestinal microbiota do not

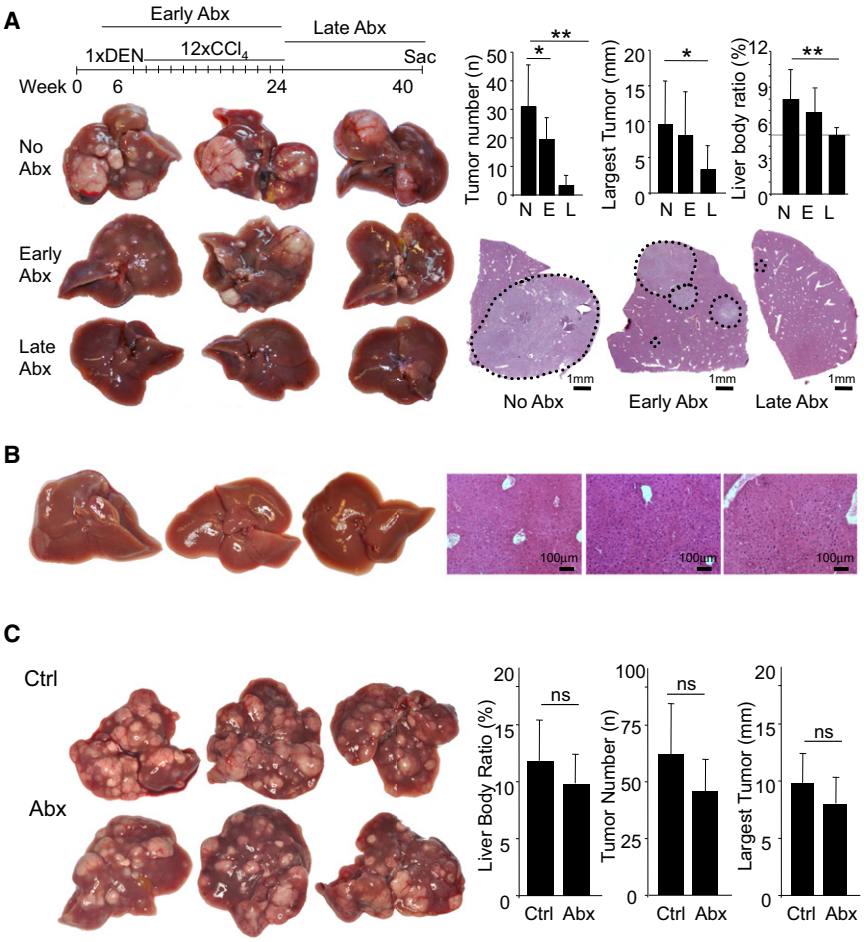

Figure 7. The Intestinal Microbiota Promotes HCC in Late Stages of Hepatocarcinogenesis

(A) Wild-type mice (C3H/HeOuJ) were treated with DEN (100 mg/kg i.p. at the age of 6 weeks) and 12 CCl_4 (0.5 ml/kg i.p.) injections and were either not gut sterilized (N, n = 7), gut sterilized starting 2 weeks before DEN injection until 2 weeks after the last CCl_4 injection (E, n = 10), or 2 weeks after the last CCl_4 injection until they were sacrificed (L, n = 8), followed by determination of tumor number, size, and liver:body weight ratio.

(B) Wild-type mice treated as described earlier were sacrificed at the time point when the gut-sterilization treatment was started to determine whether macroscopic or microscopic tumors were present.

(C) Wild-type mice were treated with DEN (25 mg/kg i.p.) at Day 15 postpartum followed by 14 weekly injections of CCl_4. After confirming the presence of tumor by ultrasound (data not shown), mice were treated with (Abx, n = 7) or without (Ctrl, n = 6) antibiotics (ampicillin, vancomycin, neomycin, and metronidazole) starting 2 weeks after the last CCl_4 injection. After 6 weeks of antibiotics, mice were sacrificed, and tumor number, size, and liver:body weight ratio was determined. Data are represented as means ± SD. *$p < 0.05$. **$p < 0.01$. ns, nonsignificant.

See also Figure S5.

promote tumor formation by increasing proliferation in nontumor liver (Figure 8A).

Both gut-sterilized and *Tlr4*^{mut} mice displayed a significant increase in cleaved-caspase 3-positive cells with predominant expression of cleaved-caspase 3 in hepatocytes in nontumor areas (Figure 8B). Notably, the number of cleaved caspase 3-positive cells was inversely and highly significantly correlated with tumor number, size, and the liver:body weight ratio (Figure 8B), further underlining the biological relevance of these findings. Significant increases in cleaved-caspase 3 positive cells and a strong and highly significant inverse correlation between cleaved-caspase 3 and tumor number, size, and liver:body weight ratio were also observed in mice that were gut-sterilized at late time points (Figures 8C and 8D). Moreover, the expression of NF-κB-regulated antiapoptotic genes *Birc3*, *Birc5*, and *Nos2* (Hatano et al., 2001; Wang et al., 1998) was reduced in nontumor areas of livers from *Tlr4*^{mut} and antibiotics-treated mice (Figure 8E), suggesting that TLR4 and the intestinal microbiota provide survival signals that are advantageous for hepatocarcinogenesis.

DISCUSSION

Chronic inflammation is a key contributor to carcinogenesis in various organs including the stomach, colon, lung, and liver (Balkwill and Mantovani, 2001; Grivennikov et al., 2010). In the liver, 80% of HCCs develop in a microenvironment characterized by chronic injury, inflammation, and fibrosis. However, mediators that are responsible for the high risk to develop HCC in the chronically injured liver are largely unknown. Translocation of bacteria and bacterial PAMPs is common in chronic liver disease (Schuppan and Afdhal, 2008; Tandon and Garcia-Tsao, 2008) and promotes inflammation and fibrosis in chronic liver injury (Seki et al., 2007).

We now provide several lines of evidence that the intestinal microbiota and TLR4 link inflammation and carcinogenesis in the chronically injured liver. Genetic TLR4 inactivation, gut sterilization, or GF status decrease HCC development by ≈80%. Conversely, prolonged treatment with low-dose LPS significantly increases HCC development. These findings are similar to intestinal tumorigenesis in which TLR4 and MyD88 drive carcinogenesis (Fukata et al., 2007; Lee et al., 2010; Rakoff-Nahoum and Medzhitov, 2007). In contrast to the intestine, the liver is not in direct contact with intestinal bacteria. However, the liver is the first target of intestinal bacteria and PAMPs translocating into the portal circulation. Moreover, translocation increases with the development of liver fibrosis and cirrhosis (Fukui et al., 1991; Lin et al., 1995; Wiest and Garcia-Tsao, 2005). Our HCC data in GF mice effectively exclude the possibility that the employed antibiotics with low systemic bioavailability might have exerted direct effects on the liver in our model. Moreover, 16s pyrosequencing demonstrated that TLR4 status and LPS treatment do not significantly change

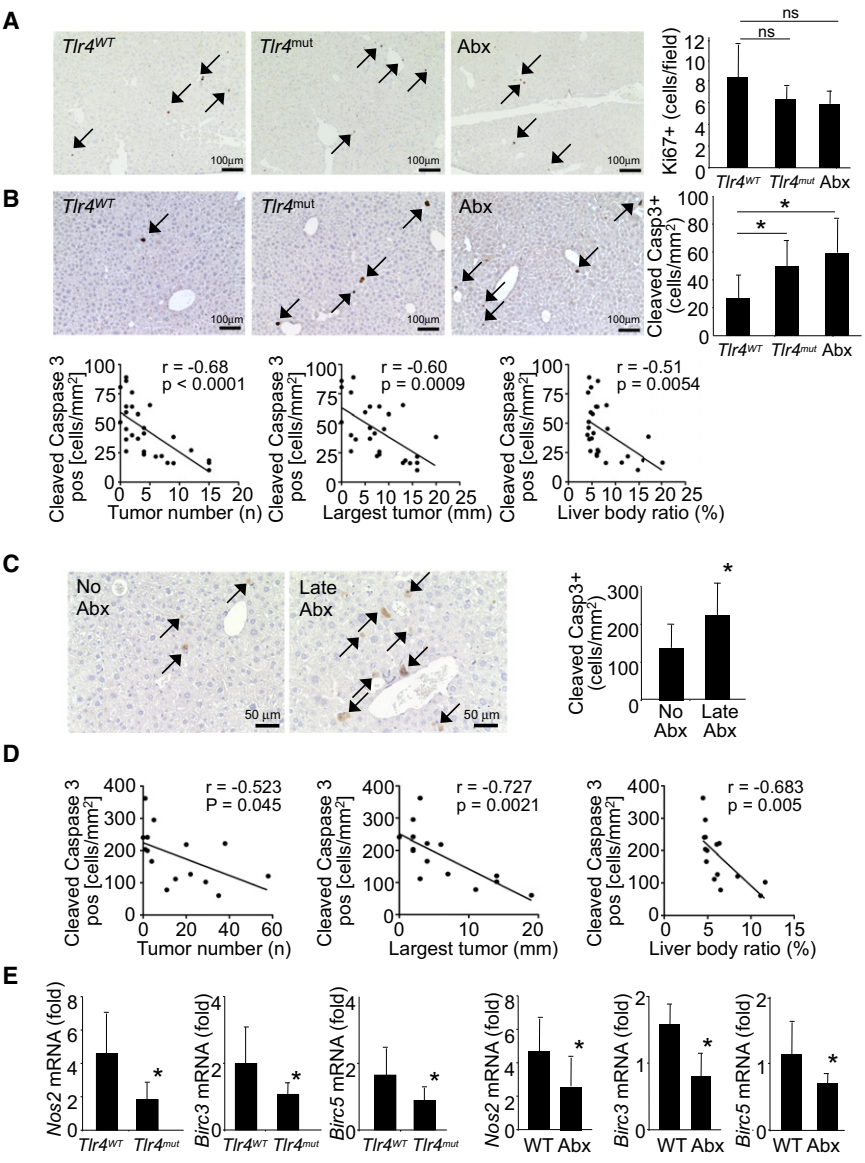

Figure 8. TLR4 and the Intestinal Microbiota Protect from Apoptosis

(A–B) Livers from *Tlr4*^{WT} (n = 11), *Tlr4*^{mut} (n = 9) or antibiotics-treated (Abx) *Tlr4*^{mut} mice (n = 7) were stained for Ki-67 (A) or cleaved-caspase 3 (B) followed by quantification. Correlation between the number of cleaved-caspase 3 positive cells and tumor number, size and liver:body weight ratio was determined.

(C–D) *Tlr4*^{WT} were either not gut sterilized (n = 7) or gut sterilized 2 weeks after the last CCl_4 injection until they were sacrificed (n = 8). Livers were stained for Ki-67 and cleaved-caspase 3 followed by quantification (C). Correlation between the number of cleaved-caspase 3 positive cells and tumor number, size, and liver:body weight ratio was determined (D).

(E) *Nos2*, *Birc3*, and *Birc5* mRNA levels were compared between livers from *Tlr4*^{WT} (n = 12) and *Tlr4*^{mut} (n = 9) mice and between untreated wild-type mice (WT, n = 9) and antibiotics-treated wild-type mice (Abx, n = 6) *Tlr4*^{WT} mice. Data are represented as means ± SD. *p < 0.05.

See also Figure S6.

the composition of the gut microbiome, with the exception of one taxon whose abundance differed between LPS- and PBS-treated mice but not between *Tlr4*^{WT} and *Tlr4*^{mut} mice.

In contrast to a previous study (Yu et al., 2010), we find no significant contribution of the intestinal microbiota and TLR4 to tumor initiation or purely genotoxic hepatocarcinogenesis but demonstrate two distinct mechanisms through which the intestinal microbiota and TLR4 promote HCC: In early stages, TLR4 deficiency and gut sterilization decrease hepatic proliferation and fibrogenesis. Accordingly, gut sterilization or LPS infusion given during early stages moderately decrease or increase hepatocarcinogenesis, respectively. Our study provides evidence that TLR4-dependent HCC promotion in the early phases is predominantly mediated by TLR4-dependent secretion of growth factors such as epiregulin by hepatic stellate cells. Thus, hepatic stellate cells might provide a link between fibrosis and HCC development by increasing growth factors. Based on previous studies showing promotion of growth factor signaling and tumor development by ECM-rich and stiff environment (Levental et al., 2009; Samuel et al., 2011), it is likely that growth factors and ECM produced by hepatic stellate cells synergize in tumor promotion. Our results are consistent with recent studies showing TLR4- and MyD88/Trif-dependent regulation of epiregulin and regeneration after injury in the intestine (Brandl et al., 2010; Hsu et al., 2010). However, HCC reduction in epiregulin-deficient mice was less pronounced than in *Tlr4*^{mut} or gut-sterilized mice, suggesting that additional mechanisms contribute to TLR4-dependent HCC promotion.

The most significant contribution of the intestinal microbiota in our study occurred during later stages of hepatocarcinogenesis independently of CCl_4-induced upregulation of growth factors and regenerative responses. These results are remarkably similar to a previous study in which NF-κB inhibition at late, but not early, stages reduced inflammation-associated HCC (Pikarsky et al., 2004). In line with this study, we detected decreased induction of NF-κB regulated genes and an increased rate of apoptosis in all groups that were protected from HCC development. Accordingly, we found that the hepatocyte compartment which had been unresponsive to LPS in healthy livers became highly sensitive to LPS in DEN plus CCl_4-injured livers. The biological relevance of increased apoptosis for HCC development is emphasized by the strong inverse correlation of tumor number, tumor size, and liver:body weight ratio with cleaved-caspase 3-positive cells in two sets of gut-sterilized mice and in *Tlr4*^{mut} mice. In addition to its role in *Abcb4*^{KO} chronic liver

injury model (Pikarsky et al., 2004), hepatocellular NF-κB also acts a promoter of hepatocarcinogenesis in lymphotoxin-driven HCC (Haybaeck et al., 2009), suggesting a requirement for hepatocellular NF-κB in HCC occurring in the setting of significant inflammation. In contrast, hepatocellular inactivation of NF-κB in genotoxic HCC models enhances hepatocarcinogenesis (He et al., 2010; Maeda et al., 2005). Finally, the complete but rather unphysiological absence of NF-κB activity by Nemo or TAK1 deletion causes chronic hepatocyte injury, liver cirrhosis, and spontaneous HCC (Bettermann et al., 2010; Inokuchi et al., 2010; Luedde et al., 2007). Thus, the presence of inflammation and the degree of NF-κB inhibition appear to be crucial factors that determine whether NF-κB promotes or inhibits hepatocarcinogenesis.

The majority of apoptosis in our study occurred in nontumor areas of the liver suggesting that prosurvival signals provided by the intestinal microbiota and TLR4 are required for the survival of tumor precursors and that apoptosis prevents the development of tumor lesions rather than leading to regression of already established tumors. Accordingly, we observed no effect of gut sterilization on already established HCCs. These results are consistent with previous findings that gene expression profiles in nontumor liver tissue, including gene sets related to NF-κB, TNFα, and interferon signaling—all downstream targets of TLR4—are crucial determinants of tumor recurrence, whereas tumor profiles have no prognostic value (Hoshida et al., 2008).

One important difference between our findings and many previous studies is the tumor-promoting effect of inflammatory signals in resident liver cells. Bone-marrow-derived cells such as macrophages are abundant sources of inflammatory cytokines and contribute to genotoxic HCC (Maeda et al., 2005). Our studies in chimeric mice demonstrate that bone-marrow-derived cells including hepatic macrophages do not mediate the tumor-promoting effects of TLR4 in both acute and long-term HCC models. Accordingly, we found that both hepatic stellate cells and hepatocytes are targets of LPS in the liver with TLR4 on hepatic stellate cells most likely mediating regenerative response after injury and TLR4 on hepatocytes preventing apoptosis of hepatocytes and premalignant cells. Oval cells represent another potential target of LPS and LPS-induced mediators such as TNFα (Brooling et al., 2005), but we found only few areas with A6- and cytokeratin-positive cells typical of oval cells in our tumor model and no influence of TLR4 status and gut sterilization on the number of these cells. Further studies in mice with conditional TLR4 deletion are required to distinguish the relative contribution of TLR4 expressed in hepatocytes versus TLR4 expressed in hepatic stellate cells to hepatocarcinogenesis.

Together with results from a previous study (Pikarsky et al., 2004), our data suggest that chronic liver injury affects the resident liver compartment and makes resident liver cells and/or tumor-forming cells more dependent on inflammatory signals for their survival. With the majority of HCCs occurring in chronically injured livers but many mouse models lacking chronic injury, it is possible that the contribution of inflammatory pathway to human HCC has been underestimated. Our results differ from a previous study in which bone-marrow-derived cell populations were suggested to promote HCC through TLR4 (Yu et al., 2010). Notably, conclusions on the contribution of bone marrow were based on acute responses to DEN instead of HCC development in that study. Moreover, TLR4- and MyD88-dependent carcinogenesis in the intestine and hepatic carcinogenesis in HCV transgenic mice are also promoted by resident cells (Hsu et al., 2010; Lee et al., 2010; Machida et al., 2009; Rakoff-Nahoum and Medzhitov, 2007). In the latter study, TLR4 promotes HCC in alcohol-treated HCV transgenic mice through the upregulation of stem cell markers. Although we observed a strong increase in the stem cell marker prominin 1/CD133 in HCCs, we observed no influence of TLR4 status on its expression in our microarray analysis, suggesting that there may be additional mechanisms by which TLR4 promotes hepatocarcinogenesis in alcohol-treated HCV transgenic mice.

To enable bone marrow transplantation studies in adult mice, our study took advantage of the high HCC susceptibility of the C3H strain and used *Tlr4*^{WT} C3H/HeOuJ and *Tlr4*^{mut} C3H/HeJ mice. We can exclude that genetic differences besides TLR4 play a role in the observed promotion of HCC by TLR4 and the intestinal microbiota based on the following findings: (a) The *Tlr4* locus is the only SNP among 2,059 tested SNPs that differs between C3H/HeOuJ and C3H/HeJ mice (www.jax.org/phenome). (b) Findings in C3H/HeOuJ and C3H/HeJ mice were confirmed in wild-type and *Tlr4*^{KO} C57Bl/6 mice. (c) A large set of experiments solely performed in C3H/HeOuJ mice such as gut sterilization and LPS infusion by osmotic pumps demonstrated the HCC-promoting role for the intestinal microbiota and the TLR4 ligand LPS.

The presented data provide conclusive evidence that the intestinal microbiota exerts a profound influence on HCC promotion in the chronically injured liver. Moreover, our study provides a strong rationale for targeting the intestinal microbiota and TLR4 for the primary or secondary prevention of HCC. The astounding reduction of HCC by gut sterilization at late stages suggests that these treatments might exert protective effects even in advanced liver disease. HCC has become the major cause of death in patients with compensated liver cirrhosis, and there is a need for more effective treatment and preventative strategies (Bruix et al., 2004). To translate our findings into clinical medicine, clinically feasible methods of targeting the intestinal microbiota or TLR4 need to be established. The quadruple combination of antibiotics used in the present study almost completely decontaminated the intestine and prevented 80% of murine HCCs but is not suitable for long-term treatment due to known side effects in patients with advanced liver disease. Our study suggests that rifaximin, a nonabsorbable antibiotic that is widely used in patients with advanced liver disease (Bass et al., 2010), may moderately reduce HCC development. Further studies are required to determine if longer treatment duration or combination with other well-tolerated antibiotics could improve the effects of rifaximin or if other approaches such as TLR4 antagonists would reduce HCC development.

EXPERIMENTAL PROCEDURES

Mice: HCC Induction and Evaluation

C3H/HeOuJ, C3H/HeJ, TLR2-deficient mice, TLR4-deficient mice (C57Bl6/10ScN), TNFR1-/IL-1R1-double deficient, and C57Bl/6 mice were purchased

from Jackson Laboratories. Ereg-deficient mice in a C57Bl/6 background were obtained from the Mouse Mutant Regional Resource Center at the University of North Carolina.

In C3H/HeOuJ and C3H/HeJ mice, HCC was induced by intraperitoneal (i.p.) injection of DEN (100 mg/kg) at ages 6-14 weeks followed by 6-12 biweekly injections of carbon tetrachloride (0.5 ml/kg i.p., dissolved in corn oil) unless stated otherwise. For Ereg-deficient mice and C57Bl/6 wild-type controls, HCC was induced by the combination of DEN (25 mg/kg i.p.) given at Day 15 postpartum and 22 weekly injections of CCl_4 (0.5 ml/kg i.p., dissolved in corn oil). For *Tlr2*^{KO} mice and C57Bl/6 wild-type controls, HCC was induced by the combination of DEN (100 mg/kg, i.p.) given at the age of 8 weeks, followed by 25 biweekly injections of CCl_4 (0.5 ml/kg, i.p., dissolved in corn oil). Gut sterilization was done as previously described (Rakoff-Nahoum et al., 2004; Seki et al., 2007) using a combination of ampicillin (1 g/l), neomycin (1 g/l), metronidazole (1 g/l), and vancomycin (500 mg/l) in drinking water. For rifaximin studies, mice received either 250 mg/l rifaximin in drinking water with rifaximin dissolved in Ora-Plus/Ora-Sweet (Cober et al., 2010) or Ora-Plus/Ora-Sweet vehicle translating to a rifaximin dose of 50 mg/kg/day. GF mouse experiments were performed at the University of North Carolina National Gnotobiotic Rodent Resource Center, Chapel Hill, NC. All mice received DEN (25 mg/kg i.p.) in the GF status at Day 15 postpartum. One week after DEN, 50% of mice were moved to an SPF environment. Four weeks after the DEN injection, GF and SPF mice received a total of 10 CCl_4 injections (1 injection per week, at 0.5 ml/kg i.p. in corn oil). GF status was confirmed by biweekly monitoring for the presence of bacteria in the feces by aerobic and anaerobic culture as well as Gram staining of the stool. Mice were sacrificed 30 weeks after the initial DEN injection.

Evaluation of tumor number and size was determined as described by counting the number of visible tumors and measuring the size of the largest tumor with a caliper (Naugler et al., 2007). After sacrifice, livers were explanted, digitally photographed, and weighed to calculate the liver:body weight ratio. To evaluate acute effects of TLR4 and the intestinal microbiota, adult mice were treated with DEN (100 mg/kg i.p.) alone or in combination with either two or four injections of CCl_4 (0.5 ml/kg i.p.), two injections of thioacetamide (400 mg/kg i.p.) or 4 weeks of a choline-deficient L-amino-acid-defined diet. For some experiments, mice were treated with lipsomomal clodronate or liposome vehicles (200 μl i.p.). For some experiments, liver fibrosis was induced by ligating the common bile duct as previously described (Kluwe et al., 2010; Seki et al., 2007). All animal procedures were in accordance to guidelines by the National Institutes of Health and approved by the Institutional Animal Care and Use Committee at Columbia University and the Institutional Animal Care and Use Committee at the University of North Carolina, Chapel Hill.

Human Samples and Cells

Patients with clinical, analytical, and histological features of alcoholic hepatitis were prospectively obtained in the Liver Unit of the Hospital Clínic, Barcelona, between January 2009 and December 2010 (n = 10). Liver biopsies were obtained using a transjugular approach. In all patients, liver specimens were analyzed by an expert liver pathologist. Fragments of normal livers were obtained from optimal cadaveric liver donors (n = 2) or resection of liver metastases (n = 2). All controls had normal serum aminotransferase levels and normal liver histology. Human hepatic stellate cells were isolated by density gradient-based centrifugation from normal liver as described (Kluwe et al., 2010) and used between passages 3 and 5. Procedures involving human materials were approved by the Investigational Review Board of the Hospital Clínic of Barcelona, and informed consent was obtained from all subjects.

Primary Cell Isolations

Primary hepatic stellate cells, Kupffer cells, and hepatocytes were isolated from either normal or DEN plus 2× CCl_4-treated mice using retrograde liver perfusion and isolation techniques as previously described (Seki et al., 2007). For some experiments, hepatic stellate cells were infected with an adenovirus expressing IκB superrepressor (AdIκBsr) or an empty control adenovirus as described elsewhere (Seki et al., 2007).

ACCESSION NUMBERS

Microarray information was deposited at the Gene Expression Omnibus database (http://www.ncbi.nlm.nih.gov/geo/) with the accession number GSE33446.

SUPPLEMENTAL INFORMATION

Supplemental Information includes six figures and Supplemental Experimental Procedures and can be found with this article online at doi:10.1016/j.ccr.2012.02.007.

ACKNOWLEDGMENTS

This study was supported by NIH grants R01DK076920, U54CA163111, and R01AA020211 (to R.F.S.). GF studies were supported by NIH grant P40RR018603 (to R.B.S.). D.H.D. was supported by NIH fellowship 1F31 DK091980-01. J.P. was supported by a postdoctoral fellowship from the Fondation Recherche Medicale. H.K. and R.R. were supported by R01 LM010140 and U54 CA121852. We thank Drs. Ken Olive and Stephen Sastra (Columbia University) for help with ultrasound screening of tumors, Drs. Valentina Factor and Snorri Thorgeirsson (National Cancer Institute, National Institutes of Health) for providing A6 antibody, and Dr. Bo Liu (University of North Carolina) for help with GF mice. D.H.D. performed animal experiments including HCC induction, antibiotics, and LPS treatments, primary cell isolations, immunohistochemistry, and mRNA analysis. A.M. performed HCC induction and BMT experiments. G.G. performed animal experiments including HCC induction, antibiotics treatments, and mRNA analysis. J.P. performed immunohistochemistry and BMT. M.J. performed acute hepatocarcinogenesis studies. I.M. performed ultrasound studies, isolations of primary cells, and 16s determinations. J.M.C. performed 16s studies and immunohistochemistry. H.K. performed 16s analysis. A.A. performed studies on epiregulin secretion in hepatic stellate cells. R.B. performed studies in patients with alcoholic hepatitis. J.H.L. graded tumors. M.B. performed GF studies. R.F. performed statistical and functional analysis for microarray studies. R.B.S. designed GF studies. R.R. performed 16s analysis. R.F.S. designed and coordinated the study; performed mRNA analysis; contributed to experimental set-up, data analysis, and interpretation; and drafted and edited the manuscript.

Received: August 10, 2011
Revised: November 12, 2011
Accepted: February 1, 2012
Published: April 16, 2012

REFERENCES

Balkwill, F., and Mantovani, A. (2001). Inflammation and cancer: back to Virchow? Lancet *357*, 539–545.

Bass, N.M., Mullen, K.D., Sanyal, A., Poordad, F., Neff, G., Leevy, C.B., Sigal, S., Sheikh, M.Y., Beavers, K., Frederick, T., et al. (2010). Rifaximin treatment in hepatic encephalopathy. N. Engl. J. Med. *362*, 1071–1081.

Bettermann, K., Vucur, M., Haybaeck, J., Koppe, C., Janssen, J., Heymann, F., Weber, A., Weiskirchen, R., Liedtke, C., Gassler, N., et al. (2010). TAK1 suppresses a NEMO-dependent but NF-kappaB-independent pathway to liver cancer. Cancer Cell *17*, 481–496.

Brandl, K., Sun, L., Neppl, C., Siggs, O.M., Le Gall, S.M., Tomisato, W., Li, X., Du, X., Maennel, D.N., Blobel, C.P., and Beutler, B. (2010). MyD88 signaling in nonhematopoietic cells protects mice against induced colitis by regulating specific EGF receptor ligands. Proc. Natl. Acad. Sci. USA *107*, 19967–19972.

Broitman, S.A., Gottlieb, L.S., and Zamcheck, N. (1964). Influence of neomycin and ingested endotoxin in the pathogenesis of choline deficiency cirrhosis in the adult rat. J. Exp. Med. *119*, 633–642.

Brooling, J.T., Campbell, J.S., Mitchell, C., Yeoh, G.C., and Fausto, N. (2005). Differential regulation of rodent hepatocyte and oval cell proliferation by interferon gamma. Hepatology *41*, 906–915.

Bruix, J., Boix, L., Sala, M., and Llovet, J.M. (2004). Focus on hepatocellular carcinoma. Cancer Cell *5*, 215–219.

Cirera, I., Bauer, T.M., Navasa, M., Vila, J., Grande, L., Taurá, P., Fuster, J., García-Valdecasas, J.C., Lacy, A., Suárez, M.J., et al. (2001). Bacterial translocation of enteric organisms in patients with cirrhosis. J. Hepatol. *34*, 32–37.

Cober, M.P., Johnson, C.E., Lee, J., and Currie, K. (2010). Stability of extemporaneously prepared rifaximin oral suspensions. Am. J. Health Syst. Pharm. *67*, 287–289.

Dolganiuc, A., Norkina, O., Kodys, K., Catalano, D., Bakis, G., Marshall, C., Mandrekar, P., and Szabo, G. (2007). Viral and host factors induce macrophage activation and loss of toll-like receptor tolerance in chronic HCV infection. Gastroenterology *133*, 1627–1636.

Engelhardt, N.V., Factor, V.M., Yasova, A.K., Poltoranina, V.S., Baranov, V.N., and Lasareva, M.N. (1990). Common antigens of mouse oval and biliary epithelial cells. Expression on newly formed hepatocytes. Differentiation *45*, 29–37.

Fattovich, G., Stroffolini, T., Zagni, I., and Donato, F. (2004). Hepatocellular carcinoma in cirrhosis: incidence and risk factors. Gastroenterology *127* (5, Suppl. 1), S35–S50.

Fukata, M., Chen, A., Vamadevan, A.S., Cohen, J., Breglio, K., Krishnareddy, S., Hsu, D., Xu, R., Harpaz, N., Dannenberg, A.J., et al. (2007). Toll-like receptor-4 promotes the development of colitis-associated colorectal tumors. Gastroenterology *133*, 1869–1881.

Fukui, H., Brauner, B., Bode, J.C., and Bode, C. (1991). Plasma endotoxin concentrations in patients with alcoholic and non-alcoholic liver disease: reevaluation with an improved chromogenic assay. J. Hepatol. *12*, 162–169.

Grivennikov, S.I., Greten, F.R., and Karin, M. (2010). Immunity, inflammation, and cancer. Cell *140*, 883–899.

Hatano, E., Bennett, B.L., Manning, A.M., Qian, T., Lemasters, J.J., and Brenner, D.A. (2001). NF-kappaB stimulates inducible nitric oxide synthase to protect mouse hepatocytes from TNF-alpha- and Fas-mediated apoptosis. Gastroenterology *120*, 1251–1262.

Haybaeck, J., Zeller, N., Wolf, M.J., Weber, A., Wagner, U., Kurrer, M.O., Bremer, J., Iezzi, G., Graf, R., Clavien, P.A., et al. (2009). A lymphotoxin-driven pathway to hepatocellular carcinoma. Cancer Cell *16*, 295–308.

He, G., Yu, G.Y., Temkin, V., Ogata, H., Kuntzen, C., Sakurai, T., Sieghart, W., Peck-Radosavljevic, M., Leffert, H.L., and Karin, M. (2010). Hepatocyte IKKbeta/NF-kappaB inhibits tumor promotion and progression by preventing oxidative stress-driven STAT3 activation. Cancer Cell *17*, 286–297.

Hoshida, Y., Villanueva, A., Kobayashi, M., Peix, J., Chiang, D.Y., Camargo, A., Gupta, S., Moore, J., Wrobel, M.J., Lerner, J., et al. (2008). Gene expression in fixed tissues and outcome in hepatocellular carcinoma. N. Engl. J. Med. *359*, 1995–2004.

Hsu, D., Fukata, M., Hernandez, Y.G., Sotolongo, J.P., Goo, T., Maki, J., Hayes, L.A., Ungaro, R.C., Chen, A., Breglio, K.J., et al. (2010). Toll-like receptor 4 differentially regulates epidermal growth factor-related growth factors in response to intestinal mucosal injury. Lab. Invest. *90*, 1295–1305.

Inokuchi, S., Aoyama, T., Miura, K., Osterreicher, C.H., Kodama, Y., Miyai, K., Akira, S., Brenner, D.A., and Seki, E. (2010). Disruption of TAK1 in hepatocytes causes hepatic injury, inflammation, fibrosis, and carcinogenesis. Proc. Natl. Acad. Sci. USA *107*, 844–849.

Kluwe, J., Pradere, J.P., Gwak, G.Y., Mencin, A., De Minicis, S., Osterreicher, C.H., Colmenero, J., Bataller, R., and Schwabe, R.F. (2010). Modulation of hepatic fibrosis by c-Jun-N-terminal kinase inhibition. Gastroenterology *138*, 347–359.

Lee, S.H., Hu, L.L., Gonzalez-Navajas, J., Seo, G.S., Shen, C., Brick, J., Herdman, S., Varki, N., Corr, M., Lee, J., and Raz, E. (2010). ERK activation drives intestinal tumorigenesis in Apc(min/+) mice. Nat. Med. *16*, 665–670.

Levental, K.R., Yu, H., Kass, L., Lakins, J.N., Egeblad, M., Erler, J.T., Fong, S.F., Csiszar, K., Giaccia, A., Weninger, W., et al. (2009). Matrix crosslinking forces tumor progression by enhancing integrin signaling. Cell *139*, 891–906.

Lin, R.S., Lee, F.Y., Lee, S.D., Tsai, Y.T., Lin, H.C., Lu, R.H., Hsu, W.C., Huang, C.C., Wang, S.S., and Lo, K.J. (1995). Endotoxemia in patients with chronic liver diseases: relationship to severity of liver diseases, presence of esophageal varices, and hyperdynamic circulation. J. Hepatol. *22*, 165–172.

Luedde, T., Beraza, N., Kotsikoris, V., van Loo, G., Nenci, A., De Vos, R., Roskams, T., Trautwein, C., and Pasparakis, M. (2007). Deletion of NEMO/IKKgamma in liver parenchymal cells causes steatohepatitis and hepatocellular carcinoma. Cancer Cell *11*, 119–132.

Luedde, T., and Schwabe, R.F. (2011). NF-κB in the liver—linking injury, fibrosis and hepatocellular carcinoma. Nat. Rev. Gastroenterol. Hepatol. *8*, 108–118.

Machida, K., Tsukamoto, H., Mkrtchyan, H., Duan, L., Dynnyk, A., Liu, H.M., Asahina, K., Govindarajan, S., Ray, R., Ou, J.H., et al. (2009). Toll-like receptor 4 mediates synergism between alcohol and HCV in hepatic oncogenesis involving stem cell marker Nanog. Proc. Natl. Acad. Sci. USA *106*, 1548–1553.

Maeda, S., Kamata, H., Luo, J.L., Leffert, H., and Karin, M. (2005). IKKbeta couples hepatocyte death to cytokine-driven compensatory proliferation that promotes chemical hepatocarcinogenesis. Cell *121*, 977–990.

Naugler, W.E., Sakurai, T., Kim, S., Maeda, S., Kim, K., Elsharkawy, A.M., and Karin, M. (2007). Gender disparity in liver cancer due to sex differences in MyD88-dependent IL-6 production. Science *317*, 121–124.

Nolan, J.P., and Leibowitz, A.I. (1978). Endotoxins in liver disease. Gastroenterology *75*, 765–766.

Pikarsky, E., Porat, R.M., Stein, I., Abramovitch, R., Amit, S., Kasem, S., Gutkovich-Pyest, E., Urieli-Shoval, S., Galun, E., and Ben-Neriah, Y. (2004). NF-kappaB functions as a tumour promoter in inflammation-associated cancer. Nature *431*, 461–466.

Rakoff-Nahoum, S., and Medzhitov, R. (2007). Regulation of spontaneous intestinal tumorigenesis through the adaptor protein MyD88. Science *317*, 124–127.

Rakoff-Nahoum, S., Paglino, J., Eslami-Varzaneh, F., Edberg, S., and Medzhitov, R. (2004). Recognition of commensal microflora by toll-like receptors is required for intestinal homeostasis. Cell *118*, 229–241.

Rutenburg, A.M., Sonnenblick, E., Koven, I., Aprahamian, H.A., Reiner, L., and Fine, J. (1957). The role of intestinal bacteria in the development of dietary cirrhosis in rats. J. Exp. Med. *106*, 1–14.

Sakata, H., Takayama, H., Sharp, R., Rubin, J.S., Merlino, G., and LaRochelle, W.J. (1996). Hepatocyte growth factor/scatter factor overexpression induces growth, abnormal development, and tumor formation in transgenic mouse livers. Cell Growth Differ. *7*, 1513–1523.

Samuel, M.S., Lopez, J.I., McGhee, E.J., Croft, D.R., Strachan, D., Timpson, P., Munro, J., Schröder, E., Zhou, J., Brunton, V.G., et al. (2011). Actomyosin-mediated cellular tension drives increased tissue stiffness and β-catenin activation to induce epidermal hyperplasia and tumor growth. Cancer Cell *19*, 776–791.

Santoni-Rugiu, E., Preisegger, K.H., Kiss, A., Audolfsson, T., Shiota, G., Schmidt, E.V., and Thorgeirsson, S.S. (1996). Inhibition of neoplastic development in the liver by hepatocyte growth factor in a transgenic mouse model. Proc. Natl. Acad. Sci. USA *93*, 9577–9582.

Schuppan, D., and Afdhal, N.H. (2008). Liver cirrhosis. Lancet *371*, 838–851.

Seki, E., De Minicis, S., Osterreicher, C.H., Kluwe, J., Osawa, Y., Brenner, D.A., and Schwabe, R.F. (2007). TLR4 enhances TGF-beta signaling and hepatic fibrosis. Nat. Med. *13*, 1324–1332.

Seki, E., De Minicis, S., Gwak, G.Y., Kluwe, J., Inokuchi, S., Bursill, C.A., Llovet, J.M., Brenner, D.A., and Schwabe, R.F. (2009). CCR1 and CCR5 promote hepatic fibrosis in mice. J. Clin. Invest. *119*, 1858–1870.

Takami, T., Kaposi-Novak, P., Uchida, K., Gomez-Quiroz, L.E., Conner, E.A., Factor, V.M., and Thorgeirsson, S.S. (2007). Loss of hepatocyte growth factor/c-Met signaling pathway accelerates early stages of N-nitrosodiethylamine induced hepatocarcinogenesis. Cancer Res. *67*, 9844–9851.

Tandon, P., and Garcia-Tsao, G. (2008). Bacterial infections, sepsis, and multiorgan failure in cirrhosis. Semin. Liver Dis. *28*, 26–42.

Toyoda, H., Komurasaki, T., Uchida, D., Takayama, Y., Isobe, T., Okuyama, T., and Hanada, K. (1995). Epiregulin. A novel epidermal growth factor with mitogenic activity for rat primary hepatocytes. J. Biol. Chem. *270*, 7495–7500.

Vijay-Kumar, M., Aitken, J.D., Carvalho, F.A., Cullender, T.C., Mwangi, S., Srinivasan, S., Sitaraman, S.V., Knight, R., Ley, R.E., and Gewirtz, A.T. (2010). Metabolic syndrome and altered gut microbiota in mice lacking Toll-like receptor 5. Science *328*, 228–231.

Wang, C.Y., Mayo, M.W., Korneluk, R.G., Goeddel, D.V., and Baldwin, A.S., Jr. (1998). NF-kappaB antiapoptosis: induction of TRAF1 and TRAF2 and c-IAP1 and c-IAP2 to suppress caspase-8 activation. Science *281*, 1680–1683.

Wiest, R., and Garcia-Tsao, G. (2005). Bacterial translocation (BT) in cirrhosis. Hepatology *41*, 422–433.

Yu, L.X., Yan, H.X., Liu, Q., Yang, W., Wu, H.P., Dong, W., Tang, L., Lin, Y., He, Y.Q., Zou, S.S., et al. (2010). Endotoxin accumulation prevents carcinogen-induced apoptosis and promotes liver tumorigenesis in rodents. Hepatology *52*, 1322–1333.

also point out for the first time a specific contribution of p110γ to the survival and growth of a hematologic malignancy. This is new, because the only PI3K isoform thought to be involved in leukemia and lymphomas so far was PI3Kδ, a direct effector of tyrosine phosphorylation events downstream of CD28 and CD19 in T and B cells, respectively. The involvement of p110δ in B cell tumors such as chronic lymphocytic leukemia has recently gained great attention, as selective inhibitors such as CAL-101 have provided encouraging results in combined phase I/II clinical trials with cases of full remission (So and Fruman, 2012). Third, these results pave the way for novel therapeutic targeting in T-ALL. Indeed, Subramaniam et al. (2012) went on to prove this point. They tested derivative compounds of CAL-101 and found that CAL-130 works as a specific dual inhibitor of p110γ and p110δ. When given to mice, CAL-130 closely reproduced the thymic phenotype of double *Pik3cg*- and *Pik3cd* null mutants. Strikingly, and more importantly, CAL-130 prolonged survival of PTEN null mice and reduced human T-ALL growth by inducing apoptosis due to a block of the AKT-mediated survival pathway. Although further experimentation and clinical trials are required to fully access the efficacy and toxicity, mice treated with the currently available compound did not show major signs of toxicity. The future possibility of treating patients with a p110γ/p110δ dual inhibitor that in principle avoids the undesirable systemic effects that may be linked to pan-PI3K inhibition, such as diabetes, is particularly attractive. Whether this approach can be widened to other T lymphomas, which may also depend on both p110γ and p110δ for their growth, or if it is effective only in PTEN-deficient T-ALL remains to be established. Future studies will likely better define the spectrum of efficacy of PI3Kδ and PI3Kγ targeting in T-ALL with different genetic defects as well as in a larger set of hematological malignancies.

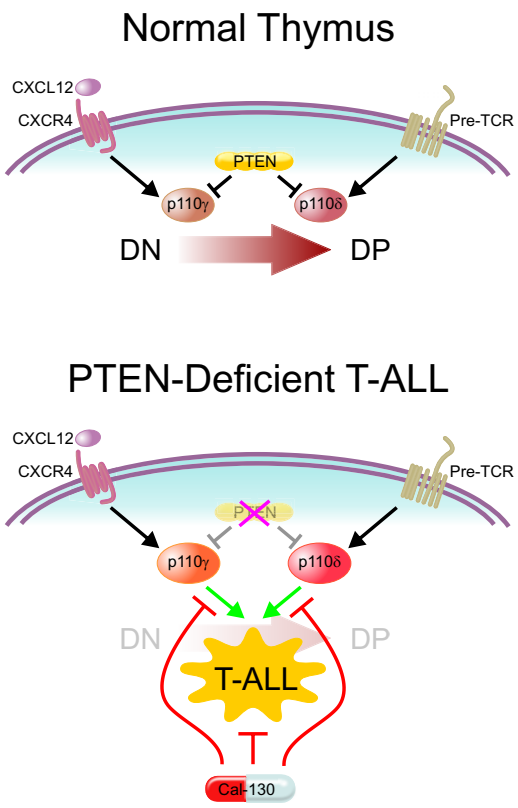

Figure 1. Role of PI3Kδ and PI3Kγ Isoforms in the Development of Normal Thymocytes and T-ALL

(Top) Signal transduction events leading to differentiation of T cells from the double negative (DN) to the double positive (DP) stage.

(Bottom) Loss of PTEN leads to unrestrained p110γ and δ activity and T-ALL. The use of the drug CAL-130 inhibits these two p110 PI3K isoforms, thus blocking T-ALL.

REFERENCES

Aifantis, I., Raetz, E., and Buonamici, S. (2008). Nat. Rev. Immunol. *8*, 380–390.

Ciraolo, E., Iezzi, M., Marone, R., Marengo, S., Curcio, C., Costa, C., Azzolino, O., Gonella, C., Rubinetto, C., Wu, H., et al. (2008). Sci. Signal. *1*, ra3.

Ghigo, A., Damilano, F., Braccini, L., and Hirsch, E. (2010). Bioessays *32*, 185–196.

Jia, S., Liu, Z., Zhang, S., Liu, P., Zhang, L., Lee, S.H., Zhang, J., Signoretti, S., Loda, M., Roberts, T.M., and Zhao, J.J. (2008). Nature *454*, 776–779.

Kang, S., Denley, A., Vanhaesebroeck, B., and Vogt, P.K. (2006). Proc. Natl. Acad. Sci. USA *103*, 1289–1294.

Martin, D., Galisteo, R., Molinolo, A.A., Wetzker, R., Hirsch, E., and Gutkind, J.S. (2011). Cancer Cell *19*, 805–813.

Schmid, M.C., Avraamides, C.J., Dippold, H.C., Franco, I., Foubert, P., Ellies, L.G., Acevedo, L.M., Manglicmot, J.R., Song, X., Wrasidlo, W., et al. (2011). Cancer Cell *19*, 715–727.

So, L., and Fruman, D.A. (2012). Biochem. J. *442*, 465–481.

Subramaniam, P.S., Whye, D.W., Efimenko, E., Chen, J., Tosello, V., De Keersmaecker, K., Kashishian, A., Thompson, M.A., Castillo, M., Cordon-Cardo, C., et al. (2012). Cancer Cell *21*, this issue, 459–472.

Wong, K.K., Engelman, J.A., and Cantley, L.C. (2010). Curr. Opin. Genet. Dev. *20*, 87–90.